NATIONAL TECHNICAL UNIVERSITY OF ATHENS
SCHOOL OF CIVIL ENGINEERING
GEOTECHNICAL DEPARTMENT

ΕΘΝΙΚΟ ΜΕΤΣΟΒΙΟ ΠΟΛΥΤΕΧΝΕΙΟ
ΣΧΟΛΗ ΠΟΛΙΤΙΚΩΝ ΜΗΧΑΝΙΚΩΝ
ΤΟΜΕΑΣ ΓΕΩΤΕΧΝΙΚΗΣ

NUMERICAL INVESTIGATION OF LATERALLY LOADED PILES IN CLAYEY SOILS

ΑΡΙΘΜΗΤΙΚΗ ΔΙΕΡΕΥΝΗΣΗ ΤΗΣ ΕΓΚΑΡΣΙΑΣ ΦΟΡΤΙΣΗΣ ΠΑΣΣΑΛΟΥ ΣΕ ΑΡΓΙΛΙΚΑ ΕΔΑΦΗ

DOCTORAL THESIS
of
KONSTANTINOS P. TZIVAKOS
Diploma of Civil Engineering, NTUA
M.Sc. National Technical University of Athens

ΔΙΔΑΚΤΟΡΙΚΗ ΔΙΑΤΡΙΒΗ
του
ΚΩΝΣΤΑΝΤΙΝΟΥ Π. ΤΖΙΒΑΚΟΥ
Διπλ. Πολιτικός Μηχανικός ΕΜΠ
Μ.Δ.Ε. Εθνικό Μετσόβιο Πολυτεχνείο

Supervisor:
Michael J. Kavvadas
Associate Professor, NTUA

Επιβλέπων:
Μιχαήλ Ι. Καββαδάς
Αναπληρωτής Καθηγητής ΕΜΠ

Athens, June 2017

Αθήνα, Ιούνιος 2017

ΕΘΝΙΚΟ ΜΕΤΣΟΒΙΟ ΠΟΛΥΤΕΧΝΕΙΟ
ΣΧΟΛΗ ΠΟΛΙΤΙΚΩΝ ΜΗΧΑΝΙΚΩΝ
ΤΟΜΕΑΣ ΓΕΩΤΕΧΝΙΚΗΣ

ΑΡΙΘΜΗΤΙΚΗ ΔΙΕΡΕΥΝΗΣΗ ΤΗΣ ΕΓΚΑΡΣΙΑΣ ΦΟΡΤΙΣΗΣ ΠΑΣΣΑΛΟΥ ΣΕ ΑΡΓΙΛΙΚΑ ΕΔΑΦΗ

ΔΙΔΑΚΤΟΡΙΚΗ ΔΙΑΤΡΙΒΗ

ΚΩΝΣΤΑΝΤΙΝΟΥ Π. ΤΖΙΒΑΚΟΥ

Διπλ. Πολιτικός Μηχανικός ΕΜΠ

Μ.Δ.Ε. Εθνικό Μετσόβιο Πολυτεχνείο

Η διατριβή υποβάλλεται στη Σχολή Πολιτικών Μηχανικών του Εθνικού Μετσόβιου Πολυτεχνείου προς εκπλήρωση των προϋποθέσεων του τίτλου του Διδάκτορος Μηχανικού

ΤΡΙΜΕΛΗΣ ΣΥΜΒΟΥΛΕΥΤΙΚΗ ΕΠΙΤΡΟΠΗ:

1. Μ. ΚΑΒΒΑΔΑΣ, Αν. Καθηγητής ΕΜΠ (Επιβλέπων)
2. Γ. ΜΠΟΥΚΟΒΑΛΑΣ, Καθηγητής ΕΜΠ
3. Ν. ΓΕΡΟΛΥΜΟΣ, Αν. Καθηγητής ΕΜΠ

ΕΠΤΑΜΕΛΗΣ ΕΞΕΤΑΣΤΙΚΗ ΕΠΙΤΡΟΠΗ:

1. Μ. ΚΑΒΒΑΔΑΣ, Αν. Καθηγητής ΕΜΠ (Επιβλέπων)
2. Γ. ΜΠΟΥΚΟΒΑΛΑΣ, Καθηγητής ΕΜΠ
3. Ν. ΓΕΡΟΛΥΜΟΣ, Αν. Καθηγητής ΕΜΠ
4. Γ. ΓΚΑΖΕΤΑΣ, Καθηγητής ΕΜΠ
5. Γ. ΜΥΛΩΝΑΚΗΣ, Καθηγητής Πανεπ. Πατρών
6. Β. ΓΕΩΡΓΙΑΝΝΟΥ, Αν. Καθηγήτρια ΕΜΠ
7. Α. ΠΑΠΑΔΗΜΗΤΡΙΟΥ, Επίκ. Καθηγητής ΕΜΠ

Αθήνα, Ιούνιος 2017

NATIONAL TECHNICAL UNIVERSITY OF ATHENS
SCHOOL OF CIVIL ENGINEERING
GEOTECHNICAL DEPARTMENT

NUMERICAL INVESTIGATION OF LATERALLY LOADED PILES IN CLAYEY SOILS

DOCTORAL THESIS

KONSTANTINOS P. TZIVAKOS

Dipl. Civil Engineer, National Technical University of Athens
M.Sc. National Technical University of Athens

The thesis is submitted to the School of Civil Engineering of the National Technical University of Athens in fulfilment of the requirements for the Degree of Doctor of Philosophy

ADVISORY COMMITTEE:

1. M. KAVVADAS, Assoc. Professor NTUA (Supervisor)

2. G. BOUCKOVALAS, Professor NTUA

3. N. GEROLYMOS, Assoc. Professor NTUA

EXAMINATION COMMITTEE:

1. M. KAVVADAS, Assoc. Professor NTUA (Supervisor)

2. G. BOUCKOVALAS, Professor NTUA

3. N. GEROLYMOS, Assoc. Professor NTUA

4. G. GAZETAS, Professor NTUA

5. G. MYLONAKIS, Professor Un. of Patras

6. V. GEORGIANNOU, Assoc. Professor NTUA

7. A. PAPADIMITRIOU, Asst. Professor NTUA

Athens, June 2017

This document was created using LaTeX.

Thesis Structure \ Δομή Τεύχους Διατριβής

Στην οικογένειά μου,

Πέτρο, Βενετία, Ζαφείρη και Σταύρο

Προλεγόμενα

«Πάμε στον κόσμο υπέροχα μονάχοι, μ' ένα παλιό τραγούδι χαρωπό, το τραγουδάνε οι θαλασσομάχοι και λέει στον γλυκό του τον σκοπό πως μάταιο ταξίδι δεν υπάρχει» έγραψε κάποτε ο στιχουργός - το ¨ποιητής¨ δεν του άρεσε, τέτοιο υπήρξε το μεγαλείο της ταπεινοφροσύνης του - Βαγγέλης Λιάρος (κατά κόσμον Άλκης Αλκαίος). Κάθε που έβρισκα τα σκούρα λοιπόν σε όλη τη διάρκεια του διδακτορικού, οι παραπάνω στίχοι μαζί με το μότο ζωής του πατέρα μου «υπομονή κι επιμονή» αποτέλεσαν τη ρεζέρβα μου λίγο πριν ξεμείνω από δυνάμεις. Η πορεία του διδακτορικού υπήρξε για εμένα ένα πολυδιάστατο ταξίδι, γεμάτο πρόσωπα και εμπειρίες που συνθέτουν ένα πανέμορφο παζλ. Κομμάτια αυτού του παζλ θα σας εξιστορήσω μέσα στις επόμενες παραγράφους.

Όλα ξεκίνησαν το μακρινό 2009, όταν ο επιβλέπων μου, Αναπληρωτής Καθηγητής κ. Μιχάλης Καββαδάς με δέχτηκε εγκάρδια στην ερευνητική του ομάδα και μου ανέθεσε το θέμα της διατριβής. Δάσκαλε, θέλω να σας ευχαριστήσω από τα βάθη της καρδιάς μου για την εμπιστοσύνη που δείξατε όλα αυτά τα χρόνια στο πρόσωπό μου καθώς και για την ευκαιρία που μου δώσατε να ζήσω αυτό το μοναδικό ταξίδι! Η ενασχόλησή μου με τη διδασκαλία και η συμμετοχή μου σε συνέδρια, ερευνητικά προγράμματα, επιστημονικές και επαγγελματικές συναντήσεις όλα αυτά τα χρόνια αποτέλεσαν για εμένα μάθημα ζωής. Τα χρωστάω όλα πρωτίστως στο γεγονός ότι πιστέψατε σε εμένα και σας είμαι ευγνώμων. Υπόσχομαι να μην ξεχάσω ποτέ τα παρακάτω λόγια σας: «Κωνσταντίνε, τη γνώση που παράγουμε πρέπει να τη μοιραζόμαστε. Το οφείλουμε στην ανθρωπότητα ως αντάλλαγμα του δώρου της ευστροφίας που τόσο απλόχερα μας χάρισε η φύση!». Εύχομαι κάποια στιγμή στη ζωή μου να αποκτήσω την οξυδέρκειά σας ως μηχανικός και τη διπλωματία σας ως άνθρωπος! Να είστε πάντα καλά!

Επιπρόσθετα, οφείλω να ευχαριστήσω τα άλλα δύο μέλη της τριμελούς συμβουλευτικής επιτροπής μου, τον Καθηγητή κ. Γιώργο Μπουκοβάλα και τον Αναπληρωτή Καθηγητή κ. Νίκο Γερόλυμο που πίστεψαν στις δυνάμεις μου και με καθοδήγησαν σοφά κατά τη διάρκεια της προσπάθειάς μου. Στη συνέχεια, θέλω να εκφράσω τις ευχαριστίες μου και προς τους υπόλοιπους καθηγητές που συνέθεσαν

την επταμελή εξεταστική επιτροπή της διατριβής μου, τους Καθηγητές κ. Γιώργο Γκαζέτα και κ. Γιώργο Μυλωνάκη, την Αναπληρώτρια Καθηγήτρια κα. Βασιλική Γεωργιάννου και τον Επίκουρο Καθηγητή κ. Αχιλλέα Παπαδημητρίου. Επίσης θέλω να ευχαριστήσω όλα τα υπόλοιπα μέλη ΔΕΠ του Τομέα μας που δεν αναφέρθηκαν παραπάνω, τόσο για την επιστημοσύνη όσο και για το ήθος που τους διακρίνει. Πριν ξεκινήσω με τους συναδέλφους μου, θέλω να πω ακόμα ένα ευχαριστώ στις γραμματείς μας, κα. Σίσσυ, Ελίζα, Γιασεμή και Ναταλία καθώς και στη γραμματέα της σχολής, υπεύθυνη για θέματα Υ/Δ κα. Λία Θεοφανίδου που πάντα υπήρξαν πρόθυμες να με εξυπηρετήσουν στα ζητήματα γραφειοκρατίας.

Με τους στυλοβάτες της ομάδας Καββαδά τότε είχα εξοικειωθεί από το καλοκαίρι του 2007, όταν εκπονούσα τη διπλωματική κι έναν χρόνο μετά τη μεταπτυχιακή μου εργασία. Ο λόγος για τους αυτοκόλλητους Γιώργο Προυντζόπουλο και Πέτρο Φορτσάκη. Υπό την καθοδήγηση του Γιώργου - με κωδική ονομασία "Idol No2" - έκανα τα πρώτα μου ερευνητικά βήματα και τον ευχαριστώ θερμά για τη μύηση (< 3)! Γιώργο, είμαστε πλέον 10 χρόνια φίλοι - στα 15 μπουνιές. Με τον Πέτρο είχα την ευκαιρία να ανταλλάξω απόψεις επιστημονικού και μη χαρακτήρα, καθώς και να συνεργαστώ αρκετές φορές στα πρώτα χρόνια του διδακτορικού. Πέτρο, πώς κατάφερε φίλε να σε φουσκώσει αυτό το ένα κομμάτι περγαμόντο μετά το τσιμπούσι στην Κόρινθο ακόμα το έχω απορία, για όνομα του Θεού! Το ουσιαστικό δέσιμο και με τους δύο ήρθε εκείνο το βράδυ στο Άμστερνταμ, μετά το συνέδριο EURO:TUN 2009 στο Μπόχουμ, το οποίο μας έχει μείνει αξέχαστο.

Έτσι αβίαστα και τελείως φυσικά ξεκίνησε η περίοδος του «γραφείου» στον Τομέα Γεωτεχνικής, ο οποίος τολμώ να πω ότι αποτέλεσε το σπίτι μου τα τελευταία 7 χρόνια - στο φυσικό μου σπίτι μόνο για έναν ύπνο πήγαινα για ένα μεγάλο διάστημα του διδακτορικού. Ο πρώτος άνθρωπος που γνώρισα στο γραφείο ήταν η Χαρά Παπαχατζάκη, η πάντα ευγενική και διακριτική Χαρά, η οποία με υποδέχτηκε θερμά και την ευχαριστώ. Στη συνέχεια, γνωρίστηκα με τον Αλέξανδρο Καλό, έναν άνθρωπο με μοναδική μαθηματική αντίληψη, γείτονά μου εξ' αριστερών στο γραφείο και συνταξιδιώτη όλα αυτά τα χρόνια σε μαθήματα, διπλωματικές εργασίες και ερευνητικές προσπάθειες. Αλέξανδρε, σ' ευχαριστώ πολύ για την κριτική σου διάθεση απέναντι στους προβληματισμούς μου καθώς και για την καθοριστική συμβολή σου σε ένα πολύ σημαντικό μέρος της διατριβής. Να ξέρεις επίσης ότι για τη lemon pie που μας έμαθες, ο ουρανίσκος μου θα σε ευγνωμονεί για πάντα! Εύχομαι να καταφέρεις όλες σου τις επιστημονικές επιδιώξεις, χωρίς όμως να αμφιβάλλεις για τα πάντα - φιλική και πάντα καλοπροαίρετη συμβουλή, με αγάπη! Τον τέταρτο της «συγκατοίκησης», Παναγιώτη Σιταρένιο, τον αφήνω γι' αργότερα, όντας ένας από τους τρεις σωματοφύλακες... Στο σημείο αυτό, θέλω να ευχαριστήσω τα υπόλοιπα μέλη της ερευνητικής ομάδας Καββαδά, ξεκινώντας από

τους αρχαιότερους. Αγαπητέ Γιώργο Μπελόκα, δε θα ξεχάσω τα ακόλουθα δύο γεγονότα: τη μέρα που σε γνώρισα στην παρουσίαση της διατριβής σου (τρομερά αμήχανη στιγμή) και την αποκάλυψή σου σε δεινό ψήστη σ' εκείνο το πρώτο barbeque έξω από το κυλικείο. Σ' ευχαριστώ πολύ για όλες σου τις συμβουλές αυτά τα χρόνια και σε θαυμάζω για την ήρεμη δύναμη που σε διακρίνει. Μιχάλη Μπαρδάνη και Σμαράγδα Ευθυμίου, αν και δεν είχαμε την ευκαιρία να συναναστραφούμε αρκετά στην περίοδο του διδακτορικού, θέλω να σας ευχαριστήσω και τους δύο για το κουράγιο που μου δίνατε όποτε σας συναντούσα. Παρέα με τους δύο νεότερους ερευνητές της ομάδας, τον Δημήτρη Λίτσα και τον Φίλιππο Χόρτη, ζήσαμε μεγάλες στιγμές εντός κι εκτός συνόρων. Μήτσο μπουλντόζα, σ' ευχαριστώ πολύ που κάλυπτες τα νώτα μου σε θέματα Excel και VBA. Μα τι ωραία περάσαμε στο Old Traford, στη Ρώμη, στο Σαν Φρανσίσκο ρε φίλε... Κύριε Χόρτη μας (FC), μου θυμίζετε πολύ εμένα στη διάρκεια των δύσκολων ετών του διδακτορικού, τότε που πάλευα να του δώσω συγκεκριμένη μορφή και να πάρω την απόφαση να το τελειώσω. Σε προτρέπω να κάνεις αυτή τη γενναία κίνηση χωρίς φόβο και θα διαπιστώσεις ότι το φως στην άλλη άκρη των δίδυμων σηράγγων σου είναι πολύ πιο κοντά απ' όσο νομίζεις... Είσαι εγγυητής και θα τα καταφέρεις!

Από τις υπόλοιπες ερευνητικές ομάδες του Τομέα γνώρισα πολύ κόσμο, αλλά οι αναμνήσεις που έζησα με συγκεκριμένους ανθρώπους θα έρχονται πάντα στον νου μου όταν γυρίζω στα χρόνια του διδακτορικού. Ο Γιάννης Χαλούλος και ο Δημήτρης Καραμήτρος είναι οι δύο πρώτοι, έχουν ξεχωριστή θέση στην καρδιά μου και θα αναφερθώ σε αυτούς αργότερα, όντας οι άλλοι δύο σωματοφύλακες! Κι αφού ξεκινήσαμε με την ομάδα Μπουκοβάλα, θέλω να ευχαριστήσω τον αεροπόρο - υπηρετεί τώρα το παιδί - και μέγα φωτογράφο Γιάννη Τσιάπα, ο οποίος με τις φωτογραφίες του κράτησε ζωντανές μοναδικές κι ανεπανάληπτες στιγμές που ζήσαμε στον Τομέα. Ευχαριστώ επίσης τον Κωνσταντίνο Μπαζαίο για τις πάντα καλοδεχούμενες μουσικές του παρεμβάσεις στην ομολογουμένως πηγμένη καθημερινότητα των τελευταίων δύο ετών. Μπαζαίε, σε προ(σ)καλώ να κανονίσουμε επιτέλους να πάμε μαζί σε ένα λάιβ ρε φίλε, έλεος. Από την ίδια ομάδα, δε μπορούν να λείπουν οι φιλοφρονήσεις προς την Κική Δημητριάδη για την ευγένειά της, τον Αλέξανδρο Βαλσαμή για τον μειλίχιο και βαθύτατα καλλιεργημένο χαρακτήρα του και τον Γιώργο Κουρετζή ("THE IDOL") γιατί έτσι! Και συνεχίζω... Πώς να ξεχάσει κανείς τον μεγάλο «μπαλαδόρο» Θανάση Ζαφειράκο, τη φωνή της λογικής Γιώτα Τασιοπούλου, το αγόρι Σπύρο Γιαννακό και τη μεγάλη αναρριχήτρια Μαριάννα Λώλη; Εξίσου ευχαριστώ και τη Γεωργίτσα μας την Αγαπουλάκη για την τόνωση του ηθικού σ' εκείνο το συνέδριο στο Εδιμβούργο. Τελευταίο, αλλά καθόλου καταϊδρωμένο (εξαιρώντας την ημέρα της παρουσίασής του που δεν αγχώθηκε καθόλου) άφησα τον γιο της Ψυχραιμίας, μυαλό-ξουράφι και ταλέντο στην

αραγματική, Παύλο Αστερίου. Παύλε μου το 2013 στην Πολωνία επεράσαμε όμορφα, αλλά τα καλοκαίρια στην Αίγινα περνάμε ομορφότερα, να τα λέμε κι αυτά! Σ' ευχαριστώ πολύ που σε κάθε αλληλεπίδρασή μας μου θυμίζεις τι θα πει να είσαι cool και να παιδεύεις το μυαλό σου με τα απολύτως απαραίτητα - ενίοτε και με λιγότερα από αυτά, για να είμαστε ακριβοδίκαιοι.

Και κάπου εδώ κάνουν την εμφάνισή τους οι τρεις σωματοφύλακες! Ο λόγος για τους: Γιάννη Χαλούλο, Παναγιώτη Σιταρένιο και Δημήτρη Καραμήτρο. Πλάι τους, ως άλλος Ντ' Αρτ-αρνιάν (καλά διαβάσατε, δεν είναι τυπογραφικό λάθος) μαθήτευσα σε πολλά και διαφορετικά επιμέρους σχολεία, εντός κι εκτός των στενών επιστημονικών ορίων του διδακτορικού. Οι τέσσερίς μας τολμώ να πω ότι διαμορφώσαμε ένα κλίμα άνευ προηγουμένου στον Τομέα Γεωτεχνικής τα χρόνια που οι τροχιές μας συμπέσανε. Τι να πρωτοθυμηθώ; Τις ραδιοφωνικές εκπομπές στο γραφείο, τα ψητούρια στο «μπαλκονάκι», τα Bacardia στο κυλικείο; Όλα ήρθαν κι έδεσαν όμως εκείνο το μαγικό βράδυ Πέμπτης του 2012, όπου μετά από ένα «συμβατικό» Rock Pourri πήραν φωτιά τα όργανα και τα ποτήρια και μαζί μ' αυτά οι ψυχές μας που από τότε έχουν μείνει αχώριστες κατά τη δική μου ρομαντική εκδοχή...

Θα ξεκινήσω από τον Δημήτρη, με τον οποίο κυρίως μοιραστήκαμε κοινά ενδιαφέροντα μουσικής, αστρονομικής και τεχνολογικής φύσεως. Αγαπημένε μου Πουφ, σ' ευχαριστώ που (παρέα με τον Γιάννη) μου μετέδωσες μέσα σε ελάχιστες ώρες τις βασικές θεωρητικές αρχές των μουσικών κλιμάκων και συγχορδιών. Για την ευγενική παραχώρηση του τηλεσκοπίου σου και τις βραδιές αστρονομίας στη Θεολογάρα δε βρίσκω λόγια για να σε ευχαριστήσω. Μιας κι αναφέρθηκα στον Θεολόγο, ασπάζομαι σταυρωτά τον αδερφό σου Αντρέα και τον ευχαριστώ για τα όμορφα βράδια στο λοφτ (HM, keep up the great work!). Περισσότερο απ' όλα όμως Δημήτρη, σου είμαι ευγνώμων γιατί στο πρόσωπό σου βρήκα έναν άνθρωπο με πολυσχιδή προσωπικότητα και όρεξη να «τερματίζει» το κάθε αντικείμενο με το οποίο καταπιάνεται. Σε είχα πάντα στο μυαλό μου όταν προσπαθούσα μέσα σ' αυτά τα χρόνια να συνδυάσω δουλειά, ενδιαφέροντα και προσωπική ζωή. Δεν ξέρω πόσο καλά τα κατάφερα σε όλα εν τέλει, αλλά πάντα θα ηχεί στ' αυτιά μου η εξής φράση σου: «Το πρόβλημα με την πάρτη μας είναι ότι θέλουμε και να περνάμε καλά!». Για όλα τα παραπάνω σ' ευχαριστώ φίλε και σου εύχομαι να είσαι πάντα ευτυχισμένος - γιατί πετυχημένος είσαι σίγουρα!

Περνάω στον Παναγιώτη, με τον οποίο συγκατοικήσαμε στο γραφείο - μαζί και με τον Αλέξανδρο Κ. - κατά το μεγαλύτερο διάστημα εκπόνησης της διατριβής. Για αρχή θέλω να τον ευχαριστήσω που με έπεισε (εντάξει, δε δυσκολεύτηκε κι ιδιαίτερα) να χρησιμοποιήσω τη LaTeXάρα για τη συγγραφή αυτού του τεύχους - ΤΕΡΑΣΤΙΑ ΥΠΟΧΡΕΩΣΗ! Νομίζω ότι με τον Πάνο μοιραστήκαμε τους

περισσότερους κοινούς προβληματισμούς, άγχη κι έγνοιες όλα αυτά τα χρόνια αναφορικά με την πορεία των διδακτορικών μας. Όλο αυτό μας έφερε τόσο κοντά που μετά από πολύ λίγο καιρό συναναστροφής εφευρίσκαμε αντίστοιχες κοινές διεξόδους εκτόνωσης της πίεσης. Άλλοτε παίρναμε τα βουνά για σκι, άλλοτε τις θάλασσες για ιστιοπλοΐα, άλλοτε τα γήπεδα για τον Ολυμπιακό κι άλλοτε δυο ποτηράκια ουίσκι για να σβήσουμε τον καημό μας. Το κοινό μας πάθος για ταξίδια μας έφερε συνταξιδιώτες πολλές φορές (Ιταλία, Αγγλία, Αμερική αλλά και Κύθνο, Τζιά και Μύκονο), ακριβώς όπως συμπορευτήκαμε και στα διδακτορικά. Ο ορισμός της σχέσης «κράτα με να σε κρατώ ν' ανεβούμε στο βουνό» (κι εδώ σου κλείνω το μάτι για την ανάβαση του Έβερεστ αν δεν το κατάλαβες)! Στο σημείο αυτό θέλω να εξαίρω την αντίληψη του Παναγιώτη ως μηχανικού, του οποίου οι παρεμβάσεις και οι συμβουλές υπήρξαν καίριες για την ολοκλήρωση της διατριβής μου. Όντας εξοικειωμένος με το επάγγελμα του μηχανικού στην πράξη τα χρόνια πριν και κατά τη διάρκεια του διδακτορικού του, προσπάθησε να εμφυσήσει στην ερευνητική μας ομάδα τη σημασία της φυσικής σκέψης στο οποιοδήποτε πρόβλημα και νιώθω την ανάγκη - τουλάχιστον προσωπικά - να τον ευχαριστήσω θερμά γι' αυτό. Φίλε Πάνο, σου εύχομαι από εδώ καλό κατευόδιο στη γείτονα χώρα. Είμαι βέβαιος ότι και σε αυτό το βήμα της επιστημονικής σου σταδιοδρομίας θα τα πας τόσο περίφημα, όπως σε όλα τα προηγούμενα, γιατί το αξίζεις!

Για τον Γιάννη και τη σχέση που έχουμε αναπτύξει όλα αυτά τα χρόνια ό,τι και να πω θα είναι λίγο. Γι' αυτό θα το τραβήξω στα όρια της υπερβολής μήπως και καταφέρω να αποδώσω ένα σεβαστό μέρος της πραγματικότητας. Αδυνατώ να θυμηθώ πότε δώσαμε τα χέρια για πρώτη φορά και είπαμε τις γνωστές τυπικούρες, αλλά μου έρχεται στη μνήμη εκείνο το καλοκαίρι του 2010 στις Σπέτσες να κόβει και να ράβω μέσα στην παρέα. Κάπως έτσι νομίζω ότι άρχισαν όλα! Τα πήγαινε-έλα στο κυλικείο, οι χαβαλέδες, οι ανταλλαγές μουσικών απόψεων αλλά και οι πάντα εύστοχες υποδείξεις όταν τις επιζητούσα από εκείνον κατά τη διάρκεια της διατριβής. Αποκορύφωμα της χημείας μας - την οποία είμαι σίγουρος ότι θα αρνηθεί διαβάζοντας αυτές τις γραμμές - ήταν η εκπομπή που παρέα κάναμε (εκείνος ως παραγωγός κι εγώ ως τεχνικός) σε έναν διαδικτυακό ραδιοφωνικό σταθμό του ΕΜΠ επί δύο χρόνια και κάτι τα βράδια Πέμπτης. Εκείνα τα βράδια υπό το σύνθημα «κάθε Πέμπτη Τσικνοπέμπτη» θα μας θυμίζουν πώς μία κοπιαστική μέρα δουλειάς μπορεί να εξελιχθεί σε μια εύθυμη νύχτα διασκέδασης, στον ίδιο ακριβώς χώρο, με τα ίδια ακριβώς πρόσωπα, αρκεί να υπάρχει ένα και μόνο χαρακτηριστικό: η σπίθα της ευτυχίας. Τη σπίθα αυτή τη βρίσκαμε άλλοτε στις μουσικές (έχει κάνει άλλη εκπομπή αφιέρωμα Nirvana-Παπάζογλου άραγε;), άλλοτε στο αλκοόλ ("αν ψάχνεις τον θεό ρώτα έναν μεθυσμένο") κι άλλοτε στην ψησταριά του Ζαφείρη (ο μοναδικός άνθρωπος που σούβλισε γουρουνόπουλο στο

πάρκινγκ του Τομέα για να ταΐσει 50 άτομα εκείνη την αξέχαστη Πρωτομαγιά)! Το επιστέγασμα της στενής φιλίας μου με τον Γιάννη είναι πλέον η μεταφορά αυτού του κλίματος και εκτός συνόρων Τομέα: στις συναυλίες, στις βραδινές ρακιές, στις διακοπές, στα τραγούδια που στέλνουμε ο ένας στον άλλο σε ανύποπτο χρόνο. Επιτρέψτε μου να πιστεύω ότι αυτό που μας ένωσε έτσι είναι το κοινό μας δόγμα: «Πρώτα άνθρωπος, μετά επιστήμονας!». Φίλε μου καλέ κι αγαπημένε, σ' ευχαριστώ από τα βάθη της καρδιάς μου που ήσουν πλάι μου στα πάντα αυτά τα όμορφα χρόνια του διδακτορικού κι εύχομαι κάποια στιγμή στο μέλλον οι πορείες μας να διασταυρωθούν και πάλι...

Κλείνοντας με τα του Τομέα, θέλω να ευχαριστήσω όλους εκείνους τους φοιτητές που είχα τη χαρά να συνεπιβλέψω κατά τη διάρκεια των διπλωματικών τους εργασιών με τον καθηγητή μου κ. Καββαδά. Νίκη, Κώστα, Δήμητρα, Αντιγόνη, Ερμιόνη, Δημήτρη και Νικόλ σας ευχαριστώ πολύ που με τη δουλειά σας βάλατε ο καθένας κι η καθεμία το λιθαράκι σας στην ερευνητική μου προσπάθεια αυτών των ετών.

Προτελευταίους και με ξεχωριστή θέση στην καρδιά μου άφησα τους φίλους που μου συμπαραστάθηκαν και ήταν κοντά μου σαν οικογένεια στον μακρύ κι ανηφορικό αυτό δρόμο του διδακτορικού. Ο λόγος για τα «αδέρφια» μου Πέτρο και Άλεξ, την κοπέλα μου Βάλια και την αγαπημένη μου φίλη Μαριάννα που απέναντι σε κάθε μου στραβοπάτημα, σε κάθε μου παραξενιά, σε κάθε δυσκολία, δρούσαν ως πυροσβέστες με την αγάπη, την καλή τους διάθεση, τη συντροφικότητα και το χαμόγελό τους. Λένε ότι τους ανθρώπους που σε αγαπούν αληθινά τους διακρίνεις από τον αυθορμητισμό με τον οποίο χαίρονται στις χαρές σου, όχι από τη συμπόνια τους στις λύπες σου. Ακριβώς γι' αυτό θέλω να ευχαριστήσω μέσα από αυτή την παράγραφο τους παραπάνω ανθρώπους. Άλεξ και Πέτρο, Πέτρο κι Άλεξ, σας ευχαριστώ εκ βαθέως που με πήρατε συνταξιδιώτη σας σε ανεξερεύνητα για εμένα μουσικά μονοπάτια, που ήπιαμε μαζί τόσες μπύρες και καφέδες σε ένα σωρό μαγαζιά εντός κι εκτός Αθηνών, που είδαμε τόσες και τόσες μπάντες live και που μοιραστήκαμε αδιακρίτως όλους μας τους προβληματισμούς αυτά τα χρόνια. Οι απλές και καθημερινές χαρές της ζωής είναι που καλλιεργούν την ευτυχία μέσα μας, όχι το κυνήγι των μεγαλεπήβολων σχεδίων - για τα οποία, κακά τα ψέματα, οι συμπαντικές δυνάμεις έχουν το κακό συνήθειο να μας τα χαλάνε, αλλά εμείς δεν το βάζουμε κάτω. Μαριάννα μου, το πηγαίο σου γέλιο και η μονίμως εύθυμη αντιμετώπιση των πάντων - ακόμα και στις δυσκολότερες στιγμές - μου έμαθαν πώς είναι να μην εγκαταλείπει κανείς το πνεύμα και το χιούμορ του, ό,τι κι αν συμβεί. Σ' ευχαριστώ πολύ γι' αυτό κι ελπίζω κάποια στιγμή να σου το ανταποδώσω. Βάλια μου γλυκιά, το τι πρέπει να τράβηξες αυτή τη διετία με τις εναλλαγές της ψυχολογίας και την κυκλοθυμία μου μόνο εσύ το ξέρεις - άντε και σ' έναν βαθμό μερικοί άλλοι (βλ. «για μπύρα είμαι εγώ τώρα;»). Σ' ευχαριστώ πολύ που ήσουν

δίπλα μου 24/7, πραγματικός χορηγός θετικής ενέργειας, στις ωραίες στιγμές αλλά και στα δύσκολα. Σου εύχομαι να είσαι πάντα τόσο δυνατή και χαμογελαστή, συμπαρασύροντας στην ευτυχία όλους όσους βρίσκονται γύρω σου!

Κλείνοντας, νιώθω τη βιολογική και ψυχική ανάγκη να ευχαριστήσω τους ανθρώπους εκείνους που βρέθηκαν στην πρώτη γραμμή «κρούσης» αυτού του πολυετούς ταξιδιού, αληθινοί πλωριοί ναύτες που φυλάνε την πορεία του καραβιού από τις ξέρες και τις κακοτοπιές. Αναφέρομαι προφανώς στη φυσική μου οικογένειά, η οποία με την αγάπη, τη διακριτικότητα και τις λοιπές αρετές που την χαρακτηρίζουν υποστήριξε την προσπάθεια του διδακτορικού μου χωρίς να περιμένει το παραμικρό αντάλλαγμα. Αυθόρμητα λοιπόν, οφείλω ένα μεγάλο ευχαριστώ στον πατέρα μου Πέτρο για τη διορατικότητα και τη συμβουλευτική του (βγαλμένη από το πεζοδρόμιο όπως συνηθίζει να λέει και με κάνει τρομερά υπερήφανο που με μεγάλωσε ένας τέτοιος άνθρωπος), στη μητέρα μου Βενετία για τη στοργή και την καθημερινή επιμέλεια του τορβά μου (¨μανούλα μου…¨, που λέει κι ο Ιάκωβος Καμπανέλλης), τον αδερφό μου Ζαφείρη (Ρ.Μ.) για την αστείρευτη ενέργειά του και το πρώτο εκείνο ψητούρι στο αίθριο του Τομέα - εξ' αιτίας σου με μάθανε εκεί μέσα, σιγά που νοιάστηκε κανένας για τις ερευνητικές μου ικανότητες, χαχα - και τον Βενιαμίν μας, σ.σ. τον Σταύρακα, για τη σπάνια καλοσύνη της ψυχής του και τη γαλήνη που πάντα μου εμφυσούσε (γλυκέ μας τύραννε…). Ο «πολυτεχνίτης» παππούς Ζαφείρης κι ο θηλυκός Τσελεμεντές γιαγιά Άννα έκαναν κι εκείνοι τα ¨μαγικά¨ τους στην πορεία αυτών των ετών και τους ευχαριστώ θερμότατα. Τέλος, νιώθω την ανάγκη να ευχαριστήσω τον ιθύνοντα νου όλης της εκπαιδευτικής μου πορείας ως τώρα, τον άνθρωπο της οικογένειας που μου καλλιέργησε το ¨μικρόβιο¨ του μηχανικού και με ώθησε να το σπουδάσω μέχρι το ανώτατο αυτό επίπεδο: θείε Θανάση, σε έχω μέσα στην καρδιά μου και σου είμαι βαθύτατα ευγνώμων για τις παροτρύνσεις σου!

Στου αιώνα την παράγκα
στρώσε τ΄ όνειρό σου μάγκα
στα κρυφά και ταπεινά
ψάξε τα παντοτινά

Κωνσταντίνος Π. Τζιβάκος
Αθήνα, Ιούνιος 2017

Η παρούσα έρευνα έχει χρηματοδοτηθεί από:

- Το Ίδρυμα Κρατικών Υποτροφιών (Ι.Κ.Υ) μέσω διδακτορικής υποτροφίας εσωτερικού, για την περίοδο Οκτώβριος 2010 - Απρίλιος 2014.
- Το ερευνητικό πρόγραμμα "NeTTUN: New Technologies for Tunnelling and UNderground works" χρηματοδοτούμενο από την Ευρωπαϊκή Επιτροπή (7th Framework Programme - FP7), για την περίοδο Σεπτέμβριος 2012 - Φεβρουάριος 2017.

Ο συγγραφέας αισθάνεται την υποχρέωση να ευχαριστήσει όλους τους εμπλεκόμενους φορείς για την υποστήριξή τους.

Abstract

During pile design, the engineer usually focuses on its response in axial (usually vertical) and lateral (usually horizontal) loading. Lateral loading is particularly significant because it is related mainly to unforseen phenomena (earthquakes, storms, impacts, landslides), for which the design requirements are generally increased and associated with a high rate of uncertainty (compared to axial loading that is imposed to the piles by the vertical loads of the upper structure as well as its horizontal loads, undertaken by the deep foundation through force pairs - compressive and extensive). As a consequence, the study of the lateral pile response is necessary for the foundation of a wide variety of structures (tall buildings, bridge piers, wind turbines, offshore platforms, harbor piers, etc.), pointing out the need for computational tools that will result in a practical, reliable and effective pile design.

The current dissertation attempts to provide the engineer with clear guidelines for the design of laterally loaded piles in clayey soils through numerically derived (3D FEA) p-y curves. Two (2) main objectives are pursued towards this direction. The first is to develop a sophisticated and reliable three-dimensional finite element model in the commercial code Simulia Abaqus for the realistic simulation of a single, laterally loaded pile in clayey soils. The second is to propose a new set of upgraded p-y curves through the results of "numerical experiments", using the undrained shear strength distribution of the clayey soil as criterion (NC and OC soils). Thus, the proposed p-y curves of the present thesis correlate the lateral response of the soil-pile system with widely used strength and compressibility parameters of clayey soils.

The main characteristics of the proposed monotonic p-y curves for clayey soils are summarized in the following points:

1. The proposed p-y curves follow the notations of renowned corresponding international literature methodologies, regarding the initial stiffness K_i and the ultimate lateral soil resistance p_u. The parameters of the problem affecting these two main features are described in the next points.

2. The methodology distinguishes between soft, normally consolidated (NC) and

stiff, overconsolidated (OC) clayey soils. The criterion of this categorization is the distribution of the undrained shear strength c_u with depth, i.e. linearly increasing for NC and constant for OC soils. It is noted here that we may come across stiff NC as well as soft OC clays in nature. However, the thesis adopts the practical consideration that most NC clayey soils are soft while OC ones are stiff. The proposed p-y curves for NC soils are an exponential function of K_i and p_u, which exhibits clear plateau for extensive lateral displacement y - typical characteristic of soft soils. On the other hand, the p-y curves proposed for OC soils follow the renowned hyperbola - used by many other literature methods - between y, K_i and p_u, which is quite representative of soils with hardening comportment.

3. The initial stiffness K_i is affected by the compressibility parameters of the soil (C_c, C_r) for both clay types. Furthermore, it increases linearly with depth correspondingly to the Young's modulus of the soil that also follows the same pattern, according to the utilized poroelasticity framework (the Modified Cam-Clay (Roscoe & Burland, 1968) constitutive law - MCC - simulates the fully saturated clay behavior in the 3D FEA).

4. The dimensionless coefficient of ultimate lateral soil resistance $N_p = p_u/(c_u \cdot D)$ - non-dimensional p_u form - correlates with various parameters of the problem for the two clayey soil types under investigation (soft NC, stiff OC):

    i. for soft NC clayey soils N_p depends entirely from the adhesion factor α between the pile and the surrounding soil.

    ii. for stiff OC clayey soils the parameters that influence N_p are the following (in order from the most to the less significant one): the average undrained shear strength $c_{u,\,avg}$ from ground surface to a depth z=10D, the pile diameter D, the adhesion factor α of the pile-soil interaction and the slope κ=C_r / ln 10 of the recompression line from the oedometer test curve $v - \ln p'$ - $v = 1 + e$ the specific volume, e the void ratio and p' the mean effective stress of the soil.

5. Particular attention is given to the effect of small-strain stiffness (relatively small strains, $\varepsilon < 0.1\%$) and strength degradation - after a certain level of deformation (strain softening) - on the numerical p-y curves for stiff, OC clays. The following findings occurred from this thorough investigation:

    i. intense changes in soil stiffness at relatively small strains (small-strain stiffness) do not affect respectively equally the K_i of the p-y curves.

ii. undrained shear strength degradation greater than 20% (with reference to peak strength) transforms the form of the p-y curve from hyperbolic to exponential. The corresponding reduced value of p_u correlates exclusively with the strength reduction factor $RF = c_{u,\,\mathrm{res}}/c_{u,\,\mathrm{peak}}$. It is obvious that for the cases of stiff OC clays without any strain softening one shall consider RF=1.

For the validation and evaluation of the proposed p-y curves the dissertation carries out the following works:

1. A 2D simulation of the pile-soil system as a Beam on Non-linear Winkler Foundation (BNWF) - beam on p-y curves - is designed in the finite element code Simulia Abaqus, aiming to predict the lateral pile response (pile head lateral load-displacement curve, bending moment, horizontal displacement and/or curvature distribution along the pile) of physical lateral load tests in clayey soils under undrained conditions. For the initial verification of the simulation, we compare the pile response of the 2D BNWF model incorporating the proposed p-y curves with the corresponding 3D FEA that produce these curves. These comparisons display that the BNWF simulation is reliable and can predict successfully the lateral response of the pile. As a result, it is capable of simulating with accuracy the real experiments.

2. Through the aforementioned BNWF technique, four (4) lateral pile load tests are simulated. The experiments involve piles of various materials and dimensions installed in clayey soils with a wide range of strength and compressibility parameters. More accurately:

   i. for the evaluation of the proposed p-y curves for soft NC clayey soils two centrifuge tests are modelled (Doyle et al., 2004; Ilyas et al., 2004), involving metallic laterally loaded piles of physical diameters D=0.8, 2.5m. The soil profile of the NC materials was represented by kaolin slurry layering in the model container of the centrifuge tests.

   ii. for the assessment of the proposed p-y curves for stiff OC clayey soils two full-scale tests are simulated (Rollins et al., 1998; Stewart et al., 2007), involving steel and reinforced concrete piles, of diameters D=0.3, 2.0m in real soil profiles with undrained shear strength range c_u=40-200kPa.

3. Apart from the validation of the proposed p-y curves, the thesis attempts to evaluate their predictions of the lateral pile response in comparison with corresponding predictions that utilize typical p-y methods of the international literature. For

this particular purpose, we chose literature p-y curves around the upper and the lower bound of the total range and applied these curves on the aforementioned BNWF model. Thus, comparisons of the lateral pile response occurred (bending moments, lateral forces, horizontal displacements and curvature) between the predictions of the proposed and the literature p-y curves.

The aforementioned validation process of the proposed p-y curves proved the developed numerical tools trustworthy and in accordance with the exhibited experimental behaviour of centrifuge and full-scale lateral pile load tests in clayey soils. Consequently, the main points of the current thesis are summarized in the following:

1. Comparative assessment of the literature methodologies up to depth z=10D reveals significant divergence of the existing p-y curves for clayey soils. Indicatively, the comparison demonstrates differences up to two orders of magnitude for the initial stiffness K_i and up to 150% for the ultimate lateral soil resistance p_u. The aforementioned deviations refer to z=3D (the lateral soil response is more critical close the ground surface).

2. The proposed p-y curves for soft, NC clayey soils correlate with: slopes λ and κ of the virgin compression and the unloading-recompression lines respectively, Poisson's ratio ν and the pile-soil adhesion factor α ($\tau_{u,\,\text{interface}} = \alpha \cdot c_u$). The slope of the critical state line (CSL) M and the pile diameter D do not affect essentially these p-y curves.

3. The proposed p-y curves for stiff, OC clayey soils correlate with: the slope κ of the unloading-recompression line, Poisson's ratio ν, the pile-soil adhesion factor α, the pile diameter D and the average undrained shear strength $c_{u,\,avg}$ from ground surface to a depth z=10D. Strength degradation of the OC soil due to strain softening is not reflected on the corresponding p-y curves (residual strength down to 30% of peak strength.

4. Fixity conditions of the pile head (fixed, free) and geometrical non-linearities of the problem (large strain analysis) do not influence the numerical development of p-y curves for clayey soils under undrained loading.

5. Pseudostatic cyclic lateral displacement of the pile head $y_h = 5-50\%D$ does not affect significantly the numerical p-y curves, as they were derived from 3D FEA that simulate the clayey soils of the current dissertation through the MCC and the sophisticated model by Kalos 2014 (with small-strain stiffness and structure

degradation features). However, the application of constant, two-way cyclic lateral force on the pile head delivers differentiated shallow post-cyclic p-y curves in terms of K_i for the OC clays, compared to the monotonic ones.

6. The proposed p-y curves simulate very accurately the lateral pile response (horizontal displacement, bending moment, curvature) in soft NC and stiff OC clayey soils through the simplistic 2D BNWF model, as it occurs from comparisons with real experimental data. Despite the fact that the 3D FEA of the present thesis assume a fully elastic pile behavior, the numerically developed p-y curves predict successfully deformations and bending moments along the piles of the physical load tests that carry on even after failure of the pile material (plastic hinge).

7. The current thesis supports the modern aspect that the design of piles under lateral loading is over-conservative. Thus, it encourages the use of p_u around the upper bound of the literature methodologies for a safe, accurate and cost-effective design, as long as a thorough geotechnical investigation has taken place before. The existing p-y curve methods overlook the effect of certain soil parameters (C_c, C_r, ν), leading to conservative design solutions. On the contrary, the proposed p-y curves of the current thesis incorporate the aforementioned effects, thus improving the cost and the reliability of the design.

Future research can focus on two different axes, namely: a) improving the numerical tools utilized for the development of the p-y curves (finite element types, soil/ pile constitutive laws) and b) broaden the field of application regarding the proposed p-y curves (ground conditions/ geometry, loading type). The following shortcomings of the present thesis form the corresponding needs for further research:

1. The use of higher order finite elements (quadratic C3D20P) is required for a more detailed numerical simulation of the problem under investigation. The numerical analyses of the current dissertation utilize linear, three-dimensional finite elements with pore-pressure calculation (C3D8P) because the use of quadratic elements demands higher computational cost and usually causes numerical instabilities of the code under the regime of extensive deformation and material failure - for the estimation of p_u in the p-y curves.

2. Certain features of the poroelasticity theory and the MCC constitutive law imposed the assumption of specific distributions on some soil parameters that are investigated:

    i. assuming constant slope κ of the unloading-recompression line, the 3D FEA simulate a linearly increasing soil Young's modulus with depth. Increasing

κ with depth is required for the simulation of constant modulus of elasticity.

ii. constant yield surface magnitude is utilized to simulate almost constant c_u of OC clayey soils with depth. This assumption sometimes leads to excessive (non-realistic) overconsolidation ratios (OCR) close to ground surface, especially during the simulated cases of hard clayey formations ($c_u > 200$kPa).

3. The constitutive laws of the 3D FEA in the current thesis (simplified but classic Modified Cam-Clay law and an advanced model recently proposed by Kalos 2014) are based on Critical State Soil Mechanics and do not incorporate fatigue features, required to simulate potential hysteresis loops of the soil-structure interaction curves during cyclic loading of many cycles. In addition, the developed numerical simulation is pseudostatic and does not account for time dependent phenomena. Therefore, the conclusions for the influence of cyclic loading (with few cycles) on the numerical p-y curves are more or less qualitative and reflect the limitations of the utilized constitutive laws regarding this type of loads. The guidelines by Andersen (2015) hold as a potential reference in an attempt to quantify the effect of cyclic loads on the corresponding numerically developed p-y curves.

4. Further investigation of the effect of the partially saturated surficial soil zone on the proposed p-y curves is highly recommended. The present thesis examines fully saturated clayey soils ($S_r = 100\%$) and thus probably neglects potential strength increase of the soil close to ground surface due to partial saturation - an area that is crucial for the lateral response of the pile-soil system. Research carried out by Georgiadis et al. (2003), Jostad et al. (2015), Bardanis (2016) and Sitarenios (2016) could offer significant aid towards the specific direction.

5. The proposed p-y curves of the thesis assume horizontal ground surface. However, it is possible to construct piles in sloping ground and certain modifications shall apply on the p-y curves in that case (see Georgiadis & Georgiadis, 2010; Matlock & Reese, 1960). Therefore, improvement of the numerically developed p-y curves of the dissertation is required towards this direction.

6. The dissertation overlooks potential alterations of the soil stress field due to the pile installation. As a result, the proposed p-y curves mainly refer to bored piles. However, the proposed p-y curves also performed satisfactorily in physical lateral load tests of driven piles by predicting their lateral response quite accurately. The specific performance is probably attributed to the extended soil area that reacts to the lateral loading of the pile. The pile installation process affects only the vicinity of the pile and thus its effects are localized at the closely surrounding

clayey soil. Nevertheless, further investigation of the specific pile-soil interaction and its influence on numerically developed p-y curves for such soils is required and research conducted by Chaloulos et al. (2013) on sandy soils could prove very useful referring to this goal.

Περίληψη

Κατά τον σχεδιασμό πασσάλων ο μηχανικός μελετά την απόκρισή τους υπό αξονική (κατακόρυφη) και εγκάρσια (οριζόντια) φόρτιση. Η εγκάρσια φόρτιση είναι ιδιαιτέρως σημαντική επειδή σχετίζεται κυρίως με τυχηματικά φαινόμενα (σεισμοί, καταιγίδες, προσκρούσεις, κατολισθήσεις), για τα οποία οι σχεδιαστικές απαιτήσεις είναι εν γένει αυξημένες και χαρακτηρίζονται από υψηλό βαθμό αβεβαιότητας (σε αντίθεση με την αξονική φόρτιση που προκαλούν τα κατακόρυφα φορτία αλλά και εγκάρσιες δράσεις της ανωδομής που αναλαμβάνονται από τη θεμελίωση μέσω ζευγών – θλιπτικών και εφελκυστικών – δράσεων). Συνεπώς, η μελέτη της εγκάρσιας συμπεριφοράς πασσάλων είναι απαραίτητη για τη θεμελίωση πληθώρας κατασκευών (ψηλά κτίρια, βάθρα γεφυρών, ανεμογεννήτριες, θαλάσσιες πλατφόρμες, λιμενοβραχίονες, κλπ.), με αποτέλεσμα την ανάγκη υπολογιστικών εργαλείων που να καθιστούν τη μελέτη αυτή αξιόπιστη, εύκολη και αποτελεσματική.

Οι καμπύλες p-y αποτελούν μία πολύ συνήθη πρακτική για τον υπολογισμό εντατικών και παραμορφωσιακών μεγεθών κατά μήκος πασσάλων υπό εγκάρσια φόρτιση (καμπτικές ροπές, τέμνουσες δυνάμεις, οριζόντιες μετατοπίσεις, κλπ.), κατά την ακόλουθη προσομοίωση:

- Ο πάσσαλος προσομοιώνεται ως «δοκός επί μη-γραμμικού ελατηριωτού εδάφους Winkler» (BNWF).
- Οι καμπύλες p-y περιγράφουν τη σχέση κατανεμημένου φορτίου-μετατόπισης των μη-γραμμικών ελατηρίων. Τα εδαφικά ελατήρια θεωρούνται πακτωμένα στο ένα τους άκρο, ενώ στο άλλο άκρο συνδέονται με τον πάσσαλο-δοκό.
- Τα φορτία του συστήματος εδάφους-πασσάλου ασκούνται είτε στο πακτωμένο άκρο των ελατηρίων (κινηματικά) είτε στην κεφαλή του πασσάλου (εξωτερικά ανωδομής).

Έτσι επιλύεται το σύνθετο, τριδιάστατο πρόβλημα της οριζόντιας φόρτισης πασσάλου ως διδιάστατο, αντικαθιστώντας την οριζόντια εδαφική αντίδραση σε διάφορα βάθη με μη-γραμμικά ελατήρια. Αν κατορθώσουμε να βαθμονομήσουμε

σωστά αυτά τα ελατήρια ως προς την παραμορφωσιμότητα και την αντοχή τους, οι ανωτέρω υπολογισμοί καθίστανται γρήγοροι και αντιπροσωπευτικοί της πραγματικής εγκάρσιας απόκρισης του πασσάλου. Κύρια προϋπόθεση για τη ρεαλιστική προσομοίωση του προβλήματος με τη μέθοδο αυτή είναι η πυκνή τοποθέτησή τους κατά μήκος του πασσάλου, διότι τα εδαφικά ελατήρια είναι μη-συζευγμένα (η παραμόρφωση του κάθε ελατηρίου δεν επηρεάζει τα γειτονικά του).

Συγκριτική αξιολόγηση των βιβλιογραφικών μεθοδολογιών μέχρι βάθους $10D$ αποκαλύπτει πολύ μεγάλες αποκλίσεις των υφιστάμενων καμπυλών p-y για αργιλικά εδάφη. Ενδεικτικά αναφέρεται ότι παρατηρούνται διαφορές μέχρι και δύο τάξεων μεγέθους για την αρχική κλίση K_i ενώ σε ότι αφορά την οριακή εγκάρσια εδαφική αντίδραση p_u παρατηρούνται αποκλίσεις έως και 150%. Οι διαφορές αυτές αναφέρονται σε βάθος $z = 3D$ (η οριζόντια εδαφική απόκριση κοντά στην επιφάνεια του εδάφους είναι πιο κρίσιμη) και επηρεάζουν σημαντικά την κατανομή εντατικών και παραμορφωσιακών μεγεθών στον πάσσαλο.

Η παρούσα διδακτορική διατριβή ερευνά την εγκάρσια απόκριση μεμονωμένου, εξωτερικά φορτιζόμενου πασσάλου σε οριζόντια αργιλικά εδάφη μέσω του κώδικα ΠΣ Simulia Abaqus, επιχειρώντας την επίτευξη των ακόλουθων δύο (2) κύριων στόχων:

- να αναπτύξει ένα προηγμένο και αξιόπιστο, τριδιάστατο αριθμητικό προσομοίωμα ΠΣ για τη διερεύνηση της εγκάρσιας συμπεριφοράς μεμονωμένου πασσάλου σε αργιλικά εδάφη μέσω συζευγμένων αναλύσεων ενεργών τάσεων - ικανό να αναπαράγει τους μηχανισμούς της εν λόγω απόκρισης

- να προτείνει νέες, βελτιωμένες, καμπύλες p-y από τα αποτελέσματα των «αριθμητικών πειραμάτων» και να αξιολογήσει τις αντίστοιχες, υφιστάμενες μεθοδολογίες ανάλογα με τον σχεδιασμό πασσάλου που προβλέπουν (συντηρητικό ή ρεαλιστικό) για την ανάληψη εξωτερικών εγκάρσιων φορτίσεων.

Στα πλαίσια των παραπάνω στόχων, η διατριβή αναπτύσσει αριθμητική μεθοδολογία για τον υπολογισμό καμπυλών p-y μέσω σύνθετων τριδιάστατων αναλύσεων πεπερασμένων στοιχείων. Η μεθοδολογία αυτή χρησιμοποιεί προχωρημένα αριθμητικά εργαλεία, απαραίτητα για τη ρεαλιστική προσομοίωση της εγκάρσιας φόρτισης πασσάλου σε αργιλικά εδάφη υπό αστράγγιστες συνθήκες (συζευγμένες αναλύσεις, φόρτιση σε πραγματικό χρόνο, διεπιφάνειες, προχωρημένα καταστατικά προσομοιώματα).

Προτείνεται νέα εκθετική συνάρτηση μονοτονικών καμπυλών p-y για μαλακά, NC αργιλικά εδάφη, η οποία αποδίδει ικανοποιητικά την αντίστοιχη εγκάρσια

εδαφική αντίδραση. Οι προτεινόμενες καμπύλες p-y συσχετίζονται με τις κλίσεις λ και κ των γραμμών φόρτισης και αποφόρτισης-επαναφόρτισης αντίστοιχα, με τον λόγο Poisson ν και με τον συντελεστή συνάφειας πασσάλου-εδάφους α (η διατμητική τάση μεταξύ πασσάλου-εδάφους ορίζεται ως τ_{max}=$\alpha \cdot c_u$). Η κλίση της γραμμής κρίσιμης κατάστασης M και η διάμετρος του πασσάλου D δεν επηρεάζουν ουσιαστικά τις καμπύλες αυτές.

Οι προτεινόμενες καμπύλες p-y για στιφρά, OC αργιλικά εδάφη συσχετίζονται με την κλίση κ της γραμμής αποφόρτισης-επαναφόρτισης, με τον λόγο Poisson ν, με τον συντελεστή συνάφειας πασσάλου-εδάφους α, με τη διάμετρο D του πασσάλου και με τη μέση αστράγγιστη διατμητική αντοχή του εδάφους $c_{u,\,avg}$ από την επιφάνεια μέχρι βάθος $10D$. Πτώση της αντοχής του εδάφους μετά από εκτεταμένη παραμόρφωση δεν αντικατοπτρίζεται στη μορφή των καμπυλών p-y (μέχρι παραμένουσα αντοχή ίση με το 30% της μέγιστης). Η τασική χαλάρωση των OC εδαφών επηρεάζει την οριακή εγκάρσια εδαφική αντίδραση p_u.

Οι προτεινόμενες καμπύλες p-y προσομοιώνουν με επιτυχία την εγκάρσια απόκριση πασσάλων (οριζόντιες μετατοπίσεις, καμπτικές ροπές) σε μαλακά και στιφρά αργιλικά εδάφη με χρήση του μοντέλου «δοκού επί μη-γραμμικού ελατηριωτού εδάφους», όπως προέκυψε από σύγκριση με πειραματικά αποτελέσματα. Παρά το γεγονός ότι οι αριθμητικές αναλύσεις της διατριβής θεωρούν πλήρως ελαστικό πάσσαλο, οι προτεινόμενες καμπύλες p-y υπολογίζουν ικανοποιητικά εντατικά και παραμορφωσιακά μεγέθη κατά μήκος πασσάλων από πειράματα που τους φορτίζουν εγκάρσια μέχρι να αστοχήσει το υλικό τους (πλαστική άρθρωση).

Από την αριθμητική διερεύνηση της παρούσας διδακτορικής διατριβής προκύπτουν οι ακόλουθες δευτερεύουσες παρατηρήσεις:

- Οι συνοριακές συνθήκες κεφαλής του πασσάλου (πακτωμένη, ελεύθερη) και οι γεωμετρικές μη-γραμμικότητες του προβλήματος (large strain analysis) δεν επηρεάζουν την αριθμητική ανάπτυξη καμπυλών p-y για αργιλικά εδάφη υπό αστράγγιστες συνθήκες.

- Ανακυκλική οριζόντια φόρτιση της κεφαλής του πασσάλου $H_c = 30 - 50\% H_u$ δεν επηρεάζει ουσιαστικά τις αριθμητικές καμπύλες p-y μαλακών, NC αργιλικών εδαφών. Αντίστοιχη φόρτιση σε στιφρά, OC εδάφη φαίνεται να αυξάνει την K_i των καμπύλων p-y σε μικρά βάθη μετά την ανακύκληση, χωρίς καμία επιρροή όμως στην p_u.

- Η παρούσα διατριβή ενισχύει την αντίληψη ότι ο σχεδιασμός πασσάλων υπό εγκάρσια φόρτιση με χρήση καμπυλών p-y της βιβλιογραφίας που θεωρούν

p_u κοντά στο άνω όριο του εύρους δεν είναι απαγορευτικός, αλλά με κατάλληλη διερεύνηση των εδαφικών παραμέτρων μπορεί να πραγματοποιηθεί με ασφάλεια, ακρίβεια και οικονομία. Οι υφιστάμενες μεθοδολογίες υπολογισμού καμπυλών p-y παραγνωρίζουν την επίδραση συγκεκριμένων εδαφικών παραμέτρων (π.χ. C_c, C_r), οδηγώντας σε υπερβολικά συντηρητικές σχεδιαστικές λύσεις. Αντίθετα, οι προτεινόμενες καμπύλες ενσωματώνουν τις παραπάνω επιδράσεις βελτιώνοντας τόσο την αξιοπιστία όσο και το κόστος του σχεδιασμού.

Στα πλαίσια βελτίωσης της προτεινόμενης αριθμητικής μεθοδολογίας προκύπτουν οι ακόλουθες προτάσεις για περαιτέρω έρευνα:

- Για την ακριβέστερη αριθμητική προσομοίωση του προβλήματος απαιτείται χρήση πεπερασμένων στοιχείων ανώτερης τάξης (C3D20P). Οι αριθμητικές αναλύσεις της παρούσας διδακτορικής διατριβής χρησιμοποιούν γραμμικά τριδιάστατα πεπερασμένα στοιχεία (C3D8P) καθότι η χρήση στοιχείων ανώτερης τάξης απαιτεί πολλαπλάσιο υπολογιστικό κόστος και οδηγεί συνήθως σε αριθμητικές αστάθειες του κώδικα υπό καθεστώς εκτεταμένων παραμορφώσεων και αστοχίας υλικών – για την εκτίμηση του p_u των καμπυλών p-y.

- Τα καταστατικά προσομοιώματα των αριθμητικών αναλύσεων της παρούσας διατριβής (απλοποιημένο αλλά κλασσικό μοντέλο Modified Cam Clay και προηγμένο μοντέλο που προτάθηκε προσφάτως από τον Kalos (2014) βασίζονται στην Εδαφομηχανική Κρίσιμης Κατάστασης και δε διαθέτουν (MCC) ή δεν έχουν ενεργοποιημένα (SSS-SD) χαρακτηριστικά κόπωσης (fatigue) και χρονικά εξαρτημένων φαινομένων όπως ο ρυθμός επιβολής της ανακυκλικής φόρτισης (rate dependency). Για τον λόγο αυτό τα συμπεράσματα για την επιρροή της ανακυκλικής φόρτισης (λίγων κύκλων) στις καμπύλες p-y είναι περισσότερο ποιοτικά και αντανακλούν τους περιορισμούς των καταστατικών προσομοιωμάτων ως προς αυτού του είδους τις φορτίσεις.

- Απαιτείται η διερεύνηση της επιρροής της μη-κορεσμένης επιφανειακής ζώνης στις προτεινόμενες καμπύλες p-y. Η παρούσα διατριβή εξετάζει πλήρως κορεσμένα αργιλικά εδάφη ($S_r = 100\%$), με αποτέλεσμα να αγνοεί πιθανή αύξηση της αντοχής λόγω του μερικού κορεσμού για τα επιφανειακά εδαφικά στρώματα – περιοχή ιδιαίτερα κρίσιμη για την εγκάρσια απόκριση του συστήματος εδάφους-πασσάλου.

- Δεν λαμβάνονται υπόψη μεταβολές στο τασικό πεδίο λόγω της εγκατάστασης του πασσάλου, με αποτέλεσμα οι προτεινόμενες καμπύλες να αφορούν κυρίως έγχυτους πασσάλους. Ωστόσο, η εφαρμογή των προτεινόμενων καμπυλών σε πειραματικές δοκιμές στις οποίες χρησιμοποιήθηκαν πάσσαλοι εκτοπίσεως, έδειξε ότι προβλέπουν αρκετά ικανοποιητικά την απόκριση του πασσάλου. Αυτό πιθανώς να αποδίδεται στο γεγονός ότι η πλευρική φόρτιση αφορά μια ευρεία περιοχή εδαφικής μάζας, με αποτέλεσμα να μην επηρεάζεται έντονα από την εγκατάσταση του πασσάλου, οι επιδράσεις της οποίας περιορίζονται τοπικά στον πάσσαλο. Ωστόσο, απαιτείται περαιτέρω διερεύνηση.

Εκτενής Περίληψη

1 Το πρόβλημα

Κατά τον σχεδιασμό πασσάλων ο μηχανικός μελετά την απόκρισή τους υπό αξονική (κατακόρυφη) και εγκάρσια (οριζόντια) φόρτιση. Η εγκάρσια φόρτιση είναι ιδιαιτέρως σημαντική επειδή σχετίζεται κυρίως με τυχηματικά φαινόμενα (σεισμοί, καταιγίδες, προσκρούσεις, κατολισθήσεις), για τα οποία οι σχεδιαστικές απαιτήσεις είναι εν γένει αυξημένες και χαρακτηρίζονται από υψηλό βαθμό αβεβαιότητας (σε αντίθεση με την αξονική φόρτιση που προκαλούν τα κατακόρυφα φορτία αλλά και εγκάρσιες δράσεις της ανωδομής που αναλαμβάνονται από τη θεμελίωση μέσω ζευγών – θλιπτικών και εφελκυστικών – δράσεων). Ενδεικτικά, το Σχήμα 1 παρουσιάζει αστοχίες πασσάλων υπό εγκάρσια φόρτιση σε διάφορα μέρη του κόσμου. Συνεπώς, η μελέτη της εγκάρσιας συμπεριφοράς πασσάλων είναι απαραίτητη για τη θεμελίωση πληθώρας κατασκευών (ψηλά κτίρια, βάθρα γεφυρών, ανεμογεννήτριες, θαλάσσιες πλατφόρμες, λιμενοβραχίονες, κλπ.), με αποτέλεσμα την ανάγκη υπολογιστικών εργαλείων που να καθιστούν τη μελέτη αυτή αξιόπιστη, εύκολη και αποτελεσματική.

Οι καμπύλες p-y αποτελούν μία πολύ συνήθη πρακτική για τον υπολογισμό εντατικών και παραμορφωσιακών μεγεθών κατά μήκος πασσάλων υπό εγκάρσια φόρτιση (καμπτικές ροπές, τέμνουσες δυνάμεις, οριζόντιες μετατοπίσεις, κλπ.), κατά την ακόλουθη προσομοίωση:

- Ο πάσσαλος προσομοιώνεται ως «δοκός επί μη-γραμμικού ελατηριωτού εδάφους Winkler» (BNWF).
- Οι καμπύλες p-y περιγράφουν τη σχέση κατανεμημένου φορτίου-μετατόπισης των μη-γραμμικών ελατηρίων. Τα εδαφικά ελατήρια θεωρούνται πακτωμένα στο ένα τους άκρο, ενώ στο άλλο άκρο συνδέονται με τον πάσσαλο-δοκό.
- Τα φορτία του συστήματος εδάφους-πασσάλου ασκούνται είτε στο πακτωμένο άκρο των ελατηρίων (κινηματικά) είτε στην κεφαλή του πασσάλου (εξωτερικά ανωδομής).

Σχήμα 1: Αστοχίες πασσάλων υπό εγκάρσια φόρτιση.

Έτσι επιλύεται το σύνθετο, τριδιάστατο πρόβλημα της οριζόντιας φόρτισης πασσάλου ως διδιάστατο, αντικαθιστώντας την οριζόντια εδαφική αντίδραση σε διάφορα βάθη με μη-γραμμικά ελατήρια (Σχήμα 2). Αν κατορθώσουμε να βαθμονομήσουμε σωστά αυτά τα ελατήρια ως προς την παραμορφωσιμότητα και την αντοχή τους, οι ανωτέρω υπολογισμοί καθίστανται γρήγοροι και αντιπροσωπευτικοί της πραγματικής εγκάρσιας απόκρισης του πασσάλου. Κύρια προϋπόθεση για τη ρεαλιστική προσομοίωση του προβλήματος με τη μέθοδο αυτή είναι η πυκνή τοποθέτησή τους κατά μήκος του πασσάλου, διότι τα εδαφικά ελατήρια είναι μη-συζευγμένα (η παραμόρφωση του κάθε ελατηρίου δεν επηρεάζει

τα γειτονικά του).

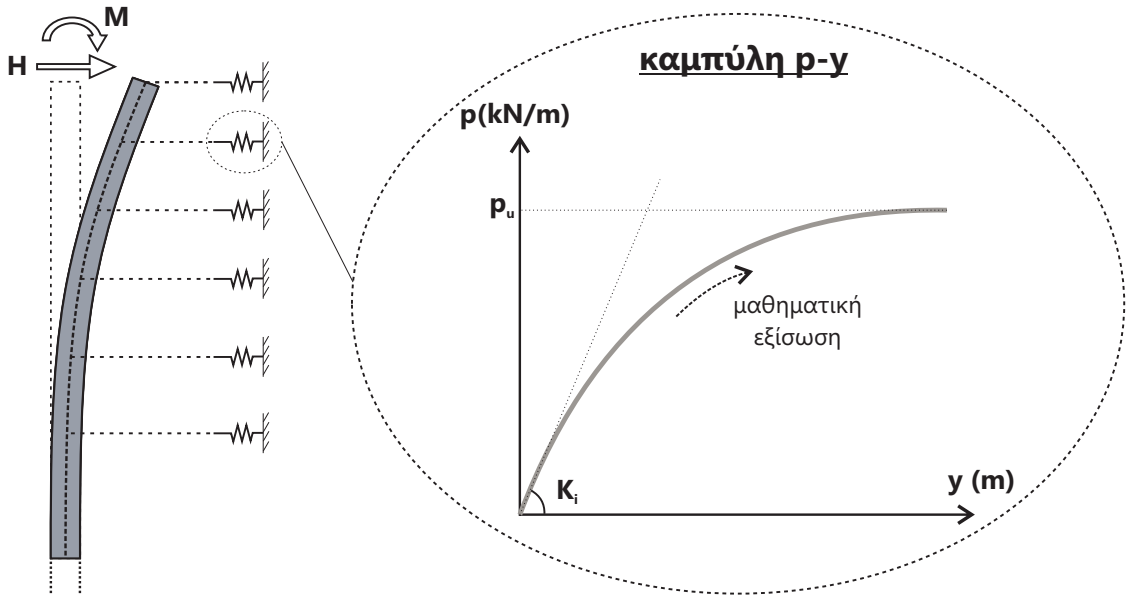

Σχήμα 2: Σχηματική απεικόνιση της ενσωμάτωσης καμπυλών p-y στο προσομοίωμα «δοκού επί μη-γραμμικού ελατηριωτού εδάφους Winkler» (BNWF).

Καθότι οι οριζόντιες δράσεις επί των πασσάλων είναι οιωνεί-στατικές (ανεμοπιέσεις, τροχοπεδήσεις), ανακυκλικές (κυματικές φορτίσεις) και δυναμικές (προσκρούσεις, σεισμοί) προτείνονται στη διεθνή βιβλιογραφία αντίστοιχες καμπύλες p-y. Ωστόσο, ιδιαίτερα σημαντική θεωρείται η εύστοχη πρόβλεψη των στατικών καμπυλών p-y επειδή χρησιμεύουν στη διαμόρφωση αντίστοιχων καμπύλων για ανακυκλική και δυναμική φόρτιση.

Πλήθος πειραμάτων και δοκιμαστικών φορτίσεων πασσάλων συμβάλλουν με τις μετρήσεις τους στον προσδιορισμό των καμπύλων p-y. Στη διεθνή βιβλιογραφία συναντώνται δύο (2) κύριες κατηγορίες πειραμάτων εγκάρσιας φόρτισης πασσάλου για τη χάραξη καμπυλών p-y: (i) πραγματικά πειράματα, πεδίου (φυσική κλίμακα) ή φυγοκεντριστή (υπό κλίμακα) και (ii) «αριθμητικά πειράματα» σε Η/Υ. Οι πρώτες προτάσεις καμπυλών p-y βασίζονταν σε δοκιμαστικές φορτίσεις για τη θεμελίωση θαλάσσιων εξεδρών, οι δε προτεινόμενες καμπύλες p-y αποδείχτηκαν ιδιαίτερα συντηρητικές. Τα πειράματα φυγοκεντριστή αποτελούν εναλλακτική της δοκιμαστικής φόρτισης φυσικής κλίμακας αλλά ειδικά για αργιλικά υλικά είναι εξαιρετικά δύσκολο να προσομοιώσουν με ακρίβεια το εδαφικό προφίλ ενώ έχουν και αυτά αυξημένο κόστος. Τα τελευταία χρόνια, με την εξέλιξη της τεχνολογίας και τη διαρκώς αυξανόμενη υπολογιστική ισχύ, διαδόθηκε η δυνατότητα αριθμητικής προσομοίωσης του προβλήματος της εγκάρσιας φόρτισης πασσάλου με πεπερασμένα στοιχεία (ΠΣ), πεπερασμένες διαφορές (ΠΔ), κλπ. Στην περίπτωση

αυτή προκύπτουν ισοδύναμες καμπύλες p-y, οι οποίες είναι τόσο αξιόπιστες όσο και το καταστατικό προσομοίωμα που χρησιμοποιήθηκε για το έδαφος, για τις ιδιότητες του υλικού του πασσάλου, για τη διεπιφάνεια εδάφους-πασσάλου καθώς και για τις υδραυλικές συνθήκες του προβλήματος.

Κρίσιμη κατά τον σχεδιασμό πασσάλων υπό εγκάρσια φόρτιση είναι κυρίως η συμπεριφορά του συστήματος εδάφους – πασσάλου μέχρι ενός βάθους περίπου ίσο με 10 φορές τη διάμετρο (D) του πασσάλου (Gazetas & Dobry, 1984). Μία συγκριτική αξιολόγηση των υφιστάμενων μεθοδολογιών ειδικά μέχρι βάθους $10D$, αποκαλύπτει πολύ μεγάλες αποκλίσεις των προτεινόμενων καμπυλών p-y για αργιλικά εδάφη. Ενδεικτικά, το Σχήμα 3 απεικονίζει την έντονη διασπορά καμπυλών p-y της βιβλιογραφίας σε βάθος $z = 3D$, τόσο για μαλακά όσο και για στιφρά αργιλικά εδάφη (η οριζόντια εδαφική απόκριση πιο κοντά στην επιφάνεια του εδάφους είναι πιο κρίσιμη). Αναφορικά με τα δύο κύρια μέρη της καμπύλης p-y (Σχήμα 2), παρατηρούνται διαφορές μέχρι και δύο τάξεων μεγέθους για την αρχική κλίση K_i και έως 150% για την οριακή εγκάρσια εδαφική αντίδραση p_u. Είναι φανερό ότι οι αποκλίσεις των υφιστάμενων μεθοδολογιών καθιστούν τον σχεδιασμό ιδιαιτέρως επισφαλή.

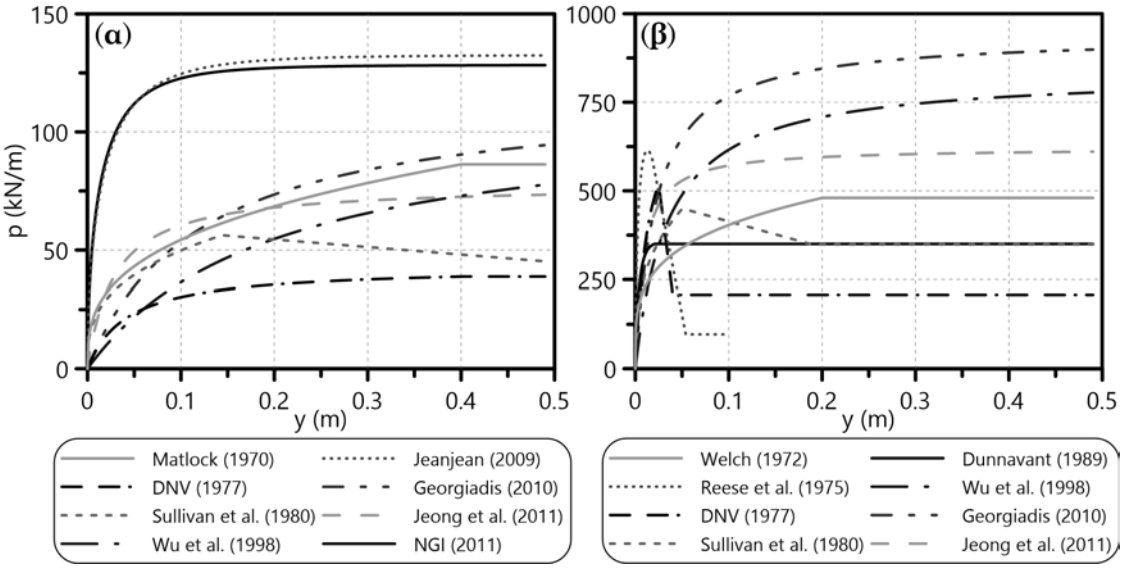

Σχήμα 3: Καμπύλες p-y της διεθνούς βιβλιογραφίας που εφαρμόζονται σε (α) μαλακά, κανονικά στερεοποιημένα και (β) στιφρά, υπερστερεοποιημένα αργιλικά εδάφη (z =3m, D =1m).

2 Σκοπός της διατριβής

Όπως προέκυψε από την περιγραφή του προβλήματος, οι καμπύλες p-y για αργιλικά υλικά απαιτούν περαιτέρω διερεύνηση. Παρά ταύτα, η διεξαγωγή έρευνας πάνω στο συγκεκριμένο αντικείμενο με χρήση φυσικών πειραμάτων (κλίμακας 1:1 ή φυγοκεντριστή) έχει αποδειχθεί ιδιαίτερα απαιτητική οικονομικά και χρονικά, ενώ ταυτόχρονα αδυνατεί να προσομοιώσει το μεγάλο εύρος παραμέτρων του προβλήματος. Επιπρόσθετα, τα συμπεράσματα που προέκυψαν από τέτοια πειράματα θεωρήθηκαν από πλήθος ερευνητών προσανατολισμένα στο εκάστοτε πεδίο εφαρμογής. Η αλματώδης πρόοδος στις αριθμητικές μεθόδους (πεπερασμένα στοιχεία, πεπερασμένες διαφορές) μέσω Η/Υ μαζί με την ανάπτυξη προχωρημένων καταστατικών μοντέλων που προσομοιώνουν με ακρίβεια την εδαφική συμπεριφορά, ακόμα και υπό συνθήκες έντονης φόρτισης (π.χ. σεισμός, ερπυσμός, ρευστοποίηση), επιτρέπουν τη ρεαλιστική και αξιόπιστη προσομοίωση διάφορων γεωτεχνικών προβλημάτων οριακών τιμών (βλ. φέρουσα ικανότητα). Τα παραπάνω «εργαλεία» δίνουν τη δυνατότητα στον ερευνητή να ξεπεράσει πολλούς περιορισμούς της φυσικής προσομοίωσης και αποτελούν μία εναλλακτική λύση για την παραμετρική διερεύνηση της μεθοδολογίας p-y. Η παρούσα διδακτορική διατριβή ερευνά την εγκάρσια απόκριση μεμονωμένου, εξωτερικά φορτιζόμενου πασσάλου σε οριζόντια αργιλικά εδάφη (Σχήμα 4) μέσω του κώδικα ΠΣ Simulia Abaqus, επιχειρώντας την επίτευξη των ακόλουθων δύο (2) κύριων στόχων:

- να αναπτύξει ένα προηγμένο και αξιόπιστο, τριδιάστατο αριθμητικό προσομοίωμα ΠΣ για τη διερεύνηση της εγκάρσιας συμπεριφοράς μεμονωμένου πασσάλου σε αργιλικά εδάφη μέσω συζευγμένων αναλύσεων ενεργών τάσεων - ικανό να αναπαράγει τους μηχανισμούς της εν λόγω απόκρισης

- να προτείνει νέες, βελτιωμένες, καμπύλες p-y από τα αποτελέσματα των «αριθμητικών πειραμάτων» και να αξιολογήσει τις αντίστοιχες, υφιστάμενες μεθοδολογίες ανάλογα με τον σχεδιασμό πασσάλου που προβλέπουν (συντηρητικό ή ρεαλιστικό) για την ανάληψη εξωτερικών εγκάρσιων φορτίσεων.

Το προς ανάπτυξη αριθμητικό προσομοίωμα αποτελεί μέρος της ευρύτερης συντονισμένης ερευνητικής προσπάθειας του Τομέα Γεωτεχνικής στο Εθνικό Μετσόβιο Πολυτεχνείο, με στόχο τη διερεύνηση της συμπεριφοράς βαθιών θεμελιώσεων υπό διάφορες φορτίσεις σε πλήθος εδαφών. Για τη ρεαλιστική προσομοίωση των αργιλικών εδαφών στις αναλύσεις ΠΣ απαιτείται η χρήση ενός ανάλογου, ακριβούς και ταυτόχρονα σταθερού καταστατικού προσομοιώματος. Οι

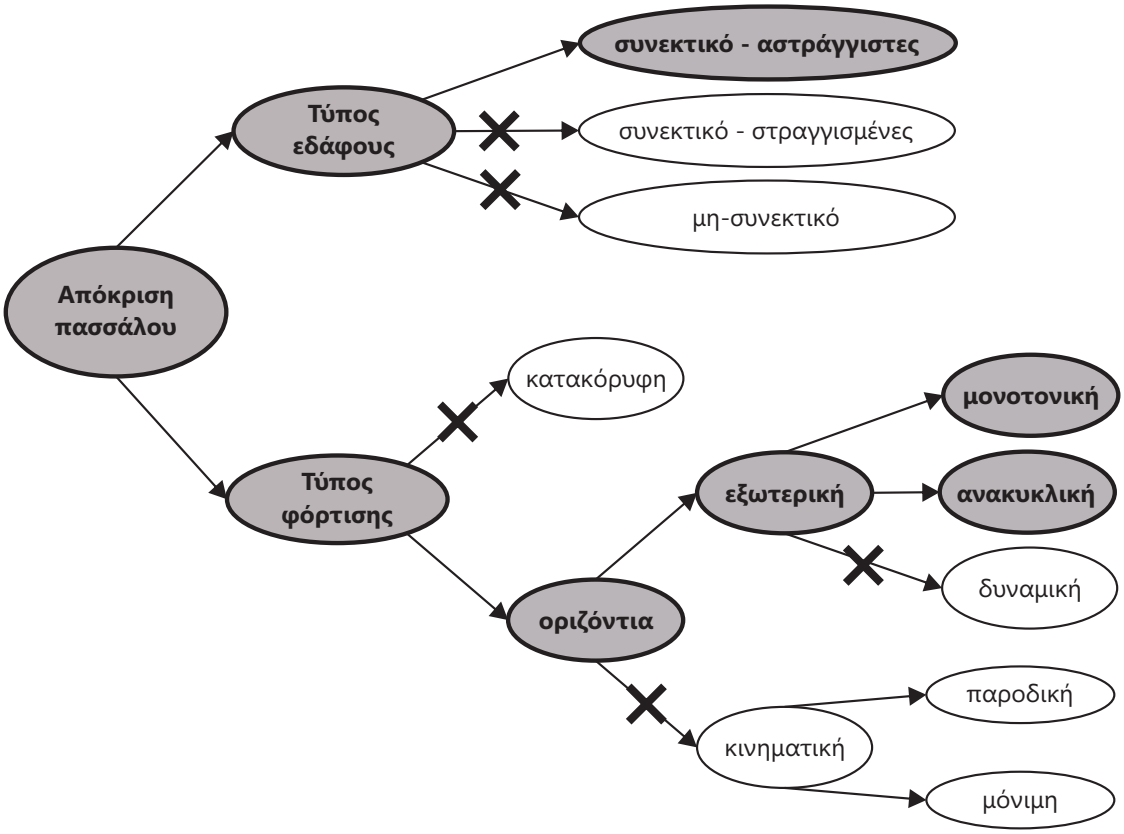

Σχήμα 4: Διαφορετικοί συνδυασμοί τύπου εδάφους και τύπου φόρτισης που επιδρούν στην απόκριση του πασσάλου και κατ' επέκταση στη μορφή των p-y. (Με «Χ» σημειώνονται οι περιπτώσεις εδάφους και φόρτισης που δεν απασχολούν την παρούσα διατριβή).

περισσότερες από τις προηγούμενες προτάσεις καμπυλών p-y που αναπτύχθηκαν με αριθμητικές μεθόδους, υιοθέτησαν απλουστευτικά καταστατικά μοντέλα εδαφικής συμπεριφοράς (Mohr-Coulomb, Von Mises), προσπαθώντας έτσι να αποφύγουν ενδεχόμενες αριθμητικές αστάθειες του εκάστοτε κώδικα επίλυσης. Η έρευνα των Kavvadas & Amorosi (2000), Belokas & Kavvadas (2011) και Kalos (2014) παρέχει στην παρούσα διατριβή τα απαραίτητα καταστατικά εργαλεία για την επιτυχή σύνδεση της εξωτερικά επιβαλλόμενης φόρτισης (σταδιακή αύξηση τάσης) με τις αντίστοιχες παραμορφώσεις που συσσωρεύονται στο έδαφος. Ασφαλώς η λεπτομερής συγκριτική αξιολόγηση μεταξύ διάφορων αποτελεσμάτων των αναλύσεων ΠΣ είναι απαραίτητη για να υπάρχει εμπιστοσύνη στο καταστατικό προσομοίωμα που χρησιμοποιείται.

Ακολουθεί επιγραμματική περιγραφή των επιμέρους **ερευνητικών ενοτήτων (ΕΕ)** της παρούσας διδακτορικής διατριβής για την επίτευξη των στόχων της:

ΕΕ 1 Εκτενής βιβλιογραφική ανασκόπηση των υφιστάμενων καμπυλών p-y για αργιλικά εδάφη (μαλακά, στιφρά) υπό αστράγγιστες συνθήκες, όπως αυτές προέκυψαν μέσω διάφορων μεθόδων (δοκιμές εγκάρσιας φόρτισης πασσάλου, αριθμητικές αναλύσεις, επί τόπου δοκιμές). Η παραπάνω αναδρομή συμπεριλαμβάνει γνωστές διερευνήσεις για τα δύο κύρια χαρακτηριστικά των καμπυλών p-y, την αρχική δυσκαμψία K_i και την οριακή εγκάρσια εδαφική αντίδραση p_u.

ΕΕ 2 Σχεδιασμός και βαθμονόμηση της τριδιάστατης αριθμητικής προσομοίωσης του προβλήματος εγκάρσιας φόρτισης πασσάλου (πεπερασμένα στοιχεία, καταστατική προσομοίωση εδάφους) για την ανάπτυξη καμπυλών p-y αργιλικών εδαφών υπό αστράγγιστες συνθήκες. Αξιολόγηση της επιρροής διαφόρων στοιχείων της προσομοίωσης (γεωμετρία και κάνναβος ΠΣ, διεπιφάνεια εδάφους-πασσάλου, γεωμετρικές μη-γραμμικότητες) στις καμπύλες p-y που προκύπτουν από τις αριθμητικές αναλύσεις. Σύγκριση με πειραματικά αποτελέσματα για τον έλεγχο εγκυρότητας του τελικού προσομοιώματος ΠΣ.

ΕΕ 3 Παραμετρική διερεύνηση διαφόρων παραμέτρων εδάφους, πασσάλου και της διεπιφάνειας αυτών που ενδέχεται να επηρεάζουν τις μονοτονικές, αριθμητικές καμπύλες p-y. Αναλύεται η συμπεριφορά δύο τύπων αργιλικού εδάφους: μαλακό, κανονικά στερεοποιημένο (NC) και μέτριο έως στιφρό, υπερστερεοποιημένο (OC), ανάλογα με την κατανομή της αστράγγιστης διατμητικής αντοχής c_u με το βάθος - γραμμική αύξηση της c_u ($c_u \approx 0$ στην επιφάνεια) και σχεδόν σταθερή c_u για NC και OC εδάφη αντίστοιχα. Ειδικά για τη δεύτερη εδαφική κατηγορία μελετάται η επιρροή χαρακτηριστικών δυσκαμψίας σε πολύ μικρές παραμορφώσεις (small-strain stiffness) και πτώσης της αντοχής λόγω αποδόμησης (structure degradation) στις αριθμητικές καμπύλες p-y. Τέλος, επιχειρείται η αριθμητική προσομοίωση ανακυκλικής εγκάρσιας φόρτισης πασσάλου μέσω ψευδοστατικών αναλύσεων ΠΣ, αποβλέποντας στην ποιοτική αποτίμηση της επίδρασης τέτοιων φορτίσεων στις καμπύλες p-y (πάντα αναφορικά με τη συγκεκριμένη αριθμητική μέθοδο).

ΕΕ 4 Κριτική αξιολόγηση της προτεινόμενης μεθοδολογίας μέσω συγκρίσεων με πειραματικά αποτελέσματα - από δοκιμές εγκάρσιας φόρτισης - τα οποία

καταγράφουν την εγκάρσια απόκριση του πασσάλου σε όρους εντατικών (καμπτικές ροπές, τέμνουσες δυνάμεις) και παραμορφωσιακών (οριζόντιες μετατοπίσεις, καμπυλότητα) μεγεθών. Επιπλέον, αξιολογείται η αποτελεσματικότητα των προτεινόμενων καμπυλών p-y ως προς τις αντίστοιχες υφιστάμενες σχέσεις της διεθνούς βιβλιογραφίας.

3 Βιβλιογραφική ανασκόπηση

Η πρώτη ερευνητική ενότητα (ΕΕ 1) αφορά στην εκτενή βιβλιογραφική αναδρομή και κατανόηση της προσομοίωσης με χρήση μονοτονικών (στατικών) και ανακυκλικών καμπυλών p-y. Οι μη-γραμμικές καμπύλες p-y της διεθνούς βιβλιογραφίας για αργιλικά εδάφη χωρίζονται σε τέσσερις μεγάλες κατηγορίες:

i. καμπύλες p-y για μαλακές αργίλους (Jeanjean et al., 2009; Matlock, 1970; Nichols et al., 2014)

ii. καμπύλες p-y για στιφρές αργίλους (Dunnavant & O'Neill, 1989; Reese et al., 1975; Welch & Reese, 1972)

iii. ενοποιημένες καμπύλες p-y για αργίλους, ανεξάρτητες από τη εδαφική στιφρότητα (DNV, 1977; Georgiadis & Georgiadis, 2010; Jeong et al., 2011; Sullivan et al., 1979; Wu et al., 1998) και

iv. καμπύλες p-y για αργίλους με χρήση αποτελεσμάτων από επιτόπου δοκιμές (Bouafia, 2013; Briaud et al., 1983; Frank, 2009; Gabr et al., 1994; Guo et al., 2014; Kim et al., 2016; Robertson et al., 1989).

Η συγκεκριμένη ερευνητική ενότητα συνιστά την απαιτούμενη για την εκπόνηση της διατριβής βιβλιογραφική ανασκόπηση των υφιστάμενων καμπυλών p-y για αργιλικά εδάφη, χωρίς να αντιγράφει συστηματικά τις διαθέσιμες πηγές. Αντιθέτως, παρουσιάζει τις βιβλιογραφικές μεθοδολογίες με μία διδακτική και ταυτόχρονα πρακτική προσέγγιση αναφορικά με το πεδίο εφαρμογής τους. Οι βασικές παράμετροι των ανωτέρω μεθοδολογιών είναι: η αστράγγιστη διατμητική αντοχή c_u του αργιλικού εδάφους, η χαρακτηριστική αξονική παραμόρφωση ε_{50} υπό τάση ίση με το ήμισυ της θλιπτικής αντοχής του εδαφικού υλικού (υπό αστράγγιστες συνθήκες), ο συντελεστής συνάφειας εδάφους-πασσάλου α, η διάμετρος D και η δυσκαμψία EI του πασσάλου. Η ΕΕ 1 καταλήγει στη συγκριτική απεικόνιση των υφιστάμενων καμπυλών p-y για μαλακά και στιφρά αργιλικά εδάφη, η οποία καταδεικνύει τη μεγάλη διασπορά τους (Σχήμα 3). Έτσι οριοθετείται ο σκοπός της διδακτορικής διατριβής στη διερεύνηση του συγκεκριμένου προβλήματος με χρήση σύνθετων αριθμητικών αναλύσεων.

4 Αριθμητική μεθοδολογία

Στις ακόλουθες παραγράφους παρουσιάζεται η αριθμητική μεθοδολογία της διατριβής τόσο για την ανάπτυξη καμπυλών p-y όσο και για τη γενικότερη μελέτη της εγκάρσιας απόκρισης μεμονωμένου πασσάλου σε αργιλικά εδάφη υπό αστράγγιστες συνθήκες. Πιο συγκεκριμένα, η αριθμητική μεθοδολογία χωρίζεται στα ακόλουθα μέρη:

- Αριθμητική προσομοίωση της εξωτερικά επιβαλλόμενης εγκάρσιας φόρτισης πασσάλου (ΕΕ 2).
- Παραμετρική διερεύνηση της εγκάρσιας απόκρισης πασσάλου σε μαλακά, NC αργιλικά εδάφη (ΕΕ 3).
- Παραμετρική διερεύνηση της εγκάρσιας απόκρισης πασσάλου σε μέτριας στιφρότητας ως στιφρά, OC αργιλικά εδάφη (ΕΕ 3).
- Αριθμητική διερεύνηση της ανακυκλικής εγκάρσιας φόρτισης πασσάλου σε αργιλικά εδάφη (ΕΕ 3).

4.1 Αριθμητική προσομοίωση της εγκάρσιας φόρτισης πασσάλου

Το τριδιάστατο προσομοίωμα του Σχήματος 5 σχεδιάστηκε στον κώδικα πεπερασμένων στοιχείων Simulia Abaqus για την εκτέλεση αριθμητικών αναλύσεων μονοτονικής εγκάρσιας φόρτισης πασσάλου σε οριζόντιο αργιλικό έδαφος υπό αστράγγιστες συνθήκες - με τον υδροφόρο ορίζοντα στην επιφάνεια του εδάφους (ΕΕ 2). Για λόγους συμμετρίας του προβλήματος και αποσκοπώντας στην ελαχιστοποίηση του υπολογιστικού χρόνου των αναλύσεων, κατασκευάστηκε το ήμισυ του συνολικού μοντέλου πασσάλου-εδάφους. Ακολουθεί η συνοπτική περιγραφή των κυριότερων χαρακτηριστικών του προσομοιώματος, καθώς και της επιρροής (ή μη) διαφόρων παραμέτρων στις αριθμητικές καμπύλες p-y.

Το αργιλικό έδαφος προσομοιώνεται με τριδιάστατα, οκταεδρικά, εξακομβικά πεπερασμένα στοιχεία τύπου C3D8P, τα οποία λαμβάνουν υπόψη την εξέλιξη της πίεσης και του δείκτη πόρων. Ως αποτέλεσμα, επιτρέπουν την ανάλυση του γεωτεχνικού προβλήματος σε όρους ενεργών τάσεων. Το συγκεκριμένο χαρακτηριστικό είναι ιδιαίτερα σημαντικό εξαιτίας της έντονης παρουσίας νερού στα αργιλικά υλικά (κορεσμένα ή μη) ενώ ταυτόχρονα επιτρέπει τη χρήση προχωρημένων καταστατικών μοντέλων για τη ρεαλιστική προσομοίωση της εδαφικής συμπεριφοράς. Στις αριθμητικές αναλύσεις της παρούσας διδακτορικής

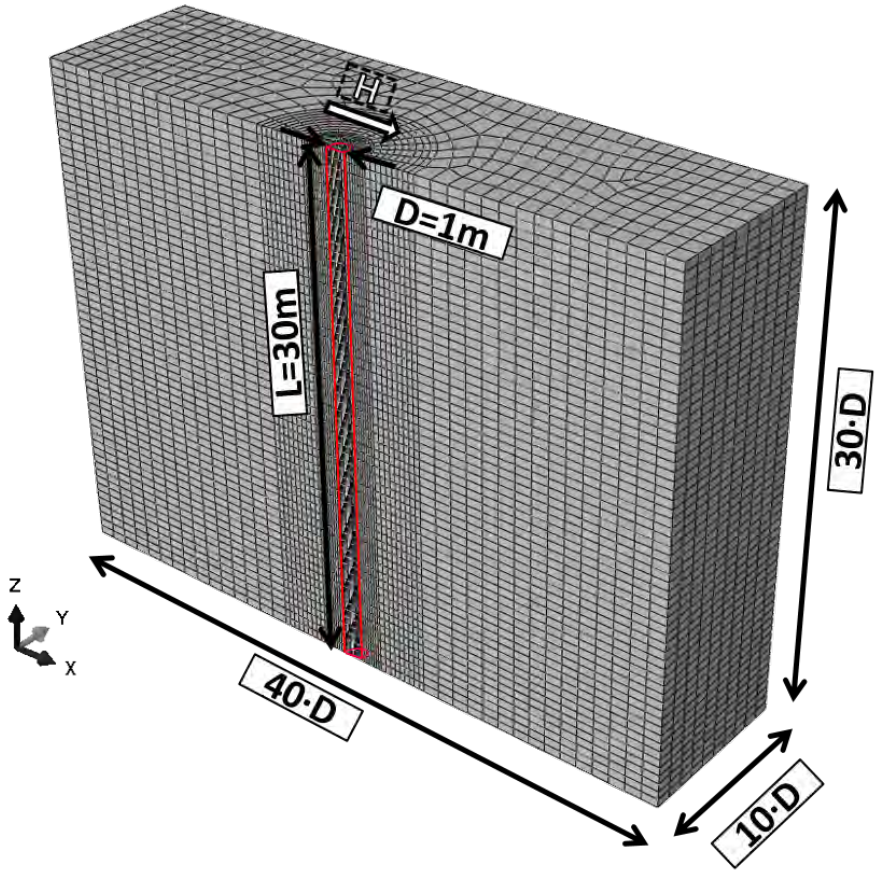

Σχήμα 5: Διαστάσεις και διακριτοποίηση του τριδιάστατου προσομοιώματος πεπερασμένων στοιχείων που χρησιμοποιήθηκε στις αριθμητικές αναλύσεις της διατριβής.

διατριβής χρησιμοποιούνται δύο καταστατικά προσομοιώματα για το έδαφος, βασισμένα στην Εδαφομηχανική Κρίσιμης Κατάστασης: το βασικό προσομοίωμα Modified Cam Clay (MCC) (Roscoe & Burland, 1968) και ένα σύνθετο από τον Kalos (2014) που βασίζεται στη θεωρία πλαστικότητας οριακής επιφάνειας και υιοθετεί στοιχεία της έρευνας των Kavvadas & Amorosi (2000) και Belokas & Kavvadas (2011) (Σχήμα 6). Πιο συγκεκριμένα, το σοφιστευμένο αυτό καταστατικό μοντέλο προσομοιώνει χαρακτηριστικά δυσκαμψίας σε πολύ μικρές παραμορφώσεις (small-strain stiffness, SSS) και μείωσης της αντοχής λόγω καταστροφής της δομής του εδάφους (structure degradation, SD) - και τα δύο πολύ χρήσιμα ιδιαίτερα την προσομοίωση στιφρών OC αργιλικών εδαφών. Η ενσωμάτωσή του στον κώδικα πεπερασμένων στοιχείων πραγματοποιήθηκε μέσω κατάλληλα διαμορφωμένης υπορουτίνας UMAT.

Η εγκάρσια φόρτιση επιβάλλεται στην ελεύθερα στρεπτή κεφαλή του πασσάλου υπό μορφή οριζόντιας μετακίνησης. Όλα τα αργιλικά εδάφη των αριθμητικών προσομοιώσεων έχουν πολύ χαμηλή διαπερατότητα ($k = 10^{-10}$m/s), η οποία σε

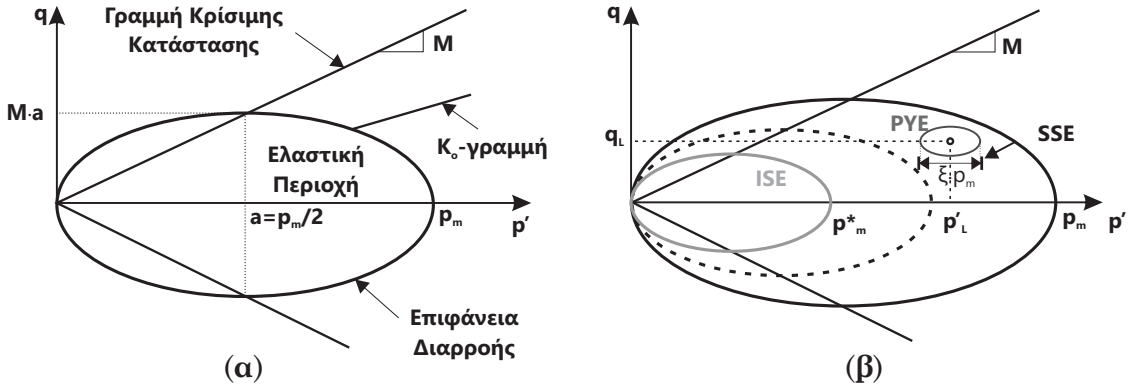

Σχήμα 6: Τα καταστατικά προσομοιώματα (α) Modified Cam Clay (MCC) (Roscoe & Burland, 1968) και (β) SSS-SD Kalos (2014) που χρησιμοποιήθηκαν στις αριθμητικές αναλύσεις της διατριβής.

συνδυασμό με την ταχεία επιβολή της εγκάρσιας μετατόπισης (εντός 1 ημέρας) εξασφαλίζει τις αστράγγιστες συνθήκες φόρτισης του εκάστοτε εδάφους. Οι αριθμητικές αναλύσεις επιλύουν ταυτόχρονα το μηχανικό (έδαφος) και το υδραυλικό πρόβλημα (υδατική ροή). Τα διαγράμματα $p-q$ και $q-\varepsilon_q$ εδαφικού στοιχείου μπροστά από τον πάσσαλο - κατά τη φορά φόρτισης - επιβεβαιώνουν την ορθή προσομοίωση του εδάφους μέσω των προαναφερθέντων καταστατικών νόμων, τόσο για μαλακά NC όσο και για στιφρά OC αργιλικά εδάφη (Σχήμα 7). Η μηδενική ογκομετρική παραμόρφωση (ε_{vol}) και η διαρκής ανάπτυξη υπερπίεσης πόρων (Δ_u) κατά τη διάρκεια των αριθμητικών αναλύσεων[1] αποδεικνύουν ότι η εγκάρσια φόρτιση του πασσάλου επιβάλλεται υπό αστράγγιστες συνθήκες.

Η αριθμητική προσομοίωση του πασσάλου συνδυάζει στερεά στοιχεία (C3D8) και στοιχεία δοκού (B31). Τα πρώτα διαμορφώνουν το σώμα του πασσάλου - απαραίτητο για την προσομοίωση της διεπιφάνειας εδάφους-πασσάλου - ενώ τα δεύτερα (στο κέντρο του πασσάλου) προσομοιώνουν τη δυσκαμψία του πασσάλου και συνδέονται με τους κόμβους των στερεών στοιχείων μέσω άκαμπτων συνδέσμων (MPC). Με τον τρόπο αυτό εξασφαλίζεται το «απαραμόρφωτο» της διατομής του πασσάλου και καθίσταται εφικτός ο υπολογισμός εντατικών μεγεθών κατά μήκος του. Τα στερεά στοιχεία διαθέτουν πολύ χαμηλό μέτρο ελαστικότητας 100kPa ώστε να μην επιδρούν στη δυσκαμψία του πασσάλου. Για λόγους συμβατότητας με την προσομοίωση του μισού μοντέλου, τα στοιχεία δοκού έχουν μισή επιφάνεια διατομής και ροπή αδράνειας από την πραγματική του εκάστοτε πασσάλου.

Η πλειοψηφία των αριθμητικών αναλύσεων της παρούσας διατριβής αναφέρεται σε πάσσαλο ελεύθερης κεφαλής από οπλισμένο σκυρόδεμα (E_p=30GPa, ν=0.20), μήκους L=30m και διαμέτρου D=1m. Για όλα τα αργιλικά εδάφη της αριθμητικής

[1] δεν παρουσιάζονται για λόγους συντομίας

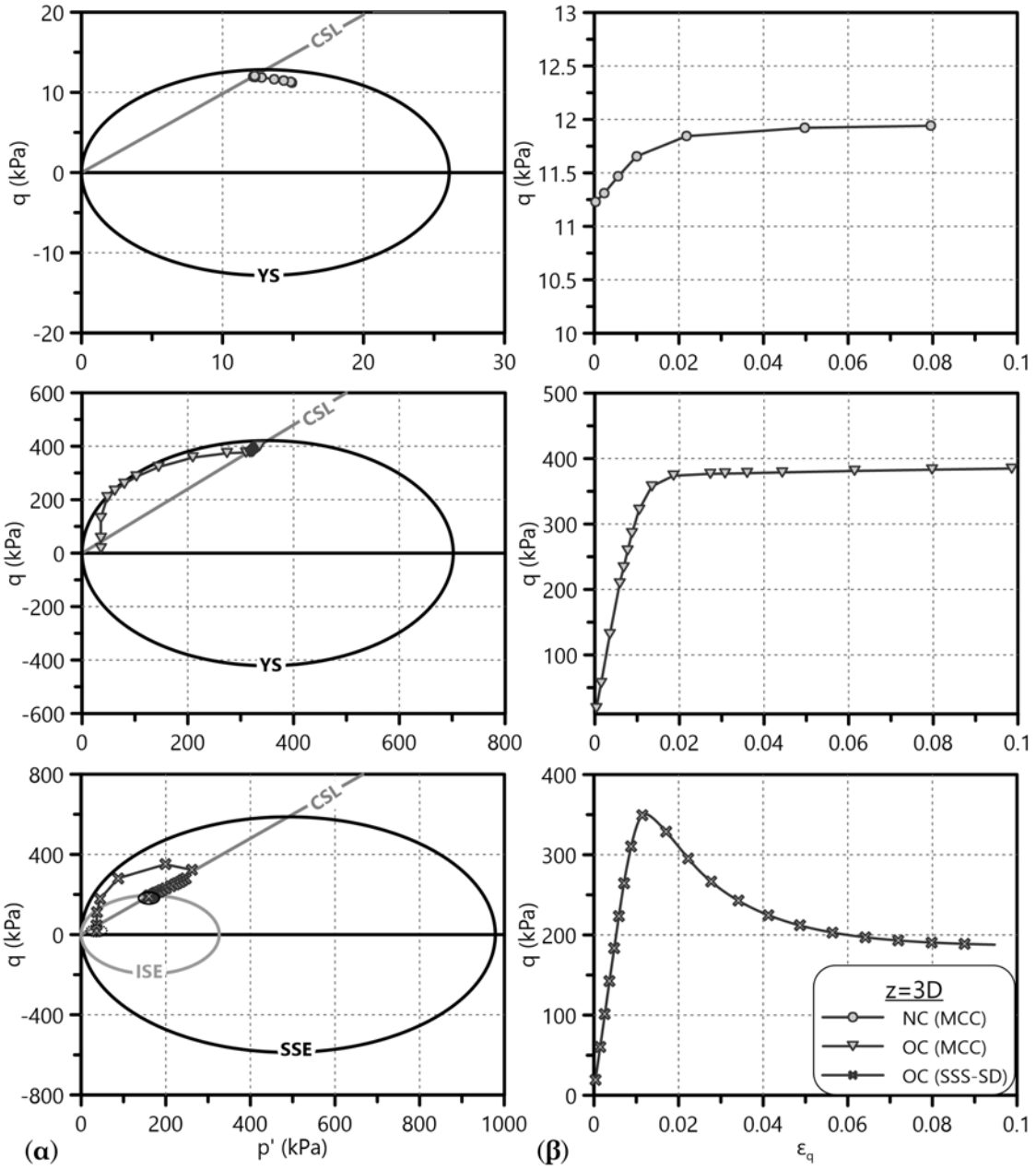

Σχήμα 7: Διαγράμματα (α) $p-q$ και (β) $q-\varepsilon_q$ από εδαφικό στοιχείο σε βάθος $z = 3D$ μπροστά από τον πάσσαλο (D =1m). Προσομοίωση του μαλακού NC εδάφους με το καταστατικό προσομοίωμα MCC. Προσομοίωση του στιφρού OC εδάφους με το MCC και το σύνθετο SSS-SD (Kalos, 2014).

διερεύνησης ο πάσσαλος είναι μακρύς - αστοχεί σε κάμψη - με μέσο λόγο ενεργού μήκους προς διάμετρο L_c/D=10-15 (Gazetas, 1991). Επειδή όμως ο σχεδιασμός σε οριακή κατάσταση λειτουργικότητας απαιτεί την ελαστική συμπεριφορά της θεμελίωσης, ο πάσσαλος προσομοιώνεται ως πλήρως ελαστικός στις αριθμητικές αναλύσεις. Στη συγκεκριμένη προσομοίωση συνάδει και η επιβολή μεγάλης οριζόντιας μετατόπισης της κεφαλής του πασσάλου (έως και $3D$), η οποία είναι αναγκαία για να αστοχήσει σε εκτεταμένο βάθος το έδαφος και έτσι να προκύψει οριακή εγκάρσια εδαφική αντίδραση p_u των αντίστοιχων καμπυλών p-y.

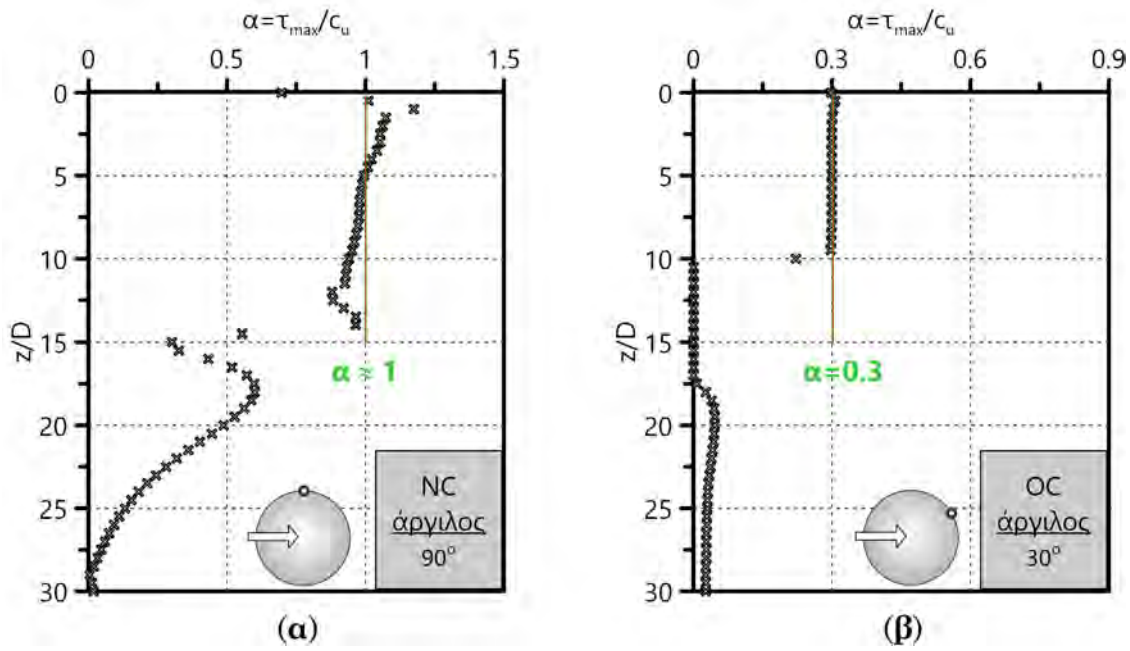

Σχήμα 8: Επαλήθευση του συντελεστή συνάφειας α κατά μήκος πασσάλου υπό εγκάρσια φόρτιση σε (α) μαλακό, NC και (β) στιφρό, OC αργιλικό σχηματισμό.

Η διεπιφάνεια πασσάλου-εδάφους διέπεται από συγκεκριμένους νόμους ως προς τη διεύθυνση των ορθών και διατμητικών τάσεων που παραλαμβάνει. Στην ορθή διεύθυνση επιτρέπεται η αποκόλληση του πασσάλου από το περιβάλλον έδαφος - αν κι εφόσον έχει επαρκή αντοχή c_u για να σταθεί κατακόρυφο. Επιπλέον, η διεπιφάνεια επιτρέπει την ολίσθηση του εδάφους επί της παράπλευρης επιφάνειας του πασσάλου με την υπέρβαση της διατμητικής τάσης τ_{max}=$\alpha \cdot c_u$, όπου α ο συντελεστής συνάφειας πασσάλου-εδάφους. Η διατμητική τάση συνάφειας που αναπτύσσεται στον πάσσαλο από αργιλικά εδάφη (υπό αστράγγιστες συνθήκες) εξαρτάται από το υλικό του πασσάλου. Για τον λόγο αυτό προσομοιώθηκαν συντελεστές α=0.3-1.0 που καλύπτουν εύρος παράπλευρων επιφανειών πασσάλων από λείες (π.χ. μεταλλικοί - 0.3) έως τραχείες (π.χ. σκυροδέματος - 1.0). Το Σχήμα 8 δείχνει την εκτίμηση του α από τις διατμητικές

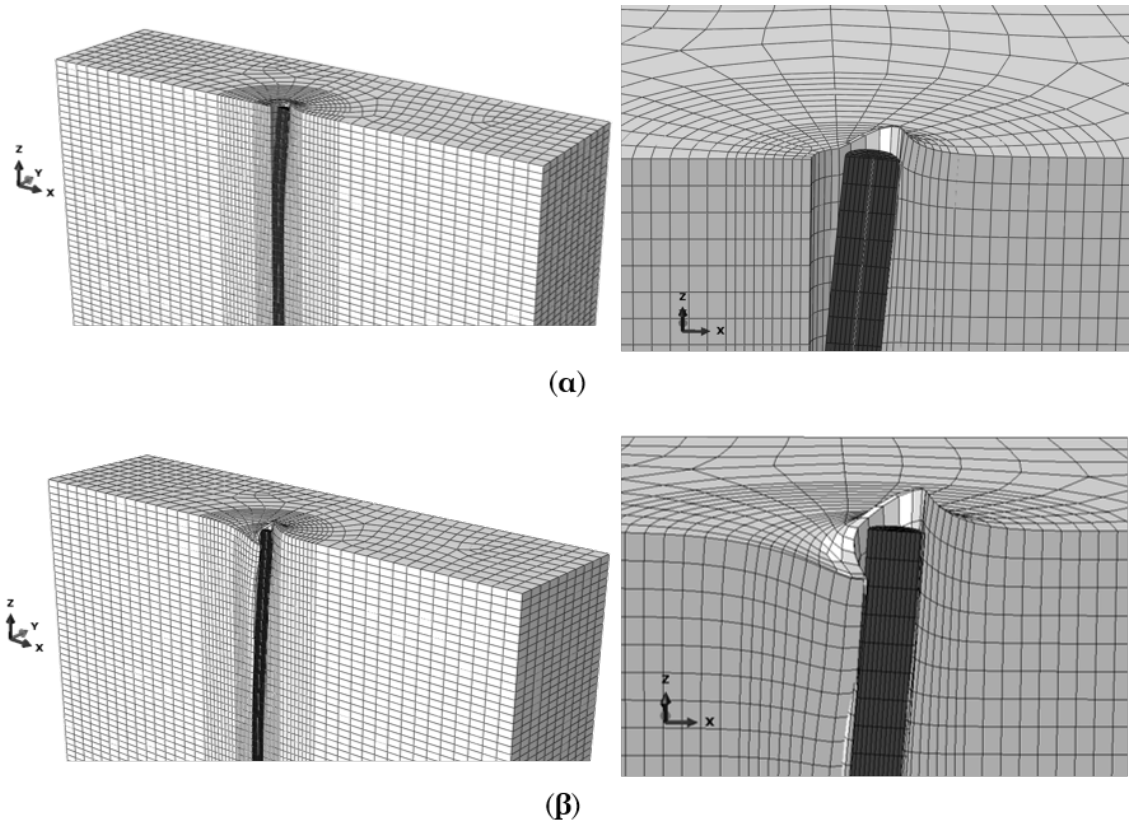

Σχήμα 9: Διεπιφάνεια εδάφους-πασσάλου από τις αναλύσεις ΠΣ. (α) Αποκόλληση του πασσάλου από το έδαφος σε στιφρή άργιλο και (β) σχετική ολίσθηση σε μαλακή άργιλο.

τάσεις που μετρώνται στην παράπλευρη επιφάνεια του πασσάλου κατά τη διάρκεια των αριθμητικών αναλύσεων και επιβεβαιώνει την ορθότητα της προσομοίωσης. Στο ίδιο συμπέρασμα οδηγεί και η μορφή του παραμορφωμένου δικτύου πεπερασμένων στοιχείων του Σχήματος 3.16, όπου φαίνεται τόσο η αποκόλληση του πασσάλου από το περιβάλλον έδαφος για στιφρούς σχηματισμούς όσο και η ολίσθηση επί μαλακών εδαφών.

Σκοπός των σύνθετων αριθμητικών αναλύσεων είναι ο κατά το δυνατόν ακριβέστερος υπολογισμός καμπυλών p-y από τα αντίστοιχα αποτελέσματα. Η οριζόντια μετατόπιση y υπολογίζεται απευθείας στο κέντρο της διατομής του πασσάλου (επικόμβια μετατόπιση στοιχείων δοκού) για κάθε επιμέρους προσαύξηση της εξωτερικά επιβαλλόμενης εγκάρσιας φόρτισης. Για την εξαγωγή της οριζόντιας εδαφικής αντίδρασης p - υπό μορφή κατανεμημένου φορτίου (kN/m) - από τις αναλύσεις κατά μήκος του πασσάλου εντοπίσαμε τις ακόλουθους τρεις (3) μεθόδους:

- με παραγώγιση της κατανομής των τεμνουσών δυνάμεων - στα σημεία ολοκλήρωσης των στοιχείων δοκού - κατά μήκος του πασσάλου $p_1 = \mathrm{d}Q/\mathrm{d}z$

(Σχήμα 10),

- με άθροιση των συνιστωσών των (ολικών) δυνάμεων στη διεπιφάνεια εδάφους-πασσαλου κατά την οριζόντια διεύθυνση (Σχήμα 11) και διαίρεση του αθροίσματος με το αντίστοιχο μήκος επιρροής επί του πασσάλου $p_2 = \sum (\mathrm{CNFx}_i + \mathrm{CSFx}_i)/\,\mathrm{d}z$
- με αναγωγή της ολικής οριζόντιας τάσης του εδάφους σε κατανεμημένο φορτίο, μέσω των επιμέρους συνιστωσών των τάσεων στην οριζόντια διεύθυνση $p_3 = \sum (u_i \cdot l_{y,i} + \sigma_{xx,i} \cdot l_{y,i} + \tau_{xy,i} \cdot l_{x,i} + \tau_{xz,i} \cdot l_{x,i})$ (Σχήμα 12).

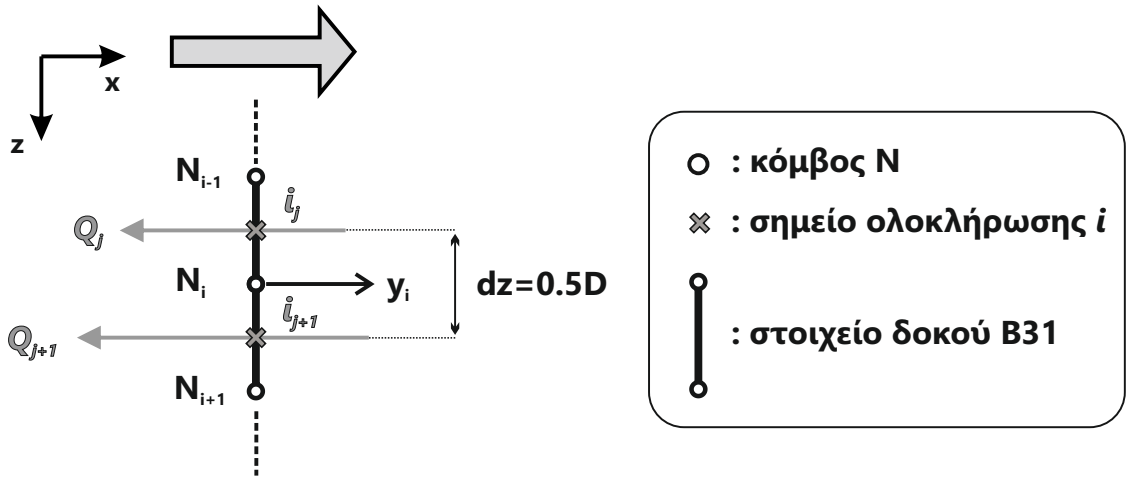

Σχήμα 10: Υπολογισμός της οριζόντιας εδαφικής αντίδρασης p μέσω της τέμνουσας δύναμης δύο διαδοχικών στοιχείων δοκού B31.

Σημειώνεται εδώ ότι η p που προκύπτει και από τις τρεις παραπάνω μεθόδους αναφέρεται στην ημιδιατομή του πασσάλου (συμμετρικό προσομοίωμα). Συνεπώς, για την πραγματική p επί του πασσάλου απαιτείται ο διπλασιασμός των ανωτέρω υπολογισμών. Συγκρίνοντας τις καμπύλες p-y από τις τρεις μεθόδους για δύο διαφορετικά βάθη ($z = 2,6D$) και για τα δύο κύρια αργιλικά εδάφη της διερεύνησης (NC, OC) προκύπτει απόλυτη ταύτισή τους στο μικρό βάθος και μικρές διαφοροποιήσεις της τρίτης μεθόδου από τις άλλες δύο στο μεγάλο βάθος, σύμφωνα με το Σχήμα 13. Επιλέγεται τελικά ο υπολογισμός p_1 για την εξαγωγή αριθμητικών καμπυλών p-y στο υπόλοιπο της διδακτορικής διατριβής, όντας ο λιγότερο πεπλεγμένος, με σκοπό την ελαχιστοποίηση του υπολογιστικού χρόνου καθώς και των πιθανών σφαλμάτων σε πράξεις.

Για τις κυριότερες παραμέτρους της παραπάνω αριθμητικής προσομοίωσης ακολούθησε ανάλυση ευαισθησίας, η οποία κατέδειξε τα χαρακτηριστικά που επηρεάζουν τις αριθμητικές καμπύλες p-y καθώς κι εκείνα που δεν τις

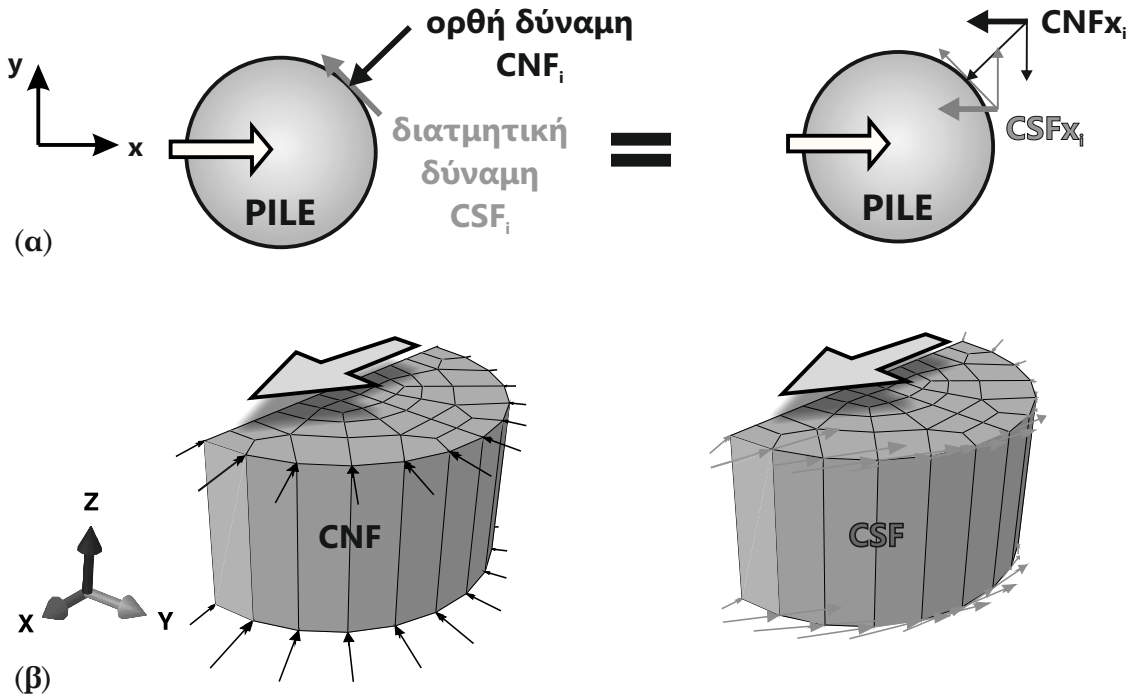

Σχήμα 11: Υπολογισμός της οριζόντιας εδαφικής αντίδρασης p μέσω των (ολικών) δυνάμεων επί της διεπιφάνειας εδάφους πασσάλου. Επεξήγηση (α) των συνιστωσών των ορθών (CNF) και διατμητικών (CSF) δυνάμεων καθώς και (β) των συνισταμένων τους δράσεων επί ενός διακριτοποιημένου τμήματος του πασσάλου.

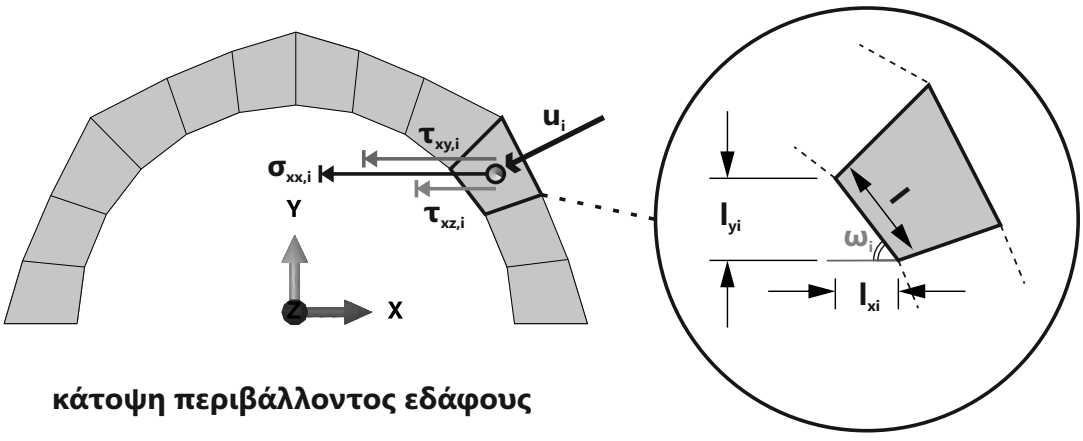

Σχήμα 12: Υπολογισμός της οριζόντιας εδαφικής αντίδρασης p μέσω των τάσεων του εδάφους που περιβάλλει τον εγκάρσια φορτιζόμενο πάσσαλο.

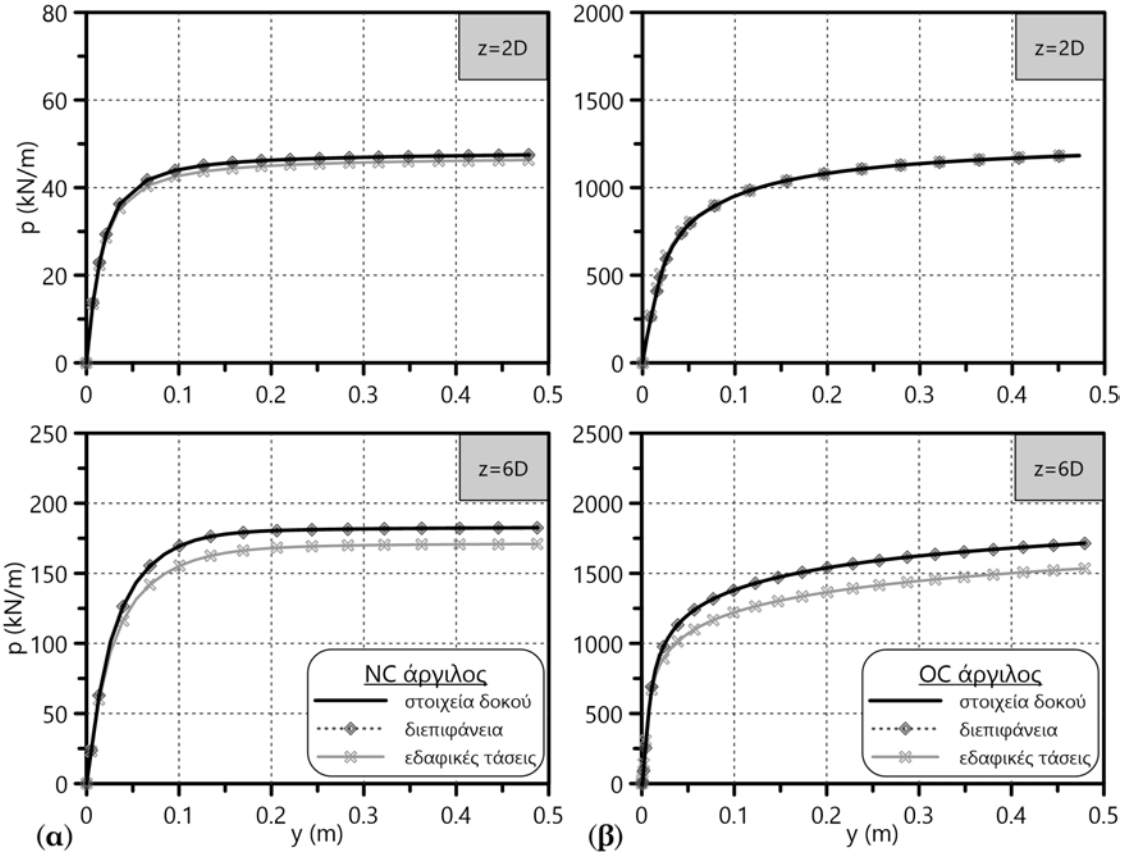

Σχήμα 13: Σύγκριση των τριών μεθόδων εξαγωγής της p από τις αναλύσεις ΠΣ - από τα στοιχεία δοκού του πασσάλου, τη διεπιφάνεια εδάφους-πασσάλου ή τις εδαφικές τάσεις γύρω από τον πάσσαλο. Καμπύλες p-y σε δύο διαφορετικά βάθη για (α) μαλακό, NC και (β) στιφρό, OC αργιλικό έδαφος (D =1m).

διαφοροποιούν ουσιαστικά. Αμελητέα επιρροή στις καμπύλες p-y έχουν: οι επιλεγμένες διαστάσεις του μοντέλου (αποστάσεις συνόρων από τον πάσσαλο), η πυκνότητα του δικτύου πεπερασμένων στοιχείων, το υλικό του πασσάλου, ο περιορισμός στροφικών βαθμών ελευθερίας της κεφαλής του πασσάλου (ελεύθερα στρεπτή ή άστρεπτη) καθώς και η προσομοίωση γεωμετρικών μη-γραμμικοτήτων μέσω κατάλληλης εντολής του κώδικα ΠΣ (NLGEOM). Αντίθετα, ο τύπος του αργιλικού εδάφους (NC, OC) - με βασικό κριτήριο την αστράγγιστη διατμητική αντοχή c_u - καθώς και η τραχύτητα της διεπιφάνειας εδάφους-πασσάλου (α) επηρεάζουν τις καμπύλες p-y σε βαθμό τέτοιο που δικαιολογεί την παραμετρική τους διερεύνηση στις ακόλουθες ερευνητικές ενότητες.

4.2 Απόκριση πασσάλου σε μαλακά NC αργιλικά εδάφη

Το παραπάνω αριθμητικό προσομοίωμα χρησιμοποιείται στην τρίτη ερευνητική ενότητα (ΕΕ 3) για την πρόταση μονοτονικών (στατικών) καμπυλών p-y σε μαλακά,

NC αργιλικά εδάφη - γραμμική αύξηση της αστράγγιστης διατμητικής αντοχής με το βάθος ($c_u \approx 0$ στην επιφάνεια). Προηγείται η παραμετρική διερεύνηση της απόκρισης εύκαμπτου πασσάλου υπό εξωτερική εγκάρσια φόρτιση. Πιο συγκεκριμένα, εξετάζουμε την επιρροή εδαφικών παραμέτρων και χαρακτηριστικών του πασσάλου στις αριθμητικές καμπύλες p-y.

Πίνακας 1: Ιδιότητες NC αργιλικού εδάφους και πασσάλου, όπως προσομοιώθηκαν στις αναλύσεις ΠΣ της παραμετρικής διερεύνησης.

Παράμετροι μαλακού NC αργιλικού εδάφους				Παράμετροι πασσάλου	
M[1]	λ[2]	λ/κ	ν	D (m)	α
0.772, 0.984, 1.2	**0.065, 0.109, 0.174**	10	0.333	**0.5, 1.0, 1.5, 2.0**	**1.0, 0.3**
0.984	0.109	**5, 20**	0.333	1.0	1.0
0.984	0.109	10	**0.1, 0.2**	1.0	1.0

[1] Οι τιμές του M αντιστοιχούν σε ϕ=20°, 25° και 30°.
[2] Οι τιμές του λ αντιστοιχούν σε C_c=0.15, 0.25 και 0.40 ($\lambda = C_c/\ln 10$).

Οι εδαφικές παράμετροι που εξετάζονται κατά την αριθμητική προσομοίωση των NC αργίλων με το MCC είναι: η κλίση της Γραμμής Κρίσιμης Κατάστασης (CSL) M, η κλίση της γραμμής παρθενικής συμπίεσης (NCL) λ ($\lambda = C_c/\ln 10$), ο λόγος των κλίσεων των γραμμών φόρτισης και αποφόρτισης $\lambda/\kappa = C_c/C_r$ και ο λόγος Poisson ν. Το σύνολο των αριθμητικών αναλύσεων μαζί με το εύρος τιμών της εκάστοτε παραμέτρου που προσομοιώθηκε φαίνονται στον Πίνακα 1. Στατιστική επεξεργασία των αποτελεσμάτων των αριθμητικών αναλύσεων καταδεικνύει σημαντική επιρροή των τριών τελευταίων παραμέτρων (λ, λ/κ και ν) στην αρχική κλίση K_i των καμπυλών p-y, όπως προκύπτει από το Σχήμα 14 για ενδεικτικό βάθος $z = 2D$. Ο συντελεστής οριζόντιων γεωστατικών τάσεων θεωρήθηκε $K_o = 0.5$ για όλα τα NC εδάφη της παραμετρικής διερεύνησης.

Αναφορικά με τον πάσσαλο, εξετάζεται παραμετρικά η επιρροή της διαμέτρου D και του συντελεστή συνάφειας εδάφους-πασσάλου α τόσο στις καμπύλες p-y όσο και στον μηχανισμό αστοχίας του περιβάλλοντος εδάφους. Το Σχήμα 15 δείχνει πώς επηρεάζεται η οριακή εγκάρσια εδαφική αντίδραση p_u μαλακών, NC αργιλικών εδαφών - αισθητά μεν, αλλά όχι ιδιαίτερα ουσιαστικά - από τη D σε βάθη z=3, 6m. Η p_u των καμπυλών p-y μεταβάλλεται κατά ένα ποσοστό 10-20% με τη συνάφεια εδάφους-πασσάλου - α=0.3 για λεία, α=1.0 για τραχεία διεπιφάνεια. Επιπλέον, στο Σχήμα 16 παρουσιάζονται οι διάφοροι μηχανισμοί αστοχίας του συγκεκριμένου τύπου εδάφους (αστοχία τύπου «σφήνας» και επίπεδης παραμόρφωσης) καθώς και ο

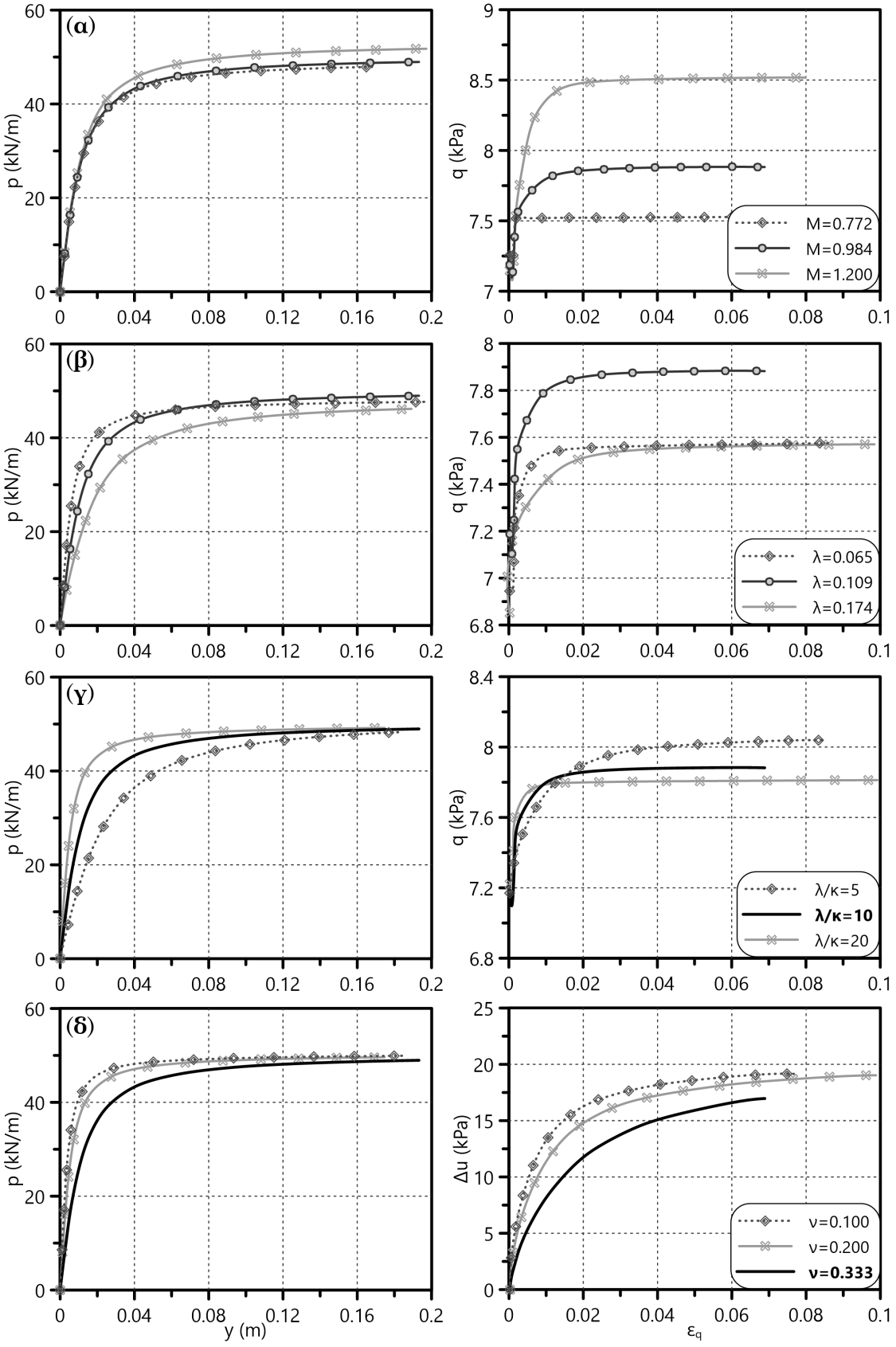

Σχήμα 14: Επιρροή (α) της κλίσης M, (β) της κλίση λ, (γ) του λόγου των κλίσεων $\lambda/\kappa = C_c/C_r$ και (δ) του λόγου Poisson ν στη συμπεριφορά του μαλακού, NC αργιλικού εδάφους (δεξιά - καμπύλες $q - \varepsilon_q$ ή $\Delta u - \varepsilon_q$) και στις καμπύλες p-y (αριστερά) για βάθος $z = 2D$.

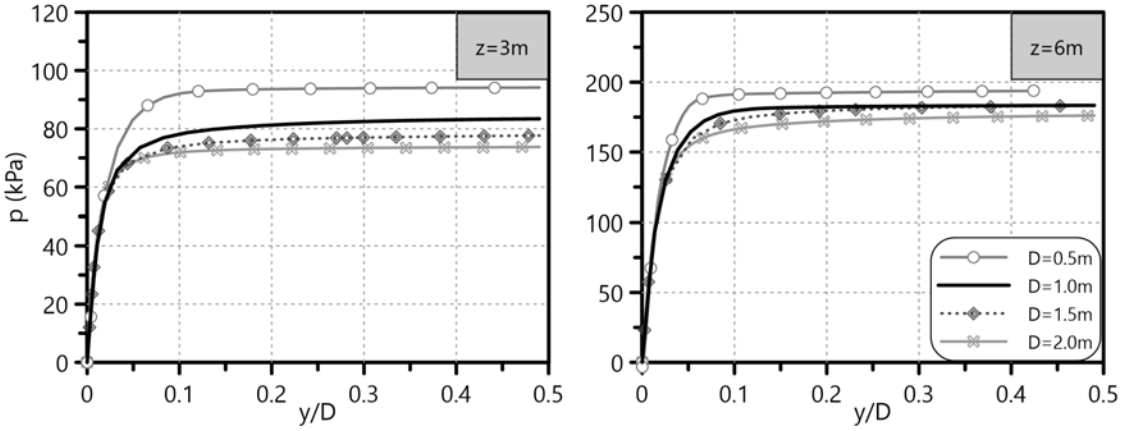

Σχήμα 15: Επιρροή της διαμέτρου D του πασσάλου στις καμπύλες $p - y/D$ (p σε kPa) σε δύο διαφορετικά βάθη μαλακού, NC αργιλικού εδάφους (z=3, 6m).

έλεγχος του βάθους «σφήνας» από τον συντελεστή συνάφειας α.

Η ανωτέρω παραμετρική διερεύνηση οδηγεί στη διατύπωση βελτιωμένων, μονοτονικών καμπυλών p-y για μαλακά, NC αργιλικά εδάφη. Οι καμπύλες αυτές ενσωματώνουν την επιρροή συγκεκριμένων χαρακτηριστικών του εδάφους και του πασσάλου ενώ συγκρίνονται και με τις αντίστοιχες βιβλιογραφικές προτάσεις. Στην ενότητα 5 της παρούσας εκτενούς περίληψης της διατριβής διατυπώνονται αναλυτικά οι καμπύλες p-y που προέκυψαν από τα αποτελέσματα των παραμετρικών αναλύσεων ΠΣ. Οι προτεινόμενες καμπύλες p-y αξιολογούνται σε αντιπαραβολή με πειραματικές μετρήσεις, ενώ παράλληλα εξετάζεται η αποτελεσματικότητά τους ως προς αντίστοιχες μεθοδολογίες της διεθνούς βιβλιογραφίας.

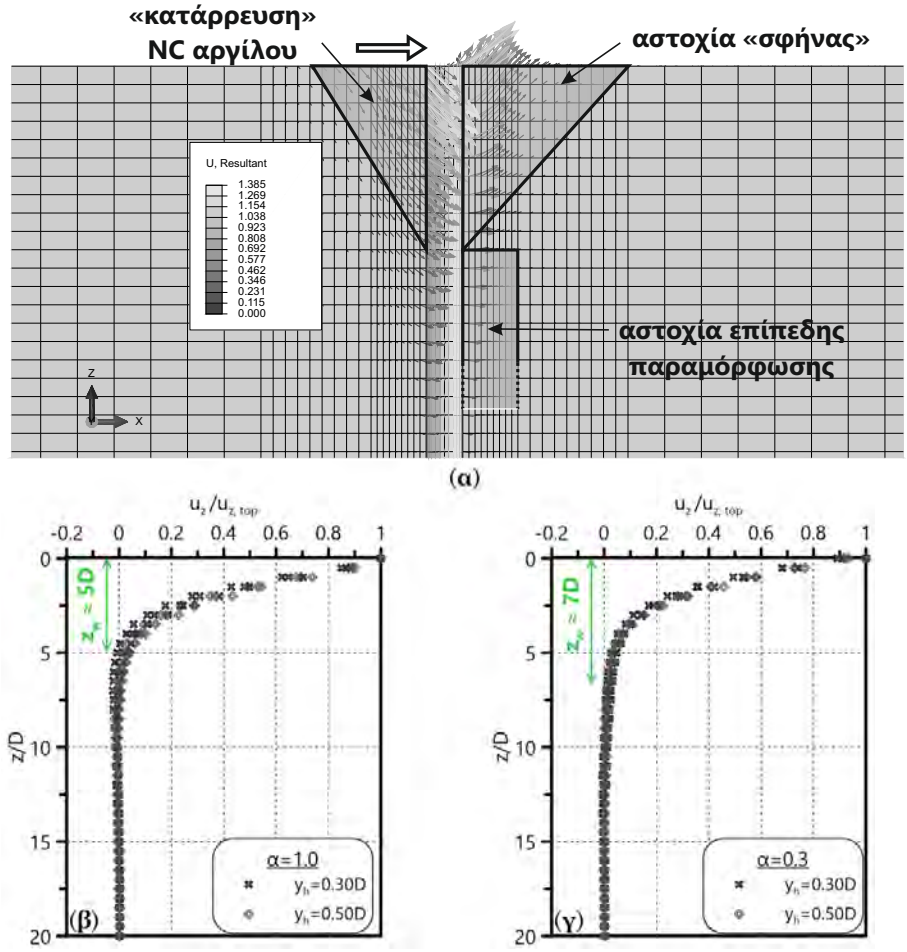

Σχήμα 16: (α) Συνισταμένες μετατοπίσεις στο μαλακό, NC αργιλικό έδαφος πέριξ του πασσάλου με εντοπισμό των διάφορων μηχανισμών αστοχίας. (β, γ) Κανονικοποιημένη κατακόρυφη μετατόπιση $u_z/u_{z,top}$ κόμβων εδάφους δίπλα στον πάσσαλο για δύο διαφορετικά επίπεδα οριζόντιας μετακίνησης κεφαλής y_h, με εντοπισμό του βάθους αστοχίας τύπου «σφήνας» σε z_w.

4.3 Απόκριση πασσάλου σε στιφρά OC αργιλικά εδάφη

Το αριθμητικό προσομοίωμα της Παραγράφου 4.1 χρησιμοποιείται στο παρόν ερευνητικό στάδιο (ΕΕ 3) για την πρόταση μονοτονικών (στατικών) καμπυλών p-y σε εν γένει στιφρά, OC αργιλικά εδάφη - σταθερής αστράγγιστης διατμητικής αντοχής με το βάθος. Προηγείται η παραμετρική διερεύνηση της απόκρισης εύκαμπτου πασσάλου υπό εξωτερική εγκάρσια φόρτιση στα συγκεκριμένα εδάφη, κατά την οποία εξετάζεται η επίδραση των χαρακτηριστικών εδάφους και πασσάλου στις αριθμητικές καμπύλες p-y. Το σύνολο των αριθμητικών αναλύσεων μαζί με το εύρος τιμών της εκάστοτε παραμέτρου που προσομοιώθηκε φαίνονται στον Πίνακα 2. Η αριθμητική προσομοίωση των OC αργιλικών εδαφών γίνεται αρχικά με το κλασικό MCC και στην πορεία με το προχωρημένο καταστατικό μοντέλο SSS-SD

Πίνακας 2: Ιδιότητες ΟC αργιλικού εδάφους όπως προσομοιώθηκαν στις αναλύσεις ΠΣ της παραμετρικής διερεύνησης. Οι αναλύσεις αφορούν πασσάλους διαμέτρου D=0.5-2.0m με συντελεστή συνάφειας εδάφους-πασσάλου α=0.3-1.0.

Παράμετροι ΟC αργιλικού εδάφους				
$c_{u,\,avg}$[1] (kPa)	κ[2]	$K_{o,\,max}$[3]	M[4]	ν
50, 95, 190, 380	**0.0033, 0.0054, 0.0065, 0.0087, 0.0108, 0.0174**	1.5	1.2	0.1
190	0.0054	**0.7, 1.0**	1.2	0.1
190	0.0054	1.5	**0.77, 0.98**	0.1
190	0.0054	1.5	1.2	**0.2, 0.333**

[1] Οι τιμές της $c_{u,\,avg}$ αναφέρονται στη μέση αστράγγιστη διατμητική αντοχή από την επιφάνεια του εδάφους μέχρι βάθος z=10D.
[2] Οι τιμές του κ αντιστοιχούν σε C_r=0.0075-0.04 ($\kappa = C_r/\ln 10$).
[3] $K_{o,\,max}$ είναι η τιμή του K_o κοντά στην επιφάνεια του εδάφους, όπου ο OCR είναι πολύ υψηλός.
[4] Οι τιμές του M αντιστοιχούν σε ϕ=20°, 25° και 30°.

του Kalos (2014). Οι αναλύσεις ΠΣ με το MCC χρησιμεύουν στη διερεύνηση της επιρροής των ακόλουθων εδαφικών χαρακτηριστικών στις καμπύλες p-y των συγκεκριμένων εδαφών:

- μέση αστράγγιστη διατμητική αντοχή $c_{u,\,avg}$ από την επιφάνεια του εδάφους μέχρι βάθος $z = 10D$
- κλίση των γραμμών αποφόρτισης-επαναφόρτισης $\kappa = C_r/\ln 10$
- μέγιστος συντελεστής οριζόντιων γεωστατικών τάσεων $K_{o,\,max}$
- κλίση της Γραμμής Κρίσιμης Κατάστασης (CSL) M
- λόγος Poisson ν

Στατιστική επεξεργασία των αποτελεσμάτων των αριθμητικών αναλύσεων καταδεικνύει σημαντική επιρροή των δύο πρώτων παραμέτρων ($c_{u,\,avg}$ και κ) στην οριακή εγκάρσια εδαφική αντίδραση p_u των καμπυλών p-y, όπως προκύπτει από το Σχήμα 17 για ενδεικτικό βάθος $z = 2D$. Αντίστοιχα, επηρεάζουν την αρχική κλίση K_i των καμπυλών η κ και ο ν του εδάφους.

Στη συνέχεια και μέσω του προχωρημένου καταστατικού προσομοιώματος (Kalos, 2014) εξετάζεται παραμετρικά πώς επιδρούν τα παρακάτω χαρακτηριστικά στιφρών αργιλικών εδαφών στις αντίστοιχες αριθμητικές καμπύλες p-y: η δυσκαμψία του εδάφους σε καθεστώς μικρών παραμορφώσεων (small-strain stiffness, **SSS**) και η

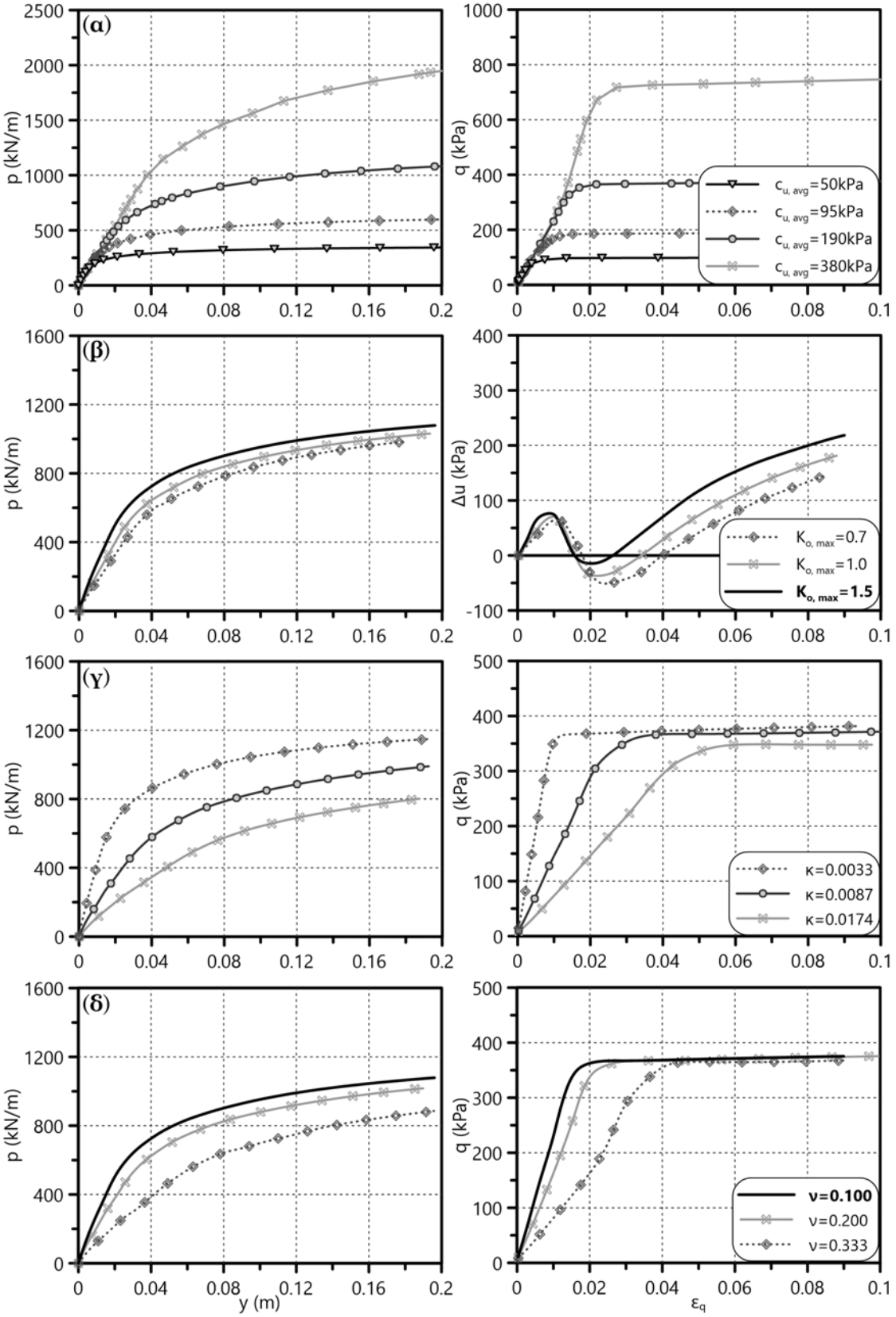

Σχήμα 17: Επιρροή (α) της μέσης αστράγγιστης διατμητικής αντοχής $c_{u,avg}$, (β) του μέγιστου συντελεστή οριζόντιων γεωστατικών τάσεων $K_{o,max}$, (γ) της κλίση της γραμμής αποφόρτισης-επαναφόρτισης κ και (δ) του λόγου Poisson ν στη συμπεριφορά του στιφρού, ΟC αργιλικού εδάφους (δεξιά - καμπύλες $q-\varepsilon_q$ ή $\Delta u-\varepsilon_q$) και στις καμπύλες p-y (αριστερά) για βάθος $z=2D$.

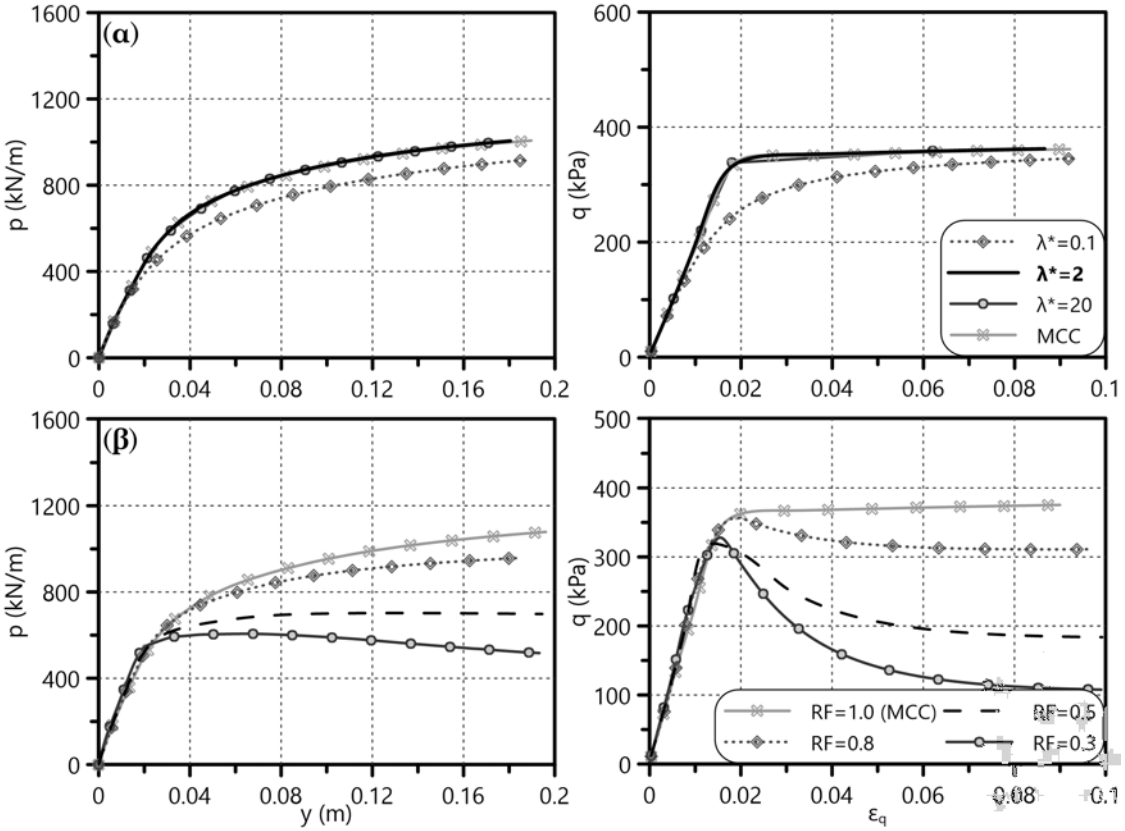

Σχήμα 18: Επιρροή (α) της παραμέτρου λ^* που ελέγχει τη δυσκαμψία σε σχετικά μικρές παραμορφώσεις (SSS) και (β) του δείκτη απομείωσης της αστράγγιστης διατμητικής αντοχής RF (SD) στο διάγραμμα διεκτροπικών τάσεων-παραμορφώσεων $q - \varepsilon_q$ (δεξιά) και στις καμπύλες p-y (αριστερά) του στιφρού, ΟC αργιλικού εδάφους για βάθος $z = 2D$.

μείωση της εδαφικής αντοχής (strength degradation, **SD**) λόγω τασικής χαλάρωσης (strain softening). Το πρώτο χαρακτηριστικό εκφράζεται μέσω της παραμέτρου λ^* που προσδιορίζει τη σχέση παρεμβολής της PYE με την SSE (βλ. Σχήμα 6β), ενώ το δεύτερο αντιπροσωπεύεται από τον βαθμό απομείωσης της αστράγγιστης διατμητικής αντοχής $RF = c_{u,\,\mathrm{res}}/c_{u,\,\mathrm{peak}}$. Οι τιμές που διερευνήθηκαν για τις δύο παραπάνω παραμέτρους είναι: λ^* =0.1, 2, 20 και RF =0.3, 0.5, 0.8 (η περίπτωση του RF=1 ισοδυναμεί με το MCC σε όρους αντοχής).

Η διερεύνηση καταλήγει στο συμπέρασμα ότι η επιρροή του RF (SD) στην p_u των καμπυλών p-y είναι πολύ ισχυρότερη από εκείνη του λ^* (SSS) στην αντίστοιχη K_i (Σχήμα 18). Επιπλέον, παρατηρούμε ότι η τασική χαλάρωση που προσομοιώνεται για τα εδάφη αυτά δε «μεταφράζεται» σε ανάλογη χαλάρωση των αντίστοιχων καμπυλών p-y. Αντιθέτως η p_u αυτών των καμπυλών εμφανίζει σαφή οριζοντίωση (πλατό). Κατά συνέπεια, οι βελτιωμένες καμπύλες p-y της διατριβής για στιφρά, ΟC αργιλικά εδάφη συμπεριλαμβάνουν μόνο τον δείκτη RF ως προς τα ανωτέρω χαρακτηριστικά. Η συγκεκριμένη παραμετρική διερεύνηση αφορά σε

τιμές του RF =0.3-0.8, για εδάφη με $c_{u,\,avg}$=95-380kPa, κ=0.0054, $K_{o,\,max}$=1.5, M=1.2, ν=0.1 και πάσσαλο διαμέτρου D=1m με α=0.3, 1.0.

Το Σχήμα 19α απεικονίζει τις καμπύλες p-y για τρεις διαφορετικές ΟC αργίλους με έντονη απομείωση της μέγιστης αντοχής (RF=0.3) σε βάθη z=2, 6D. Επιπλέον, το Σχήμα 19β δείχνει ότι μόνο τα εδαφικά στοιχεία που βρίσκονται κοντά στον πάσσαλο - μέχρι ακτινική απόσταση περίπου $2D$ - φορτίζονται τόσο ώστε να εμφανίζουν τασική χαλάρωση και να φτάνουν στην παραμένουσα αντοχή τους. Για την ακρίβεια, τα εδαφικά στοιχεία σε οριζόντια απόσταση x=3D δε φτάνουν καν στη διαρροή υπό την εκτεταμένη οριζόντια μετακίνηση $y_h = 30\%D$ της κεφαλής του πασσάλου. Η συγκεκριμένη διερεύνηση καταλήγει στο συμπέρασμα ότι η συμπεριφορά του συστήματος εδάφους-πασσάλου «κυριαρχεί» έναντι της συμπεριφοράς του εδαφικού στοιχείου, με αποτέλεσμα η τασική χαλάρωση του τελευταίου να μην αντικατοπτρίζεται στις αντίστοιχες καμπύλες p-y.

Σχετικά με τα χαρακτηριστικά του πασσάλου, εξετάζεται παραμετρικά η επιρροή της διαμέτρου D και του συντελεστή συνάφειας εδάφους-πασσάλου α τόσο στις καμπύλες p-y όσο και στον μηχανισμό αστοχίας του περιβάλλοντος εδάφους. Το Σχήμα 20 παρουσιάζει τον τρόπο με τον οποίο επηρεάζεται η οριακή εγκάρσια εδαφική αντίδραση p_u στιφρών, ΟC αργιλικών εδαφών από τη D σε βάθη z=3, 6m. Η p_u των καμπυλών p-y μεταβάλλεται κατά ένα ποσοστό 10-20% με τη συνάφεια εδάφους-πασσάλου - α=0.3 για λεία, α=1.0 για τραχεία διεπιφάνεια. Επιπλέον, στο Σχήμα 21 διακρίνονται οι δύο κύριοι μηχανισμοί αστοχίας του συγκεκριμένου τύπου εδάφους «μπροστά» από τον πάσσαλο (αστοχία τύπου «σφήνας» και επίπεδης παραμόρφωσης) καθώς και ο έλεγχος του βάθους «σφήνας» από τον συντελεστή συνάφειας α.

Η παραπάνω παραμετρική διερεύνηση οδηγεί στη διατύπωση βελτιωμένων, μονοτονικών καμπυλών p-y για μέτρια ως στιφρά, ΟC αργιλικά εδάφη, με ($RF < 1$) και χωρίς ($RF = 1$) τασική χαλάρωση. Οι καμπύλες αυτές ενσωματώνουν την επιρροή συγκεκριμένων χαρακτηριστικών του εδάφους και του πασσάλου ενώ συγκρίνονται και με τις αντίστοιχες βιβλιογραφικές προτάσεις. Στην ενότητα 5 της παρούσας εκτενούς περίληψης της διατριβής διατυπώνονται αναλυτικά οι καμπύλες p-y που προέκυψαν από τα αποτελέσματα των παραμετρικών αναλύσεων ΠΣ. Οι προτεινόμενες καμπύλες p-y αξιολογούνται σε αντιπαραβολή με πειραματικές μετρήσεις, ενώ παράλληλα εξετάζεται η αποτελεσματικότητά τους ως προς αντίστοιχες μεθοδολογίες της διεθνούς βιβλιογραφίας.

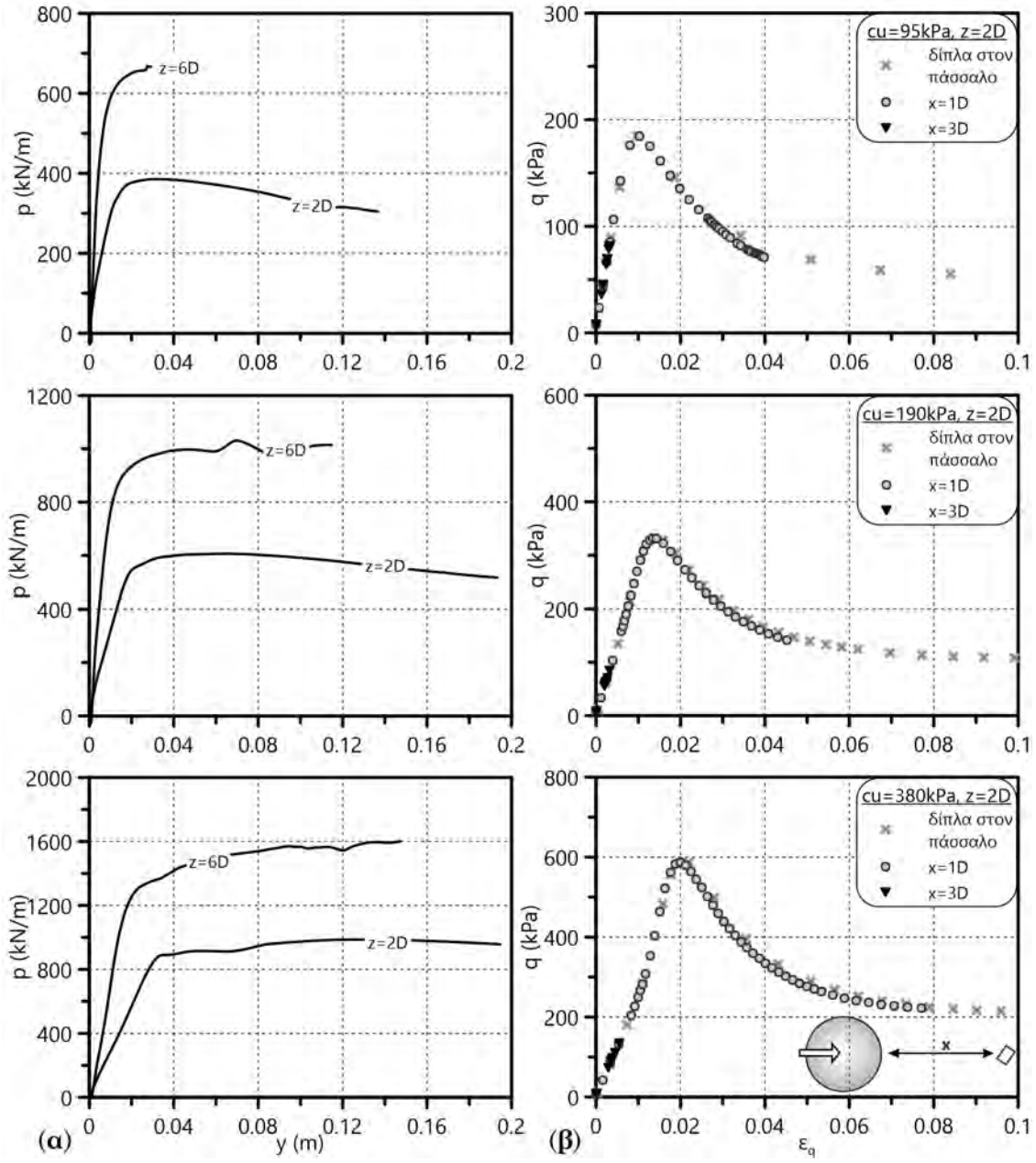

Σχήμα 19: Παράλληλη απεικόνιση (α) καμπυλών p-y σε βάθη z=2, 6D και (β) διαγραμμάτων $q-\varepsilon_q$ σε z=2D για τρεις διαφορετικές οριζόντιες αποστάσεις x=0, 1 και 3D από την παρειά του πασσάλου ($c_{u,\,avg}$=95, 190, 380kPa, RF=0.3, κ=0.0054, $K_{o,\,max}$=1.5, M=1.2, ν=0.1, D=1m). Τα αποτελέσματα των αναλύσεων ΠΣ αναφέρονται σε οριζόντια μετατόπιση του πασσάλου $y_{\text{z=2D}} = 20\%D$ (στο βάθος z=2D).

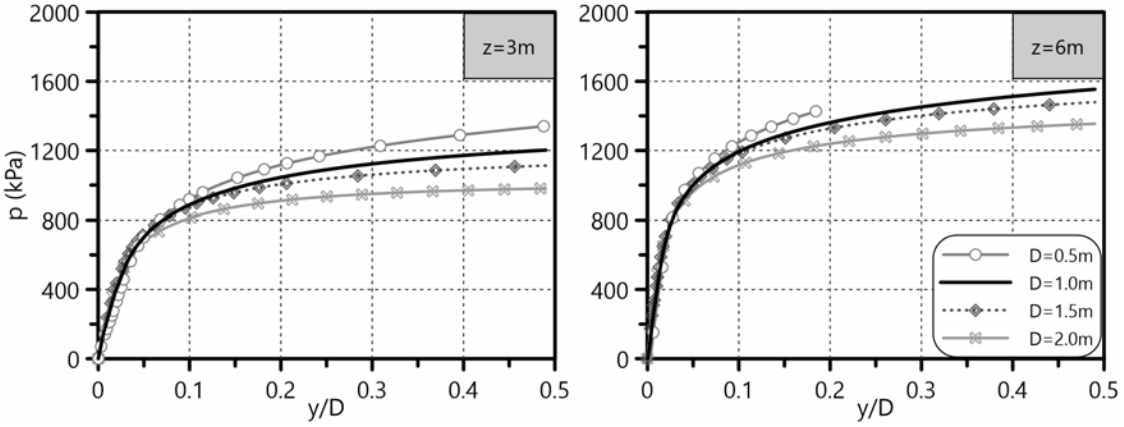

Σχήμα 20: Επιρροή της διαμέτρου D του πασσάλου στις καμπύλες $p - y/D$ (p σε kPa) σε δύο διαφορετικά βάθη στιφρού, ΟC αργιλικού εδάφους (z=3, 6m).

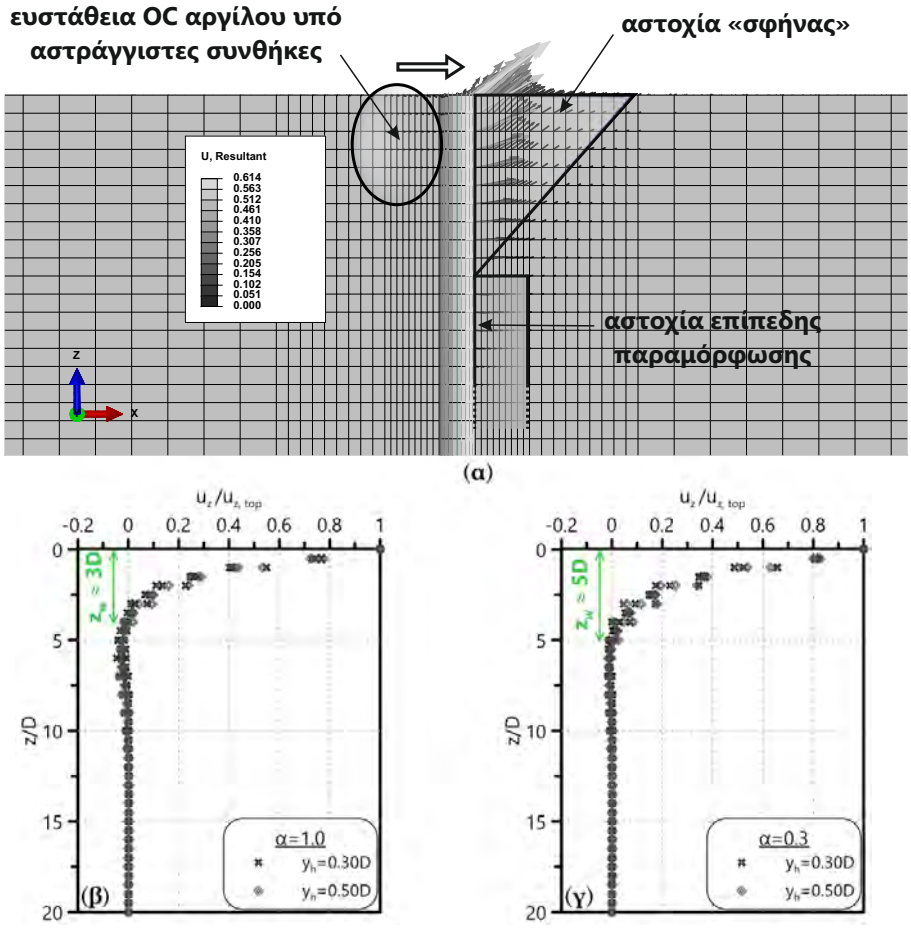

Σχήμα 21: (α) Συνισταμένες μετατοπίσεις στο στιφρό, ΟC αργιλικό έδαφος πέριξ του πασσάλου με εντοπισμό των διάφορων μηχανισμών αστοχίας. (β, γ) Κανονικοποιημένη κατακόρυφη μετατόπιση $u_z / u_{z,top}$ κόμβων εδάφους δίπλα στον πάσσαλο για δύο διαφορετικά επίπεδα οριζόντιας μετακίνησης κεφαλής y_h, με εντοπισμό του βάθους αστοχίας τύπου «σφήνας» σε z_w.

4.4 Διερεύνηση της ανακυκλικής εγκάρσιας φόρτισης πασσάλου σε αργιλικά εδάφη

Στα πλαίσια της τρίτης ερευνητικής ενότητας (ΕΕ 3) διερευνάται και η επίδραση της ανακυκλικής φόρτισης στις αριθμητικές καμπύλες p-y NC και OC αργιλικών σχηματισμών. Η ανακυκλική εγκάρσια φόρτιση πασσάλων αναφέρεται συνήθως στη μετάδοση υδάτινων κυμάτων και στην επαναληψιμότητα των ανεμοπιέσεων, προσομοιώνοντας συνδυαστικά φαινόμενα καταιγίδων που πλήττουν υπεράκτιες ανεμογεννήτριες και εξέδρες εξόρυξης ορυκτών καυσίμων. Στη διεθνή βιβλιογραφία συναντώνται διάφορες προτάσεις τόσο ανακυκλικών καμπυλών p-y (DNV, 1977; Dunnavant & O'Neill, 1989; Kim et al., 2016; Matlock, 1970; Reese et al., 1975; Sullivan et al., 1979; Welch & Reese, 1972) όσο και της επιρροής τέτοιων φορτίσεων στην εγκάρσια απόκριση του συστήματος εδάφους-πασσάλου (Chandrasekaran et al., 2010; Janoyan et al., 2006; Memarpour et al., 2012; Stewart et al., 2007; Tuladhar et al., 2008; Zhang et al., 2010; Zhang & Ng, 2016). Η πλειοψηφία των παραπάνω ερευνητικών προσπαθειών υποδεικνύει ότι 10-20 κύκλοι φόρτισης παρόμοιου μεγέθους οδηγούν σε σταθεροποίηση των βρόγχων υστέρησης.

Η παρούσα διδακτορική διατριβή εξετάζει την ικανότητα του τριδιάστατου αριθμητικού μοντέλου (ΕΕ 2) να προσομοιώσει ανακυκλικές εγκάρσιες φορτίσεις λίγων κύκλων σε αργιλικά εδάφη υπό αστράγγιστες συνθήκες. Για τον σκοπό αυτό, η ανακυκλική φόρτιση στις αναλύσεις ΠΣ επιβάλλεται ψευδοστατικά, υπό μορφή είτε οριζόντιας μετατόπισης είτε οριζόντιου συγκεντρωμένου φορτίου εκατέρωθεν της αρχικής θέσης του πασσάλου για 20 κύκλους. Με την πάροδο των 20 κύκλων φόρτισης, η κεφαλή του πασσάλου φορτίζεται εγκάρσια μέχρι την αστοχία - του εδάφους (ελαστικός πάσσαλος) - για την εξαγωγή καμπυλών p-y μετά την ανακυκλική φόρτιση. Σημειώνεται εδώ ότι η αριθμητική προσομοίωση δε λαμβάνει υπόψη ούτε τη χρονική εξέλιξη ούτε τον ρυθμό επιβολής της ανακυκλικής φόρτισης - εκτός από τις συνθήκες εξασφάλισης των αστράγγιστων συνθηκών.

Καθότι πρόκειται για μία ερευνητική προσπάθεια που δεν αποτελεί κύριο αντικείμενο της διατριβής, επιλέγονται τα ακόλουθα τρία χαρακτηριστικά εδάφη για την αριθμητική διερεύνηση της ανακυκλικής εγκάρσιας φόρτισης:

- **NC:** M=0.984, λ=0.109, λ/κ=10, K_o=0.5, ν=0.333 (MCC, SSS)
- **OC ($RF = 1$):** M=1.2, $c_{u,\,avg}$=190kPa, κ=0.0054, $K_{o,\,max}$=1.5, ν=0.1 (MCC, SSS)
- **OC ($RF = 0.5$):** M=1.2, $c_{u,\,avg}$=190kPa, κ=0.0054, $K_{o,\,max}$=1.5, ν=0.1 (SSS-SD)

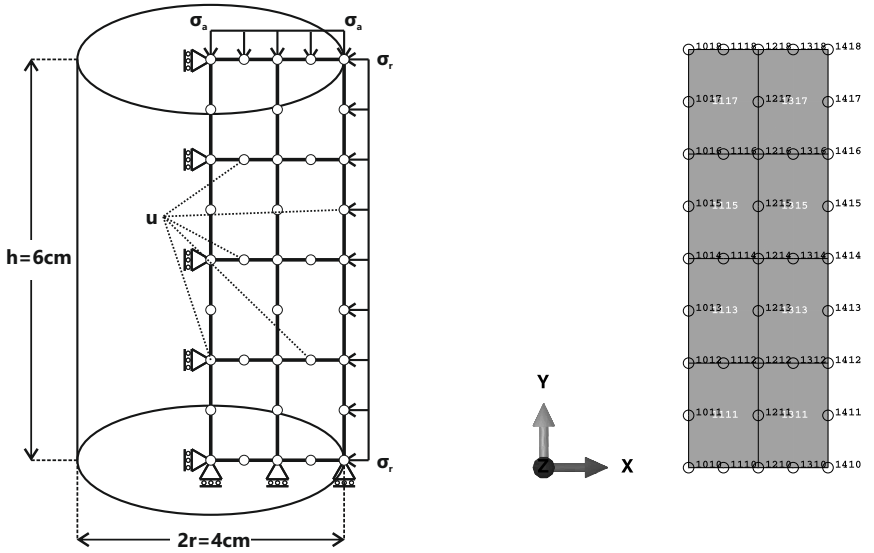

(α) (β)

Σχήμα 22: (α) Σχηματική απεικόνιση των αριθμητικών αστράγγιστων τριαξονικών δοκιμών. (β) Διακριτοποίηση του αξονοσυμμετρικού προσομοιώματος πεπερασμένων στοιχείων για τις τριαξονικές δοκιμές.

Πριν τη σύνθετη αριθμητική προσομοίωση του τριδιάστατου προβλήματος εξετάζεται η ικανότητα των καταστατικών μοντέλων που χρησιμοποιήθηκαν ως τώρα (MCC, SSS-SD) να αποδώσουν την ανακυκλική απόκριση σε επίπεδο εδαφικού στοιχείου. Για τον λόγο αυτό εκτελούνται αριθμητικές ανακυκλικές τριαξονικές δοκιμές (Σχήμα 22) στα παραπάνω εδάφη με την επιβολή 20 κύκλων εφαρμογής και αφαίρεσης αξονικής παραμόρφωσης σταθερού μεγέθους στο δοκίμιο (0-ε_a[1]). Η αρχική εντατική κατάσταση αναφέρεται σε βάθος $z = 3D$ (D=1m) και για τα τρία αργιλικά εδάφη της διερεύνησης. Τα Σχήματα 23 (NC) και 24 (OC) παρουσιάζουν την αστράγγιστη ανακυκλική απόκριση των τριών εδαφών συναρτήσει των ακόλουθων διαγραμμάτων:

(α΄) $p - q$: τασική όδευση

(β΄) $\Delta u - \varepsilon_q$: ανάπτυξη υπερπίεσης πόρων (Δu) με τη διεκτροπική παραμόρφωση (ε_q), σ.σ. ίση με την αξονική παραμόρφωση υπό αστράγγιστες συνθήκες

(γ΄) $S1 - E1$: καμπύλη τάσεων παραμορφώσεων στον γενικευμένο χώρο των τάσεων, με $S1$=$(2\sigma_y - \sigma_x - \sigma_z)/\sqrt{6}$ και $E1$=$(2\varepsilon_y - \varepsilon_x - \varepsilon_z)/\sqrt{6}$ (η ανακυκλική παραμόρφωση επιβάλλεται κατά τον άξονα y - βλ. Σχήμα 22)

(δ΄) $q - \varepsilon_{qp}$: διεκτροπική τάση - συσσωρευμένη πλαστική διεκτροπική παραμόρφωση, με ε_{qp}=$\sum d\varepsilon_{qp}$

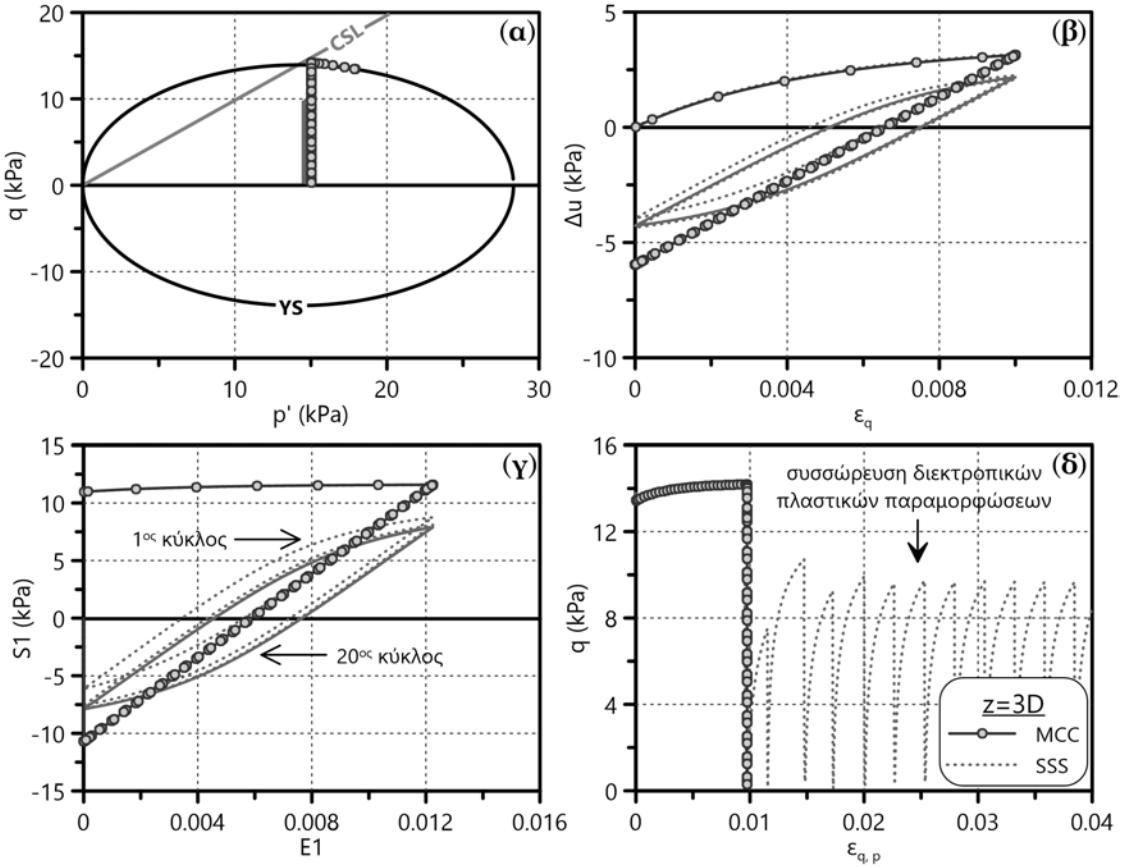

Σχήμα 23: Επιρροή της αστράγγιστης ανακυκλικής τριαξονικής φόρτισης (20 κύκλοι, ε_a=1%) στα διαγράμματα (α) $p-q$, (β) $\Delta u-\varepsilon_q$, (γ) $S1-E1$ και (δ) $q-\varepsilon_{qp}$ για εδαφικό στοιχείο NC αργίλου σε βάθος z=3D.

Για τη μαλακή, NC άργιλο φαίνεται ότι το χαρακτηριστικό της δυσκαμψίας υπό μικρές παραμορφώσεις (SSS) οδηγεί στη διαμόρφωση βρόγχων υστέρησης σε όρους τάσεων-παραμορφώσεων (Σχήματα 23β, γ). Επιπλέον, η εν λόγω ιδιότητα επιτρέπει τη συσσώρευση πλαστικών παραμορφώσεων (ε_{qp}) εξαιτίας της πολύ μικρής επιφάνειας διαρροής (PYE - βλ. Σχήμα 6β) που περικλείει την αρχική εντατική κατάσταση, σε αντίθεση με το MCC που περιορίζει την αποφόρτιση-επαναφόρτιση του εδαφικού στοιχείου στην ελαστική περιοχή εντός της επιφάνειας διαρροής YS (Σχήμα 23α). Για τις στιφρές, OC αργίλους οι παρατηρήσεις είναι αντίστοιχες με αυτές των NC, αναφορικά με την αποτελεσματικότητα του σύνθετου καταστατικού προσομοιώματος SSS-SD. Οι βρόγχοι υστέρησης και η σταθεροποίησή τους είναι εμφανείς κατά την ανακυκλική αξονική παραμόρφωση του εδαφικού στοιχείου στην αστράγγιστη τριαξονική δοκιμή. Επιπρόσθετα, διακρίνεται η πτώση της αντοχής με τη συσσώρευση διεκτροπικών πλαστικών παραμορφώσεων για την περίπτωση του $RF=0.5$ (Σχήμα 24δ).

[1] ε_a=1% και 0.5% για το NC και τα OC εδάφη αντίστοιχα

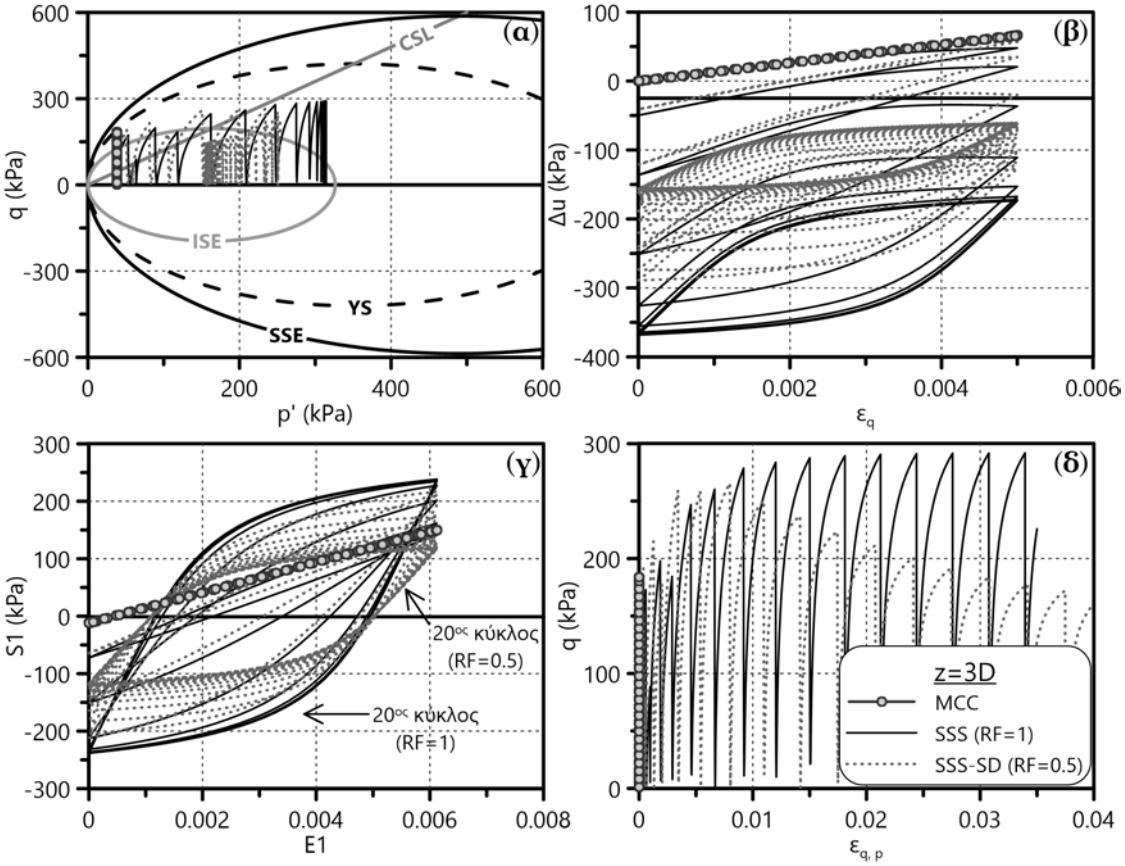

Σχήμα 24: Επιρροή της αστράγγιστης ανακυκλικής τριαξονικής φόρτισης (20 κύκλοι, ε_a=0.5%) στα διαγράμματα (α) $p-q$, (β) $\Delta u-\varepsilon_q$, (γ) $S1-E1$ και (δ) $q-\varepsilon_{qp}$ για εδαφικό στοιχείο ΟC αργίλου σε βάθος z=3D.

Έπειτα από την ανωτέρω αξιολόγηση των χρησιμοποιούμενων καταστατικών προσομοιωμάτων σε επίπεδο εδαφικού στοιχείου, η διερεύνηση περνάει στην αριθμητική προσομοίωση της ανακυκλικής εγκάρσιας φόρτισης πασσάλου διαμέτρου D =1m μέσω τριδιάστατων αναλύσεων ΠΣ (ψευδοστατικά). Αρχικά, η ανακυκλική φόρτιση προσομοιώθηκε με επιβαλλόμενη οριζόντια μετακίνηση της κεφαλής του πασσάλου. Καθότι όμως η συγκεκριμένη προσέγγιση θεωρήθηκε ότι «χειραγωγεί» την ισορροπία της ανακυκλικής απόκρισης του πασσάλου, επιλέγεται η επιβολή οριζόντιου συγκεντρωμένου φορτίου H_c σταθερού μεγέθους για την πιο ρεαλιστική προσομοίωση του προβλήματος. Το H_c που επιβάλλεται ανά περίπτωση - για 20 κύκλους φόρτισης - ισούται προσεγγιστικά με το 1/3-1/2 του οριακού εγκάρσιου φορτίου κεφαλής H_u κατά τη μονοτονική φόρτιση, ήτοι H_c=600, 3000 και 2000kN για τα αργιλικά εδάφη NC, OC με $RF=1$ και OC με $RF=0.5$ αντίστοιχα.

Το Σχήμα 25 αντιπαραβάλει την εγκάρσια μονοτονική και ανακυκλική απόκριση της κεφαλής του πασσάλου σε όρους αδιάστατης μετατόπισης -

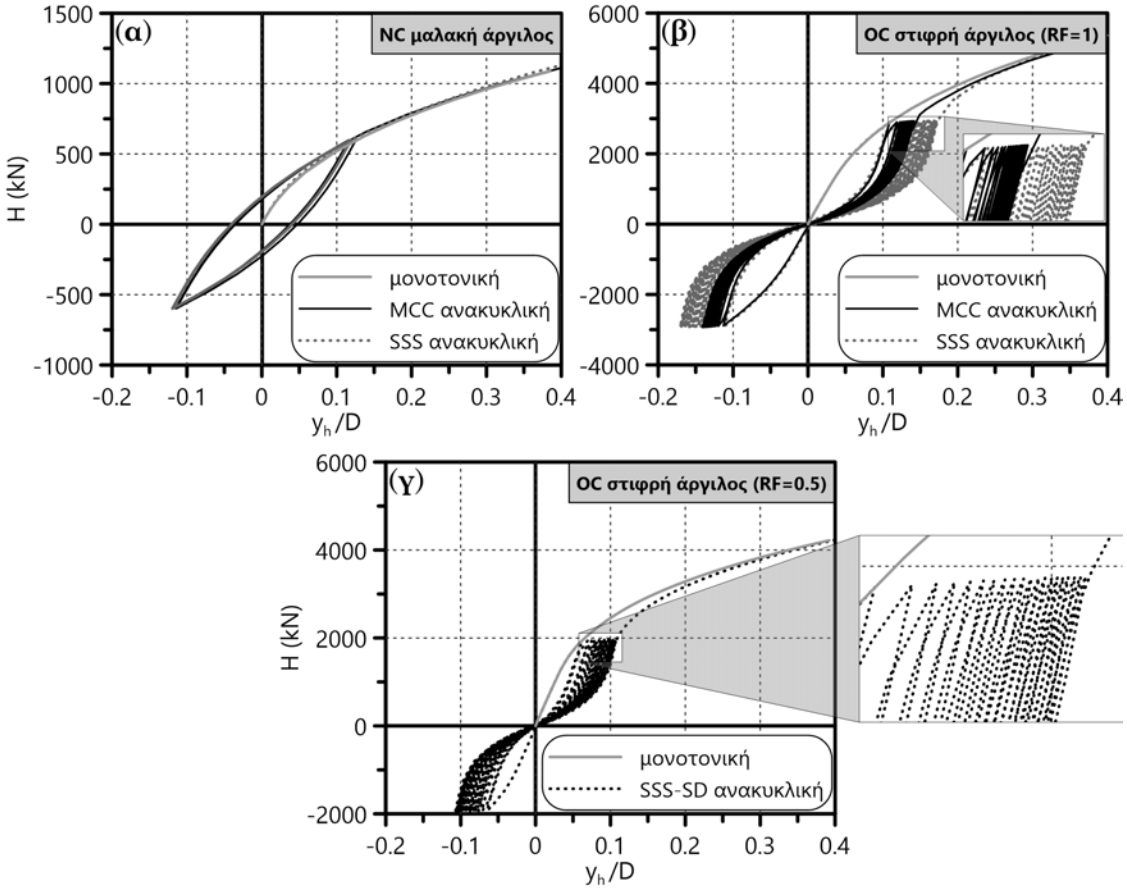

Σχήμα 25: Καμπύλες αδιάστατης μετατόπισης - οριζόντιου φορτίου κεφαλής του πασσάλου $y_h/D - H$ για μονοτονική και ανακυκλική φόρτιση (α) μαλακής, NC αργίλου και στιφρής, OC αργίλου (β) χωρίς ($RF = 1$) και (γ) με τασική χαλάρωση ($RF = 0.5$).

οριζόντιου φορτίου $y_h/D - H$ για τα τρία εδάφη της διερεύνησης. Η προσομοίωση του μαλακού, NC αργιλικού εδάφους με τα δύο διαφορετικά καταστατικά προσομοιώματα δεν εμφανίζει καμία διαφοροποίηση ως προς το συγκεκριμένο διάγραμμα (Σχήμα 25α), παρά τις διαφορές που παρατηρήθηκαν σε επίπεδο εδαφικού στοιχείου - πιθανότατα λόγω πολύ εκτεταμένων παραμορφώσεων στο έδαφος συγκριτικά με τις τριαξονικές δοκιμές. Επίσης αμελητέα φαίνεται να είναι η επιρροή της ανακυκλικής φόρτισης στο H_u (φόρτιση μέχρι την αστοχία μετά το ανακυκλικό φορτίο). Τα αντίστοιχα διαγράμματα των στιφρών, OC αργιλικών εδαφών (Σχήματα 25β, γ) παρουσιάζουν σαφείς ενδείξεις σταθεροποίησης της απόκρισης του συστήματος έπειτα από κάποιον αριθμό κύκλων φόρτισης (plastic shakedown). Επιπλέον, φαίνεται η μειωμένη ισοδύναμη δυσκαμψία του διαγράμματος $y_h/D - H$ αν λάβουμε υπόψη το διάστημα της ανακυκλικής φόρτισης καθώς και ότι το σύστημα δεν εμφανίζει χαρακτηριστικά τασικής χαλάρωσης (ανάλογα με αυτά της συμπεριφοράς του εδαφικού στοιχείου για

$RF = 0.5$).

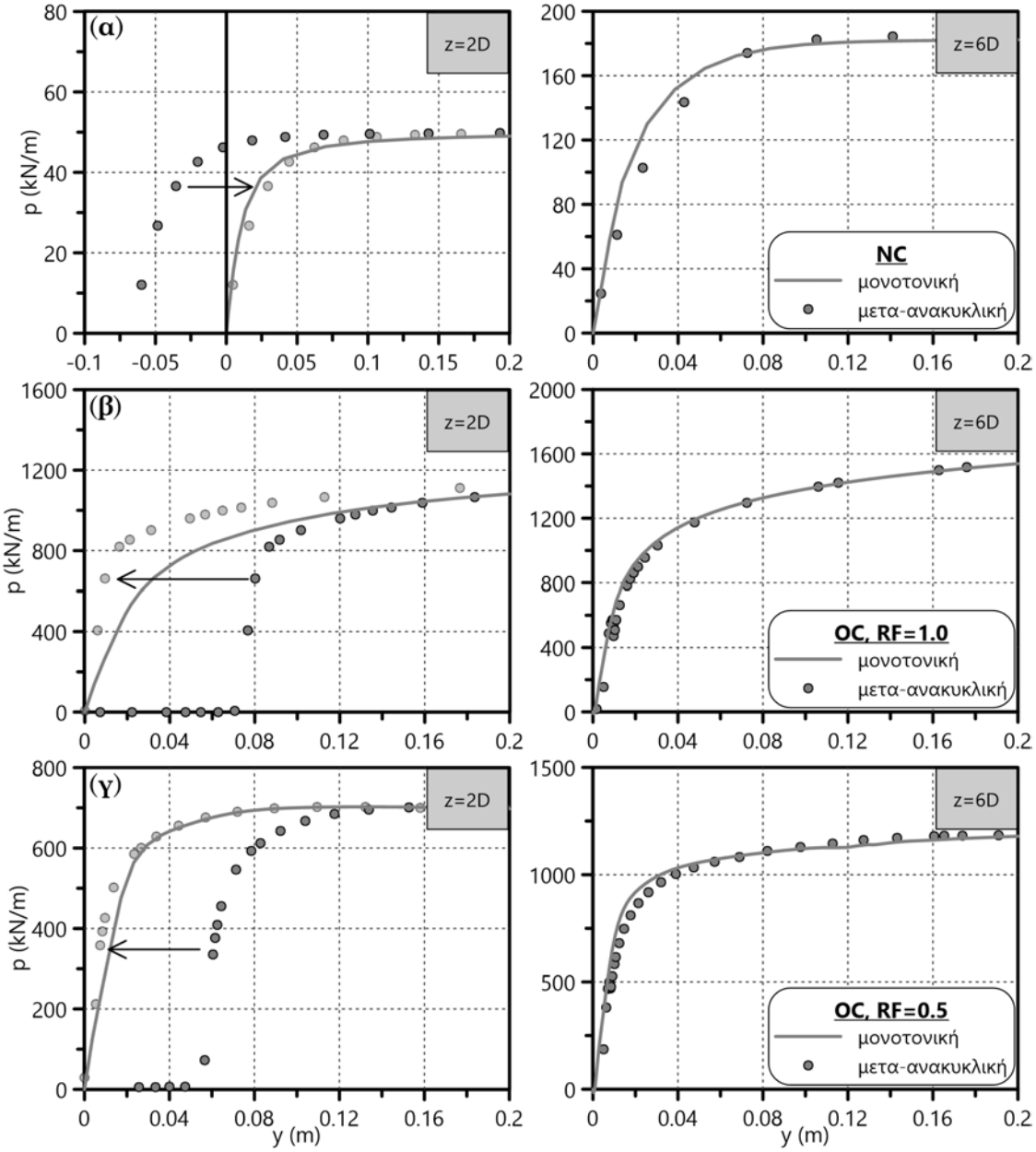

Σχήμα 26: Σύγκριση καμπυλών p-y μετά την ανακυκλική φόρτιση με τις αντίστοιχες μονοτονικές σε βάθη z=2 και $6D$ για (α) μαλακή, NC άργιλο και στιφρή, OC άργιλο (β) χωρίς ($RF = 1$) και (γ) με τασική χαλάρωση ($RF = 0.5$).

Τέλος, η διερεύνηση αυτή συγκρίνει τις καμπύλες p-y που προέκυψαν μετά την ανακυκλική φόρτιση με τις αντίστοιχες μονοτονικές σε δύο διαφορετικά βάθη $z = 2, 6D$ (Σχήμα 26). Σημειώνεται ότι ως καμπύλη p-y μετά την ανακυκλική φόρτιση νοείται το τμήμα της καμπύλης, στο οποίο η εγκάρσια εδαφική αντίδραση p μεταβαίνει από αρνητικές σε θετικές τιμές. Η καμπύλη p-y στο μεγάλο βάθος ($z = 6D$) μετά την ανακυκλική φόρτιση είναι ίδια με την αντίστοιχη μονοτονική και για τα

τρία εδάφη, καθότι το ανακυκλικό φορτίο παρά το μέγεθός του ($y_h = 0.1 - 0.2D$) δεν επηρεάζει αυτά τα βάθη. Η p_u μετά την ανακυκλική φόρτιση δε διαφέρει καθόλου από την αντίστοιχη μονοτονική σε κανένα από τα τρία εδάφη. Αναφορικά με την K_i, παρατηρείται κάποια αύξησή[1] της στα OC εδάφη και σε μικρό βάθος ($z = 2D$). Εντούτοις, η δυσκαμψία του ισοδύναμου ελατηρίου p-y για δεδομένο επίπεδο y μειώνεται με τον αριθμό των κύκλων φόρτισης, κατά αντιστοιχία με τη συμπεριφορά των διαγραμμάτων $y_h/D - H$ (Σχήμα 25).

Τέλος, υπενθυμίζεται ότι η προαναφερθείσα αριθμητική διερεύνηση της ανακυκλικής εγκάρσιας φόρτισης πασσάλου είναι ποιοτικού χαρακτήρα και θίγει ποικίλες πτυχές του προβλήματος (καταστατική προσομοίωση, συμπεριφορά συστήματος εδάφους-πασσάλου, ανακυκλικές καμπύλες p-y), αποσκοπώντας στην περαιτέρω μελέτη αυτού από μελλοντικές εργασίες.

[1] για να συγκριθούν οι K_i απαιτείται μετατόπιση της τελικής καμπύλης p-y στην αρχή των αξόνων

5 Αποτελέσματα-Αξιολόγηση

Η παραμετρική διερεύνηση της εξωτερικά επιβαλλόμενης εγκάρσιας φόρτισης πασσάλου μέσω αριθμητικών αναλύσεων πεπερασμένων στοιχείων οδήγησε στη διατύπωση των ακόλουθων βελτιωμένων μονοτονικών καμπυλών p-y για μαλακά, NC και στιφρά, OC αργιλικά εδάφη. Επιγραμματικά αναφέρονται τα τέσσερα επιμέρους σημεία ενδιαφέροντος για την περιγραφή των προτεινόμενων καμπυλών:

- μαθηματική έκφραση της καμπύλης p-y
- αρχική δυσκαμψία K_i
- οριακή εγκάρσια εδαφική αντίδραση p_u
- σύγκριση με τις προτεινόμενες καμπύλες p-y της βιβλιογραφίας.

Τέλος, οι προτεινόμενες καμπύλες p-y αξιολογούνται ως προς την ικανότητά τους να προβλέψουν την εγκάρσια απόκριση πασσάλων, όπως αυτή μετρήθηκε κατά τη διάρκεια φυσικών δοκιμαστικών φορτίσεων. Στα πλαίσια αυτής της αξιολόγησης, εξετάζεται και η αποτελεσματικότητα των προτάσεων της διατριβής συγκριτικά με αντίστοιχες υφιστάμενες βιβλιογραφικές μεθοδολογίες.

5.1 Μονοτονικές καμπύλες p-y για μαλακά NC αργιλικά εδάφη

Προτείνεται η ακόλουθη εκθετική συνάρτηση μονοτονικών καμπυλών p-y για μαλακά, NC αργιλικά εδάφη:

$$\frac{p}{p_u} = 1 - \exp\left(\frac{-K_i \cdot y}{p_u}\right) \tag{1}$$

Σύμφωνα με το Σχήμα 27, η ευρέως χρησιμοποιούμενη υπερβολική εξίσωση δεν αναπαράγει με ακρίβεια την εγκάρσια εδαφική απόκριση των μαλακών αργίλων[1], τόσο για μικρά (z=1D) όσο και για μεγάλα βάθη (z=6D) - συγκριτικά με την προτεινόμενη εκθετική σχέση. Στο Σχήμα 7 παρατηρεί κανείς δύο διαφορετικές συμπεριφορές: η NC άργιλος κρατύνεται ελάχιστα ως προς την αντίστοιχη κράτυνση της OC αργίλου. Η συγκεκριμένη διαφορά σε επίπεδο εδαφικού στοιχείου είναι ομοίως έκδηλη και στη μακροκλίμακα των καμπυλών p-y. Ως εκ τούτου, η προτεινόμενη εκθετική μορφή για τα συγκεκριμένα μαλακά εδάφη επιτρέπει τον σχηματισμό σαφούς πλατό αναφορικά με την p_u των αντίστοιχων καμπυλών. Ακολουθούν οι αντίστοιχες προτάσεις της παρούσας διατριβής για την K_i και την p_u που απαιτούνται από την Εξίσωση 1. Η αρχική δυσκαμψία $K_{i,\text{NC}}$ των

[1] οι αριθμητικές καμπύλες p-y του σχήματος αναφέρονται σε NC έδαφος με M=0.984, λ=0.109, λ/κ=10, ν=0.333 και πάσσαλο διαμέτρου D=1.0m και α=1.0

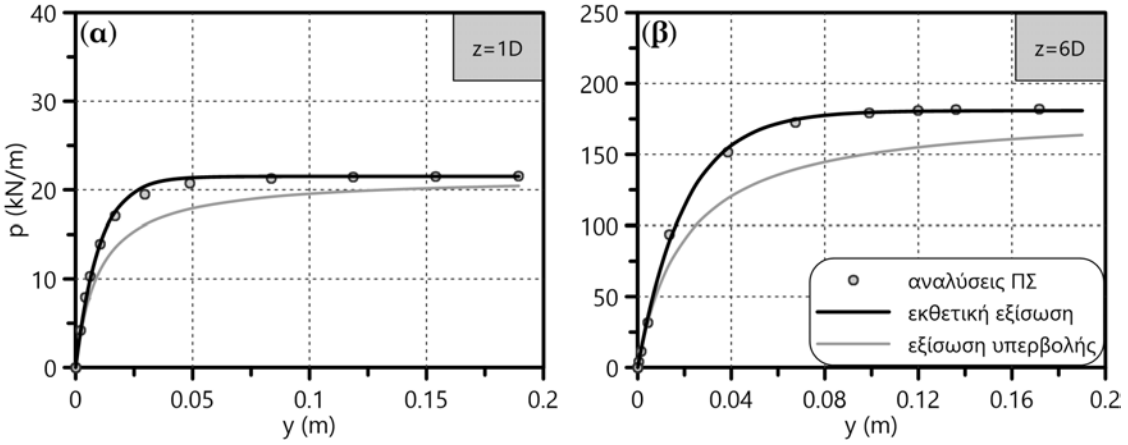

Σχήμα 27: Σύγκριση της προτεινόμενης εκθετικής σχέσης με την αντίστοιχη υπερβολική ως προς την αναλυτική προσέγγιση των καμπυλών p-y που προέκυψαν για δύο διαφορετικά βάθη (z=1, 6D) μαλακού, NC αργιλικού εδάφους από τις αναλύσεις ΠΣ.

προτεινόμενων καμπυλών p-y αποτελεί γραμμική συνάρτηση του βάθους z με κλίση n και τιμή 0 στην επιφάνεια του εδάφους, αντικατοπτρίζοντας έτσι το αντίστοιχο γραμμικά αυξανόμενο μέτρο ελαστικότητας των συγκεκριμένων εδαφών - όπως προσομοιώθηκαν στις αναλύσεις ΠΣ. Η K_i προκύπτει ως συνάρτηση των εδαφικών παραμέτρων λ, λ/κ και ν σύμφωνα με την ακόλουθη έκφραση:

$$K_{i,\mathrm{NC}}(z) = n \cdot z \quad (\mathrm{kN/m^2}) \tag{2}$$

$$n = 3.9 \cdot 10^{-7} \cdot \, n(\lambda) \cdot n(\lambda/\kappa) \cdot n(\nu) \tag{3}$$

$$n(\lambda) = 170 \cdot \lambda^{-1} \tag{4}$$

$$n(\lambda/\kappa) = 140 \cdot (\lambda/\kappa) + 200 \tag{5}$$

$$n(\nu) = 11250 \cdot \nu + 5400 \tag{6}$$

Το Σχήμα 28 παρουσιάζει την επιμέρους επιρροή των παραπάνω παραμέτρων για μαλακά, NC αργιλικά εδάφη στην αρχική κλίση K_i. Η οριακή εγκάρσια εδαφική αντίδραση p_u παρουσιάζεται συνήθως αδιαστατοποιημένη υπό τη μορφή του αντίστοιχου συντελεστή $N_p = p_u/(c_u \cdot D)$. Στατιστική επεξεργασία των αποτελεσμάτων των παραμετρικών αναλύσεων ΠΣ για τα συγκεκριμένα εδάφη καταδεικνύει αμελητέα επιρροή της κλίση της Γραμμής Κρίσιμης Κατάστασης M και της διαμέτρου D του πασσάλου στον N_p. Η ακόλουθη έκφραση που διατυπώνεται για τον $N_{p,\mathrm{NC}}$ είναι αποκλειστική συνάρτηση του συντελεστή συνάφειας εδάφους-πασσάλου α (συμφωνώντας με πολλές, αντίστοιχες

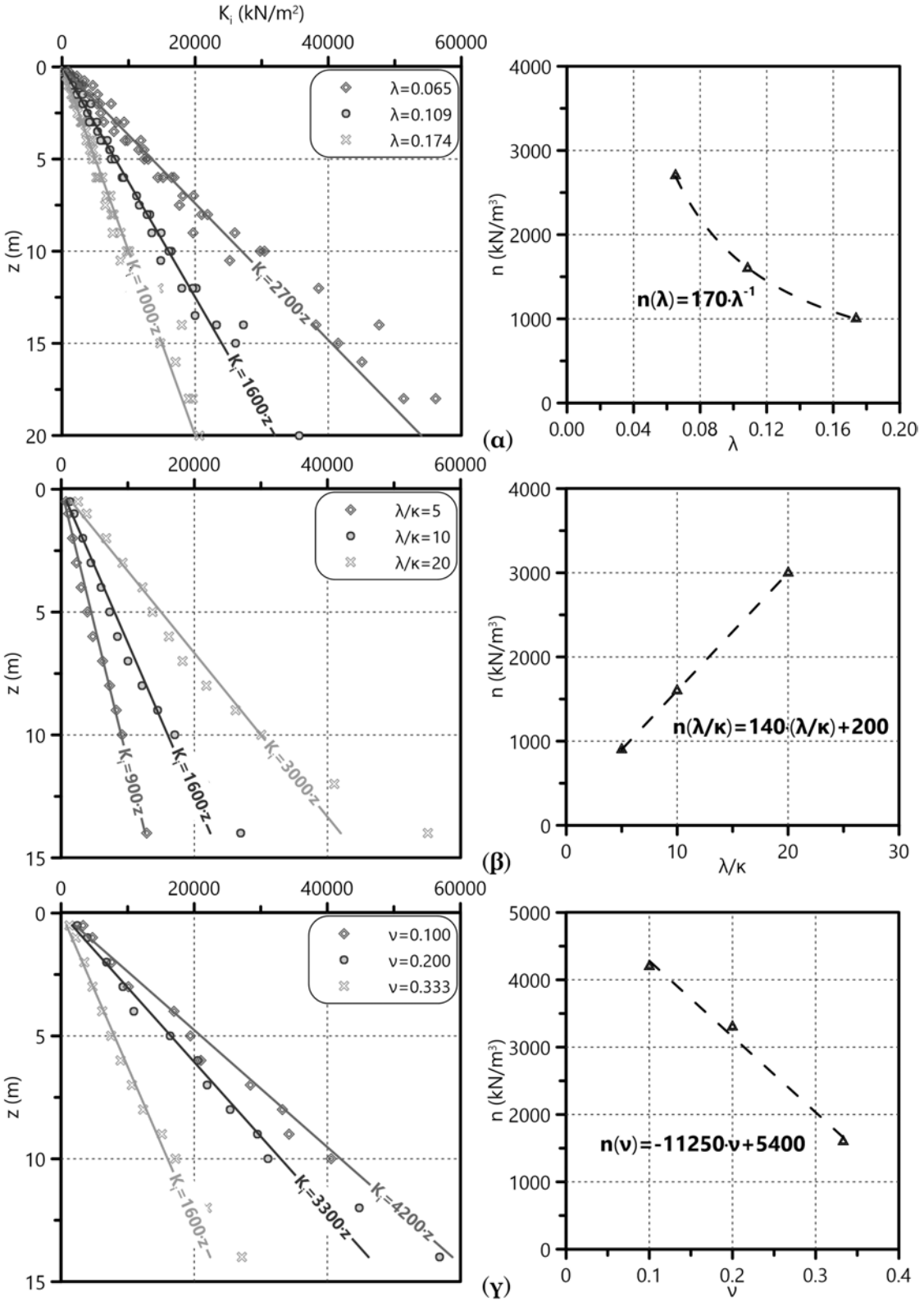

Σχήμα 28: Προσδιορισμός της κλίσης n για τη γραμμική συνάρτηση της αρχικής δυσκαμψίας $K_i(z) = n \cdot z$ των αριθμητικών καμπυλών p-y μαλακών, NC αργίλων. Επιρροή (α) της κλίσης λ της γραμμής παρθενικής συμπίεσης, (β) του λόγου λ/κ και (γ) του λόγου Poisson ν στην κλίση n.

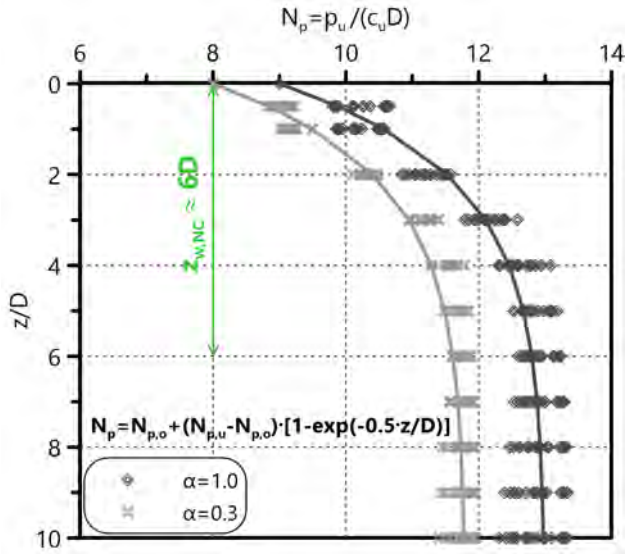

Σχήμα 29: Επιρροή του συντελεστή συνάφειας εδάφους-πασσάλου α στην κατανομή του N_p με το z/D από τις αναλύσεις ΠΣ για διάφορες διαμέτρους D σε πλήθος μαλακών, NC αργιλικών εδαφών.

διαπιστώσεις της βιβλιογραφίας):

$$N_p = \frac{p_u}{c_u \cdot D} = N_{p,o} + (N_{p,u} - N_{p,o}) \left(1 - \exp\left(-0.5\,\frac{z}{D}\right)\right) \tag{7}$$

$$N_{p,o} = 7.57 + 1.43 \cdot \alpha \tag{8}$$

$$N_{p,u} = 11.29 + 1.71 \cdot \alpha \tag{9}$$

Το Σχήμα 29 οπτικοποιεί την παραπάνω σχέση και επιβεβαιώνει την ύπαρξη δύο μηχανισμών αστοχίας του εδάφους μπροστά από τον εγκάρσια φορτιζόμενο πάσσαλο: την αστοχία τύπου «σφήνας» μέχρι το βάθος z=5-7D - εξαρτάται από την τιμή του α - και την αστοχία υπό καθεστώς επίπεδης παραμόρφωσης για μεγαλύτερα βάθη[1].

Συγκρίνοντας τις προαναφερθείσες βελτιωμένες καμπύλες p-y της διατριβής με τις αντίστοιχες της βιβλιογραφίας, φαίνεται πως η πλειοψηφία των υφιστάμενων μεθοδολογιών προτείνει συντηρητικές λύσεις για τα συγκεκριμένα εδάφη (Σχήμα 30). Η σύγκριση αναφέρεται σε πάσσαλο διαμέτρου D=1m, μήκους L=30m, συντελεστή συνάφειας εδάφους-πασσάλου α=1.0 σε μαλακή, NC άργιλο με κορεσμένο ειδικό βάρος γ=20kN/m^3, $c_u = 5 + 0.25 \cdot \sigma'_{vo}$ (kPa), λ=0.130 (C_c=0.30), λ/κ=10, ν=0.30 και στάθμη υδροφόρου ορίζοντα στην επιφάνεια του εδάφους. Σε ανάλογη διαπίστωση για τις βιβλιογραφικές καμπύλες p-y μαλακών αργιλικών

[1] Ο συντελεστής N_p παραμένει σταθερός για αδιάστατο βάθος $z/D > 6$, ίσο με το αντίστοιχο μέσο βάθος εκδήλωσης της αστοχίας τύπου «σφήνας» στα μαλακά, NC αργιλικά εδάφη των αριθμητικών αναλύσεων.

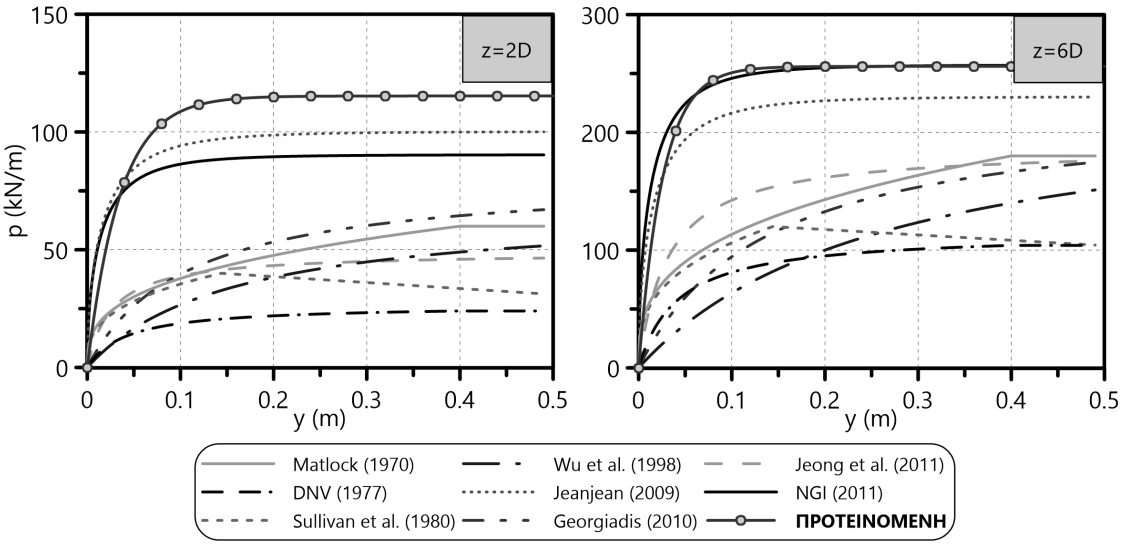

Σχήμα 30: Σύγκριση των προτεινόμενων μονοτονικών καμπυλών p-y με τις αντίστοιχες βιβλιογραφικές μεθοδολογίες για πάσσαλο διαμέτρου D=1m και συνάφειας α=1.0 σε πλήρως κορεσμένο, μαλακό, NC αργιλικό έδαφος, σε μικρό (z=2D) και μεγάλο βάθος (z=6D).

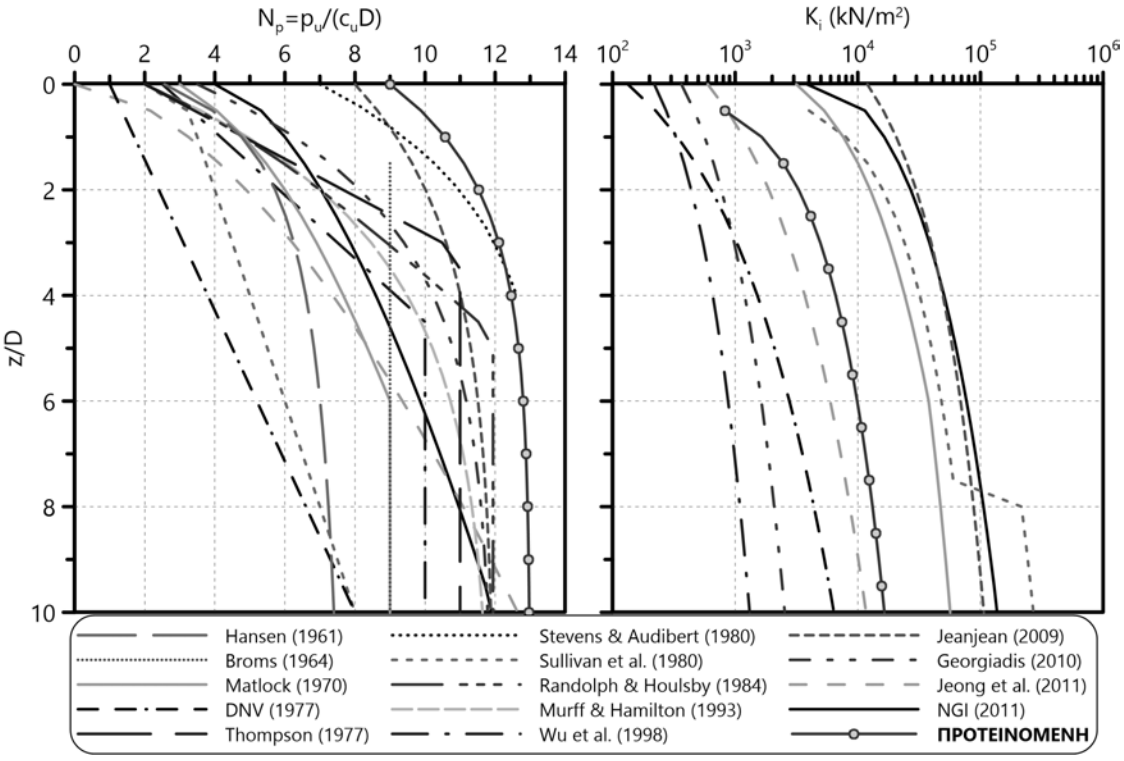

Σχήμα 31: Σύγκριση των προτεινόμενων κατανομών N_p-z/D και K_i-z/D με τις αντίστοιχες βιβλιογραφικές μεθοδολογίες για πάσσαλο διαμέτρου D=1m και συνάφειας α=1.0 σε πλήρως κορεσμένο, μαλακό, NC αργιλικό έδαφος.

εδαφών καταλήγει κανείς αν εξετάσει επιμέρους τις κατανομές των N_p και K_i με το αδιάστατο βάθος z/D (Σχήμα 31). Κατ' επέκταση, οι προτεινόμενες από τη διατριβή καμπύλες p-y συντελούν στην επίτευξη ενός ρεαλιστικού, ασφαλούς και οικονομικού σχεδιασμού πασσάλων υπό εγκάρσια φόρτιση κεφαλής σε αυτά τα εδάφη.

5.2 Μονοτονικές καμπύλες p-y για στιφρά OC αργιλικά εδάφη

Η εμφάνιση ή μη τασικής χαλάρωσης από το εκάστοτε στιφρό, OC αργιλικό έδαφος - $RF < 1$ ή $RF = 1$ αντίστοιχα[1] - καθορίζει τη μορφή των προτεινόμενων καμπυλών p-y για τους εν λόγω εδαφικούς σχηματισμούς:

RF=1: Προτείνεται η υπερβολική συνάρτηση της βιβλιογραφίας λόγω της διαρκώς κρατυνόμενης οριζόντιας απόκρισης του OC εδάφους. Η εξίσωση της υπερβολής εύκολα μετατρέπεται σε εξίσωση ευθείας σε άξονες $y - y/p$ για τον υπολογισμό των K_i (αρχική τιμή) και p_u (κλίση) της συγκεκριμένης καμπύλης p-y.

$$p = \frac{y}{\frac{1}{K_i} + \frac{y}{p_u}} \quad \Leftrightarrow \quad \frac{y}{p} = \frac{1}{K_i} + \frac{1}{p_u} \cdot y \tag{10}$$

RF<1: Προτείνεται η χρήση της εκθετικής συνάρτησης που διατυπώθηκε για τα NC αργιλικά εδάφη (Εξίσωση 1), καθότι οι καμπύλες p-y των στιφρών αργίλων της διατριβής εμφανίζουν σαφή οριζόντιο κλάδο της p_u.

$$\frac{p}{p_u} = 1 - \exp\left(\frac{-K_i \cdot y}{p_u}\right)$$

Στο σημείο αυτό, επαναλαμβάνεται η ακόλουθη διαπίστωση για τις καμπύλες p-y στιφρών, OC αργιλικών εδαφών με τασική χαλάρωση ($RF < 1$) - όπως αυτές προέκυψαν από τις αναλύσεις ΠΣ: σε αντίθεση με κάποιες βιβλιογραφικές μεθοδολογίες (DNV, 1977; Reese et al., 1975; Sullivan et al., 1979), οι αριθμητικές καμπύλες p-y στιφρών εδαφών με έντονη πτώση της αντοχής τους υπό εκτεταμένη παραμόρφωση (π.χ. RF=0.3) δεν εμφανίζουν ανάλογη μορφή με την καμπύλη τάσεων-παραμορφώσεων του εδάφους - πιθανότατα λόγω επικράτησης της συμπεριφοράς του συστήματος εδάφους-πασσάλου στην εγκάρσια απόκριση. Ακολουθούν οι αντίστοιχες προτάσεις της παρούσας διατριβής για την K_i και την p_u που απαιτούνται από τις παραπάνω εξισώσεις.

[1] $RF = c_{u,\,\mathrm{res}}/c_{u,\,\mathrm{peak}}$

Η αρχική δυσκαμψία $K_{i,\text{OC}}$ των προτεινόμενων καμπυλών p-y αποτελεί γραμμική συνάρτηση του βάθους z με κλίση n και τιμή K_{i0} στην επιφάνεια του εδάφους, αντικατοπτρίζοντας έτσι το αντίστοιχο γραμμικά αυξανόμενο μέτρο ελαστικότητας των συγκεκριμένων εδαφών - όπως προσομοιώθηκαν στις αναλύσεις ΠΣ με χρήση του MCC. Η K_i προκύπτει ως συνάρτηση των εδαφικών παραμέτρων κ και ν σύμφωνα με την ακόλουθη έκφραση:

$$K_i = n \cdot z + K_{i0} \tag{11}$$

$$n = 270 \cdot \kappa^{-0.77} \cdot (-2.07 \cdot \nu + 1.17) \tag{12}$$

$$K_{i0} = 8.4 \cdot \kappa^{-1.3} \cdot (-6.14 \cdot \nu + 2.23) \tag{13}$$

Το Σχήμα 32 παρουσιάζει την επιμέρους επιρροή των παραπάνω παραμέτρων για στιφρά, OC αργιλικά εδάφη στην αρχική κλίση K_i. Στατιστική επεξεργασία των αποτελεσμάτων των παραμετρικών αναλύσεων ΠΣ για τα συγκεκριμένα εδάφη καταδεικνύει αμελητέα επιρροή της κλίση της Γραμμής Κρίσιμης Κατάστασης M και του μέγιστου συντελεστή οριζόντιων γεωστατικών τάσεων $K_{o,\,max}$ στην p_u - και κατ' επέκταση στον N_p. Η ακόλουθη έκφραση που διατυπώνεται για τον $N_{p,\text{OC}}$ εμπεριέχει την επιρροή της μέσης αστράγγιστης διατμητικής αντοχής $c_{u,\,avg}$ - από την επιφάνεια του εδάφους μέχρι βάθος $z = 10D$ - της κλίσης των γραμμών αποφόρτισης-επαναφόρτισης κ, της διαμέτρου του πασσάλου D, του βαθμού συνάφειας εδάφους-πασσάλου α και του δείκτη απομείωσης της αστράγγιστης διατμητικής αντοχής RF στον συγκεκριμένο αδιαστατοποιημένο δείκτη της p_u:

$$p_u = N_p \cdot c_u \cdot D = \left[N_{p,o} + (N_{p,u} - N_{p,o})\left(1 - \exp\left(-0.333\,\frac{z}{D}\right)\right)\right] \cdot c_u \cdot D \tag{14}$$

$$N_{p,o} = \left(0.6 \cdot \frac{c_{u,\,avg}}{p_a} + 0.9 \cdot \alpha + 2.5\right) \cdot [0.1 \cdot \exp(2.3 \cdot RF)] \tag{15}$$

$$N_{p,u} = (F_c \cdot F_\kappa \cdot F_D) \cdot (0.6 \cdot RF + 0.4) \tag{16}$$

$$F_c = \left(\frac{c_{u,\,avg}}{p_a}\right)^{-\frac{1}{7}} \tag{17}$$

$$F_\kappa = -9.5 \cdot \kappa + 1.2 \tag{18}$$

$$F_D = 7.9 + 0.9\alpha + \left(-0.5 \cdot \frac{c_{u,\,avg}}{p_a} + 2\right)\frac{D}{D_1} \tag{19}$$

Για λόγους αδιαστατοποίησης, στις παραπάνω εκφράσεις του N_p συμμετέχει η ατμοσφαιρική πίεση στο επίπεδο της θάλασσας p_a=100kPa. Το Σχήμα 33 παρουσιάζει το σφάλμα εκτίμησης του N_p μέσω των αναλυτικών σχέσεων ως προς

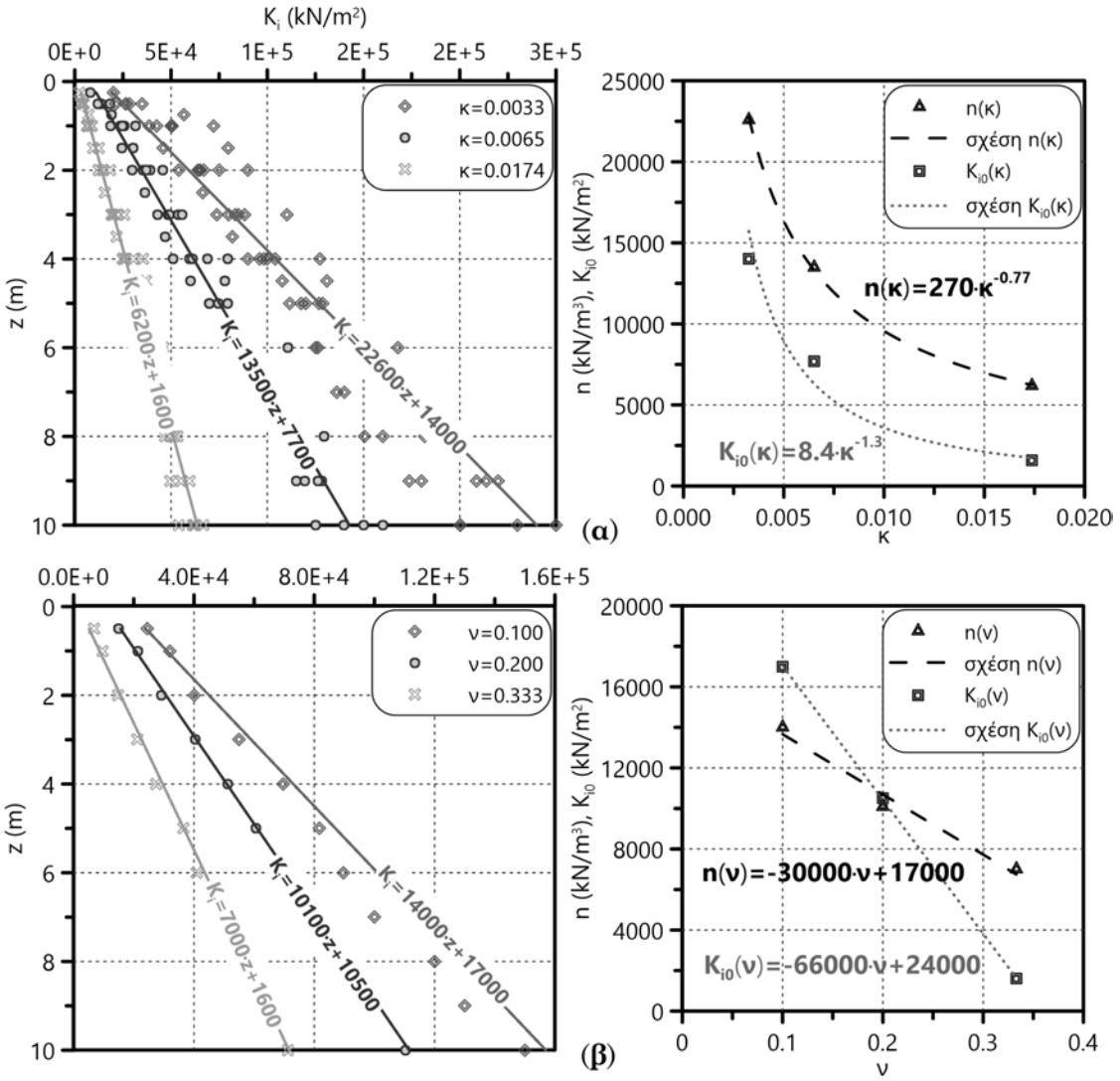

Σχήμα 32: Προσδιορισμός της κλίσης n και της αρχικής τιμής K_{i0} για τη γραμμική συνάρτηση της αρχικής δυσκαμψίας $K_i(z) = n \cdot z + K_{i0}$ των αριθμητικών καμπυλών p-y στιφρών, ΟC αργίλων. Επιρροή (α) της κλίσης κ των γραμμών αποφόρτισης-επαναφόρτισης και (β) του λόγου Poisson ν στα n και K_{i0}.

τους αντίστοιχους υπολογισμούς των αναλύσεων ΠΣ. Το σφάλμα για τα μέτρια ως στιφρά, ΟC αργιλικά εδάφη με $c_{u,\,avg}$=50-95kPa αναφέρεται σε περιπτώσεις χωρίς τασική χαλάρωση ($RF = 1$), ενώ για τα αντίστοιχα στιφρά εδάφη με $c_{u,\,avg}$=190-380kPa παρουσιάζονται οι περιπτώσεις με τασική χαλάρωση ($RF < 1$). Στο μεγάλο εύρος του N_p, το οποίο καλύπτει βάθη $z = 1 - 10D$, το σφάλμα των προτεινόμενων αναλυτικών εκφράσεων είναι εν γένει μικρότερο του 10%, άρα ικανοποιητικό. Συγκρίνοντας τις προαναφερθείσες βελτιωμένες καμπύλες p-y της διατριβής με τις αντίστοιχες της βιβλιογραφίας, φαίνεται πως η πλειοψηφία των υφιστάμενων μεθοδολογιών προτείνει συντηρητικές λύσεις για τα συγκεκριμένα

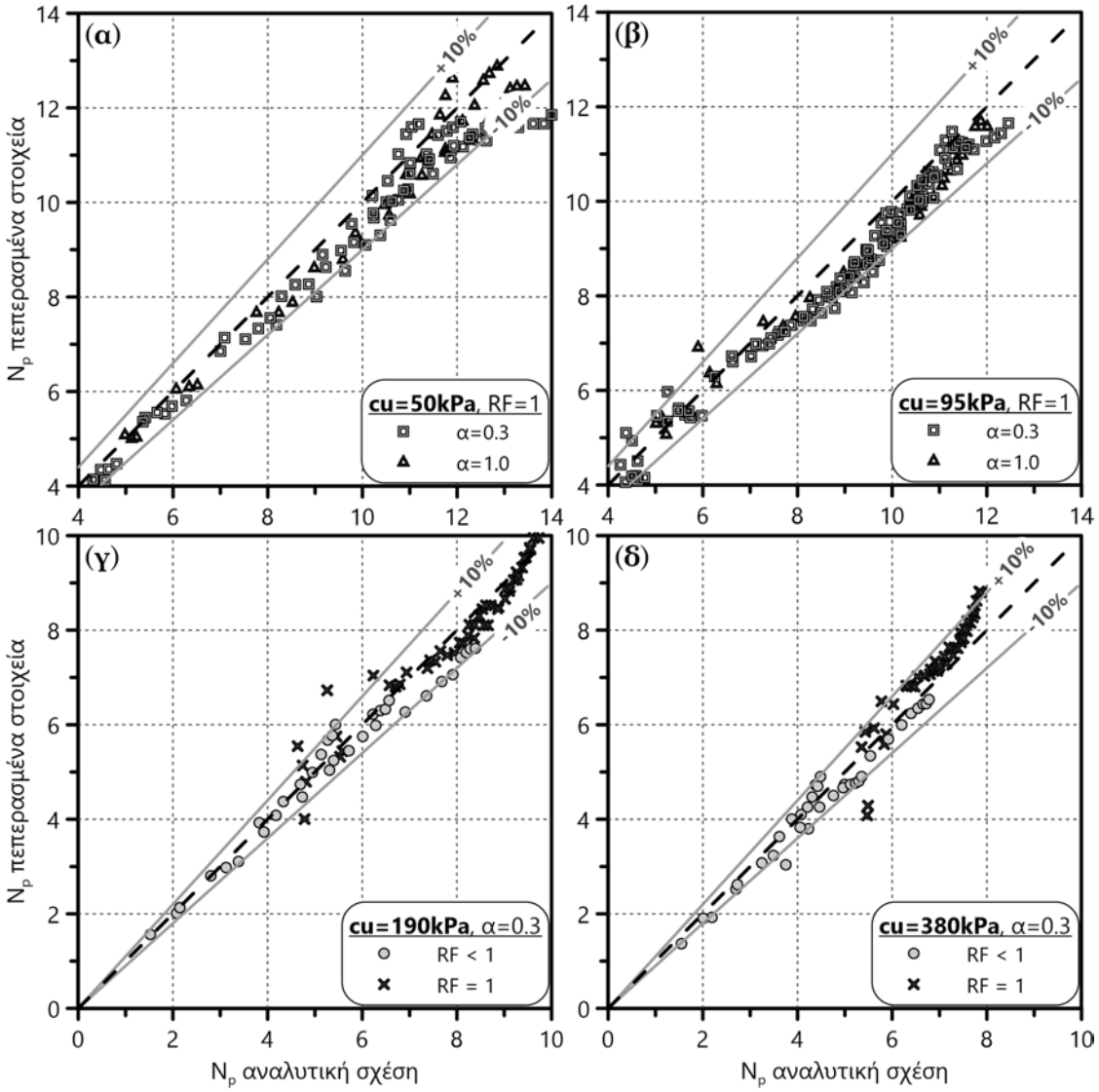

Σχήμα 33: Σύγκριση του N_p στιφρών, ΟC αργιλικών εδαφών από τις προτεινόμενες αναλυτικές σχέσεις με τους αντίστοιχους υπολογισμούς των αριθμητικών αναλύσεων. (α, β) $c_{u,avg}$=50, 95kPa και διάφορες τιμές των παραμέτρων κ, α και D. (γ, δ) $c_{u,avg}$=190, 380kPa, α=0.3, D=1m και διάφορες τιμές του $RF \leq 1$.

εδάφη (Σχήμα 34). Η σύγκριση αναφέρεται σε πάσσαλο διαμέτρου D=1m, μήκους L=30m, συντελεστή συνάφειας εδάφους-πασσάλου α=1.0 σε στιφρή, ΟC άργιλο με κορεσμένο ειδικό βάρος γ=20kN/m^3, $c_u = 100$kPa, κ=0.0054 (C_r=0.0125), ν=0.10 και στάθμη υδροφόρου ορίζοντα στην επιφάνεια του εδάφους. Σε ανάλογη διαπίστωση για τις βιβλιογραφικές καμπύλες p-y στιφρών αργιλικών εδαφών καταλήγει κανείς αν εξετάσει επιμέρους τις κατανομές των N_p και K_i με το αδιάστατο βάθος z/D (Σχήμα 35). Συνεπώς, οι προτεινόμενες από τη διατριβή καμπύλες p-y συντελούν στην επίτευξη ενός ρεαλιστικού, ασφαλούς και οικονομικού σχεδιασμού πασσάλων υπό εγκάρσια φόρτιση σε αυτά τα εδάφη.

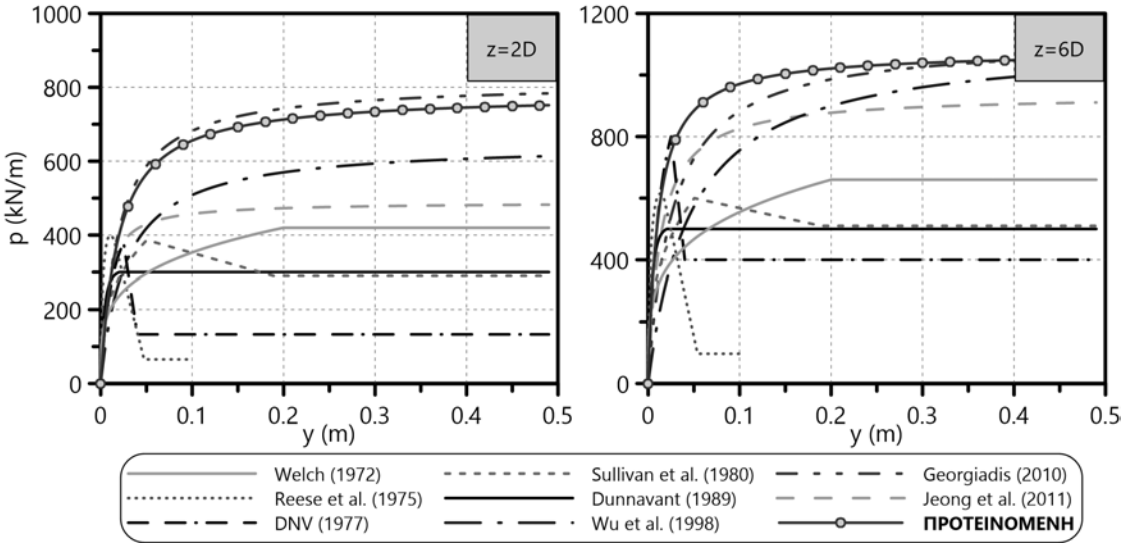

Σχήμα 34: Σύγκριση των προτεινόμενων μονοτονικών καμπυλών p-y με τις αντίστοιχες βιβλιογραφικές μεθοδολογίες για πάσσαλο διαμέτρου D=1m και συνάφειας α=0.3 σε πλήρως κορεσμένο, στιφρό, ΟC αργιλικό έδαφος, σε μικρό (z=2D) και μεγάλο βάθος (z=6D).

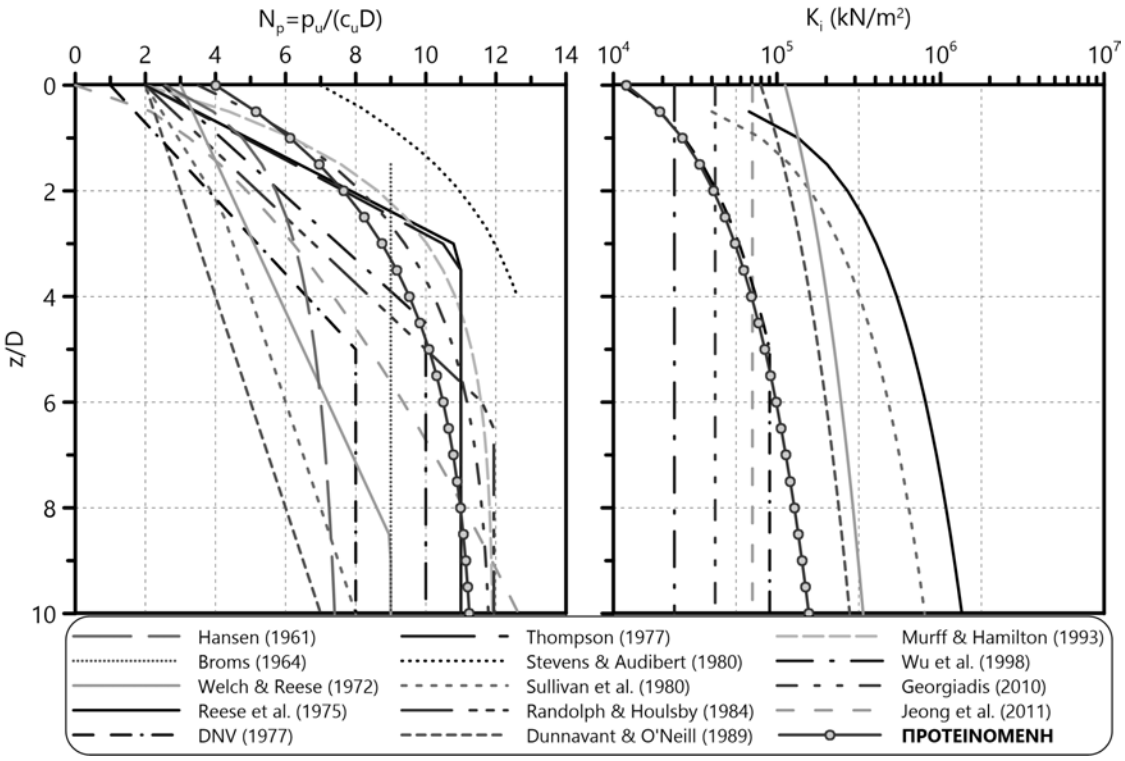

Σχήμα 35: Σύγκριση των προτεινόμενων κατανομών N_p-z/D και K_i-z/D με τις αντίστοιχες βιβλιογραφικές μεθοδολογίες για πάσσαλο διαμέτρου D=1m και συνάφειας α=0.3 σε πλήρως κορεσμένο, στιφρό, ΟC αργιλικό έδαφος.

5.3 Αξιολόγηση προτεινόμενων καμπυλών p-y με αποτελέσματα πειραματικών δοκιμών

Η τελευταία αυτή ερευνητική ενότητα (ΕΕ 4) της διδακτορικής διατριβής αξιολογεί τις προτεινόμενες καμπύλες p-y για μαλακά, NC και στιφρά, OC αργιλικά εδάφη μέσω αποτελεσμάτων από δοκιμαστικές εγκάρσιες φορτίσεις πασσάλων σε φυγοκεντριστή ή στο ελεύθερο πεδίο. Οι συγκρίσεις συμπεριλαμβάνουν διαγράμματα αδιάστατης μετατόπισης - οριζόντιου φορτίου ($y_h/D - H$) στην κεφαλή του πασσάλου, καθώς και κατανομές καμπτικών ροπών M$-z$, οριζόντιων μετατοπίσεων $y - z$ και καμπυλότητας κατά μήκος του εγκάρσια φορτιζόμενου πασσάλου. Για τη χάραξη των παραπάνω διαγραμμάτων εφαρμόζονται οι προτεινόμενες καμπύλες p-y σε κατάλληλα διαμορφωμένο διδιάστατο προσομοίωμα «δοκού επί μη-γραμμικού ελατηριωτού εδάφους Winkler» (BNWF), το οποίο λαμβάνει υπόψη τα χαρακτηριστικά εδάφους και πασσάλου όπως αναφέρονται στην εκάστοτε δοκιμή. Το Σχήμα 36 απεικονίζει ενδεικτικό τμήμα του

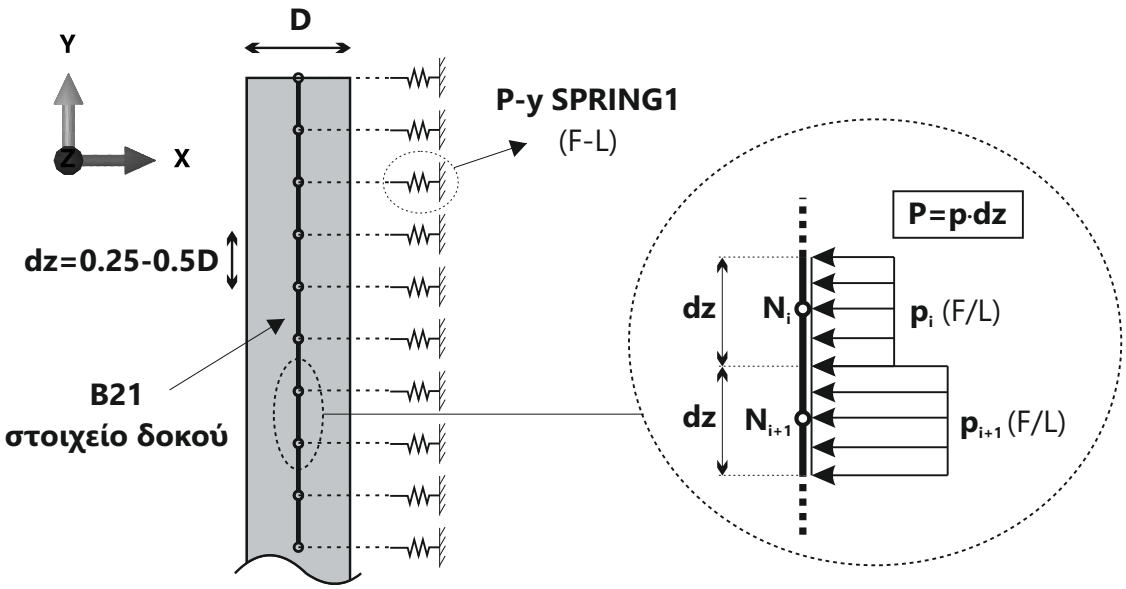

Σχήμα 36: Αριθμητική προσομοίωση του πασσάλου υπό εγκάρσια φόρτιση ως «δοκού επί μη-γραμμικού ελατηριωτού εδάφους Winkler» (BNWF) και ενσωμάτωση των καμπυλών p-y στις αναλύσεις ΠΣ.

διδιάστατου προσομοιώματος BNWF που διαμορφώθηκε στον κώδικα ΠΣ Simulia Abaqus, χρησιμοποιώντας στοιχεία δοκού B21 για τον πάσσαλο και ελατήρια SPRING1 για την εγκάρσια εδαφική απόκριση. Καθότι οι προτεινόμενες από τη διατριβή καμπύλες p-y εμπεριέχουν τις παραμέτρους συμπιεστότητας του εδάφους (λ, κ), η ακόλουθη αξιολόγηση τις προσδιορίζει από συσχετίσεις της βιβλιογραφίας[1]

[1] η πλειοψηφία τους ανακτήθηκε από τον Bowles (1988)

με φυσικά χαρακτηριστικά όπως τα όρια Atterberg (PL, LL), το ποσοστό φυσικής υγρασίας w_N, η πυκνότητα των εδαφικών κόκκων G_s και ο αρχικός δείκτης πόρων e_o - εννοείται σε περίπτωση που το πείραμα δεν αναφέρει τις παραπάνω παραμέτρους συμπιεστότητας. Ο λόγος Poisson του αργιλικού εδάφους ν λαμβάνεται ίσος με 0.10-0.30 αν δεν προσδιορίζεται από τα πειράματα.

Η προσομοίωση του πασσάλου λαμβάνει υπόψη τις ιδιότητες του υλικού του, δηλαδή το μέτρο ελαστικότητας E_p, τον λόγο Poisson ν_p, το όριο διαρροής f_y καθώς και διαγράμματα ροπής-καμπυλότητας - αν έχουν καταγραφεί κατά τη διάρκεια των πειραμάτων. Επιπλέον, στην κεφαλή του πασσάλου δεσμεύονται οι ίδιοι στροφικοί βαθμοί ελευθερίας με το κάθε πείραμα (πάσσαλοι ελεύθερα στρεπτής ή άστρεπτης κεφαλής). Έπειτα από την επιτυχή επαλήθευση[1] των αποτελεσμάτων του διδιάστατου αριθμητικού προσομοιώματος με τα αντίστοιχα των τριδιάστατων αναλύσεων ΠΣ - για ένα μαλακό, NC κι ένα στιφρό, OC αργιλικό έδαφος - ακολουθεί η αξιολόγηση της προτεινόμενης μεθοδολογίας με τα πραγματικά πειράματα.

Εκτός από την επαλήθευση των προτεινόμενων καμπυλών p-y, στη διατριβή γίνεται και η αξιολόγηση των προβλέψεών τους συγκριτικά με τις αντίστοιχες προβλέψεις που προκύπτουν με χρήση τυπικών καμπυλών p-y της διεθνούς βιβλιογραφίας. Για τον λόγο αυτό επιλέχθηκαν υφιστάμενες μεθοδολογίες που προβλέπουν καμπύλες p-y στα άνω και κάτω όρια του συνόλου των καμπυλών και εφαρμόσθηκαν στο διδιάστατο προσομοίωμα που προαναφέρθηκε. Με τον τρόπο αυτό γίνεται σύγκριση των εντατικών (M, Q) και παραμορφωσιακών μεγεθών (οριζόντιες μετακινήσεις και στροφές) κατά μήκος του πασσάλου, με τα αντίστοιχα που προέκυψαν με χρήση των καμπυλών p-y που προτείνονται από την παρούσα διατριβή.

5.3.1 Πειράματα σε μαλακά, NC αργιλικά εδάφη

Για την αξιολόγηση των καμπυλών p-y μαλακών, NC αργιλικών σχηματισμών προσομοιώθηκαν δύο πειράματα εγκάρσιας φόρτισης μεταλλικών πασσάλων φυσικών διαμέτρων D=0.8-2.5m σε φυγοκεντριστή. Το εδαφικό προφίλ των NC υλικών προσομοιώθηκε από πολτό καολίνη που τοποθετήθηκε σε στρώσεις εντός των δοχείων διεξαγωγής των πειραμάτων.

Πειράματα φυγοκεντριστή των Ilyas et al. (2004)

Οι Ilyas et al. (2004) πραγματοποίησαν πειράματα φυγοκεντριστή για την εγκάρσια απόκριση μεμονωμένου μεταλλικού πασσάλου σε μαλακή, NC άργιλο υπό επιτάχυνση 70g, στο Εθνικό Πανεπιστήμιο της Σιγκαπούρης (NUS). Αποθέτοντας

[1] δεν παρουσιάζονται για λόγους συντομίας

πολτό καολίνη (αναμεμειγμένο στο 150% του LL) σε στρώσεις, προέκυψε το NC αργιλικό προφίλ με τις ακόλουθες ιδιότητες: ειδικό βάρος $\gamma = 16kN/m^3$, φυσική υγρασία $w_N = 66\%$, όριο πλαστιμότητας $PL = 35.1\%$, όριο υδαρότητας $LL = 79.8\%$, κλίση της γραμμής παρθενικής συμπίεσης $C_c = 0.55$, κλίση της γραμμής αποφόρτισης-επαναφόρτισης $C_r = 0.16$ και διαπερατότητα $k = 2 \cdot 10^{-8} m/s$. Οι δοκιμές πενετρομέτρου τύπου T-bar (Stewart & Randolph, 1991) που πραγματοποιήθηκαν κατά τη διάρκεια της επιτάχυνσης του μοντέλου, μέτρησαν γραμμικά αυξανόμενη c_u με το βάθος από 0 στην επιφάνεια του εδάφους μέχρι 20kPa σε z=15m (κλίμακα πεδίου), αιτιολογώντας έτσι τον χαρακτηρισμό της αργίλου ως μαλακής.

Το μοντέλο πασσάλου ήταν σωλήνας αλουμινίου κοίλης τετραγωνικής διατομής, με δέκα (10) ζεύγη μετρητών παραμορφώσεων κατά μήκος του - για τη μέτρηση της καμπτικής ροπής. Στα 70g ο πάσσαλος έχει εύρος διατομής B=0.84m, μήκος εντός της αργίλου L_b=14.7m, καμπτική δυσκαμψία $E_pI_p = 922MNm^2$, τάση διαρροής f_y=110MPa ενώ το εγκάρσιο φορτίο ασκείται επί του πασσάλου στα 3.5m πάνω από την επιφάνεια του εδάφους - συνολικό μήκος πασσάλου L=18.2m.

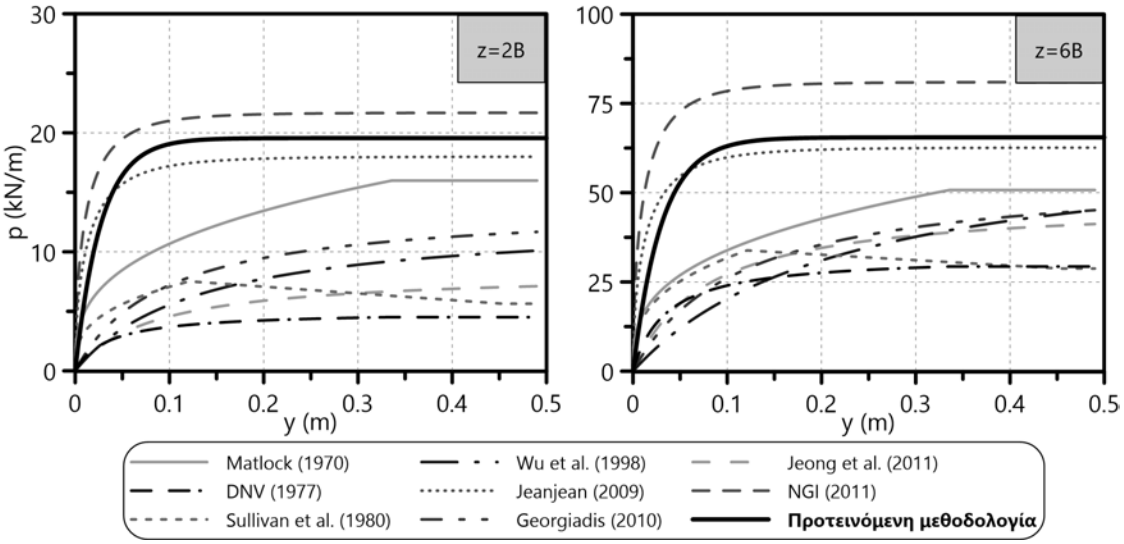

Σχήμα 37: Καμπύλες p-y σε βάθη z=2, 6B (B=0.84m) για το NC εδαφικό προφίλ των πειραμάτων φυγοκεντριστή από τους Ilyas et al. (2004).

Το Σχήμα 37 παρουσιάζει σε δύο διαφορετικά βάθη (z=2, 6B) τις καμπύλες p-y που εφαρμόζονται σε μαλακές, NC αργίλους. Από αυτές επιλέγονται οι καμπύλες των Nichols et al. (2014), της παρούσας διατριβής ($\lambda = C_c/\ln 10 = 0.24$, $\lambda/\kappa = 3.9$, $\nu = 0.3$, $\alpha = 0.3$ για πάσσαλο από αλουμίνιο) - και οι δύο κοντά στο άνω όριο του εύρους. Επίσης υιοθετήθηκαν οι καμπύλες p-y του Matlock (1970) (ε_{50} κατά Peck et al. (1974)) - τις οποίες προτείνει και το API (2007) - που βρίσκονται

περί το μέσο του εύρους των μεθοδολογιών. Εφόσον η βιβλιογραφία θεωρεί ότι οι τελευταίες καμπύλες οδηγούν σε μάλλον συντηρητικό σχεδιασμό, θεωρήσαμε την εν λόγω μεθοδολογία (Matlock, 1970) ως το κάτω όριο της συγκεκριμένης αξιολόγησης.

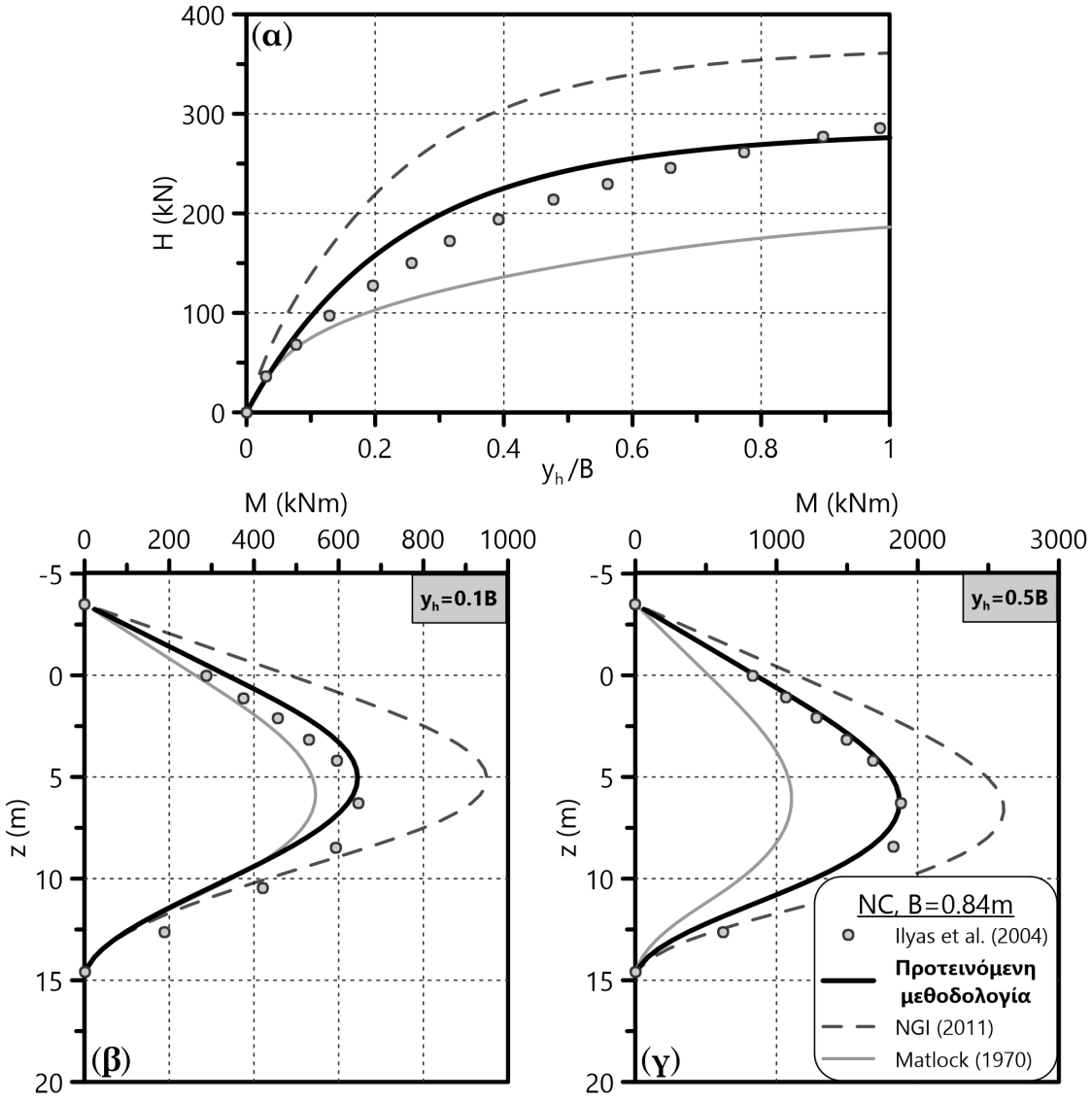

Σχήμα 38: Σύγκριση (α) διαγραμμάτων αδιάστατης οριζόντιας μετατόπισης - φορτίου κεφαλής $y_h/B - H$ και (β, γ) κατανομής της καμπτικής ροπής κατά μήκος του πασσάλου M$-z$ για δύο επίπεδα y_h=0.1, 0.5B (B=0.84m), όπως αυτά προέκυψαν από τη χρήση καμπυλών p-y στο προσομοίωμα BNWF, με τις αντίστοιχες πειραματικές μετρήσεις.

Τα διαγράμματα $y_h/B - H$ και M$-z$ (Σχήμα 38) που προκύπτουν για το προσομοίωμα BNWF χρησιμοποιώντας τις προτεινόμενες καμπύλες p-y προσεγγίζουν με μεγάλη ακρίβεια τα αντίστοιχα των πειραματικών μετρήσεων - τόσο ως προς το οριακό εγκάρσιο φορτίο κεφαλής H_u όσο και ως προς τη μέγιστη καμπτική ροπή κατά μήκος του πασσάλου M_{max} (για οριζόντια μετατόπιση

κεφαλής y_h=$0.1B$ και $0.5B$). Οι άλλες δύο μεθοδολογίες εμφανίζουν απόκλιση έως και 50% από τα πειραματικά αποτελέσματα - και οι δύο βρίσκονται άνω του μέσου όρου των καμπυλών. Σημειώνεται εδώ ότι οι αναλύσεις BNWF υποδεικνύουν αστοχία του εδάφους καθότι δεν εμφανίζεται πλαστική άρθρωση στον πάσσαλο (αστοχία κοντού πασσάλου).

Πειράματα φυγοκεντριστή των Doyle et al. (2004)

Οι Doyle et al. (2004) πραγματοποίησαν πειράματα φυγοκεντριστή για την εγκάρσια απόκριση μεμονωμένου μεταλλικού πασσάλου σε μαλακή, NC άργιλο υπό επιτάχυνση 100g, στο Πανεπιστήμιο του Cambridge. Αποθέτοντας πολτό καολίνη (αναμεμειγμένο στο 200% του LL), προέκυψε το ανώτερο NC αργιλικό προφίλ με τις ακόλουθες ιδιότητες: ειδικό βάρος $\gamma = 16.6kN/m^3$, πυκνότητα στερεών κόκκων $G_s = 2.61 - 2.64\,Mg/m^3$, φυσική υγρασία $w_N = 55\%$, όριο πλαστιμότητας $PL = 38\%$, όριο υδαρότητας $LL = 69\%$, αρχικό δείκτη πόρων e_o=$w_N \cdot G_s$=$0.55 \cdot 2.62$=1.441, κλίση της γραμμής παρθενικής συμπίεσης $C_c = 0.6$ και κλίση της γραμμής αποφόρτισης-επαναφόρτισης $C_r = 0.05$ (τα C_c, C_r κατά προσέγγιση μέσω συσχετίσεων με φυσικά χαρακτηριστικά). Οι δοκιμές πτερυγίου που πραγματοποιήθηκαν κατά τη διάρκεια της επιτάχυνσης του μοντέλου, μέτρησαν κατανομή $c_u = 2.17 \exp 0.1122z$ για το πάχος του μαλακού NC εδάφους - ελαφρώς υποστερεοποιημένο - μέχρι βάθος z=27m (κλίμακα πεδίου). Σε μεγαλύτερο βάθος θεωρήθηκε σταθερό c_u=80kPa.

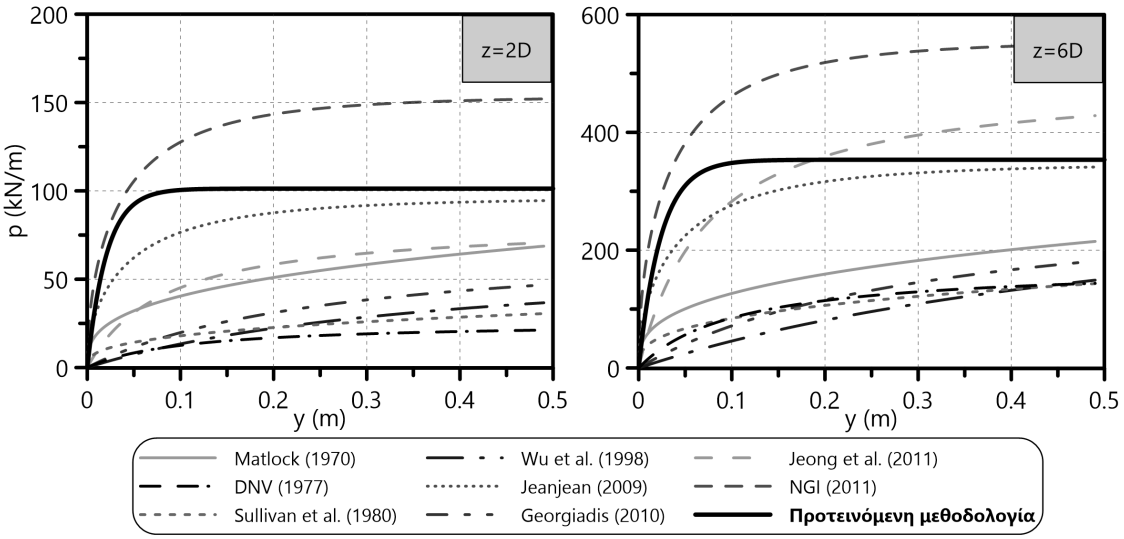

Σχήμα 39: Καμπύλες p-y σε βάθη z=2, $6D$ (D=2.54m) για το NC εδαφικό προφίλ των πειραμάτων φυγοκεντριστή από τους Doyle et al. (2004).

Το μοντέλο πασσάλου ήταν σωλήνας αλουμινίου κοίλης κυκλικής διατομής, σε τρία διαφορετικά τμήματα, με δεκαπέντε (15) ζεύγη μετρητών παραμορφώσεων

κατά μήκος του. Στα 100g ο πάσσαλος έχει διάμετρο D=2.54m, μήκος εντός της αργίλου L_b=51.5m, καμπτική δυσκαμψία $E_pI_{p,1} = 60263MNm^2$, ροπές διαρροής και αστοχίας $M_{y,1} = 156MNm$ και $M_{u,1} = 395MNm$ αντίστοιχα για το ανώτερο τμήμα, $E_pI_{p,2} = 46776MNm^2$, $M_{y,2} = 121MNm$ και $M_{u,2} = 303MNm$ για το κατώτερο τμήμα ενώ το εγκάρσιο φορτίο ασκείται επί του πασσάλου στα 7.5m πάνω από την επιφάνεια του εδάφους - συνολικό μήκος πασσάλου L=59m.

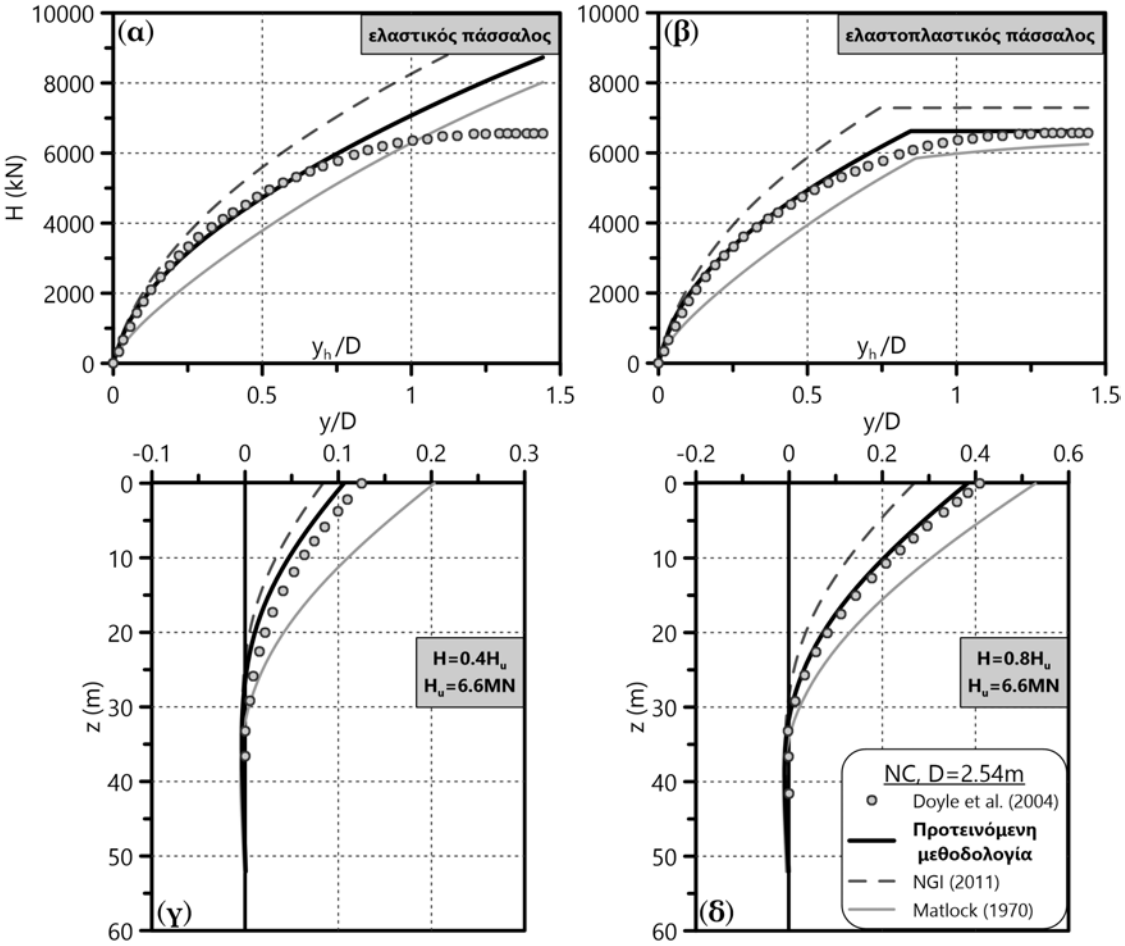

Σχήμα 40: Σύγκριση (α, β) διαγραμμάτων αδιάστατης οριζόντιας μετατόπισης - φορτίου κεφαλής $y_h/D - H$ για ελαστικό και ελαστοπλαστικό πάσσαλο και (γ, δ) οριζόντιας μετατόπισης κατά μήκος του πασσάλου $y - z$ για δύο επίπεδα H=0.4, 0.8H_u ($H_u \approx$6.6MN), όπως αυτά προέκυψαν από τη χρήση καμπυλών p-y στο προσομοίωμα BNWF, με τις αντίστοιχες πειραματικές μετρήσεις.

Το Σχήμα 39 παρουσιάζει σε δύο διαφορετικά βάθη (z=2, 6D) τις καμπύλες p-y που εφαρμόζονται σε μαλακές, NC αργίλους. Από αυτές επιλέγονται οι καμπύλες των Nichols et al. (2014), της παρούσας διατριβής ($\lambda = C_c/\ln 10 = 0.26$, $\lambda/\kappa = 12$, $\nu = 0.3$, $\alpha = 0.3$ για πάσσαλο από αλουμίνιο) - και οι δύο κοντά στο άνω όριο του εύρους. Επίσης υιοθετήθηκαν οι καμπύλες p-y του Matlock (1970) (ε_{50} κατά Peck

et al. (1974)) - τις οποίες προτείνει και το API (2007) - που βρίσκονται περί το κάτω όριο των μεθοδολογιών.

Τα διαγράμματα $y_h/D - H$ και $y - z$ (Σχήμα 40) που προκύπτουν για το προσομοίωμα BNWF χρησιμοποιώντας τις προτεινόμενες καμπύλες p-y προσεγγίζουν πολύ ικανοποιητικά τα αντίστοιχα τις πειραματικές μετρήσεις - τόσο ως προς το οριακό εγκάρσιο φορτίο κεφαλής H_u όσο και ως προς την οριζόντια μετατόπιση κατά μήκος του πασσάλου (για εγκάρσιο φορτίο κεφαλής $H = 40, 80\%H_u$ - H_u=6565kN). Οι άλλες δύο μεθοδολογίες εμφανίζουν απόκλιση από τα πειραματικά αποτελέσματα, μεγαλύτερη από αυτή των προτεινόμενων από τη διατριβή καμπυλών.

5.3.2 Πειράματα σε στιφρά, OC αργιλικά εδάφη

Για την αξιολόγηση των καμπυλών p-y στιφρών, OC αργιλικών υλικών προσομοιώθηκαν δύο πειράματα εγκάρσιας φόρτισης πασσάλων μεταλλικών και οπλισμένου σκυροδέματος, διαμέτρων D=0.3-2.0m σε πραγματικά εδαφικά προφίλ με τιμές αστράγγιστης διατμητικής αντοχής c_u=40-200kPa.

Πειράματα ελεύθερου πεδίου των Rollins et al. (1998)

Οι Rollins et al. (1998) πραγματοποίησαν δοκιμή εγκάρσιας φόρτισης μεμονωμένου, σύμμικτου, εμπηγνυόμενου πασσάλου σε μέτριας στιφρότητας, OC άργιλο με τα ακόλουθα χαρακτηριστικά[1]: ειδικό βάρος $\gamma = 15kN/m^3$, πυκνότητα στερεών κόκκων $G_s = 2.7\,Mg/m^3$, φυσική υγρασία $w_N = 30\%$, όριο πλαστιμότητας $PL = 18\%$, όριο υδαρότητας $LL = 37\%$, αρχικό δείκτη πόρων e_o=$w_N \cdot G_s$=0.30 $\cdot$ 2.7=0.81 και κλίση της γραμμής αποφόρτισης-επαναφόρτισης C_r=0.018-0.046 (κατά προσέγγιση μέσω συσχετίσεων με φυσικά χαρακτηριστικά). Το έδαφος ήταν υπερστερεοποιημένο μέχρι βάθος z=10m με αστράγγιστη διατμητική αντοχή c_u=25-100kPa. Στους παραπάνω αργιλικούς σχηματισμούς παρεμβάλλονται δύο αμμώδη στρώματα με $\phi = 36 - 38°$ και $D_r = 65 - 80\%$. Η στάθμη του υδροφόρου ορίζοντα βρέθηκε στην επιφάνεια του πρώτου αργιλικού στρώματος - έπειτα από εκσκαφή των επιφανειακών αποθέσεων πάχους 1.6m.

Ο εμπηγνυόμενος πάσσαλος ελεύθερα στρεπτής κεφαλής της δοκιμής ήταν χαλύβδινος σωλήνας διαμέτρου D=0.324m ($E_{p,s}$=200GPa, $f_{y,s}$=331MPa), πληρωμένος με σκυρόδεμα ($E_{p,c}$=17.5GPa, $f_{y,c}$=20.7MPa) πριν τη φόρτιση. Το μήκος έμπηξής του ήταν L_b=7.9m ενώ το εγκάρσιο φορτίο εφαρμόστηκε στα 0.4m πάνω από την επιφάνεια του εδάφους (μετά την αφαίρεση του επιφανειακού στρώματος αποθέσεων). Κατά την προσομοίωση του πασσάλου ως δοκού λήφθηκαν

[1] μέσες τιμές από τη γεωτεχνική αξιολόγηση

υπόψη μόνο οι ιδιότητες του χάλυβα, θεωρώντας ότι το σκυρόδεμα πλήρωσης δεν επηρεάζει σημαντικά τη δυσκαμψία - με ιδιότητες μία τάξη μεγέθους μικρότερες από τις αντίστοιχες του χάλυβα. Επιπλέον, καθότι η εγκάρσια μετατόπιση κεφαλής του πασσάλου $y_h < 0.2D$, δε φαίνεται να διαρρέει ο χάλυβας - σύμφωνα με τις παρατηρήσεις του πειράματος. Το Σχήμα 41 παρουσιάζει σε δύο διαφορετικά βάθη

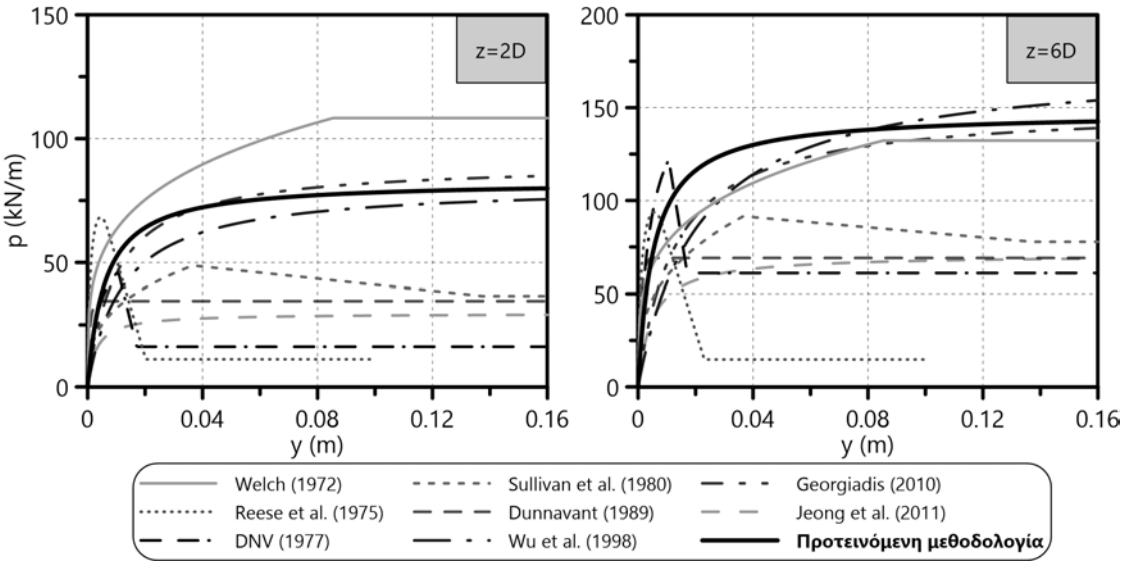

Σχήμα 41: Καμπύλες p-y σε βάθη z=2, 6D (D=0.324m) για το OC εδαφικό προφίλ των πειραμάτων πεδίου από τους Rollins et al. (1998).

(z=2, 6D) τις καμπύλες p-y που εφαρμόζονται σε μέτριες ως στιφρές, OC αργίλους. Από αυτές επιλέγονται οι καμπύλες των Georgiadis & Georgiadis (2010), της παρούσας διατριβής ($\kappa = C_r/\ln 10 = 0.008 - 0.02$, $\nu = 0.10$, $\alpha = 0.3$ για μεταλλικό πάσσαλο) - και οι δύο κοντά στο άνω όριο του εύρους. Επίσης υιοθετήθηκαν οι καμπύλες p-y των Reese et al. (1975) (ε_{50} κατά Reese et al. (1975)), των οποίων η παραμένουσα p_u σηματοδοτεί το κάτω όριο των μεθοδολογιών. Η απόκριση των ενδιάμεσων στρωμάτων άμμου, χρησιμοποιώντας είτε τις καμπύλες p-y κατά API (2011) για άμμους είτε τις παραπάνω καμπύλες για άργιλο - με c_u=50kPa (συντηρητικά) για τα εν λόγω στρώματα - δεν επηρεάζει ουσιαστικά τη συνολική εγκάρσια απόκριση του πασσάλου. Τα Σχήματα 42 αποδεικνύουν ότι η προτεινόμενη μεθοδολογία προβλέπει διαγράμματα $y_h/D - H$ και M$-z$ πολύ κοντά στις πειραματικές μετρήσεις. Επιπλέον, οι καμπύλες p-y της διατριβής για OC αργιλικά εδάφη υπολογίζουν με ακρίβεια τη μέγιστη καμπτική ροπή κατά μήκος του πασσάλου, ειδικά για εγκάρσιο φορτίο κεφαλής του πασσάλου H=53.4kN. Στο συγκεκριμένο επίπεδο φόρτισης, οι δύο άλλες μεθοδολογίες της βιβλιογραφίας προβλέπουν μέσω του BNWF προσομοιώματος M_{max} με απόκλιση 20-40% από τα πειραματικά αποτελέσματα.

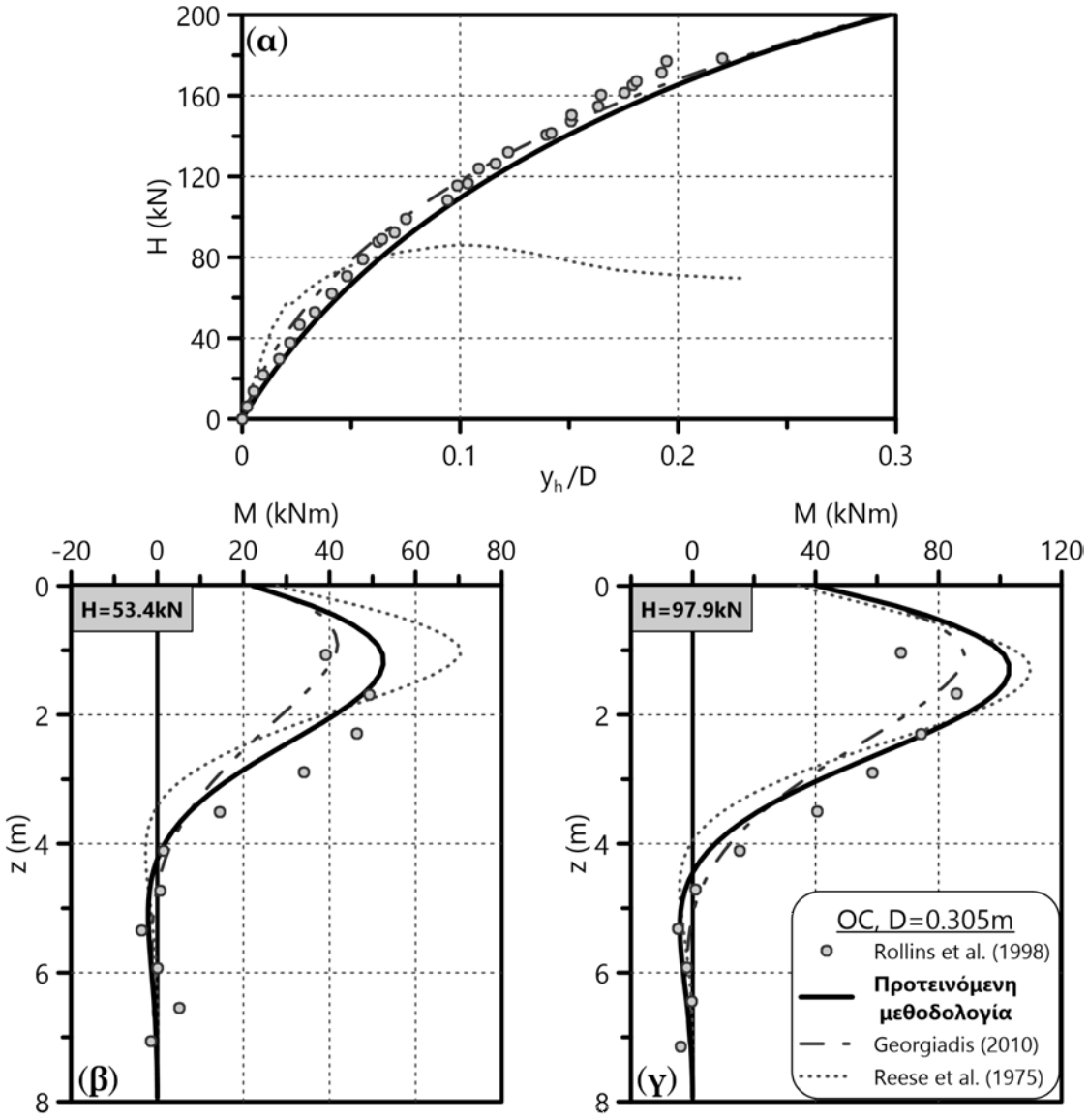

Σχήμα 42: Σύγκριση (α) διαγραμμάτων αδιάστατης οριζόντιας μετατόπισης - φορτίου κεφαλής $y_h/D - H$ και (β, γ) κατανομής της καμπτικής ροπής κατά μήκος του πασσάλου $M-z$ για δύο επίπεδα H=53.4, 97.9kN, όπως αυτά προέκυψαν από τη χρήση καμπυλών p-y στο προσομοίωμα BNWF, με τις αντίστοιχες πειραματικές μετρήσεις.

Πειράματα ελεύθερου πεδίου από το UCLA (1998-2006)

Μία ερευνητική ομάδα της σχολής πολιτικών μηχανικών του πανεπιστημίου UCLA (Janoyan et al., 2006; Lemnitzer et al., 2010; Stewart et al., 2007) στην Καλιφόρνια πραγματοποίησε τέσσερα (4) πειράματα ανακυκλικής εγκάρσιας φόρτισης σε στοιχεία βαθιάς θεμελίωσης βάθρων γεφυρών (μία ομάδα πασσάλων και τρεις μεμονωμένοι πάσσαλοι), με σκοπό τη μελέτη της εγκάρσιας απόκρισής τους σε στιφρά, OC αργιλικά εδάφη. Στα πλαίσια της παρούσας διατριβής, αξιολογήθηκαν οι προτεινόμενες καμπύλες p-y για τέτοια εδάφη ως προς τα

αποτελέσματα δοκιμαστικών φορτίσεων των μεμονωμένων πασσάλων.

Η αστράγγιστη διατμητική αντοχή του εδάφους στο πεδίο των δοκιμών θεωρήθηκε συντηρητικά c_u ≈200kPa (σταθερή με το βάθος), ενώ εκτιμήθηκε και $OCR \approx 2-6$. Οι αστράγγιστες τριαξονικές δοκιμές εργαστηρίου (UU) εμφάνισαν αστοχία των δοκιμίων υπό αξονική παραμόρφωση $\varepsilon_a = 0.6-1\%$. Επιπλέον, προσδιορίστηκαν τα ακόλουθα φυσικά χαρακτηριστικά του εδάφους: ειδικό βάρος $\gamma = 19kN/m^3$, πυκνότητα στερεών κόκκων $G_s = 2.7\,Mg/m^3$, βαθμός κορεσμού $S_r = 86-100\%$, φυσική υγρασία $w_N = 25\%$, όριο πλαστιμότητας $PL = 20\%$, όριο υδαρότητας $LL = 35\%$, αρχικό δείκτη πόρων e_o=$w_N \cdot G_s$=0.25 · 2.7=0.68 και κλίση της γραμμής αποφόρτισης-επαναφόρτισης C_r=0.015-0.044 (κατά προσέγγιση μέσω συσχετίσεων με φυσικά χαρακτηριστικά). Εντούτοις, αριθμητικές τριαξονικές δοκιμές με χρήση του συγκεκριμένου εύρους για το C_r οδήγησαν σε αρκετά αυξημένες τιμές της αξονικής παραμόρφωσης αστοχίας (ε_a), σε σχέση με τα εργαστηριακά αποτελέσματα. Για τον λόγο αυτό χρησιμοποιείται διορθωμένο C_r=0.004 στην παρακάτω αξιολόγηση, το οποίο εξασφαλίζει συμβατότητα της συμπεριφοράς τάσεων-παραμορφώσεων του εδάφους με τις εργαστηριακές μετρήσεις. Σημειώνεται ότι παρά τον (σχεδόν) πλήρη κορεσμό των ανώτερων εδαφικών στρωμάτων, ο υπόγειος υδροφόρος ορίζοντας εμφανίστηκε στα -14.6m από την επιφάνεια - κάτω από τις αιχμές όλων των πασσάλων που μελετήθηκαν.

Οι τρεις μεμονωμένοι πάσσαλοι των δοκιμαστικών φορτίσεων ήταν έγχυτοι[1] από οπλισμένο σκυρόδεμα, δύο διαφορετικών διαμέτρων D=0.61, 2.0m και με διαφορετικές συνοριακές συνθήκες κεφαλής ανά περίπτωση. Για λόγους συντομίας, παρουσιάζονται εδώ τα αποτελέσματα των συγκρίσεων ως προς τους δύο από τους τρεις πασσάλους:

- πάσσαλος άστρεπτης κεφαλής, διαμέτρου D=0.61m και μήκους L_b=7.62m εντός του εδάφους, με οριζόντια μετατόπιση κεφαλής $y_h \approx 0.16D$ να επιβάλλεται ακριβώς επί της επιφάνειας του εδάφους

- πάσσαλος ελεύθερα στρεπτής κεφαλής διαμέτρου D=2.0m εντός και D=1.8m εκτός του εδάφους, μήκους L_b=14.62m εντός του εδάφους, με οριζόντια μετατόπιση κεφαλής $y_h \approx 1.6D$ στα 12.2m από την επιφάνεια του εδάφους - ήτοι συνολικό μήκος L=26.82m.

Τα διαγράμματα ροπής-καμπυλότητας των δύο διαφορετικών διατομών φαίνονται στο Σχήμα 43. Το εξωτερικό ανακυκλικό φορτίο επιβάλλεται σταδιακά και ψευδοστατικά, με το κάθε επίπεδο οριζόντιας μετατόπισης να εφαρμόζεται προς τις

[1] κατά τη διάρκεια της κατασκευής των πασσάλων δεν παρατηρήθηκε εισροή νερού στις οπές ή διεύρυνση κυλινδρικής κοιλότητας

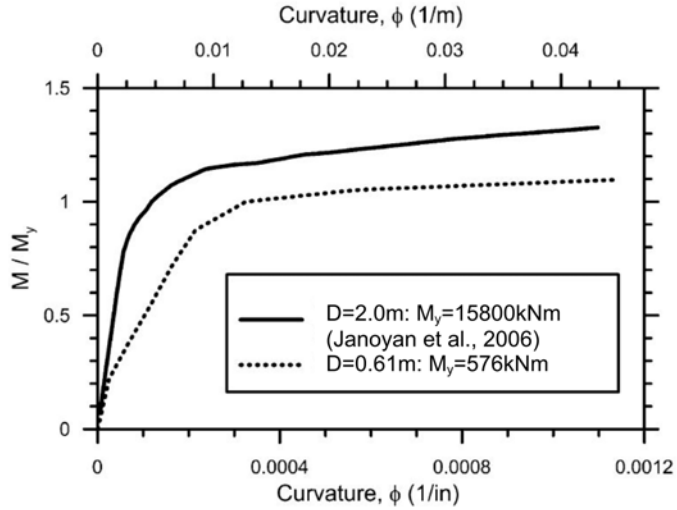

Σχήμα 43: Διαγράμματα κανονικοποιημένης ροπής - καμπυλότητας που υιοθετήθηκαν στα προσομοιώματα BNWF για τους πασσάλους οπλισμένου σκυροδέματος διαμέτρων D=0.61, 2.0m, σύμφωνα με τις πειραματικές μετρήσεις των Janoyan et al. (2006) και Stewart et al. (2007).

δύο κατευθύνσεις για τρεις (3) κύκλους. Ο συγκεκριμένος αριθμός κύκλων ήταν τόσο μικρός που πρακτικά η απόκριση των πασσάλων θεωρήθηκε στατική, ακόμα και από τους ίδιους του συγγραφείς. Για τον λόγο αυτό, η επιβολή της οριζόντιας μετατόπισης κεφαλής έγινε μονοτονικά κατά τις αριθμητικές αναλύσεις (BNWF). Το

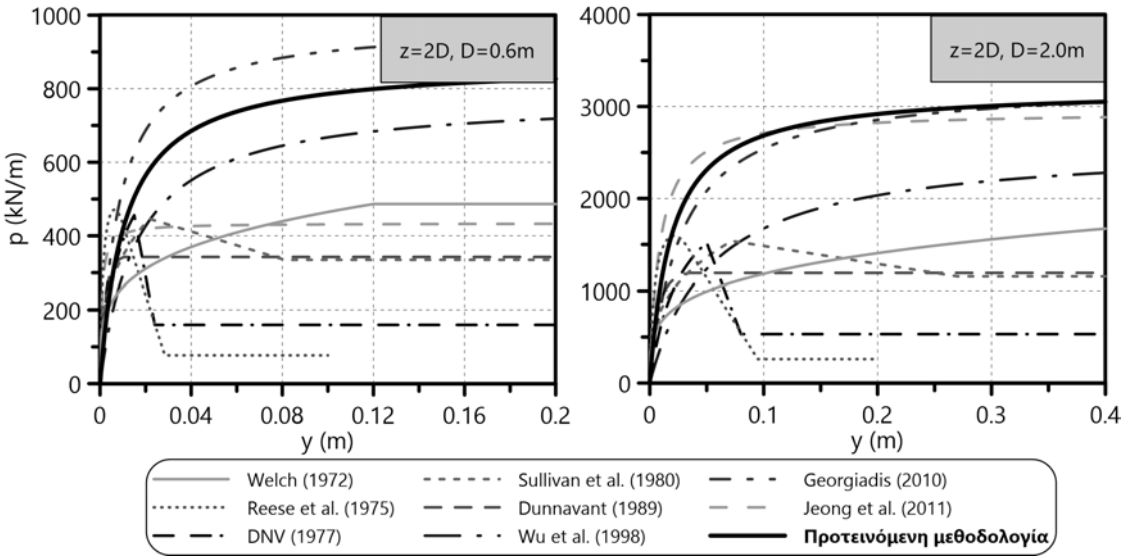

Σχήμα 44: Καμπύλες p-y σε βάθος z=2D (D=0.6, 2.0m) για το OC εδαφικό προφίλ των πειραμάτων πεδίου από τους Janoyan et al. (2006) και Stewart et al. (2007).

Σχήμα 44 παρουσιάζει σε αντιπροσωπευτικό βάθος z=2D τις καμπύλες p-y που

εφαρμόζονται σε στιφρές, ΟC αργίλους. Από αυτές επιλέγονται οι καμπύλες των Georgiadis & Georgiadis (2010) και Dunnavant & O'Neill (1989) για τον πάσσαλο με D=0.61m, των Jeong et al. (2011) (K_c=800 για μέσο OCR=4 και PI=15) και DNV (1977) για τον πάσσαλο με D=2.0m καθώς και της παρούσας διατριβής ($\kappa = C_r/\ln 10 = 0.0017$, $\nu = 0.15$, $\alpha = 1.0$ για έγχυτο πάσσαλο). Το σκεπτικό των παραπάνω επιλογών σχετίζεται με την κάλυψη του πλήρους εύρους καμπυλών p-y που προτείνονται για τον συγκεκριμένο αργιλικό σχηματισμό. Η επίλυση του

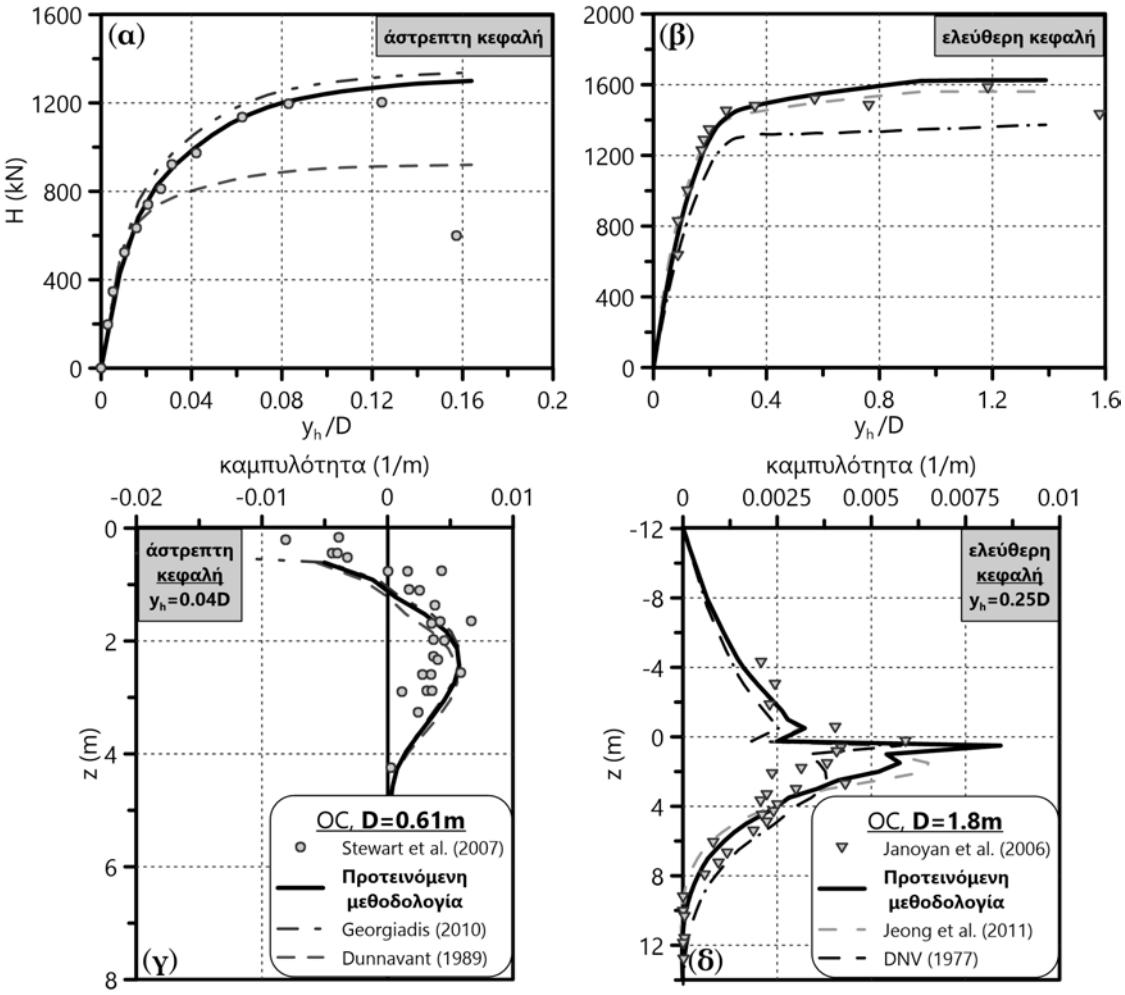

Σχήμα 45: Σύγκριση (α, β) διαγραμμάτων αδιάστατης οριζόντιας μετατόπισης - φορτίου κεφαλής $y_h/D - H$ για πάσσαλο άστρεπτης και ελεύθερα στρεπτής κεφαλής και (γ, δ) καμπυλότητας κατά μήκος του πασσάλου για διαφορετικά επίπεδα y_H, όπως αυτά προέκυψαν από τη χρήση καμπυλών p-y στα προσομοιώματα BNWF, με τις αντίστοιχες πειραματικές μετρήσεις.

προσομοιώματος BNWF με τις παραπάνω καμπύλες p-y έδωσε τα αποτελέσματα του Σχήματος 45 για τους δύο πασσάλους που προαναφέρθηκαν. Για τον μικρό πάσσαλο (D=0.61m), οι καμπύλες p-y της παρούσας διατριβής μαζί με αυτές των

Georgiadis & Georgiadis (2010) προβλέπουν διάγραμμα $y_h/D - H$[1] σχεδόν όμοιο με τα πειραματικά αποτελέσματα. Ομοίως και για τον μεγάλο πάσσαλο (D=2.0m), τα αποτελέσματα της προτεινόμενης μεθοδολογίας συμφωνούν με τις πειραματικές μετρήσεις καθώς και με τις προβλέψεις των καμπυλών p-y κατά Jeong et al. (2011) - στο άνω όριο του εύρους της βιβλιογραφίας. Αντιθέτως, οι καμπύλες p-y κατά Dunnavant & O'Neill (1989) και DNV (1977) φαίνεται να υποεκτιμούν κατά τουλάχιστον 20% το οριακό εγκάρσιο φορτίο κεφαλής H_u και των δύο πασσάλων. Αναφορικά με τα διαγράμματα καμπυλότητας κατά μήκος των πασσάλων, το Σχήμα 45 παρουσιάζει μικρές διαφοροποιήσεις μεταξύ των διάφορων μεθόδων, αλλά συμφωνία όλων με τα αποτελέσματα των δοκιμαστικών φορτίσεων - ενδεχομένως επειδή οι πάσσαλοι έχουν διαρρεύσει για την εκάστοτε επιβαλλόμενη οριζόντια μετατόπιση κεφαλής y_h.

6 Παρατηρήσεις-Προτάσεις

Τα κυριότερα συμπεράσματα της διατριβής μπορούν να συνοψιστούν ως εξής:

- Συγκριτική αξιολόγηση των βιβλιογραφικών μεθοδολογιών μέχρι βάθους $10D$ αποκαλύπτει πολύ μεγάλες αποκλίσεις των υφιστάμενων καμπυλών p-y για αργιλικά εδάφη. Ενδεικτικά αναφέρεται ότι παρατηρούνται διαφορές μέχρι και δύο τάξεων μεγέθους για την αρχική κλίση K_i ενώ σε ότι αφορά την οριακή εγκάρσια εδαφική αντίδραση p_u παρατηρούνται αποκλίσεις έως και 150%. Οι διαφορές αυτές αναφέρονται σε βάθος $z = 3D$ (η οριζόντια εδαφική απόκριση κοντά στην επιφάνεια του εδάφους είναι πιο κρίσιμη) και επηρεάζουν σημαντικά την κατανομή εντατικών και παραμορφωσιακών μεγεθών στον πάσσαλο.

- Αναπτύσσεται αριθμητική μεθοδολογία για τον υπολογισμό καμπυλών p-y μέσω σύνθετων τριδιάστατων αναλύσεων πεπερασμένων στοιχείων. Η μεθοδολογία αυτή χρησιμοποιεί προχωρημένα αριθμητικά εργαλεία, απαραίτητα για τη ρεαλιστική προσομοίωση της εγκάρσιας φόρτισης πασσάλου σε αργιλικά εδάφη υπό αστράγγιστες συνθήκες (συζευγμένες αναλύσεις, φόρτιση σε πραγματικό χρόνο, διεπιφάνειες, προχωρημένα καταστατικά προσομοιώματα).

- Προτείνεται νέα εκθετική συνάρτηση μονοτονικών καμπυλών p-y για μαλακά, NC αργιλικά εδάφη, η οποία αποδίδει ικανοποιητικά την αντίστοιχη εγκάρσια

[1] τα πειραματικά αποτελέσματα αφορούν στο μέσο εγκάρσιο συγκεντρωμένο φορτίο που μετρήθηκε κατά τον πρώτο μισό κύκλο, ανά το εκάστοτε βήμα μετατόπισης

εδαφική αντίδραση. Οι προτεινόμενες καμπύλες p-y συσχετίζονται με τις κλίσεις λ και κ των γραμμών φόρτισης και αποφόρτισης-επαναφόρτισης αντίστοιχα, με τον λόγο Poisson ν και με τον συντελεστή συνάφειας πασσάλου-εδάφους α (η διατμητική τάση μεταξύ πασσάλου-εδάφους ορίζεται ως τ_{max}=$\alpha \cdot c_u$). Η κλίση της γραμμής κρίσιμης κατάστασης M και η διάμετρος του πασσάλου D δεν επηρεάζουν ουσιαστικά τις καμπύλες αυτές.

- Οι προτεινόμενες καμπύλες p-y για στιφρά, OC αργιλικά εδάφη συσχετίζονται με την κλίση κ της γραμμής αποφόρτισης-επαναφόρτισης, με τον λόγο Poisson ν, με τον συντελεστή συνάφειας πασσάλου-εδάφους α, με τη διάμετρο D του πασσάλου και με τη μέση αστράγγιστη διατμητική αντοχή του εδάφους $c_{u,avg}$ από την επιφάνεια μέχρι βάθος $10D$. Πτώση της αντοχής του εδάφους μετά από εκτεταμένη παραμόρφωση δεν αντικατοπτρίζεται στη μορφή των καμπυλών p-y (μέχρι παραμένουσα αντοχή ίση με το 30% της μέγιστης). Η τασική χαλάρωση των OC εδαφών επηρεάζει την οριακή εγκάρσια εδαφική αντίδραση p_u.

- Οι συνοριακές συνθήκες κεφαλής του πασσάλου (πακτωμένη, ελεύθερη) και οι γεωμετρικές μη-γραμμικότητες του προβλήματος (large strain analysis) δεν επηρεάζουν την αριθμητική ανάπτυξη καμπυλών p-y για αργιλικά εδάφη υπό αστράγγιστες συνθήκες.

- Ανακυκλική οριζόντια φόρτιση της κεφαλής του πασσάλου $H_c = 30 - 50\% H_u$ δεν επηρεάζει ουσιαστικά τις αριθμητικές καμπύλες p-y μαλακών, NC αργιλικών εδαφών. Αντίστοιχη φόρτιση σε στιφρά, OC εδάφη φαίνεται να αυξάνει την K_i των καμπύλων p-y σε μικρά βάθη μετά την ανακύκληση, χωρίς καμία επιρροή όμως στην p_u.

- Οι προτεινόμενες καμπύλες p-y προσομοιώνουν με επιτυχία την εγκάρσια απόκριση πασσάλων (οριζόντιες μετατοπίσεις, καμπτικές ροπές) σε μαλακά και στιφρά αργιλικά εδάφη με χρήση του μοντέλου «δοκού επί μη-γραμμικού ελατηριωτού εδάφους», όπως προέκυψε από σύγκριση με πειραματικά αποτελέσματα. Παρά το γεγονός ότι οι αριθμητικές αναλύσεις της διατριβής θεωρούν πλήρως ελαστικό πάσσαλο, οι προτεινόμενες καμπύλες p-y υπολογίζουν ικανοποιητικά εντατικά και παραμορφωσιακά μεγέθη κατά μήκος πασσάλων από πειράματα που τους φορτίζουν εγκάρσια μέχρι να αστοχήσει το υλικό τους (πλαστική άρθρωση).

- Η παρούσα διατριβή ενισχύει την αντίληψη ότι ο σχεδιασμός πασσάλων υπό εγκάρσια φόρτιση με χρήση καμπυλών p-y της βιβλιογραφίας που θεωρούν

p_u κοντά στο άνω όριο του εύρους δεν είναι απαγορευτικός, αλλά με κατάλληλη διερεύνηση των εδαφικών παραμέτρων μπορεί να πραγματοποιηθεί με ασφάλεια, ακρίβεια και οικονομία. Οι υφιστάμενες μεθοδολογίες υπολογισμού καμπυλών p-y παραγνωρίζουν την επίδραση συγκεκριμένων εδαφικών παραμέτρων (π.χ. C_c, C_r), οδηγώντας σε υπερβολικά συντηρητικές σχεδιαστικές λύσεις. Αντίθετα, οι προτεινόμενες καμπύλες ενσωματώνουν τις παραπάνω επιδράσεις βελτιώνοντας τόσο την αξιοπιστία όσο και το κόστος του σχεδιασμού.

Αναγνωρίζεται ότι η αριθμητική μεθοδολογία της διατριβής - όπως και κάθε αριθμητική προσομοίωση γενικότερα - έχει περιθώρια βελτίωσης που συνοψίζονται στα ακόλουθα σημεία:

- Για την ακριβέστερη αριθμητική προσομοίωση του προβλήματος απαιτείται χρήση πεπερασμένων στοιχείων ανώτερης τάξης (C3D20P). Οι αριθμητικές αναλύσεις της παρούσας διδακτορικής διατριβής χρησιμοποιούν γραμμικά τριδιάστατα πεπερασμένα στοιχεία (C3D8P) καθότι η χρήση στοιχείων ανώτερης τάξης απαιτεί πολλαπλάσιο υπολογιστικό κόστος και οδηγεί συνήθως σε αριθμητικές αστάθειες του κώδικα υπό καθεστώς εκτεταμένων παραμορφώσεων και αστοχίας υλικών – για την εκτίμηση του p_u των καμπυλών p-y.

- Ορισμένες ιδιαιτερότητες της θεωρίας ποροελαστικότητας και του καταστατικού προσομοιώματος Modified Cam Clay επέβαλαν την παραδοχή συγκεκριμένων κατανομών για κάποιες από τις παραμέτρους των εδαφών που διερευνήθηκαν:

  i. Με τη θεώρηση σταθερής κλίσης κ της γραμμής αποφόρτισης-επαναφόρτισης η προσομοίωση καταλήγει σε μέτρο ελαστικότητας γραμμικά αυξανόμενο με το βάθος. Για την προσομοίωση σταθερού μέτρου ελαστικότητας απαιτείται θεώρηση αυξανόμενης κ με το βάθος.

  ii. Για την προσομοίωση περίπου σταθερής αντοχής στιφρών, OC αργιλικών εδαφών με το βάθος απαιτείται η θεώρηση σταθερού μεγέθους επιφάνειας διαρροής. Αυτό οδηγεί σε πολύ μεγάλους (μη-ρεαλιστικούς) βαθμούς προστερεοποίησης (OCR) κοντά στην επιφάνεια του εδάφους, ειδικά στις περιπτώσεις σκληρών αργιλικών σχηματισμών ($c_u > 200kPa$).

- Τα καταστατικά προσομοιώματα των αριθμητικών αναλύσεων της παρούσας διατριβής (απλοποιημένο αλλά κλασσικό μοντέλο Modified Cam Clay και προηγμένο μοντέλο που προτάθηκε προσφάτως από τον Kalos (2014)

βασίζονται στην Εδαφομηχανική Κρίσιμης Κατάστασης και δε διαθέτουν (MCC) ή δεν έχουν ενεργοποιημένα (SSS-SD) χαρακτηριστικά κόπωσης (fatigue) και χρονικά εξαρτημένων φαινομένων όπως ο ρυθμός επιβολής της ανακυκλικής φόρτισης (rate dependency). Για τον λόγο αυτό τα συμπεράσματα για την επιρροή της ανακυκλικής φόρτισης (λίγων κύκλων) στις καμπύλες p-y είναι περισσότερο ποιοτικά και αντανακλούν τους περιορισμούς των καταστατικών προσομοιωμάτων ως προς αυτού του είδους τις φορτίσεις.

- Απαιτείται η διερεύνηση της επιρροής της μη-κορεσμένης επιφανειακής ζώνης στις προτεινόμενες καμπύλες p-y. Η παρούσα διατριβή εξετάζει πλήρως κορεσμένα αργιλικά εδάφη ($S_r = 100\%$), με αποτέλεσμα να αγνοεί πιθανή αύξηση της αντοχής λόγω του μερικού κορεσμού για τα επιφανειακά εδαφικά στρώματα – περιοχή ιδιαίτερα κρίσιμη για την εγκάρσια απόκριση του συστήματος εδάφους-πασσάλου.

- Δεν λαμβάνονται υπόψη μεταβολές στο τασικό πεδίο λόγω της εγκατάστασης του πασσάλου, με αποτέλεσμα οι προτεινόμενες καμπύλες να αφορούν κυρίως έγχυτους πασσάλους. Ωστόσο, η εφαρμογή των προτεινόμενων καμπυλών σε πειραματικές δοκιμές στις οποίες χρησιμοποιήθηκαν πάσσαλοι εκτοπίσεως, έδειξε ότι προβλέπουν αρκετά ικανοποιητικά την απόκριση του πασσάλου. Αυτό πιθανώς να αποδίδεται στο γεγονός ότι η πλευρική φόρτιση αφορά μια ευρεία περιοχή εδαφικής μάζας, με αποτέλεσμα να μην επηρεάζεται έντονα από την εγκατάσταση του πασσάλου, οι επιδράσεις της οποίας περιορίζονται τοπικά στον πάσσαλο. Ωστόσο, απαιτείται περαιτέρω διερεύνηση.

Thesis Main Body

Contents

List of Figures

List of Tables

Chapter 1

Introduction

1.1 Problem description

During pile design, the engineer usually focuses on its response in axial (usually vertical) and lateral (usually horizontal) loading. Lateral loading is particularly significant because it is related mainly to unforseen phenomena (earthquakes, storms, impacts, landslides), for which the design requirements are generally increased and associated with a high rate of uncertainty (compared to axial loading that is imposed to the piles by the vertical loads of the upper structure as well as its horizontal loads, undertaken by the deep foundation through force pairs - compressive and extensive). Indicatively, Figure 1.1 presents failures of laterally loaded piles around the world. As a consequence, the study of the lateral pile response is necessary for the foundation of a wide variety of structures (tall buildings, bridge piers, wind turbines, offshore platforms, harbor piers, etc.), pointing out the need for computational tools that will result in a practical, reliable and effective pile design.

The use of p-y curves - serving as horizontal nonlinear soil springs - on a Beam on Nonlinear Winkler Foundation (BNWF) is common practice for the calculation of section forces and deformations along laterally loaded piles (bending moments, shear forces, horizontal displacements, etc.). The formulation of this method is based on the following three (3) assumptions:

- Structural elements (pile, cap, superstructure) are simulated as beam elements.
- Soil-pile interaction is represented by the p-y curves, which dictate the distributed load-displacement relationship of the corresponding lateral nonlinear soil springs. One end of the springs is attached to the pile while the other remains fixed.
- The loads of the soil-pile system are applied either at the fixed end of the

Figure 1.1: Indicative failures of laterally loaded piles around the world.

springs (kinematic) or at the structure-foundation formation - superstructure, pile, cap - (external).

As a result, the complex, three-dimensional problem of the laterally loaded pile is solved as two-dimensional through the replacement of the lateral soil reaction with nonlinear springs at various depths. If the engineer manages to calibrate these springs successfully regarding their strength and compressibility, the aforementioned calculations become quick and representative of the actual lateral pile response. The main prerequisite for a realistic simulation of the problem through the BNWF method is the use of accurate p-y curves at various depths together

with the dense application of these soil springs along the pile, since they are not conjugated (the deformation of each spring does not affect its neighbouring). The international literature proposes p-y curves for external quasi-static loading (wind, braking), cyclic loading (waves) and dynamic loading (impacts, earthquakes). However, the accurate development of static (monotonic) p-y curves is considered highly significant because it facilitates the formulation of corresponding curves for the other two loading categories (cyclic, dynamic).

Various experiments and pile load tests aid with their measurements in the development of p-y curves. Two (2) main categories of laterally loaded pile experiments are met in the international literature, resulting in specific p-y curve relationships: (i) physical experiments, either full-scale or in centrifuge and (ii) "numerical experiments" in PC. The first p-y curves were proposed based on lateral load tests of piles for the foundation design of offshore platforms. These curves proved particularly conservative from time to time, while the corresponding load tests were very costly. Centrifuge tests offer an alternative in full-scale tests, although they struggle simulating actual clayey soil profiles with accuracy. Furthermore, centrifuge tests are not that affordable compared with the large-scale ones. On the other hand, the technological evolution and constantly increasing computational power of the last decades offer the potential of advanced numerical simulations concerning the problem of the laterally loaded pile (finite elements, finite differences, etc.). In this case, the numerically developed p-y curves reflect the reliability of: the constitutive law used for the soil simulation, the properties of the pile material, the pile-soil interaction and the hydraulic conditions of the simulated problem.

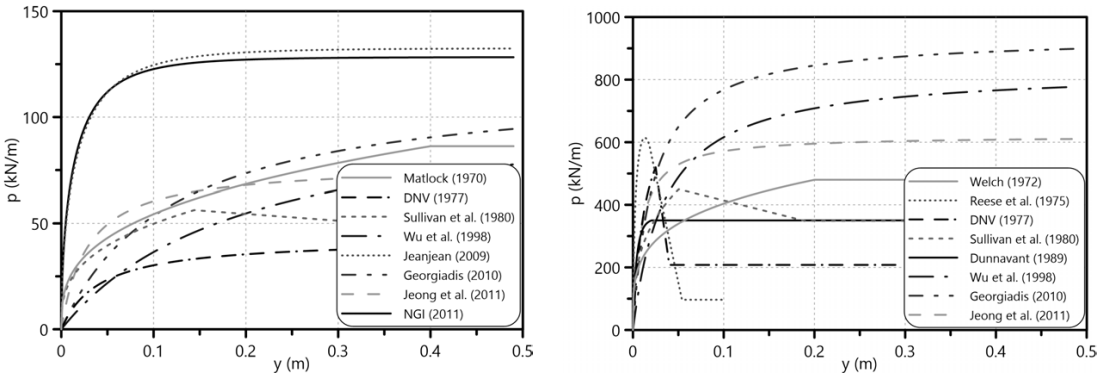

(a) **(b)**

Figure 1.2: Literature p-y curves for (a) soft, normally consolidated clays and (b) stiff, overconsolidated clays (z=3m, D=1m).

During the design of laterally loaded piles, the behavior of the soil-pile system up to a depth of approximately ten (10) times the pile diameter (D) is considered

crucial (Gazetas & Dobry, 1984). A comparative evaluation of the existing methodologies, focusing on depths shallower than $10D$, reveals very high deviation of the corresponding p-y curves for clayey soils - applicable to external loading cases of laterally loaded piles. Indicatively, Figure 1.2 depicts the p-y scatter of a soft and a stiff clay at a depth equal to $3D$ (lateral pile-soil response is more critical closer to ground surface). Regarding the main parts of the p-y curve relationships, the aforementioned observed deviation reaches up to two orders of magnitude for the initial curve stiffness K_i and up to 150% for the ultimate lateral soil resistance p_u. It is obvious that such deviation levels make the specific design particularly uncertain.

Up to date, a significant number of researchers have pointed out these differentiations and emphasized on the benefits of numerical investigations regarding p-y curves (Ahmadi & Ahmari, 2009; Brown & Shie, 1990; Chen & Poulos, 1993; Comodromos et al., 2009; Georgiadis & Georgiadis, 2010; Mylonakis et al., 1997; Templeton et al., 2009; Yang & Jeremić, 2002; Yegian & Wright, 1973). However, apart from Georgiadis & Georgiadis (2010), no upgraded p-y curves for clayey soils exist in the literature that are derived from numerical analyses.

The present doctoral thesis comes to fill this void by simulating the problem of a single, laterally loaded pile in clayey soils through advanced finite element analyses (FEA). It is important to clarify that **all the FEA carried out in the dissertation refer to external lateral loads on the piles - not kinematic**. This research distinguishes between clayey soils according to their undrained shear strength c_u distribution with depth (linear or constant) and utilizes various soil constitutive laws for verification and parametric investigation purposes. The FEA in the computer code Simulia Abaqus incorporate significant innovations compared to existing research on the specific topic. Thus, the thesis attempts to develop improved p-y curves for clayey soils, correlated with widely used strength and compressibility parameters of such soils. Hence, the proposed p-y curves shall be applicable to conventional design of laterally loaded piles.

1.2 Scope of work

The aforementioned problem description reveals that p-y curves for clayey soils require further investigation. Nevertheless, pursuing this goal through full-scale or centrifuge tests on laterally loaded piles has proved both costly and time consuming, with certain inabilities to simulate the variety of parameters involved in the problem. In addition, conclusions drawn from such tests were judged site-oriented quite a few times by various researchers in the past. Recent advances in numerical

modelling (finite elements, finite differences) along with the development of sophisticated constitutive models that simulate thoroughly the soil behavior even under extreme loading conditions (e.g. earthquake, creep, liquefaction), allow for a realistic and reliable simulation of various geotechnical boundary value problems. Thus, researchers possess a very powerful tool that overcomes many limitations of physical modelling and serves as a valuable alternative towards the parametric study of the p-y methodology. Consequently, the current dissertation decides to investigate the lateral response of a single, externally loaded pile in clayey soils through FEA in the commercial code Simulia Abaqus, attempting to achieve the following two (2) main objectives:

- develop a sophisticated and reliable three-dimensional finite element model for the realistic simulation of a single, laterally loaded pile in clayey soils through effective stress analyses, capable of capturing the mechanisms that govern the lateral pile response
- propose upgraded p-y curves from the results of thoroughly calibrated "numerical experiments", using the undrained shear strength distribution of the clayey soil as criterion (NC and OC clays) and evaluate the existing p-y curve methodologies for clayey soils according to the pile design they lead to (conservative or realistic), namely for external lateral loads.

The developed finite element model is part of a coordinated research effort, carried out during the last three decades in the Geotechnical Department of the National Technical University of Athens, aiming to investigate the behavior of deep foundations under various loading and soil conditions. Characteristic contributions include the work by Kavvadas & Gazetas (1993) on the kinematic response of free-head piles in layered soil, the development of a Winkler model for static and dynamic caisson response by Gerolymos & Gazetas (2006), the numerical simulation of slope stabilizing piles by Kourkoulis et al. (2010) and the analysis of liquefaction effects on the ultimate pile reaction to lateral spreading by Chaloulos et al. (2013).

A robust (both accurate and stable) constitutive law is required for the realistic simulation of soil behavior in the FEA. Most earlier attempts on the numerical development of p-y curves adopted simplistic constitutive models for the soil behavior (Mohr-Coulomb, Von Mises), trying to avoid numerical instabilities during the solutions. The research conducted by Kavvadas & Amorosi (2000), Belokas & Kavvadas (2011) and Kalos (2014) provides the current thesis with versatile tools in order to link successfully the externally imposed loading (i.e. stress increments) with the corresponding strains accumulating in the ground. Of course extensive benchmarking is necessary to gain confidence on the utilized constitutive law.

In more detail, **the scope of the present doctoral thesis** is outlined in the following points:

- Develop upgraded monotonic p-y curves for clayey soils under undrained loading conditions through sophisticated, three-dimensional, finite element analyses (FEA) in effective stress terms. Although p-y curves for such soils have been proposed through FEA and FDA in the past, the current dissertation shall be the first to simultaneously utilize advanced numerical tools for the simulation of the laterally loaded pile (hydromechanical coupling, real-time loading, soil-pile interface, Critical State Soil Mechanics constitutive law for the clay).

- The proposed p-y curves aim at categorizing the clayey soils based on the c_u distribution with depth and not according to its absolute magnitude (see existing methodologies). Hence, it proposes p-y curves for soft, normally consolidated (NC) and stiff, overconsolidated (OC) clayey soils, with linearly increasing and constant c_u with depth respectively.

- Correlate the initial stiffnes K_i and the ultimate lateral soil resistance p_u of the proposed p-y curves with widely used strength (c_u) and compressibility (C_c, C_r, ν) parameters of clayey soils. Especially for K_i, these correlations offer an alternative choice to the majority of the existing literature methods that assume an initial p-y stiffness mainly dependent from the characteristic axial strain ε_{50} corresponding to one-half the maximum principal stress difference during an undrained compressive test of a specimen.

- Allow for the investigation of the influence that two soil characteristics - mainly observed in stiff clays - have on the corresponding p-y curves, namely the soil stiffness under relatively small strains (small-strain stiffness) and the post-peak strength decrease due to various phenomena (e.g. structure degradation), by incorporating them in the soil constitutive law of the FEA.

- Attempt to simulate the cyclic lateral loading of a single pile through quasi-static FEA and derive some initial quantitative observations regarding the effect of few load cycles on the developed post-cyclic p-y curves.

- Evaluate the existing literature p-y curves for clayey soils and ascertain whether they lead to a conservative or realistic design of an externally laterally loaded pile in such soils.

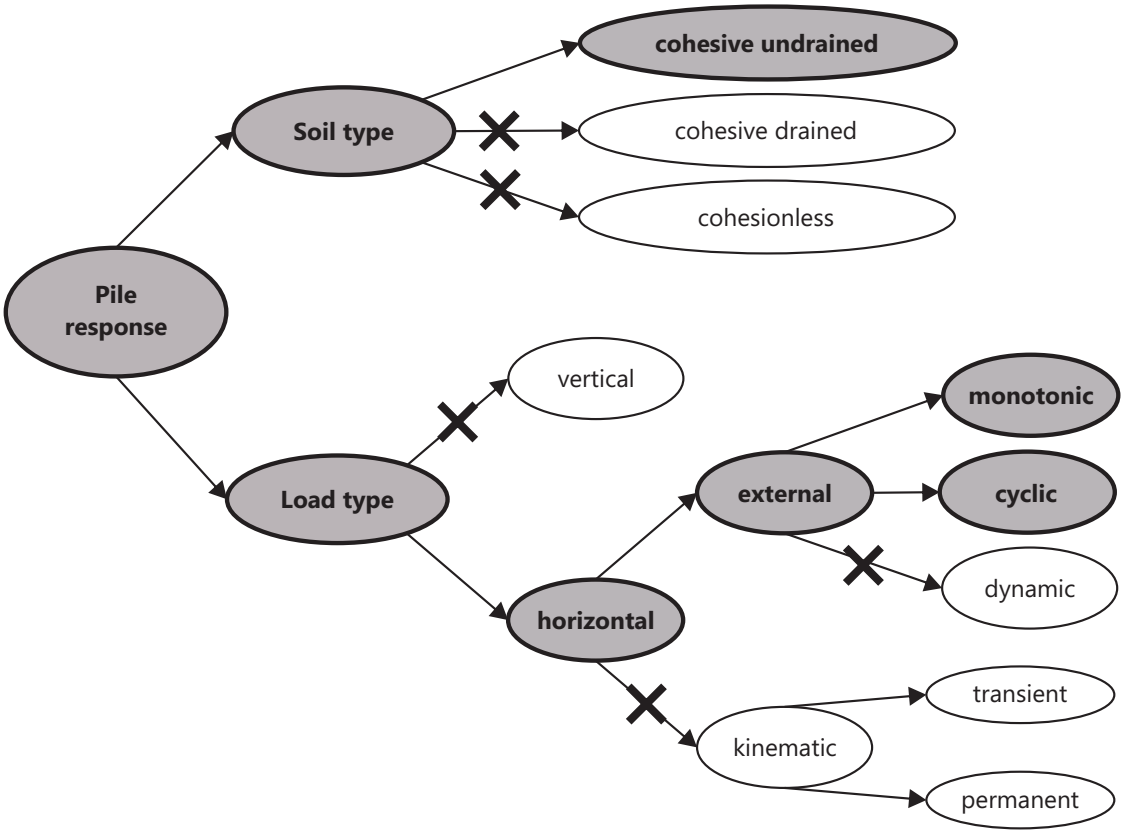

Figure 1.3: Soil types and loading conditions investigated through the FEA of the present doctoral thesis, regarding pile response.

Figure 1.3 depicts the soil types and loading conditions that the current dissertation investigates through numerical simulations, regarding the pile response and consequently the developed p-y curves.

1.3 Research methodology - Thesis outline

The research methodology to establish the proposed p-y curves for NC and OC clayey soils is summarized in the following four (4) distinct Research Steps (RS), which are reflected on the structure of the thesis:

RS 1: an extensive literature review of existing p-y curves for all types of clays (soft, stiff) derived through various procedures (lateral pile load tests, FEA, in-situ testing) followed by renowned elaborations on the main p-y parts, namely the initial stiffness K_i and the ultimate lateral soil resistance p_u. Chapter 2 carries out the aforementioned review;

RS 2: the design of the numerical simulation (finite element model, incorporated

constitutive laws) for the development of p-y curves for clayey soils under undrained loading conditions, together with the corresponding benchmarking of the output derived from the FEA. Chapter 3 presents the specific process;

RS 3: the parametric investigation of various soil and pile properties potentially affecting the numerically derived monotonic p-y curves for soft, NC and medium-to-stiff, OC clayey soils, together with a qualitative assessment on the probable modification of the curves due to cyclic pile-head loading, presented in Chapters 4, 5 and 6;

RS 4: the evaluation of the proposed methodology through comparisons with experimental measurements - from lateral load tests - on the lateral pile response (pile deformation, pile-head load-displacement curves, maximum bending moment), addressed in Chapter 7.

In more detail, **Chapter 2** carries out a thorough review of the international literature on static and cyclic p-y curves for clays and clarifies the principles of the specific simulation technique. Non-linear p-y curves of the literature for clayey soils are divided into four (4) main categories according to this chapter: (i) p-y curves for soft clays (Jeanjean et al., 2009; Matlock, 1970; Nichols et al., 2014), (ii) p-y curves for stiff clays (Dunnavant & O'Neill, 1989; Reese et al., 1975; Welch & Reese, 1972), (iii) unified p-y curves for clays (DNV, 1977; Georgiadis & Georgiadis, 2010; Jeong et al., 2011; Sullivan et al., 1979; Wu et al., 1998) and (iv) p-y curves for clays that correlate with in-situ field test measurements (Bouafia, 2013; Briaud et al., 1983; Frank, 2009; Gabr et al., 1994; Guo et al., 2014; Kim et al., 2016; Robertson et al., 1989). Although the specific chapter comprises the necessary literature review accompanying this thesis, it is attempted to avoid a strict quotation of available sources. Instead, it presents the available literature resources in a didactic and practical manner, regarding their field of application. The basic parameters of the aforementioned methodologies are: the undrained shear strength c_u of the clayey soil, the characteristic axial strain ε_{50} corresponding to one-half the maximum principal stress difference during an undrained compressive test of a specimen (in other words the strain corresponding to c_u), the soil-pile adhesion factor α, the pile diameter D and the stiffness of the pile E_pI_p. **Chapter 2** concludes to a comparative depiction of the existing p-y curves for soft and stiff clayey soils, which evinces their significant scatter. Thus, the main objective of the doctoral thesis is oriented in investigating the problem through sophisticated numerical analyses. The following five (5) chapters (Chapter 3 to 7) concern solely the original contribution of the present dissertation with respect to the aforementioned goal.

Chapter 3 describes methodically the three-dimensional (3D) finite element simulation of the single laterally loaded pile in clayey soils, designed in the commercial code Simulia Abaqus 6.12 for the numerical development of p-y curves. More specifically, the chapter presents the simulation of the soil material, the pile, the pile-soil interface and the analyses steps up to the lateral loading of the pile head. The finite element analyses (FEA) of the present dissertation are carried out in effective stress terms for the clayey soils under investigation, with simultaneous solution of the mechanical and the hydraulic problem and by mainly utilizing the Modified Cam-Clay (MCC) constitutive law for the simulation of the soil behavior. The research distinguishes between soft, normally consolidated (NC) and stiff, overconsolidated (OC) clayey soils, depending on the distribution of c_u with depth (linearly increasing distribution and $c_{u,0}$=0 on ground surface for NC, almost constant c_u >50kPa for OC). Certain FEA simulate small-strain stiffness (relatively small strains $\varepsilon < 0.1\%$) and intense strain-softening with corresponding strength degradation for specific OC clayey soils and through proper modifications on the MCC (Belokas, 2008; Kalos, 2014). **Chapter 3** closes with an extensive sensitivity analysis (geometrical boundaries and density of the finite element grid, pile-soil interface properties, fixity conditions of the pile head, large-strain analyses), which validates the efficiency of the simulation that is performed during the whole course of the thesis in order to develop p-y curves from FEA.

Chapter 4 develops monotonic p-y curves for soft, NC clayey soils through numerical "experiments" of a single laterally loaded pile, according to the simulation described in Chapter 3. A thorough parametric investigation is carried out in order to quantify the effect of certain properties of the soil (strength, compressibility), the pile (diameter) and the pile-soil interface (adhesion) on the lateral soil response and consequently on the p-y curves derived from the FEA. The observations from the aforementioned parametric investigation for various depths along the pile indicate the parameters that influence significantly both the initial stiffness K_i and the ultimate lateral soil resistance p_u of the p-y curves for the specific soil category. The chapter proposes the improved p-y curves for soft, NC clayey soils - involving the aforementioned critical parameters - and finally it compares them to the existing literature p-y curves (Chapter 2) applicable to such soils.

Chapter 5 follows the same process with Chapter 4, i.e. development of p-y curves through FEA, but for medium-to-stiff, OC clayey soils. Apart from the parametric investigation on certain design parameters of the pile-soil system (soil strength and compressibility, pile diameter, pile-soil interface), the specific chapter focuses on the effect of two important stiff clay features on the derived p-y curves: the soil stiffness at relatively small strains ($\varepsilon < 0.1\%$) and the strength degradation

due to strain-softening after significant soil deformation. An extended section within the chapter describes how these two features are controlled by certain parameters of an MCC-type constitutive law developed by Belokas (2008) and modified by Kalos (2014) - the corresponding soil behavior is verified through FEA of both undrained triaxial tests and laterally loaded single piles. Finally, the chapter proposes improved monotonic p-y curves for medium-to-stiff, OC clayey soils that take into account all the aforementioned effects and compares them to the corresponding literature curves (Chapter 2) for such soils.

Pile head lateral loading is considered monotonic up to the specific point of the thesis. **Chapter 6** investigates the influence of cyclic lateral pile head loading on the derived post-cyclic p-y curves for both soft, NC and stiff, OC clays. The performed FEA simulate cyclic loading in a pseudostatic manner, by imposing up to 20 cycles of lateral pile head lateral loading. The specific number of load cycles is indicative of the lateral pile response in cyclic loading according to literature recommendations. A monotonic loading that leads to soil failure, succeeds the cyclic loading and the p-y curves of this final load step are compared with the corresponding monotonic p-y curves of Chapters 4 and 5.

Chapter 7 validates and evaluates the proposed p-y curves of the dissertation. It verifies the p-y curves - proposed in Chapters 4 and 5 - through four (4) physical experiments of laterally loaded piles (full-scale or centrifuge tests) and compares the predictions of the Beam on Non-linear Winkler Foundation (BNWF) solution with the experimental measurements (ultimate lateral pile head load, maximum bending moment, horizontal displacement and curvature along the test pile). The experiments of the specific validation are thoroughly documented. They are chosen because they cover a significant range of mechanical parameters for clayey soils - NC and OC - as well as pile dimensions, compared to the corresponding range of the parametric investigation that delivered the numerical p-y curves of the current thesis. In addition, Chapter 7 compares the BNWF predictions of the proposed p-y curves with the corresponding calculations that occurred by the use of existing literature p-y curves. Thus, the thesis suggests a preferable range of p-y curve methodologies for a safe and cost-effective pile design.

Finally, **Chapter 8** summarizes the main points of the doctoral thesis and evaluates in total its proposed p-y curves for clayey soils. Furthermore, it formulates certain proposals for future research on the specific field, originated from the shortcomings of the present attempt and associated with the evolution of the proposed p-y curves, as well as with their implementation in practical engineering problems.

Chapter 2

The p-y curve method

2.1 General

A detailed literature review is carried out in the present chapter, in order to describe the available methodologies simulating the soil response against a laterally loaded pile. Current design practice emphasizes on the BNWF (Beam on Nonlinear Winkler Foundation) method, widely known as the *p-y method*. The *p-y method* consists of three major simulation processes:

- **Pile simulation:** The pile is simulated through beam elements, introducing the characteristics of the structural part of the problem (i.e. Young's modulus E_p, moment of inertia I_p, etc.).
- **Soil response:** The response of the soil against the laterally loaded pile is the key of a successful simulation for the specific problem. A detailed simulation of the actual soil constitutive behavior leads to a very accurate reproduction of the soil response. This nonlinear spring called p-y curve is thoroughly simulated through three parts, as depicted in Figure 2.1 : (a) the initial stiffness K_i, (b) the ultimate lateral soil resistance p_u and (c) the mathematical expression controlling the transition to yield.
- **Pile loading:** The lateral loading of the pile is applied on its head either as a concentrated load or a displacement. Furthermore, axial loading and bending moment may also apply there.

In the beginning of this chapter, it is important to clarify that most of the methods described herein characterize the clays as either soft or stiff according to mean values of the undrained shear strength c_u. However, an alternative characterization is adopted in the current dissertation, referring to the distribution of the undrained

shear strength c_u with depth. Namely, soft clays are considered with linearly increasing undrained shear strength $c_u(z)$, while stiff clays with constant undrained shear strength $c_u = ct.$ with depth.

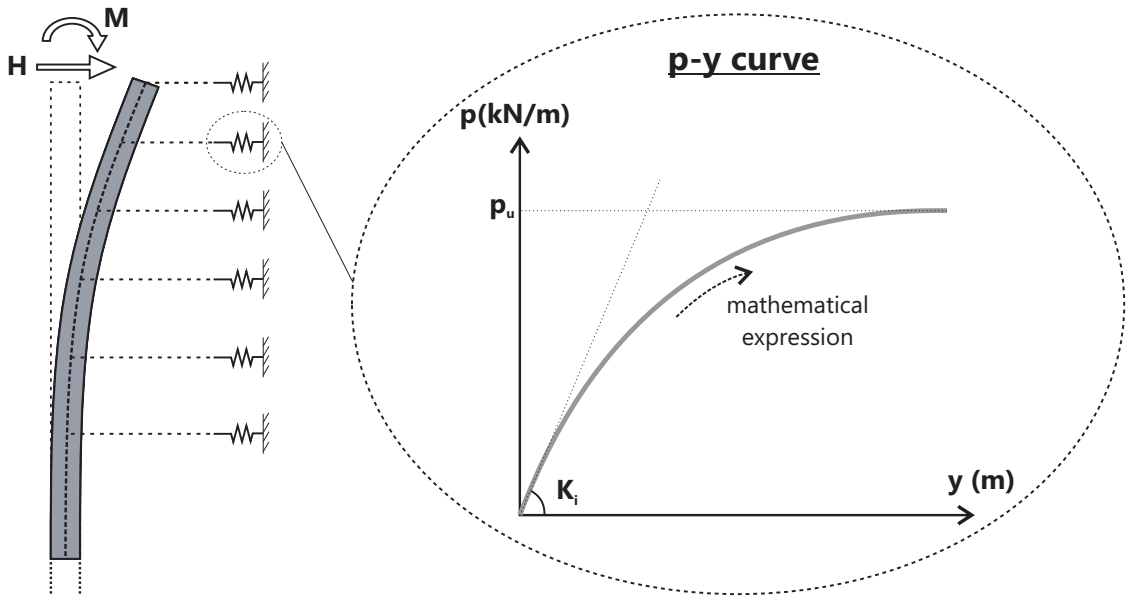

Figure 2.1: Typical form of a p-y curve.

Most of the recommendations presented for obtaining p-y curves are based on the analysis of the results of full scale experiments with instrumented piles. A comprehensive geotechnical investigation was performed at each site and the most suitable estimate of the undrained shear strength of the clay was found. The dimensions and stiffness of the test piles were calculated accurately. Experimental p-y curves were obtained by one or more of the techniques described earlier. In order to derive analytical expressions for the proposed p-y curves, theory was used to the fullest extent. As a result, the developed p-y curves, when used in a BNWF solution, yielded curves of deflection and bending moment versus depth that agreed well with the experimental values. Loading in most of the experiments was both monotonic and cyclic.

2.2 Early recommendations on p-y curves for clays

The first attempts on the simulation of a laterally loaded pile through mathematical forms - "ancestors" of p-y curves - were carried out by Skempton (1951), Terzaghi (1955) and McClelland & Focht (1958). In the following paragraphs, the recommendations of these studies with respect to saturated clays are briefly described.

2.2.1 Skempton (1951)

The theoretical considerations presented by Skempton (1951) were oriented to the prediction of load-settlement curves. Especially for saturated clays - providing a limited solution of the problem - useful conclusions were derived, reflecting the practical application of theory. These observations were based on the similarity assumed between load-deflection curves for a vertically loaded horizontal plate and a pile under lateral loading. According to the theory of elasticity, the mean settlement ρ of a foundation with width B on the surface of a semi-infinite solid is estimated by the equation:

$$\rho = qBI_{\rho}\frac{1-\nu^2}{E_s} \tag{2.1}$$

where q= foundation pressure, I_{ρ}= influence coefficient, ν= Poisson's ratio of the solid and E_s= Young's modulus of the solid. The modification of Equation 2.1 for a rigid circular footing on the ground surface of a saturated clay assumes ν=0.5 (undrained loading), I_{ρ}=$\pi/4$ and a failure stress q_f=6.8c_u (c_u= the undrained shear strength of the clay). Thus, the following expression yields, which is valid for any depth according to Skempton:

$$\frac{\rho}{B} = \frac{4c_u}{E_s}\frac{q}{q_f} \tag{2.2}$$

The axial strain during an undrained triaxial compression test is related to the failure stress of the specimen $(\sigma_1 - \sigma_3)_f$=2c_u through the following equation.

$$\varepsilon = \frac{2c_u}{E_s}\frac{(\sigma_1-\sigma_3)}{(\sigma_1-\sigma_3)_f} \tag{2.3}$$

where E_s= Young's modulus at the stress $(\sigma_1-\sigma_3)$ The comparison of Equations 2.1 and 2.3 leads to the observation that for the same ratio of applied to failure stress, the deflection of the footing (or laterally loaded pile) is related to the corresponding axial strain of the laboratory triaxial compression test through the expression:

$$\frac{\rho}{B} = 2\ \varepsilon \tag{2.4}$$

Skempton's considerations introduced the assumption of a nonlinear Young's modulus E_s for the soil, depending on the stress state of the elements below the footing - either close or far from failure. In addition, he stated that to a degree of approximation comparable with the accuracy of the assumptions, namely 20%, Equation 2.5 is applicable to either circular or square footings. However, assuming that the behavior of a laterally loaded pile is more similar to that of a strip footing, Skempton proposed the modification of the aforementioned equation according to the follow-

ing observations. Timoshenko (1934) and Terzaghi (1943) reported that for a strip footing with length to width ratio of 10, influence coefficient was I_ρ=1.26. With a bearing capacity q_f=5.3c_u for the specific footing, Equation 2.5 was rewritten:

$$\frac{\rho}{B} = 2.5\ \varepsilon \tag{2.5}$$

Finally, Skempton pointed out that the failure stress of the soil below a strip footing reaches a maximum value of q_f=9c_u. Thus, a resistance-deflection curve could be obtained for a long strip footing, by calculating deflection from Equation 2.5 - assuming that a laboratory stress-strain curve is available - and with soil resistance equal to 4.5$\Delta\sigma$.

2.2.2 Terzaghi (1955)

A number of important aspects of the subgrade reaction were discussed by Terzaghi (1955) in his paper, including the resistance of the soil to a laterally loaded pile. However, while he demonstrated significant knowledge on the problem of the pile, his recommendations lacked any experimental or analytical validation. Terzaghi noticed that the units of the lateral soil pressure p are force per unit length (F/L) and the definition of p was presented graphically (Figure 2.2). Nonetheless, the problem of the pile under lateral loading was not altered and Terzaghi simply assumed that $p = qB$.

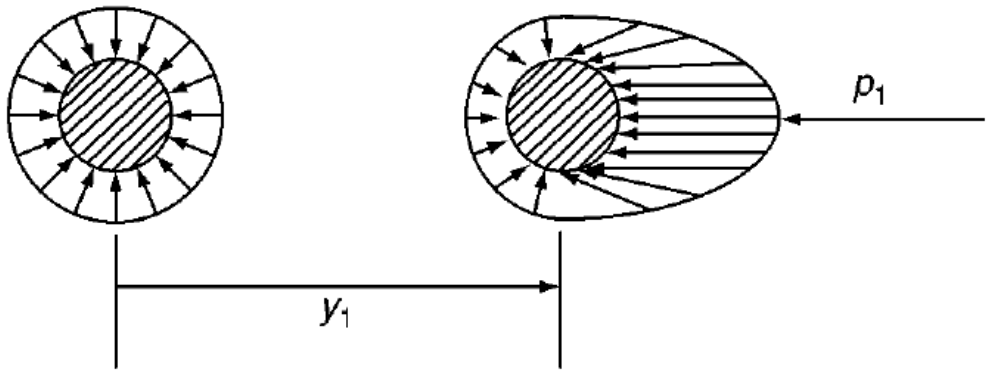

Figure 2.2: Graphical presentation of lateral soil pressure p (Terzaghi, 1955).

Especially for the coefficient of subgrade reaction for piles in stiff clays, Terzaghi's recommendations were based on his observation that the deformational characteristics of such clays are assumed constant with depth. Thus, he proposed constant p-y curves with depth, with a p to y ratio α_T depending on the unconfined compression

strength of the clay (Table 2.1). Apparently, Terzaghi recognized that the laterally loaded pile could not be deflected to an unlimited extent assuming a linear increase of soil resistance. Therefore, he pointed out that a linear p-y relationship was valid for values of p smaller than about half the lateral bearing capacity of the clay.

Table 2.1: Terzaghi's recommendations on the soil modulus α_T for laterally loaded piles in stiff clay.

Consistency of clay	Stiff	Very stiff	Hard
q_u, kPa	100-200	200-400	> 400
α_T, MPa[1]	3.2-6.4	6.4-12.8	12.8 up

[1] The values of constant α_T are independent from pile diameter - in consistency with the theory for small deflections.

2.2.3 McClelland and Focht (1958)

One of the first attempts to propose specific p-y curves for laterally loaded piles in clayey soils was carried out by McClelland & Focht (1958). The results from a full-scale, instrumented, lateral pile load test were analyzed and certain curves were derived. The study indicated that the stiffness of the p-y curves E_{py} is not exclusively a soil property, but depends on the pile diameter and the deflection as well. The paper initially recommended the performance of consolidated, undrained triaxial compression tests at various soil depths, with confinement pressure equal to the overburden. Subsequently, the soil stress-strain curves could be transformed to p-y curves - point by point - through the following equations.

$$p = 5.5\ D\ \Delta\sigma \tag{2.6a}$$

$$y = 0.5\ D\ \varepsilon \tag{2.6b}$$

where D= pile diameter, $\Delta\sigma$=$(\sigma_1 - \sigma_3)$= the deviatoric stress from the stress-strain curve and ε= the strain from the stress-strain curve. Equations 2.6a and 2.6b demonstrate similarities to the work presented by Skempton (1951) (see Paragraph 2.2.1), although only in form - not in magnitude. Referring to the ultimate value of p from the aforementioned equations, investigators observed that it was similar to that for bearing capacity well below ground surface and certain modifications were necessary to account for the influence of the latter.

2.3 P-y curves for soft clays

In the current section, p-y curves derived exclusively for soft clays are described. The following methodologies occurred either from large scale experiments on instrumented, laterally loaded piles or from thorough numerical investigation.

2.3.1 Matlock (1970)

The p-y curves proposed by Matlock (1970) were developed based on full scale experiments performed at Lake Austin and Sabine, in Texas between 1955-1965. A steel-pipe pile with a diameter of 0.319m, wall thickness of 12.7mm, a length of 12.8m and bending stiffness $E_pI_p = 31280kNm^2$ was driven twice and two complete series of free-head loadings - one static and one cyclic - were performed at Lake Austin. The clay of the specific site was slightly overconsolidated with an average undrained shear strength measured $(c_u)_{vane} = 38.3kPa$. An average value of $\varepsilon_{50} = 0.012$ - assumed constant with depth - was measured from triaxial tests. The same pile was removed and installed at a test site near the mouth of the Sabine River. Two static and two cyclic test loadings were carried out there, under both free-head and restrained-head conditions. This clay was a slightly overconsolidated marine deposit with an undrained shear strength $c_u = 14.4kPa$. Computations were carried out with a value of $\varepsilon_{50} = 0.02$, according to the suggestions of Table 2.2. The layout of the test and the pile characteristics at the Sabine site are depicted in Figure 2.3. Matlock (1970) proposed procedures for the formulation of p-y curves for short-term, static loading, for cyclic loading and for after-cyclic loading as depicted in Figures 2.4a, 2.4b and 2.4c respectively.

Table 2.2: Representative values of ε_{50} for normally consolidated clays after Skempton (1951) and Peck et al. (1974).

Consistency of clay	Average c_u (kPa)	ε_{50}
Soft	< 48	0.020
Medium	$48 - 96$	0.010
Stiff	$96 - 192$	0.005

Static loading

1. At the beginning, obtain the best possible estimate of the undrained shear strength c_u and the submerged unit weight γ with depth. Also obtain the value of ε_{50}, the axial strain corresponding to one-half the maximum principal stress difference.

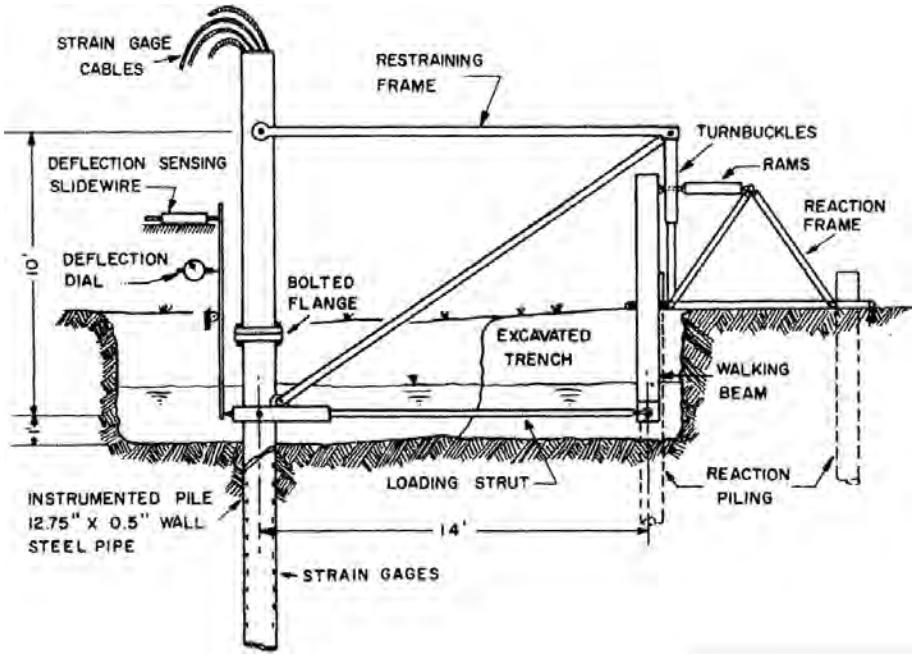

Figure 2.3: The field test layout at Sabine, using restrained-head lateral loading (Matlock, 1970).

If no laboratory test data are available for the stress-strain behavior of the clay, choose a typical ε_{50} value from Table 2.2 after Skempton (1951) and Peck et al. (1974).

2. Compute the deflection y_{50} at one-half the ultimate soil resistance from the following equation:

$$y_{50} = 2.5\ \varepsilon_{50}\ D \tag{2.7}$$

where D= the width of the pile.

3. Calculate the ultimate soil resistance per pile unit length, according to the following equation:

$$p_{ult} = min\left[3 + \frac{\gamma\,'}{c_u}\ z + \frac{J}{D}\ z,\ 9\right]\ c_u\ D \tag{2.8}$$

where $\gamma\,'$= average effective unit weight from the ground surface to the depth of the derived p-y curve, z= depth from the ground surface to the p-y curve depth and c_u= undrained shear strength at depth z. Matlock (1970) stated that the value of J ranges between 0.5 - 0.25 for soft to medium clay respectively - a value of $J = 0.5$ is frequently used. The value of p_{ult} is calculated at each depth that a p-y curve is desired, based on the in situ undrained shear strength at that depth.

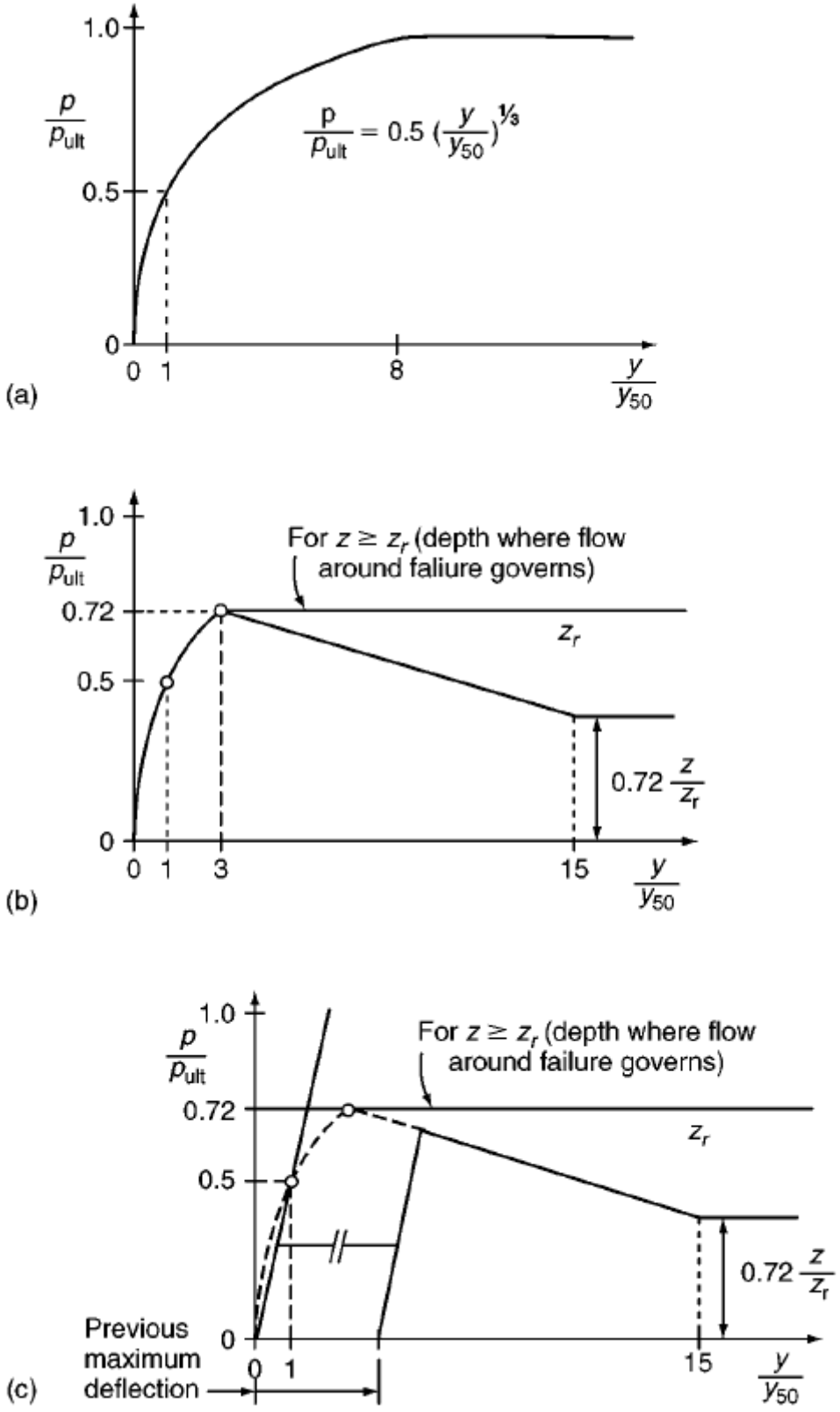

Figure 2.4: Formulation of p-y curves for soft clay in the presence of free water, (a) static loading; (b) cyclic loading; (c) after-cyclic loading (Matlock, 1970)

4. Finally, the relationship combining the previous steps and describing the p-y curve is:

$$\frac{p}{p_{ult}} = 0.5\left(\frac{y}{y_{50}}\right)^{1/3} \tag{2.9}$$

It is important to mention here that the value of p remains constant beyond $y = 8y_{50}$, as depicted in Figure 2.4a.

Cyclic loading

1. Form the p-y curve according to the aforementioned instructions for static lateral loading conditions on the pile head, for values of p less than $0.72p_{ult}$.

2. According to the method, there is a critical depth z_r, where the transition between a three-dimensional wedge-type failure and a two-dimensional flow-around failure occurs. By equating the two parts of Equation 2.8, the following expression for z_r is calculated:

$$z_r = \frac{6c_u D}{(\gamma' D + Jc_u)} \tag{2.10}$$

   This relationship calculates z_r for constant unit weight and shear strength in the upper zone. If these soil properties vary with depth, the value of z_r should be computed with parameters referring to the depth where the p-y curve is desired.

3. If the depth of the p-y curve is $z \geq z_r$, then $p = 0.72p_{ult}$ for all values of y greater than $3y_{50}$.

4. In the case that the depth of the p-y curve is $z < z_r$, the value of p decreases from $p = 0.72p_{ult}$ at $y = 3y_{50}$ to the value calculated by the following equation at $y = 15y_{50}$.

$$p = 0.72p_{ult}\left(\frac{z}{z_r}\right) \tag{2.11}$$

The value of p remains constant beyond $y = 15y_{50}$. It is important to mention here that the aforementioned methodology is adopted by many regulations and recommendations around the world, when the soft clay response against laterally loaded piles needs to be simulated. Amongst them, the recommendations of the American Petroleum Institute (API, 2007) and the Norwegian Regulations (DNV, 2010) are the most renowned for the design of offshore structures.

Due to the breakthrough of the research carried out by Matlock at that specific time, his proposed p-y curves are broadly utilized in the design of laterally loaded piles. Furthermore, Matlock's p-y equation is used as a backbone curve for the simulation of the lateral pile response according to more recent studies. However,

the methodology occurred after large scale load tests on piles of relatively small diameter, a parameter with significant effect on p_{ult} and y_{50} according to various subsequent studies. Therefore, many researchers attempted to modify certain steps of Matlock's methodology on the formulation of p-y curves for soft clays, the most renowned of which are briefly described herein.

Yegian & Wright (1973) performed finite element analyses allowing for a realistic simulation of the pile-soil interface in the shear direction. Thus, pile-soil adhesion was introduced and its influence on p_{ult} of the derived numerical p-y curves was noted. The specific study also pointed out that p-y curves can be derived from FEA as soon as soil parameters are thoroughly documented and the stress-strain relationship of the soil is rationally simulated through a mathematical form. It is important to mention that Yegian & Wright carried out the first attempt on the formulation of p-y curves from FEA. Their comparison of the aforementioned p-y curves with the ones proposed by Matlock for soft clays yielded major similarities and only some minor disagreements.

Stevens & Audibert (1979) carried out research on the effect of D and p_{ult} on the p-y curves proposed by Matlock and thus on the corresponding deflection and bending moment profile of the laterally loaded pile under concern. Large scale tests on laterally loaded piles of diameter D up to 1.5m were examined and certain conclusion were drawn. In more detail, their study proposed the following alternative equation for the computation of y_{50}:

$$y_{50} = 1.42\ \varepsilon_{50}\ \sqrt{D} \tag{2.12}$$

Although the aforementioned expression for y_{50} is not dimensionally correct, it was considered a very satisfactory empirical approximation of the specific p-y curve parameter. Furthermore, the researchers proposed a range of the ultimate lateral soil resistance factor $N_p = p_{ult}/(c_u\, D)$ based on their observations on p_{ult} from the different pile load tests they examined. Values of N_p were observed significantly greater than the ones calculated by Matlock's proposals, especially at shallow depths above $4D$, as depicted in Figure 2.5.

Lee & Gilbert (1979) proposed certain modifications on Matlock's static and cyclic p-y curves, after observations they made on a laterally loaded pile driven in very soft clay. While their p-y curve relationship was identical to the one proposed by Matlock for static lateral loading (Equation 2.9), alterations of p_{ult} and y_{50} were suggested. More accurately, it was recommended to increase 2.6 times the undrained shear strength value of the clay that was introduced in Equation 2.8. In addition

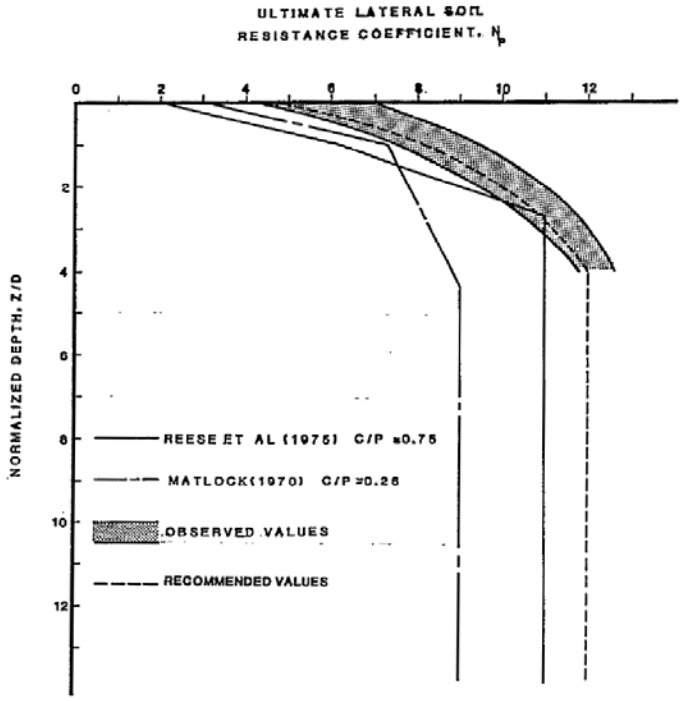

Figure 2.5: Ultimate lateral soil resistance factor N_p with dimensionless depth z/D for soft and medium clays according to Stevens & Audibert (1979)

the following expression was proposed for the calculation of y_{50}:

$$y_{50} = 0.1\ \varepsilon_{50}\ D \tag{2.13}$$

Finally, for the formulation of cyclic p-y curves Lee & Gilbert proposed the utilization of Matlock's static p-y curves - including the aforementioned modifications - up to values of $p < 0.91 p_{ult}$, corresponding to $y < 6 y_{50}$. For greater horizontal displacement y, a constant value of $p = 0.91 p_{ult}$ was recommended.

2.3.2 Jeanjean (2009)

Jeanjean et al. (2009) carried out a series of centrifuge tests on monotonic and cyclic laterally loaded steel piles in soft clay conditions. The purpose of the specific research was to examine the lateral response of offshore conductors installed in such soil types. As a result, a new p-y curve equation was proposed for monotonic loading and certain modifications on the secant modulus of the curves for cyclic (fatigue) design are recommended. The methodology is compared with corresponding FEA results and Matlock (1970)/API (2007) instructions on the design.

The soil profile of the tests was one of a lightly overconsolidated soft clay, with undrained shear strength c_u increasing linearly with depth, according to a ratio to

the in situ vertical effective stress $c_u/\sigma'_{vo}=\alpha(OCR)^{\beta}$ (α=0.19, β=0.67). The kaolin cake simulating the clay was constructed in two lifts, separated by a thin sand drainage layer for acceleration of the consolidation process[1]. Figure 2.6 depicts the c_u distribution with depth that was measured through PCPT tests in the centrifuge together with the corresponding interpreted c_u for the FEA input and the data analysis. The abrupt increase of c_u around z=11m is attributed to the intermediate sand

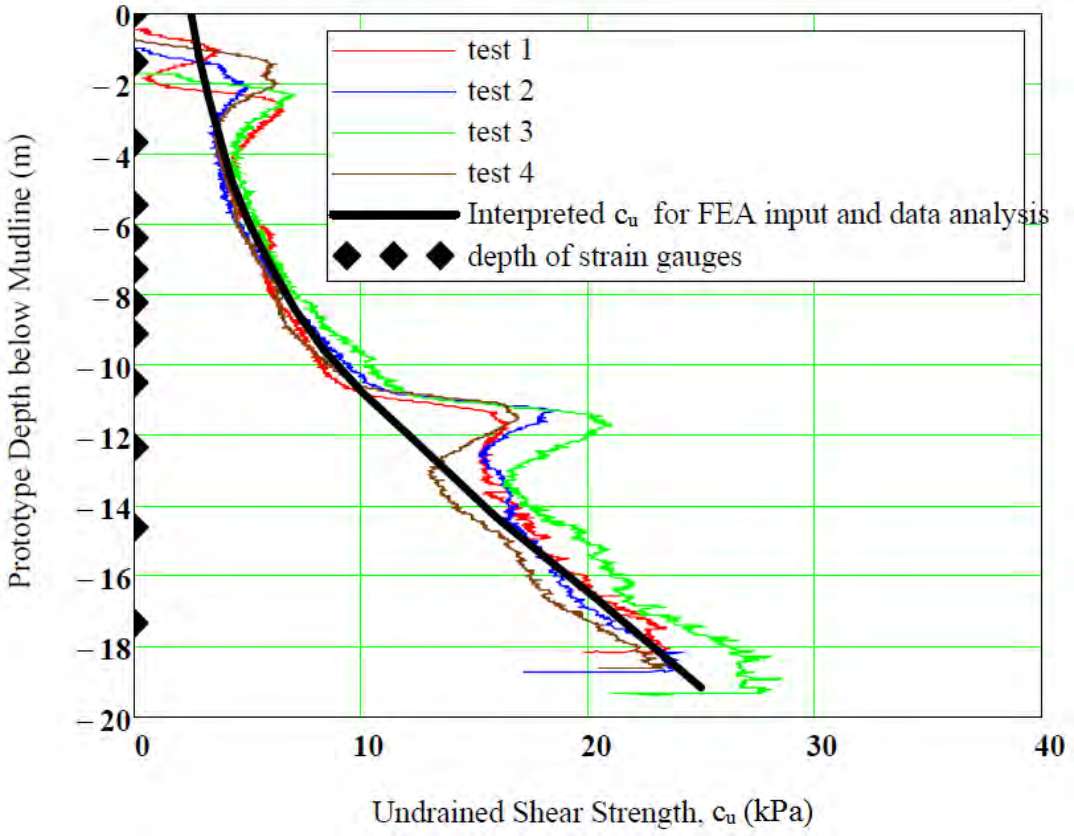

Figure 2.6: Undrained shear strength c_u of the kaolin with prototype depth from PCPT records.

layer. However, it did not affect the derived p-y curves, since they were calculated only for soil depths above this drainage layer. Soil properties of the current research were acquired from Direct Simple Shear (DSS) and Resonant Column (RC) tests in the laboratory. The methodology proposes a correction of $c_{u,DSS}$ measured from DSS tests with a dimensionless factor f_{Su}, so as to simulate more accurately the actual c_u field conditions - used as an input strength in the p-y curves. Field c_u and

[1]In order to reduce consolidation time in the centrifuge, the clay sample was pre-consolidated to about 95% of its effective vertical stress profile, prior to the centrifuge test.

factor f_{Su} are calculated according to the following equations:

$$c_u = c_{u,DSS} \cdot f_{Su} \tag{2.14}$$

$$f_{Su} = 1 + 0.1 \cdot Log_{10}\left(\frac{T_{DSS} \cdot 0.1}{T_{RC}}\right) \tag{2.15}$$

where T_{DSS}= the time period for peak shear strain, or 279 minutes for the kaolin of the centrifuge tests

T_{RC}= the time period for peak shear strain for an assumed RC test, or 3 seconds for the data set herein

The slope of the virgin compression line and the unload-reload line in v-lnp' space were measured λ=0.25 and κ=0.05 respectively for the kaolin. The coefficient of horizontal geostatic stress K_o=0.64, the plasticity index PI=26, the critical state line slope M=0.8 and the maximum shear modulus G_{max}=550c_u were also obtained for the test soil.

Four centrifuge tests were carried out - one monotonic and three cyclic (up to 1000 cycles each) with a final monotonic push to failure - in order to simulate soil failure as well as fatigue damage to the conductor. Free-head, steel, hollow-pipe conductors were tested with prototype diameter D=0.91m, wall thickness t=50.8mm and length L=20.2m. Each pile model was equipped with 13 sets of strain gauges along it - denser concentration of gauges between 6m and 12m of embedded pile length, where the highest bending moments were expected. In addition, specific instrumentation allowed for load, inclination and lateral movement measurements on the pile head. The conductor models were pushed (closed-ended) into slightly undersized pre-drilled holes prior to each test. The lateral load was applied about 4.3m - prototype distance - above mudline and water level was allowed only slightly above soil bed in order to preserve the strain gauges connection.

Pressure p and lateral displacement y of the p-y curves were derived by double differentiation and double integration of the bending moment profile obtained from the strain gauges along the test piles respectively. The acquired experimental p-y curves were used to generate a new backbone p-y curve criterion for monotonic laterally loaded piles in soft clays. For the formulation of these p-y curves, the following procedure describes the main steps:

1. The ultimate lateral pressure p_u at different depths, after a significant set of results from centrifuge tests and FEA for kaolin and Gulf of Mexico (GoM) clay (Templeton et al., 2009), is expressed according to the following equation. The

expression is similar to the framework proposed by Murff & Hamilton (1993) for a linearly increasing undrained shear strength profile with depth.

$$p_u = N_p \cdot c_u \tag{2.16}$$

where N_p= $12 - 4 \cdot exp\left(-\xi z/D\right)$

ξ= $0.25 + 0.05\lambda$ for $\lambda < 6$

ξ= 0.55 for $\lambda \geq 6$

λ= $c_{u0}/\left(c_{u1}\ D\right)$

c_{u0}= undrained shear strength on ground surface

c_{u1}= rate of increase of undrained shear strength with depth

D= pile diameter

z= depth below ground surface

The value of N_p is limited to 12 in order to be consistent with the lower bound plasticity theory solution proposed by Randolph & Houlsby (1984) for rough piles. However, higher values of the lateral bearing capacity factor N_p were measured during centrifuge tests and FEA, as depicted in Figure 2.7. It is important to mention here that the values of ultimate lateral soil resistance p_u were obtained at a normalized horizontal displacement y/D=0.20 on the p-y curves derived from the centrifuge tests and the FEA.

2. The following monotonic backbone p-y curve, proposed by the current methodology, is inspired from the equation proposed by Dunnavant & O'Neill (1989) for laterally loaded piles in submerged, stiff clays (see Paragraph 2.4.3):

$$\frac{p}{p_u} = \tanh\left[\frac{G_{max}}{100\ c_u} \cdot \left(\frac{y}{D}\right)^{0.5}\right] \tag{2.17}$$

where p_u= the ultimate lateral soil pressure derived from Equation 2.16

G_{max}= the maximum shear modulus of the soil

c_u= the undrained shear strength at the depth of the desired p-y curve

D= pile diameter

For cyclic loading conditions, the following expression is proposed for the degradation of the secant modulus as a function of the number of load cycles.

$$\frac{M_n}{M_1} = \frac{0.9}{0.9 + 2.5\ \tanh\left(0.7 \cdot log(n)\right)} \tag{2.18}$$

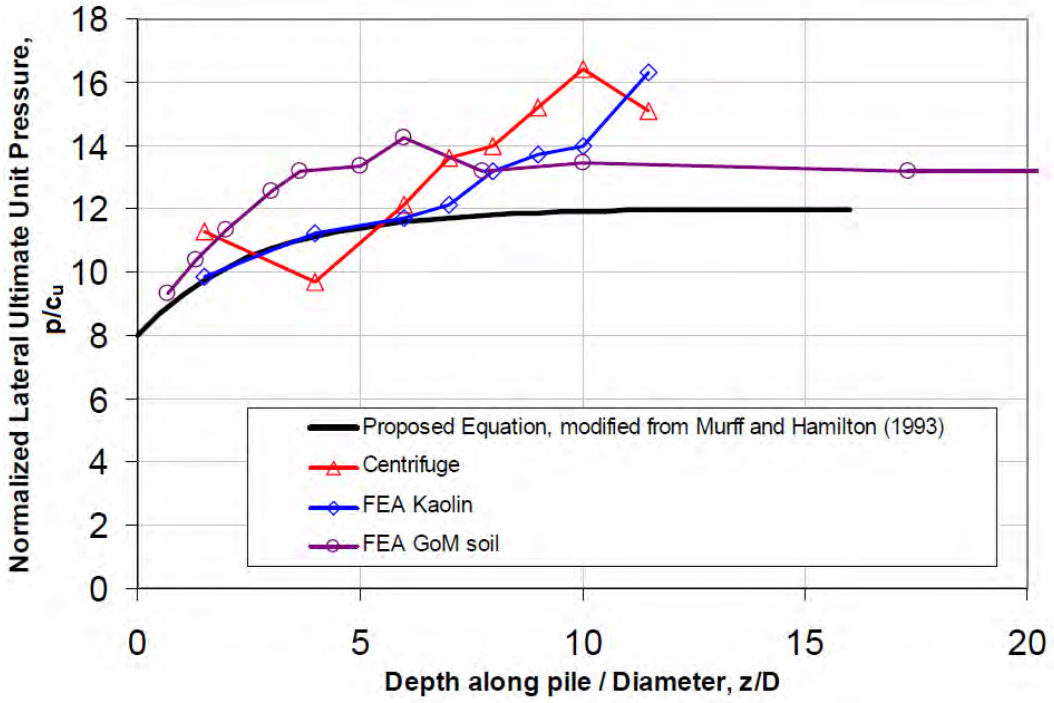

Figure 2.7: Proposed ultimate normalized unit pressure with depth compared with measurements from centrifuge test 1 and FEA.

where M_n= the secant modulus of the nth load cycle

M_1= the secant modulus of the 1st load cycle

n= the number of load cycles

The ratio of the secant modulus - derived from the centrifuge test p-y curves - of each unload-reload cycle over the tangent modulus at mid-range load on the monotonic backbone curve is far greater than unity, even for more than 100 loading cycles (Figure 2.8). Thus, the tangent modulus approach adopted by structural software for the calculation of cyclic loading soil displacements - and therefore the cyclic stresses in the pile - is judged conservative. Another observation confirms that small amplitude load cycles do not seem to affect in a negative way subsequent large load-displacement behavior, regardless of the soil consolidation allowed. The same applies to subsequent small amplitude load-displacement behavior if reasonable soil consolidation occurs. Regarding the pile head cyclic lateral response, it was measured stiffer and with higher ultimate pile head resistance after a significant number of load cycles compared to the corresponding response in monotonic loading. According to the current research, this behavior - potentially attributed to soil hardening under cyclic loads - could be of major importance when re-assessing the ultimate capacity of offshore foundations that have been in service for many years.

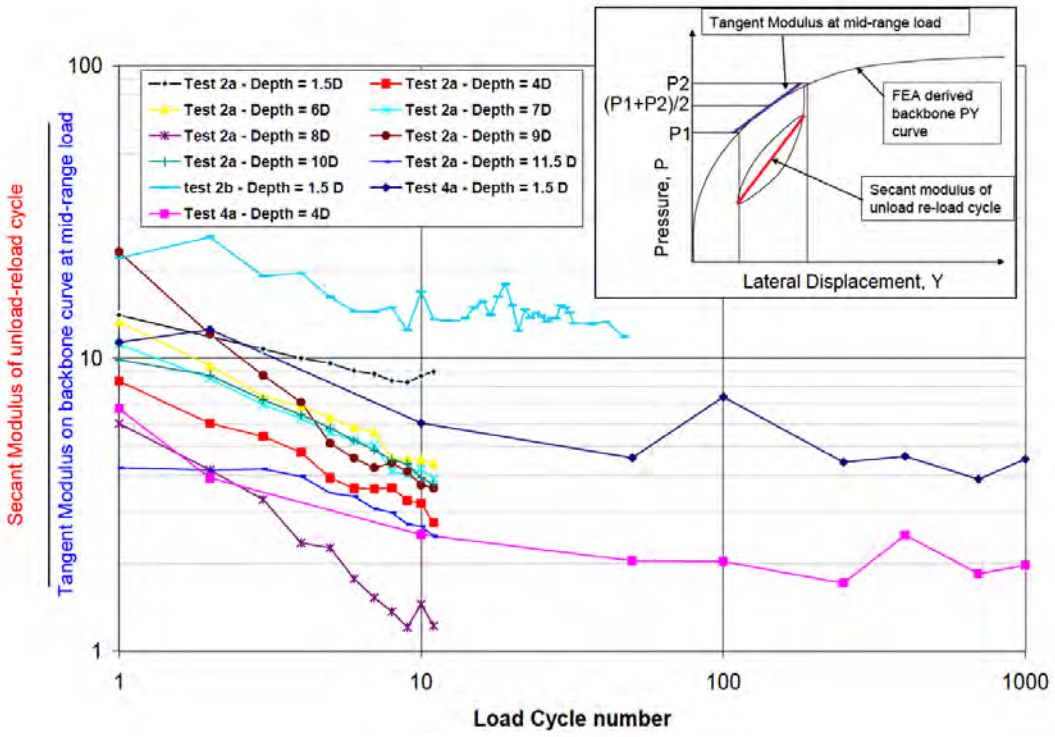

Figure 2.8: Ratio of the secant p-y modulus (cyclic centrifuge tests) of unload-reload cycles over the tangent modulus at mid-range load on the corresponding monotonic backbone curve.

2.3.3 NGI-11 (2014)

The research group of the specific methodology suspected potentially higher pile lateral capacity for pile load tests and foundation performance in the Gulf of Mexico during hurricane events, compared with the values calculated by the API (2007) recommendations. Therefore, Petronas Carigali Sdn Bhd (PCSB) together with the Norwegian Geotechnical Institute (NGI) carried out a study on the development of a new method called NGI-11 for the calculation of static p-y curves applicable to soft, normally consolidated clays. The aforementioned research incorporated literature review, review of field lateral load data and advanced numerical modeling for the calibration of the proposed p-y curves. The procedure for the proposal of a realistic and acceptable p-y method to model soft clay lateral behavior is summarized in the following steps (Nichols et al., 2014):

1. Undertake literature review

2. Compare p-y results using various methods

3. Compare the calculated response with actual pile load test data

4. Undertake calibration of the selected p-y method using non-linear 3D FEA

5. Review results to establish improvement to p-y curves

6. Perform pushover analyses using the SPLICE and the USFOS software

A common observation of the current thesis and the study of Nichols et al. (2014) is that the soil data provided by field tests of laterally loaded piles in soft clays do not refer to clearly normally consolidated soils. Particularly the ratio of the undrained shear strength to the in situ vertical effective stress c_u/σ'_{vo} at 2/3 of the depth to the maximum embedded bending moment of the pile received values much higher than the range 0.25-0.35 of normally consolidated clays. For all the reviewed tests the research group observed higher measured stiffness of the piles subjected to static lateral loading compared with the ones calculated by the method of API (2007). This difference is mainly attributed to the absence of significant amount of soil strength data and the large scatter in the measured strength values for the field tests under investigation. The proposed p-y curves for static lateral loading of piles in soft clays were derived from a set of 3D non-linear finite element analyses (FEA) carried out by NGI. The PLAXIS software was used for the FEA in combination with NGI's own soft clay material model. These analyses were performed in two different soil profiles: a "normally consolidated (NC)" and a "lightly overconsolidated (LOC)". Two pile diameters were analyzed, namely of 1.067m (42") and 1.829m (72"). The piles were rotationally restrained at the mudline to represent the jacket and were loaded by a horizontal force at their heads. Referring to the interface properties of the simulation, the piles were allowed to form a gap with the soil at their back side. The NGI clay material model for the FEA is based on anisotropic undrained shear strengths determined from triaxial compression (${c_u}^C$), direct simple shear (${c_u}^{DSS}$) and triaxial extension (${c_u}^E$) laboratory tests. The strength ratios used for the study were ${c_u}^{DSS}/{c_u}^C$ =0.66-0.72 and ${c_u}^E/{c_u}^C$ =0.50-0.55, with the lowest ratios referring to the NC clay profile. The steps for the formulation of p-y curves applying for static laterally loaded piles in soft clay according to NGI-11 are described through the following general instructions:

1. The ultimate lateral pressure p_u at different depths, after a significant set of results from the FEA and remarks of exact plasticity theory for a rough pile (Randolph & Houlsby, 1984), is expressed as:

$$p_u = min\left[N_p c_u + \gamma' z,\ 11.9 c_u^{DSS}\right] \tag{2.19}$$

   where N_p= lateral bearing capacity factor

c_u= undrained shear strength at depth z, $c_u = 0.5(c_u{}^{DSS} + c_u{}^{E})$

γ'= average submerged unit weight

z= depth below ground surface

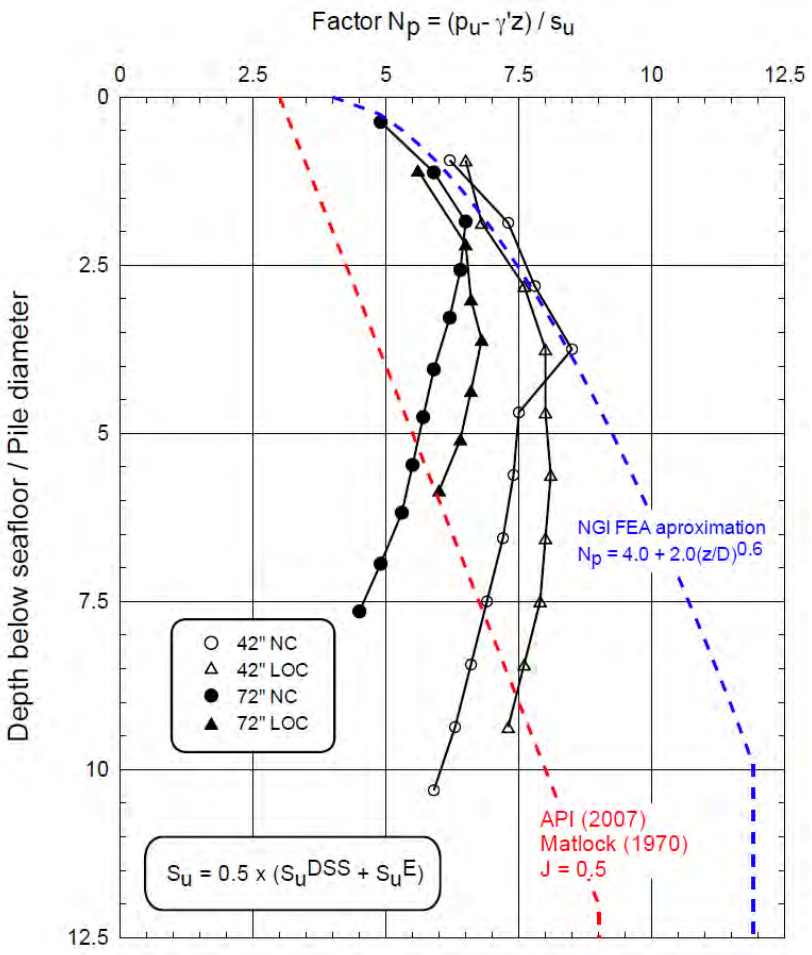

Figure 2.9: Lateral bearing capacity factor N_p: FEA output calculations and proposed expression with dimensionless depth.

The unit ultimate lateral capacity of the derived p-y curve is $p_u \cdot D$ - expressed in F/L units - where D is the pile diameter. Derivation of the calculated shear forces along the pile from the FEA was used to estimate the N_p factor in Equation 2.19, assuming that the ultimate lateral soil resistance has been reached at the examined depth. The calculated N_p factors for the two soil profiles and the two pile types are plotted against the normalized depth z/D in Figure 2.9. It was observed that the ultimate lateral resistance against the piles of the FEA was only reached for shallow depths - up to 2-4 times the pile diameter. Thus, the

proposed expression for the N_p factor is:

$$N_p = 4.0 + 2.0(z/D)^{0.6} \tag{2.20}$$

It is mentioned here that the undrained shear strength c_u used in Equation 2.19 is the average of direct simple shear and triaxial extension tests. Figure 2.9 includes also the N_p factor proposed by Matlock/API-07 for comparison purposes, although the comparison is not totally valid since the reference strength c_u is not equivalent for the two methodologies.

2. The FEA solutions and p-y based solutions were compared with field data and the following p-y curve relationship - introduced by Jeanjean et al. (2009) (see Paragraph 2.3.2) - is proposed:

$$\frac{p}{p_u} = \tanh\left[0.01\left(\frac{G_0}{c_u}\right)\cdot\left(\frac{y}{D}\right)^{0.5}\right] \tag{2.21}$$

where p= lateral stress for displacement y

p_u= ultimate lateral stress (Equation 2.19)

G_0/c_u= initial shear stiffness ratio

y= lateral pile displacement

D= pile diameter

$\tanh(x) = (e^{2x} - 1.0)/(e^{2x} + 1.0)$

3. Finally, an appropriate G_0/c_u ratio needs to be determined for the p-y curves. Figure 2.10 depicts the p-y curves calculated by Equation 2.21 for different G_0/c_u ratios and compares the results with the p-y curve proposed by Matlock/API-07. Trial calculations with the NGI-11 p-y model were compared with the FEA bending moment and lateral displacement distributions along the pile. These comparisons led to the conclusion that satisfactory agreement between the two sets of output occurred through incorporation of $\mathbf{G_0/c_u = 600}$, for both soil types and for both pile diameters.

Comparison of the NGI-11 method with the recommendations by API-07 on the Sabine River static pile tests (Matlock, 1970) showed that the latter overestimates the maximum bending moment along the pile up to 25%. On the contrary, the proposed NGI p-y curves for soft clay closely "predict" the measured values (Figure 2.11).

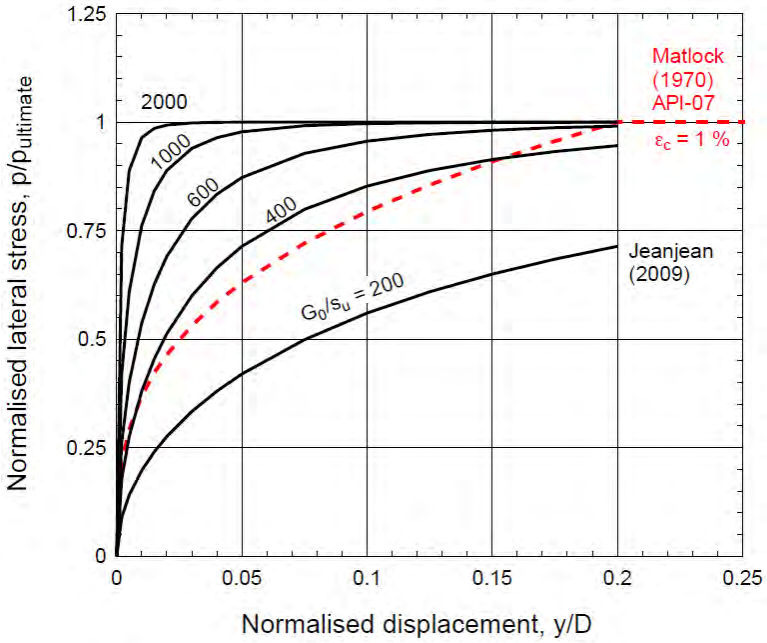

Figure 2.10: Comparison of p-y curves for different initial shear stiffness ratios G_0/c_u.

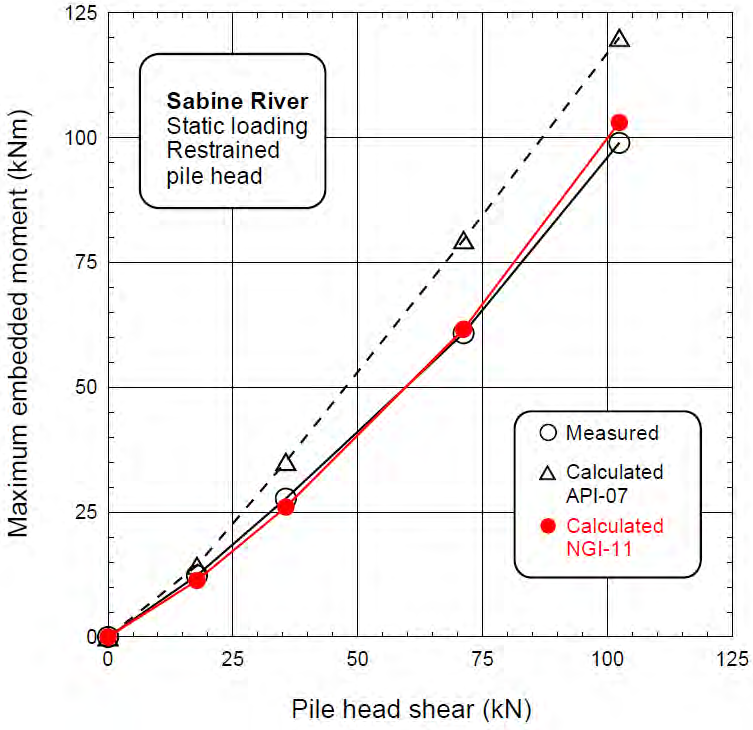

Figure 2.11: Comparison of NGI-11 and API-07 predictions on the maximum bending moment along the pile tested at the Sabine River site.

2.4 P-y curves for stiff clays

2.4.1 Welch and Reese (1972)

The results from a test of a laterally loaded bored pile in Houston, Texas were reported by Welch & Reese (1972). The response of stiff clay with no free water was then simulated through specific p-y curves for static and cyclic lateral loading of the pile. A brief report of this test is also presented by Reese & Welch (1975).

The bored pile of the test, with a diameter of 0.762m and a penetration length of 12.8m, was a rather complex construction with an instrumented steel pipe forming its core. The bending stiffness of the pile was measured during testing by reading the strain gauges output on opposite sides of the instrumented pipe and computed $E_pI_p = 4.0 \cdot 10^5 kNm^2$. The soil properties of the site correspond to a stiff, over-consolidated clay - called Beaumont clay locally - with a well developed secondary structure. The water table was found at a depth of 5.5m during the period of the field tests. The undrained shear strength of the clay - measured by unconsolidated undrained triaxial tests with confining pressure equal to the overburden - ranged between c_u =76-163kPa along the pile embedment length. A value of $\varepsilon_{50} = 0.005$ was assumed from the review of laboratory stress-strain curves, coming in agreement with the suggestions of Table 2.4.

Both static and cyclic loads were applied at 0.076m above the ground surface. The same pile was used without re-driving to obtain results for both loading types. At each increment of lateral load during cyclic loading, readings were obtained at 1, 5, 10 and 20 cycles - the latter for the larger loads.

Static loading

The procedure described herein is for the formulation of p-y curves corresponding to short-term static lateral loading of the pile (Figure 2.12):

1. Obtain values of the undrained shear strength c_u, soil unit weight γ and pile diameter D. In addition, specify the values of ε_{50} from laboratory stress-strain curves. In absence of the latter, a range of $\varepsilon_{50} = 0.005 - 0.010$ is suggested according to Table 2.4, the larger value leading to a more conservative behavior.

2. Calculate the ultimate soil resistance p_{ult} per pile unit length, according to the following equation:

$$p_{ult} = min \left[3 + \frac{\gamma}{c_u} z + \frac{J}{D} z,\ 9 \right] c_u\ D \tag{2.22}$$

where γ= average unit weight from the ground surface to the depth of the derived

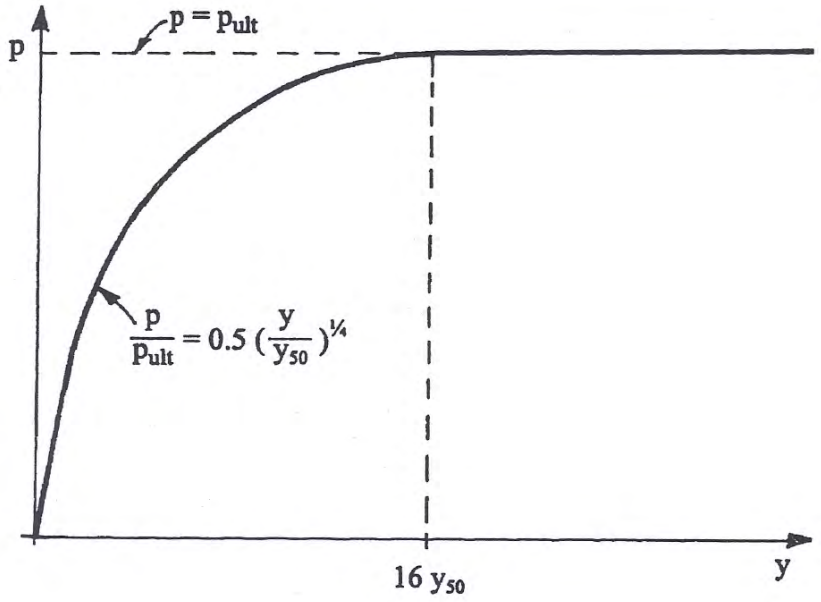

Figure 2.12: Formulation of p-y curves for static loading in stiff clay with no free water (Welch & Reese, 1972).

p-y curve (reflecting the position of the water table), z= depth from the ground surface to the p-y curve depth, $J = 0.5$ and c_u= average undrained shear strength from ground surface to depth z.

3. Compute the deflection y_{50} at one-half the ultimate soil resistance from the following equation:

$$y_{50} = 2.5\ \varepsilon_{50}\ D \tag{2.23}$$

where D= the width of the pile.

4. Develop the p-y curve for the selected depth z according to the relationship below:

$$\frac{p}{p_{ult}} = 0.5\left(\frac{y}{y_{50}}\right)^{1/4} \tag{2.24}$$

5. Beyond $y = 16y_{50}$, p is equal to p_{ult} for all values of y.

Cyclic loading

The procedure described herein is for the formulation of p-y curves corresponding to cyclic lateral loading of the pile (Figure 2.13):

1. Select a depth and develop the p-y curve for short-term static loading, as described through the aforementioned steps.

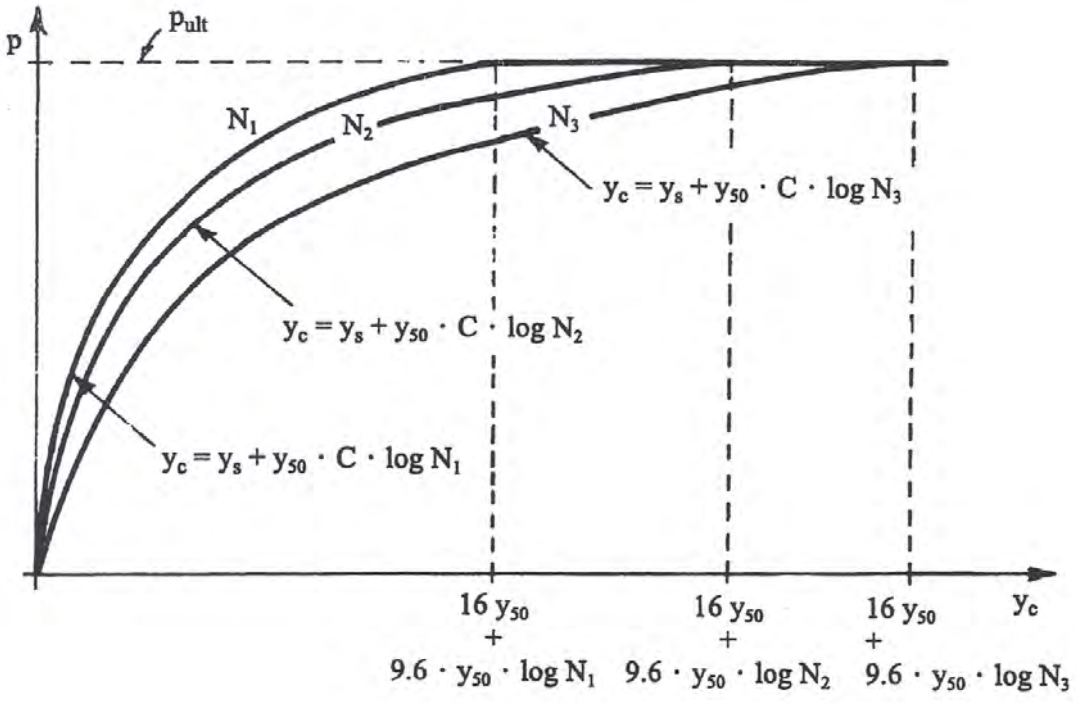

Figure 2.13: Formulation of p-y curves for cyclic loading in stiff clay with no free water (Welch & Reese, 1972), with y_s and y_c referring to the static and cyclic lateral displacement respectively.

2. Determine the number of times the design load will be applied to the laterally loaded pile.

3. For several p/p_{ult} ratios obtain the value C corresponding to the effect of cyclic loading on deformation, either from a relationship developed by laboratory tests (see Welch & Reese, 1972) or from the following equation:

$$C = 9.6 \left(\frac{p}{p_{ult}} \right)^4 \tag{2.25}$$

4. At the value of p corresponding to the p/p_{ult} ratios selected in Step 3, compute corrected values of y for cyclic loading from the following equation:

$$y_c = y_s + y_{50} C log N \tag{2.26}$$

   where y_c= deflection under N-cycles of load, y_s= deflection under short-term static load and y_{50} calculated after Equation 2.23.

5. The developed p-y curve defines the soil response after N-cycles of lateral load.

2.4.2 Reese et al. (1975)

Reese et al. (1975) proposed a set of p-y curves for static and cyclic lateral loading of piles in stiff clays in the presence of free water. The formulation of the p-y curves described in the current section are based on full scale experiments performed at Manor, Texas (1968). Two steel-pipe, 15.2m long piles driven in stiff clay were tested, with upper and lower section diameter 0.641m and 0.610m respectively. The experimental p-y curves derived from the tests carried out at Manor are depicted in Figure 2.14.

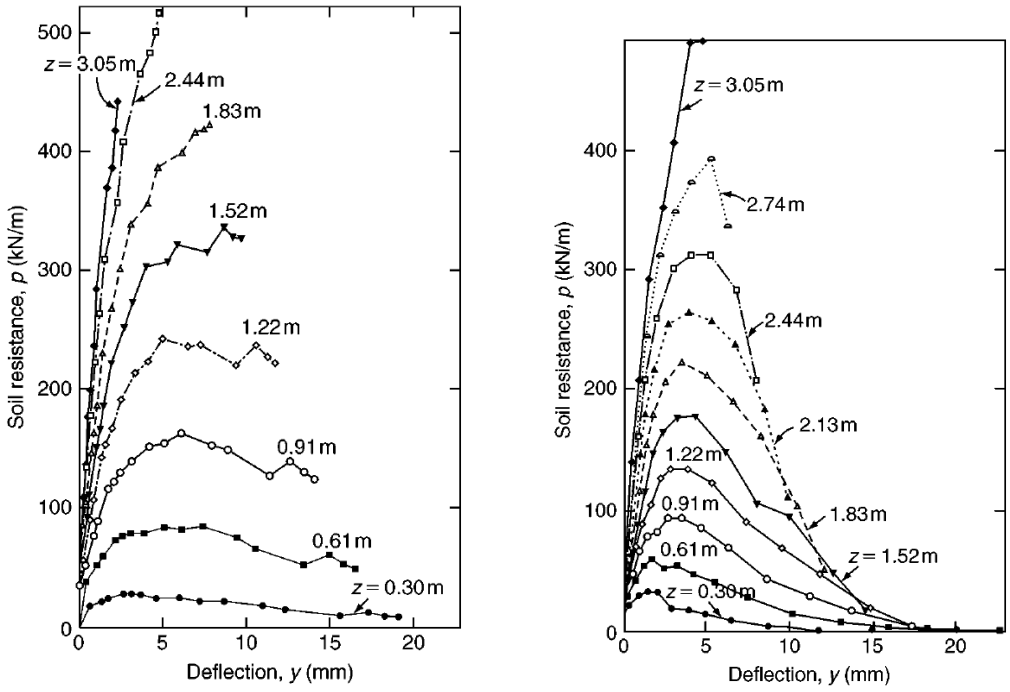

Figure 2.14: Reese et al. (1975) (a) static and (b) cyclic p-y curves derived from full scale tests at Manor.

The soil properties of the Manor site correspond to a stiff, highly overconsolidated clay with a well developed secondary structure. The undrained shear strength of the clay - measured by unconsolidated undrained triaxial tests with confining pressure equal to the overburden - ranged between c_u =25-1100kPa from z =0-20m respectively. For the same depth range, values of $\varepsilon_{50} = 0.004 - 0.007$ were acquired from Table 2.4, decreasing from ground surface to deeper strata. The values of ε_{50} obtained from experiments demonstrated great scatter - potentially due to the secondary structure of the clay - but were generally in agreement with the aforementioned suggestions. It is mentioned here that the site was excavated to a depth of about 1m and water was kept above the surface of the site for several weeks prior

to obtaining data for soil properties.

The piles of the tests were both instrumented with strain gauges for the measurement of bending moment along them. The lateral load was applied at 0.305m above ground level on both piles. One pile was tested under static lateral loading, with the load increasing in increments and the test being terminated when the bending moment was measured near the yield moment value $M_y = 1757kNm$. The second pile underwent cyclic loading with the load cycling at each increment until deflections were stabilized. An order of 100 cycles were applied during the cyclic lateral loading of this pile at a rate of about two cycles per minute.

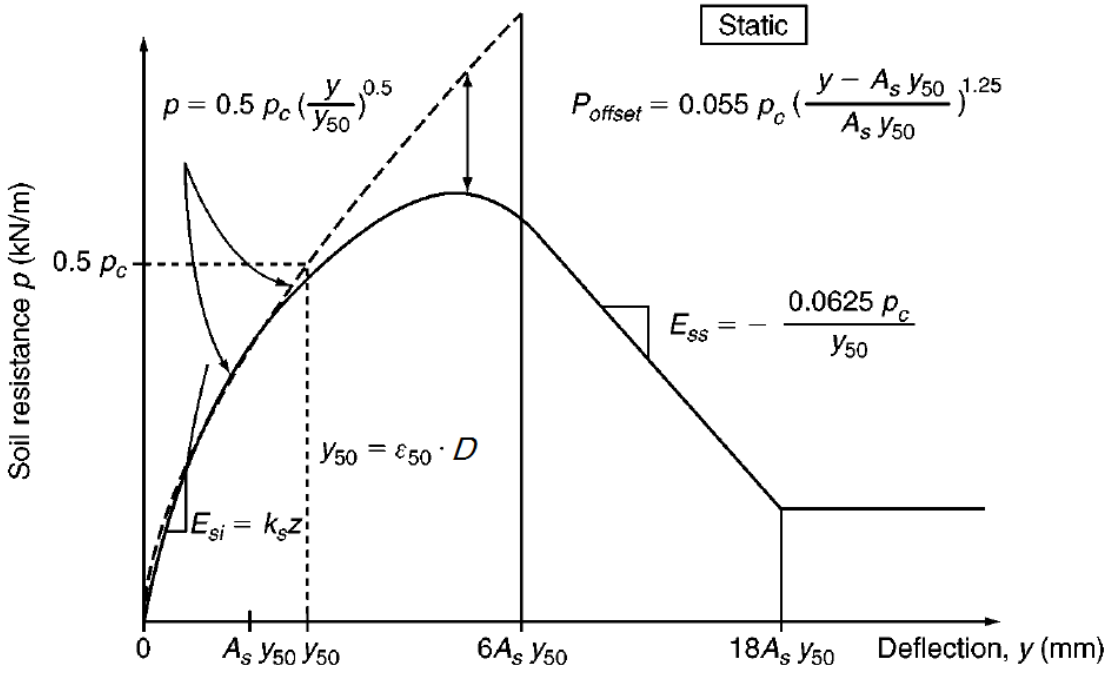

Figure 2.15: Formulation of p-y curves for static loading in stiff clay in the presence of free water (Reese et al., 1975).

Static loading

The characteristic shape of p-y curves for static loading in stiff clay in the presence of free water is depicted in Figure 2.15. The following steps are proposed for the formulation of the aforementioned p-y curves:

1. Obtain the best possible estimate of the undrained shear strength c_u and the submerged unit weight γ' with depth. Specify pile diameter D and depth z of the desired p-y curve.

2. Calculate the average undrained shear strength c_a over the depth z and the value c_u at the specific depth.

3. The ultimate lateral soil resistance p_c per unit length of the pile is computed according the equation below:

$$p_c = min\left[2c_aD + \gamma' Dz + 2.83c_az,\ 11c_uD\right] \tag{2.27}$$

4. Choose the appropriate value of A_s (static loading) from Figure 2.16 for the non-dimensional depth z/D of the desired p-y curve.

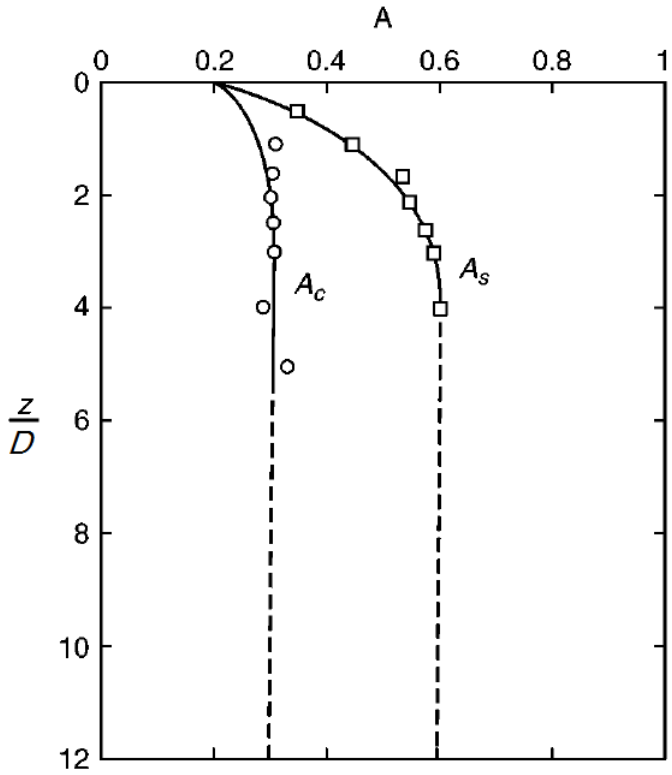

Figure 2.16: Values of constants A_s and A_c with non-dimensional depth z/D.

5. Form the initial straight-line portion of the p-y curve, using the appropriate value of k_s from Table 2.3.

$$p = (k_sz)\,y \tag{2.28}$$

6. Compute the displacement y_{50}, using an appropriate value of ε_{50} from results of undrained triaxial laboratory tests or - in absence of the latter - from Table 2.4.

$$y_{50} = \varepsilon_{50}D \tag{2.29}$$

Table 2.3: Representative values of k_{py} for overconsolidated clays.

	Average c_u (kPa)[1]		
	50-100	100-200	300-400
k_{pys}(static) MN/m^3	135	270	540
k_{pyc}(cyclic) MN/m^3	55	110	540

[1] The average shear strength should be computed from the shear strength of the clay to a depth of 5 pile diameters. It should be defined as half the total maximum principal stress difference in an unconsolidated undrained triaxial test.

Table 2.4: Representative values of ε_{50} for overconsolidated clays.

	Average c_u (kPa)		
	50-100	100-200	300-400
ε_{50}	0.007	0.005	0.004

7. Establish the first parabolic part of the p-y curve according to the following equation and obtaining p_c from Equation 2.27.

$$p = 0.5 p_c \left(\frac{y}{y_{50}}\right)^{0.5} \tag{2.30}$$

Equation 2.30 defines the portion of the p-y curve from the intersection point with Equation 2.28 to a point where $y = A_s y_{50}$ (see the note after Step 10).

8. Form the second parabolic part of the p-y curve:

$$p = 0.5 p_c \left(\frac{y}{y_{50}}\right)^{0.5} - 0.055 p_c \left(\frac{y - A_s y_{50}}{A_s y_{50}}\right)^{1.25} \tag{2.31}$$

Equation 2.31 defines the portion of the p-y curve from the point where $y = A_s y_{50}$ to a point where $y = 6A_s y_{50}$ (see the note after Step 10).

9. Establish the next straight-line portion of the p-y curve according to:

$$p = 0.5 p_c \left(6A_s\right)^{0.5} - 0.411 p_c - \frac{0.0625}{y_{50}} p_c \left(y - 6A_s y_{50}\right) \tag{2.32}$$

Equation 2.32 defines the portion of the p-y curve from the point where $y = 6A_s y_{50}$ to a point where $y = 18A_s y_{50}$ (see the note after Step 10).

10. Establish the final straight-line portion of the p-y curve according to:

$$p = p_c \left(1.225\sqrt{A_s} - 0.75A_s - 0.411\right) \tag{2.33}$$

Equation 2.33 defines the portion of the p-y curve for all points where $y \geq 18A_s y_{50}$ (see following note).

Note: The aforementioned step-by-step procedure and the corresponding Figure 2.15 premise an intersection between Equations 2.28 and 2.30. However, there may occur no intersection of Equation 2.28 with any of the rest equations defining the p-y curve. In that case, Equation 2.28 stands for the definition of the p-y curve until it intersects with one of the other equations.

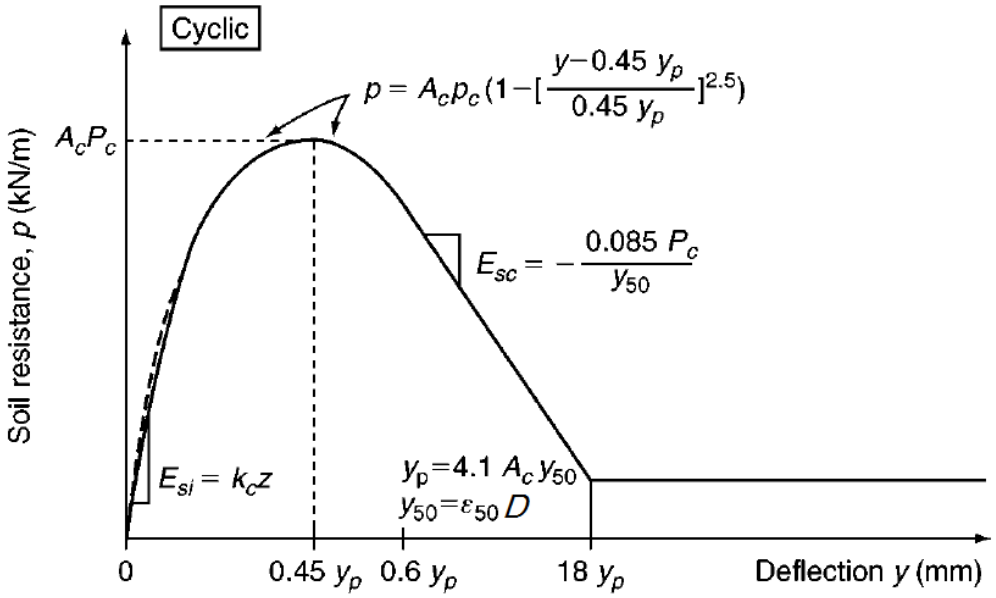

Figure 2.17: Formulation of p-y curves for cyclic loading in stiff clay in the presence of free water (Reese et al., 1975).

Cyclic loading

The characteristic shape of p-y curves for cyclic loading in stiff clay in the presence of free water is depicted in Figure 2.17. The following steps are proposed for the formulation of the aforementioned p-y curves:

1. Steps 1, 2, 3, 5 and 6 are identical to the ones described for static loading.

4. Choose the appropriate value of A_s (cyclic loading) from Figure 2.16 for the non-dimensional depth z/D of the desired p-y curve. Then, compute the expression:

$$y_p = 4.1 A_c y_{50} \tag{2.34}$$

7. Form the parabolic part of the p-y curve after the following:

$$p = A_c p_c \left[1 - \left| \frac{y - 0.45 y_p}{0.45 y_p} \right|^{0.25} \right] \tag{2.35}$$

   Equation 2.35 defines the portion of the p-y curve from the intersection point with Equation 2.28 to a point where $y = 0.6 y_p$ (see the note after Step 9).

8. Establish the next straight-line portion of the p-y curve according to:

$$p = 0.936 A_c p_c - \frac{0.085}{y_{50}} p_c \left(y - 0.6 y_p \right) \tag{2.36}$$

   Equation 2.36 defines the portion of the p-y curve from the point where $y = 0.6 y_p$ to a point where $y = 1.8 y_p$ (see the note after Step 9).

9. Establish the final straight-line portion of the p-y curve according to:

$$p = 0.936 A_c p_c - \frac{0.102}{y_{50}} p_c y_p \tag{2.37}$$

   Equation 2.37 defines the portion of the p-y curve for all points where $y \geq 1.8 y_p$ (see following note).

Note: The aforementioned step-by-step procedure and the corresponding Figure 2.17 premise an intersection between Equations 2.28 and 2.35. However, there may occur no intersection of Equation 2.28 with any of the rest equations defining the p-y curve. In that case, the equation that computes the smallest value of p for any value of y should be employed.

Stevens & Audibert (1979) proposed certain modifications on the ultimate lateral soil resistance and the lateral soil displacement y_{50} of p-y curves for soft (Matlock, 1970) and medium-to-stiff clays (Reese et al., 1975). Their recommendations were briefly described at the end of Paragraph 2.3.1.

2.4.3 Dunnavant and O'Neill (1989)

A p-y criterion was proposed by Dunnavant & O'Neill (1989) for laterally loaded piles in submerged, stiff clays. The model is particularly well-suited to large-diameter piles. Findings of the analyses by Gazioglu & O'Neill (1984) demonstrated that existing p-y curves for stiff clays below the water table, proposed by Reese et al. (1975) incorporated great uncertainty. This was attributed to the expansive nature of the stiff clay at Manor site (see Paragraph 2.4.2), in which the pile load tests of the corresponding p-y curves took place. Thus, a new set of full scale pile load

tests were performed and recommendations on the formulation of p-y curves for stiff clays were presented. Both static and cyclic pile load tests were carried out at the University of Houston Foundation Test Facility.

The soil properties of the test site correspond to a natural, overconsolidated, saturated, CL to CH clay. It is mentioned here that the pile load tests were performed in a 0.6m deep pit, flooded with water for the absolute saturation of the soil. The undrained shear strength of the clay - measured by unconsolidated (UU) and isotropically consolidated (CIU) undrained triaxial compression tests, as well as from cone penetration test (CPT) and field vane test results - was assumed to increase linearly from c_u=50kPa at the bottom of the test pit to c_u=135kPa at z=5.5m below the pit. Constant values of c_u=135kPa, 115kPa and 200kPa were attributed to soil depth ranges z=5.5-7.4m, 7.4-8.5m and 8.5-12.0m respectively. For the same depth range, values of $\varepsilon_{50} = 0.002 - 0.059$ were acquired from UU and CIU triaxial tests, indicating significant scatter among them. Therefore, the interpreted profile of ε_{50} depicted in Figure 2.18 was finally attributed to the clay.

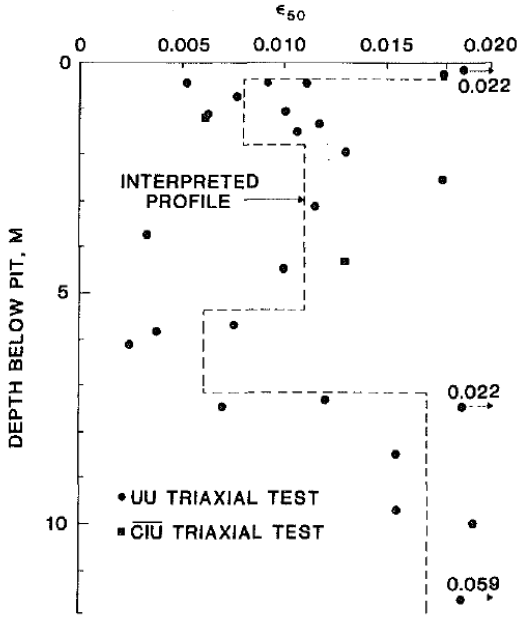

Figure 2.18: The profile of ε_{50} for the test site.

Three free-head piles of varying diameter and flexural stiffness were tested, instrumented with strain gauges for the measurement of bending moment along them. Piles 1 and 2 were open-ended, steel, driven piles, with length L=11.8m and 11.4m, diameter D=0.273m and 1.22m, wall thickness t=9.27mm and 15.9mm and flexural stiffness $E_pI_p = 138MNm^2$ and $358.6{\cdot}10^6MNm^2$ respectively. Pile 3 was a reinforced concrete, bored pile with length L=11.4m, diameter D=1.83m and flexural

stiffness $E_pI_p = 2.53 \cdot 10^7 MNm^2$ and $1.98 \cdot 10^7 MNm^2$ above and below 0.76m respectively. Piles 1 and 2 were driven into a pit that was flooded for five months prior to driving, while Pile 3 was bored in a dry area that was then excavated and flooded for eight months prior to testing. Most pile loads were applied using two-way displacement-controlled cycling, with cycle periods ranging from 1 to 100s.

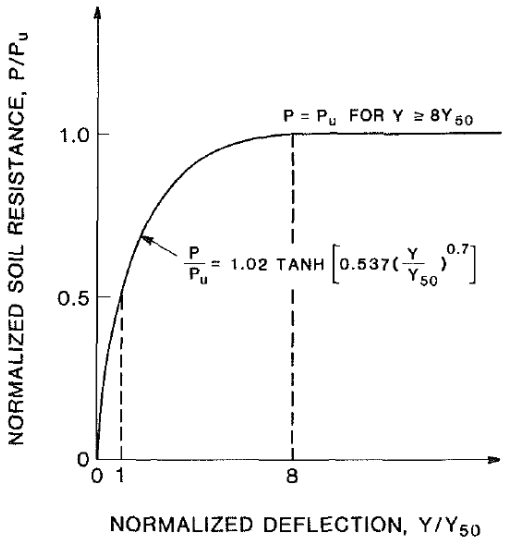

Figure 2.19: Typical shape of static p-y curves proposed by Dunnavant & O'Neill (1989) for submerged, stiff clays.

Static loading

The procedure described herein is for the formulation of p-y curves corresponding to short-term static lateral loading of the pile. Figure 2.19 demonstrates the shape and particular points of the proposed static p-y curves, as they were best fitted to the experimental results.

1. The ultimate lateral soil resistance p_u is expressed as:

$$p_u = N_p \, c_u \, D \tag{2.38}$$

where c_u= the undrained shear strength of the soil at the depth of the desired p-y curve, D= the pile diameter and N_p= the lateral bearing capacity factor.

2. The ultimate lateral soil resistance factor is calculated according to the following equation.

$$N_p = 2 + \frac{\sigma_v^{'}}{c_{ua}} + 0.4\frac{z}{D} \leq 9 \tag{2.39}$$

where σ_v'= the in situ vertical effective stress at the depth of the p-y curve and c_{ua}= the average undrained shear strength from the ground surface to depth

z. Although an upper limit of N_p=9 is set, the lateral bearing capacity factor never received values greater than 6 during the pile load tests. The investigators attribute this behavior to the inability of mobilizing ultimate lateral soil resistance p_u at significant depth due to limited lateral pile head displacement.

3. Compute the deflection y_{50} at one-half the ultimate soil resistance from the following equation:

$$y_{50} = 0.0063\ \varepsilon_{50} D K_R{}^{-0.875} \tag{2.40}$$

where ε_{50}= the axial strain corresponding to one-half the peak principal stress difference in an undrained triaxial compression test and K_R= the relative pile-soil stiffness (see following step).

4. Calculate the relative pile-soil stiffness from the equation:

$$K_R = \left(\frac{E_p I_p}{E_s L^4}\right) \tag{2.41}$$

where E_s= a strength correlated soil modulus, L= the pile length - limited numerically to the "critical pile length" $L_{cr} = 3D(E_p I_p / E_s D^4)^{0.286}$ (Gazioglu & O'Neill, 1984) - beyond which additional pile length affects negligibly the pile-head behavior. The introduction of K_R is supported by former analytical results reported by Baguelin et al. (1977), suggesting that the initial stiffness of the p-y curve increases with the increase of relative pile-soil stiffness.

5. The relationship combining the previous steps and describing the p-y curve is:

$$p = 1.02\ p_u\ \tanh\left[0.537\left(\frac{y}{y_{50}}\right)^{0.70}\right]\ ,\quad y \leq 8y_{50} \tag{2.42}$$

For values of lateral displacement $y > 8y_{50}$, the soil reaction p remains constant and equal to the ultimate lateral soil resistance p_u at the specific depth.

Cyclic loading

The instructions for the formulation of p-y curves, representative of cyclic lateral loading of piles in submerged, stiff clays, are summarized in the following steps. Figure 2.20 depicts the shape and particular points of the proposed cyclic p-y curves. Indexes 'cm' and 'r' refer to the peak and residual lateral soil reaction during cyclic loading of the pile respectively.

1. The peak cyclic lateral soil resistance p_{cm} is expressed as:

$$p_{cm} = N_{cm}\ c_u\ D \tag{2.43}$$

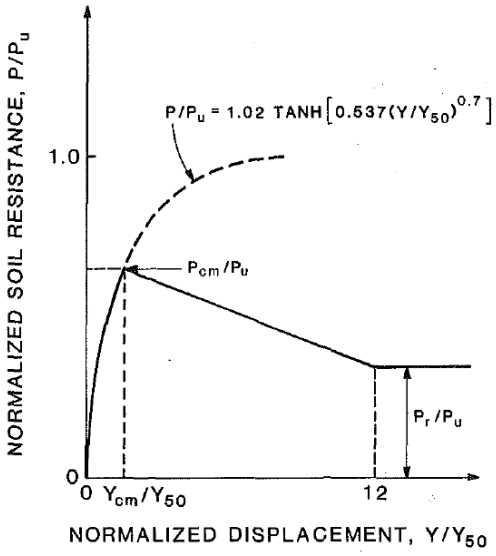

Figure 2.20: Typical shape of cyclic p-y curves proposed by Dunnavant & O'Neill (1989) for submerged, stiff clays.

2. The ratio of the cyclic to the static ultimate lateral soil resistance factor N_{cm}/N_p is calculated according to the following equations, either for 100 load cycles or for a random number of cycles N.

$$\frac{N_{cm}}{N_p} = 0.1 + 0.36\frac{z}{z_o} \leq 0.76 \quad (100 \text{ load cycles}) \tag{2.44}$$

$$\left(\frac{N_{cm}}{N_p}\right)_N = 1 - \left(0.45 - 0.18\frac{z}{z_o}\right) logN \leq 1 \quad (N \text{ load cycles}) \tag{2.45}$$

where z= the depth of the p-y curve and z_o=1m.

3. Cyclic lateral soil reaction p builds up to p_{cm} according to Equation 2.42. Attention!: The ultimate lateral soil resistance p_u still refers to static loading and is calculated from Equation 2.38.

4. The ratio of the residual to the peak cyclic lateral soil resistance p_r/p_{cm} is calculated according to the following equations, either for 100 load cycles or for a random number of cycles N. The residual cyclic lateral soil reaction p_{cm} is reached for a lateral displacement $y = 12y_{50}$ according to the current methodology (Figure 2.20).

$$\frac{p_r}{p_{cm}} = 0.5 + 0.14\frac{z}{z_o} \leq 1 \quad (100 \text{ load cycles}) \tag{2.46}$$

$$\left(\frac{p_r}{p_{cm}}\right)_N = 1 - \left(0.25 - 0.07\frac{z}{z_o}\right) logN \leq 1 \quad N \text{ load cycles}) \tag{2.47}$$

For values of lateral displacement $y > 12y_{50}$, the soil reaction p remains constant and equal to the residual cyclic lateral soil resistance p_r at the specific depth. It is important to point out the cycle-dependent form of the cyclic criterion, implying that degradation of the lateral soil response continues with increasing number of cycles.

2.5 Unified p-y curves for clays

2.5.1 Det Norske Veritas -DNV- (1977)

The current Norwegian Regulations for the design of offshore structures (DNV, 2010) adopt the methodology proposed by Matlock (1970) for the formulation of p-y curves for cohesive soils. However, an older version of Det Norske Veritas (DNV, 1977) introduced its own procedure for the construction of p-y curves in clays, both for static and cyclic laterally loaded piles. The proposed methodology mainly refers to offshore piles with diameter typically between D=1.0 and 1.5m. Prior to any design attempt for the laterally loaded piles, the regulations recommend a thorough investigation of the soil properties in both lateral and vertical directions down to a depth of at least 10 pile diameters.

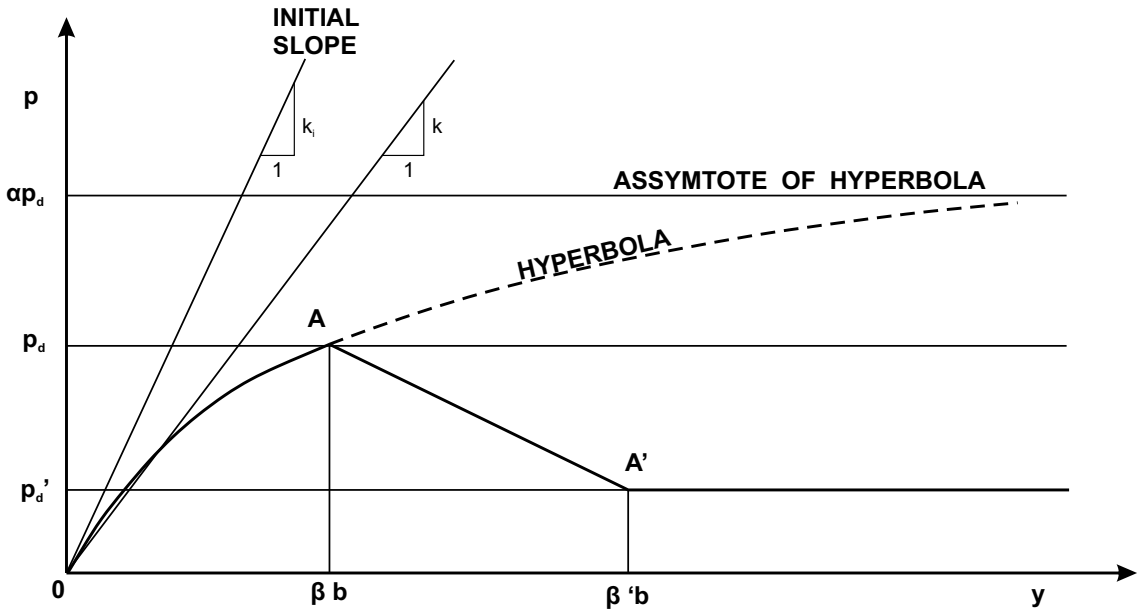

Figure 2.21: Typical form of the p-y curves proposed by DNV (1977).

The steps for the formulation of p-y curves applying for static and cyclic lateral loading of piles in clay according to the current methodology are described through the following procedure:

1. Calculate the peak design lateral soil resistance pressure p_d - either static (p_{ds}) or cyclic (p_{dc}) - from the equation:

$$p_d = N_p \frac{c_u}{\gamma_{mc}} \tag{2.48}$$

where c_u= the characteristic undrained shear strength[1] of the soil at depth z of the desired p-y curve, representing the loading conditions of the design (static or cyclic), γ_{mc}= a material coefficient for plastic analysis of the pile, otherwise γ_{mc}=1.0, and N_p= a lateral bearing capacity factor increasing linearly with depth from 1 (static) or 0 (cyclic) at ground surface to 8 at a depth of $10D$ or $5D$ below mudline, for normally consolidated and overconsolidated clays respectively.

2. The residual design lateral soil resistance pressure $p_d^{'}$ - either static $p_{ds}^{'}$ or cyclic $p_{dc}^{'}$ - is determined from Equation 2.48, by using a residual value of the undrained shear strength c_{ur} instead of c_u. Therefore, the static laboratory tests have to be carried out to significantly large strains, enough to define the aforementioned residual strength c_{ur}. In absence of laboratory test results for c_{ur}, the current methodology suggests c_{ur}/c_u (static) and c_{ur}/c_{uc} (cyclic) residual to peak strength ratios increasing linearly with depth from 0.25 at ground surface to 0.5 at a depth of $10D$ or $5D$ below mudline, for normally consolidated and overconsolidated clays respectively. These recommendations may be either conservative for some clays or unsafe for others, indicating the need for laboratory tests in order to determine c_{ur}.

3. Calculate the initial straight-line portion of the p-y curve, using the following equation:

$$k_i = \xi \frac{p_d}{D\ (\varepsilon_{50})^{0.25}} \tag{2.49}$$

where D= the pile diameter, p_d= the peak design lateral soil resistance pressure

[1]For the determination of the characteristic undrained shear during the design of offshore piles that shall withstand cyclic loads, DNV (1977) recommend: undrained cyclic triaxial or simple shear tests on soil samples consolidated to the in situ stress field and a static undrained test on the same sample after completion of the cyclic. This cyclic shear strength is termed c_{uc} and by substituting c_u in Equation 2.48 it calculates the peak design lateral soil resistance pressure p_{dc} for cyclic loading. For piles subjected to pure static loading, the aforementioned cyclic part of the laboratory tests is omitted. Thus, the peak design lateral soil resistance pressure p_{ds} for static loading is calculated.

- either static (p_{ds}) or cyclic (p_{dc}), ε_{50}= the axial strain corresponding to one-half the maximum principal stress difference and ξ= an empirical coefficient depending on the overconsolidation ratio (OCR) of the clay, obtained from Table 2.5.

Table 2.5: Recommended values for coefficients ξ, β and β' for clay.

Parameter	Load type	Type of clay[1]	
		Normally consolidated	Over-consolidated
ξ	Static	10	30
β	Static	20 ε_{50}	5 ε_{50}
β'	Static	80 ε_{50}	8 ε_{50}
ξ	Cyclic	10	30
β	Cyclic	7.5 ε_{50}	2.5 ε_{50}
β'	Cyclic	20 ε_{50}	5 ε_{50}

[1] In case of a slightly overconsolidated clay, the set of parameters leading to the most conservative response shall be used.

4. The proposed p-y curve for clayey soils consists of three parts, as depicted in Figure 2.21:

   - For $p \leq p_d$ and $y \leq \beta D$ the curve is described by the hyperbola:

   $$\frac{y}{p} = \frac{1}{k_i} + \frac{y}{\alpha\, p_d} \tag{2.50}$$

   - For $\beta D < y \leq \beta' D$ the curve is formed by a linear part from point A to point A', corresponding to the transition from peak (p_d) to residual lateral soil resistance pressure p'_d.
   - For $y > \beta' D$ no further reduction in lateral soil resistance is assumed, thus $p = p'_d$.

   Coefficients β and β' depend on the overconsolidation ratio (OCR) of the clay and the loading conditions of the pile (static or cyclic) and are obtained from Table 2.5. For $\beta D \leq p_d/k_i$ the hyperbola may be replaced by a straight line.

5. The intersection point A between the hyperbola and the following linear part of the p-y curve is related to coefficient α, which for $p = p_d$ and $y = \beta D$ in Equation 2.50 becomes:

$$\alpha = \frac{1}{1 - \dfrac{p_d}{k_i \ \beta \ D}} \tag{2.51}$$

2.5.2 Sullivan et al. (1979)

The current section describes the attempt of Sullivan et al. (1979) to unify the aforementioned methodologies by Matlock (1970) and Reese et al. (1975) in a single set of proposed p-y curves for clayey soils. Based on the satisfactory agreement of the analytical predictions with the experimental results of laterally loaded piles in both types of clay, the unified p-y curves perform quite satisfactorily. According to Sullivan's remarks, the proposed method is applicable to cases of short term and repeated loading and can be utilized for the analysis of piles of any geometry, stiffness and pile head fixity conditions.

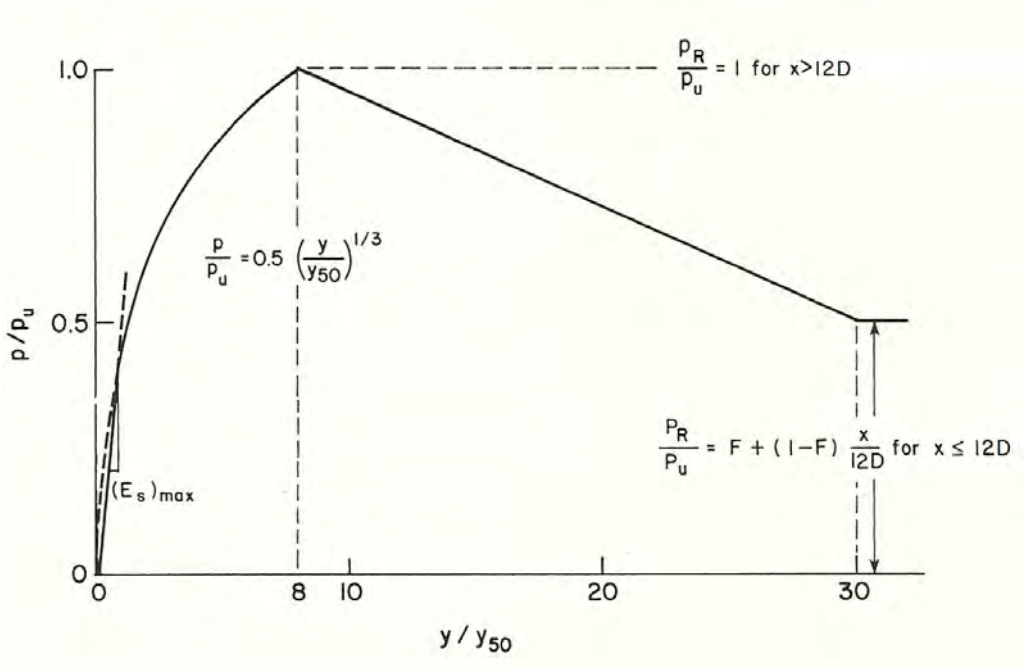

Figure 2.22: Formulation of p-y curves for static loading with unified clay criteria (Sullivan et al., 1979).

Static loading

The procedure described herein is for the formulation of unified p-y curves corresponding to short-term static lateral loading of the pile. Figure 2.22 demonstrates the shape and particular points of the proposed static p-y curves.

1. The ultimate soil resistance per pile unit length is calculated according to the following expression:

$$p_u = min \left[\left(2 + \frac{\gamma'}{(c_u)_{avg}} z + \frac{0.833}{D} z \right) (c_u)_{avg} D, \left(3 + \frac{0.5}{D} z \right) c_u D, \ 9 c_u D \right] \tag{2.52}$$

where γ'= average effective unit weight from the ground surface to the depth of the derived p-y curve, z= depth from the ground surface to the p-y curve depth, $(c_u)_{avg}$= average undrained shear strength above depth z and c_u= undrained shear strength at depth z. The general idea of the aforementioned expression was to incorporate ultimate lateral clay resistance values with depth that were suggested by various experimental and theoretical studies prior to the proposal of the unified p-y curve methodology. Suggestions on the ultimate lateral soil resistance factor $N_p = p_u/(c_u D)$ were gathered for three representative depths, namely at ground surface, at $z = 3D$ and $12D$. The proposed relationship for p_u takes these observations into account.

2. The initial part of the p-y curve is linear and is described by the equation:

$$p = (E_s)_{max} y \tag{2.53}$$

where $(E_s)_{max}$ is the limiting maximum value of the soil Young's modulus. If $(E_s)_{max}$ is not defined experimentally, it can be computed through the equation:

$$(E_s)_{max} = kz \tag{2.54}$$

with representative values of k - dependent on the in situ undrained shear strength c_u - according to Table 2.6.

3. The displacement y_{50} is calculated according to the following equation:

$$y_{50} = A \, \varepsilon_{50} \, D \tag{2.55}$$

with values of ε_{50} obtained either from undrained triaxial tests or from Table 2.7. The estimation of parameter A is discussed at the end of the current methodology.

4. The first curved portion of the p-y curve - after the initial linear one - is formed

Table 2.6: Representative values of k for unified p-y curves after Sullivan et al. (1979).

c_u (kPa)	k (MN/m^3)
12 - 25	8
25 - 50	27
50 - 100	80
100 - 200	270
200 - 400	800

Table 2.7: Representative values of ε_{50} for unified p-y curves after Sullivan et al. (1979).

c_u (kPa)	ε_{50}
12 - 25	0.02
25 - 50	0.01
50 - 100	0.007
100 - 200	0.005
200 - 400	0.004

according to equation:

$$\frac{p}{p_u} = 0.5\left(\frac{y}{y_{50}}\right)^{1/3} \tag{2.56}$$

that is identical to Equation 2.9 recommended by Matlock (1970).

5. The lateral soil resistance after large deformation is computed by the minimum of the two following equations.

$$p_R = p_u\left[F + (1-F)\frac{z}{12D}\right] \quad \text{for} \quad z < 12D \tag{2.57a}$$

$$p_R = p_u \quad \text{for} \quad z > 12D \tag{2.57b}$$

The estimation of parameter F depends on the stress-strain characteristics of the soil and will be discussed at the end of the current methodology. The selection of $y = 30y_{50}$ as the lateral displacement, at which the residual resistance is reached, as well as the increase of p_R/p_u with depth are not justified in the study of Sullivan et al. (1979). However, the shape of the proposed p-y curves (Figure

2.22) was applied in the analytical solution and the calculated values along the piles came in good agreement with the ones acquired from the experiments.

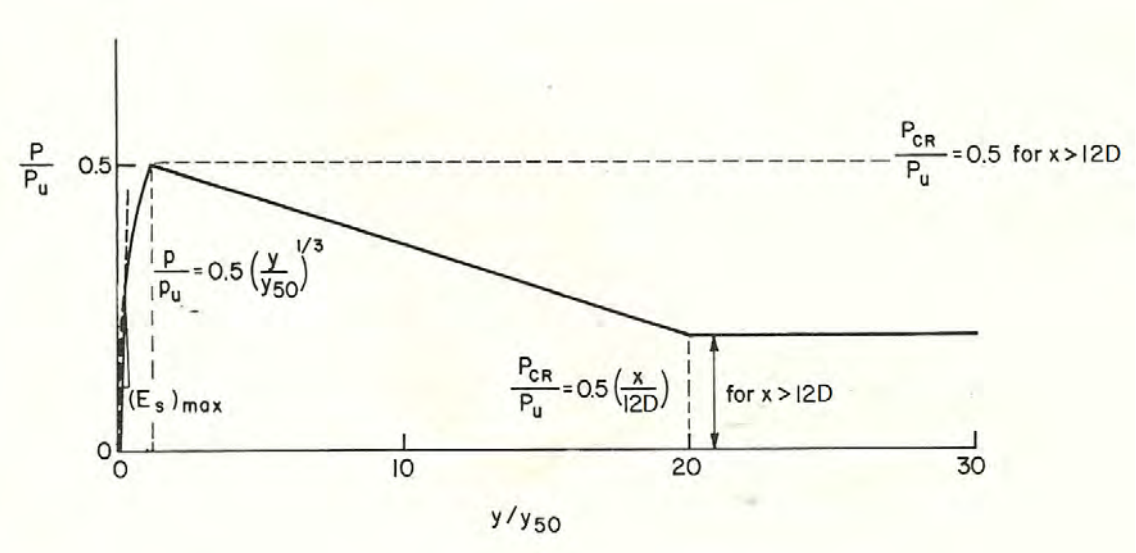

Figure 2.23: Formulation of p-y curves for cyclic loading with unified clay criteria (Sullivan et al., 1979).

Cyclic loading

Figure 2.23 demonstrates the shape and particular points of the proposed unified p-y curves corresponding to cyclic lateral loading of the pile. According to Sullivan et al. (1979), the recommended shape is completely empirical and has features consistent with the recommendations of Matlock (1970) for cyclic p-y curves. The efficiency of the proposed cyclic p-y curves is validated against measured values along test piles of full scale experiments.

Equations 2.55 and 2.57a for the definition of the static p-y curve contain the parameters A and F. These were determined empirically from results of load tests at Sabine (Matlock, 1970) and Manor (Reese et al., 1975) and are given in Table. The specific table also includes information on other soil parameters such as the overconsolidation ratio (OCR), the sensitivity (S_t), the liquidity limit (w_L), the plasticity index (PI) and the liquidity index (LI). In order to estimate parameters A and F for any given clay, the author of this unified methodology recommends the following procedure:

(a) Determine as many of the following properties of the clay as possible: c_u, ε_{50}, OCR, w_L, PI, LI, degree of saturation, degree of fissuring, failure from stress-strain curves and ratio of residual to peak strength.

(b) Compare the properties of the soil in question with the properties of the clays at Sabine and Manor site listed in Table 2.8.

(c) If the properties are similar to either the Sabine or Manor clay properties, use A and F corresponding to these two soil profiles. Otherwise, estimate A and F using engineering judgement and Table 2.8 for guidance.

Table 2.8: Curve parameters A and F for the unified p-y curves.

Site	Sabine River	Manor
Clay description	inorganic, intact $(c_u)_{avg} = 15kPa$ $\varepsilon_{50} = 0.007$ $OCR \approx 1$ $S_t \approx 2$ $w_L = 92$ $PI = 68$ $LI = 1$	inorganic, very fissured $(c_u)_{avg} = 115kPa$ $\varepsilon_{50} = 0.005$ $OCR > 10$ $S_t \approx 1$ $w_L = 77$ $PI = 60$ $LI \approx 0.2$
A	2.5	0.35
F	1.0	0.5

Note: The aforementioned procedures for the unified p-y curves in clays (Figures 2.22 and 2.23) assume an intersection between Equations 2.53 and 2.56. If no such intersection occurs, the p-y curve is computed by Equation 2.53 until there is an intersection with the equations defining the p-y curve at greater lateral pile displacements.

2.5.3 Wu et al. (1998)

The recommendations of Wu et al. (1998) on the design of static laterally loaded piles in cohesive soils include a thoroughly described process for the formulation of corresponding p-y curves. The proposed hyperbolic p-y criterion is based on results from lateral pile load tests in Shanghai, PRC that were carried out in a medium stiff clay. This research aimed to improve former design methods using p-y curves for clayey soils.

In more detail, the test site was located on the left bank of Huangpu River with a soil profile consisting of stiff, fissured, overconsolidated clay in the upper 4m and of stratified, stiff, silty clay below that. The water table was always above the bottom of the test trenches, thus simulating fully saturated soil conditions. The undrained shear strength of the clay was measured by unconsolidated (UU) and anisotropically consolidated (ACU) undrained triaxial compression tests in the laboratory, as well as from cone penetration tests (CPT), field vane tests and pressuremeter tests in situ. Results from the laboratory and the vane tests together with the assumed undrained shear strength distribution with depth are depicted in Figure 2.24. The in situ coefficient of the horizontal geostatic stress ranged between K_o=0.55-0.60. The strain ε_{50} at half the failure stress of the investigated soil samples was measured between 0.0143 and 0.0170.

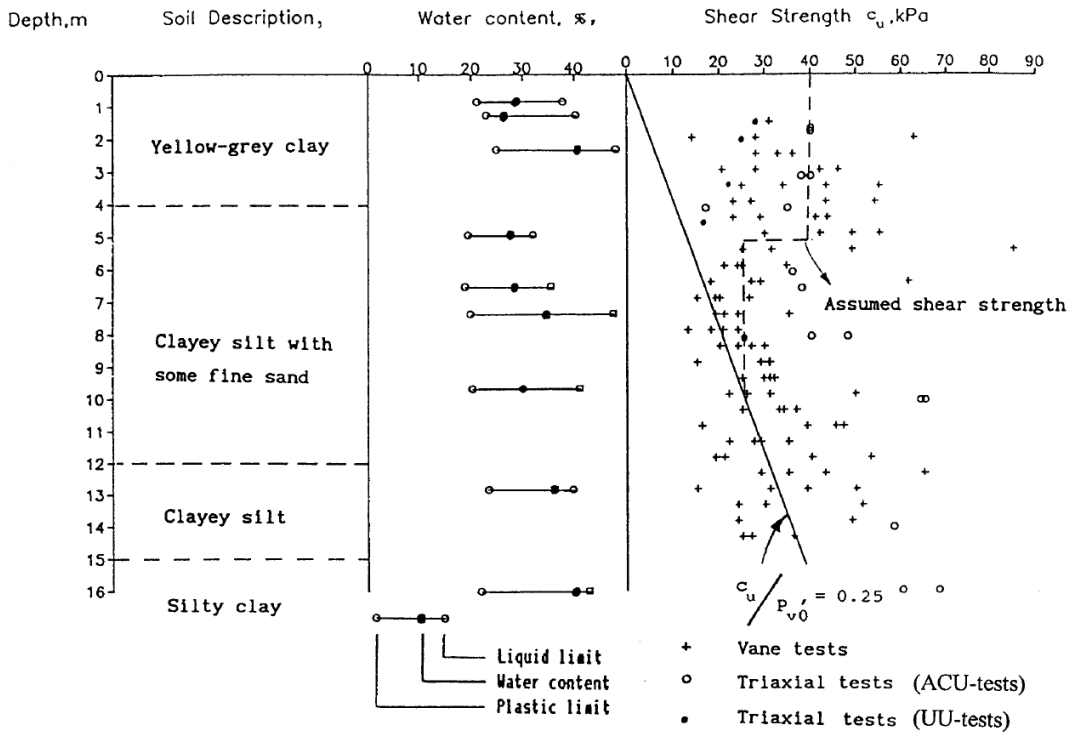

Figure 2.24: Soil profile at the Huangpu River test site.

The pile load tests involved steel pipes with diameter D=0.09-0.60m, wall thickness t=4-10mm and pile stiffness E_pI_p=0.182-153.3MNm^2. All the piles were equipped with strain gauges and had sufficient embedded length to behave as infinitely long during lateral loading. Moreover, the bottom of the test piles was sealed to prevent water and soil from entering the pipe during driving. A hydraulic jack applied the lateral load on the pile head in ten increments, keeping it constant for 10 to 60

minutes depending on the load level - as recommended by ASTM (D3966-81).

The hyperbolic shape of p-y curves that is described in the following procedure, fitted best to the pile load test results. Before processing with the proposed p-y curves, two new parameters referring to the soil deformation are introduced. Parameters $\beta = \varepsilon_{100}/\varepsilon_{50}$ (for stress-strain curves) and $\beta^{'} = y_{100}/y_{50}$ (for p-y curves) are used to express the strain and displacement ratio of the total to half the soil failure stress respectively. The steps for the formulation of p-y curves applying for static laterally loaded piles in cohesive soils according to the current methodology are described through the following procedure:

1. The ultimate lateral soil resistance p_u is calculated as:

$$p_u = N_p \; c_u \; D \tag{2.58}$$

where D= the pile diameter, N_p= a lateral bearing capacity factor increasing linearly with depth from 2 to 3 at ground surface to 9 to 11 at a depth of $4D$ to $5D$ and c_u= the undrained shear strength of the soil at the depth of the desired p-y curve. The engineer needs to evaluate the derived p_u values and potentially reduce the estimated undrained shear strength when the clay is overconsolidated, according to Table 2.9.

Table 2.9: Recommended reduction of the undrained shear strength c_u.

OCR	Triaxial tests UU-tests	Field vane tests	CPTs
1 - 2	0	0	0
2 - 8	15%	50%	25%
> 8	30%	75%	50%

2. Calculate the lateral soil displacement y_{50} at half the ultimate lateral soil resistance p_u according to the equation:

$$y_{50} = A \; \varepsilon_{50} \; D \tag{2.59}$$

where $A = N_p$ for normally consolidated clays and $A = 0.77N_p$ for heavily overconsolidated clays, as depicted in Figure 2.25.

3. Determine the coefficient β from undrained triaxial tests (UU-, CU- or ACU-tests). Otherwise, assume β=8 for soft clay, β=9 for medium stiff clay and β=11-12 for stiff clay.

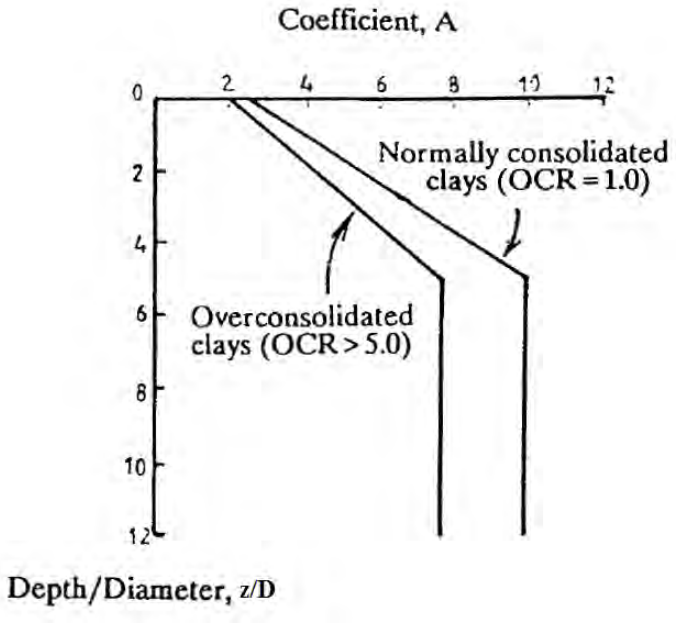

Figure 2.25: Coefficient A with dimensionless depth z/D and overconsolidation ratio OCR of the clay.

4. The proposed static p-y curve including the aforementioned parameters and assuming that $\beta' = \beta$ is:

$$\frac{p}{p_u} = \frac{y/y_{50}}{\dfrac{\beta'}{\beta'-1} + \dfrac{\beta'-2}{\beta'-1}\, y/y_{50}} \tag{2.60}$$

The p-y criteria proposed by Wu et al. (1998) were applied to the large-scale pile load tests carried out by Matlock (1970) at Lake Austin and Sabine and by Reese et al. (1975) at Manor. The results of maximum bending moment along the pile and pile head displacement predicted with the current methodology are compared with the corresponding measurements of the piles tested at the aforementioned sites in Figures 2.26 and 2.27. The comparison demonstrates a very satisfactory agreement between the predictions of the p-y criteria by Wu et al. and the test measured curves.

A certain modification process on the p-y curves by Wu et al. was proposed by Dewaikar et al. (2009), referring to laterally loaded piles in stiff clays both under static and cyclic loading conditions. In more detail, the following modifications were proposed for p-y curves in stiff clays:

1. The lateral bearing capacity factor N_p is calculated as:

$$N_p = 1.298A \quad \text{with } A = 0.9 + 1.1727\frac{z}{D} \tag{2.61}$$

For the calculation of the ultimate lateral soil resistance (Equation 2.58) use the average undrained shear strength c_u up to the depth of the desired p-y curve.

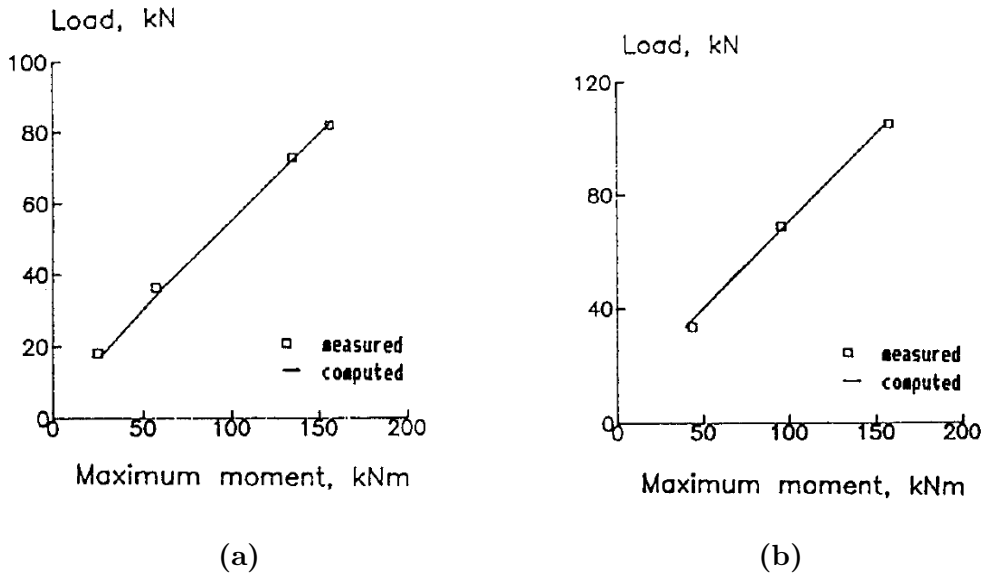

Figure 2.26: Measured (Matlock, 1970) versus computed (Wu et al., 1998) maximum bending moment along the pile tested at (a) Lake Austin and (b) Sabine site.

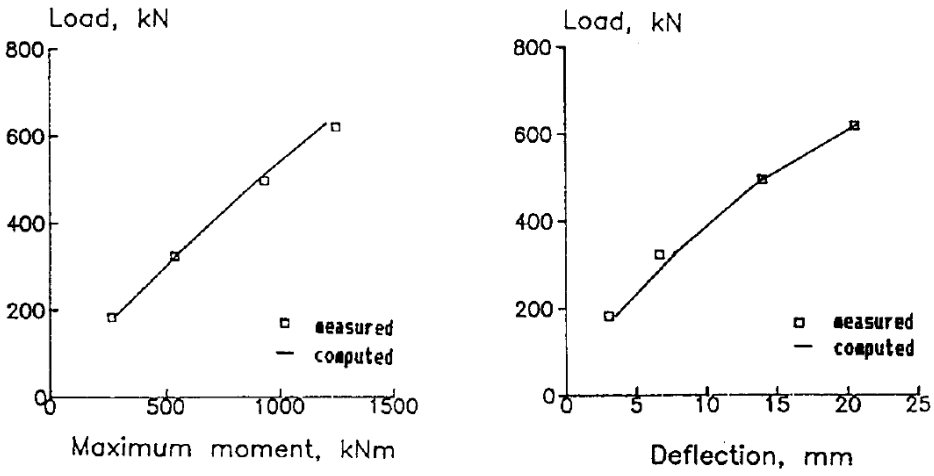

Figure 2.27: Measured (Reese et al., 1975) versus computed (Wu et al., 1998) maximum bending moment and pile head deflection at Manor site.

2. The lateral displacement y_{50} is calculated as:

$$y_{50} = \varepsilon_{50}\ D \tag{2.62}$$

with ε_{50} retrieved from Table 2.4 in absence of corresponding data from undrained triaxial tests.

3. Determine coefficient β from undrained triaxial tests. Assume β=9 for medium stiff clay and β=11 to 12 for stiff clay in absence of triaxial test data.

4. The modified p-y curve expression proposed by Dewaikar et al. (2009) is:

$$\frac{p}{p_u} = \frac{\alpha_1\, B\, y/y_{50}}{\dfrac{\beta' - 1.6}{\beta' + \alpha_2} + \dfrac{\beta' - 1}{\beta'}\, y/y_{50}} \tag{2.63}$$

where α_1 and α_2 are constants differing for static and cyclic loading and B is a coefficient depending on y and y_{50}.

$$log(B) = 0.004 \left(\frac{y}{y_{50}}\right)^2 - 0.157 \left(\frac{y}{y_{50}}\right) + 0.087 \tag{2.64}$$

For static loading: $\alpha_1 = 1.71B$ and $\alpha_2 = 2$. For cyclic loading: $\alpha_1 = 0.65C$ and $\alpha_2 = 0.5$, with $C = 0.55B$ for $y < 0.6y_{50}$ and $C = 0.033$ for $y \geq 0.6y_{50}$.

2.5.4 Georgiadis (2010)

The methodology proposed by Georgiadis & Georgiadis (2010) refers to the static undrained lateral response of piles, without separating soft from stiff clay conditions. Thus, it is presented in the current section together with other unified p-y curves for clays. The study refers to the effect of sloping ground on the undrained response of laterally loaded piles. However, a framework of static p-y curves for the case of horizontal ground surface is initially proposed. This framework is described in the current section. The following recommendations on the formulation of p-y curves for clays were derived from sophisticated FEA, the features of which are presented herein. The finite element software Plaxis 3D Foundation V2.2 was used for a variety of geometrical pile characteristics and soil properties.

In particular, the soil was simulated as a linear elastic - perfectly plastic Tresca material. Since the loading was undrained, Poisson's ratio $\nu_u = 0.49$ was assigned to the clay. The majority of the numerical analyses were carried out with undrained shear strength c_u =50kPa constant with depth, submerged unit weight

$\gamma = 18kN/m^3$ and ratio of the undrained elasticity modulus to the undrained shear strength E_u/c_u =200. The effect of the aforementioned clay parameters on the derived p-y curves was studied with values ranging between:

- c_u=25-100kPa for the undrained shear strength
- γ=16-20kN/m^3 for the submerged unit weight and
- E_u/c_u=100-400 for the ratio of the undrained elasticity modulus to the undrained shear strength.

Two pile lengths $L = 12$m and 20m and three pile diameters $D = 0.5$m, 1m and 2m were simulated in the FEA. The pile material was assumed linearly elastic with a Young's modulus $E_p = 2.9 \cdot 10^7$kPa and Poisson's ratio $\nu_p = 0.1$. Potential pile-soil separation was simulated by assigning zero tensile strength to a thin zone of 10cm around the pile. In addition, the limiting pile-soil adhesion was assumed $\tau = \alpha c_u$, with three adhesion factor values $\alpha = 0.3, 0.5$ and 1 taken into account for the interface. The steps for the formulation of p-y curves applying for static laterally loaded piles in clay according to the current methodology are described through the following general instructions:

1. The ultimate lateral soil resistance p_u depends on the type of failure mechanism developed in front of the pile - wedge type or plane strain failure - and is expressed as:

$$p_u = N_p \; c_u \; D \tag{2.65}$$

where c_u= the undrained shear strength of the soil at the depth of the desired p-y curve, D= the pile diameter and N_p= a lateral bearing capacity factor increasing from a value N_{po} at ground surface to a maximum value N_{pu} at greater depth according to the following equation for horizontal ground surface:

$$N_p = N_{pu} - (N_{pu} - N_{po})\, e^{-\lambda(z/D)} \tag{2.66}$$

The ultimate bearing capacity factor N_{pu} is calculated according to the lower bound solution of Randolph & Houlsby (1984) from the following equation:

$$N_{pu} = \pi + 2\Delta + 2\cos\Delta + 4\left(\cos\frac{\Delta}{2} + \sin\frac{\Delta}{2}\right) \tag{2.67}$$

where $\Delta = \sin^{-1}\alpha$. Output from the FEA showed that factors N_{po} and λ are also expressed as linear functions of the pile-soil adhesion factor α:

$$N_{po} = 2 + 1.5\alpha \tag{2.68}$$

$$\lambda = 0.55 - 0.15\alpha \tag{2.69}$$

Factors N_{pu}, N_{po} and λ depend on the friction developed on the pile-soil interface. For undrained loading of clays, the ultimate shear stress developed between the pile and the soil is commonly calculated as the product of the in situ undrained shear strength c_u and the adhesion factor α. The latter varies from 1 for soft clays to 0.3 for very stiff clays with higher c_u. Another approach on the adhesion factor associates $\alpha = 1$ with rough pile-soil interaction, while $\alpha = 0.3$ refers to a smooth one. This methodology suggests the usage of a lower bound for the adhesion factor α recommended by various studies on axially loaded piles, as depicted in Figure 2.28.

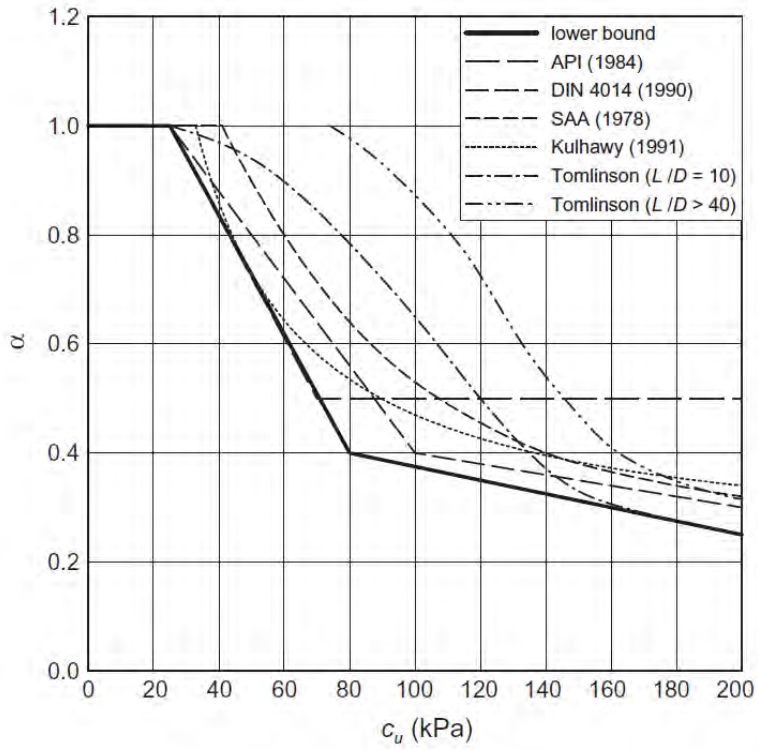

Figure 2.28: Adhesion factor α with the undrained shear strength c_u for axially loaded piles.

2. The initial stiffness K_i of the p-y curves for level ground is related to the soil elasticity modulus E_{50} at 50% the failure stress, the pile diameter D and the pile bending stiffness E_pI_p according to the following equation:

$$K_i = 3E_{50}\left(\frac{E_{50}D^4}{E_pI_p}\right)^{1/12} \tag{2.70}$$

The methodology claims that according to Equation 2.70 and to the FEA results, pile diameter D is rather insignificant for the estimation of the initial stiffness K_i of the p-y curves.

3. The hyperbolic relationship combining the previous steps and describing the p-y curve is:

$$p = \frac{y}{\frac{1}{K_i} + \frac{y}{p_u}} \tag{2.71}$$

The p-y criteria proposed by Georgiadis & Georgiadis (2010) were applied to some well documented large-scale pile load tests, among which the tests carried out by Matlock (1970) at Lake Austin and Sabine and the ones reported by Wu et al. (1998) in Shanghai. The results of pile head load-displacement curves $y_o - H_o$ predicted with the current methodology and other literature p-y curves are compared in Figure 2.29 with the corresponding measurements of three piles tested in Shanghai. The comparison demonstrates a very satisfactory agreement between the predictions of the p-y criteria by Georgiadis K. & M. and the test measured load-displacement curves. Similar observations are drawn from the comparisons concerning the rest of the pile load tests.

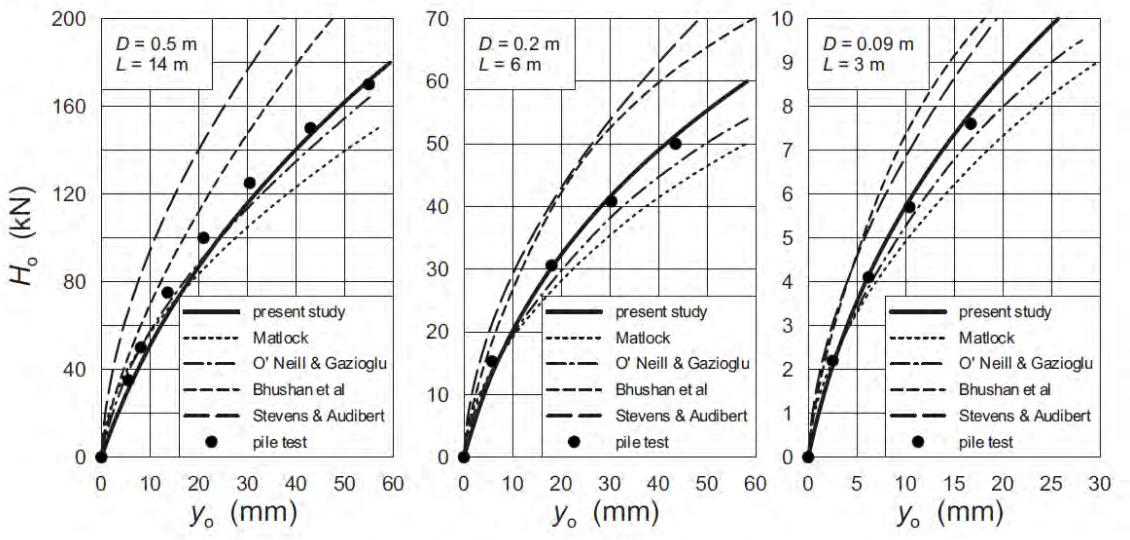

Figure 2.29: Comparison of Georgiadis & Georgiadis (2010) and other literature p-y criteria predictions with measured load-displacement curves for three test piles in Shanghai (Wu et al., 1998).

2.5.5 Jeong et al. (2011)

A complete methodology for the formulation of p-y curves applied to static laterally loaded piles in clayey soils was presented by Jeong et al. (2011), based on results from large-scale field tests and laboratory model tests. More accurately, four pile load tests were carried out at the Incheon bridge site (Korea) and four more in the Geotechnical Testing Lab (Yonsei University, Korea). The field of the large-scale pile tests consisted mainly of normally to lightly overconsolidated marine clay with undrained shear strength c_u=18kPa and 42kPa and axial strain corresponding to one-half the maximum principal stress difference ε_{50}=0.02 and 0.01 for the upper and the lower layer respectively. Silty clay, residual soil, weathered rock and soft rock were met in the borehole specimen close to the test site and below the aforementioned marine clay layers. Two pile types were imposed to static lateral load tests at the site (Figure 2.30): driven steel-pipe piles with diameter D=1.02m, wall thickness t=16.0mm, length L=26.6m (1m above ground surface) and bending stiffness $E_pI_p = 1.26 \cdot 10^6 kNm^2$ and a drilled concrete shaft with diameter D=2.4m, length L=44.3m (9.1m above ground surface) and bending stiffness $E_pI_p = 42.35 \cdot 10^6 kNm^2$.

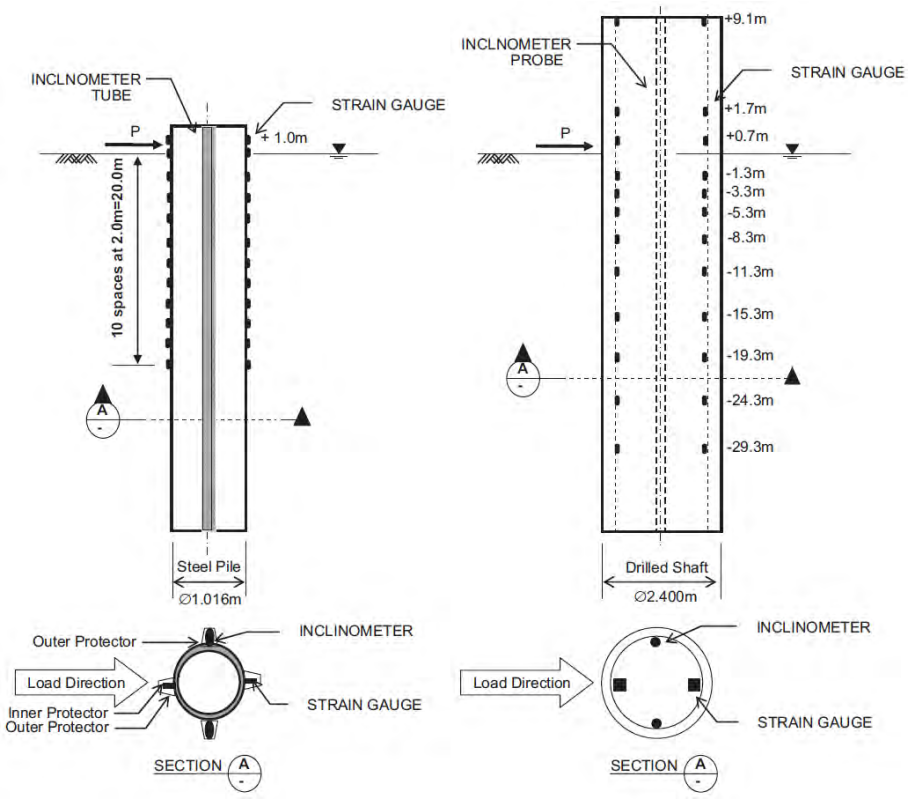

Figure 2.30: Vertical and horizontal sections of the steel driven piles (left) and the drilled concrete shaft (right) subjected to lateral load tests at the Incheon bridge site.

Two 32mm-diameter aluminium model piles with a hollow circular cross-section,

one 450mm and another 600mm long, were tested in the laboratory pit (Figure 2.31). Two different soil profiles were prepared in the lab test pit, one with c_u=18kPa and another with 42kPa, thus imitating both marine clay layers of the field site and simulating either flexible or rigid pile behavior combined with the two aforementioned model pile lengths.

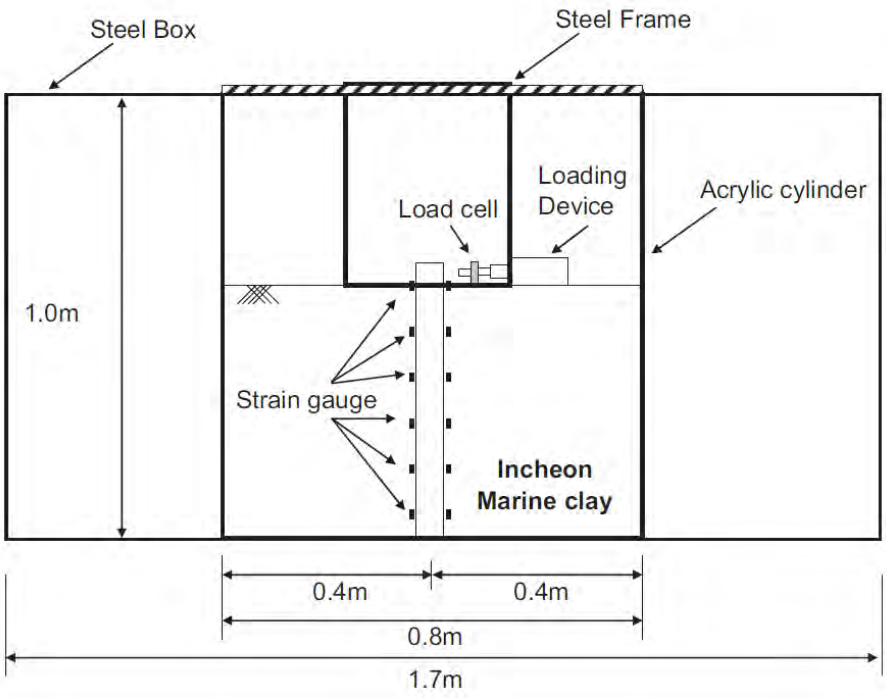

Figure 2.31: Configuration of the laboratory model pile lateral load tests in the Geotechnical Testing Lab of Yonsei University.

Results from the aforementioned field and laboratory pile lateral load tests were used for the formulation of p-y curves corresponding to short-term static lateral loading, according to the following procedure:

1. Determine the subgrade reaction modulus K of the pile-soil interaction according to the expression:

$$K = 17.4 \, \frac{E}{1-\nu^2} \sqrt{\frac{D}{D_{ref}}} \left[\frac{E \, D^4}{E_p \, I_p} \right]^{0.66} \tag{2.72}$$

   where E= the soil Young's modulus, ν= the soil Poisson's ratio and D_{ref}= a reference pile diameter equal to 1m.

2. Calculate the ultimate lateral soil resistance p_u according to the following equa-

tion.

$$p_u = 3.25 c_u \, D \left(\frac{z}{z_{ref}} \right)^{0.59} \tag{2.73}$$

where z_{ref}= a reference soil depth equal to 1m.

3. The hyperbolic p-y curve expression combining K and p_u from the previous steps is:

$$p = \frac{y}{\frac{1}{K} + \frac{y}{p_u}} \tag{2.74}$$

Figure 2.32 depicts the satisfactory agreement between the measured and the proposed p-y curves, both for the field and the laboratory pile load tests. Furthermore, the current research concluded that p-y curves characteristics affect the lateral response of flexible piles more significantly than the corresponding response of rigid piles.

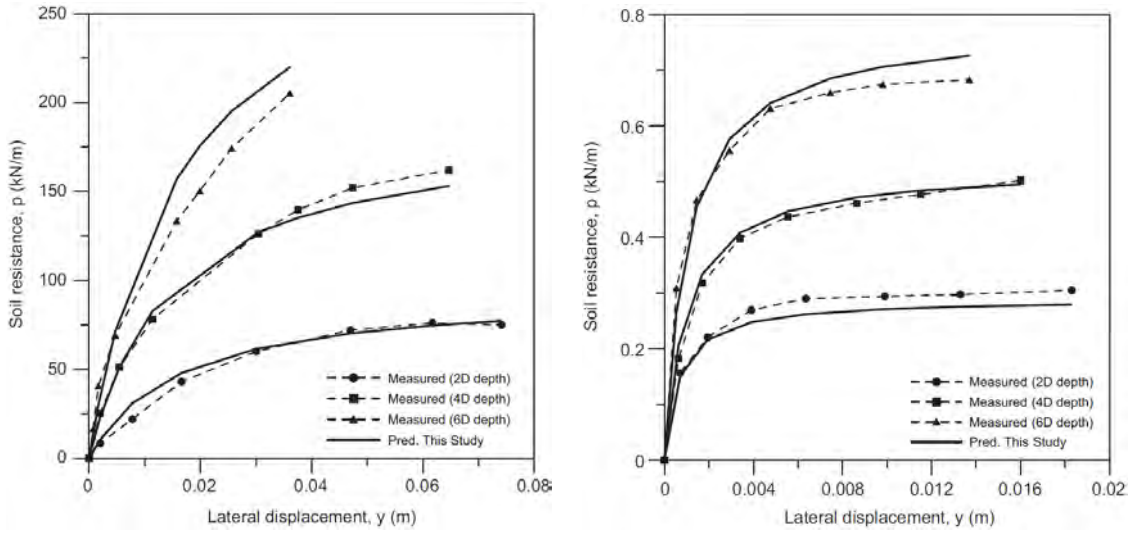

Figure 2.32: Comparison of measured and proposed p-y curves for (a) a field load test and (b) a laboratory load test (Jeong et al., 2011).

Credits need to be attributed to Liang et al. (2007) for their elaboration on a hyperbolic p-y criterion for intermediate cohesive geomaterial - neither soft nor stiff - proposed prior to the study by Jeong et al. P-y curves were derived from 3D FEA and verified with six large scale lateral pile load tests. Equation 2.74 was used as the backbone curve, including the initial stiffness K_i (not the secant subgrade reaction modulus K) and the ultimate lateral soil resistance p_u. The aforementioned p-y curve parameters of the hyperbolic criterion were calculated according to the

following expressions:

$$K_i = 0.943 \left(\frac{z}{z_{ref}}\right)^{0.016} \left(\frac{D}{D_{ref}}\right) \nu^{-0.078} {E_s}^{1.036} {E_p}^{-0.031} \tag{2.75}$$

where z_{ref} and D_{ref} are reference values of the p-y curve depth and the pile diameter, both equal to 1.0m, ν= the Poisson's ratio of the soil, E_s= the Young's modulus of the soil and E_p= the Young's modulus of the pile.

$$p_u = min \left[3 + \frac{\gamma'}{c_u} z + \frac{J}{D} z,\ 10\right] c_u D \tag{2.76}$$

with the expression almost identical to the recommendations by Matlock (1970) for soft clays, except for the ultimate lateral bearing capacity factor - equal to 10 instead of 9 by Matlock.

2.6 P-y curves for clays from in situ testing

2.6.1 PMT-based p-y curves

2.6.1.1 Briaud et al. (1983)

In their paper Briaud et al. (1983) presented a methodology for the derivation of p-y curves from pressuremeter test (PMT) curves. The specific method distinguishes between the frictional behavior of the pile-soil interaction and the resistance in front of the pile. Combining the derived resistance curves from the two mechanisms mentioned before, the p-y curve at the desired depth is formed.

The investigators noticed that friction developing around the laterally loaded pile is an important component of the total resistance and that this frictional resistance is fully mobilized before the resistance in front of the pile. Therefore, they concluded in incorporating both parts of the resistance in the derived p-y curve, pointing out that friction is all important at working loads. The proposed methodology is summarized in the following simple steps.

1. Calculate the resistance Q in front of the pile through measurements of the PMT pressure p_{PMT}, according to the equation:

$$Q = p_{PMT} \cdot B \cdot s_Q \tag{2.77}$$

where B= the pile diameter or width and s_Q= a shape factor equal to 1.0 for square piles loaded parallel to their sides and 0.8 for circular piles or square piles

not loaded parallel to their sides.

2. Calculate the frictional resistance F of the pile-soil interaction according to the equation:

$$F = \tau_s \cdot B \cdot s_F \tag{2.78}$$

where τ_s= the soil shear stress obtained through the subtangent method on the PMT curve and s_F= a shape factor equal to 2.0 for square piles loaded parallel to their sides and 1.0 for circular piles or square piles not loaded parallel to their sides.

3. The horizontal displacement y of the p-y curve is calculated through the following equation.

$$y = \frac{y_{PMT}}{R_{PMT}} R \tag{2.79}$$

where y_{PMT}= the increase in radius of the soil cavity during the PMT, R_{PMT}= the initial radius of the soil cavity of the PMT and R= the radius of the pile.

4. The lateral soil pressure p per unit length of the pile is considered the sum of Q and F. Combined with the horizontal pile displacement y, the desired p-y curve is formed.

5. In order to account for low confinement pressure close to the ground surface, reduction factor RF (Figure 2.33b) is applied only on Q resistance up to a depth of reduced resistance D_c (Figure 2.33a).

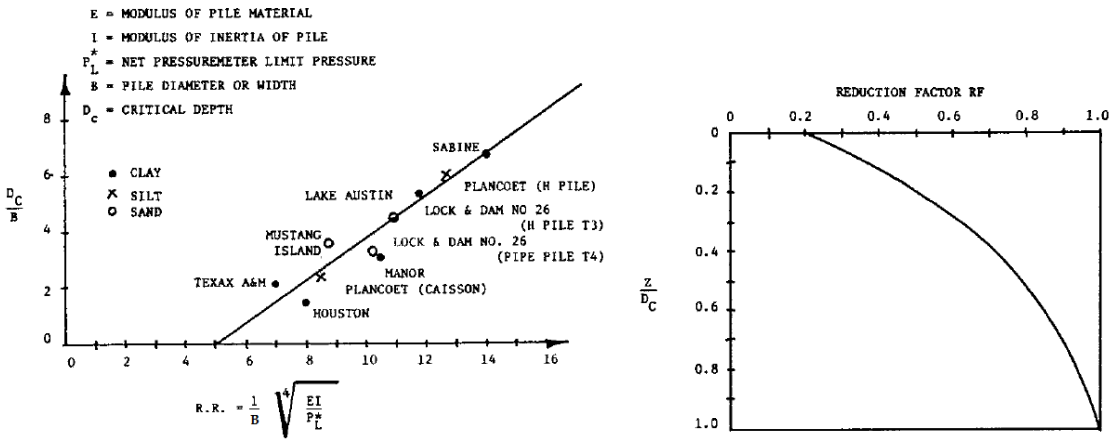

Figure 2.33: Determination of (a) the depth D_c of reduced resistance and (b) the reduced factor RF applied on Q for the aforementioned depth (Briaud et al., 1983).

The proposed methodology was verified for soft clays through the p-y and pile response curves derived from the Sabine site, Texas (see Paragraph 2.3.1). The

comparison between the predicted and measured curves was judged satisfactory in general, with minor divergence in the p-y curves of certain depths. Finally, it was noted that p-y curves were derived either from the first load or the reload PMT curves. From the limited evidence of the current study, it was recommended to use PMT first load curves for the p-y curves of drilled shafts or piles that do not plug, whereas PMT reload curves were considered more suitable for p-y curves of driven piles or piles that plug.

2.6.1.2 Frank (2009)

Part of the work presented by Frank (2009) on the use of the Menard Pressuremeter (MPM) tests for the design of foundations in France, referred to laterally loaded piles and the derivation of corresponding p-y curves. Figure 2.34 depicts the p-y curve of a single pile under long-duration lateral loading at a given depth. The results of MPM test are utilized for the formulation of the aforementioned curve.

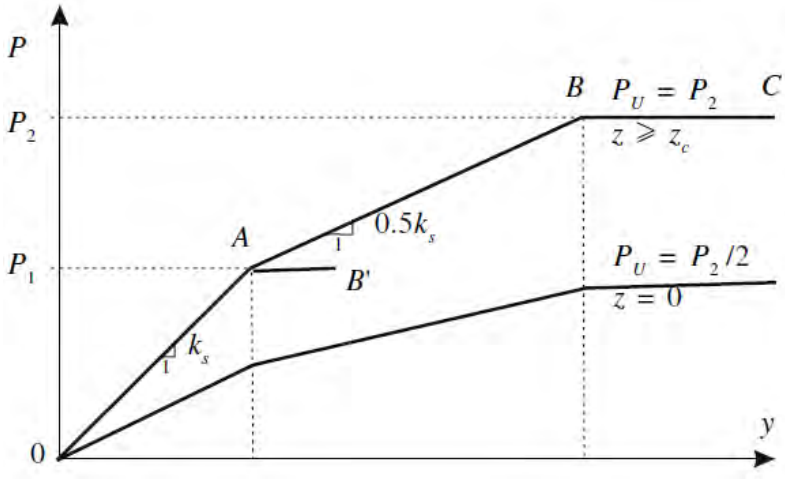

Figure 2.34: The p-y curve derived from MPM tests for piles under long-duration lateral loads (Frank, 2009).

In more detail, the subgrade reaction modulus $k_s = p/y$ of part OA is obtained from the Menard settlement Equation 2.80, assuming $q - \sigma_v = p$, $s = y$, $E_c = E_d = E_M$ - E_M is the MPM modulus - and calculations for a strip footing with λ_c=1.5 and λ_d=2.65.

$$s = (q - \sigma_v) \left[\frac{2D_o \left(\lambda_d \frac{D}{D_o} \right)^{\alpha}}{9E_d} + \frac{\alpha \lambda_c \, D}{9E_c} \right] \tag{2.80}$$

where D= the pile diameter, D_o=0.60m and α= a rheological coefficient based on structure and time.

Table 2.10: Average limit pressure values p_l of cohesive soils measured from MPM tests.

Soil	Type		p_l (MPa)
Clay & Silt	A	Soft	< 0.7
	B	Stiff	1.2-2
	C	Hard (clay)	> 2.5

For p values greater than creep pressure p_f - $p_f = p_l/2$ is a satisfactory estimate, with p_l from Table 2.10 for cohesive soils - effects of soil nonlinearity are taken into account and the slope of part AB is assumed equal to one-half the slope of part OA (Figure 2.34). The ultimate lateral soil resistance component BC of the p-y curve is taken equal to the limit pressure measured with the MPM. However, engineering practice demands that creep pressure $p_f = p_l/2$ is not exceeded and thus OAB' curve is utilized for the design of piles loaded laterally through concentrated forces on the pile head - although a rather conservative recommendation. Especially for cohesive soils, the derived p-y curves are modified for depths shallower than a critical depth z_c=2D. At ground surface (z=0) pressure p is divided by 2 for the same displacement y, with linearly interpolated corresponding p values until $z = z_c$.

2.6.1.3 Bouafia (2013)

Another attempt to derive p-y curves from pre-bored pressuremeter test (PMT) measurements was presented by Bouafia (2013). The contributions of Menard deformation modulus E_M, net PMT limit pressure p_l^*, pile slenderness ratio L/D and relative lateral pile-soil stiffness in the p-y curve formulation are thoroughly analyzed in this study. The proposed p-y curves were then validated versus some well-documented large scale tests of laterally loaded piles.

The following step-by-step procedure is proposed, in order to form p-y curves from PMT data:

1. Subdivide the soil surrounding the pile into N zones of thickness h_i, thin enough to assume that PMT data (E_M, p_l) vary linearly within each zone. Acquire the mean values of the aforementioned parameters for each zone i.

2. Assume a rigid or semi-rigid pile, namely with embedded length L equal to the effective embedded length L_e, beyond which the pile does not deform.

3. Compute the characteristic soil modulus E_c through the following expression.

$$E_c = \frac{1}{L_e} \int_0^{L_e} E_M(z)\,\mathrm{d}z = \frac{\sum_{i=1}^{N} E_M^i\, h_i}{L_e} \tag{2.81}$$

4. Calculate the lateral pile-soil stiffness ratio K_R according to the equation:

$$K_R = \frac{E_p\, I_p}{E_c\, {L_e}^4} \tag{2.82}$$

where $E_p\, I_p$= the pile stiffness.

5. Compute modulus K_E^i per soil layer i through the following equation, obtaining coefficients a and n from Table 2.11.

$$K_E^i = a\left(K_R^i\right)^n \tag{2.83}$$

Table 2.11: Values of coefficients a, n, b, c and m for laterally loaded piles with slenderness ratio $L/D \geq 5$ in cohesive soils.

Soil	a	n	b	c	m
Clay	1.85	-0.2	0.3	1.0	1.0
Silt	5.50	0.0	2.3	0.0	0.0
Organic clay	3.7	0.0	1.4	0.0	0.0

6. Calculate the average lateral reaction modulus E_{ti}^i per soil layer i in the middle of each pile segment through the expression:

$$E_{ti}^i = \frac{1}{h_i} \int E_{ti}(z)\,\mathrm{d}z = \frac{K_E^i}{h_i} \int E_M(z)\,\mathrm{d}z = K_E^i\, E_M^i \tag{2.84}$$

7. The characteristic lateral reaction modulus E_{ti}^c of the equivalent homogeneous soil, namely the average reaction modulus, is calculated from the equation:

$$E_{ti}^c = \frac{1}{L_e} \int_0^{L_e} E_{ti}(z)\,\mathrm{d}z = \frac{\sum_{i=1}^{N} K_E^i\, E_M^i\, h_i}{L_e} \tag{2.85}$$

8. Compute the elastic (or transfer) length L_0 of the pile through the following equation.

$$L_0 = \sqrt[4]{\frac{E_p\, I_p}{E_{ti}^c}} \tag{2.86}$$

Then calculate the effective embedded length of the pile $L_e = \min[L,\ \pi L_0]$. If L_0 from Equation 2.86 leads to $L > L_e$, namely to a flexible pile, follow an iterative process through steps 3 to 8 until the computation of K_R converges.

9. Compute the lateral reaction modulus E_{ti} of the p-y curve from the expression:

$$E_{ti} = K_E\, E_M \tag{2.87}$$

where K_E is calculated according to Equation 2.83.

10. Compute the ultimate lateral soil resistance p_u of the p-y curve from the following equations, obtaining coefficients b, c and m from Table 2.11.

$$p_u = K_p\, p_l^*\, D \tag{2.88a}$$

$$K_p = b + cK_R^m \tag{2.88b}$$

11. Finally, obtain the desired p-y curve through the renowned hyperbolic form:

$$p = \frac{y}{\dfrac{1}{E_{ti}} + \dfrac{|y|}{p_u}} \tag{2.89}$$

Measured load-deflection response of single laterally loaded piles from full-scale tests was compared with the corresponding response derived from the application of the developed p-y curves on a BNWF solution. The results of the comparison demonstrated very satisfactory prediction capability of the lateral pile response through the proposed p-y curve methodology.

2.6.2 DMT-based p-y curves

2.6.2.1 Robertson et al. (1989)

The study of Robertson et al. (1989) aimed at the correlation of flat dilatometer test (DMT) measurements with static p-y curves for driven, laterally loaded piles in cohesive and cohesionless soils. As far as this thesis is concerned, the proposals for

the lateral response of clayey soils is of interest and will be presented herein. Before describing the proposed DMT-based p-y curves of the current methodology, a brief introduction is attempted on the main index parameters derived from DMT measurements. Two readings are extracted every 200mm in depth from the deformation of the flexible membrane of the dilatometer, which are corrected to pressures P_0 and P_1. These two pressures are used to calculate the following three index parameters, proposed by Marchetti (1980):

$$I_D = \frac{P_1 - P_0}{P_0 - u_0} = \text{material index} \tag{2.90a}$$

$$K_D = \frac{P_0 - u_0}{\sigma'_{vo}} = \text{horizontal stress index} \tag{2.90b}$$

$$E_D = 34.6\,(P_1 - P_0) = \text{dilatometer modulus} \tag{2.90c}$$

where u_0= the in situ hydrostatic water pressure and σ'_{vo}= the in situ vertical effective stress. Experience on DMT has shown that the test provides a satisfactory indication of soil type and reasonable values of the undrained shear strength c_u, the coefficient of horizontal geostatic stress K_o and the overconsolidation ratio OCR for soft to medium, uncemented, insensitive clays.

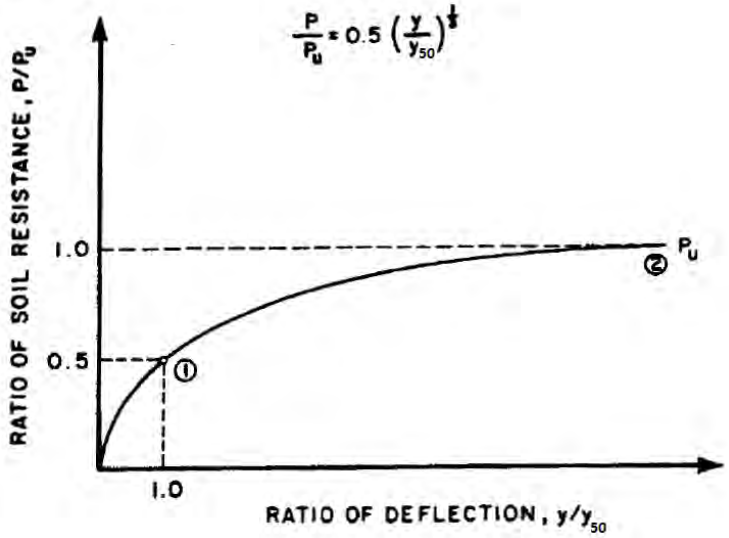

Figure 2.35: The cubic parabola DMT-based p-y curve by Robertson et al. (1989).

The framework proposed by Matlock (1970) was used as a baseline for the DMT-based p-y curves of the current methodology for cohesive soils ($I_D \leq 1.0$). However, some modifications were judged necessary and were incorporated in the following

procedure for the formulation of these p-y curves:

1. Obtain values of the undrained shear strength c_u from the correlation with the DMT test results.

2. Calculate the ultimate lateral soil resistance p_u after the equation:

$$p_u = N_p \; c_u \; D \tag{2.91}$$

where $N_p = min \left[3 + \frac{\gamma'}{c_u} z + \frac{J}{D} z, \; 9 \right]$ from Matlock (1970) (see Paragraph 2.3.1) and D= the pile diameter.

3. Estimate the initial tangent modulus E_i of the stress-strain curve from DMT data, according to the equation:

$$E_i = F_c \; E_D \tag{2.92}$$

where F_c= empirical stiffness factor approximately equal to 10 as an initial approach and E_D= the DMT modulus from Equation 2.90c.

4. Calculate the axial strain corresponding to one-half the maximum principal stress difference ε_{50} from the following equation:

$$\varepsilon_{50} = \frac{1.67 \; c_u}{E_i} \tag{2.93}$$

5. Compute the deflection y_{50} at one-half the ultimate soil resistance from the following equation, proposed by Stevens & Audibert (1979):

$$y_{50} = B \; \varepsilon_{50} \; D^{0.5} \xrightarrow[\text{Equations 2.92, 2.93}]{\text{B=14.2cm (empirical)}} y_{50} = \frac{23.67 \; c_u \; D^{0.5}}{F_c \; E_D} \tag{2.94}$$

where the pile diameter D in cm and the derived y_{50} also in cm. It is important to mention here that Equation 2.94 is not dimensionally correct. However, the findings of Stevens & Audibert (1979) persuaded the investigators of the current methodology to use the specific equation for y_{50}.

6. The following DMT-based p-y criterion (Figure 2.35) combines the aforementioned calculated parameters into the corresponding cubic parabola proposed by Matlock (1970):

$$\frac{p}{p_u} = 0.5 \left(\frac{y}{y_{50}} \right)^{1/3} \tag{2.95}$$

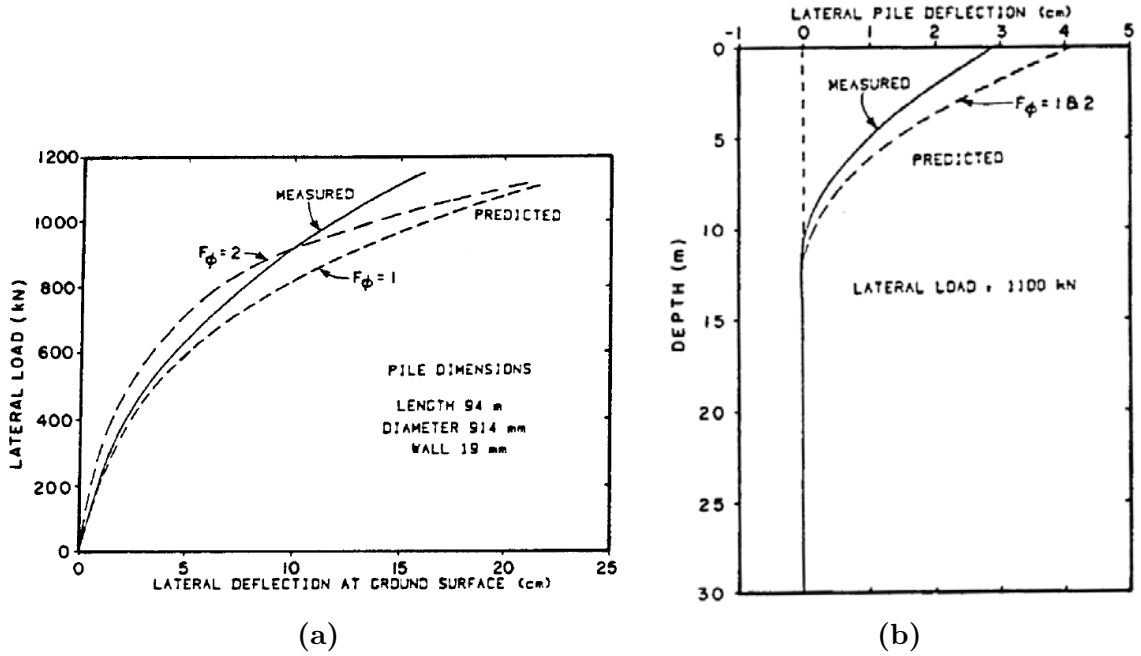

Figure 2.36: Predicted and measured (a) pile head load-displacement curves and (b) horizontal displacement along the pile for pile head lateral load H=1100kN of the static laterally loaded 914mm-diameter test pile at UBCPRS. F_ϕ is an empirical stiffness factor for DMT-based p-y curves in sands.

The DMT-based p-y criteria proposed by Robertson et al. (1989) were applied to three large-scale lateral pile load tests at the University of British Columbia pile research site (UBCPRS) (Davies, 1987). The test site soil profile consisted of clean river sand in the upper 2 to 4m, with a deposit of soft organic silty clay extending underneath it and to a depth of 15m below ground surface. A deposit of medium dense sand to a depth of about 30m underlies the clay layer and a deep deposit of normally consolidated clayey silt with thin interbedded sand layers extends below the aforementioned sand. Three driven steel pipe piles with length L=94.0, 16.8 and 31.1m, diameter D=914 and 324mm (two piles) and wall thickness t=19.0, 9.5 and 11.5mm respectively underwent static monotonic lateral load tests. Averaged values of the ultimate lateral soil resistance p_u and the deflection y_{50}, derived from correlations with the DMT data, were used as input to form p-y curves according to the aforementioned process and import them into a BNWF simulation. Indicatively for the 914mm-diameter pile, the curves of pile head load-displacement and horizontal displacement along the pile (for pile head lateral load H=1100kN) predicted with the current methodology were compared with the corresponding field measured curves (Figure 2.36). The comparison demonstrates a very satisfactory agreement between the prediction of the DMT-based p-y criteria and the measurements of the large-scale test, although the predicted horizontal deflection of the pile head at the

specific load increment was 25% overestimated. Similar observations were made for the lateral response of the other two test piles. Finally, the predicted bending moment profile using the DMT-based p-y curves was overestimated compared to the corresponding moments that were measured from the field tests, for all three test piles.

2.6.2.2 Gabr et al. (1994)

The methodology proposed by Gabr et al. (1994) uses data from DMT for the formulation of static p-y curves in clay deposits. A hyperbolic p-y curve equation is proposed and certain instructions are given on the calculation of the ultimate lateral soil resistance p_u and the initial modulus of subgrade reaction k_h, defining the aforementioned curve. Furthermore, the study focuses on installation effects of a close-ended pile on the soil properties around the pile that are used for the formulation of the p-y curves. Three very well documented test sites - one in Norway and two in England - and corresponding static laterally loaded test piles were examined. Test data from the Norway site were used for the evaluation of p_u and k_h as well as for the proposal of a new DMT-based p-y relationship. The other two test sites - in England - allowed for the verification of the proposed methodology versus the acquired test results.

The first test site was located at Haga, Norway and consisted mainly of lean medium marine clay deposits. The undrained shear strength c_u profile, derived from various in situ and laboratory tests, increased from 25kPa at ground surface to 40kPa at a depth of 1.5m and remained almost constant for greater depths. A generally high overconsolidation ratio OCR was detected at the specific site, decreasing from 35 at ground surface to 2 at a depth of 7m. Overconsolidation of the clay was attributed to the removal of 6m of overburden from the site approximately 10 years prior to the pile tests. The test pile was a 4.15m-long, closed-ended pile, jacketed in the ground, with diameter D=0.153m and eight strain gauge bridges along it. Six earth pressure cells and equal pore pressure cells were also installed on the test pile. The maximum lateral load of the pile was 30kN, applied at a point about 0.30m above the pile head and in increments of 2.5kN each. For reliability purposes, the aforementioned load was imposed towards both opposite loading directions and the presented results were the average of data obtained from both tests.

The procedure described herein is for the formulation of DMT-based p-y curves corresponding to short-term static lateral loading of piles in clay:

1. Obtain values of the undrained shear strength c_u and the overconsolidation ratio OCR with depth.

2. In case of a driven, closed-ended pile - the current study refers to such piles - multiply the obtained c_u value with a correction factor corresponding to the OCR at the depth of the desired p-y curve, as depicted in Figure 2.37. Thus, a corrected undrained shear strength $c_{u,c}$ occurs and installation effects of the pile on soil strength are taken into account.

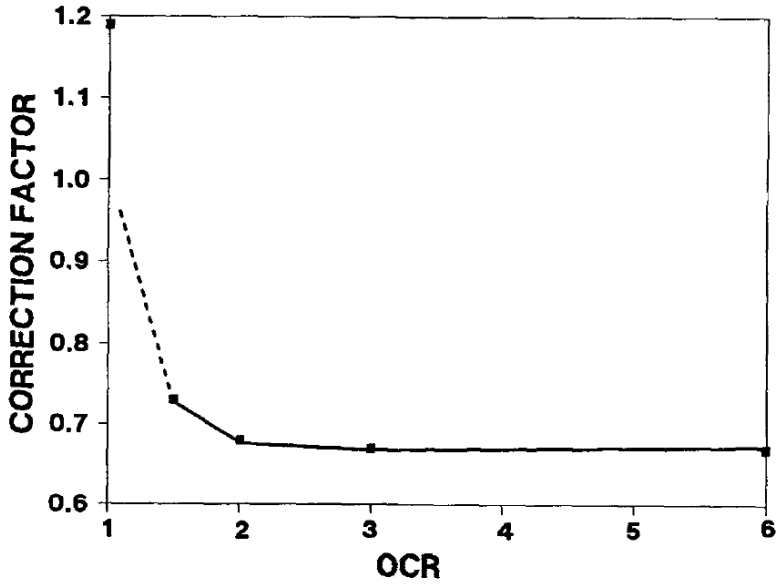

Figure 2.37: Correction factor of the undrained shear strength c_u at Haga site, depending on OCR.

3. Calculate the ultimate lateral soil resistance p_u after the equation:

$$p_u = N_p \, c_{u,c} \, D \tag{2.96}$$

where $N_p = min \left[3 + \frac{\gamma'}{c_{u,c}} z + \frac{J}{D} z, \; 9 \right]$ from Matlock (1970) (see Paragraph 2.3.1) and D= the pile diameter.

4. Compute the initial tangent coefficient of subgrade reaction for the clay from DMT data, according to the equation:

$$k_{hi} = \frac{6.5 \, (p_o - \sigma_h)}{t_{hb}} \tag{2.97}$$

where p_o= a pressure calculated from DMT readings, σ_h= in situ total lateral soil pressure at rest and t_{hb}= half the dilatometer blade thickness. The initial modulus of subgrade reaction k_h is actually k_{hi} multiplied with the pile diameter D.

5. According to the measured field p-y curves, the equation proposed for a corresponding DMT-based p-y criterion is the following:

$$p = p_u \cdot \tanh\left[\frac{k_{hi}\,(z \text{ or } D)}{p_u} \cdot y\right] \tag{2.98}$$

Note: The correction factor for the in situ undrained shear strength c_u (Figure 2.37) refers to driven, closed-ended piles and exclusively to the specific test site (Haga, Norway). For other pile types and clay properties, a corresponding investigation on pile installation effects needs to take place.

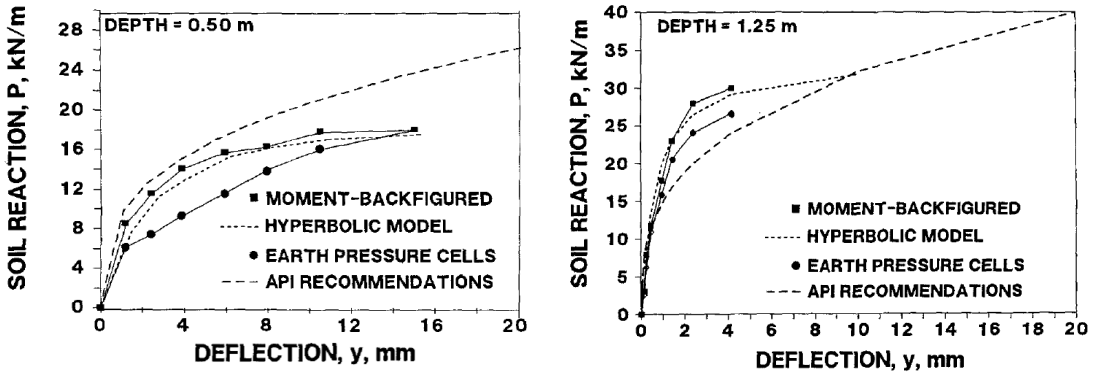

(a) (b)

Figure 2.38: Measured and predicted p-y curves at Haga site for (a) a shallow depth and (b) a greater depth.

For the verification of the DMT-based p-y criterion, the proposed p-y curves were compared with the p-y curves derived from the strain gauges measurements along the pile[1], the results from earth pressure cells and the predicted p-y curves according to the recommendations by API (1991) - actually the p-y curves by Matlock (1970) (see Paragraph 2.3.1). Figure 2.38 depicts the aforementioned comparison for a shallow and a greater depth. It is observed that the DMT-based p-y curves simulate very accurately the recorded lateral soil behavior, while the p-y curves proposed by API (1991) systematically underestimate p for the range of y noticed during the tests. Respective conclusions are drawn for the pile head load-displacement curve and the bending moment distribution along the pile (Figure 2.39).

In order to evaluate the proposed DMT-based p-y curves, the results from two other large-scale lateral pile load tests with DMT measurements were examined. In more detail, the lateral response of a tubular, steel, 17.5m-long and 0.406m-in-diameter pile at Brent Cross, England, was of concern from the first test site.

[1]Double integration for the lateral displacement y and double derivation for lateral soil reaction p.

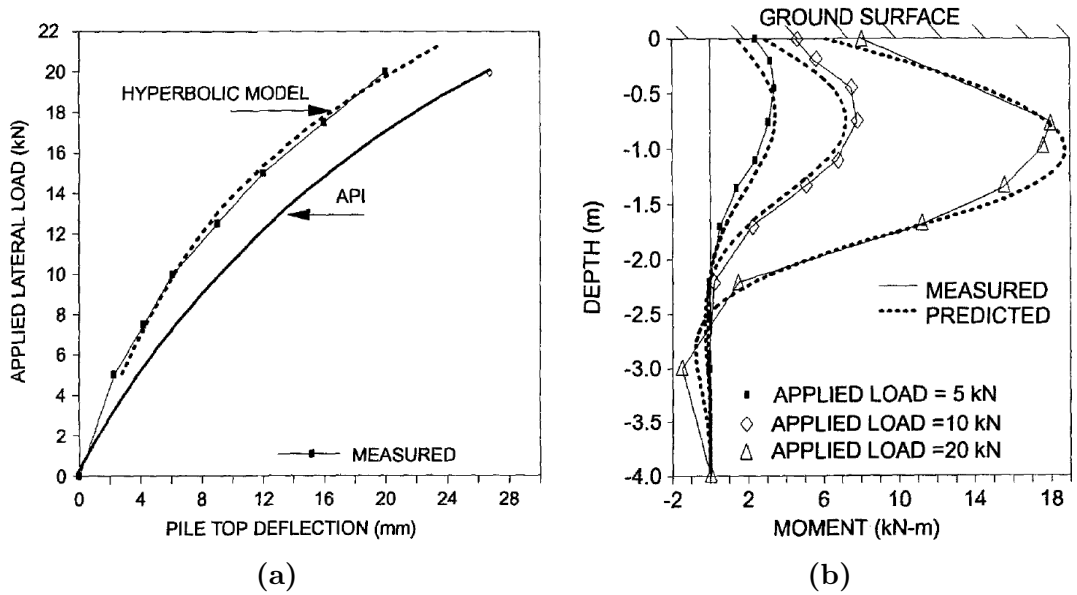

Figure 2.39: Measured and predicted lateral pile response at Haga site in terms of (a) pile head load-displacement curves and (b) bending moment distribution along the pile.

This pile was installed in London clay with undrained shear strength c_u increasing parabolically from 10kPa at ground surface to 50kPa at a depth of 5m and retaining the latter value for greater depths. Measured and predicted - through a BNWF solution with the current p-y curve methodology - pile head load-displacement curves and bending moment distribution curves along the pile matched very accurately, as demonstrated in Figure 2.40. At the second test site, namely Canons Park in England, a bored cast in place, 4.5m-long and 0.17m-in-diameter pile was tested in stiff and slightly gravelly London clay. While pile head load-displacement curves show a satisfactory agreement between measured and predicted values for Canons Park test site, the bending moment profile derived from the p-y curve simulation seems underestimated compared to field observations (Figure 2.41).

In general, the DMT-based p-y curves proposed by Gabr et al. (1994) resulted in satisfactory agreement between predicted and measured lateral pile responses for three different case studies. By estimating the ultimate lateral soil resistance p_u and the initial tangent coefficient of subgrade reaction k_{hi}, one can form the p-y curve at the desired depth according to the current methodology. However, further investigation is required for the formulation of DMT-based p-y curves for large diameter piles, since all the aforementioned pile tests refer to relatively small diameters - of an order of magnitude similar to the dilatometer width.

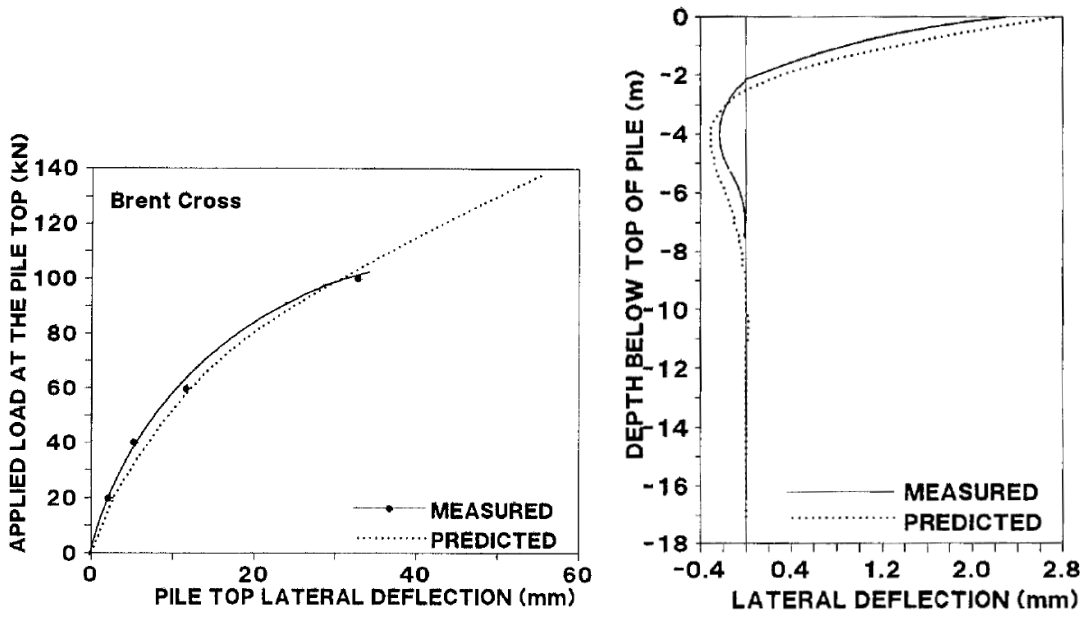

Figure 2.40: Measured and predicted lateral pile response at Brent Cross site in terms of (a) pile head load-displacement curves and (b) bending moment distribution along the pile (Gabr et al., 1994).

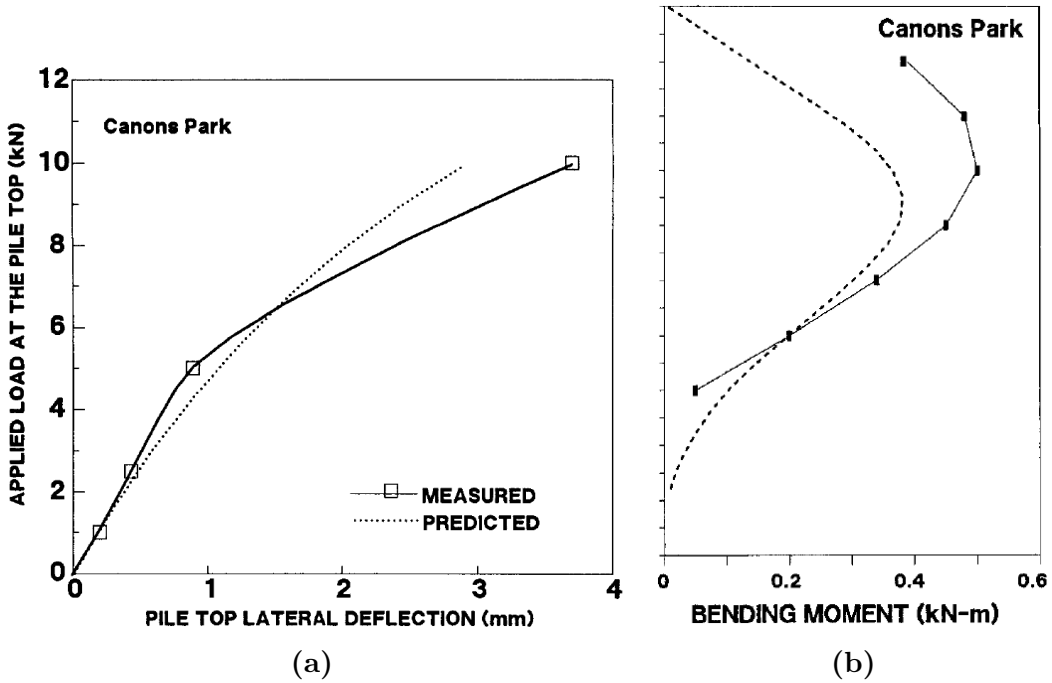

Figure 2.41: Measured and predicted lateral pile response at Canons Park site in terms of (a) pile head load-displacement curves and (b) bending moment distribution along the pile (Gabr et al., 1994).

2.6.3 CPT-based p-y curves

2.6.3.1 Guo and Lehane (2014)

Guo et al. (2014) carried out two centrifuge tests on static laterally loaded aluminium piles in kaolin slurry. The purpose of the specific research was to examine the lateral response of piles in soft, normally to lightly overconsolidated clays. As a result, experimentally derived CPT-based p-y curves were proposed for static laterally loaded piles in such soil types. The methodology is compared with corresponding centrifuge test results by Jeanjean et al. (2009) (see Paragraph 2.3.2) and recommendations of API (2011) on p-y curves for clays.

Two centrifuge tests were carried out; one in a normally consolidated kaolin sample at a centrifuge acceleration of 80g (T1) and another in a lightly overconsolidated - OCR=2 - corresponding sample at 40g (T2). Both kaolin samples were progressively topped up as consolidation carried on, with the final consolidated kaolin prototype thickness equal to 13.2m and 6.6m for T1 and T2 respectively. It is important to mention that after the driving process of the test pile, the kaolin sample was allowed to rest for a period of at least 4 hours - long enough to allow for installation induced excess pore pressures to dissipate and lead to at least 90% completion of consolidation. CPT tests were performed before and after the lateral loading of the test pile and the net cone penetration resistance (q_{net}) was measured (Figure 2.42b). The observed CPT test measurements demonstrated an almost linear increase of q_{net} with depth at a rate of 19.6kPa/m and 30.3kPa/m for OCR=1 and 2 respectively.

The test pile was an aluminium tube with outer diameter D=11mm - including the epoxy coating preserving the strain gauges - and embedment length L=130mm (Figure 2.42a) that represented a 0.88m-wide/ 10.4m-long prototype pile at 80g (T1) and a 0.44m-wide/ 5.2m-long prototype pile at 40g (T2). The length to diameter ratio for both tests was L/D=11.8, thus corresponding to rigid pile behavior. The lateral load was applied through a loading arm and via a cubic lightweight hollow cap on the pile head, at a prototype undrained rate of 0.028m/s and 0.014m/s during T1 and T2 respectively. The corresponding prototype vertical eccentricity of the applied lateral load was e_1=1.52m (T1) and e_2=0.76m (T2).

Pressure p and lateral displacement y of the p-y curves were derived by double differentiation and double integration of the bending moment profile obtained from the strain gauges along the test pile respectively. The acquired experimental p-y curves were used to generate a new CPT-based p-y curve equation for static laterally loaded piles in soft clays. Figure 2.43 depicts the normalized lateral soil pressure with the net CPT resistance p/q_{net} versus the normalized lateral displacement with the pile diameter y/D at different depth to diameter ratios z/D and for both centrifuge

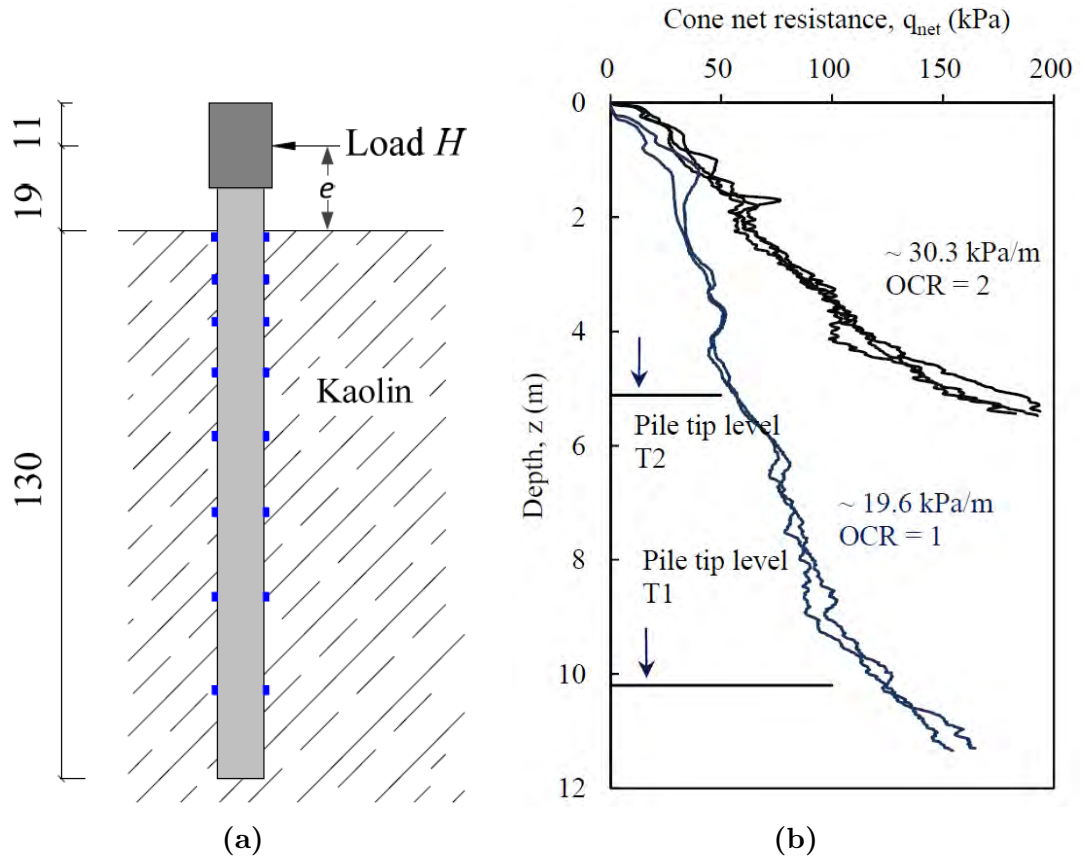

Figure 2.42: (a) Centrifuge tests setup (units in mm) and (b) net CPT resistance with depth for both tests.

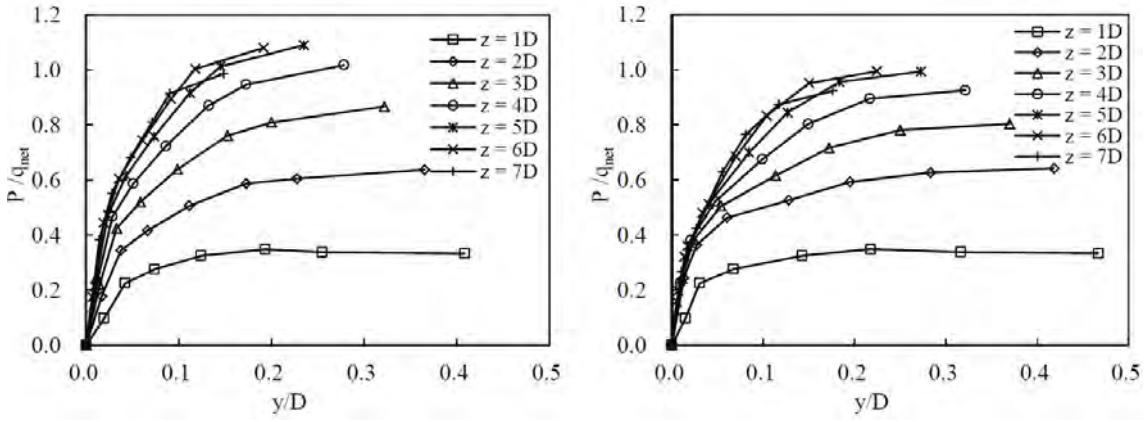

Figure 2.43: Normalized experimental p-y curves for various z/D ratios, derived from centrifuge test T1 (left) and T2 (right).

tests. The lateral bearing capacity factor N_{pq} is introduced - equal to the ratio of the ultimate lateral soil resistance to the net CPT resistance p_u/q_{net} - and plotted versus z/D for both OCR of T1 and T2 in Figure 2.44. The following equation is

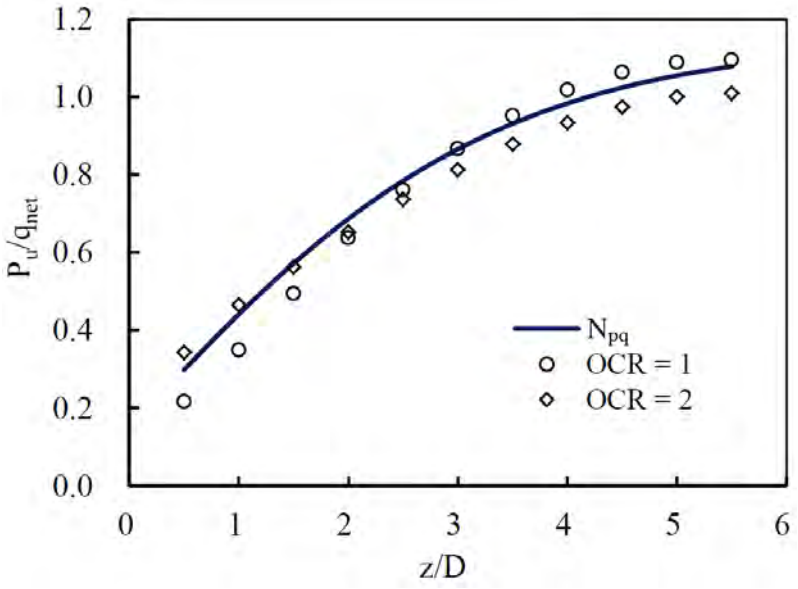

Figure 2.44: Experimental and analytical N_{pq} factor with dimensionless depth z/D for both centrifuge tests.

proposed for N_{pq}, providing a satisfactory match to the test data.

$$N_{pq} = \frac{p_u}{q_{net}} = 0.2 + \tanh[0.3(z/D)] \tag{2.99}$$

A transition of the soil failure mechanism from wedge-type to flow-around-type is observed at $z/D \approx 3$[1] and the following p-y curves, inspired by Dunnavant & O'Neill (1989) (see Paragraph 2.4.3), are proposed.

$$\frac{p}{p_u} = \tanh\left[8.80\left(\frac{z}{D}\right)^{-0.30} \cdot \left(\frac{y}{D}\right)^{0.68}\right] \quad \text{for} \quad 0 < z/D \leq 3 \tag{2.100a}$$

$$\frac{p}{p_u} = \tanh\left[6.34\left(\frac{y}{D}\right)^{0.68}\right] \quad \text{for} \quad z/D \geq 3 \tag{2.100b}$$

The formulation of the aforementioned CPT-based p-y curves for soft clays requires only the net CPT resistance q_{net} as input parameter.

Both N_{pq} and the p-y curve equations of the current methodology are compared to corresponding proposals of the literature. To compare the conventional lateral

[1]Values of ultimate lateral soil resistance p_u are almost equal to the net CPT resistance q_{net} for z/D greater than 3, as depicted in Figure 2.43.

bearing capacity factor N_p with N_{pq}, the following equation is introduced:

$$N_p = \frac{p_u}{c_u} = N_{pq} \cdot N_{kt} \tag{2.101}$$

where N_{kt}= the ratio q_{net}/c_u of the net CPT resistance to the in situ undrained shear strength. The equivalent N_p of the current methodology seems to agree in a satisfactory manner with the observations of Jeanjean et al. (2009) on his centrifuge tests (see Paragraph 2.3.2) for a value of N_{kt}=12, as depicted in Figure 2.45a. Referring to the shape of the CPT-based p-y curves, Figure 2.45b compares Equation 2.100b - for $z/D > 3$ - with the corresponding p-y curves recommended by API (2011) using two values of the axial strain corresponding to one-half the maximum principal stress difference, namely ε_{50}=0.0075 and 0.02. It is observed that ε_{50}=0.02, corresponding to soft clays, leads to a much more ductile lateral soil response than the observed one, whereas API (2011) p-y curves with ε_{50}=0.0075 come to very good agreement with the CPT-based ones.

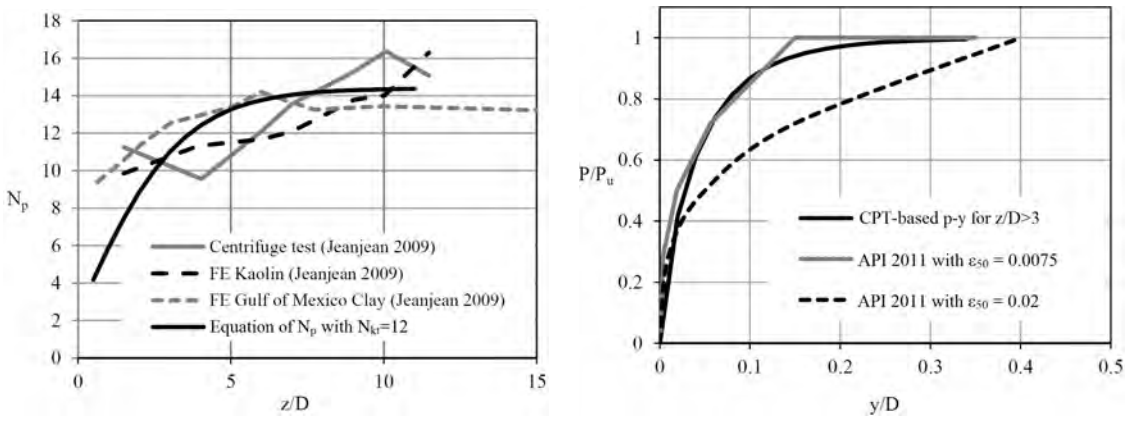

(a) **(b)**

Figure 2.45: (a) Comparison of lateral bearing capacity factor N_p by Jeanjean et al. (2009) with the corresponding factor from Equation 2.101 for N_{kt}=12 and (b) normalized CPT-based p-y curve for $z/D > 3$ versus the corresponding curve recommended by API (2011) with ε_{50}=0.0075 and 0.02.

2.6.3.2 Kim et al. (2016)

The study of Kim et al. (2016) proposes a p-y criterion based on the cone resistance measured from CPT tests in clayey soils. Both static and cyclic p-y curves are proposed and validated through large-scale tests. The derived pile head lateral load-displacement curves, the maximum bending moment and the horizontal displacement measured along the test piles were compared with the corresponding predictions of BNWF solutions incorporating the proposed p-y criterion as well as

the p-y curves by Matlock (1970), Reese et al. (1975) and Dunnavant & O'Neill (1989).

The key component for CPT-based correlations in clays is the fact that both the undrained shear strength c_u and the cone resistance q_c depend on the in situ effective stress σ'_{vo}. In more detail, the following relationship (Lee et al., 2010) correlates the aforementioned parameters:

$$c_u = \frac{q_c - u_0}{N_e} = \frac{q_e}{N_e} \tag{2.102}$$

where N_e= effective cone factor equal to 16

q_c= cone resistance from CPT test

u_0= pore water pressure

q_e= effective cone resistance

Static loading

The procedure described herein is for the formulation of p-y curves corresponding to short-term static lateral loading of the pile (Figure 2.46a):

1. Obtain values of the undrained shear strength c_u from the correlation with the CPT test results, according to Equation 2.102.

2. Calculate the ultimate lateral soil resistance p_u, which after introducing the effective cone factor N_e becomes:

$$p_u = N_p \; c_u \; D = \frac{N_p}{N_e} \; q_e \; D \tag{2.103}$$

where $N_p = min\left[3 + \frac{\gamma'}{c_u}z + \frac{J}{D}z, \; 9\right]$ from Matlock (1970) (see Paragraph 2.3.1) and D= the pile diameter.

3. Calculate the reference strain ε_{CPT} from the following equation:

$$\varepsilon_{CPT} = 0.185 \left(\frac{q_e}{p_A}\right)^{-0.124} \leq 0.02 \tag{2.104}$$

where p_A= atmospheric pressure as a reference stress assumed equal to 100kPa.

4. The following CPT-based p-y criterion combines the aforementioned calculated parameters into the corresponding curve proposed by Matlock (1970):

$$\frac{p}{p_u} = 0.5\left(\frac{y}{2.5 \; \varepsilon_{50} \; D}\right)^{1/3} \xrightarrow[\varepsilon_{50}=\varepsilon_{CPT}]{\text{Equation 2.103}} p = 0.368 \left(\frac{N_p}{N_e}\right) q_e \left(\frac{yD^2}{\varepsilon_{CPT}}\right)^{1/3} \tag{2.105}$$

5. The value of $p = p_u$ remains constant beyond $y = 8y_{50}$ - with y_{50}=$2.5 \cdot \varepsilon_{50} \cdot D$ and ε_{50}= the axial strain corresponding to one-half the maximum principal stress difference - as depicted in Figure 2.46a.

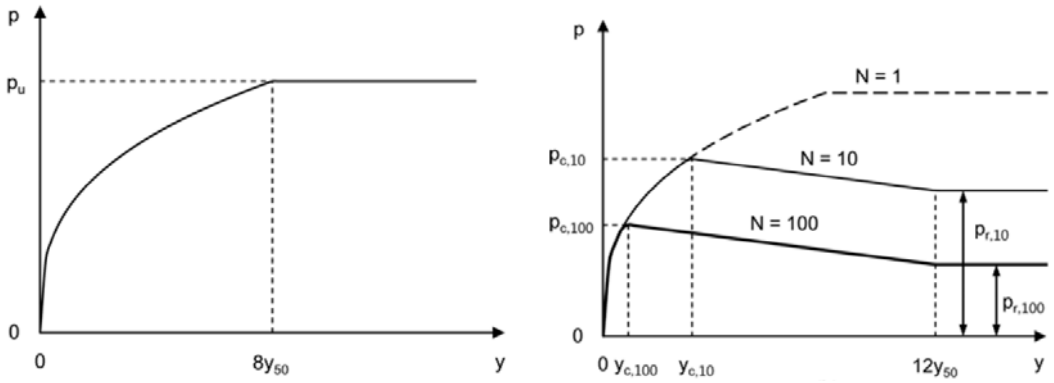

(a) **(b)**

Figure 2.46: Kim et al. (2016) (a) static and (b) cyclic CPT-based p-y curves.

Cyclic loading

The procedure described herein is for the formulation of p-y curves corresponding to cyclic lateral loading of the pile (Figure 2.46b). The proposals of Dunnavant & O'Neill (1989) - see Paragraph 2.4.3 - were adopted in order to take into account the effect that the number of load cycles has on the peak and residual cyclic lateral soil resistance.

1. Form the cyclic p-y curve exactly as the corresponding static curve of Equation 2.105 until the point of the peak cyclic lateral soil resistance p_c.

2. The peak cyclic lateral soil resistance p_c after a certain number of load cycles N is expressed as:

$$p_c = \left(\frac{N_p}{N_e}\right)\left[1 - \left(0.45 - 0.18\frac{z}{z_o}\right) logN\right] \; q_e \; D \leq p_u \tag{2.106}$$

where z= the depth of the p-y curve, z_o=1m and p_u= the ultimate lateral soil resistance for static conditions according to Equation 2.103.

3. Calculate the lateral displacement y_c corresponding to the peak cyclic lateral soil resistance p_c from the equation:

$$y_c = 20 \; \varepsilon_{CPT} \; D \; \left(\frac{p_c}{p_u}\right)^3 \tag{2.107}$$

4. The peak cyclic lateral soil resistance p_c degrades linearly to a residual cyclic lateral soil resistance p_r from $y = y_c$ to $y = 12 \cdot y_{50}$ (Figure 2.46b). The residual cyclic lateral soil resistance p_r is calculated from the following equation.

$$p_r = p_c \left[1 - \left(0.25 - 0.07\frac{z}{z_o}\right) logN\right] \leq p_c \tag{2.108}$$

5. The value of $p = p_r$ remains constant beyond $y = 12y_{50}$.

The CPT-based p-y criteria proposed by Kim et al. (2016) were applied to two well documented large-scale lateral pile load tests, one static at the Incheon bridge construction site (Kim & Jeong, 2010) and one cyclic at Salt Lake City, US (Rollins et al., 2006). The test site of the static load test consisted mainly of low-plasticity clays and silty clays from ground surface up to a depth of 22.0m, with CPT resistances lower than 1MPa for the upper 7m of the marine clay and higher corresponding measurements for greater depths. Values of the undrained shear strength c_u ranged between 18kPa and 60kPa at the specific site. The lateral load imposed to the test pile, with diameter D=1.016m and embedded length L=26.6m, was applied 0.5m above ground surface. The results of pile head load-displacement curves and horizontal displacement curves along the pile (for pile head lateral load H=700kN) predicted with the current methodology, with FEA and through BNWF solutions with the p-y curves by Matlock (1970) and Dunnavant & O'Neill (1989) are compared in Figure 2.47 with the corresponding measurements of the large-scale test. The comparison demonstrates a very satisfactory agreement between the predictions of the CPT-based p-y criteria, the calculations derived from FEA and the corresponding test measured curves. On the contrary, the predictions of Matlock and Dunnavant and O'Neill were judged conservative for the specific load test.

At the test site of the cyclic load test, medium stiff clay and sand layers existed down to a depth of 5m with a soft clay layer below them. The CPT resistances within the clay layers were measured lower than 5MPa, whereas the corresponding measurements for sand were significantly higher. Values of the undrained shear strength c_u ranged between 70kPa and 105kPa for medium stiff clay, while soft clay had a $c_u \approx$ 35kPa. Two closed-ended steel piles were tested, with diameters D=0.324m, 0.610m and embedded lengths L=11.5m, 11.2m respectively. Fifteen (15) lateral load cycles were applied at 0.38m above ground surface. The results of pile head load-displacement curves and maximum bending moment-pile head load curves predicted with the CPT-based criteria and through BNWF solutions with the p-y curves by Matlock (1970), Reese et al. (1975) and Dunnavant & O'Neill (1989) for the 15$^{\text{th}}$ load cycle are compared for the 0.610m diameter pile in Figure

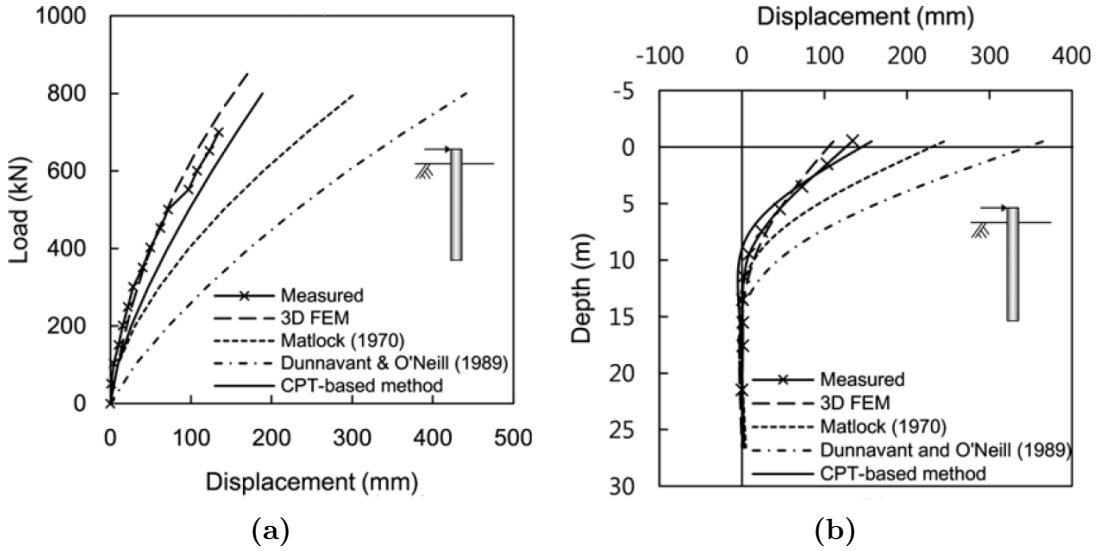

Figure 2.47: Predicted and measured (a) pile head load-displacement curves and (b) horizontal displacement along the pile for pile head lateral load H=700kN of the static laterally loaded pile test (Incheon site).

2.48 with the corresponding measurements of the large-scale test. The lateral soil response for sand layers was simulated through p-y curves proposed by API (2007). The comparison demonstrates a very satisfactory agreement between the predictions of the CPT-based p-y criteria, Matlock's p-y curves and the corresponding test measured curves. On the contrary, the predictions of Reese et al. and Dunnavant and O'Neill were judged conservative for the cyclic load test.

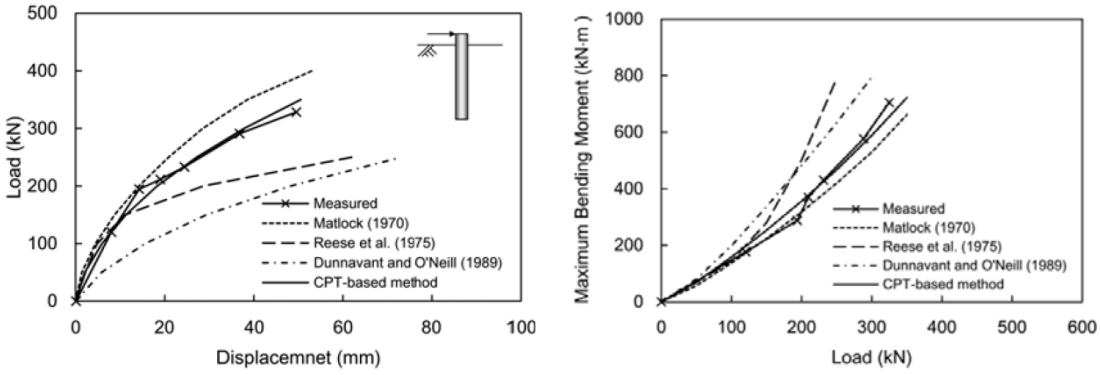

Figure 2.48: Predicted and measured (a) pile head load-displacement and (b) maximum bending moment-pile head load curves for the 15th cycle of the cyclic laterally loaded 0.610m-diameter pile (Salt Lake City, US).

2.7 The ultimate lateral soil resistance

In the current section, studies on solely the ultimate lateral soil resistance p_u of p-y curves for cohesive soils are presented. Many researchers have attempted to evaluate experimental results, field observations or output from numerical simulations and compare them with analytical solutions. Herein, the most renowned studies on the specific topic are enlisted and briefly described, followed by a comparative depiction.

2.7.1 Broms (1964)

The method presented by Broms (1964) was one of the first attempts to estimate the ultimate lateral resistance of piles in cohesive soils. Assuming a specific distribution of this resistance with depth, the proposed methodology allows for the calculation of the ultimate lateral pile load and maximum bending moment through static equilibrium equations. The aforementioned calculations were carried out for free-head and fixed-head piles of various lengths (short, intermediate, long) and are presented herein, along with graphs that group the derived solutions.

Free-head piles

For **short free-head** piles, the assumed distributions of ultimate lateral soil resistance, shear force and bending moment along the pile are depicted in Figure 2.49.

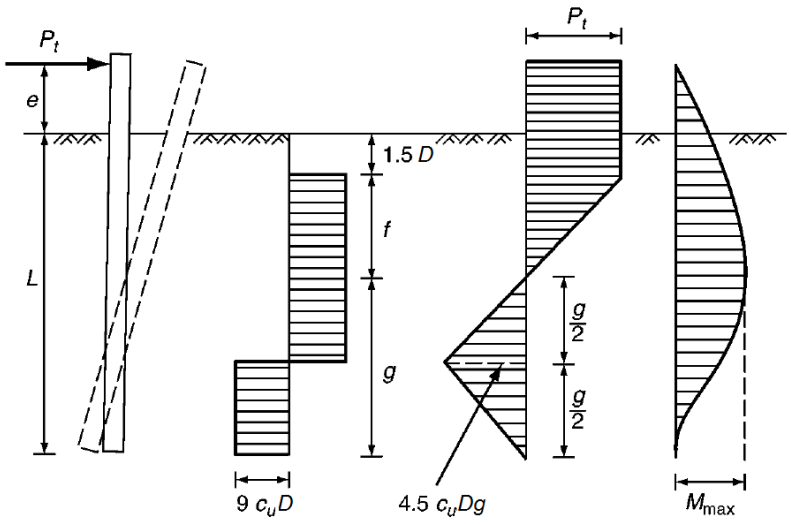

Figure 2.49: Distribution of soil resistance, shear force and bending moment for a short free-head pile in cohesive soil (Broms, 1964).

Integration of the upper part of the shear force diagram to the point of zero shear

(i.e., maximum bending moment) yields the following expression:

$$M_{max} = P_t(e + 1.5D + f) - \frac{9c_u D f^2}{2} \tag{2.109}$$

However, the point of zero shear force is located at:

$$f = \frac{P_t}{9c_u D} \tag{2.110}$$

and therefore Equation 2.109 is now written:

$$M_{max} = P_t(e + 1.5D + 0.5f) \tag{2.111}$$

By integrating the lower part of the shear force diagram, the following expression of the maximum bending moment also occurs:

$$M_{max} = 2.25c_u D g^2 \tag{2.112}$$

Finally, it is obvious from Figure 2.49 that the embedded length of the short pile verifies the expression:

$$L = (1.5D + f + g) \tag{2.113}$$

By solving Equations 2.110 through 2.113, the ultimate lateral load $P_{t,ult}$ of the pile that will lead to soil failure is calculated. After the calculation of $P_{t,ult}$, the maximum bending moment M_{max} is computed and compared with the moment capacity of the pile. If the value of the latter is greater than M_{max}, then the short pile shall fail due to soil failure. In his study, Broms included a set of curves for directly solving the corresponding problem through the pile and soil properties (Figure 2.50).

For **long free-head** piles, failure under lateral loading in cohesive soils occurs with the formation of a plastic hinge at a depth of $1.5D + f$. Equation 2.111 can then be used to calculate $P_{t,ult}$, assuming that the maximum bending moment is equal to the yield moment of the pile ($M_{max} = M_y$). Although the shape of the laterally loaded long pile is different from the one demonstrated in Figure 2.49, the static equilibrium equations remain the same for the upper part of the pile - above the plastic hinge. Figure 2.51 depicts the set of curves for the estimation of $P_{t,ult}$ for long, free- and fixed-head piles, depending on the yield moment of the pile, the pile diameter and the undrained shear strength of the soil.

It is important to consider the right pile failure mechanism - either short or long pile - for the estimation of the correct ultimate lateral load, according to the current

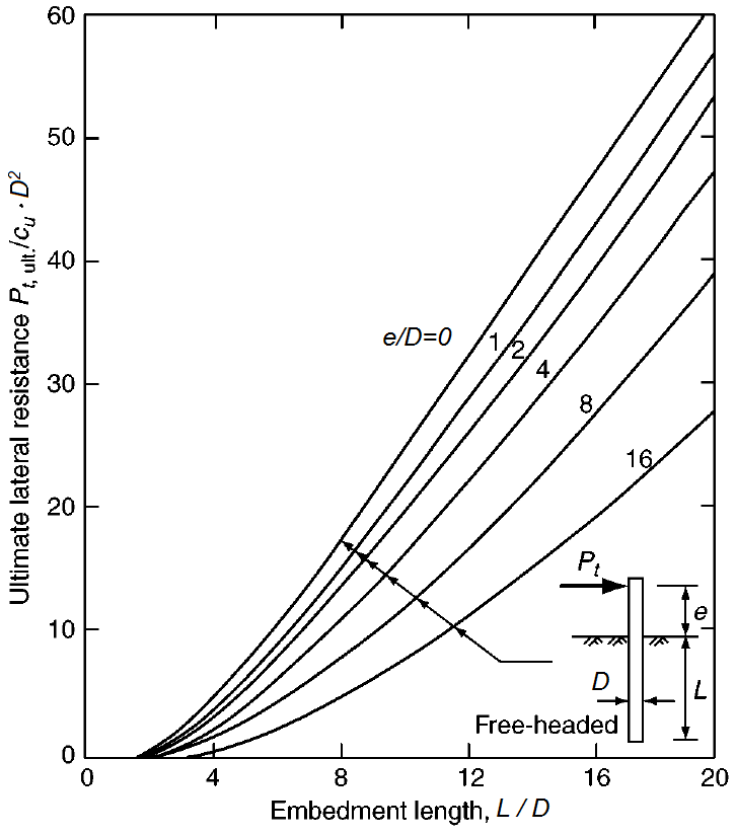

Figure 2.50: Design curves for short free-head piles under lateral loading in cohesive soil.

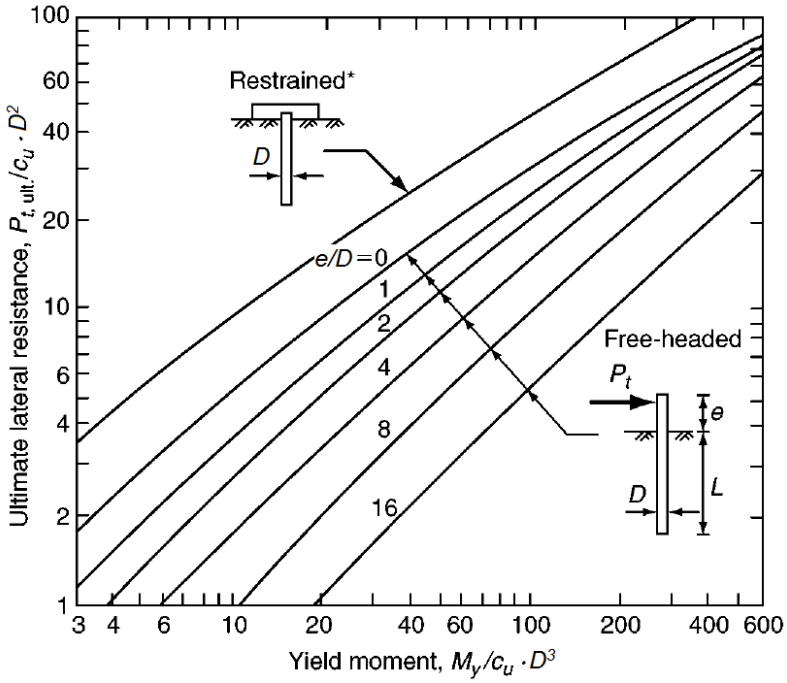

Figure 2.51: Design curves for long free- and fixed-head piles under lateral loading in cohesive soil.

methodology. In order to calculate the critical length differentiating the two pile behaviors, Equations 2.110 through 2.113 can be solved assuming that $M_{max} = M_y$. Piles longer than this critical length shall fail by yielding. Otherwise, a particular solution may initiate using the short-pile equations; if the resulting $M_{max} > M_y$, the long-pile solution is to be used.

Fixed-head piles

For **short fixed-head** piles, failure occurs through a horizontal movement of the pile with the full lateral soil resistance developing over the embedded length of the pile except for the top $1.5D$ that is not taken into account. The following simple equation calculates the ultimate lateral load $P_{t,ult}$ of this failure mode of the pile through a simple force equilibrium:

$$P_{t,ult} = 9c_u D(L - 1.5D) \tag{2.114}$$

For **intermediate fixed-head** piles, the assumed distributions of ultimate lateral soil resistance, shear force and bending moment along the pile are depicted in Figure 2.52. As the pile length increases from short to intermediate, a plastic hinge is formed on top of the pile. The top of the pile shall rotate and a point of zero deflection will exist somewhere along the pile. The following expression calculates the maximum

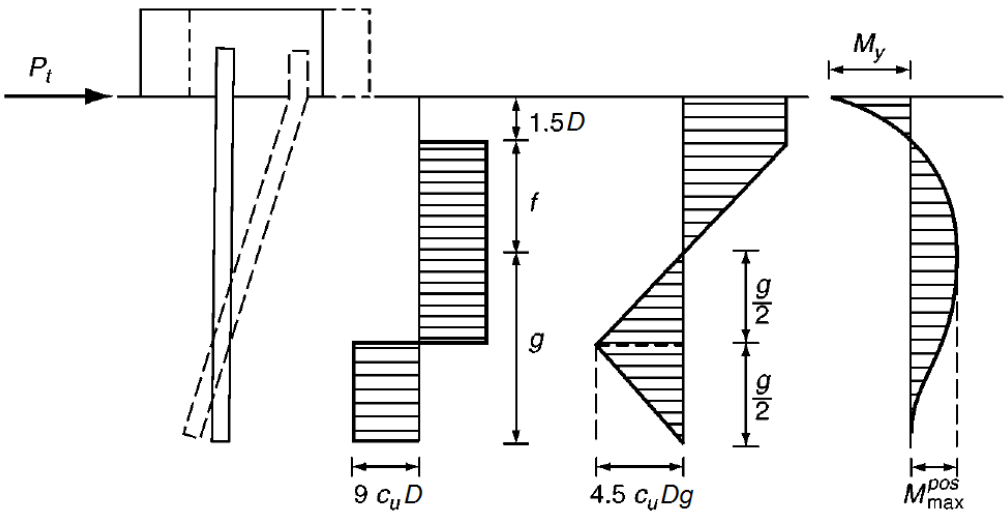

Figure 2.52: Distribution of soil resistance, shear force and bending moment for an intermediate fixed-head pile in cohesive soil (Broms, 1964).

positive moment for the point of zero shear force:

$$M^{pos}_{max} = P_t(1.5D + f) - f\,(9c_u D)\left(\frac{f}{2}\right) - M_y \tag{2.115}$$

By substituting the value of f from equation

$$f = \frac{P_t}{9c_u D} \tag{2.116}$$

the aforementioned expression of M_{max}^{pos} becomes:

$$M_{max}^{pos} = P_t(1.5D + 0.5f) - M_y \tag{2.117}$$

Integration of the shear force distribution for the lower portion of the pile delivers:

$$M_{max}^{pos} = 2.25c_u D g^2 \tag{2.118}$$

Finally, it is obvious from Figure 2.52 that the embedded length of the intermediate fixed-head pile verifies the expression:

$$L = (1.5D + f + g) \tag{2.119}$$

The solution of Equations 2.116 through 2.119 leads to the calculation of the ultimate lateral load $P_{t,ult}$ for the intermediate fixed-head pile.

For **long fixed-head** piles, failure under lateral loading in cohesive soils occurs with the formation of a plastic hinge at the point of the maximum positive moment. Equation 2.117 can then be used to calculate $P_{t,ult}$, assuming that $M_{max} = M_y$:

$$P_t = \frac{2M_y}{1.5D + 0.5f} \tag{2.120}$$

By solving Equations 2.120 and 2.116, $P_{t,ult}$ is obtained for the long fixed-head pile.

Broms finally commented on the influence of repetitive loading in the ultimate lateral soil resistance of cohesive soils. More specifically, he claimed that the gradual degradation of soil shear strength caused by cyclic loading may decrease the ultimate lateral soil resistance to about one-half its initial value.

2.7.2 Limit Equilibrium Method (LEM)

Various false estimations of the ultimate lateral soil resistance p_u were attempted during the early years in the analysis of laterally loaded piles. Engineers failed to adopt Terzaghi's recommendations that values of p_u could not exceed half the bearing capacity of the soil (Terzaghi, 1955). Therefore, lacking rational methods for the computation of the lateral bearing capacity, the following two simplistic simulations were applied for solving the problem through limit equilibrium equations.

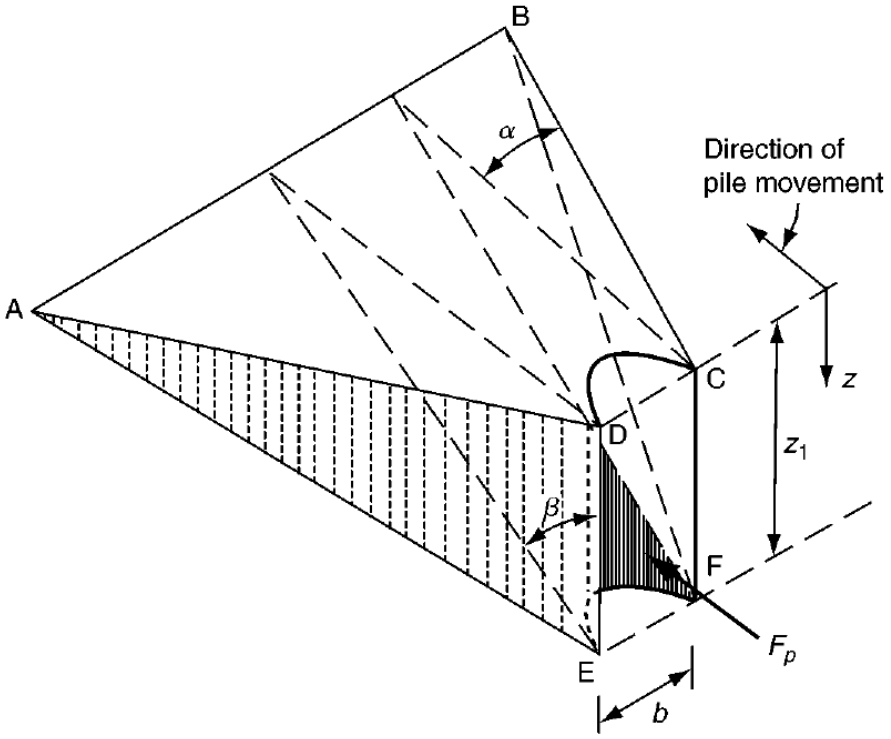

Figure 2.53: Model of the wedge failure mechanism in front of a laterally loaded pile (Reese & Van Impe, 2010).

The first model assumed a soil wedge forming in front of the laterally loaded pile for relatively shallow depths (Figure 2.53). The ultimate lateral force F_p acting on the soil wedge from the pile may be computed by integrating the horizontal components of the frictional resistances on the sliding surfaces and taking the wedge weight into account. Through differentiation of F_p with depth z below ground surface, an expression for the ultimate lateral soil resistance p_u along the pile is derived. Although the simplicity of the wedge model is evident, the resulting solutions shown in Figure 2.55 demonstrate that pile diameter D, depth z and soil properties have significant effect in p_u. Specifically for a fully saturated cohesive soil subjected to undrained lateral pile loading, the derivative of F_p with respect to z, assuming angle α=0, yielded the following p_u expression per pile unit length.

$$p_{u,1} = c_a\ D\left[\tan\beta + (1+\kappa_c)\cot\beta\right] + \gamma D z + 2c_a\ z(\tan\beta\sin\beta + \cos\beta) \qquad (2.121)$$

where c_a= the average undrained shear strength over the wedge depth and κ_c= a shearing resistance reduction factor along the pile face. Assuming κ_c=0 - reasonable for cyclic loading, where little relative pile-soil movement occurs - as well as angle

β=45^o, Equation 2.121 becomes:

$$p_{u,1} = 2c_a\ D + \gamma Dz + 2.83c_a\ z \tag{2.122}$$

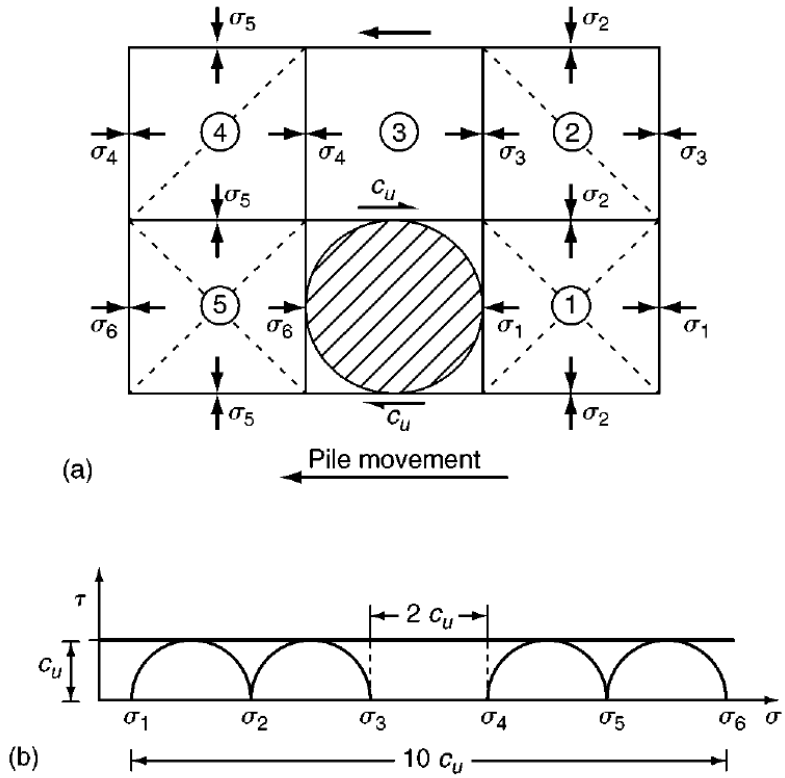

Figure 2.54: Model of the plane strain failure mechanism of a laterally loaded pile at great depth (Reese & Van Impe, 2010). (a) Horizontal section and (b) Mohr-Coulomb failure of the model for cohesive soils under undrained loading conditions.

It is reasonable to assume that below a specific depth the wedge failure mechanism will give way to a flow-around-pile plane strain failure form. Thus, the second simulation (Figure 2.54a) depicts a horizontal section of a cylindrical pile along with five blocks of soil around it and the normal and shear stresses developed between all the previous. This model is also rather simple and based on the assumption that Blocks 1, 2, 4 and 5 fail by shearing, while Block 3 fails by sliding. The ultimate lateral pressure is then calculated as the difference between the stresses σ_6 and σ_1. Figure 2.54b depicts the corresponding Mohr-Coulomb circles at failure for a clay under undrained loading conditions, which were used to derive equations representative of the aforementioned plane strain failure mechanism. In more detail and assuming constant undrained shear strength c_u with depth, $(\sigma_6 - \sigma_1)$ is found equal to $10c_u$ although other work - not shown here - pointed out that a value of $11c_u$

would be more rational.

$$p_{u,2} = (\sigma_6 - \sigma_1)\ D = 11\ c_u\ D \tag{2.123}$$

Thompson (1977) in his dissertation differentiated Equation 2.121 with respect to z and evaluated the resulted expressions numerically. Figure 2.55 depicts his findings with continuous lines, assuming negligible influence of the term γ/c_a and for values of κ_c=0 and 1. Equations 2.122 and 2.123 are demonstrated in the same figure, also under the assumption of an insignificant γ/c_a term. Solving for the intersection of the aforementioned equations, the depth for the transition from a wedge to a plane strain failure mechanism is equal to about $3.2D$. For comparative purposes, Figure 2.55 includes the distribution of p_u with depth, recommended by Hansen (1961a, 1961b) according to Equation 2.124. Hansen's proposals agree very satisfactorily with the p_u estimations based on the LEM close to the ground surface (wedge-type failure); however, for greater depths significant difference is observed between the two approaches.

$$\frac{p_u}{c_u\ D} = \frac{2.567 + 5.307\ \dfrac{z}{D}}{1 + 0.652\ \dfrac{z}{D}} \tag{2.124}$$

Ashour et al. (1998, 2000) presented a thoroughly developed strain wedge (SW) model, which results in the formulation of p-y curves through an analytical solution of the pile-soil interaction problem. The proposed SW model is capable of simulating the effects of soil layering, pile bending stiffness, pile cross-sectional shape, pile-head fixity and pile-head embedment on the derived p-y curves. However, it addresses the problem of the laterally loaded pile from an analytical aspect that exceeds the purpose of the current literature review.

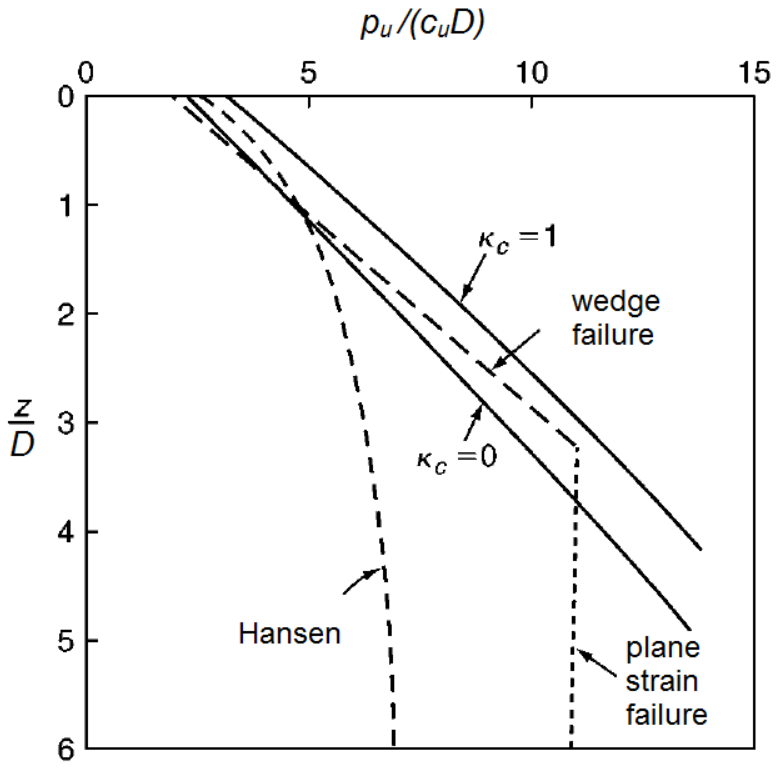

Figure 2.55: Elaboration on the ultimate lateral resistance of cohesive soils by Thompson (1977).

2.7.3 Randolph and Houlsby (1984)

The study carried out by Randolph & Houlsby (1984) refers to the limiting pressure acting on a circular, laterally loaded pile in cohesive soil. Modelling the soil as a perfectly plastic, cohesive material and assuming flow-around failure along the pile reduces the pile-soil interaction to a plane strain problem. Thus, lower bound and upper bound approaches of plasticity theory were utilized and the collapse load of a cylindrical pile moving laterally through an infinite medium was calculated analytically. It has to be stated in advance that the solutions developed herein refer to a rigid, perfectly plastic response of the soil, with a shear strength c independent of the in situ total stress field and the assumption of a constant volume deformation mechanism (associated flow rule). At the end of the study, approximate calculations of the same collapse load using cavity expansion theory and wedge failure assumption near soil surface were compared with the aforementioned plasticity theory solutions.

The lower bound solution assumes a stress distribution in the soil that comes in equilibrium with an applied lateral load. Provided that the aforementioned stress field does not violate the failure criterion of the soil, the applied load will be less than or equal to the true failure load. A geometry of characteristics - namely slip

lines representing planes, on which the observed shear stress is maximized - used in the current lower bound solution, is depicted in Figure 2.56. Three different mesh zones are defined (EQC, CQFA and FAF') for one quadrant of the pile-soil interaction and the corresponding normal and shear components on the characteristics are calculated. Summation of the forces on each of the four quadrants shows that whereas shear strength terms are additive, mean stress terms cancel, thus indicating no effect of the latter on the failure load of the pile. The ultimate lateral soil resistance per unit length of the pile from the lower bound solution was calculated:

$$\frac{p_{u,l}}{c \cdot D} = \pi + 2\Delta + 2\cos\Delta + 4\left[\cos\left(\frac{\Delta}{2}\right) + \sin\left(\frac{\Delta}{2}\right)\right] \tag{2.125}$$

where D= the pile diameter and $\Delta = \sin^{-1}\alpha$, with α the pile-soil adhesion[1] factor $(0 < \alpha < 1)$.

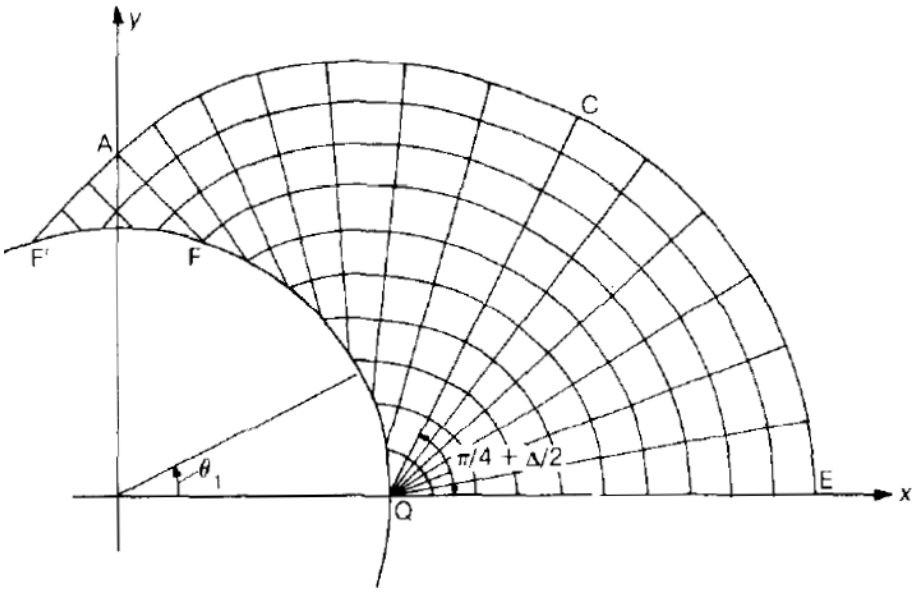

Figure 2.56: Characteristic mesh of the lower bound solution.

In the upper bound solution, a failure mechanism is postulated and the collapse load is calculated through the equation of the rate of energy dissipation within the deforming soil mass with the work produced by the external load. The velocity field associated with the postulation of the failure mechanism is mapped and five separate deformation mechanisms are observed on the quadrant of the pile-soil interaction (Figure 2.57). The following calculated ultimate lateral soil resistance from the upper bound solution matched exactly the corresponding expression according to

[1]The shear strength mobilized on the pile-soil interface is called adhesion and is assumed equal to the product $\alpha \cdot c_u$ in undrained conditions.

the lower bound solution (Equation 2.125).

$$\frac{p_{u,u}}{c \cdot D} = \pi + 2\Delta + 4\cos\psi \left(\sqrt{2} + \sin\psi\right) \tag{2.126}$$

where $\psi = \pi/4 - \Delta/2$.

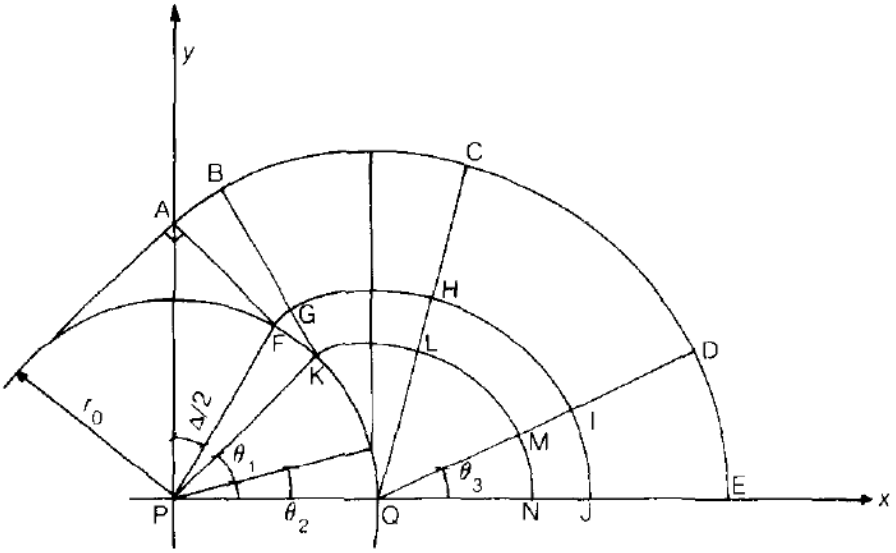

Figure 2.57: Deformation mechanism of the upper bound solution.

Taking into account former literature proposals on the ultimate lateral soil resistance for cohesive soils, the current study attempted to expand its recommendations by raising the issues of the wedge failure mechanism close to ground surface and of cavity expansion. These observations together with the analytical solutions of plasticity theory are summarized into the following:

- For shallow soil depths up to $z \approx 3D$, a wedge failure mechanism is assumed to develop in front of the pile. The ultimate lateral soil resistance for this depth range is calculated according to the equation:

$$\frac{p_u}{c \cdot D} = 2 + \frac{\sigma_{vo}}{c} + 1.5\ \frac{z}{D} \tag{2.127}$$

  where σ_{vo}= the vertical geostatic stress of the soil at the desired depth z, either total or effective, depending on the level of the water table.

- For a cavity expansion failure mechanism developed anywhere along the pile, the following expression is proposed:

$$\frac{p_u}{c \cdot D} = 7 + \frac{\sigma_{ho}}{c} \tag{2.128}$$

where σ_{ho}= the horizontal geostatic stress of the soil at the desired depth z, either total or effective, depending on the level of the water table.

- For flow-around failure mechanism along the pile, analytical lower and upper bound solutions of plasticity theory (Equations 2.125 and 2.126 respectively) yielded the following expression, assuming an average adhesion factor α=0.4:

$$\frac{p_u}{c \cdot D} = 10.5 \tag{2.129}$$

Since different soil failure mechanisms may develop along the pile, the study suggests that the aforementioned expressions are plotted with depth and the minimum value of the three is chosen.

2.7.4 Murff and Hamilton (1993)

Another study to estimate the ultimate undrained lateral soil resistance of cohesive soils, using the upper bound approach of plasticity theory, was carried out by Murff & Hamilton (1993). The failure mechanism of the soil surrounding the laterally loaded pile was captured for shallow (wedge) as well as for greater depths (plane strain). Furthermore, the effect of complex conditions such as pile-head fixity, pile-soil adhesion, suction behind the pile, soil layering and varying soil strength with depth was examined. After deriving the upper bound solution for the collapse load of the pile, centrifuge tests were performed to verify it and an empirical fit on the analytical results was proposed.

Various simulations took place to investigate the effect of the aforementioned parameters on the ultimate lateral soil resistance. Initially, the effect of soil strength distribution was examined on a rigidly translating pile through the soil (no rotation). Figure 2.58 depicts the comparison of the lateral bearing capacity factor N_p for uniform and linearly increasing undrained shear strength with the corresponding proposed values by Matlock (1970) and Reese et al. (1975) (see Paragraphs 2.3.1 and 2.4.2 respectively). Distinct differences are observed between the two strength distributions, as well as between the literature recommendations and the values derived from the upper bound solution. Another simulation referring to the effect of pile rotation showed negligible influence of the latter on the ultimate lateral soil resistance, in consistency with corresponding findings by Matlock (1970). The effect of pile-soil adhesion was also investigated, with the interaction considered only for the front of the pile during the current simulation. Results of N_p with depth for a smooth and a rough pile - no and full adhesion respectively - demonstrate a

significant effect of the specific feature on the ultimate lateral soil resistance (Figure 2.59).

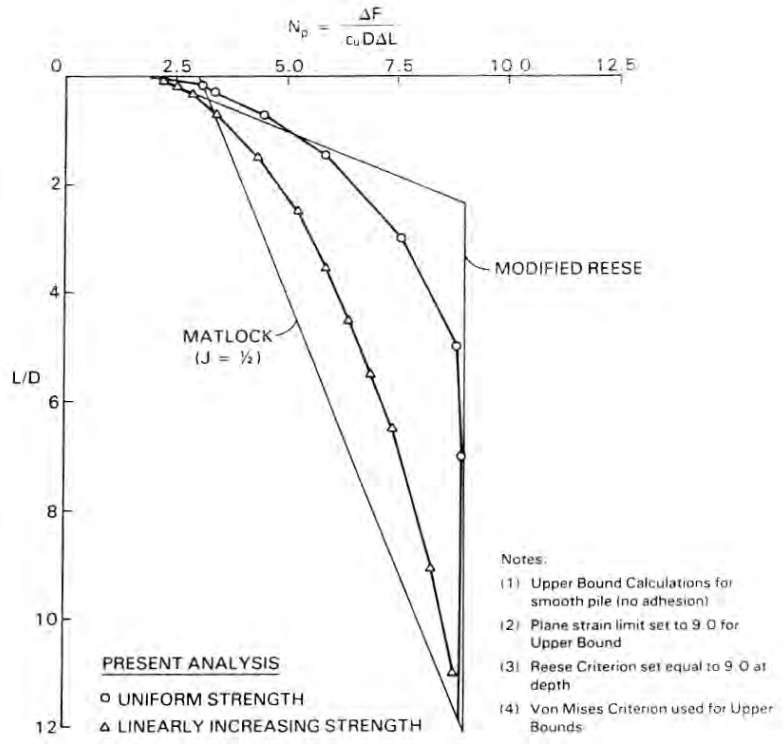

Figure 2.58: Effect of c_u distribution with depth on the lateral bearing capacity factor N_p.

The results of the previously mentioned studies allowed for a better understanding of suction behind the pile and tip-rotational resistance, along with the mechanisms developed around the pile with these components. Suction can develop on the back of a pile during abrupt monotonic lateral loading, thus "triggering" an active failure mode in that soil region. The model of the current study idealized this mechanism through an active wedge on the backside of the pile, which significantly increased the increase rate of ultimate lateral soil resistance close to the ground surface and caused the plane strain failure type to occur at shallower depths. Tip-rotational resistance was accommodated to the proposed model through a spherical segment on the tip, with a center at the rotational center of the mechanism. In this way, significant resistance developing at the tip of a short, rigid, laterally loaded pile can be taken into account.

Centrifuge tests on rigid, monotonic laterally loaded, model piles were carried out at Cambridge University in order to verify the predictions of the proposed analytical model on the ultimate lateral resistance of clayey soils. In more detail, the experiments were performed in a sedimented kaolin clay with undrained shear

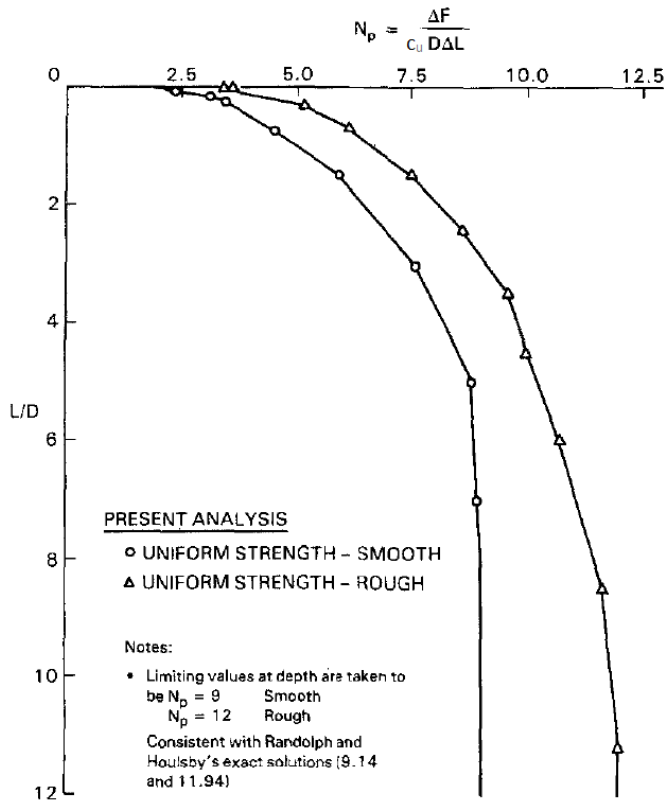

Figure 2.59: Effect of the pile-soil adhesion on the lateral bearing capacity factor N_p.

strength c_u=9kPa at the surface and a rate of increase equal to 1.4kPa/m with depth. Lateral displacement of 0.5 pile diameters was applied on the fixed heads of the test piles, allowing for development and measurement of the ultimate lateral soil resistance to depths greater than the wedge failure mechanism - sometimes to over 10 diameters below ground surface. It is important to mention that a wide range of prototype pile diameters were tested, up to 2.45m for the highest centrifuge acceleration imposed to the model. Figure 2.60 depicts the lateral bearing capacity factor N_p with dimensionless depth z/D distribution derived from three different sources: centrifuge test results, the proposed analytical solution (including suction effects and full pile-soil adhesion) and values suggested by Matlock (1970). Despite the scatter of centrifuge test results up to a depth of one pile diameter below the mudline, the conclusion is drawn that limiting values of the ultimate lateral soil resistance appear not deeper than two pile diameters, apparently as proposed by the failure mechanism of the current study. Furthermore, these values were obtained approximately equal to 11 c_u D, thus matching the recommendations of Reese et al. (1975) and Randolph & Houlsby (1984). Full pile-soil adhesion conditions were confirmed along the test piles after the completion of the centrifuge tests.

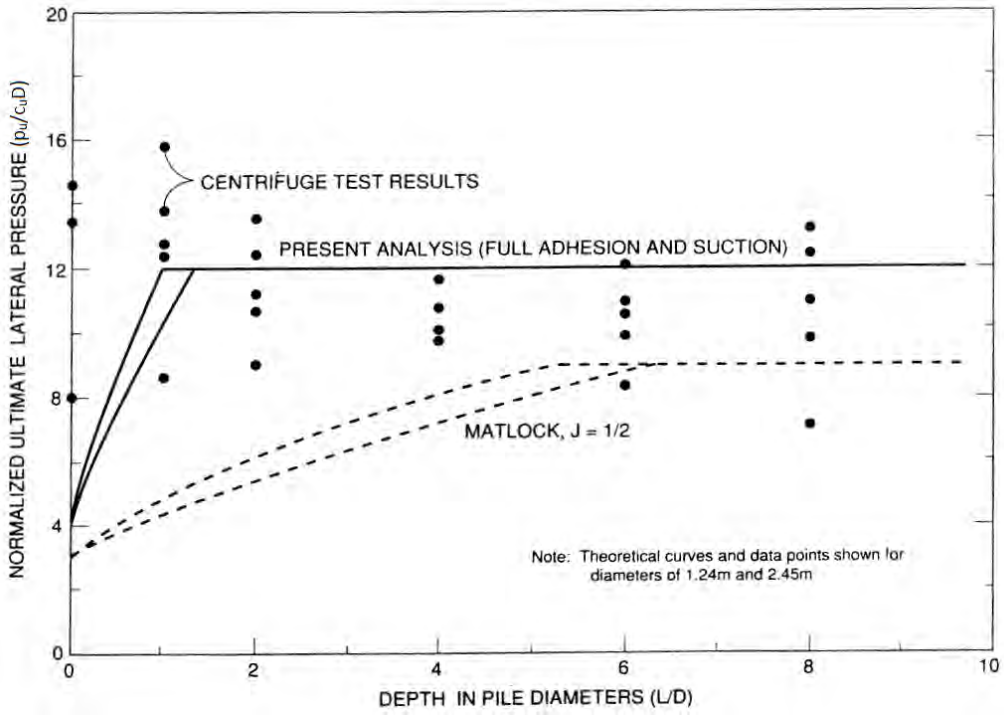

Figure 2.60: Experimental versus predicted N_p.

Finally, an empirical fit on the derived upper bound solution of the current study was proposed, according to the following steps:

1. The non-dimensional lateral bearing capacity factor N_p of a cohesive soil with linearly increasing undrained shear strength with depth depends on the depth to diameter ratio z/D, the undrained shear strength at ground surface $c_{u,0}$ and the linear rate of strength increase with depth $c_{u,1}$.

2. Define parameter ξ for the soil according to the following equations:

$$\xi = 0.25 + 0.05\lambda \quad \text{for} \quad \lambda < 6 \tag{2.130a}$$

$$\xi = 0.55 \quad \text{for} \quad \lambda \geq 6 \tag{2.130b}$$

   where $\lambda = c_{u,0}/(c_{u,1}D)$. In case of either negligible $c_{u,0}$ or uniform c_u with depth (i.e., $c_{u,1} \approx 0$), ξ=0.25 and 0.55 respectively.

3. The following empirical function of N_p is proposed:

$$N_p = N_1 - N_2 \, exp\left(-\frac{\xi z}{D}\right) \tag{2.131}$$

where N_1= the limiting value of N_p at great depth (i.e., plane strain failure) and $(N_1 - N_2)$= the value of N_p at ground surface.

4. The ultimate lateral soil pressure along the pile is defined as:

$$p_u = N_p \, c_u + \gamma' z \tag{2.132}$$

A series of calculations was performed in order to estimate the lateral force required for the failure of a laterally loaded pile in a cohesive soil with linearly increasing undrained shear strength, both with the upper bound solution and the aforementioned empirical fit. The comparison demonstrated in Figure 2.61 for various values of parameter λ was judged almost excellent.

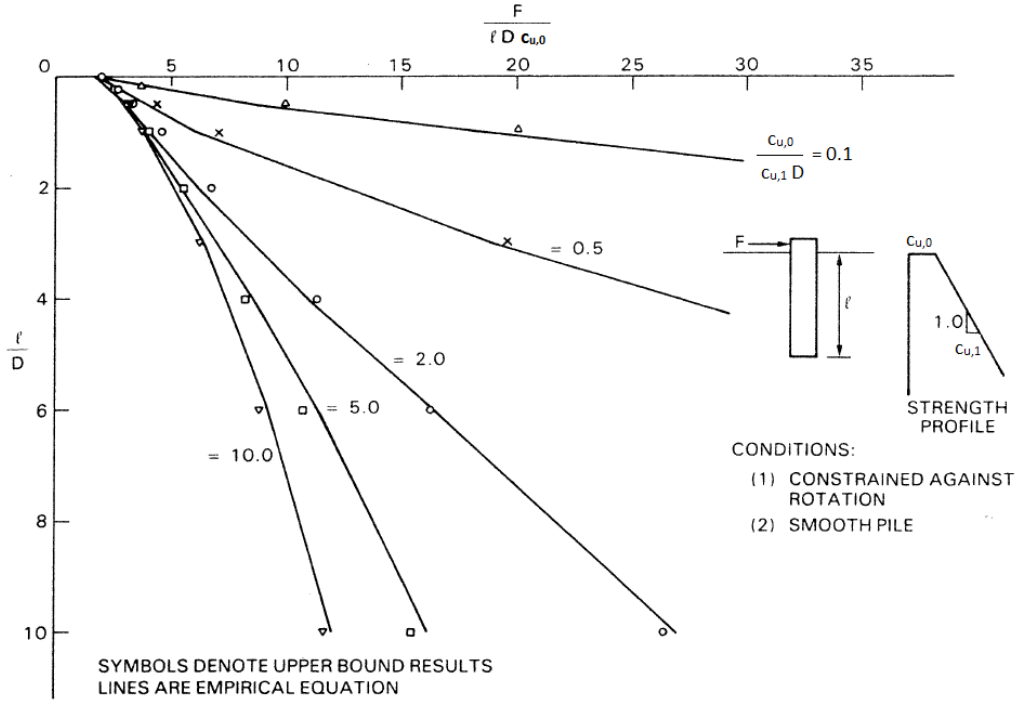

Figure 2.61: Empirical fit on the upper bound solution results for linearly increasing c_u with depth.

Certain equations were derived during this study also for a laterally loaded pile in a two-layer cohesive soil. However, they exceed the research field of the current literature review and therefore are not described herein.

2.8 The initial subgrade reaction modulus

P-y curves are generally defined by the ultimate lateral soil resistance p_u and the initial curve stiffness K_i. The latter is discussed in the current section and certain

clarifications on its estimation are presented. It is important to point out that K_i is actually the coefficient of the initial horizontal subgrade reaction of the soil (units F/L^3) multiplied by the pile width. Thus, according to Terzaghi (1955), Scott (1981), Reese & Van Impe (2010) and many other researchers, K_i of the p-y curves (per unit length of a pile) is not expected to vary with pile width.

Although many literature references have elaborated on the horizontal subgrade reaction modulus, it is either the chord or the secant p-y curve modulus that they refer to (Terzaghi (1955), Broms (1964), Poulos (1971), Baguelin et al. (1977), Scott (1980), Bowles (1988) et al.). Such stiffness estimations are very useful in terms of working loads of laterally loaded piles. However, engineering practice has shown that the design of such piles is primarily controlled by limit-state stresses and thus lateral loads are limited either by maximum bending moment or combined stress and maximum deflection restrictions. Therefore, it is important to clarify that the initial subgrade reaction modulus K_i is of concern when aiming in the formulation of p-y curves.

Certain p-y curve methodologies presented in Sections 2.3, 2.4 and 2.5 propose specific values of K_i, depending on the undrained shear strength c_u of the clay and the pile-soil relative stiffness. However, certain mathematical formulas on the initial, small-strain elasticity modulus of the soil - and subsequently on K_i - were not detected in literature. Thus, the reader is directed to the aforementioned Sections for specific estimations on K_i. In the case of p-y curve methodologies that do not propose a K_i expression directly, single differentiation of the corresponding p-y curve equation with respect to displacement y and under the assumption of a significantly low initial y_i will yield a decent estimation of the desired K_i.

2.9 Concluding remarks on the p-y method

The following figures depict a general comparison of the p-y curve methodologies applicable to soft, normally consolidated clays (Figure 2.62) and the corresponding proposals on the ultimate lateral soil resistance factor N_p and the initial p-y curve stiffness K_i (Figure 2.63), as described in the current chapter. For the literature recommendations lacking a profound equation on the estimation of K_i, the initial subgrade reaction modulus is estimated as the first derivative dp/dy of the p-y curve equation for an infinitesimal value of y.

In correspondence to the comparison for soft clays, the following figures compare the p-y curve methodologies applicable to stiff, overconsolidated clays (Figure 2.64) and the corresponding proposals on the ultimate lateral soil resistance factor N_p and

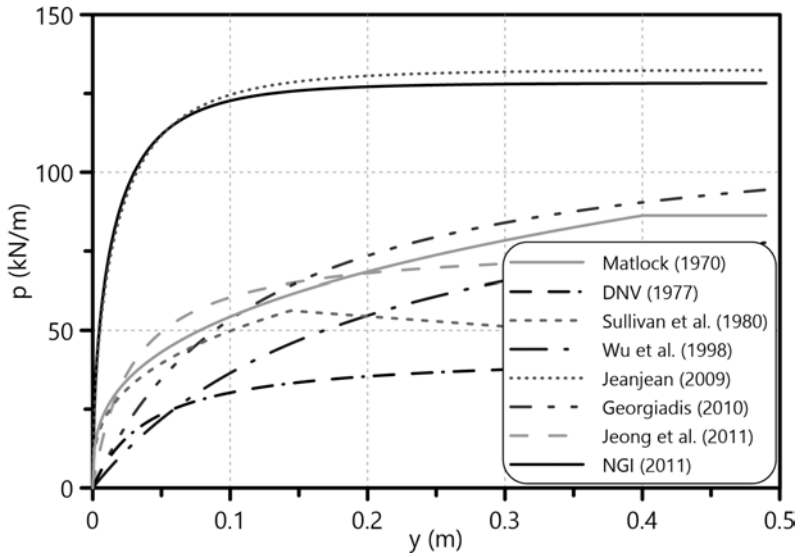

Figure 2.62: Literature p-y curves for soft, normally consolidated clays (z=3m, D=1m).

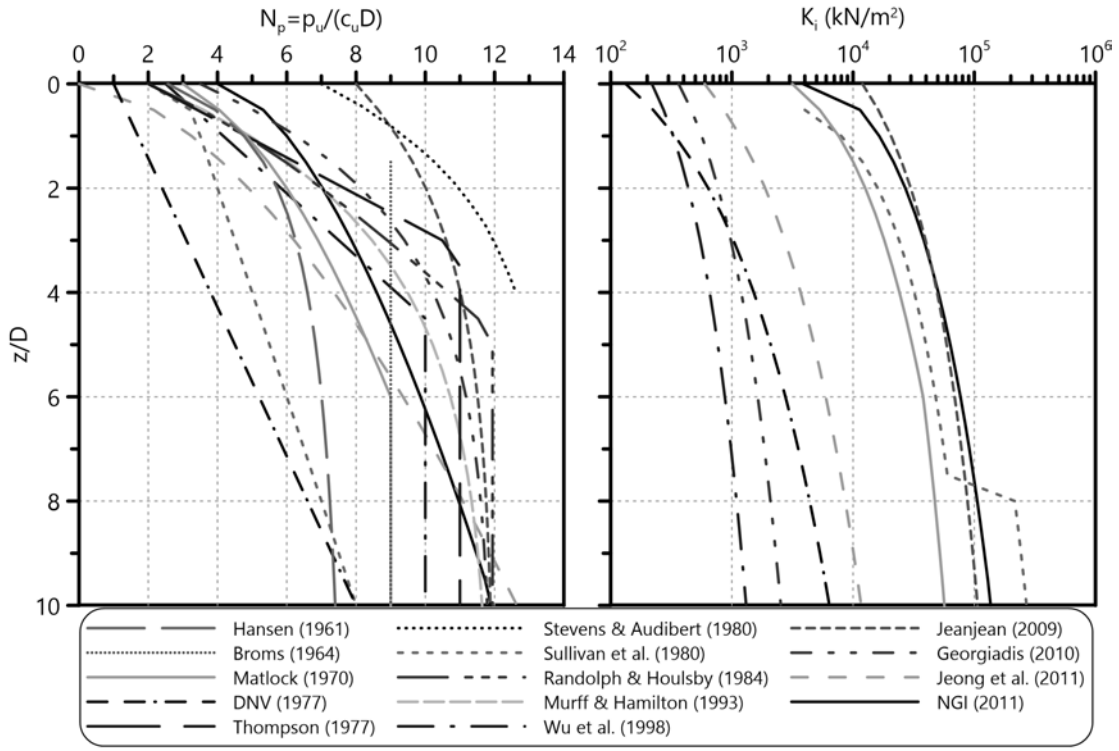

Figure 2.63: Literature proposals on the ultimate lateral soil resistance factor N_p and the initial p-y curve stiffness K_i for soft, normally consolidated clays.

the initial p-y curve stiffness K_i (Figure 2.65), as described in the current chapter.

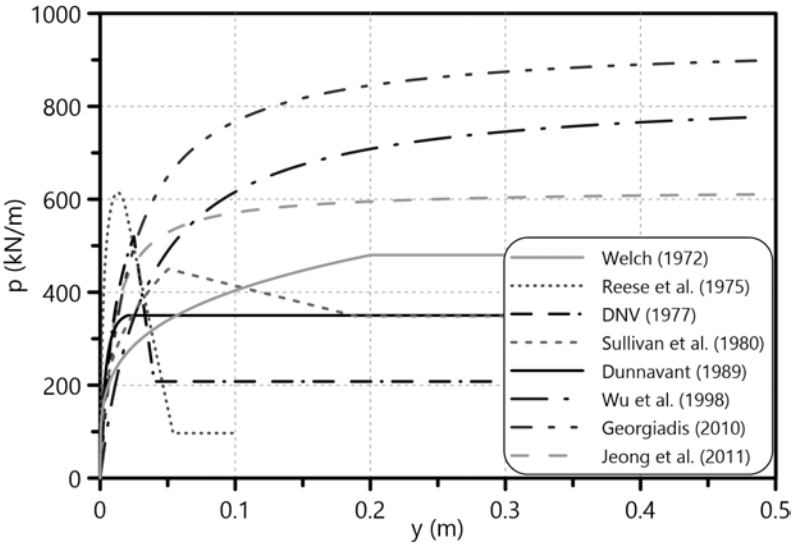

Figure 2.64: Literature p-y curves for stiff, overconsolidated clays (z=3m, D=1m).

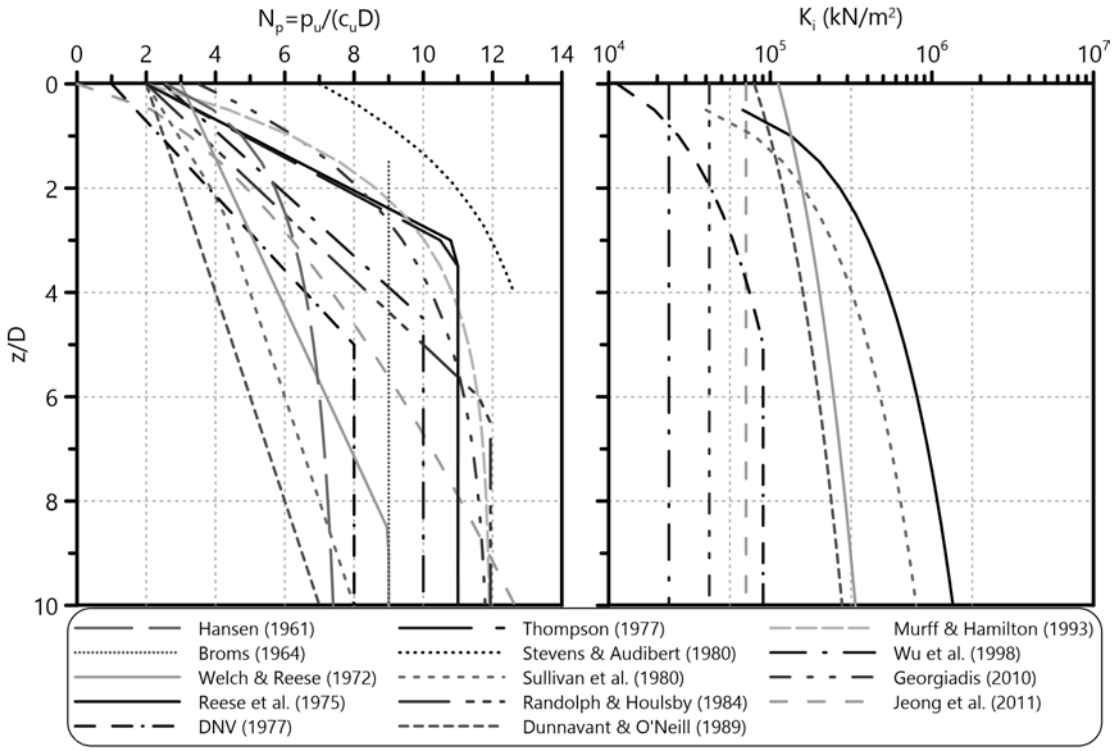

Figure 2.65: Literature proposals on the ultimate lateral soil resistance factor N_p and the initial p-y curve stiffness K_i for stiff, overconsolidated clays.

The general conclusion is drawn that a very intense scatter exists among the literature p-y curves and their major characteristics - p_u and K_i. Regarding these

two main parts of the p-y curve relationships, the aforementioned observed deviation reaches up to two orders of magnitude for the initial curve stiffness K_i and up to 150% for the ultimate lateral soil resistance p_u. It is obvious that such deviation levels make the design of laterally loaded piles in such soils particularly uncertain. Therefore, an extensive numerical investigation of the specific topic is judged necessary and is presented in the following chapters through the current dissertation.

Chapter 3

Numerical development of p-y curves for clays

3.1 General

This introductive paragraph briefly presents past research on the numerical development of p-y curves for clayey soils. The section focuses on simulation parameters potentially improved through the current dissertation and points out the motivation of this research attempt.

The p-y curve methodology proposed by Jeanjean et al. (2009) for soft clays (see Paragraph 2.3.2) involves the performance of FEA for calibration purposes. Nichols et al. (2014) developed corresponding p-y curves from FEA in the code PLAXIS 3D, utilizing an NGI clay material model for the simulation of the soft clay. Finally, Georgiadis & Georgiadis (2010) proposed unified p-y curves - either for soft or stiff clays (Paragraph 2.5.4) - that they developed directly from 3D total stress FEA in PLAXIS 3D, incorporating an elastic-perfectly plastic Tresca constitutive law to simulate the clayey soil.

The FEA configuration developed herein generally refers to effective stress, coupled numerical analyses with parallel solution of the mechanical and the hydraulic problem. Moreover, the current dissertation adopts Critical State Soil Mechanics with corresponding constitutive laws for the soil simulation. Since the existing FEA (Georgiadis & Georgiadis, 2010; Jeanjean et al., 2009; Nichols et al., 2014) for the numerical development of p-y curves in clays lack such sophisticated soil simulation, we became motivated by potential comparisons of our findings with the aforementioned methodologies. Going through the era of immense computational power, the modern engineer needs to evaluate the problem variables and determine the amount of this power required in order to solve his problem cost effectively. Solely for the

functional configuration of coupled FEA with complex soil-pile interface simulations, one must investigate thoroughly several numerical benchmark problems. Furthermore, the thesis attempts to simulate certain crucial features of stiff OC clays such as small-strain stiffness and structure degradation that play a significant role especially in the cyclic lateral pile response.

The present chapter describes the base-model for the numerical simulation of a laterally loaded pile under undrained loading conditions - examined in the current dissertation. Moreover, this section parametrically investigates the influence of the following properties and characteristics of the model on the derived p-y curves:

- Soil simulation
- Pile simulation
- The process of the p-y curves derivation
- FEA mesh density and boundary effects
- Soil-pile interaction properties
- Geometrical nonlinearity
- Pile head fixity
- Soil constitutive law

3.2 The FEM numerical model

The following paragraphs describe the numerical model that we designed and analyzed through Simulia Abaqus 6.12. In more detail, we present herein the geometry of the numerical model, the boundary conditions, the soil and pile simulation along with the soil-pile interface properties. In addition, we briefly describe the main constitutive laws utilized for the clay simulation during the FEA. Finally, the section enlists the analysis steps for the performance of a monotonic lateral pile loading - the general loading case of the current dissertation.

3.2.1 Geometry-Boundaries

A 3D finite element model is designed in order to simulate the single laterally loaded pile. The model simulates half the cross-section of the pile and the surrounding soil block for symmetry reasons (Figure 3.1), with either a concentrated lateral load H or a lateral displacement y_h applying on the pile head. The center of the pile

head cross-section coincides with the origin of the coordinate system xyz. The mesh generator descritized the simulated pile-soil system in $0.5D$-long elements along z-axis, where D the pile diameter.

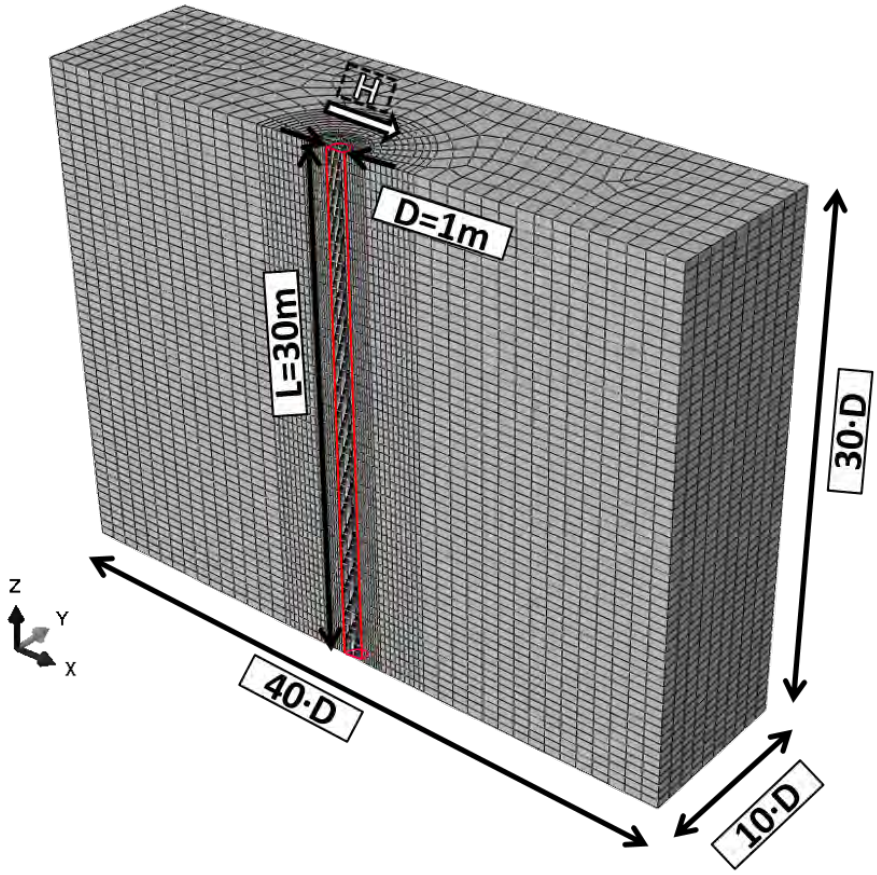

Figure 3.1: Dimensions and mesh of the 3D FEM numerical model basically analyzed in the current dissertation.

The FEM model restricts displacements along x- and y-axis on yz and xz planes respectively, thus simulating roll boundary conditions on the aforementioned planes. It also restrains vertical displacements on xy plane at the pile tip level, while allowing ground surface to deform freely. In addition, the rotation of the nodes of all structural elements about x-axis on the plane of symmetry are restrained. Finally, the simulation imposes hydraulic boundary conditions to the soil block; none of the model sides allows for water flow through it apart from the ground surface that is assigned zero pore water pressure and thus free drainage conditions.

Figure 3.1 depicts the boundaries of the numerical simulation, determined after sensitivity analysis on their distance from the laterally loaded pile. In more detail, we examined various distances of the soil block boundaries on the xy plane[1] and

[1]The FEM numerical model always considers z-dimension equal to the pile length L. Since the

ended up with the base-model dimensions (see Paragraph 3.3.2).

3.2.2 Soil constitutive laws

The current paragraph describes the constitutive laws assigned to the soil in the current dissertation. It initially analyzes the Modified Cam Clay (MCC) constitutive model. Subsequently, we present a set of modifications on the MCC, introduced by Kalos (2014) for the incorporation of small-strain stiffness and structure degradation in the constitutive model.

3.2.2.1 The Modified Cam Clay

The Cambridge models, Cam Clay (Roscoe et al., 1958; Schofield & Wroth, 1968) and Modified Cam Clay (Roscoe & Burland, 1968), represent some of the early attempts to develop comprehensive constitutive laws for soils. They are the outcome of an extensive research conducted in the University of Cambridge, including experimental investigation of the mechanical behavior of the clay from Cam river, after which the models are named. Within the aforementioned research, one should consider the work of Hvorslev and that of Rendulic of great importance. It was their work that leaded to the development of the Critical State Soil Mechanics (CSSM) (Schofield & Wroth, 1968), a generalized framework capable of describing in a unified way the mechanical behavior of soils under different stress paths and initial conditions. Critical State Soil Mechanics is based on the observation that a boundary surface exists for reconstituted soils in the $v-p-q$ space, the State Boundary Surface (SBS), defining the boundary between accessible and not accessible material states.

At first we shall examine the behavior of a reconstituted soil subjected to an isotropic consolidation test. It is convenient to plot the results of compression tests on the $v-p$ plane, where $v = 1 + e$ the specific volume and p the mean effective stress. In Figure 3.2 we may see the results of an isotropic compression test on a sample of reconstituted Kaolin Clay, involving loading by increasing p from A to B, unloading to D and then reloading along D-B-C. The observed behavior, neglecting the small loop in the unloading and reloading cycle B-D-B, can be idealized by two straight lines on the $v-\ln p$ plane. Researchers found that all compression tests on most reconstituted clayey soils can be similarly idealized and represented by:

- A straight line on the $v-\ln p$ plane, called the Isotropic Normal Compression Line (NCL), mathematically represented through $v = N_{iso} - \lambda \ln p$, where λ

pile is flexible and laterally loaded, no further soil profile is needed below the pile tip.

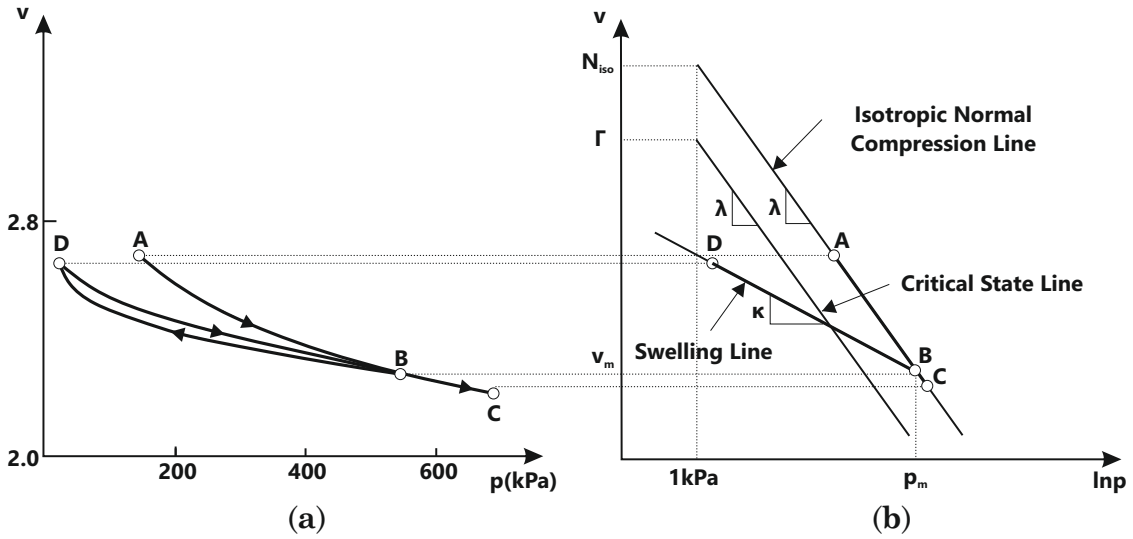

Figure 3.2: (a) An isotropic compression test on a Kaolin clay (Amerasinghe, 1973) (after Atkinson & Bransby (1977)). (b) The idealized compressibility framework on the $v - \ln p$ plane.

defines the slope, and N_{iso} the position of the NCL in the $v - \ln p$ plane. A soil state lying on the NCL represents a normally loaded (normally consolidated) soil, where its current stress state is also the maximum stress state ever imposed on the given soil. Soil states to the right of the isotropic NCL line cannot be attained[1] and thus it comprises a state boundary line.

- A set of parallel unloading - reloading lines (also called swelling lines), representing pre-loaded (overconsolidated) material states. The slope of the swelling lines is represented by κ and their position can be defined through the maximum mean effective stress p_m imposed in the soil under consideration. In the examined case, p_m, which is also called the preconsolidation pressure corresponds to the soil state at B.

Parameters κ, λ and N_{iso} are regarded as soil constants. Their value depends on the particular soil and is experimentally determined. Burland (1990) proposed the term intrinsic to describe soil properties of reconstituted clays. Intrinsic states can be used as a reference frame, to compare the structured behavior of natural soils with, allowing for a quantification of the effect of structure (due to ageing, thixotropy, bonding). Following Burland's definition, a material state lying on the aforementioned NCL can be characterized as intrinsic, while the corresponding compression line as an Intrinsic Compression Line (ICL).

[1]Structured soil states may exist on the right of the NCL, but at this point the presented analysis is restricted only to sructurless states

After describing the behavior of an isotropically compressed reconstituted material, we examine the behavior of isotropically consolidated soils loaded in triaxial compression tests to failure. In doing so, it is convenient to start from the behavior of normally consolidated soil samples that are triaxially compressed under drained or undrained conditions. Considering different tests initiating from various initial conditions (p, v), sheared under either drained or undrained conditions, the following comments can been made:

- Specimens which where initially compressed in higher p values sustain higher values of deviatoric stress q at failure, but the shape of the deviatoric stress (q) - deviatoric strain (ε_q) curves are similar.
- The data points at failure, plotted all together, define a single straight line passing through the origin on the $p-q$ plane and also a single curved line on the $v-p$ plane. It turns out that the latter is a line parallel to the normal compression line on the $v-\ln p$ plane. This single and unique line in the $v-p-q$ space is defined as the Critical State Line (CSL). It is the obvious that the CSL defines the failure of all normally consolidated samples, irrespective of the initial conditions and the stress path followed. It represents the state of the soil at which large shear strains accumulate under constant stress state (p, q) and constant specific volume v.
- The stress paths followed under both drained and undrained conditions seem to follow a unique surface in the $v-p-q$ space connecting the isotropic normal compression line with the critical state line, called the Roscoe surface. Roscoe surface has been found to be a limiting surface, where all the stress paths of normally or even lightly overconsolidated soils during shear should finally lay on, while states outside of it cannot be achieved. Therefore, Roscoe Surface is also a State Boundary Surface (SBS).

The following equation describes the critical state line on the $p-q$ plane:

$$q = M \cdot p \tag{3.1}$$

where M represents the CSL slope, which is idealized as a straight line, parallel to the normal compression line in the $v-\ln p$ it, described by:

$$v_{cs} = \Gamma - \lambda \ln p \tag{3.2}$$

where λ the already defined slope of the NCL and Γ the v_{cs} at $p = 1kPa$. The following expression calculates the CSL slope as a function of the internal friction

angle ϕ of the clay:

$$M = \frac{6\sin\phi}{3-\sin\phi} \text{ (triaxial compression)} \tag{3.3a}$$

$$M = \frac{6\sin\phi}{3+\sin\phi} \text{ (triaxial extension)} \tag{3.3b}$$

Figure 3.3a depicts the Hvorslev state boundary surface that similarly describes the behavior of overconsolidated soils in a unified way. Test paths of overconsolidated soil specimens move above the projection of the critical state line on the $p-q$ plane exhibiting a peak strength followed by a post peak strain-softening behavior before reaching their residual strength, also laying on the critical state line. The Hvorslev surface represents the peak strength. In addition, it intersects with the Roscoe surface at the critical state line, while towards the origin of the $p-q$ plane it is limited by the tension failure plane representing the maximum value that the q/p ratio may obtain if the soil is assumed incapable of withstanding any true tensile stress.

Figure 3.3b portrays the complete State Boundary Surface, using a normalization procedure based on Hvorslev equivalent pressure p_e:

$$p_e = \exp\left(N_{iso} - v\right) \ \lambda \tag{3.4}$$

constant v sections of the complete SBS can be plotted in the $p/p_e - q/q_e$ plane. Figure 3.3b presents such a plot. Based on the mechanical framework of Critical

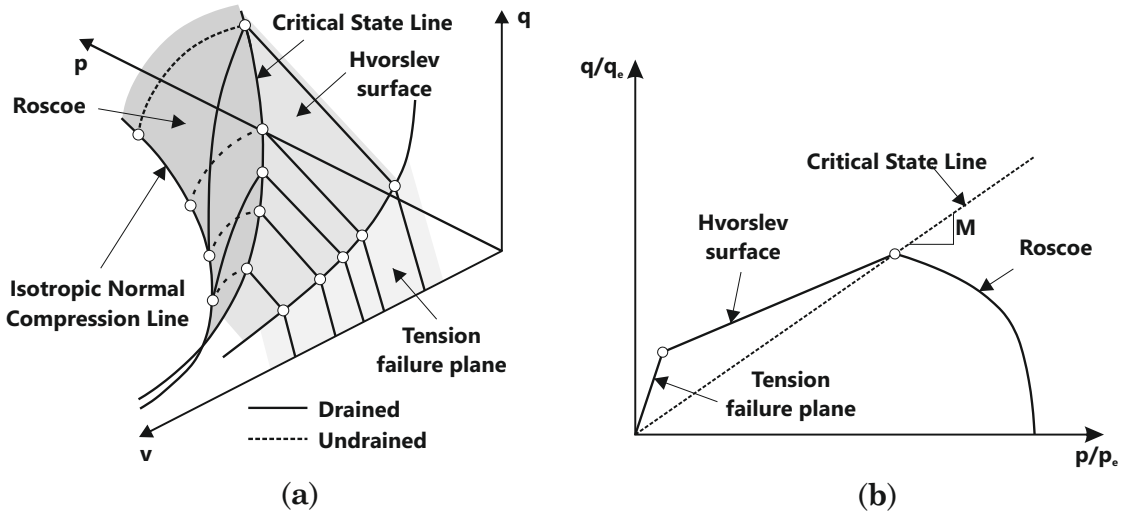

Figure 3.3: The complete state boundary surface (Roscoe-Hvorslev); (a) in the $p-q-v$ space and (b) on the normalized $p/p_e - q/q_e$ plane.

State Soil Mechanics, Roscoe et al. (1958) introduced the Cam Clay constitutive model. Roscoe & Burland (1968) later enhanced it, with an eye towards increased mathematical stability, to the well known Modified Cam Clay constitutive model. MCC adopts an ellipsoidal yield surface on the $p-q$ plane, symmetric about the hydrostatic axis, that is assumed to harden only isotropically (without changing its shape) by expanding homothetically with respect to the p, q axis intersection. The following yield function describes the adopted yield surface (see Figure 3.4) in the $p-q$ plane:

$$f(p',\ q,\ p_m) = q^2 + M^2\, p'\,(p' - p_m) = 0 \tag{3.5}$$

where p_m the hardening variable corresponding to the size of the ellipse on p-axis and M the CSL slope. Comparing Figures3.3b and 3.4, we observe that the MCC

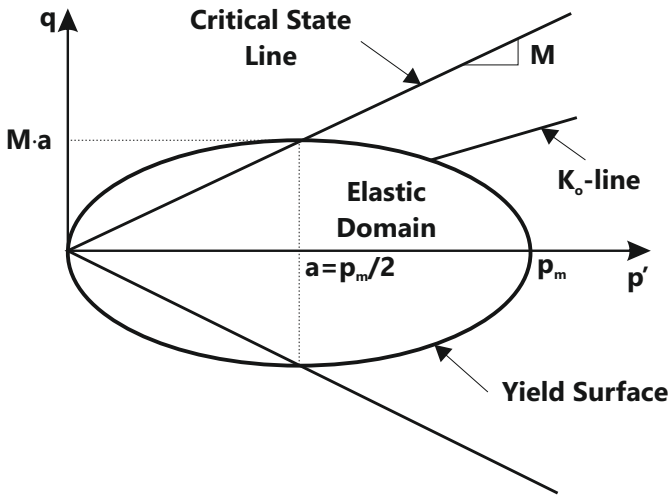

Figure 3.4: The yield surface of the Modified Cam Clay constitutive model.

yield surface approximates a constant volume section of the Hvorslev-Roscoe SBS, while by employing a volumetric hardening rule the complete SBS in the $p-q-v$ space can be simulated.

MCC adopts an associated flow rule and thus the yield surface also represents the plastic potential surface. The so called "poroelasticity" simulates the elastic behavior within the Yield Surface. Poroelasticity is formulated based on the observed behavior during unloading and reloading stress paths under isotropic and uniaxial conditions. As already discussed, a family of swelling lines on the $v-\ln p$ plane approximates the volumetric behavior of unloaded and reloaded soil specimens (see Figure 3.2). Let's assume an initially elastic state (p, v) lying on a swelling line with

slope κ. The aforementioned swelling line can be mathematically described as:

$$v = v_m - \kappa \ln \frac{p'}{p_m} \tag{3.6}$$

while by considering the theory of elasticity we define the tangent bulk modulus K:

$$K = \frac{v\ p'}{\kappa} \tag{3.7}$$

It is evident that the derived bulk modulus is a pressure dependant modulus which depends on the current mean effective stress p' and specific volume v. Hence, as during loading both quantities undergo changes, the bulk modulus evolves and poroelasticity predicts non-zero values of the second order work along a full loading-unloading cycle. Such a behavior is regarded as conservative Belokas (2008). As far as the shear modulus is concerned it can be defined as:

$$G = \frac{1}{2}\left(\frac{2G}{K}\right) K \tag{3.8}$$

where the quantity $2G/K$ is assumed a material constant directly related to Poisson's ratio through the expression:

$$\frac{2G}{K} = \frac{3\,(1-2\nu)}{1+\nu} \tag{3.9}$$

The isotropic hardening rule of MCC can be defined in a similar manner based on the isotropic NCL. The state of an isotropically NCL should lay on the isotropic normal compression line in the $v - \ln p$ plane and also on the tip of the yield surface (along the isotropic axis) corresponding to p_m. Any infinitesimal loading under isotropic conditions should make the yield surface expand and also the material state on the $v - \ln p$ to move along the isotropic NCL towards a higher stress value. Starting from the governing equation of the NCL where current stress p' is assumed equal to p_m, we may write:

$$v = N_{iso} - \lambda \ln p_m \tag{3.10}$$

According to the MCC constitutive relationships the predicted mechanical behavior can be separated in the following two zones:

- **Wet side**: The wet side corresponds to states at the right hand side of the CSL on the $p - q$ plane, where $p' - a > 0$ - strain-hardening response is expected. Hence, a triaxially sheared soil specimen at the wet side will yield upon reaching the yield surface, elastoplastic strains will start accumulating and the yield surface will expand. Deviatoric stress will continuously increase

until the state reaches the CSL where $p'-a=0$ corresponding to a failure state. At the same time the associated flow rule assumed represents a contractant behavior.

- **Dry side**: On the dry side, at the left hand side of the CSL, $p'-a<0$ and thus strain-softening behavior is reproduced. In that end a soil specimen that is triaxially sheared from an initially elastic state, upon reaching the yield surface on the dry side, will have reached its peak strength value. Further plastic loading will result in the contraction of the yield surface (strain-softening), reproducing a decrease of the deviatoric stress towards the residual strength, finally reached when the material state reaches the critical state line. A dilatant behavior is reproduced.

Figure 3.5 schematically summarizes the aforementioned behavior, demonstrating the stress path of two drained triaxial compression tests, one on the wet side and the other on the dry side. We also need to mention that in MCC the CSL apart from defining the failure states also plays the role of a Phase Transformation Line (PTL), where the transition between dilatant and contractant behavior takes place.

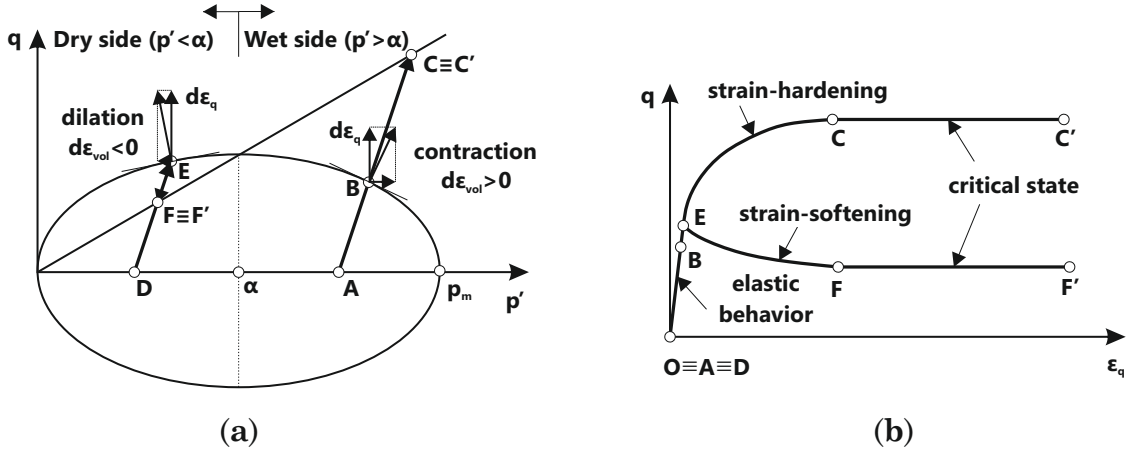

Figure 3.5: Two typical drained triaxial compression tests and the corresponding MCC model's predictions at the wet and the dry side. (a) Stress paths on the $p-q$ plane and (b) the corresponding stress strain curves.

The MCC is a simple but at the same time very efficient constitutive model. It has been based on the sound and solid mechanical framework of the Critical State Soil Mechanics theory, and thus can represent essential features of the mechanical behavior of isotropically consolidated structureless soils, with parameters easily accessible through conventional laboratory tests (i.e., isotropic compression test, triaxial drained and undrained compression tests).

At the same time, considering that MCC is one of the first attempts for a comprehensive description of soil behavior, it is reasonable to expect that it will not be able to represent complex mechanical characteristics that natural soils usually exhibit due to anisotropy, structure, small-strain stiffness, partial saturation or viscous effects. Following MCC principles a lot of researches have presented more complex constitutive models to address some of the aforementioned types of behavior. For instance, Kavvadas & Amorosi (2000) presented a constitutive model for structured soils, Belokas (2008) proposed a constitutive law for structured anisotropic soils and Kalos (2014) demonstrated a constitutive model for soils with viscous time-dependent behavior.

3.2.2.2 Small-strain stiffness and structure degradation

Small-strain stiffness (SSS) and structure degradation (SD) are two very significant features of OC clays. However, the MCC fails reproducing both of them, even at high $OCRs$. Therefore, Kalos (2014) formed a constitutive law based on the equations and the yield surface of MCC for the simulation of these characteristics. The MCC-type constitutive model applicable to OC clays, simulating SSS and SD, incorporates the following characteristic surfaces:

- Intrinsic Strength Envelope (ISE)
- Structure Strength Envelope (SSE)
- Plastic Yield Envelope (PYE)

The Intrinsic Strength Envelope solely represents a reference surface for the destructuring mechanism. Hence, the assumption of two characteristic surfaces establishes the elastoplastic underlying framework of the model: the Structure Strength Envelope and the Plastic Yield Envelope corresponding to the two levels of yielding based on the concept of Vaughan et al. (1988) and Malandraki & Toll (1994). The SSE encloses all possible states for the given structure and anisotropy simulated while the PYE encloses all possible elastic states assuming the general elastoplastic behavioral framework. Figure 3.6 demonstrates the aforementioned characteristic surfaces on the $p - q$ plane.

The **Intrinsic Strength Envelope (ISE)** encloses all structureless states of the geomaterial. Considering that it comprises the state that the material falls into after the accumulation of substantial strains associated with critical state, the intrinsic anisotropy is null due to the chaotic distribution of the soil particle orientation at the initiation of failure. Regardless, whether a preferred orientation does occur after

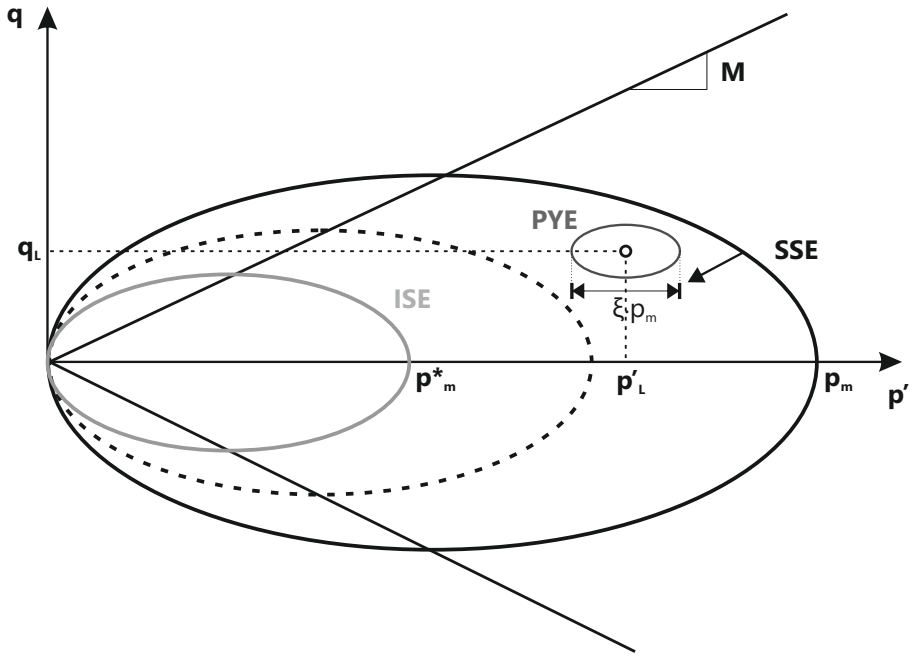

Figure 3.6: Characteristic surfaces of the constitutive law reproducing small-strain stiffness and structure degradation features for OC clays (Kalos, 2014).

the shear banding forms thus leading to a macroscopic failure the proposed constitutive model will not focus on the post residual mechanical behavior of geomaterials. Every structureless state characterized as intrinsic can be described solely by the stress history and void ratio. The following expression portrays the mathematical formulation of the intrinsic strength envelope:

$$f^*(p',\ q,\ p^*_m) = q^2 + M^2\, p'\,(p' - p^*_m) = 0 \tag{3.11}$$

The star "*" superscript applies to denote the intrinsic measures. The parameter p^*_m stands for the size of the ISE oriented along the isotropic axis illustrated in Figure 3.6. Orientation of the intrinsic strength envelope is along the isotropic p-axis. The ISE is allowed to harden isotropically by associating the size of the ISE with undergoing alterations on the void ratio due to the accumulation of volumetric plastic strains. The kinematic hardening of the ISE is of no major significance considering that the only measure of the intrinsic strength envelope required within the formulation of the constitutive model is its size p^*_m to define the asymptote for the destructuring process of SSE undertaken during plastic deformation.

The **Structure Strength Envelope (SSE)** portrays the effect of bonding on the soil fabric (Figure 3.6). It defines the available strength due to bonding formation and hence encloses the ISE. The selected shape of the SSE is considered analogous to

the Intrinsic since primary anisotropy is not simulated in this version of the model. Considering it encloses the ISE its size is allowed to degrade but at no time should it cross the intrinsic surface thus justifying its limit bound on the down side. The selected expression for the Structure Strength Envelope is given below:

$$f(p',\ q,\ p_m) = q^2 + M^2\, p'\,(p' - p_m) = 0 \tag{3.12}$$

The size of the SSE is denoted p_m and the ratio $B = p_m/p_m^*$ is always greater than unity considering that the ISE comprises the lower bound of the Structure Strength Envelope. At times when chemical or biological transformations have been undertaken throughout the bonding formation it is not unusual for the ratio to reach the residual size value of the intrinsic, at least for the strain levels measured in the laboratory. Hence, conforming with the Dafalias & Popov (1975) postulate the SSE comprises the bounding envelope and the ISE represents a characteristic surface coinciding with the SSE in the complete absence of structure (no primary anisotropy is considered).

The **Plastic Yield Envelope (PYE)** defines the infinitesimal purely elastic domain, where the accumulated strains are recoverable upon removal of the loading increment. As a consequence, the plastic yield surface of this domain is only but a fraction of the SSE. Even strains of the order of 0.001-0.01% may be considered irreversible and hence inelastic (Georgiannou, 1988; Jardine, 1995; Smith et al., 1992). In the formulation of the proposed model the PYE and the SSE are similar associated through a similarity ratio denoted ξ. The similarity ratio is considered constant throughout plastic or elastic loading increments undertaken. Here follows the mathematical formulation of the PYE on the $p-q$ plane:

$$f(p',\ q,\ p_L^{'},\ q_L,\ p_m) = (q - q_L)^2 + M^2 \left(p' - p_L^{'}\right)\left[\left(p' - p_L^{'}\right) - \xi \cdot p_m\right] = 0 \tag{3.13}$$

where $p_L^{'},\ q_L$ the center of PYE, controlled through a kinematic hardening law and thus employed as a state variable that may translate towards the SSE assuming an elastic-plastic loading increment. The proportionality ratio controls the size of the PYE and is assumed to be a fraction of the SSE, usually $\xi = 0.1 - 5\%$. It is noted that the strain increment imposed in the numerical analysis is not independent of the proportionality ratio. Small proportionality ratios shall result to a small PYE and consequently the elastic increment to adjust the stress state on PYE shall be equally small. Hence, the proportionality ratio for the numerical solution to be precise needs to be somewhere in the aforementioned range assuming that the imposed strain increment employed within the numerical programming is of the

order of $10^{-6} - 10^{-5}$.

After the aforementioned description of the characteristic surfaces involved in the "enhanced" MCC-type constitutive law, we shall present briefly the SSS and SD features of the model and how the interaction of the surfaces triggers them.

- **Small-strain stiffness (SSS)** is controlled by the size of PYE - absolutely proportional to that of the SSE - and the interpolation rule between PYE and SSE (λ^*). The PYE moves towards SSE and right after the moment the two surfaces come in contact they begin moving together towards the ISE.

- The **structure degradation (SD)** process begins for the soil after the point of peak strength. The ISE increases through volumetric hardening while the SSE decreases its size through the accumulation of plastic deviatoric strains. As a result, the two surfaces coincide at a specific loading frame and the destructuring process begins. There are certain parameters of the model controlling the SD. The most important parameter controlling the residual strength of the soil is the ratio B of the SSE to the ISE size. Another crucial issue is the determination of the OC clay peak strength relatively to the corresponding strength according to the MCC. What we need to decide prior to the SD simulation is whether the peak or the residual strength of this sophisticated constitutive law coincides with the MCC peak strength for the OC clay.

3.2.2.3 Undrained triaxial constitutive behavior

The numerical investigation presented in the current thesis involves a single laterally loaded pile in clays under undrained loading conditions. Therefore, prior to the verification of the complete numerical model, it is essential to comprehend the undrained behavior of a single soil specimen simulated according to the aforementioned constitutive laws. For the specific cause, we simulated four different constitutive behaviors in a numerical undrained triaxial compression test.

The FEM numerical model resembles a typical cylindrical soil specimen tested in the common triaxial laboratory apparatus. We form the model using eight axisymmetric, 8-node, second order solid, pore pressure elements with 9 integration points (CAX8P). Either the Simulia Abaqus in-built MCC or the developed UMAT subroutine incorporating SSS and SD features simulate the constitutive behavior of the soil elements. Figure 3.7 presents the model dimensions and the applied boundary conditions. A total axial (σ_a) and radial (σ_r) stress applies to the specimen, corresponding to the actual geostatic stress field at a specific soil depth. The aforementioned stresses come to equilibrium with the initial effective stress field (σ') and

the pore water pressure (u) assigned to the soil elements. Undrained loading conditions primarily take place due to the combination of very low clay permeability $k = 10^{-11}$m/s with load application in a short time period, namely t=6 days. By applying the so-called "no-flow" hydraulic boundaries around the specimen, we also ensure that the loading is undrained. Axial loading is then imposed through axial strains $\varepsilon_a = 5 - 20\%$.

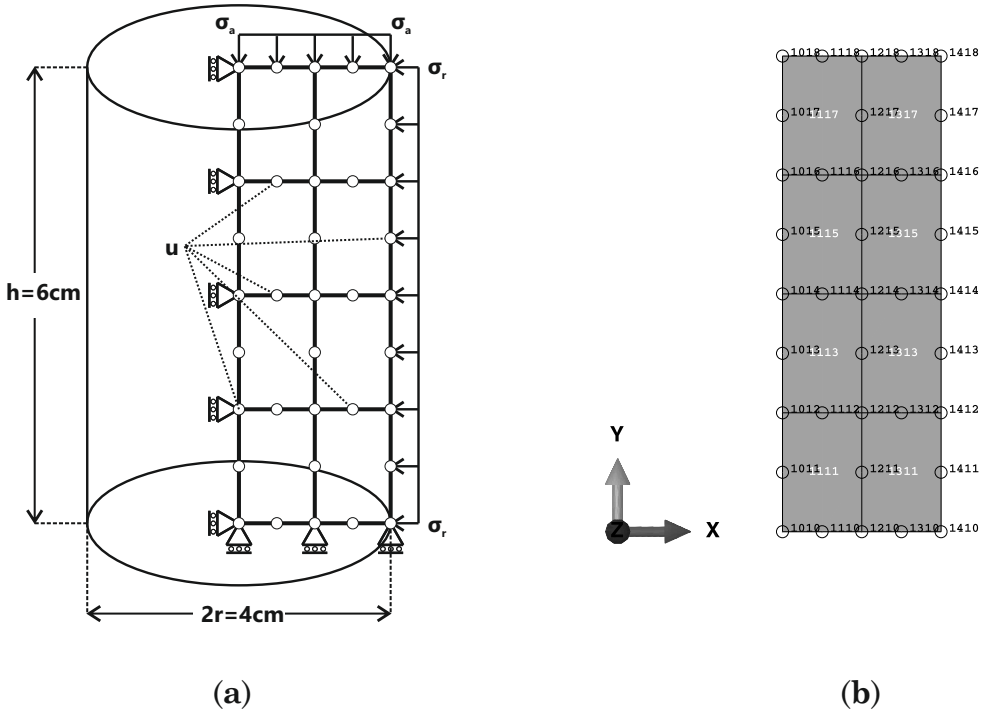

Figure 3.7: (a) Schematic representation of the numerically simulated undrained triaxial tests. (b) FEA axisymmetric mesh of the triaxial tests.

The current paragraph presents through stress paths ($p - q$) and stress-strain curves ($q - \varepsilon_q$) the clay response during these triaxial tests, in order to verify the following four constitutive simulations:

- NC clay undrained triaxial behavior through the MCC.
- OC clay undrained triaxial behavior through the MCC.
- OC clay undrained triaxial behavior with SSS.
- OC clay undrained triaxial behavior with SSS and SD.

Table 3.1 demonstrates the main characteristics of the aforementioned simulations for NC and OC clay specimens at a depth z=4m.

Table 3.1: Clay properties of the numerical undrained triaxial tests.

Law	Clay	M	λ	λ/κ	ν	p_m (kPa)	B	ξ	λ^*
MCC	NC	0.98	0.174	10	0.333	35	-	-	-
	OC					702	-	-	-
SSS	OC	1.20	0.109	20	0.100	702	1	0.001-20	0.1-20
SSS & SD	OC					702, 2106	3	0.05	2

Figure 3.8 depicts a typical behavior of a NC clay. The undrained stress path of the triaxial test starts from the K_o-line (see Figure 3.4) and ends up to the CSL at failure. The course of the stress path on the YS confirms the undrained loading conditions.

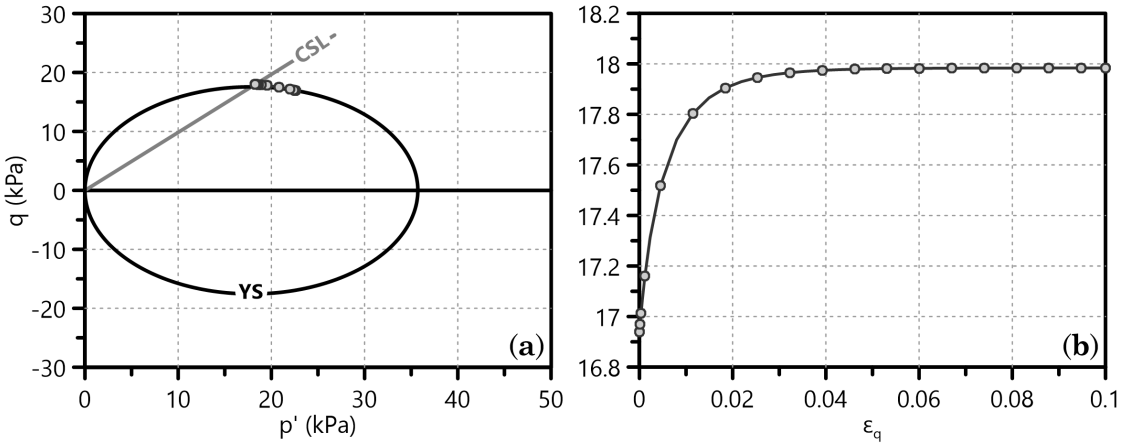

Figure 3.8: (a) Stress path and (b) deviatoric stress-strain curve of a numerical undrained triaxial test on a NC clay specimen. Constitutive behavior of the NC clay controlled by the MCC.

Figure 3.9 demonstrates the constitutive behavior of a highly OC clay ($OCR \approx 20$). The corresponding undrained stress path develops from the elastic domain (inside the YS), vertically towards the YS and then to the CSL at failure. It is obvious that the equivalent $c_u = q_u/2$ of the OC clay is greater than the corresponding strength of the NC by many orders of magnitude.

In order to verify the SSS, we degenerated the sophisticated constitutive law described in Paragraph 3.2.2.2 into a MCC with a PYE - characteristic surface SSE coincides with the ISE (B=1). In Figures 3.10a,b we observe no actual influence of the PYE size ($\xi \cdot p_m$), neither on the stress path nor on the derived $q - \varepsilon_q$ curve of the simulated OC clay. On the other hand, Figures 3.10c,d demonstrate a significant effect of parameter λ^* - interpolation rule between PYE and SSE≡ISE.

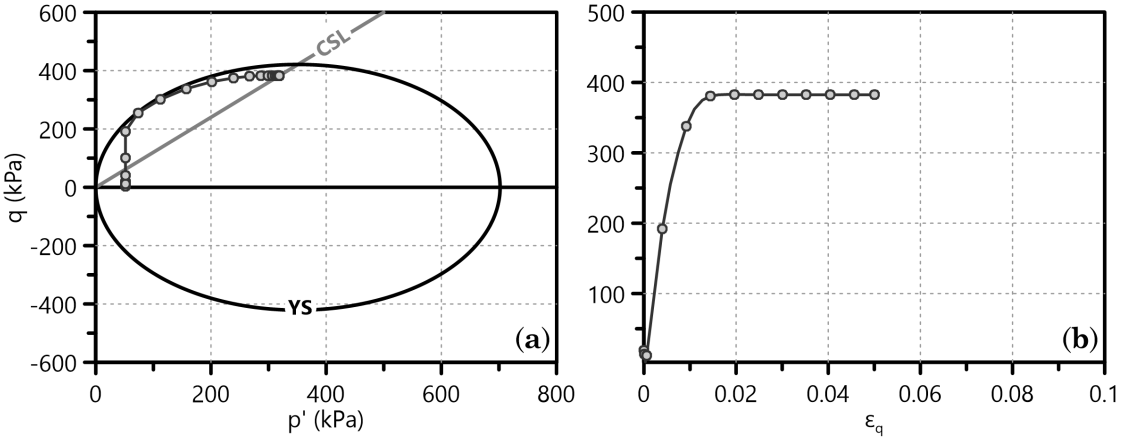

Figure 3.9: (a) Stress path and (b) deviatoric stress-strain curve of a numerical undrained triaxial test on an OC clay specimen. Constitutive behavior of the OC clay controlled by the MCC.

In more detail, we discern intense decrease of the small-strain stiffness for λ^*=0.1. Therefore, the value of λ^* we are going to use during our numerical investigation depends on the clay stiffness we want to reproduce. Two more remarks occur from the SSS triaxial test; the one refers to the path the PYE follows, while the other to the comparison between the degenerated SSS and SD constitutive law with the Abaqus in-built MCC. Figure 3.10 shows that the stress path begins from the center of PYE (the initial position of PYE is close to the isotropic p-axis), then onto PYE and finally on the CSL. It is important to note that PYE moves along the stress path and contacts SSE≡ISE on the corresponding conjugate point of the latter. Comparison of the $q - \varepsilon_q$ curves derived from the SSS triaxial tests (for $\lambda^* > 2$) with the corresponding curve of the MCC triaxial test (Figure 3.9) leads to absolute coincidence of the two. Thus, we verify that the SSS and SD constitutive model can be successfully downgraded to a simple MCC after the removal of the aforementioned advanced features and that the developed UMAT is fully functional.

The fully featured simulation (SSS and SD) of the OC clay specimen under undrained triaxial loading is presented in Figure 3.11. We investigated two different peak and residual strength assumptions, although both with the same ratio B=3 ($B = p_m/p_m^*$): one considering that the peak strength of the sophisticated constitutive law coincides with that of the MCC simulation and another assuming that the MCC peak strength is equal to the residual strength of the advanced model. Figure 3.11 (left) depicts the stress path of the first simulation. The second simulation follows a respective stress path, only with greater ISE and SSE sizes. In the general case, the ISE tends to increase its size due to volumetric hardening while the SSE shrinks after the accumulation of deviatoric strains. However, volumetric

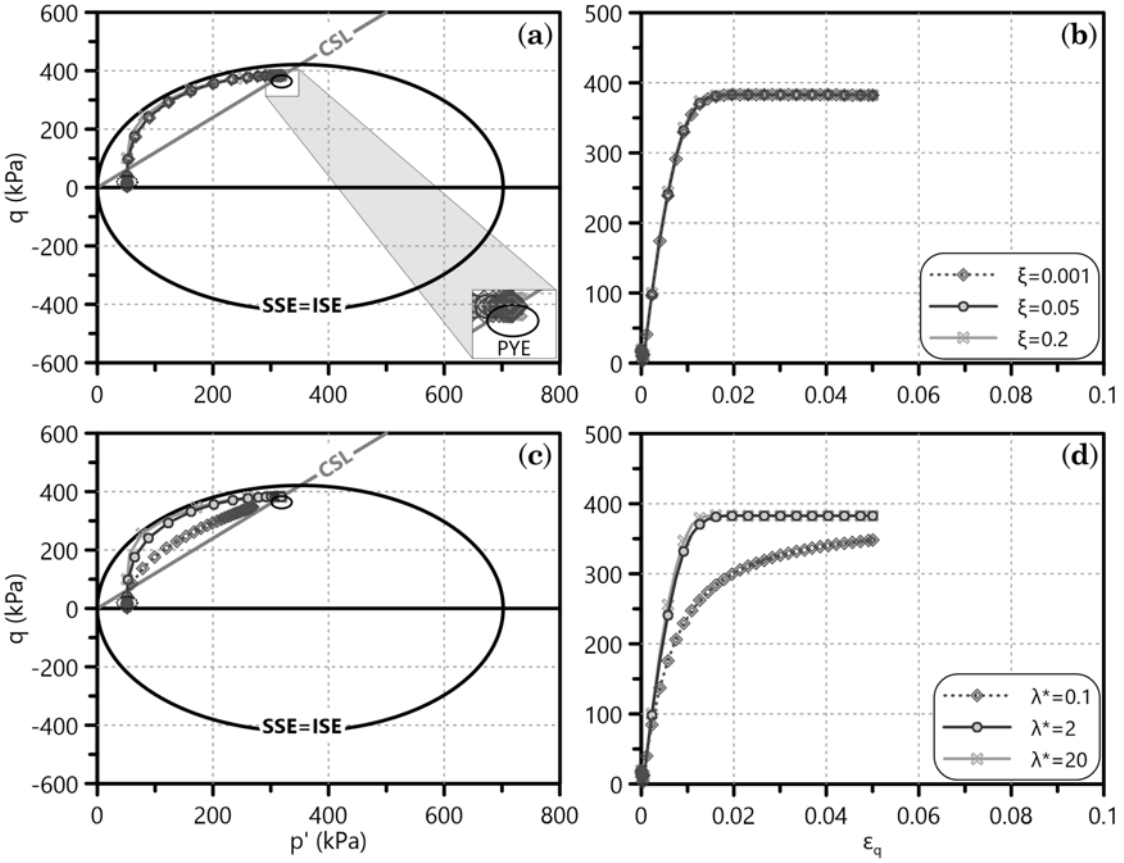

Figure 3.10: (a,c) Stress paths and (b,d) deviatoric stress-strain curves of numerical undrained triaxial tests on an OC clay specimen. Constitutive behavior of the OC clay controlled by the sophisticated constitutive law, only with the SSS feature activated. Effect of the PYE size ($\xi \cdot p_m$) (a,b) and the PYE-SSE interpolation rule parameter λ^* (c,d) on the triaxial behavior.

strains are infinitesimal during undrained loading, thus the ISE barely expands. On the contrary, extensive deviatoric strains trigger the shrinking of the SSE that is divided in two phases:

- the "peak strength" phase when the stress path reaches the CSL and
- the "residual strength" phase after the end of the destructuring process - "hook"-type part of the stress path along the CSL until the SSE meets the ISE.

Finally, we compare the $q - \varepsilon_q$ curves derived from the aforementioned simulations with the corresponding MCC curve of the OC clay (Figure 3.11b). We observe that both simulations of the undrained triaxial test using the sophisticated SSS and SD constitutive law perform exactly as aimed in terms of peak and residual strength. Therefore, we conclude that this advanced constitutive model simulates successfully

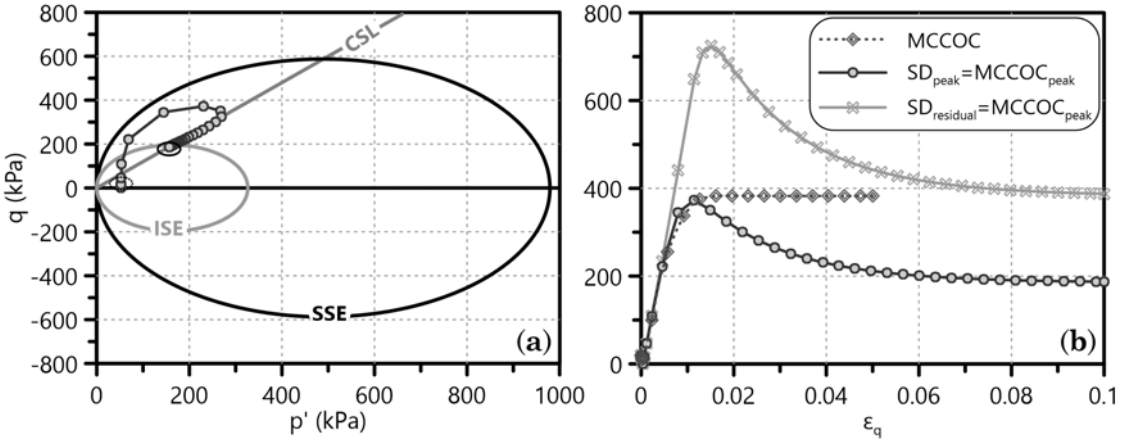

Figure 3.11: (a) Stress paths and (b) deviatoric stress-strain curves of numerical undrained triaxial tests on an OC clay specimen. Constitutive behavior of the OC clay controlled by the sophisticated constitutive law, incorporating the SSS and SD features. (b) Two different simulations of the peak and residual strength of the clay compared with the corresponding MCC behavior in terms of $q - \varepsilon_q$ curves.

both small-strain stiffness and structure degradation features of OC clays.

3.2.3 Soil simulation

The numerical simulation described in Paragraph 3.2.1 carries out three-dimensional, fully coupled, effective stress FEA. The FEA we performed during the current dissertation refer to undrained loading conditions of fully saturated clayey soils with the water table at ground level. Either the Simulia Abaqus in-built MCC or the developed UMAT subroutine incorporating SSS and SD features (see Paragraph 3.2.2) represent the clay constitutive behavior. In the present paragraph we describe the corresponding finite elements used for the simulation of the clay, as well as the process followed for the simulation of NC and OC clay behavior in the FEA through the aforementioned constitutive laws.

3.2.3.1 Soil finite elements

Solid, 8-node, full integration (8 integration points close to the corresponding nodes) pore pressure elements (C3D8P) are used to model the clay in the current numerical investigation. Figure 3.12 depicts the face and integration point numbers assigned to the corresponding entities of a single C3D8P element (Simulia, 2012). The FEA solve two problem types simultaneously for the soil elements:

- The mechanical problem regarding the mechanical properties and the constitutive behavior of the soil.

- The hydraulic problem taking into account the water properties and Darcy flow rule through the soil with certain permeability k.

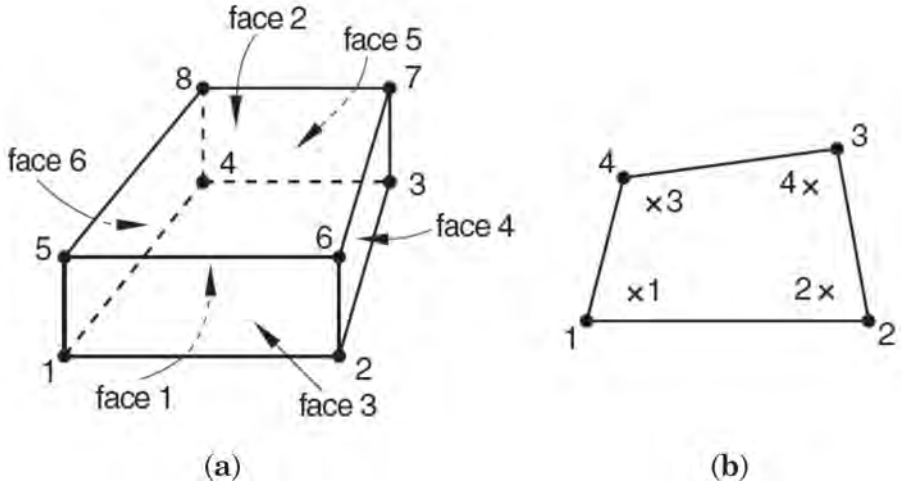

Figure 3.12: (a) Face numbering and (b) integration point numbering of a solid 8-node pore pressure element C3D8P (Simulia, 2012). Integration points in the second layer of the solid element are numbered consecutively.

3.2.3.2 NC and OC clay simulation

In order to simulate NC and OC clay conditions for the soil profile along the laterally loaded pile, we carry out a procedure balancing the geostatic stress field with certain mechanical properties and physical characteristics of the soil. What we describe in the following paragraphs is an exercise of balance between the fundamental principles of the so called "poroelasticity" and the MCC constitutive model. All the calculations evolve assuming a fully saturated soil with the water table on ground surface.

NC clay (OCR=1)

The simulation of a NC clay behavior for the soil - increasing strength with depth - introduces the following steps, controlled by the MCC constitutive law:

1. At the beginning, we assume the following physical characteristics and mechanical properties for the NC clay: density of the soil grains $\rho_s = 2.65kN/m^3$, water density $\rho_w = 1.0kN/m^3$, saturation ratio $S_r = 100\%$, NCL slope $\lambda = C_c/\ln 10$, slope of swelling lines $\kappa = C_r/\ln 10$, CSL slope M, Poisson's ration ν and coefficient of horizontal geostatic stress $K_o = 0.5$. NCL intercept at p=1kPa on the $v - \ln p$ plane is assigned values $N_{iso} = 2.0 - 3.0$ in order to receive realistic void ratio values e=0.8-1.2 of the NC clay after the following process.

2. We assume an initial common nodal void ratio e per depth z. We apply the following equations for the physical characteristics of the soil in order to calculate the average void ratio $\bar{e}$ and soil density values - dry ρ_d and saturated ρ - per element row of the numerical model (see Paragraph 3.2.1).

$$\bar{e} = \frac{e_{z_i} + e_{z_{i+1}}}{2} \tag{3.14a}$$

$$\rho_s \cdot w = S \cdot \bar{e}\rho_w \tag{3.14b}$$

$$\rho = \rho_s \frac{1+w}{1+\bar{e}} \xrightarrow{\text{Equation 3.14b}} \rho = \frac{\rho_s + S \cdot \bar{e}\rho_w}{1+\bar{e}} \tag{3.14c}$$

$$\rho_d \overset{w=0}{=} \rho_s \frac{1}{1+\bar{e}} \tag{3.14d}$$

where w=the soil humidity. Figure 3.13 demonstrates the actual points of the aforementioned calculations for e, $\bar{e}$, ρ and ρ_d between two subsequent soil element rows.

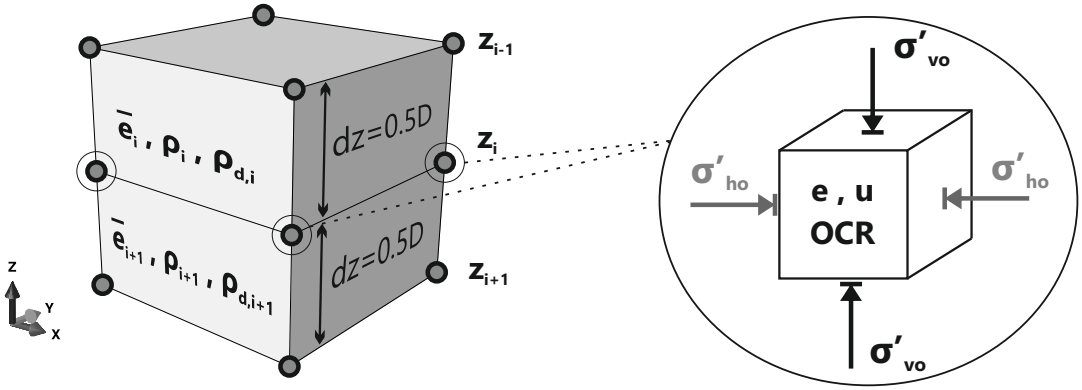

Figure 3.13: The calculated $\bar{e}$, ρ and ρ_d per soil element row (left). Calculation of the nodal e, OCR and geostatic stresses - u, σ'_{vo} and σ'_{ho} - (right).

3. We calculate the following stresses per nodal depth z: pore water pressure u, vertical effective stress σ'_{vo}, horizontal effective stress $\sigma'_{ho} = K_o \cdot \sigma'_{vo}$, mean effective stress $p' = (\sigma'_{vo} + 2 \cdot \sigma'_{ho})/3$ and deviatoric stress $q = \sigma'_{vo} - \sigma'_{ho}$.

4. Since the soil we simulate is a NC clay (OCR=1), each geostatic $p - q$ stress state per nodal depth is located on the K_o-line of the MCC yield surface (Figure 3.14). As a result, Equation 3.5 calculates the size p_m of the YS ellipse on the

isotropic p-axis as:

$$p_m = \frac{q^2 + M^2 \cdot p'^2}{M^2 \cdot p'} \tag{3.15}$$

It is obvious that p_m increases with depth, thus simulating a realistic NC clay behavior.

5. For the equilibrium between the mechanical and physical characteristics of the soil, we assume that all the aforementioned p_m states lay on the NCL for NC clays - λ-slope (Figure 3.14). Thus, Equation 3.10 calculates a new specific volume v, referring to p_m at the specific depth. The new corresponding value for $e = v - 1$ returns to Step 2 and through this **iterative procedure** the desired equilibrium is achieved.

6. The following equation (Wood, 1990) calculates the equivalent undrained shear strength c_u of each nodal depth:

$$c_u = \frac{M}{2} \cdot p' \cdot \left(\frac{PQOCR}{2} \right)^{\left(1 - \frac{\kappa}{\lambda}\right)} \tag{3.16}$$

where $PQOCR{=}p_m/p'$ is an equivalent OCR on the isotropic p-axis. This equivalent c_u is verified against both numerical undrained triaxial test and 3D failure of the clay surrounding the laterally loaded pile in the FEA (see Paragraph 3.3.6).

7. Another value we control through this geostatic stress equilibrium process - through CSL slope M more accurately - is the ratio $A = c_u/\sigma'_{vo}$ with depth. Values of A=0.25-0.35 are reported in the literature for NC clays in general.

8. Finally, we calculate the initial undrained Young's modulus E_u of the clay with depth through the following equation:

$$E_u = \frac{9 \cdot K \cdot (1 - 2\nu)}{2 \cdot (1 + \nu)} \tag{3.17}$$

where K the bulk modulus of the soil at the specific depth from Equation 3.7.

OC clay $(OCR > 1)$

The simulation of an OC clay behavior for the soil - almost constant strength with depth - introduces the following steps, controlled by the MCC constitutive law:

1. At the beginning, we assume the following physical characteristics and mechanical properties for the OC clay: density of the soil grains $\rho_s = 2.65kN/m^3$, water density $\rho_w = 1.0kN/m^3$, saturation ratio $S_r = 100\%$, NCL slope $\lambda = C_c/\ln 10$,

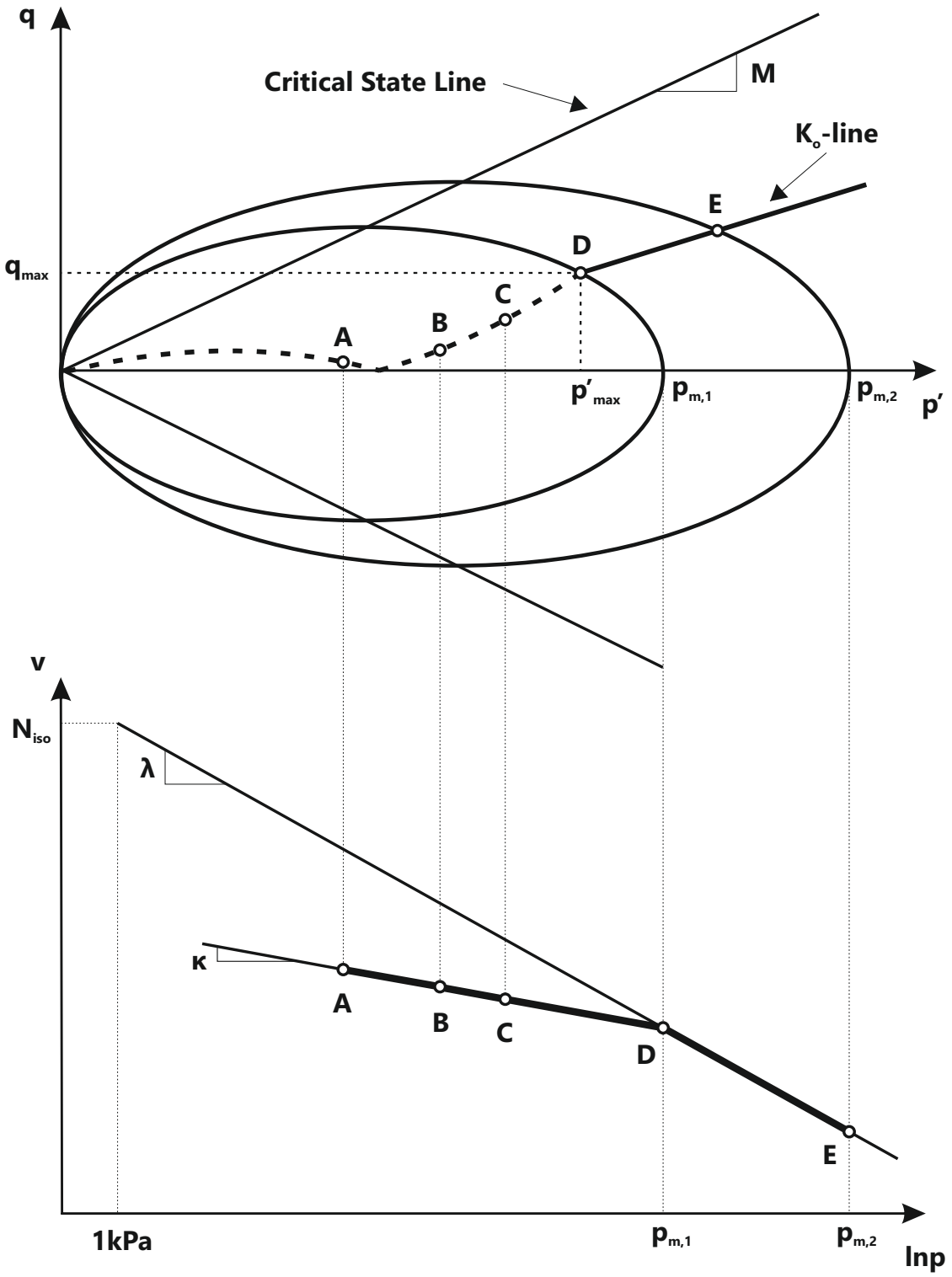

Figure 3.14: NC and OC clay geostatic stress states: on the $p - q$ plane with respect to the MCC yield surface (up); on the $v - \ln p$ plane with respect to the NCL and the swelling lines (down). States D and E correspond to the simulation of a NC clay, while A, B and C to that of an OC clay.

slope of swelling lines $\kappa = C_r/\ln 10$, CSL slope M, Poisson's ration ν and coefficient of horizontal geostatic stress for the NC soil $K_{o,\,NC} = 0.5$. NCL intercept at p=1kPa on the $v - \ln p$ plane is assigned values $N_{iso} = 2.0 - 3.0$ in order to receive realistic void ratio values $e \approx 0.7$ of the OC clay after the following process.

2. We assume an initial common nodal void ratio e and OCR per depth z. We apply the following equations for the physical characteristics of the soil in order to calculate the average void ratio $\bar{e}$ and soil density values - dry ρ_d and saturated ρ - per element row of the numerical model (see Paragraph 3.2.1).

$$\bar{e} = \frac{e_{z_i} + e_{z_{i+1}}}{2} \tag{3.18a}$$

$$\rho_s \cdot w = S \cdot \bar{e}\rho_w \tag{3.18b}$$

$$\rho = \rho_s \frac{1+w}{1+\bar{e}} \xrightarrow{\text{Equation 3.18b}} \rho = \frac{\rho_s + S \cdot \bar{e}\rho_w}{1+\bar{e}} \tag{3.18c}$$

$$\rho_d \overset{w=0}{=} \rho_s \frac{1}{1+\bar{e}} \tag{3.18d}$$

where w=the soil humidity. Figure 3.13 demonstrates the actual points of the aforementioned calculations for e, $\bar{e}$, ρ and ρ_d between two subsequent soil element rows.

3. The size of the MCC yield surface p_m shall correspond to certain values of the average undrained shear strength $c_{u,\,avg}$ of the OC clay along a pile length of $10D$. This p_m represents the strength variable of the OC clay and is assumed constant with depth as long as the clay remains OC, i.e. $OCR > 1$. In case the soil becomes NC after a certain depth - as it is common for many clay profiles - the equations mentioned before for such clays are valid from the specific depth and below on the $v - \ln p$ and $p - q$ plane[1].

4. We calculate the following stresses per nodal depth z: pore water pressure u, vertical effective stress σ'_{vo}, horizontal effective stress $\sigma'_{ho} = K_o \cdot \sigma'_{vo}$, mean effective stress $p' = (\sigma'_{vo} + 2 \cdot \sigma'_{ho})/3$ and deviatoric stress $q = |\sigma'_{vo} - \sigma'_{ho}|$. It is important to point out the following assumption on K_o:

$$K_o = \begin{cases} K_{o,\,NC}, & \text{if } OCR = 1 \\ K_{o,\,OC} = K_{o,\,NC} \cdot \sqrt{OCR} \leq 1.5, & \text{if } OCR > 1 \end{cases} \tag{3.19}$$

[1]For NC clays p_m is assumed to increase with depth.

5. Since the soil we simulate is an OC clay ($OCR > 1$), each geostatic $p - q$ stress state per nodal depth is located on the K_o-line but inside the MCC yield surface (Figure 3.14). Equation 3.5 calculates the assumed p_m of the YS ellipse on the isotropic p-axis as:

$$p_m = \frac{q_{\max}^2 + M^2 \cdot {p'}_{\max}^2}{M^2 \cdot {p'}_{\max}^2} \tag{3.20}$$

where ${p'}_{\max}$ and $q_{\max}$ the maximum p' and q of the specific YS respectively (see Figure 3.14), calculated according to the following equations:

$${p'}_{\max} = \frac{\sigma_{vp}^{'} + 2\,\sigma_{hp}^{'}}{3} = \frac{\sigma_{vp}^{'} + 2\,K_{o,\,NC}\,\sigma_{vp}^{'}}{3} \tag{3.21a}$$

$$q_{\max} = \sigma_{vp}^{'} - \sigma_{hp}^{'} = \sigma_{vp}^{'}\,(1 - K_{o,\,NC}) \tag{3.21b}$$

with $\sigma_{vp}^{'}$ and $\sigma_{hp}^{'}$ the vertical and horizontal preconsolidation stress of the OC clay at this depth respectively. It is rational to assume that $K_{o,\,NC}$ applies to the preconsolidation stresses.

6. Through simultaneous solution of Equations 3.20 and 3.21 we calculate $\sigma_{vp}^{'}$:

$$\sigma_{vp}^{'} = \frac{p_m \cdot M^2 \cdot \left(\dfrac{1 + 2\,K_{o,\,NC}}{3}\right)}{\left(1 - K_{o,\,NC}\right)^2 + M^2 \cdot \left(\dfrac{1 + 2\,K_{o,\,NC}}{3}\right)^2} \tag{3.22}$$

For soil depths that the OC clay becomes NC, $\sigma_{vp}^{'}$=$\sigma_{vo}^{'}$ from Step 3.

7. For the equilibrium between the mechanical and physical characteristics of the soil, we distinguish between OC (close to ground level) and NC states (potential at greater depth). Thus, the following equations calculate a new specific volume v, referring to p_m at the specific depth - either on κ- or on λ-slope of the $v - \ln p$ diagram (Figure 3.14).

$$v = \begin{cases} N_{iso} - \lambda \ln p_m, & \text{if } OCR = 1 \\ N_{iso} - \lambda \ln p_m - \kappa \ln \dfrac{p'}{p_m}, & \text{if } OCR > 1 \end{cases} \tag{3.23}$$

The new corresponding value for $e = v - 1$ returns to Step 2 together with the newly calculated $OCR = \sigma_{vp}^{'}/\sigma_{vo}^{'}$ and through this **iterative procedure** the desired equilibrium is achieved.

8. The following equation (Wood, 1990) calculates the equivalent undrained shear strength c_u of each nodal depth:

$$c_u = \frac{M}{2} \cdot p' \cdot \left(\frac{PQOCR}{2} \right)^{\left(1-\frac{\kappa}{\lambda}\right)} \tag{3.24}$$

where $PQOCR{=}p_m/p'$ is an equivalent OCR on the isotropic p-axis. This equivalent c_u is verified against both numerical undrained triaxial test and 3D failure of the clay surrounding the laterally loaded pile in the FEA (see Paragraph 3.3.6).

9. Finally, we calculate the initial undrained Young's modulus E_u of the clay with depth through the following equation:

$$E_u = \frac{9 \cdot K \cdot (1 - 2\nu)}{2 \cdot (1 + \nu)} \tag{3.25}$$

where K the bulk modulus of the soil at the specific depth from Equation 3.7.

3.2.4 Pile simulation

The majority of the FEA results in the current dissertation refer to a laterally loaded free-head, reinforced concrete pile with length L=30m and diameter D=1m, i.e. flexible pile (Figure 3.1). Structural serviceability limit state design demands the elastic behavior of the pile. Moreover, focusing on the derivation of p-y curves for clays in the current thesis, we are mainly concerned on the lateral soil behavior rather than the pile design. Therefore, the pile is considered elastic with Young's modulus E_p=30GPa and Poisson's ratio ν=0.20.

The numerical simulation of the single pile in the FEA combines structural and solid finite elements. Figure 3.15 depicts the aforementioned configuration that involves beam elements (B31) connected with rigid truss elements (MPC) to the solid elements (C3D8) forming the volume of the pile. While the beam elements are used for the calculation of forces and bending moments along the pile, solid elements are also essential for the formulation of the soil-pile interface - since a robust surface interaction between beam and solid elements was not available. Truss elements ensure that no noticeable deformation is allowed on the pile cross-section. It is important to mention that the C3D8 elements were assigned very low Young's modulus - namely 100kPa - in the FEA, thus not affecting the stiffness of the pile. For consistency reasons, half the pile cross-sectional area $A_p/2$ and half the corresponding moment of inertia $I_p/2$ were assigned to the beam elements simulating the pile.

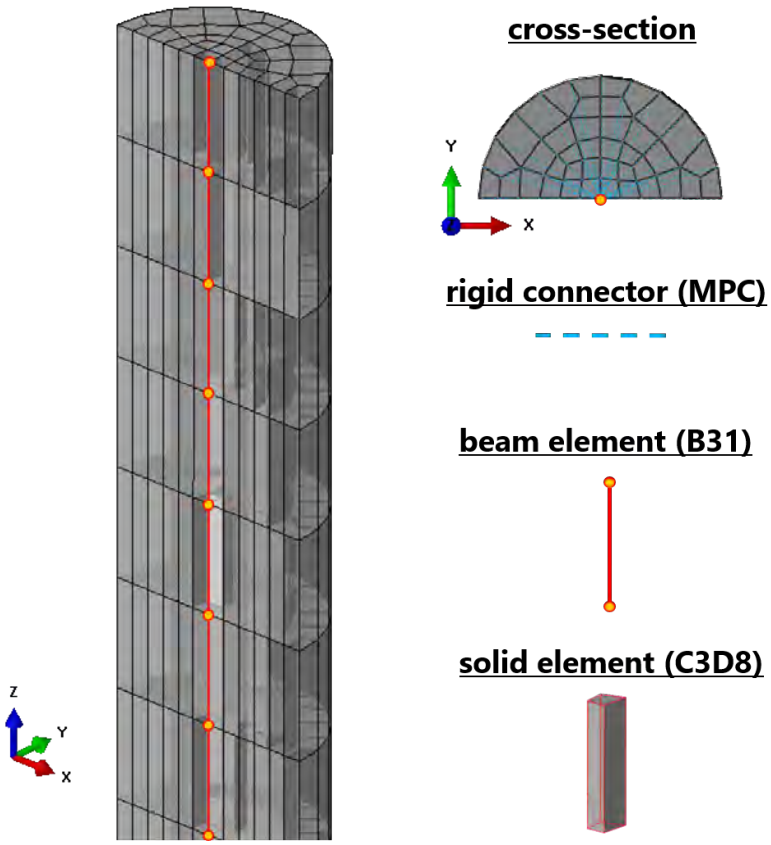

Figure 3.15: Numerical simulation of the laterally loaded pile in the 3D FEA of the current dissertation.

3.2.5 Soil-pile interface simulation

The normal stress[1] interaction between the pile and the surrounding soil allows for the formulation of a gap behind the pile (Figure 3.16) – as long as the undrained shear strength c_u of the soil suffices for it to stand vertical. The accurate contact pressure simulation on the pile-soil interface follows the exponential law depicted in Figure 3.17, in order to avoid potential numerical instabilities caused by a corresponding hard contact simulation. According to this law, contact pressure starts to build up between the two interacting surfaces at infinitesimal clearance c_o. The contact pressure transmitted between the surfaces then increases exponentially as the clearance continues to diminish. The following equations express the formulation of

[1]Normal and shear stresses along the soil-pile interface are total stresses because pile C3D8 elements - forming the surrounding pile surface - do not take poroelasticity into account.

this pressure-overclosure law.

$$p = 0 \quad \text{for} \quad h \leq -c_o \tag{3.26a}$$

$$p = \frac{p_o}{(\exp(1) - 1)} \left[\left(\frac{h}{c_o} + 1 \right) \left(\exp\left(\frac{h}{c_o} + 1 \right) - 1 \right) \right] \quad \text{for} \quad h > -c_o \tag{3.26b}$$

The normal stiffness k_n of the exponential pressure-overclosure law at different contact regimes - depending on the overclosure h - is expressed as:

$$\frac{dp}{dh} = 0 \quad \text{for} \quad h \leq -c_o \tag{3.27a}$$

$$\frac{dp}{dh} = \frac{p_o}{(\exp(1) - 1)} \left[\frac{1}{c_o} \left(\frac{h}{c_o} + 2 \right) \exp\left(\frac{h}{c_o} + 1 \right) - \frac{1}{c_o} \right] \quad \text{for} \quad h > -c_o \tag{3.27b}$$

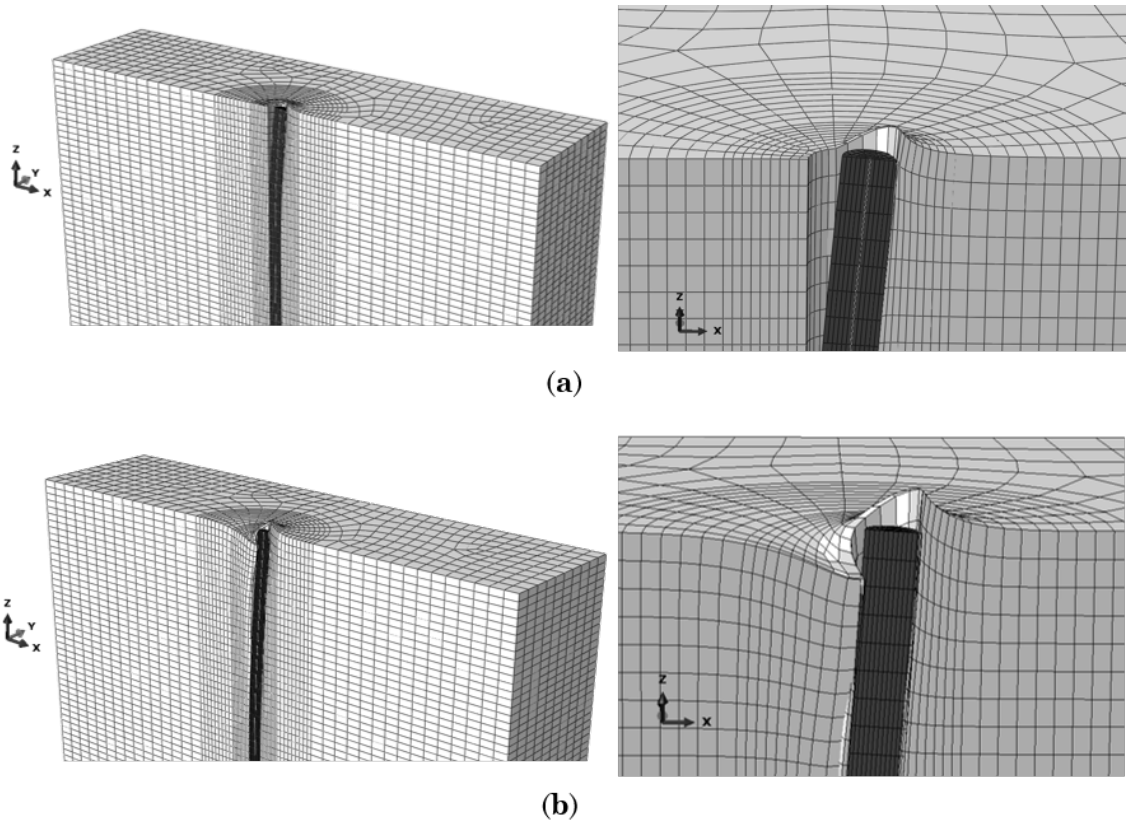

Figure 3.16: Soil-pile interface behavior of the 3D FEA laterally loaded pile. (a) Soil-pile separation in a stiff clay and (b) relative slip in a soft clay.

For the FEA of the current study, clearance c_o=10^{-4}m and pressure p_o=0.4kPa were systematically assigned to the aforementioned exponential law. Assuming that k_n is calculated at the moment of zero overclosure (h=0), Equation 3.27b results in

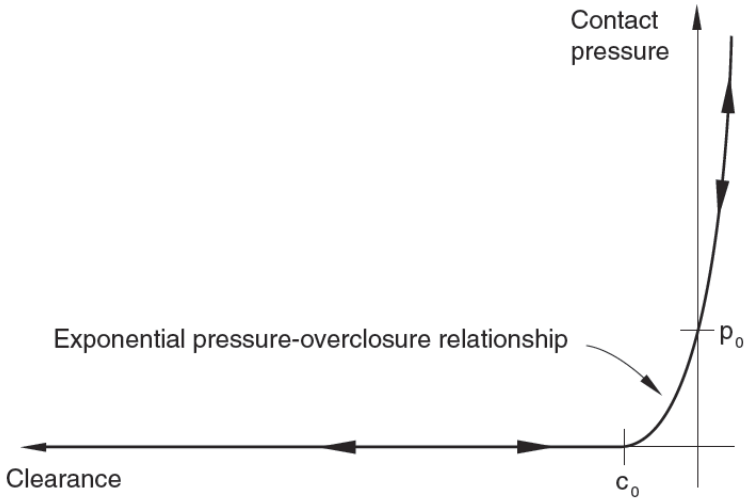

Figure 3.17: Exponential pressure-overclosure law used in the 3D FEA for the simulation of the soil-pile normal stress interaction.

k_n=$10^4\,kN/m^3$ for this set of c_o, p_o.

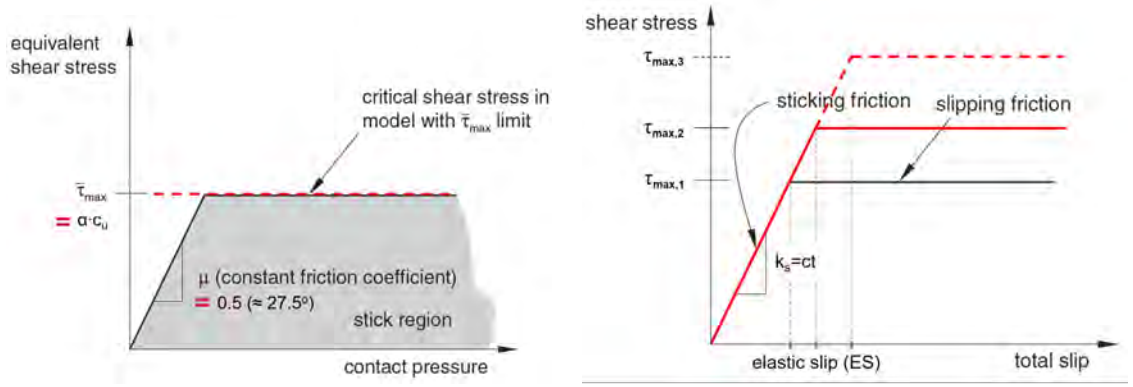

(a) **(b)**

Figure 3.18: Soil-pile interface simulation of (a) the shear stress-contact pressure and (b) the shear stress-slip behavior (Simulia, 2012).

An initial Coulomb friction law simulates the surface interaction between the pile and the surrounding soil in the shear direction, reaching an ultimate frictional resistance τ_{max}=$\alpha \cdot c_u$ (Figure 3.18a) - where α is the soil-pile adhesion factor. As Georgiadis & Georgiadis (2010) depicted in Figure 2.28, many researchers assume values of α close to unity for soft clays, while the factor generally diminishes around 0.3-0.4 for stiff clays. In the current dissertation we examined adhesion factor values α=0.3 and 1.0, thus accounting for smooth and rough soil-pile interface respectively. A frictional constant μ=0.5 - representing an interface friction angle of δ=27.5^o - is

assigned to the initial part of the friction-pressure curve. Relative slip between the pile and the surrounding soil occurs once the aforementioned ultimate shear stress τ_{max} is reached at the interface. Abaqus simulates the shear stress-slip behavior through the elastic-perfectly plastic law of Figure 3.18b. A parameter called elastic slip (ES) controls the shear stiffness k_s of the sticking friction part and is calculated as:

$$k_s = \frac{\tau_{max}}{\text{ES}} \tag{3.28}$$

In order to assign constant k_s=k_n=$10^4\, kN/m^3$ along the soil-pile interface - for consistence reasons - we calculated and inserted certain τ_{max}-ES pairs in the FEM code, according to the α chosen for the specific clay type (soft or stiff).

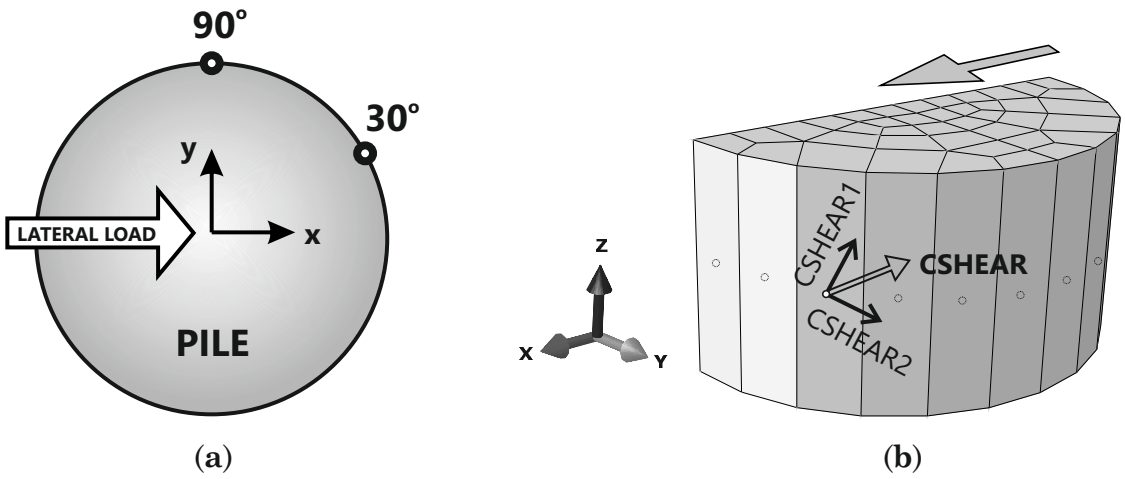

Figure 3.19: (a) Points of adhesion factor verification on the plan view of the pile. (b) Shear stress measurement on the surrounding surface of a pile slice.

We verified the assigned adhesion factor α for the laterally loaded pile both in soft NC (M=0.98, λ=0.174, λ/κ=10, ν=0.333) and stiff OC ($c_{u,avg}$=190kPa, κ=0.00543, λ/κ=20, ν=0.10) clay. We assumed α=1 and 0.3 for the NC and OC clay respectively in the verification analyses. In order to check the shear stress developing on the soil-pile interface, we check these stresses along the pile at two specific angles from the axis of the applied lateral load, namely at 30° and 90°, as depicted in Figure 3.19. The prerequisite output from the FEA refers to the nodal contact shear stress components (CSHEAR1 and CSHEAR2) developed on the plane of the soil-pile interface at the aforementioned angles along the pile. These values are inserted per depth into a worksheet and α=τ/c_u is calculated for the specified increment. The shear stress developed on the interface is calculated - independently from the local axes of the shear components - as:

$$\tau = \sqrt{\text{CSHEAR1}^2 + \text{CSHEAR2}^2} \tag{3.29}$$

In an increment with relative slip between the pile and the soil, the calculated τ is equal to the assigned τ_{max}, thus leading to the simulated α. Figure 3.20 confirms the validity of the applied numerical simulation.

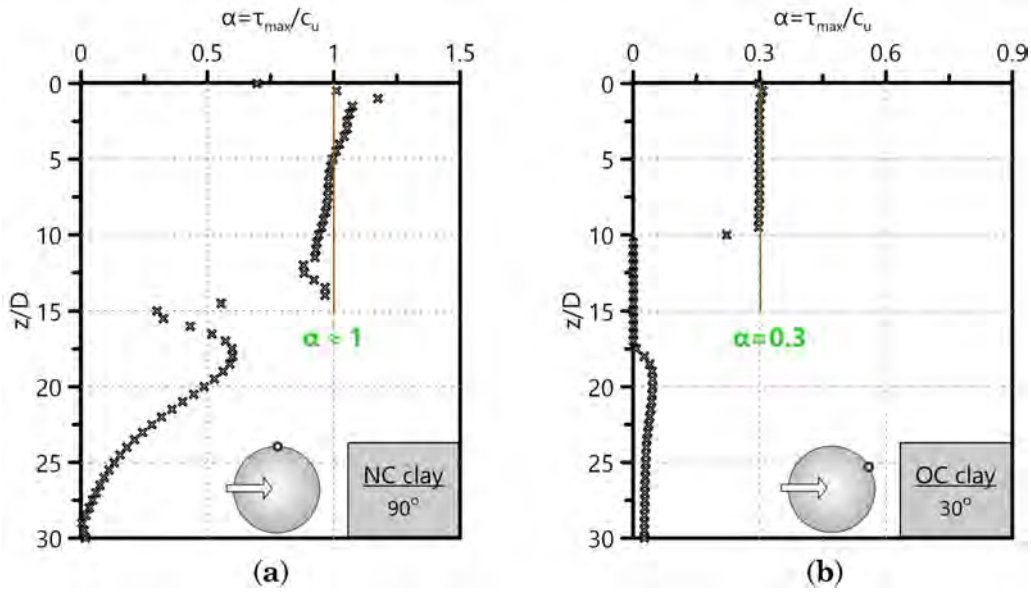

Figure 3.20: Verified adhesion factor α developing along a laterally loaded pile in (a) NC clay and (b) OC clay.

3.2.6 FEA steps of a laterally loaded pile

The effective stress, coupled FEA carried out in the current dissertation simulate the lateral loading of a generally flexible pile in a clayey soil under undrained conditions. In order to simulate the actual physical problem, we performed the FEA through the four following steps:

- **STEP 1:** The so-called geostatic step that generates the geostatic stress field in the FEM model. This step attempts the equilibrium of gravitational forces imposed on the solid elements with predefined initial stress conditions. All pile elements and soil-pile interfaces are removed during the specific step. After the completion of the geostatic step, we observed insignificant vertical and horizontal displacements of an order of magnitude 10^{-4}m and 10^{-5}m respectively. Thus, the FEA generates the geostatic stress field and subsequent steps are ready for calculation.

- **STEP 2:** The pile-soil interchange step. During this step, we replace the solid soil elements in the pile shaft with the solid pile elements of low Young's modulus (see Paragraph 3.2.4) and activate the beam elements of the pile. In addition,

the soil-soil interface - namely a rough, hard contact interaction - of the geostatic step is replaced by the soil-pile interface described in Paragraph 3.2.5.

- **STEP 3:** The consolidation step prior to the application of the lateral load. This is a dummy step that allows the soil of the FEM model to consolidate for 1000 days or until it reaches steady state, whichever happens first. The steady-state criterion is actually the dissipation of excess pore water pressure potentially developed during STEP 2.

- **STEP 4:** The step of the lateral pile loading. The pile is laterally loaded during the specific step by imposing either a concentrated load or a horizontal displacement on the pile head. Depending on the pile head fixity state (free-head or fixed-head), corresponding boundary conditions are assigned to the specific point. It is important to point out that we impose the monotonic lateral load within a time period of 1 day. This duration of the loading process combined with the very low permeability assigned to the clay ($k = 10^{-10}$m/s - see Paragraph 3.2.3) ensures undrained loading conditions.

3.3 Verification of the numerical model

The current section verifies the procedure for the numerical development of p-y curves derived in the present dissertation. The following paragraphs examine three potential processes for the derivation of p-y curves through the current FEA. In addition, we investigate the effect of the FEA mesh density, boundary distances from the pile, soil-pile interface properties, geometrical nonlinearity, pile head fixity and clay type (soft NC or stiff OC) of the problem on the derived p-y curves. The aforementioned sensitivity analysis is carried out for a laterally loaded pile both in a soft NC clay (M=0.98, λ=0.174, λ/κ=10, ν=0.333) and a stiff OC clay ($c_{u,avg}$=190kPa, κ=0.00543, λ/κ=20, ν=0.10). We assumed adhesion factor α=1 and 0.3 for the NC and OC clay respectively in the verification analyses. The thesis investigates separately the effect of soil and pile properties on the proposed p-y curves for NC and OC clays in Chapters 4 and 5 respectively.

3.3.1 The process of the p-y curves development

In the current section we describe potential procedures for the numerical development of p-y curves in the dissertation. The lateral displacement y of the pile is always the FEA output of the horizontal deflection $U1_i$ at the central node of the pile cross-section at the depth of the desired p-y curve (Figure 3.21. On the other

hand, the current paragraph verifies three different approaches for the calculation of the corresponding lateral soil reaction p. Finally, we determine the most appropriate method of the three for the derivation of p-y curves through our parametric study. All soil reaction calculations of the current paragraph refer to half the pile cross-section - as described in Paragraph 3.2.1. In order to determine the actual p, the corresponding calculation doubles the aforementioned reaction.

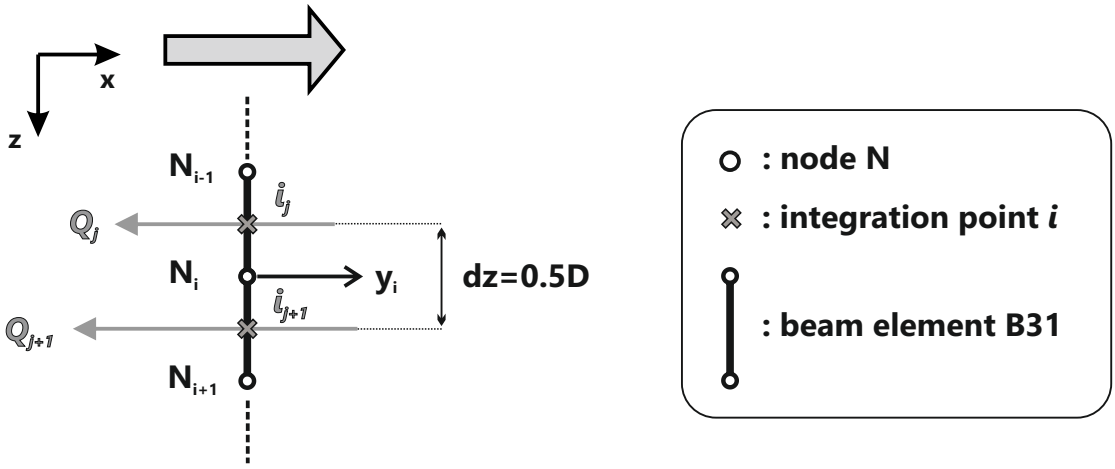

Figure 3.21: Calculation of p from FEA shear force output on two subsequent beam elements B31.

The first method is the classic beam on elastic foundation method proposed by Hetényi (1971) and expanded in the calculation of the soil reaction, considering the pile as an elastic beam on a surrounding soil simulated with lateral springs. This method considers the soil reaction p against a laterally loaded pile equal to the first derivative of the shear force of the pile-beam at the specific depth:

$$p_1 = \frac{\mathrm{d}Q}{\mathrm{d}z} = \frac{Q_{j+1} - Q_j}{z_{j+1} - z_j} \tag{3.30}$$

FEA calculate the developed shear force on the beam elements of the pile simulation (see Paragraph 3.2.4) per loading increment. The shear force in the FEA is calculated at the integration point of each B31 beam element[1]. The difference dQ between two subsequent elements divided by the length of the beam element, i.e. dz=0.5 D, delivers the soil reaction p at the depth of the node connecting these two elements, as explained schematically in Figure 3.21.

The second method introduced in the current dissertation concerns direct soil reaction horizontal forces on the soil-pile interface. As we mentioned in the description of the soil-pile interface simulation (Paragraph 3.2.5), total forces and stresses

[1]The integration point of the B31 beam elements is located on their mid-length (Simulia, 2012).

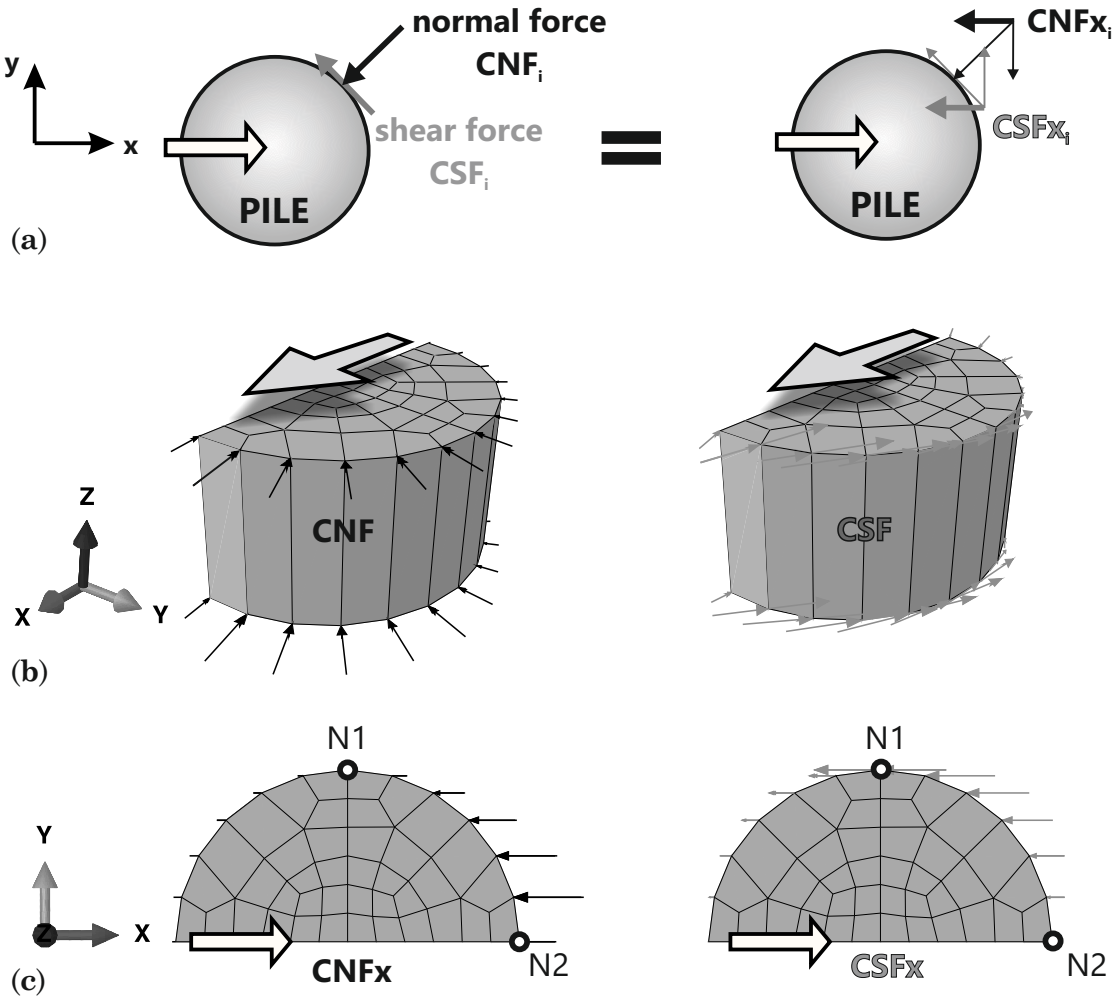

Figure 3.22: Calculation of p from FEA interface output on a pile slice. Explanation of (a) contact normal (CNF) and shear (CSF) forces, (b) their resultants and (c) their components acting in the direction of the lateral load.

are calculated on the surface interaction. Figure 3.22 depicts the interface nodes, on which the contact forces are measured. More accurately, we extract the normal (CNFx) and shear (CSFx) interface force components in the direction of global x-axis, calculated during the FEA at the depth of the desired p-y curve. By summing vectorially the aforementioned interface output and dividing it with its pile length of influence, i.e. $\mathrm{d}z{=}0.5\,D$, we calculate the corresponding soil reaction p as a distributed load along the pile (kN/m).

$$p_2 = \frac{\sum (\mathrm{CNFx}_i + \mathrm{CSFx}_i)}{\mathrm{d}z} \tag{3.31}$$

In Figure 3.22 (down) depicting the horizontal components of contact forces calculated through the FEA, note that node N1 actually delivers just a shear component

while node N2 just a normal component - as expected due to the nature of the problem.

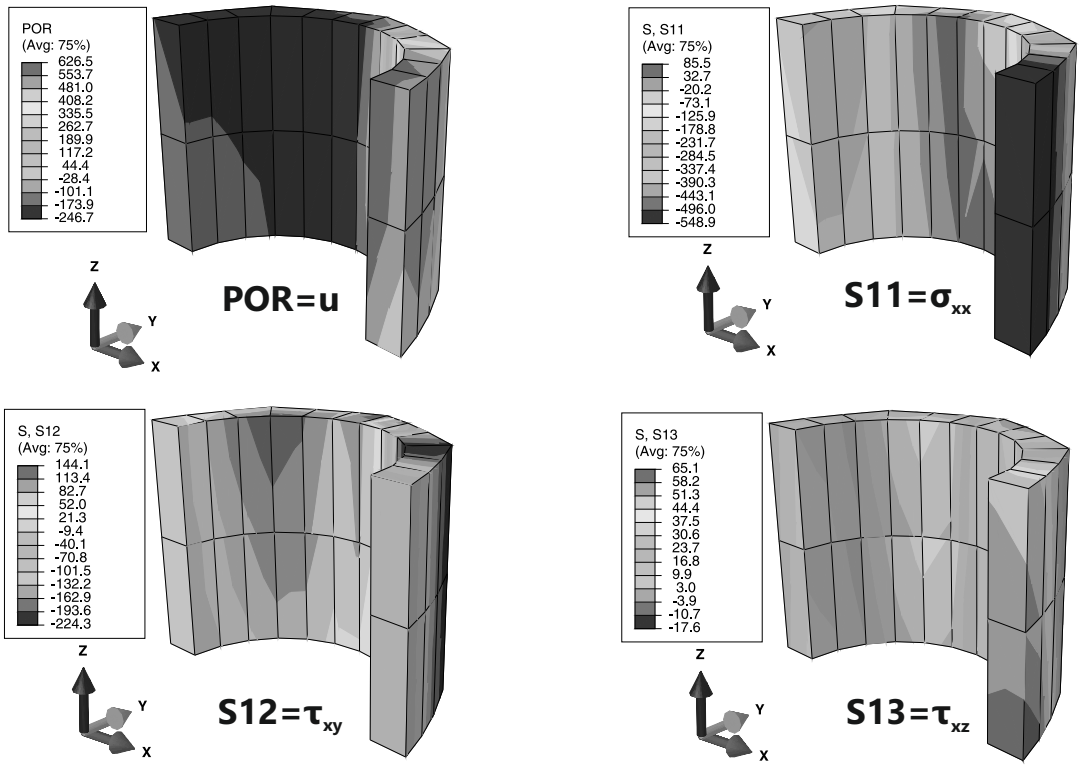

Figure 3.23: FEA contours of pore water pressure u and effective soil stress components σ_{xx}, τ_{xy}, τ_{xz} for two subsequent soil "rings" in direct contact with the laterally loaded pile.

In order to verify the accuracy of the soil reaction calculated through the two aforementioned approaches, we introduce a third method for p measurement through the FEA outputa. In this method we calculate the total pressure parallel to the loading direction developing at specific soil "rings" surrounding the laterally loaded pile. For this calculation we extract the FEA output for all the effective normal and shear stress components (σ_{xx}, τ_{xy}, τ_{xz}) in the direction of global x-axis at the centroid[1] of each soil element around the pile. Moreover, we take into account the corresponding FEA computations on the (isotropic) pore water pressure development (u). Figure 3.23 depicts FEA output contours of the stresses involved in the specific calculation of p for two subsequent soil "rings".

In order to convert x-stress components to distributed load components per soil element, we multiply normal and shear stress components with the xy plan

[1]The centroid of C3D8 and C3D8P solid elements is located on their center of gravity (Simulia, 2012).

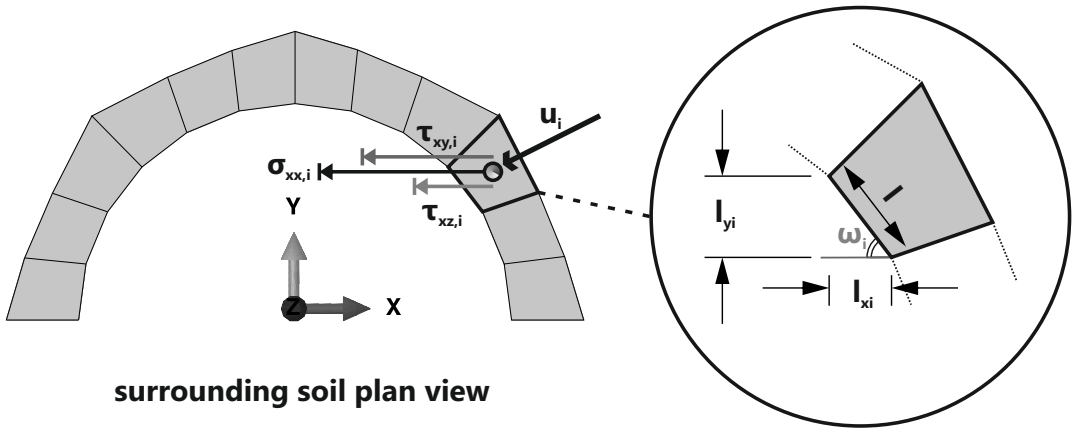

Figure 3.24: Calculation of p from FEA stress output on a soil "ring" surrounding the laterally loaded pile.

view projection on global y-axis on which they apply (Figure 3.24). The same multiplication applies to the isotropic pore water pressure. Through the following equations we calculate the aforementioned distributed load components per element of the soil "ring":

$$P_{ux,i} = u_i \cdot l_{y,i} = u \cdot (l \cdot \sin \omega_i) \tag{3.32a}$$

$$P_{xx,i} = \sigma_{xx,i} \cdot l_{y,i} = \sigma_{xx,i} \cdot (l \cdot \sin \omega_i) \tag{3.32b}$$

$$P_{xy,i} = \tau_{xy,i} \cdot l_{x,i} = \tau_{xy,i} \cdot (l \cdot \cos \omega_i) \tag{3.32c}$$

$$P_{xz,i} = \tau_{xz,i} \cdot l_{x,i} = \tau_{xz,i} \cdot (l \cdot \cos \omega_i) \tag{3.32d}$$

with l= the soil element length on xy plan view in contact with the pile - equal for all soil "ring" elements - (Figure 3.24) and ω_i= the acute angle between l and global x-axis. Subsequently, we calculate soil reaction p as the algebraic sum of the aforementioned components - distributed load along the pile (kN/m):

$$p_3 = \sum (P_{ux,i} + P_{xx,i} + P_{xy,i} + P_{xz,i}) \tag{3.33}$$

The centroid position of elements constituting a single soil "ring" does not coincide with the depth of the lateral deflection y measurement, thus not allowing for the exact p calculation at the desired depth. Therefore, in the specific approach we calculate p as the average lateral soil reaction measured from two soil "rings" above and below the depth of the p-y curve.

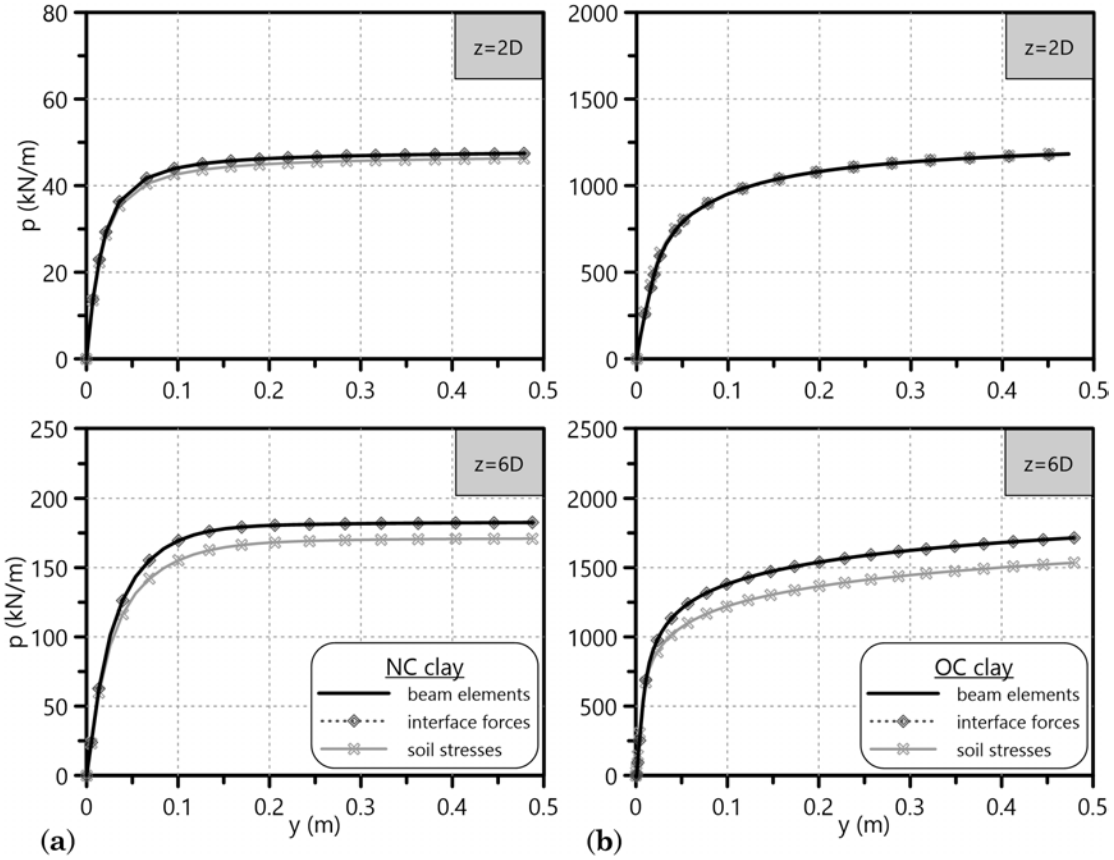

Figure 3.25: Comparison of three methods - beam elements shear forces, interface normal and shear forces and soil stresses - for the derivation of p-y curves. Calculated p-y curves for two different depths of (a) NC clay and (b) OC clay.

Comparison of the three aforementioned methods for the p-y curve derivation shows absolute coincidence of the first (beam) and the second (interface) method (Figure 3.25). The third (stress) method also delivers p-y curves very close to the previous two that almost coincide for the shallow depth ($z = 2D$). However, due to certain assumptions of this method (stresses measured on the element centroid, approximate length of stress application, etc.) the derived p-y curves demonstrate lower p for greater depth ($z = 6D$). The specific satisfactory comparison shall stand as a validation process of the numerically developed p-y curves depicted herein in the current dissertation. We decide to use p_1-method for the derivation of p-y curves herein in this thesis due to its simplicity and minimum time consumption.

3.3.2 Effect of FEA mesh density and boundaries

The current paragraph demonstrates the sensitivity analysis carried out in order to evaluate the effect of mesh density and the boundaries distance from the pile on the

derived p-y curves for NC and OC clays. In more detail, we compare the p-y curves calculated for the standard FEM model (see Paragraph 3.2) at two different depths ($z = 2D$ and $6D$) with the corresponding curves retrieved from two other FEA:

- One FEA with a grid of finite elements twice as dense as the standard model (Figure 3.26a). The so-called dense model involves almost 80000 solid elements - the standard model includes almost 40000 elements - and the mesh grid of the soil block is much denser than the standard one. However, the mesh densities at the proximity of the pile, i.e. $5D$-radius around the pile, are equivalent for both simulations.

- Another FEA with extended boundaries distance from the laterally loaded pile (see Figure 3.26b) compared to the corresponding distance of the base model (see Figure 3.1). Apart from the boundaries of the model on the xy plane, we extend the vertical dimension of the model adding a $5D$-thick soil layer below the pile tip, i.e. z-dimension equal to $35D$.

The comparison results in the absolute coincidence of the p-y curves computed through all three aforementioned FEA for NC as well as OC clays, as depicted in Figure 3.27. Therefore the mesh density and the boundaries of the standard model are judged adequate for the accuracy level of the current dissertation and thus this simulation is used herein in the thesis.

3.3.3 Effect of soil-pile interface properties

This section refers to the effect of different soil-pile interface parameters, namely the interface stiffness in the normal (k_n) and the shear (k_s) direction as well as the adhesion factor α controlling the interface shear strength (see Paragraph 3.2.5), on the p-y curves derived from the FEA.

The standard configuration properties for the interface stiffness are $k_n = 10^4\ kN/m^3$, $k_s = 10^4\ kN/m^3$. Numerical instabilities occur during the FEA if the interface is either very stiff or very soft compared to the relative stiffness of the soil-pile system. In addition, if the interface is very soft we encounter loss of normal and shear forces transmitted through this interaction due to intense strain accumulation of the interface. Therefore, this paragraph carries out a sensitivity analysis for the effect of k_n and k_s on the derived p-y curves for NC and OC clays. Especially for k_n, values lower than standard $k_n = 10^4\ kN/m^3$ result in numerical instabilities even from Step 2 of the FEA (see Paragraph 3.2.6), attributed potentially to the large surface overclosure allowed between the pile and the surrounding soil by such small k_n values. For this reason, the current verification examines only k_n values higher

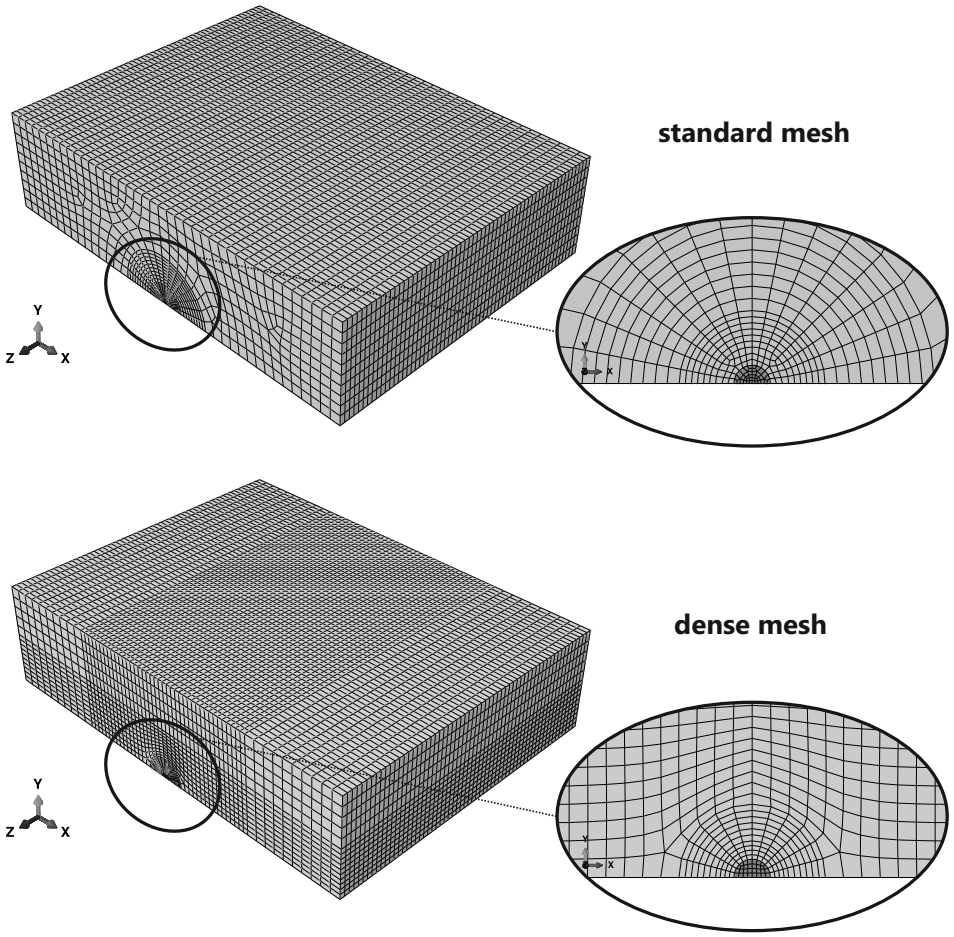

(a)

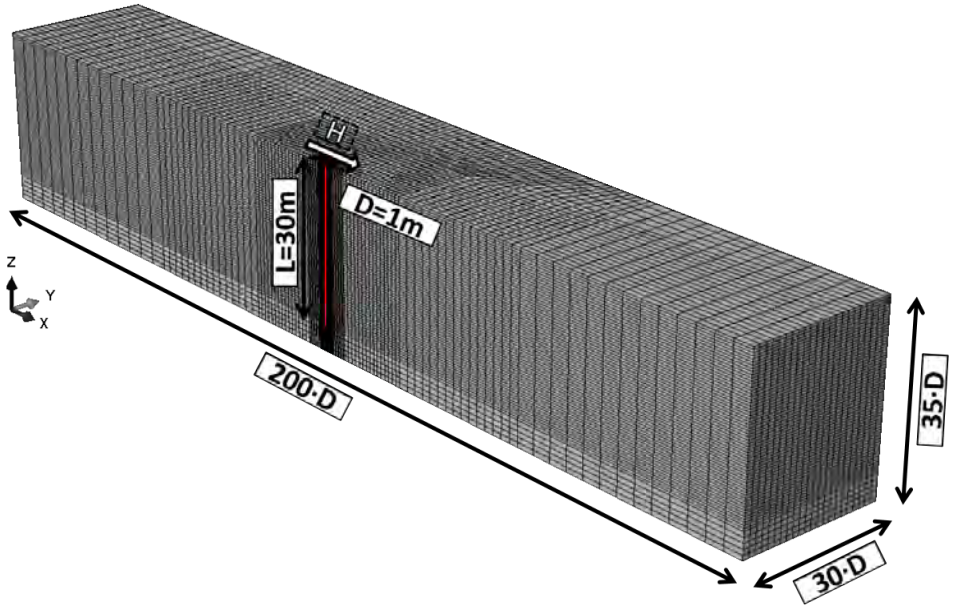

(b)

Figure 3.26: (a) Standard and dense mesh grid of the FEA. (b) Mesh grid of the FEA with extended boundary distances from the laterally loaded pile.

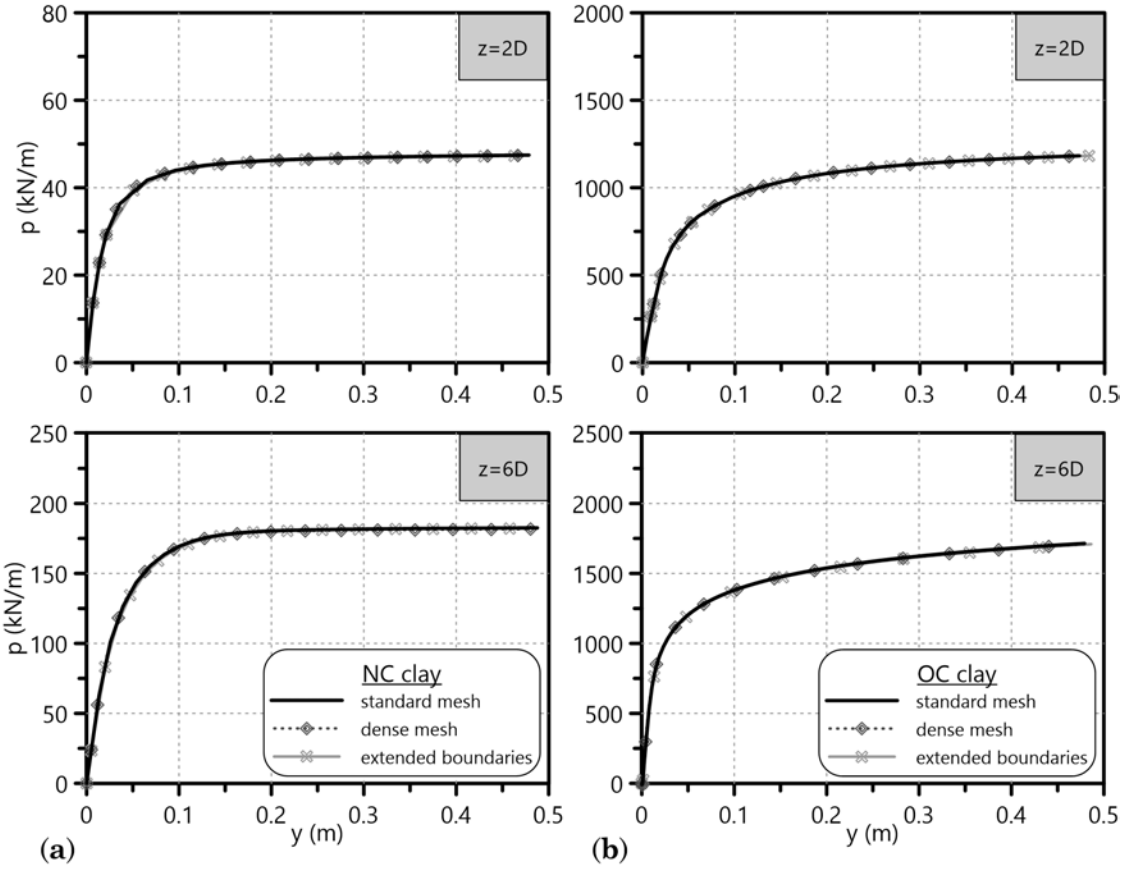

Figure 3.27: Effect of mesh density and boundaries distance from the pile on the numerical p-y curves. Calculated p-y curves for two different depths of (a) NC clay and (b) OC clay.

than standard. We perform three FEA with altered k_n and k_s values compared to the standard ones:

- One FEA with $k_n = 10^8\ kN/m^3$ and $k_s = 10^4\ kN/m^3$ to notice the effect of higher k_n.
- Another FEA with $k_n = 10^4\ kN/m^3$ and $k_s = 10^1\ kN/m^3$ to notice the effect of lower k_s.
- A third FEA with $k_n = 10^4\ kN/m^3$ and $k_s = 10^8\ kN/m^3$ to notice the effect of higher k_s.

Figure 3.28 depicts the comparison of the p-y curves calculated from the aforementioned FEA with the corresponding ones from the standard FEA at two different depths ($z = 2D$ and $6D$) of the NC and OC clay examined in the current verification process. We initially observe that alterations of the interface stiffness exclusively affect the ultimate lateral soil resistance p_u of the curves. For the NC clay, the

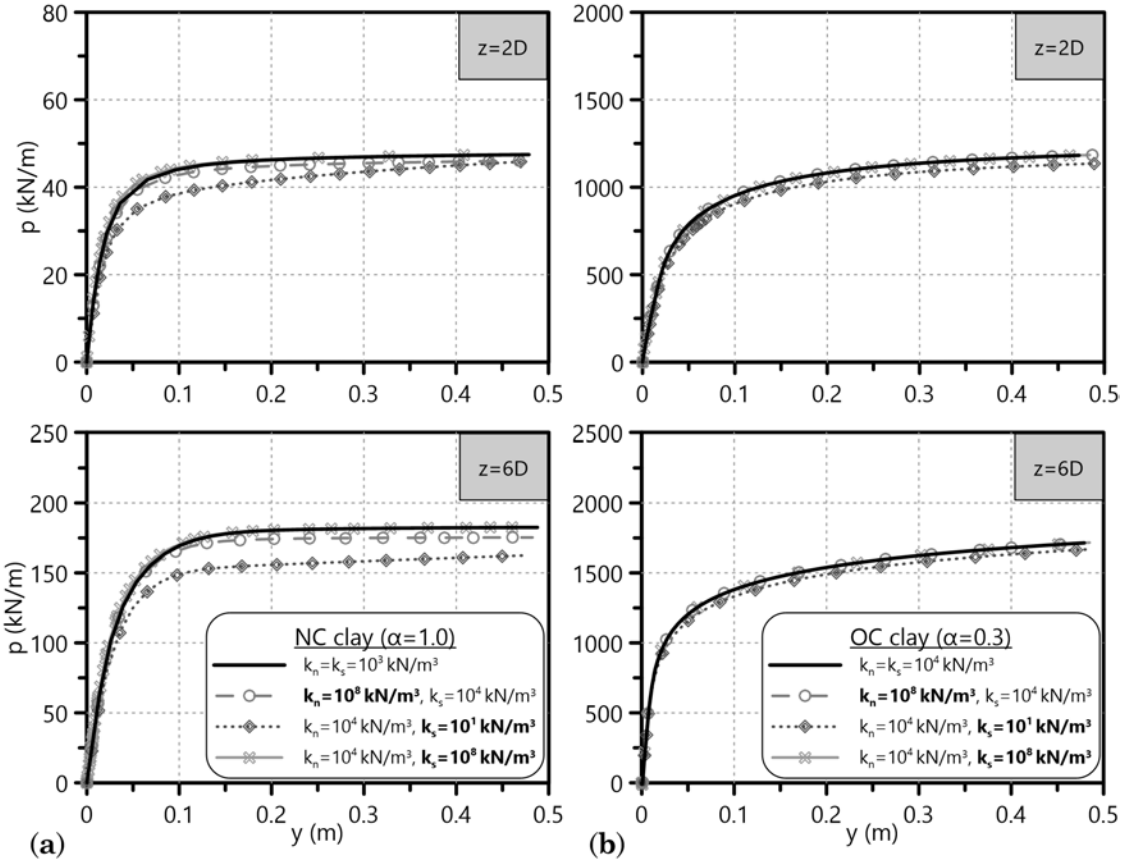

Figure 3.28: Effect of the normal k_n and shear k_s interface stiffness on the numerical p-y curves. Calculated p-y curves for two different depths of (a) NC clay and (b) OC clay.

derived p-y curves with significantly higher k_n and k_s appear very close to or even on the corresponding curves of the standard FEM configuration; very low k_s seems to deliver the lowest p_u due to extensive interface deformation. For the OC clay, only significantly low k_s narrowly influences the p_u of the p-y curves.

For the standard FEA of the current chapter, adhesion factor α=1 and 0.3 is assumed for the NC and OC clay respectively. In order to evaluate the effect of the interface on the derived p-y curves, we compare the corresponding FEA results with and without any interface at various depths (Figure 3.29). The simulation of a realistic pile-soil interaction (with slipping and detachment properties) has limited effect on soft NC clays - FEA without interface overestimate p_u by 20-25%. The specific observation is rather anticipated since such soils tend to follow pile deformation due to their very low c_u. On the other, interface simulation is essential for stiff OC clays because the numerical p-y curves without it exhibit p_u overestimation even by 100% - no interface neglects pile-soil separation. As a consequence, all the numerical simulations of the thesis incorporate interface simulation. Furthermore, we compare the FEA results of both adhesion factors applied on both soils to quantify

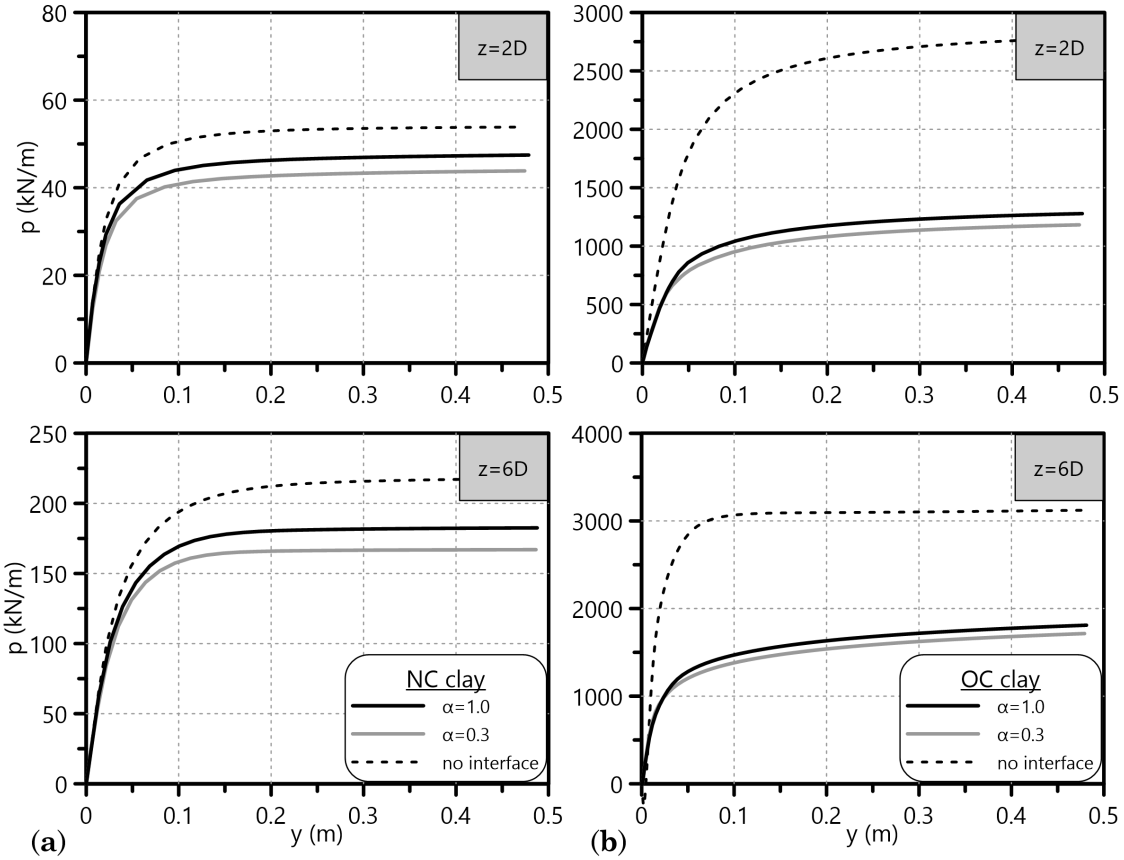

Figure 3.29: Effect of the interface simulation and the adhesion factor α on the numerical p-y curves. Calculated p-y curves for two different depths of (a) NC clay and (b) OC clay.

the effect of α on the numerical p-y curves. Figure 3.29 presents this comparison, demonstrating some differentiation of p_u between the p-y curves derived for the two different adhesion factors - thus confirming the observations of various researchers on the specific effect (see Chapter 2).

According to the aforementioned remarks, we assume that the interface simulation of the standard FEA regularly carried out in the current dissertation (k_n = 10^4 kN/m^3=k_s = 10^4 kN/m^3 and α=1 and 0.3 for NC and OC clay respectively) is successfully verified for its effect on the numerically developed p-y curves. Characteristic frames of the FEA that depict the realistic pile-soil interface simulation are included in Appendix C.

3.3.4 Effect of geometrical nonlinearity

The numerical derivation of p-y curves from FEA output requires very large lateral load or displacement imposed on the pile head. The reason for such a simulation is the required development of ultimate lateral soil resistance p_u of the calculated p-y

curves up to a critical depth of 6-8D. As a result, large deformations occur on the FEA mesh leading to potential geometrical nonlinearities of the simulation when the surrounding soil reaches its failure stress. Therefore, we consider taking into account the updated coordinates of the FEA nodes throughout the loading step by introducing the nonlinear geometry feature (NLGEOM) in the specific step (Simulia, 2012). Figure 3.30 depicts the dimensionless lateral displacement output y/D along the pile of the FEA with horizontal head displacement y_h equal to 10%D, 30%D and 50%D in a soft NC and a stiff OC clay, with and without the geometrical nonlinearity feature. It is obvious that the NLGEOM feature has no significant influence on the horizontal deflection profile of the laterally loaded pile. The comparison of derived

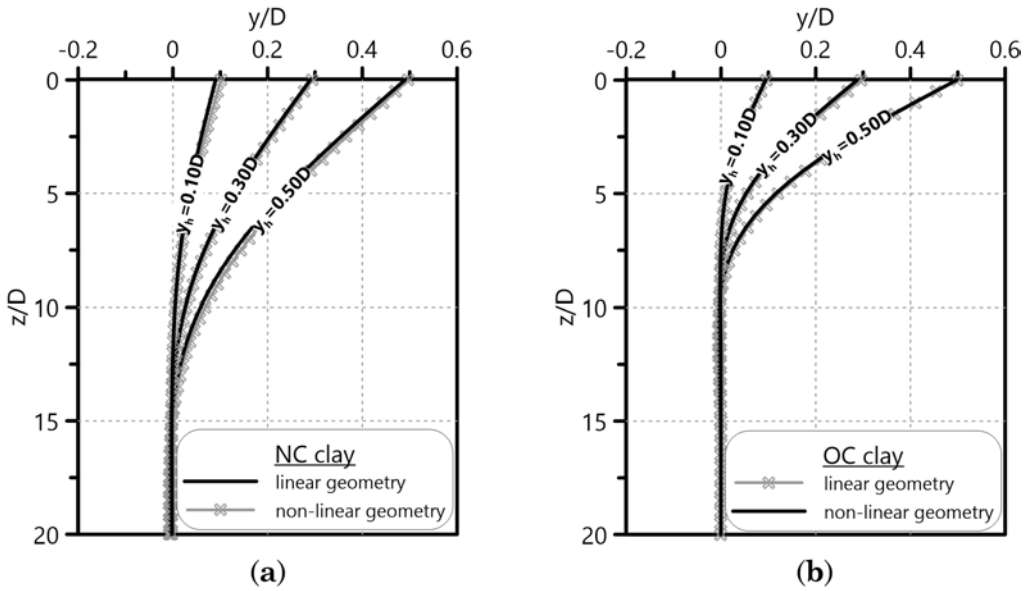

Figure 3.30: Dimensionless lateral displacement y/D along the pile for various horizontal displacements y_h imposed on the pile head. Horizontal deflection profile of the laterally loaded pile in (a) a soft NC and (b) a stiff OC clay.

p-y curves with and without the NLGEOM feature shows certain differences between them, especially for the NC clay. These differences are attributed to the inability of the FEA soil constitutive laws (see Paragraph 3.2.2) to adopt to the stress-strain field defined under the geometrical nonlinearities regime (Piola-Kirchhoff stresses). The fundamental principle of the constitutive laws assigned to the soil in the FEA of the current dissertation is the separation of a strain increment into two components, an elastic and a plastic one. Since the FEA calculations with the NLGEOM feature refer to the incrementally updated geometry of the mesh, the specific analysis calculates the aforementioned strain - and consequently stress - increments with respect to this updated geometry. Therefore, the current paragraph considers the stress calculations between the small-strain assumption (utilized constitutive laws) and the

large-strain theory (geometrical nonlinearity) inconsistent regarding the FEA of this thesis. In order to exploit the potentials of the constitutive laws used in the current dissertation for an advanced simulation of NC and OC clays, the adopted numerical simulation presented herein develops p-y curves according to the small-strain assumption and thus without the geometrical nonlinearity feature.

3.3.5 Effect of pile characteristics

The following verification examines potential effect of the pile stiffness E_pI_p and the fixity conditions of the pile head on the numerically developed p-y curves.

3.3.5.1 Effect of pile stiffness

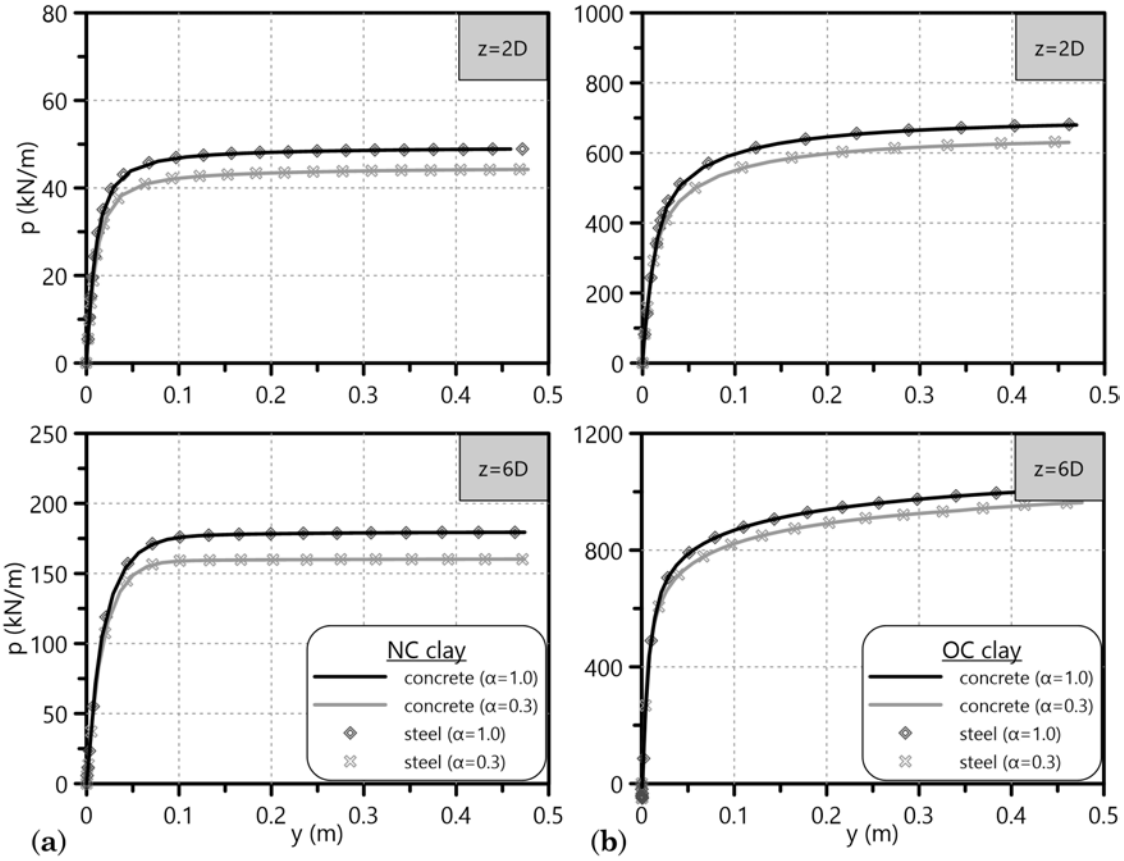

Figure 3.31: Effect of the pile stiffness E_pI_p (elastic pile) on the numerical p-y curves. Calculated p-y curves for two different depths of (a) NC clay and (b) OC clay.

The current paragraph examines if the flexural rigidity of the elastic pile affects the p-y curves that are derived from the FEA. In more detail, the investigation refers to two pile types of outer diameter D=1.0m:

- a reinforced concrete pile with solid cross-section and $E_pI_{p,\text{conc}} = 1500MNm^2$ and
- a steel pile with hollow cross-section and $E_pI_{p,\text{steel}} = 960MNm^2$ (wall thickness t=12.7mm).

Figure 3.31 compares the numerical p-y curves derived for the two pile types (concrete, steel) at two different depths ($z = 2D$ and $6D$) of a NC and an OC clay, for the whole adhesion range of the numerical investigation (α=0.3-1.0). It is evident that the pile stiffness does not affect the p-y curves derived from the corresponding FEA.

3.3.5.2 Effect of pile head fixity

Another issue that the current FEM model verification investigates is the effect of pile head fixity conditions - and as a result the effect of the lateral loading conditions - on the numerically developed p-y curves. As Figure 3.32 depicts, we distinguish between the following lateral loading regimes of a pile:

- **Free-head:** Concentrated lateral load or displacement on a pile head free to rotate. This simulation corresponds either to single free-head piles or piles that belong to a group without a pile cap.
- **Fixed-head:** Concentrated lateral load or displacement on a pile head restrained against rotation. This simulation corresponds either to single fixed-head piles or piles that belong to a group with a pile cap.
- **Uniform displacement:** Uniform lateral displacement along a pile. This simulation corresponds to piles undergoing large uniform displacement along them, i.e. slope stabilizing piles or piles in a laterally spreading soil.

Figure 3.33 demonstrates the derived p-y curves from FEA simulating the three aforementioned loading conditions of a laterally loaded pile in a NC clay (M=0.98, λ=0.109, λ/κ=10, ν=0.333) and an OC clay ($c_{u,avg}$=190kPa, κ=0.00543, λ/κ=20, ν=0.10). We observe infinitesimal differences between the p-y curves of a free-head and a fixed-head pile[1], while uniform lateral displacement delivers lower ultimate lateral soil resistance p_u. Especially for the NC clay, we notice a post-peak behavior with decreasing lateral resistance that is not physically explained - since we observe detachment from the soil at the back of the pile after a certain value of the uniform

[1] Appendix C contains characteristic FEA frames that depict the simulation of the pile head constraints.

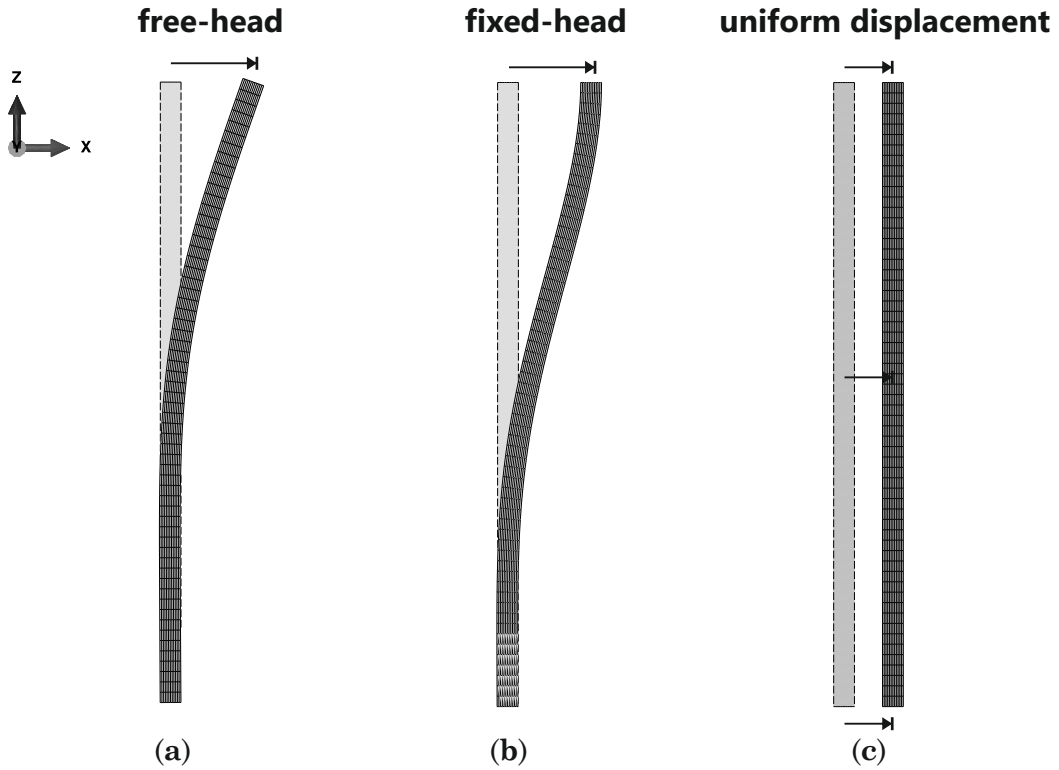

Figure 3.32: Three different pile head fixity conditions: lateral load applied on top of a free-head (left) or fixed-head (middle) pile and uniform lateral displacement along the pile (right).

lateral displacement. Thus, the present verification judges the FEA output of the "uniform displacement" case as uncertain after a lateral displacement around $10\%D$.

3.3.6 Constitutive laws reliability

The current paragraph attempts a summarizing verification of the utilized constitutive laws during the FEA of this thesis. Initially, we plot certain curves for a specific soil element under compression in front of the pile and at a depth z=3D (D=1m). For the centroid of the element intoned in Figure 3.34, we demonstrate the constitutive behavior during the lateral loading of the pile.

Either the MCC (NC and OC clay) or the sophisticated constitutive law incorporating SSS and SD features (OC clay) controls this behavior. The MCC parameters are the ones listed at the beginning of the verification process, while for the SSS-SD model we simulate peak strength equal to that of the MCC OC clay and residual strength assuming B=3 (see Paragraph 3.2.2.2). Stress paths together with $q-\varepsilon_q$, $\varepsilon_{\text{vol}}-\varepsilon_q$ and $\Delta u-\varepsilon_q$ curves are plotted for the three aforementioned constitutive simulations. Figures 3.35, 3.36 and 3.37 depict constitutive behaviors totally analo-

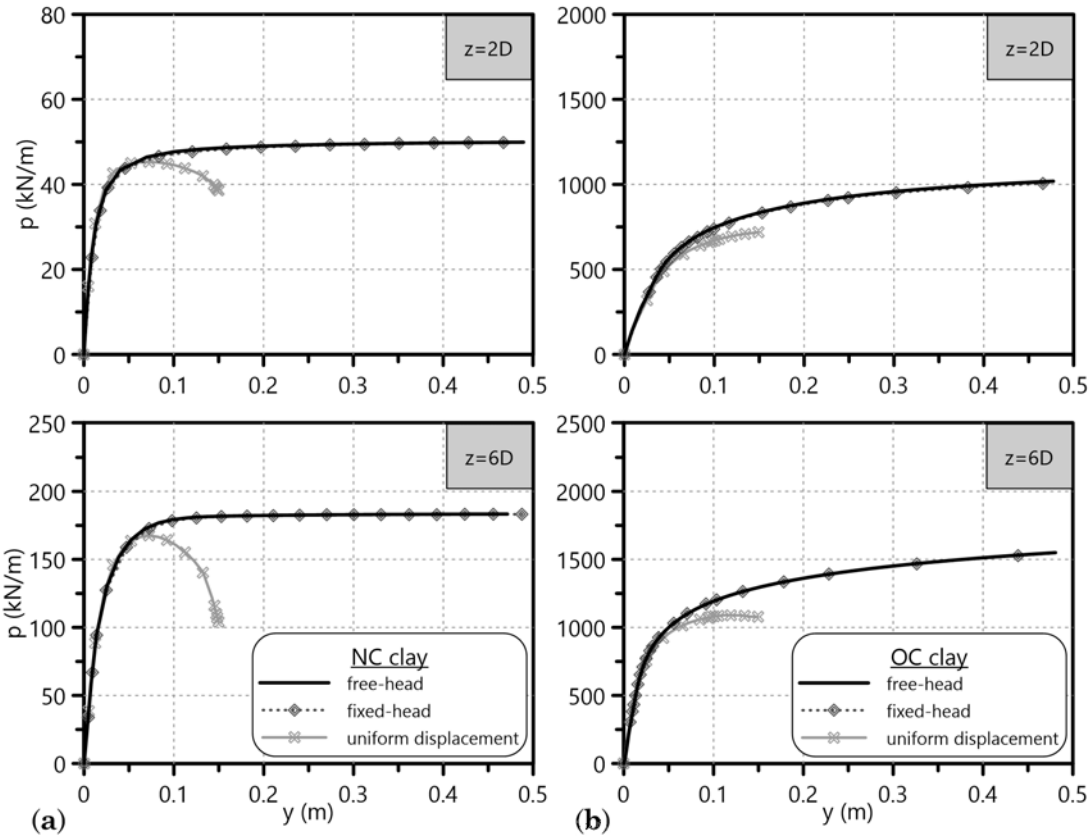

Figure 3.33: Effect of pile head fixity conditions on the numerical p-y curves. Calculated p-y curves for two different depths of (a) NC clay and (b) OC clay.

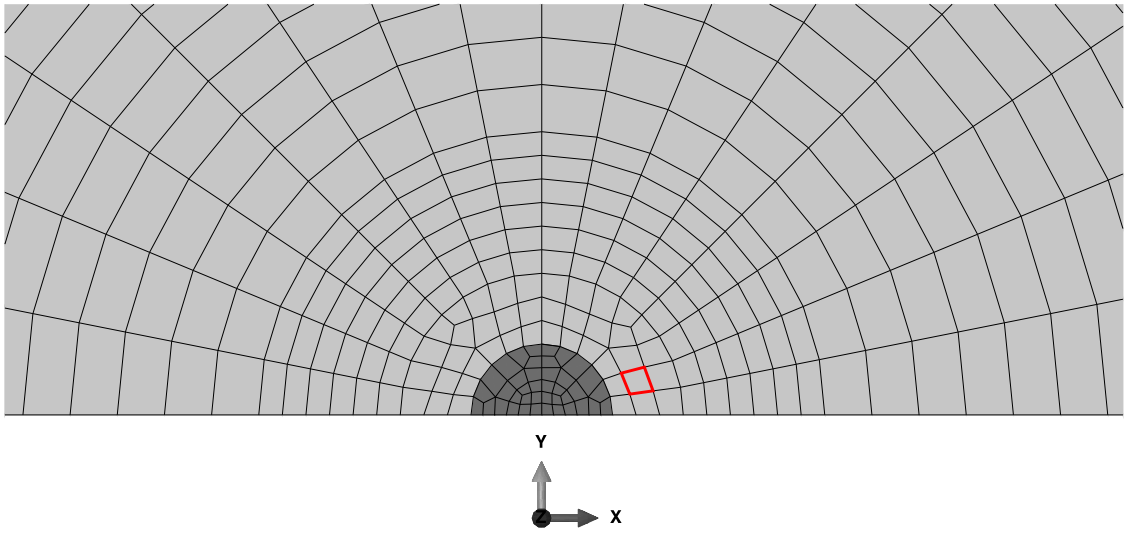

Figure 3.34: Soil element in front of the laterally loaded pile for the verification of the FEA constitutive laws reliability.

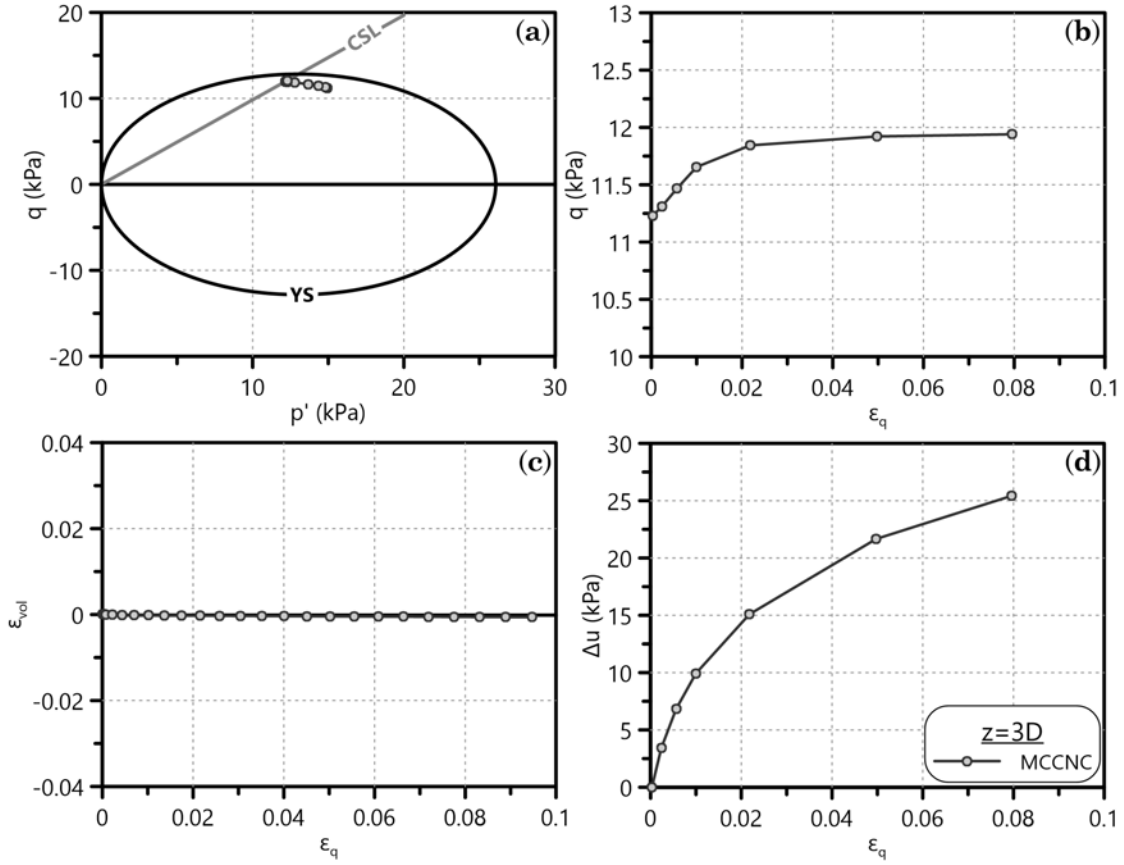

Figure 3.35: (a) Stress path, (b) deviatoric stress-strain curve, (c) volumetric-deviatoric strain curve and (d) pore water overpressure development of a specific NC clay element under compression in front of the laterally loaded pile (z=3D). Constitutive behavior controlled by the MCC.

gous to the corresponding numerical undrained triaxial tests presented in Paragraph 3.2.2.3.

It is very important to notice that apart from the expected constitutive behavior in $p-q$ and $q-\varepsilon_q$ planes, we validate the lateral loading of the pile under actual undrained conditions during the FEA. Diagrams $\varepsilon_{\text{vol}}-\varepsilon_q$ and $\Delta u-\varepsilon_q$ demonstrate that through both the infinitesimal volumetric strains $\varepsilon_{\text{vol}} \approx 0$ and the pore water overpressure development Δu of the examined soil element. Thus, these plots verify that the assigned permeability-loading duration combination of the FEA ensures the desired undrained loading regime.

Finally, we carry out a couple of total stress FEA using the Mohr-Coulomb constitutive model for the soil simulation in order to validate the p-y curves derived through the MCC and the SSS-SD model simulations. These FEA simulate both NC and OC clay behaviors assuming a c_u distribution with depth according to Paragraph 3.2.3.2. We also assume an undrained Young's modulus E_u=300 $\cdot$ c_u -

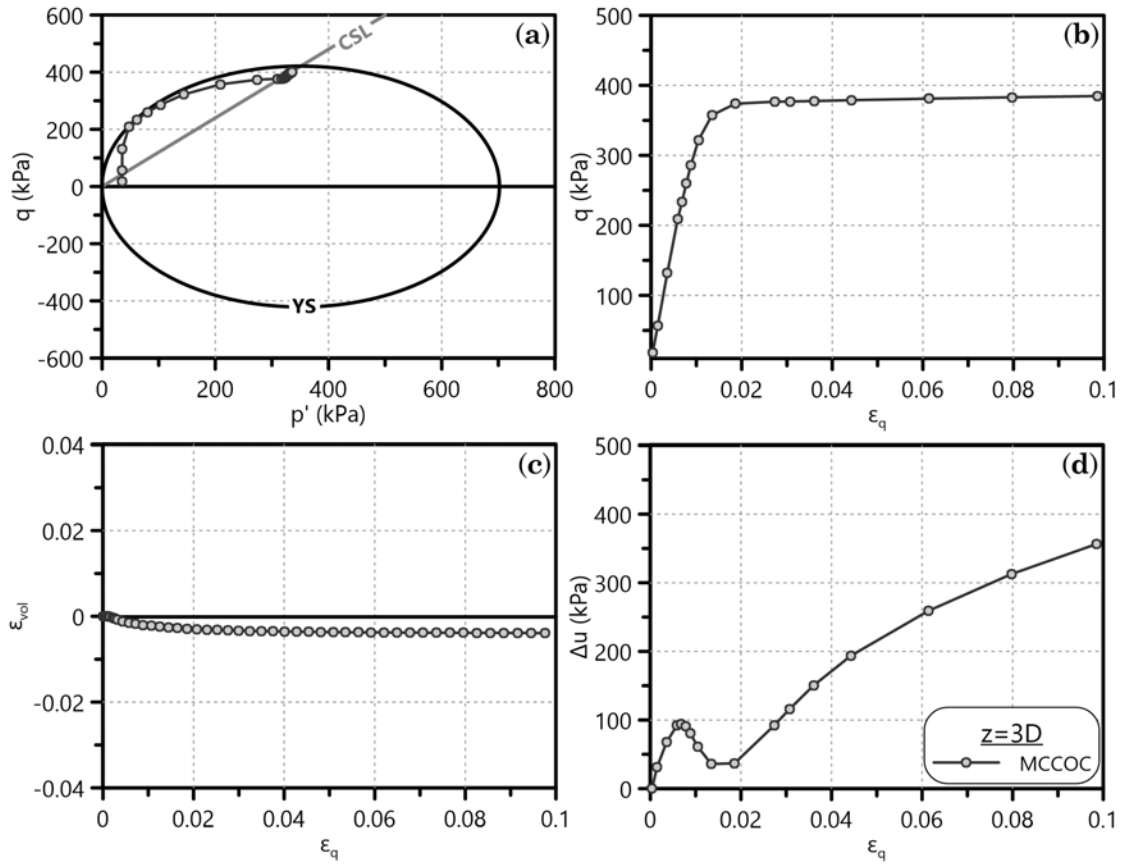

Figure 3.36: (a) Stress path, (b) deviatoric stress-strain curve, (c) volumetric-deviatoric strain curve and (d) pore water overpressure development of a specific OC clay element under compression in front of the laterally loaded pile (z=3D). Constitutive behavior controlled by the MCC.

as a conservative approximation from literature - and a Poisson's ratio ν=0.5 in order to simulate undrained loading conditions. Figure 3.38 depicts that the p-y curves derived from the MCC and the Mohr-Coulomb FEA generally agree for the NC clay at all the examined soil depths. On the contrary, the p-y curves of the two different constitutive simulations show striking differences for all the depths of the OC clay apart from z=4D. We observe that the clay constitutive law affects the initial stiffness K_i as well as the ultimate lateral soil resistance p_u of the p-y curves. However, this observation does not cancel the importance of the current verification process. As a matter of fact, we validate here that the advanced MCC - compared with the elastic-perfectly plastic Mohr-Coulomb - can predict reliable numerical p-y curves. Although the MCC p-y curves almost match the corresponding Mohr-Coulomb curves for the NC clay, it is very significant to propose such numerical curves after a constitutive model with certain complexities (effective stress analysis, poroelasticity, critical state soil mechanics, etc.). Thus, we have the opportunity to

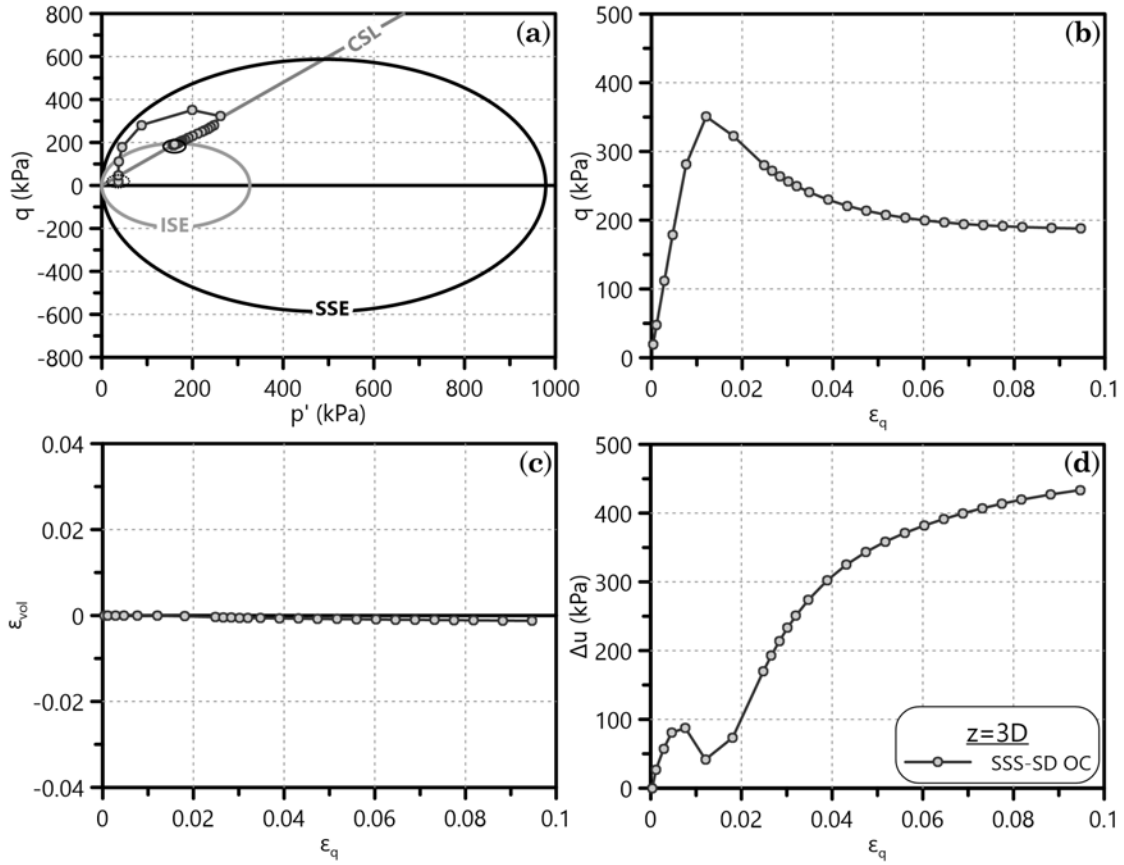

Figure 3.37: (a) Stress path, (b) deviatoric stress-strain curve, (c) volumetric-deviatoric strain curve and (d) pore water overpressure development of a specific OC clay element under compression in front of the laterally loaded pile (z=3D). Constitutive behavior controlled by the sophisticated SSS-SD model.

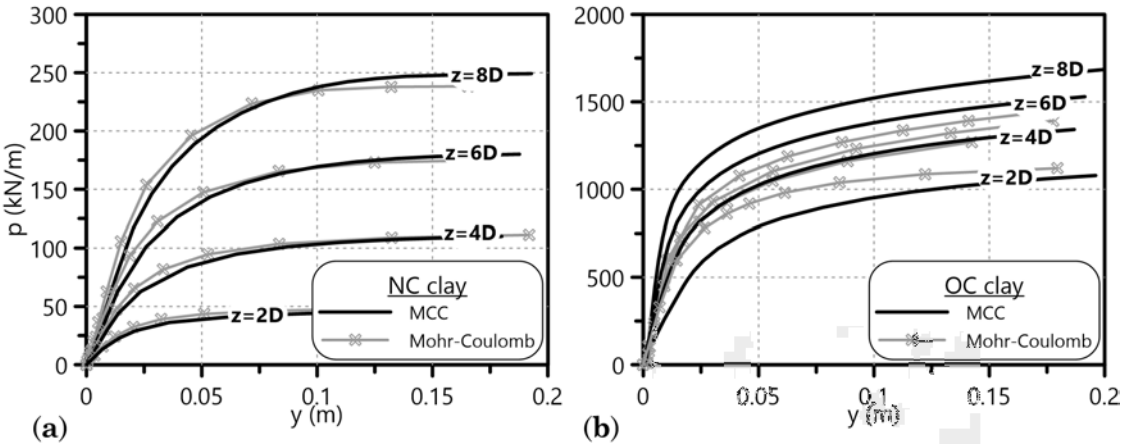

Figure 3.38: MCC numerically developed p-y curves for various depths compared with the corresponding ones from total stress FEA with the Mohr-Coulomb constitutive model; (a) NC clay simulation; (b) OC clay simulation.

solve potential benchmark problems of the FEA and move on with confidence to the simulation of OC clays through a sophisticated constitutive law that reproduces the physical features of small-strain stiffness (SSS) and structure degradation (SD) exhibited by such soils at the field.

3.3.7 Validation with experimental results

This final paragraph of the chapter attempts to validate the developed numerical simulation through comparisons with centrifuge test results of laterally loaded piles in soft, NC clays. These comparisons involve charts of the non-dimensional pile head lateral displacement vs. shear force ($y_h/B - H$) as well as the distribution of bending moment ($M - z$) along the laterally loaded pile. To do so, we enter the soil and pile properties of each load test in the 3D FEA and compare the output of the latter with the corresponding test measurements.

The FEA predictions are validated with the results of two centrifuge tests in soft, NC clays:

- centrifuge test by Kitazume (1994)
- centrifuge test by Ilyas et al. (2004)

Kitazume (1994) carried out a series of centrifuge tests on the PHRI (Port and Harbour Research Institute) geotechnical centrifuge under 25g acceleration field. The model pile of the tests was plate-shaped, of prototype width B=0.5m, various thicknesses d and various flexural rigidities E_pI_p. The following validation chooses Test 5 (AL-5) on an aluminium model pile of prototype stiffness $E_pI_p = 4.9MNm^2$ for comparison with the FEA results. The pile had a prototype embedment length L_b=10.0m in the soft clay and horizontal displacement y_h up to $0.7B$ was imposed at constant speed of 1.15mm/min on the pile top (at a height of 2.5m above ground level, thus resulting in a total pile length L=12.5m). The soil of the specific centrifuge tests was a fully saturated (water table above ground level), soft, NC clay with the following properties: plastic limit $PL = 16.8\%$, liquid limit $LL = 59.0\%$ and estimates[1] of the virgin compression line slope $C_c = 0.50$ and the unloading-reloading line slope $C_r = 0.10$. The undrained shear strength c_u of the aforementioned soil increased linearly from 1kPa at ground level to around 10kPa at prototype depth z=10m.

On the other hand, Ilyas et al. (2004) carried out a series of centrifuge model tests in order to examine the behavior of laterally loaded pile groups in normally

[1] according to correlations with the Atterberg limits by Bowles (1988)

consolidated and overconsolidated kaolin clay. Apart from pile groups, lateral load tests were also conducted to single piles. All the tests were performed at 70g on the National University of Singapore (NUS) Geotechnical Centrifuge. The model pile was a hollow aluminum square tube instrumented with ten levels of strain gauges to enable bending moment measurements along the pile shaft. At 70g, the simulated prototype pile has a width B=0.84m, embedded length L_b=14.7m in the clay, flexural rigidity $E_pI_p = 922MNm^2$ and lateral displacement y_h=B was imposed at constant speed of 0.05mm/s on the pile head (3.5m above ground surface, thus resulting in a total pile length L=18.2m). The kaolin clay used to prepare the soft, NC clay profile in the test container had the following properties: average bulk unit weight $\gamma = 16kN/m^3$, average water content $w_N = 66\%$, plastic limit $PL = 35.1\%$, liquid limit $LL = 79.8\%$, virgin compression line slope $C_c = 0.55$, unloading-reloading line slope $C_r = 0.16$ and permeability $k = 2 \cdot 10^{-8}m/s$. The c_u of the NC clay increased linearly with depth from 0 at ground surface to about 20kPa at prototype depth z=15m.

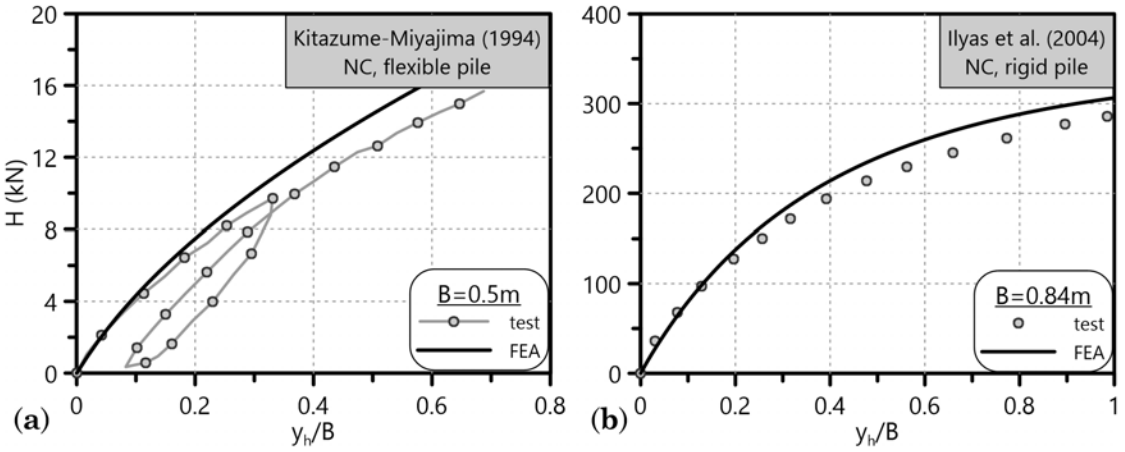

Figure 3.39: Comparison of the pile head lateral dimensionless displacement-load curves $y_h/B - H$ between the 3D FEA output and the centrifuge test measurements (a) by Kitazume (1994) and (b) by Ilyas et al. (2004).

It is important to mention that for both numerical simulations, the pile was considered elastic with aluminium Young's modulus E_p=70GPa and appropriate moment of inertia I_p of the cross-section to result in the corresponding stiffness E_pI_p of each experiment.

Figures 3.39 and 3.40 depict a very satisfactory agreement of the numerical predictions with the centrifuge test measurements. Some divergence observed between the latter (especially with the test results by Kitazume (1994)) is attributed either to the soil properties incorporated in the FEA or to the totally elastic behavior of

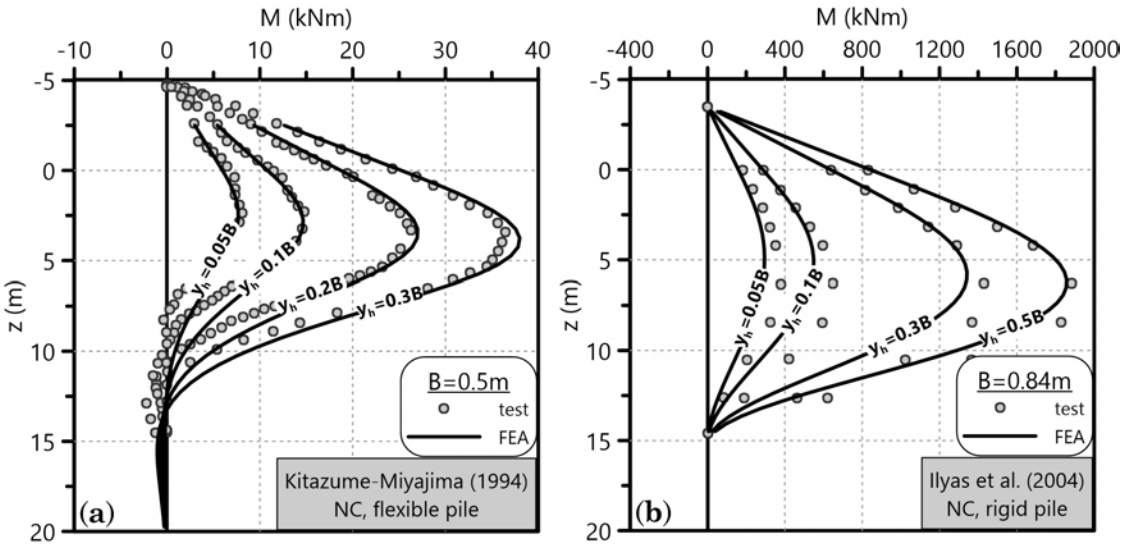

Figure 3.40: Comparison of bending moment distributions $M - z$ along the laterally loaded pile between the 3D FEA output and the centrifuge test measurements (a) by Kitazume (1994) and (b) by Ilyas et al. (2004).

the pile - although both centrifuge tests did not document any pile failures. As a conclusion, the numerical simulation developed by the thesis is judged robust and capable of predicting actual pile behavior with significant accuracy. Therefore, confidence is gained on the designed FEA, which allows the investigation to move on with the numerical parametric study of p-y curves for clayey soils.

3.4 Concluding remarks

Chapter 3 concludes in the following observations, regarding the capabilities of the numerical simulation utilized to develop p-y curves applicable to clayey soils:

- The chapter describes all aspects of the effective stress, coupled FEA performed in the computer software Simulia Abaqus 6.12 for the parallel solution of the mechanical and the hydraulic problem, when processing the simulation of a laterally loaded pile under undrained conditions. A certain permeability and load duration combination ($k = 10^{-10}$m/s and 1-day loading period) ensures undrained conditions of the clay surrounding the pile.

- While the simulation retrieves lateral displacement y as the horizontal deflection of the pile center, it offers three potential calculation ways of the lateral pressure p. The numerical p-y curves developed herein in the dissertation incorporate a p equal to the derivative of the shear force Q measured along the pile - simulated with beam elements.

- Two constitutive laws based on the Critical State Soil Mechanics theory simulate NC and OC clayey soils: the renowned MCC and a three-surface model - in the $p-q$ space - reproducing small-strain stiffness and structure degradation. We assign certain critical state parameters (M, p_m, etc.) as well as poroelasticity parameters (λ, κ, e, etc.) to the soil elements. Verification analysis shows that the FEA simulate realistically the anticipated undrained clay behavior.

- According to an extensive verification process, the mesh density and boundaries along the lateral loading direction of the adopted numerical simulation do not affect the derived numerical p-y curves.

- The magnitude of the adhesion factor α affects only the ultimate lateral soil resistance p_u of the p-y curves, with a fractional difference around 15% between low and high α values. The normal and shear stiffness of the soil-pile interface incorporated in the FEA do not influence the developed p-y curves.

- Since the FEA for the numerical development of p-y curves demand significant lateral displacement of the pile head ($>> 0.5D$), the current chapter investigated the effect of geometrical nonlinearities. Comparison of the horizontal pile displacement profiles with and without the large-strain feature shows infinitesimal differences. Thus, the FEA presented herein solve the problem of the laterally loaded pile according to the linear geometry rules, without any significant effect on the derived p-y curves.

- Pile head rotational constraints (free-head or fixed-head) have no effect at all on the developed p-y curves. Uniform lateral displacement of the pile refers to a totally different physical problem, i.e. kinematic lateral loading, that exceeds the limits of the current dissertation.

To sum up, the developed, sophisticated, three-dimensional finite element model of the present doctoral thesis proves reliable and capable of simulating realistically a single, laterally loaded pile in clayey soils through effective stress analyses. In addition, it captures the mechanisms that govern the lateral pile response. With the aforementioned observations at hand, the dissertation moves on to specific numerically developed p-y curves for NC and OC clayey soils within the following chapters.

Chapter 4

Parametric investigation of monotonic p-y curves for NC clays

4.1 Introduction

The present chapter develops numerical p-y curves for monotonic laterally loaded piles in NC clay - linearly increasing c_u with depth - under undrained loading conditions, through effective stress coupled FEA. We investigate the effect of various soil and pile parameters on the two main parts of the p-y curves, namely the initial stiffness K_i and the ultimate lateral soil resistance p_u. The FEM code Simulia Abaqus 6.12 is utilized to simulate the problem, with the MCC constitutive law reproducing the NC clay behavior in the aforementioned FEA.

As a result, the chapter delivers a new, exponential form of p-y curves for such soils, including certain strength, stiffness and geometry features of both the pile and the clay. The proposed p-y curve relationship for NC clays is compared with corresponding literature recommendations and its advantages and defects versus the latter are pointed out. Finally, the reader is referred to Chapter 7 for a validation of the proposed p-y curves with large-scale or centrifuge experimental results.

4.2 Parametric investigation of p-y curves for NC clays

In the current section we examine the parameters of the MCC constitutive law simulating the NC clay behavior (M, p_m, λ, etc.) as well as the features of the simulated laterally loaded pile (D, α, etc.). Furthermore, we investigate their effect on the numerically developed p-y curves, derived from the FEA. The following soil

and pile parameters are of concern in this research attempt on p-y curves for NC clays:

- Poroelasticity parameters λ, κ and their ratio λ/κ
- Critical state line slope M
- Poisson's ratio ν
- Pile diameter D
- Pile-soil adhesion factor α
- Depth of differentiation for the NC clay failure mechanism z_w

Table 4.1 depicts the range of the aforementioned parameters[1] - apart from z_w - used in the FEA of the current chapter for the simulation of different NC clays surrounding various laterally loaded piles. Appendix A contains the full table of the parametric FEA carried out for NC clayey soils. The following paragraphs thoroughly examine the influence of these parameters in the numerically derived p-y curves for NC clays.

Table 4.1: NC clay and pile properties of the FEA parametric investigation.

NC clay parameters				Pile parameters	
M[1]	λ[2]	λ/κ	ν	D (m)	α
0.772, 0.984, 1.200	**0.065, 0.109, 0.174**	10	0.333	**0.5, 1.0, 1.5, 2.0**	**1.0, 0.3**
0.984	0.109	**5, 20**	0.333	1.0	1.0
0.984	0.109	10	**0.10, 0.20**	1.0	1.0

[1] M values correspond to ϕ=20°, 25° and 30° (Equation 3.3).
[2] λ values correspond to C_c=0.15, 0.25 and 0.40 ($\lambda = C_c/\ln 10$).

4.2.1 NC clay parameters

The current paragraph describes the NC clay parameters examined in the current numerical simulation. The following parametric investigation indicates which NC clay properties it is necessary to take into account for the formulation of the corresponding numerical p-y curves. Prior to presenting an extensive investigation of the

[1] Appendix A contains the full extent of the parametric FEA carried out for NC clayey soils.

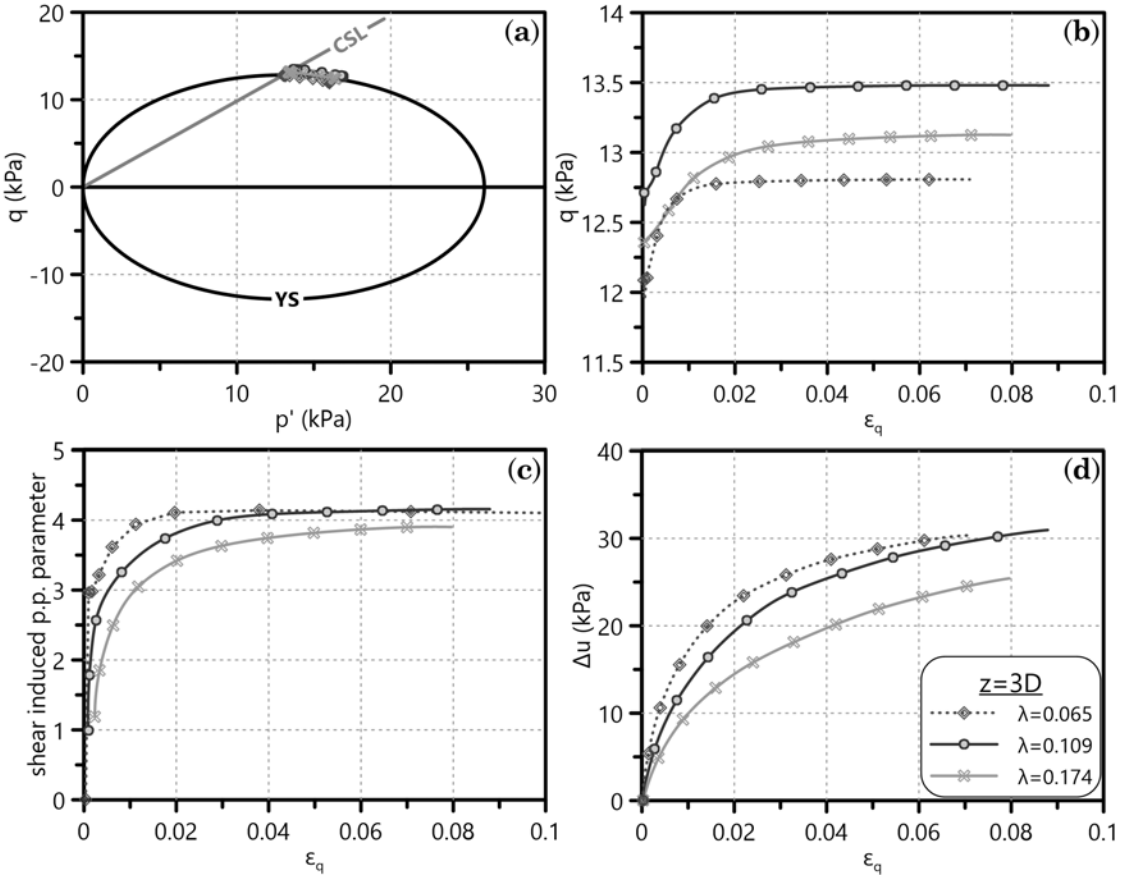

Figure 4.1: Effect of different NCL slopes λ (λ/κ=10, M=0.984, ν=0.333) on (a) stress paths, (b) deviatoric stress-strain curves, (c) shear induced pore pressure parameter-deviatoric strain curves and (d) excess pore water pressure development of a specific NC clay element under compression in front of the laterally loaded pile (z=3D).

effect these properties (λ, λ/κ, M, ν) have on the NC clay p-y curves, we deliver the following graphs at an average depth z=3D[1] (see Figure 3.34) of the FEA:

- stress paths $p-q$
- deviatoric stress-strain curves $q-\varepsilon_q$
- shear induced pore pressure parameter with the deviatoric strain $U_q-\varepsilon_q$[2]
- excess pore water pressure development with the deviatoric strain $\Delta u-\varepsilon_q$

Figures 4.1, 4.2, 4.3, and 4.4 depict the effect of λ, λ/κ, M and ν respectively on the aforementioned graphs. NCL slope λ and the ratio λ/κ affect the initial slope of the

[1]Assuming that the lateral loading of the pile affects the soil up to a depth $z \approx 6-8D$.

[2]The shear induced pore pressure parameter U_q stands for the percentage of the developed excess pore pressure Δu attributed to the shear stress. Assuming that $\Delta u = \Delta p + U_q \cdot \Delta q$ - where Δp=the difference in mean **total** stress - we calculate $U_q = -\Delta p^{'}/\Delta q$.

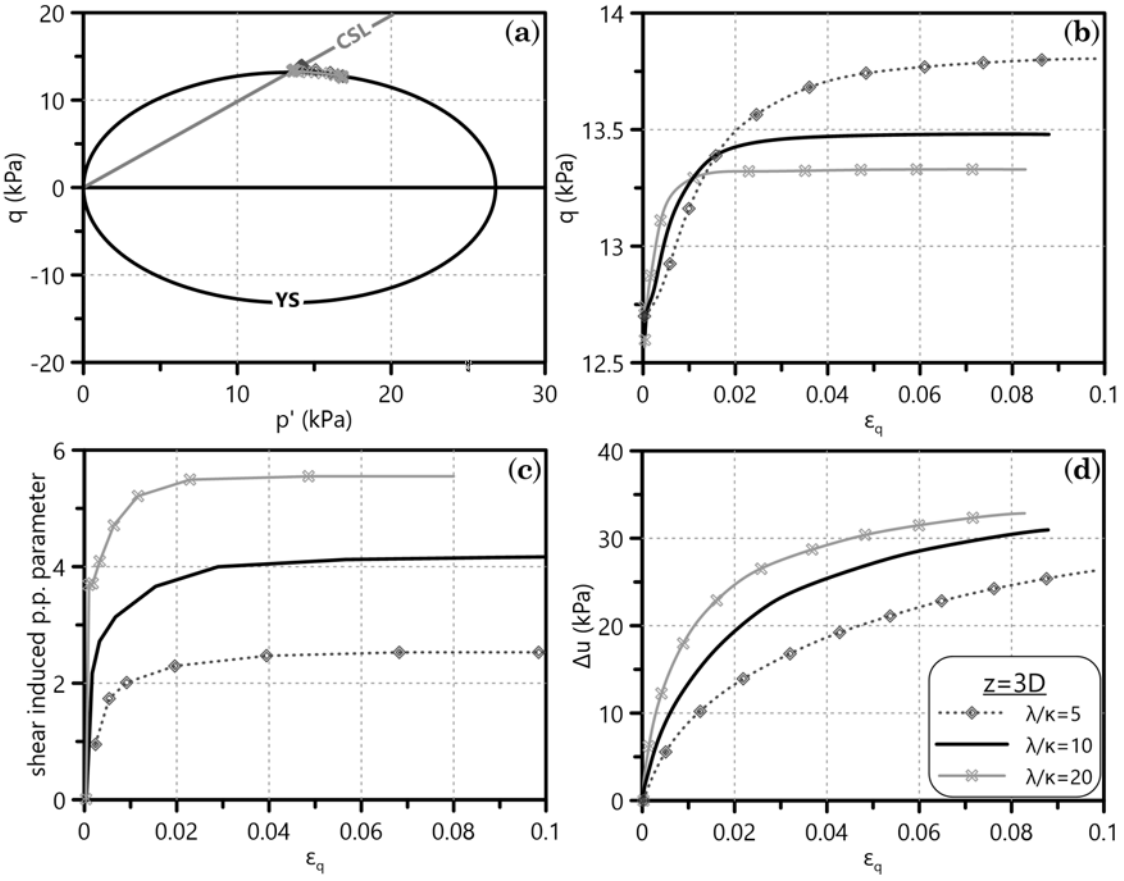

Figure 4.2: Effect of different λ/κ ratios (λ=0.109, M=0.984, ν=0.333) on (a) stress paths, (b) deviatoric stress-strain curves, (c) shear induced pore pressure parameter-deviatoric strain curves and (d) excess pore water pressure development of a specific NC clay element under compression in front of the laterally loaded pile (z=3D).

$q-\varepsilon_q$ and $\Delta u-\varepsilon_q$ curves. On the other hand, CSL slope M seems to affect the peak strength of the $q-\varepsilon_q$ curves more intensively - although relatively insignificantly compared to the corresponding strength range. Finally, while Poisson's ratio ν shows no influence on the $q-\varepsilon_q$ plots, its effect on $\Delta u-\varepsilon_q$ curves is rather measurable.

The aforementioned NC clay simulation parameters demonstrate certain effect on the soil constitutive behavior. Thus, the following paragraphs present this effect on the numerically developed p-y curves parallel to $q-\varepsilon_q$ graphs for λ, λ/κ, M and parallel to $\Delta u-\varepsilon_q$ graphs for ν at depths z=2D, 4D, 6D and 8D.

4.2.1.1 Poroelasticity parameters (λ, κ)

As Paragraph 3.2.3.2 points out (see Figure 3.14), the poroelasticity and strength parameters assigned to the clay are very important for its lateral response. NCL slope λ together with the size of the MCC YS p_m determine the initial geostatic state

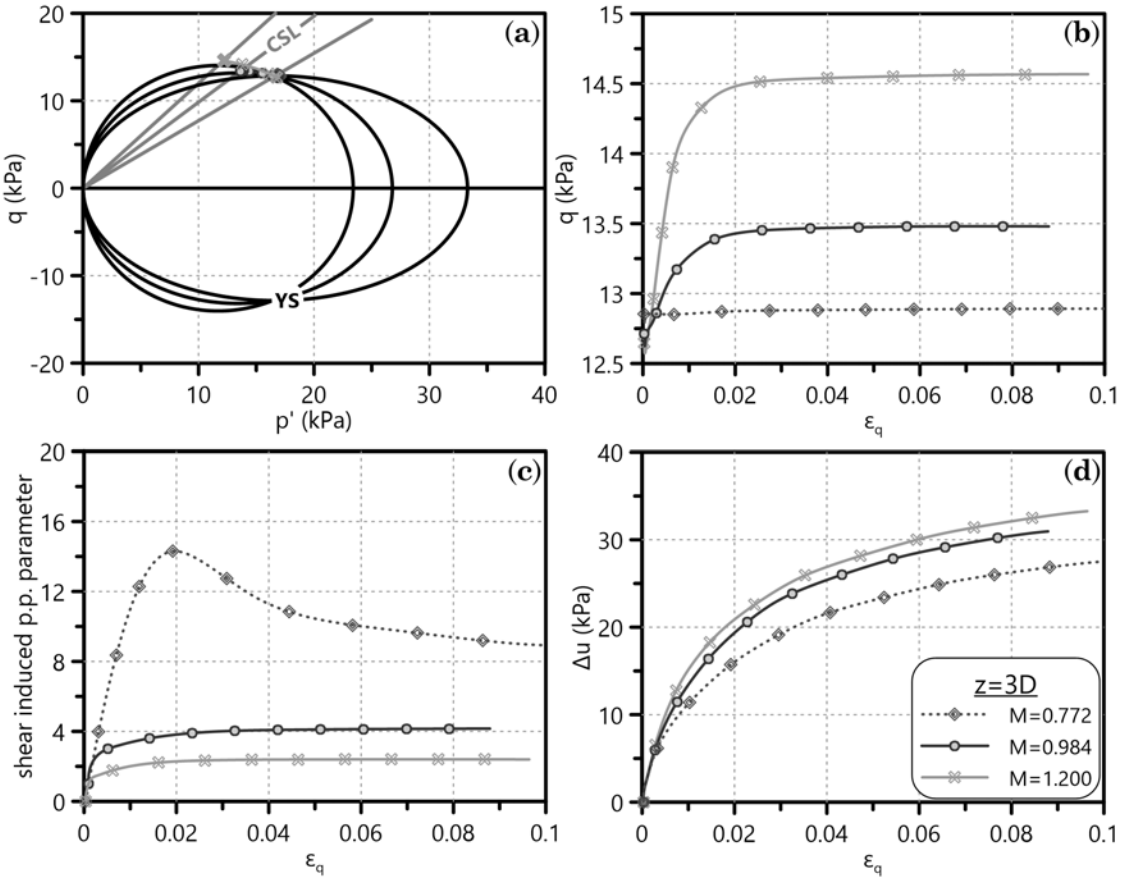

Figure 4.3: Effect of different CSL slopes M (λ=0.109, λ/κ=10, ν=0.333) on (a) stress paths, (b) deviatoric stress-strain curves, (c) shear induced pore pressure parameter-deviatoric strain curves and (d) excess pore water pressure development of a specific NC clay element under compression in front of the laterally loaded pile (z=3D).

of the NC clay on the $v - \ln p$ plane. During the lateral loading of the pile and since the clay under investigation is NC in the present chapter ($OCR = 1$), we assume that soil elements under compression (in front of the pile) undergo hardening, although slight due to undrained conditions and thus infinitesimal volumetric strain. NCL slope λ actually controls the YS size at different depths of the NC clay. Figure 4.5a presents the difference in initial stiffness K_i of p-y curves at the examined depths due to different λ of the NC clay. We assume λ/κ=10 for the specific investigation. The stiffness differentiation of the NC clay $q - \varepsilon_q$ curves (Figure 4.5b) clearly affects K_i of the numerical p-y curves. On the contrary, variation of λ hardly affects p_u of the p-y curves.

Apart from λ, the current paragraph investigates the effect of the swelling lines slope κ on the derived p-y curves for NC clays. More accurately, this verification examines the effect of three different λ/κ ratios on the numerical p-y curves, namely λ/κ=5, 10 and 20, for a NC clay with M=0.984 and λ=0.109 - midrange of the

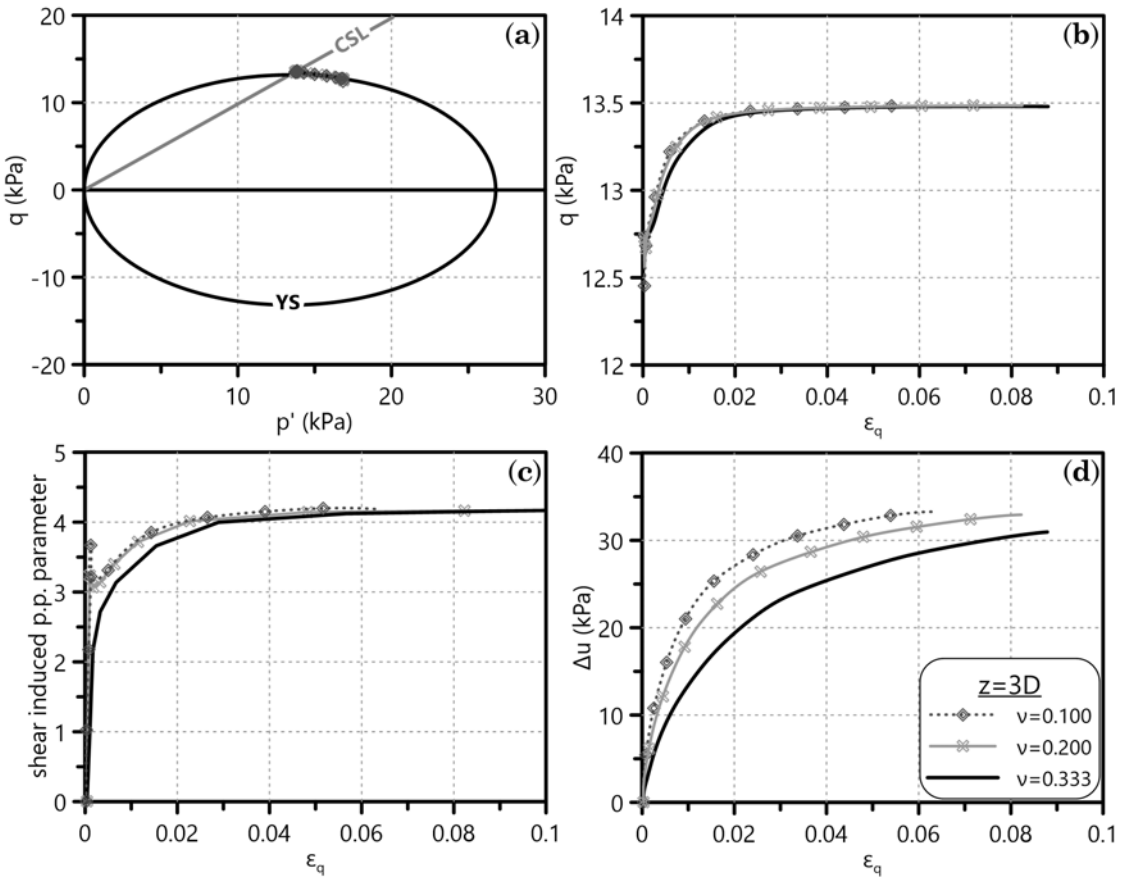

Figure 4.4: Effect of different Poisson's ratios ν (λ=0.109, λ/κ=10, M=0.984) on (a) stress paths, (b) deviatoric stress-strain curves, (c) shear induced pore pressure parameter-deviatoric strain curves and (d) excess pore water pressure development of a specific NC clay element under compression in front of the laterally loaded pile (z=3D).

specific parameters from Table 4.1. According to Terzaghi et al. (1996), most values of the ratio C_c/C_r - thus λ/κ - are in the range of 5 to 50. Very high values of the ratio, even higher than 50, correspond to highly structured and bonded soft clay and silt deposits whereas low values refer to micaceous silts and fissured stiff clays and shales. Thus, the λ/κ ratios of the current numerical investigation are within the range recommended by the literature.

It is very important to determine the most appropriate λ/κ ratio for a realistic simulation of the NC clay, in terms of stress-strain behavior. Triaxial tests on such clay specimens exhibit peak strength at axial deformation ε_a=2-4%. Assuming $\varepsilon_a \approx \varepsilon_q$ for the soil elements in front of the pile (see Figure 3.34) - since they are loaded under an almost triaxial regime - $q-\varepsilon_q$ curves for these element centroids at different depths prove very helpful for the determination of an appropriate NC clay λ/κ ratio. Figure 4.6b demonstrates that for λ/κ=10 peak NC clay strength occurs at $\varepsilon_q \approx 3\%$, whereas the corresponding deformation is around 6% and 1% for λ/κ=5 and 20

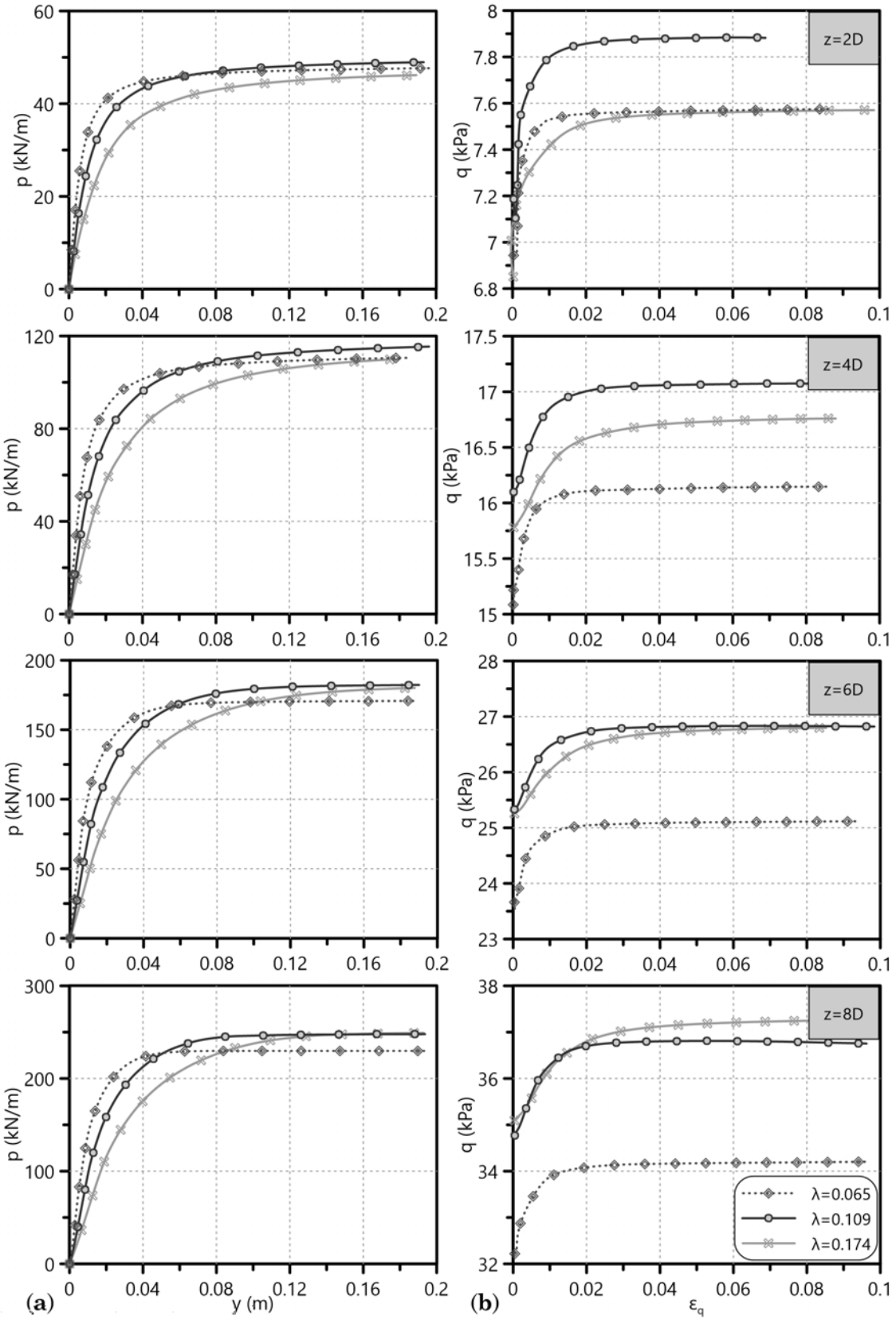

Figure 4.5: Effect of NCL slope λ on (a) the p-y curves and (b) the $q - \varepsilon_q$ curves at different depths of NC clay, derived from FEA output.

respectively. Taking into account that the parametric investigation of this chapter examines λ values higher and lower than the one of the aforementioned verification (λ=0.109), the NC clay simulation assuming λ/κ=10 seems rather rational and realistic. Finally, Figure 4.6a depicts the actual influence of λ/κ ratio on the derived FEA p-y curves. Paragraph 4.3 handles quantitatively this effect by proposing a certain monotonic p-y curve equation for NC clays through the findings of this chapter.

4.2.1.2 Critical state line slope (M)

As Figure 4.3 denotes, CSL slope M generally affects the NC clay peak total strength - $q-\varepsilon_q$ and $\Delta u-\varepsilon_q$ diagrams. It remains to investigate whether the variation of M also influences the ultimate lateral soil resistance p_u of the numerical p-y curves. The examined M values - corresponding to clay friction angles ϕ=20°, 25° and 30° (Equation 3.3) - also control the ratio of the undrained shear strength difference to the in situ vertical effective stress $\Delta c_u/\sigma'_{vo}$. M=0.772, 0.984 and 1.200 refer to $\Delta c_u/\sigma'_{vo}$=0.25, 0.27 and 0.29 respectively, thus simulating typical linear c_u distributions with depth for NC clays. Figure 4.7 depicts in parallel the FEA derived p-y curves and soil $q-\varepsilon_q$ graphs at depths z=2D, 4D, 6D and 8D. The comparison shows a rather insignificant effect of M differentiation on p_u (less than 10%). However, for consistency reasons Paragraph 4.3 investigates the actual M influence on the main parts - p_u and K_i - of the developed p-y curves for NC clays.

Another issue on the effect CSL slope M has on the p-y curves is its differentiation in compression (M_c) and extension (M_e) (see Equation 3.3). In order to investigate this effect, we carry out a FEA with M_e=0.8 · M_c (λ=0.109, λ/κ=10, M=0.984, ν=0.333) and compare the derived p-y curves with the corresponding ones from the standard numerical simulation of the NC clays. Figure 4.8 locates the difference between the two constitutive behaviors on p_u of the numerical p-y curves, with the standard simulation (M_e=M_c) generating an ultimate lateral NC clay resistance 5-8% greater than the current (M_e=0.8 · M_c).

4.2.1.3 Poisson's ratio (ν)

The current paragraph exhibits the effect of Poisson's ratio ν on the FEA derived p-y curves for NC clays. This verification tests three values of Poisson's ratio, namely ν=0.10, 0.20 and 0.333 for a NC clay with M=0.984, λ=0.109 and λ/κ=10, in terms of p-y and $\Delta u-\varepsilon_q$ curves - the latter for soil elements under compression in front of the pile (Figure 3.34). Although the lateral loading of the pile is undrained with $\varepsilon_{\text{vol}} \approx 0$ and thus $\nu_u \approx 0.5$ (see Paragraph 3.3.6), the actual ν of the soil controls

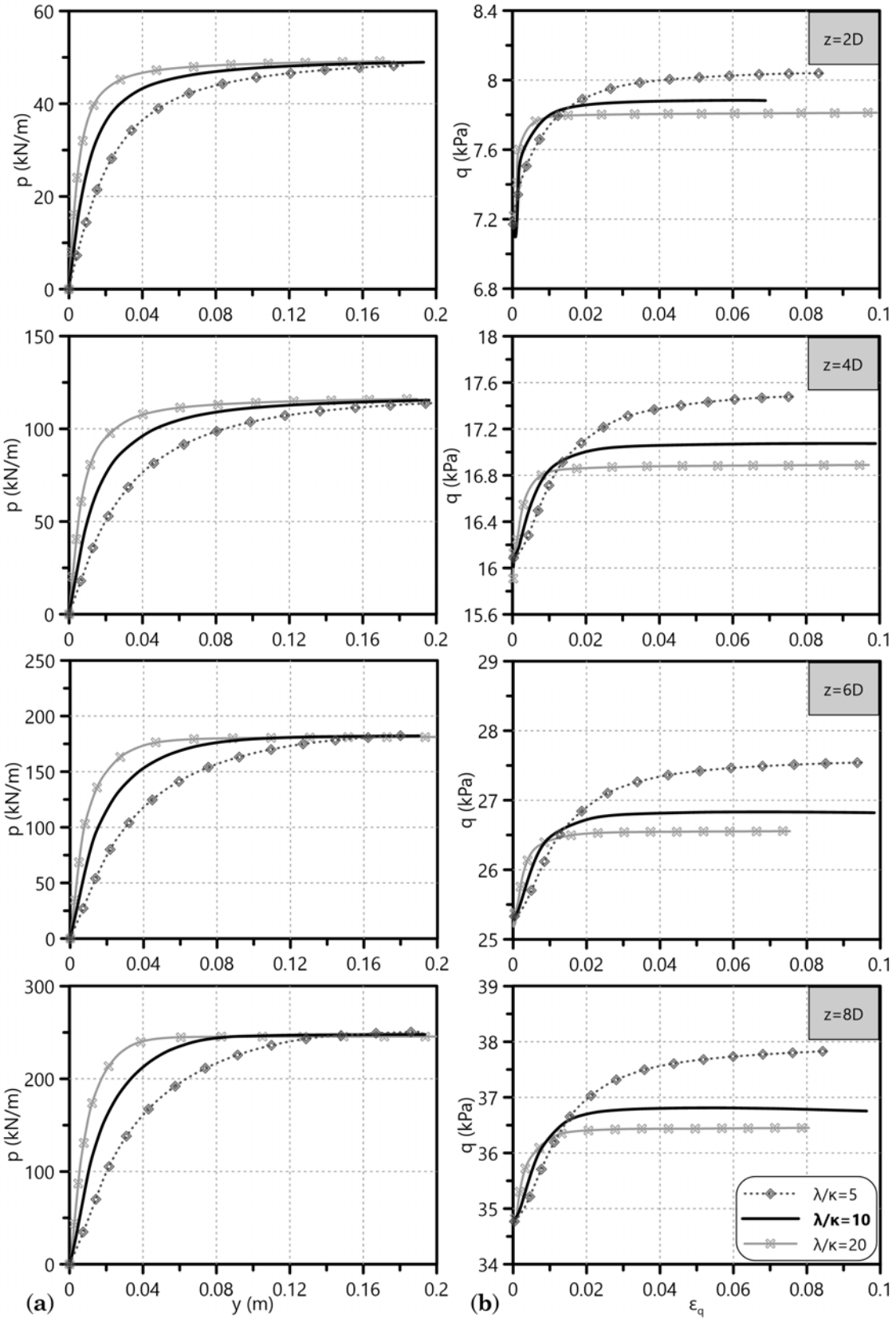

Figure 4.6: Effect of λ/κ ratio on (a) the p-y curves and (b) the $q-\varepsilon_q$ curves at different depths of NC clay, derived from FEA output.

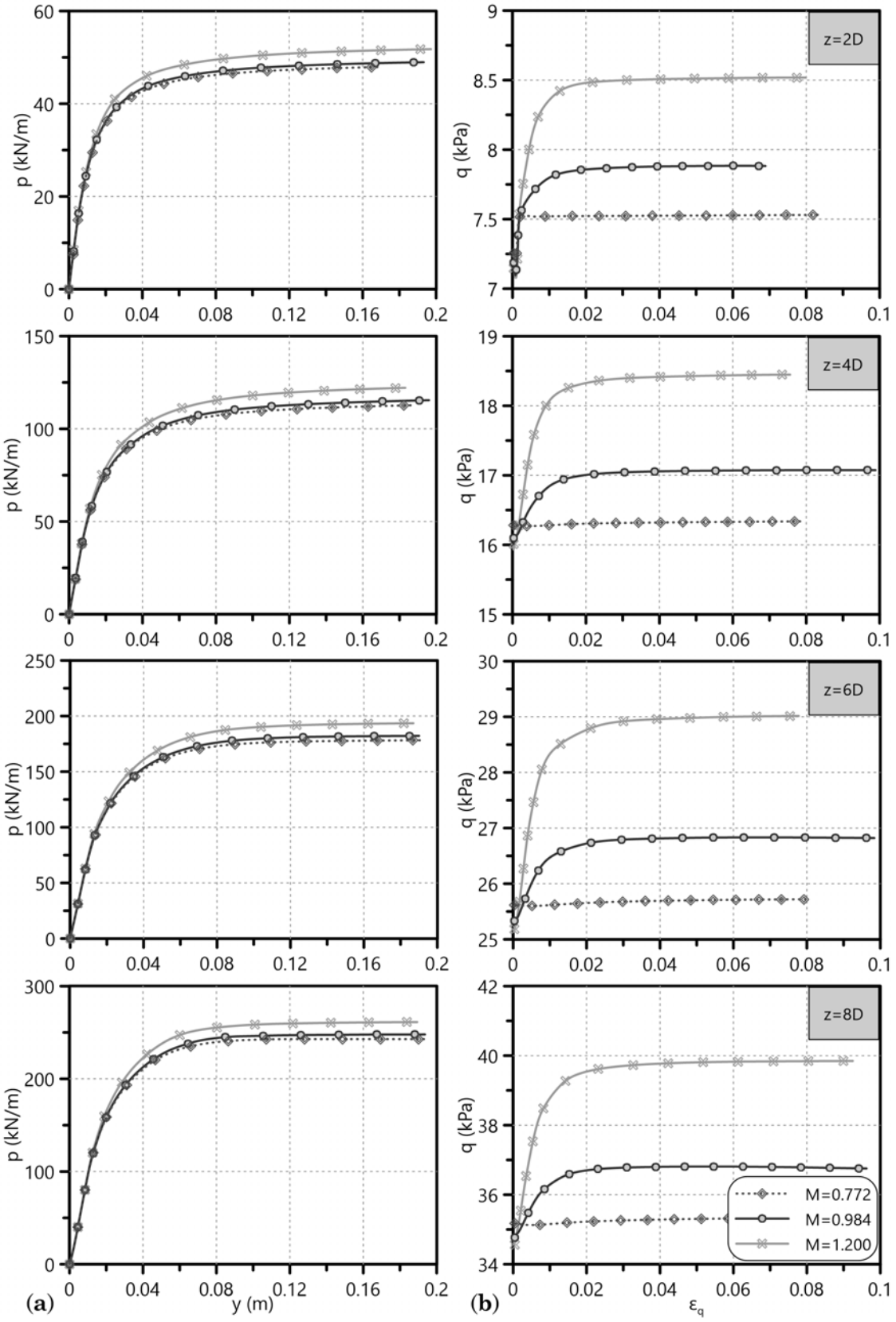

Figure 4.7: Effect of CSL slope M on (a) the p-y curves and (b) the $q - \varepsilon_q$ curves at different depths of NC clay, derived from FEA output.

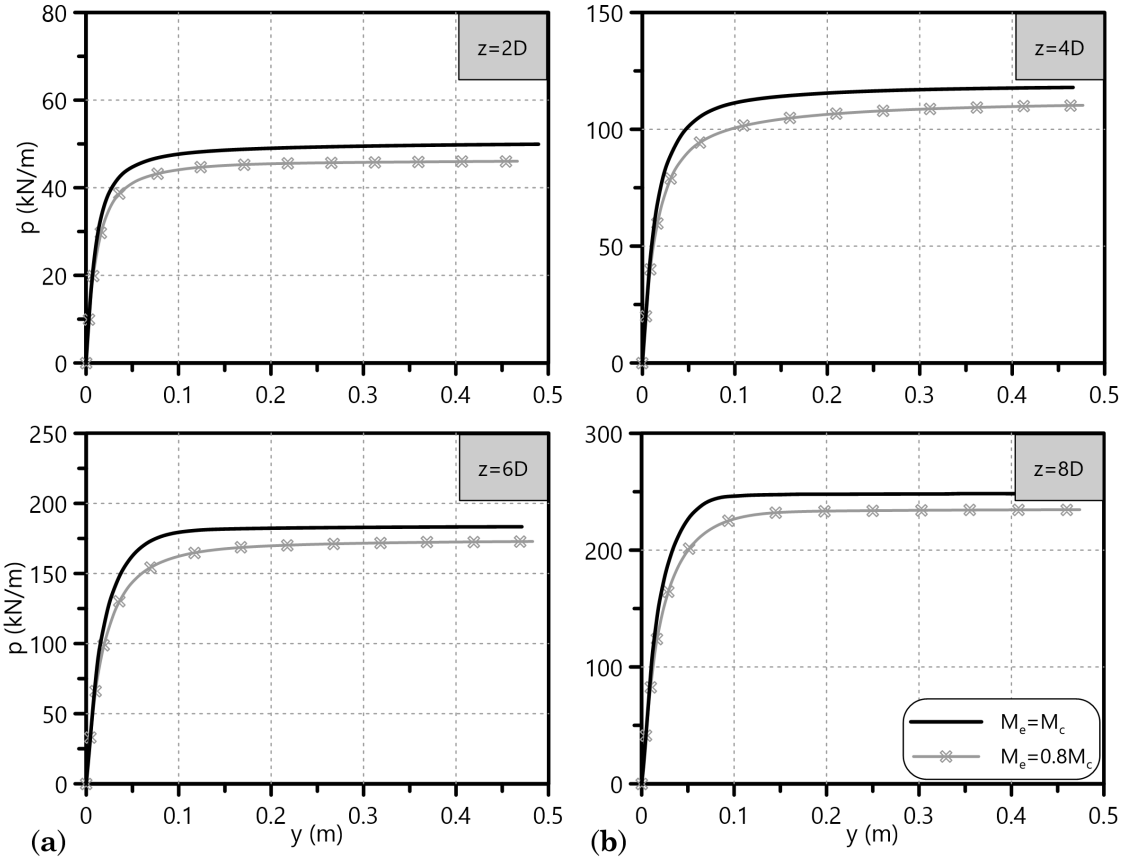

Figure 4.8: Effect of CSL slope M_e under extension on the numerical p-y curves for NC clays at various depths.

its initial stiffness through the $2G/K$ ratio (Equation 3.9). Figure 4.9 depicts the following correlation between the system and the soil element behavior: while ν seems to have no significant influence on the stress-strain curves of the soil (see Figure 4.4b), it clearly affects K_i of the numerical p-y curves derived from the FEA output (Figure 4.9a). However, the thesis mentions that the derived p-y curves refer to the total stress soil response on the laterally loaded pile. As long as the ν differentiation provokes different $\Delta u - \varepsilon_q$ curves for the NC clay (Figure 4.9b), the specific behavior explains the corresponding variation in K_i of the FEA derived p-y curves.

To sum up, while CSL slope M plays no significant role on the p-y curves for undrained lateral pile loading in NC clays, poroelasticity slopes of NCL and the swelling lines λ and κ respectively affect the initial stiffness K_i of the derived curves. In addition, Poisson's ratio also influences K_i since it controls the excess pore water pressure development Δu. Finally, differentiation of M in compression and extension affects p_u of the p-y curves for NC clays, although not crucially.

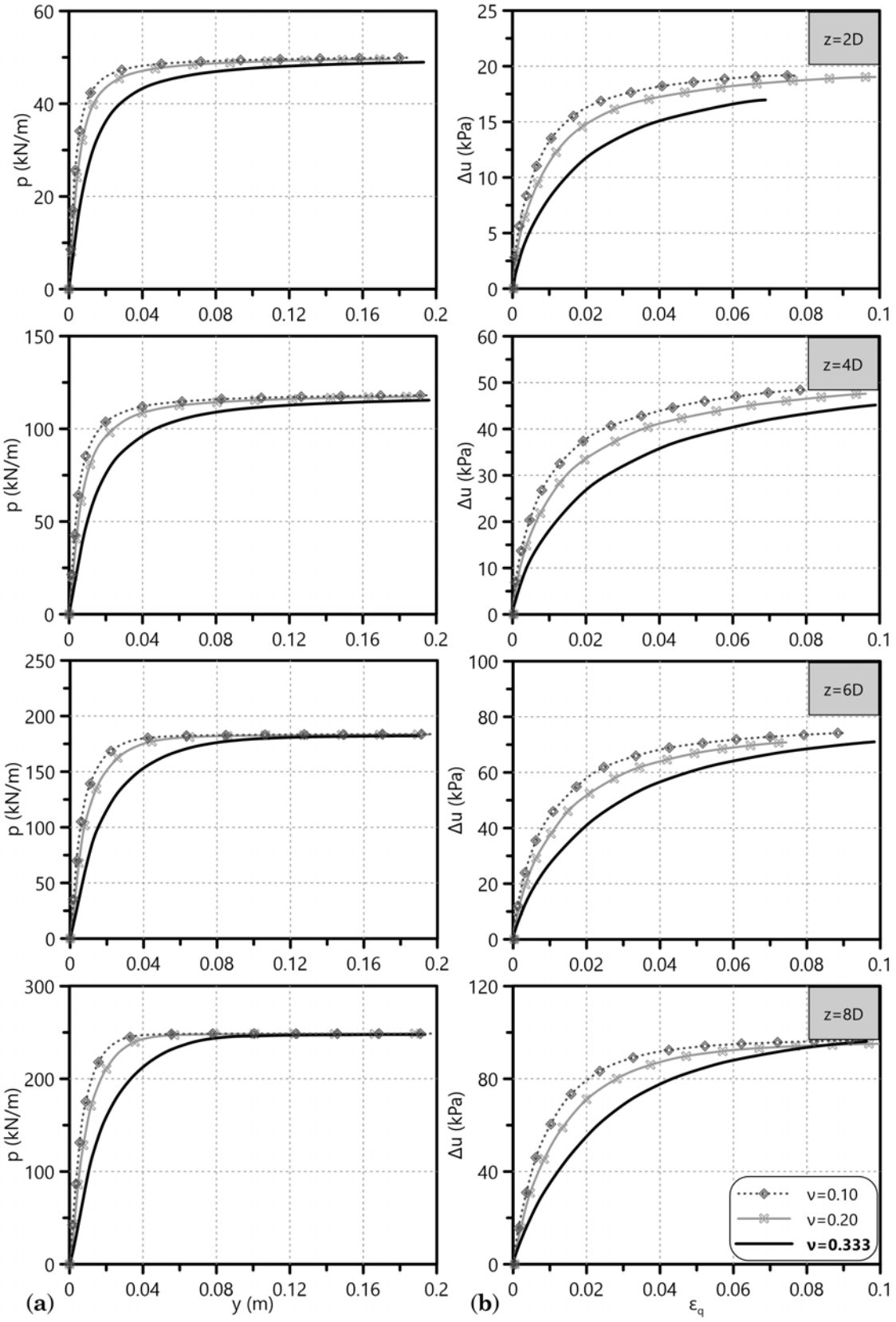

Figure 4.9: Effect of Poisson's ratio ν on (a) the p-y curves and (b) the $\Delta u - \varepsilon_q$ curves at different depths of NC clay, derived from FEA output.

4.2.2 Pile parameters

The current paragraph describes the laterally loaded pile parameters taken into account in the current numerical investigation. More accurately, it examines the effect the pile diameter D and the soil-pile adhesion factor α have on the derived p-y curves for NC clays.

4.2.2.1 Pile diameter (D)

The main principle of p-y curves formulation is the multiplication of the lateral soil pressure by the pile diameter D. Thus, the specific formulation calculates p in a distributed load form along the laterally loaded pile. The analytical expressions for p-y curves proposed in the literature (see Chapter 2) indicate that the term for the pile diameter appears as either a linear or a nonlinear function of D. The current investigation is rather qualitative. Paragraph 4.3 shall introduce a certain analytical function of D in the p-y curves proposed for NC clays through this chapter, if necessary.

Figure 4.10a demonstrates what one naturally expects in terms of lateral soil response for piles of different diameter at the same depth; the larger the D, the greater the ultimate lateral resistance p_u (kN/m) that the clay mobilizes. This observation is totally rational since we multiply the lateral soil pressure with D in order to acquire p as a distributed load (kN/m) along the pile at both depths z=3 and 6m. The investigation examines four different pile diameters, namely D=0.5, 1, 1.5 and 2m, in a NC clay with M=0.984, λ=0.109, λ/κ=10 and ν=0.333. Notice that the horizontal axis of these p-y curves is the non-dimensional ratio of the lateral soil-pile displacement y to the pile diameter D for proportionality purposes. For the effect of D on p-y curves for NC clays to be more evident, Figure 4.10b depicts p as pressure (kPa) at the aforementioned depths. The specific depiction implies that D might affect the ultimate lateral NC clay resistance p_u at shallow depths (z=3m) in a more profound manner than at greater depths (z=6m). A thorough parametric investigation of the effect D has on K_i and p_u of such p-y curves follows in Paragraph 4.3.

4.2.2.2 Pile-soil adhesion factor (α)

The FEA of the current dissertation simulate the pile-soil adhesion as a function of the clay undrained shear strength c_u, since they investigate the undrained lateral pile response. Therefore, we have introduced the so-called adhesion factor α, controlling the shear strength on the pile-soil interface (see Paragraph 3.2.5). Figure 4.11 depicts

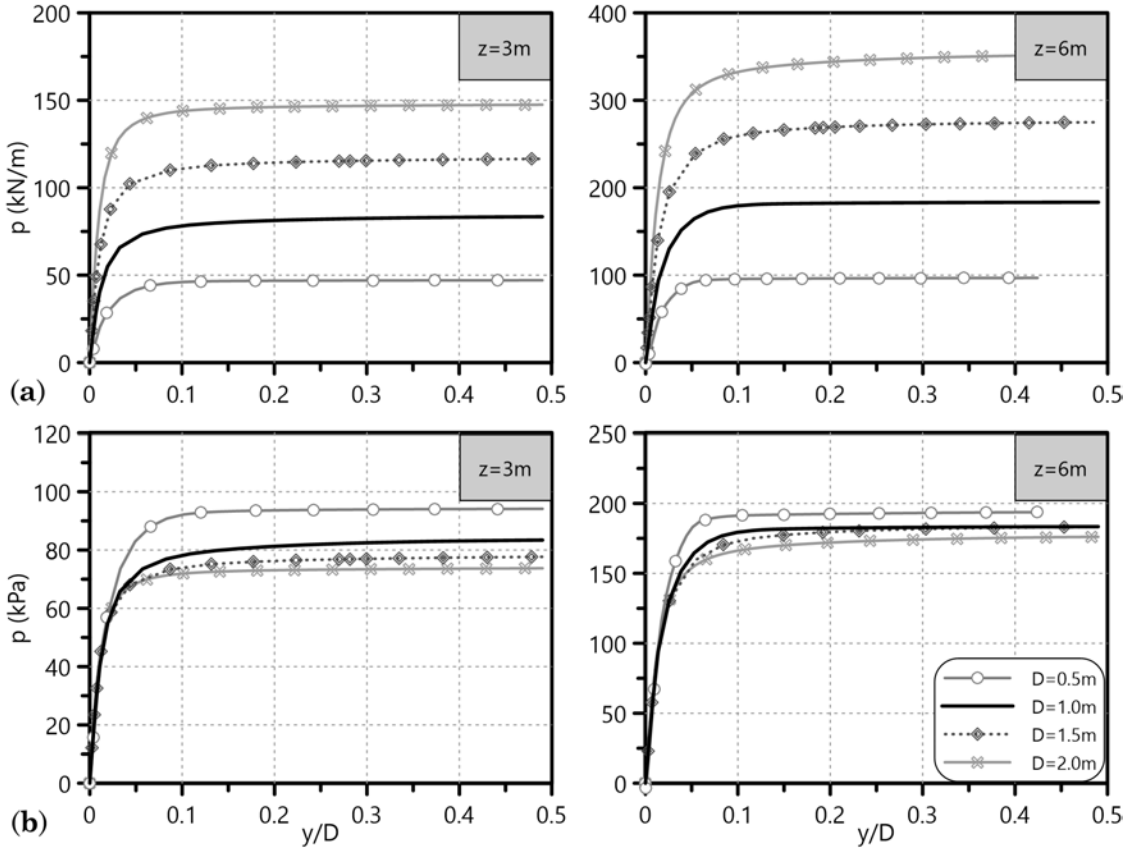

Figure 4.10: Effect of pile diameter D on the numerical p-y curves for NC clays at depth z=3 and 6m. Calculation of p as (a) distributed load (kN/m) - up - and (b) pressure (kPa) - down - along the laterally loaded pile.

the differences in p_u between the p-y curves of a smooth (α=0.3) and a rough (α=1.0) pile-soil interaction. The NC clay properties of the current investigation are the same with the ones used to examine the pile diameter effect on the corresponding p-y curves. Figure 4.11 shows that p_u of the rough pile-soil interface is almost 10% higher than that of the corresponding smooth interface (D=1m, λ=0.109, λ/κ=10, M=0.984, ν=0.333).

O'Neill (2001) states that the estimation of α in clayey soils is quite uncertain for reasons associated with the characterization of shear strength profiles and the pile construction details. Therefore, the parametric investigation of the present chapter examines both smooth and rough pile-soil interactions for the numerical development of p-y curves in NC clays. Although the softer the clay, the closer α to unity, the pile-soil interaction also concerns the pile surface and consequently Paragraph 4.3 proposes NC clay p-y curves for a range of adhesion factor α=0.3-1.0.

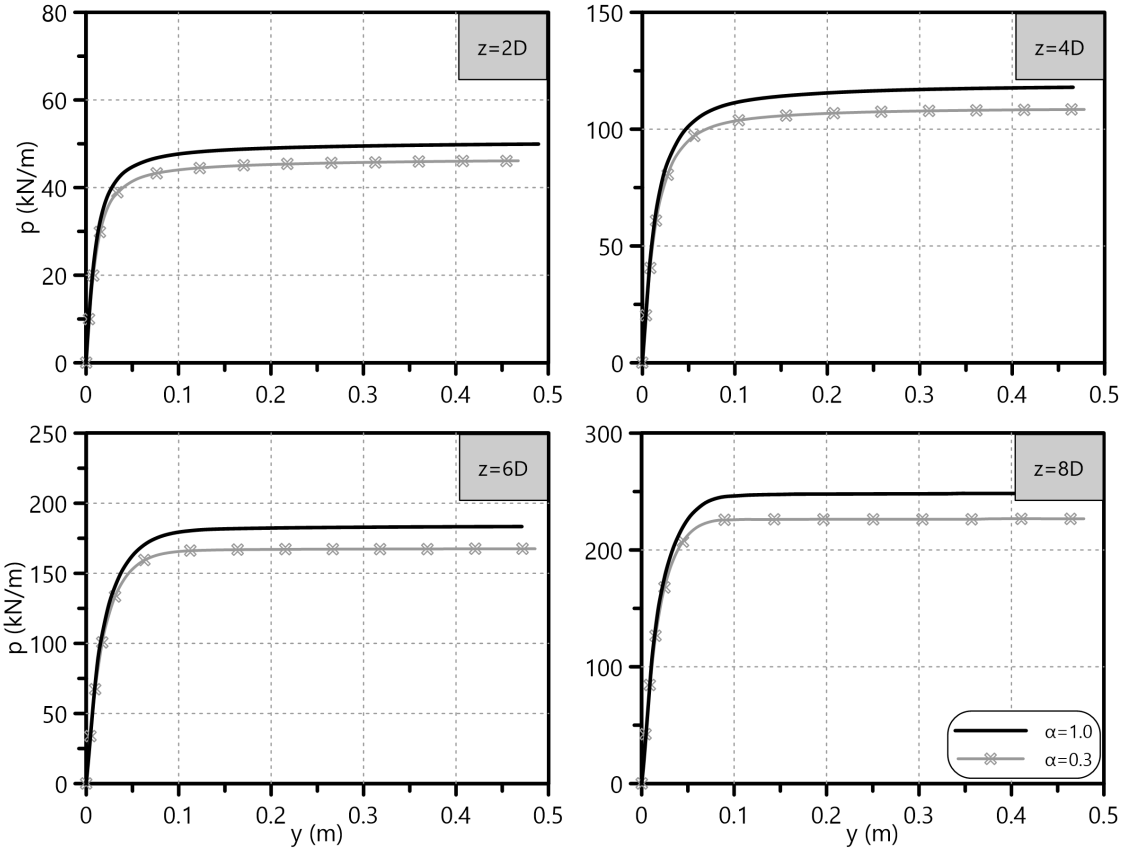

Figure 4.11: Effect of pile-soil adhesion factor α on the numerical p-y curves for NC clays at various depths.

4.2.3 NC clay failure mechanisms

The present paragraph distinguishes between two different failure mechanisms of the NC clay surrounding the laterally loaded pile, namely a shallow and a deep one. The shallow failure mechanism refers to a soil wedge in front of the pile that moves upwards when the clay reaches its ultimate lateral resistance. This failure type forms up to a certain depth, which the current investigation attempts to specify for various NC clay properties, pile diameters and pile-soil adhesion factors. For depths greater than the later the soil fails under plane-strain conditions. Figure 4.12 depicts the undeformed shape of the NC clay resultant displacements at a FEA loading frame with horizontal pile head deflection y_h equal to $50\%D$ - great enough to cause lateral NC clay failure up to a depth of $8D$. These displacements of the surrounding soil demonstrate two characteristic deformation schemes:

- The distinction between a shallow wedge-type and a deep plane-strain failure mechanism in front of the pile. Figure 4.12 locates the transition from one failure type to the other at the depth where the vertical component u_z of the

resultant soil displacement fades out.

- The collapse of the NC clay at the back of the pile, obviously due to low soil strength that does not allow the clay to stand upright during a potential pile-soil detachment.

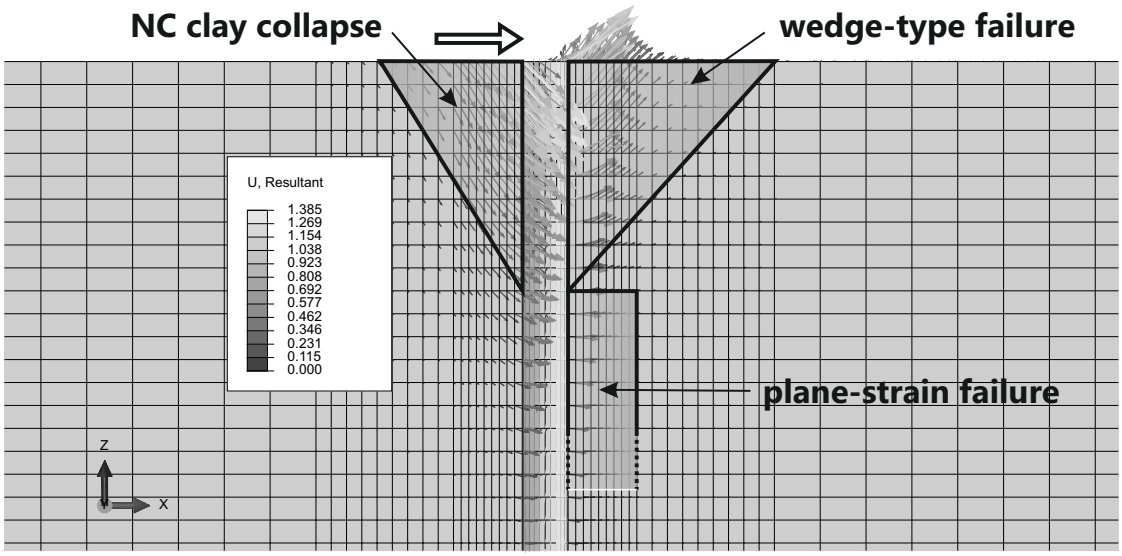

Figure 4.12: Undeformed shape of the NC clay resultant displacements at a FEA loading frame with horizontal pile head deflection y_h equal to 50%D (D=1m, α=1). Identification of various failure mechanisms of the NC clay surrounding the laterally loaded pile.

For the determination of the aforementioned transition depth from the wedge-type to the plane-strain failure mechanism, we depict the the vertical NC clay displacement u_z normalized with the corresponding displacement of the ground surface $u_{z,top}$ - naturally assuming that the vertical deflection of the clay is maximum there - for FEA grid nodes in front of but not adjacent to the laterally loaded pile. These nodes represent all depths z of the same $x-y$ plan view point in the FEA. More accurately, Figure 4.13 plots the $u_z/u_{z,top}$ ratio of the soil nodes with the depth to pile diameter ratio z/D. The specific depiction refers to two different FEA loading frames with horizontal pile head deflection y_h=30%D and 50%D - significant in order to mobilize the ultimate lateral soil resistance p_u up to z=8D. We tested all the potential M, λ and α combinations (λ/κ=10, ν=0.333) of Table 4.1 for the NC clay. However, Figure 4.13 depicts FEA output of the 1m-diameter pile in NC clays with M=0.984 and all λ values for brevity. Furthermore, this depiction also includes piles of D=0.5, 1.5 and 2.0m in a NC clay with M=0.984 and λ=0.109. Thus, this investigation approximates the depth z_w of the failure wedge for both smooth and rough pile-soil interaction.

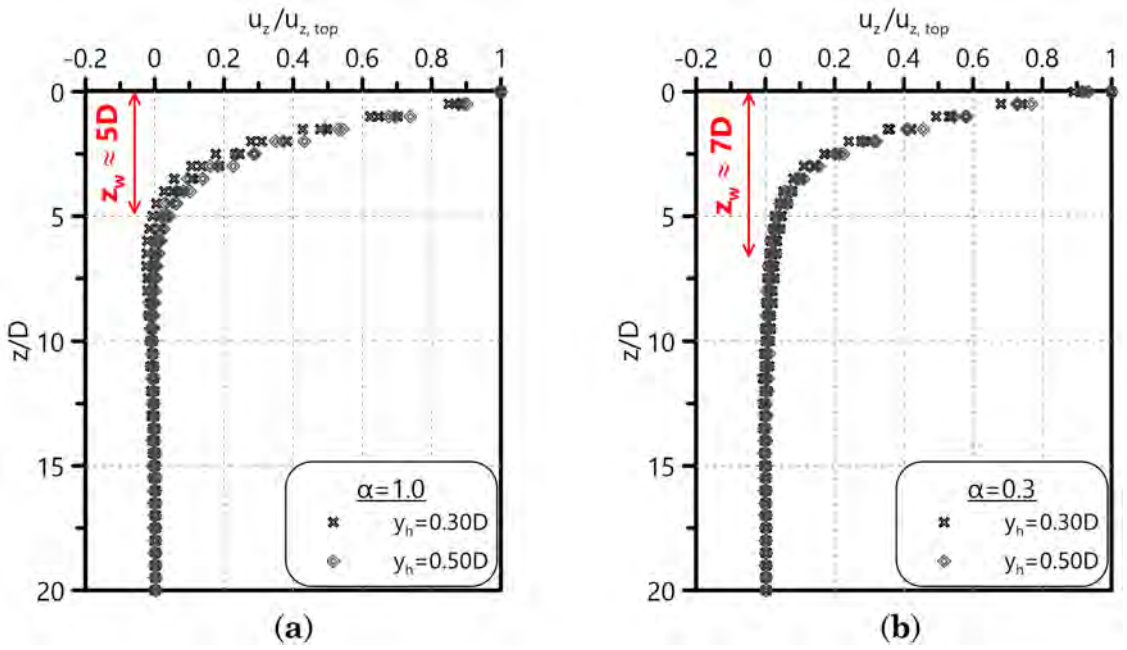

Figure 4.13: Normalized NC clay vertical displacement with the non-dimensional depth at two different FEA loading frames with horizontal pile head deflection y_h=30%D and 50%D. Parameters: M=0.984, λ=0.065-0.174, λ/κ=10, ν=0.333, D=0.5-2.0m. Estimation of the wedge-type failure depth (a) $z_w \approx 5D$ for rough (α=1.0) and (b) $z_w \approx 7D$ for smooth (α=0.3) pile-soil interaction.

The major observation of Figure 4.13 is that z_w differs between the smooth and the rough pile-soil interface simulation. More precisely, Figure 4.13a demonstrates minimization of $u_z/u_{z,top}$ at $z_w \approx 5D$ for the rough pile-soil interaction (α=1.0) while Figure 4.13b shows a $z_w \approx 7D$ for the corresponding smooth one (α=0.3). The specific behavior is natural - a simple analysis of the forces developing on the soil wedge clarifies that; the greater the friction between the pile and the clay, the shorter the wedge moving upwards during soil failure in front of the pile. A rough approximation of the transition depth from the wedge-type to the plane-strain failure mechanism indicates an average $z_{w,\mathrm{NC}} \approx 6D$ for NC clays according to the findings of the current numerical investigation, regardless of the soil-pile adhesion factor α. Characteristic frames of the FEA that depict the realistic simulation of the pile-soil interaction for NC clayey soils are included in Appendix C.

4.3 Monotonic p-y curves for NC clays

The current section presents the formulation procedure of p-y curves for NC clays, namely with linear strength distribution with depth, according to the corresponding numerical investigation of the dissertation. It introduces a new approach of the p-y curve equation for such soils and relates its main components - initial stiffness K_i and ultimate lateral soil resistance p_u - to certain soil and pile properties. Finally, the section develops a step-by-step procedure for the formulation of NC clay p-y curves and compares the findings of the FEA with corresponding literature proposals. Thus, the engineer distinguishes between conservative and inconstant p-y curve methodologies for such clays.

The curve fitting process of the FEA derived p-y curves (see Paragraph 3.3.1) requires the definition of three variables:

- the mathematical formulation
- the initial stiffness K_i and
- the ultimate lateral soil resistance p_u of the p-y curve.

Literature frequently adopts the following renowned hyperbolic equation for the formulation of p-y curves in clayey soils (DNV, 1977; Georgiadis & Georgiadis, 2010):

$$p = \frac{y}{\frac{1}{K_i} + \frac{y}{p_u}}$$

A curve fitting on the FEA p-y output utilizing the aforementioned equation results in a satisfactory representation of K_i and p_u. However, the hyperbola does not reproduce accurately the transition from the initial elastic to the ultimate lateral NC clay response, both for shallow (z=1D, Figure 4.14a) and greater depth (z=6D, Figure 4.14b). This dissertation proposes the following exponential p-y equation that fits almost flawlessly the numerically derived p-y curves.

$$\frac{p}{p_u} = 1 - \exp\left(\frac{-K_i \cdot y}{p_u}\right) \tag{4.1}$$

Figure 4.14 depicts the curve fitting comparison of the hyperbolic with the exponential form at two different depths, showing the clear superiority of the latter for NC clay p-y curves[1]. This contrast reflects the differences in hardening potential of a

[1]The FEA derived p-y curves of Figure 4.14 refer to a NC clay with M=0.984, λ=0.109, λ/κ=10, ν=0.333 and a pile with D=1.0m and α=1.0. However, the current investigation identifies

NC versus an OC clay. Comparing Figure 3.35a with Figure 3.36a one observes two different hardening behaviors; the NC clay hardens slightly compared to the corresponding OC clay hardening. This differentiation in the soil element scale is also evident in the macroscale of the p-y curves. As a result, the proposed exponential form allows for a more profound p_u plateau in contrast with the hyperbola asymptote - referring to constantly hardening soils such as sands and OC clays. Therefore, the following paragraphs propose certain K_i and p_u correlations with soil and pile characteristics for the formulation of NC clay p-y curves through Equation 4.1.

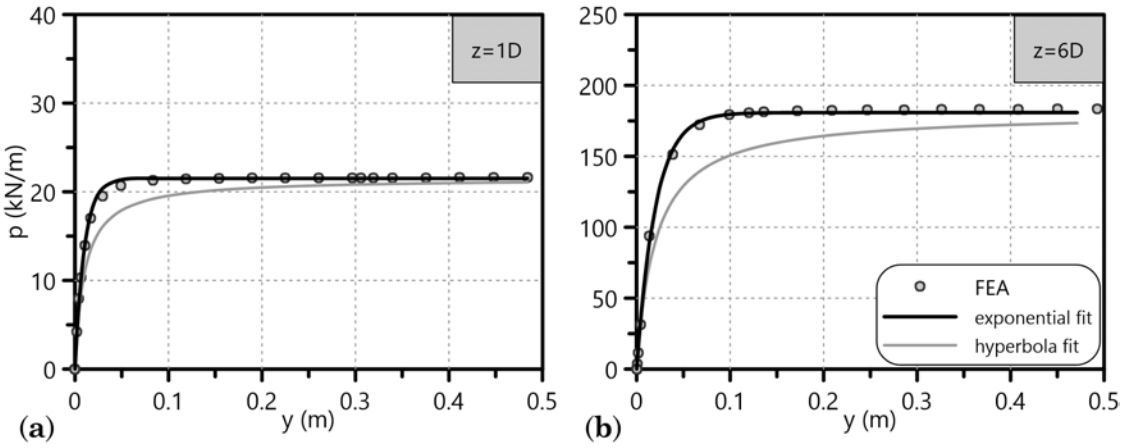

Figure 4.14: Exponential and hyperbolic fit on the FEA derived p-y curves for (a) shallow (z=1D) and (b) deep (z=6D) lateral NC clay response.

4.3.1 Initial stiffness K_i of p-y curves for NC clays

Prior to describing the estimation process of K_i through the FEA output, the current paragraph reconsiders the practical use of the specific p-y parameter. One needs to recall that p-y curves actually serve as non-linear springs along the laterally loaded pile under investigation. Thus, the structural engineer calculates lateral displacements and rotations after imposing certain forces and moments to the pile (or vice-versa). However, since p-y curves commonly depict p as a distributed load along the pile - the lateral pressure is multiplied by the pile width or diameter - (kN/m), the corresponding initial stiffness K_i comes in kN/m^2. In order to determine the equivalent spring stiffness (kN/m), the engineer multiplies the aforementioned stiffness with the pile length dl that the corresponding p-y curve represents.

Paragraphs 4.2.1.1 and 4.2.1.3 imply that the poroelasticity parameters (λ, λ/κ) and the Poisson's ratio (ν) of the NC clay simulation affect significantly K_i of the p-y

the specific p-y curve trend in all the potential soil and pile property combinations of Table 4.1 and thus generalizes these findings.

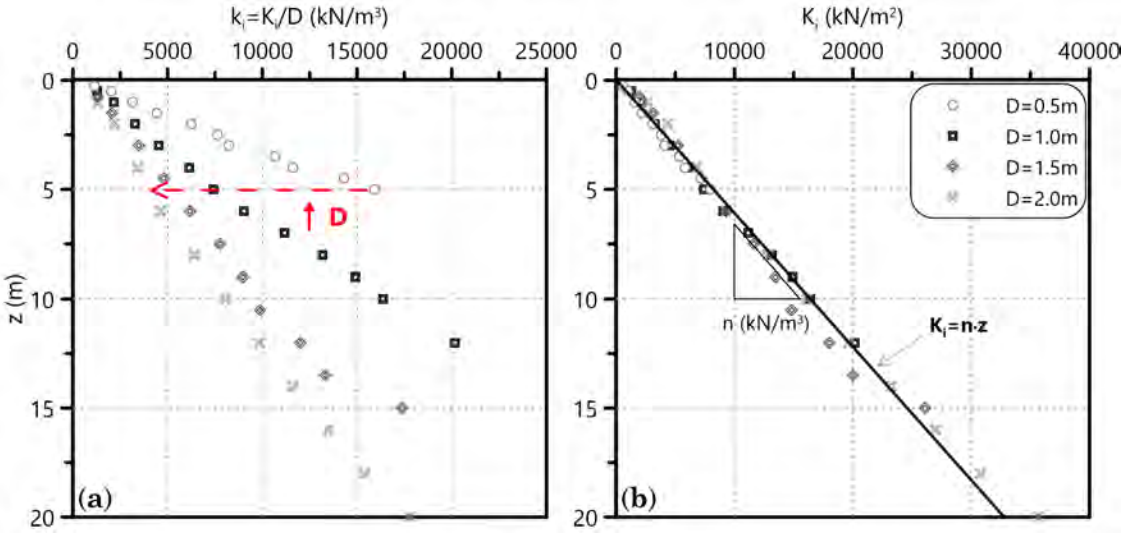

Figure 4.15: Diameter effect on the initial stiffness of the p-y curves for NC clays. Distribution of the initial FEA p-y stiffness with depth z in two different forms: (a) initial lateral subgrade reaction modulus $k_i = K_i/D$ (kN/m^3) and (b) initial stiffness K_i (kN/m^2) for p in pressure and distributed load units respectively.

curves. In addition, Figure 4.10 recommends to take a notice on the effect pile diameter D might have on K_i. For the clarification of the latter, Figure 4.15 depicts two forms of the initial stiffness distribution with depth z through the aforementioned curve fitting process, for all the pile diameters of the current numerical investigation (D=0.5, 1.0, 1.5 and 2.0m), in a specific NC clay[1] (M=0.984, λ=0.109, λ/κ=10 and ν=0.333). In more detail, Figure 4.15a presents the equivalent of the initial lateral subgrade reaction modulus $k_i = K_i/D$ (kN/m^3) with z, i.e. the initial stiffness of the p-y curves with p in terms of pressure - independent of D. The specific figure depicts the general principle that the subgrade reaction modulus is not a soil property but depends on the dimensions of the foundation pressing the soil. With that in mind, the trend of k_i to decrease at a certain depth with the increase of D seems totally rational. On the other hand, K_i estimations assuming the newly proposed exponential p-y curve relationship for NC clays (Equation 4.1) - according to the common p-y form with p in kN/m - demonstrate a linear distribution with z for all the examined D, starting from the origin of the axes (Figure 4.15b). What remains is the determination of a mathematical form for the slope n (kN/m^3) of the linear $K_i(z)$ function, incorporating the effect of λ, λ/κ and ν.

Figures 4.16a, b and c summarize the curve fitting process for the estimation

[1]Since neither M (Figure 4.7) nor α (Figure 4.11) affect the initial stiffness of the p-y curves, the current paragraph considers them constant (M=0.984, α=1.0) in the parametric investigation for the determination of K_i.

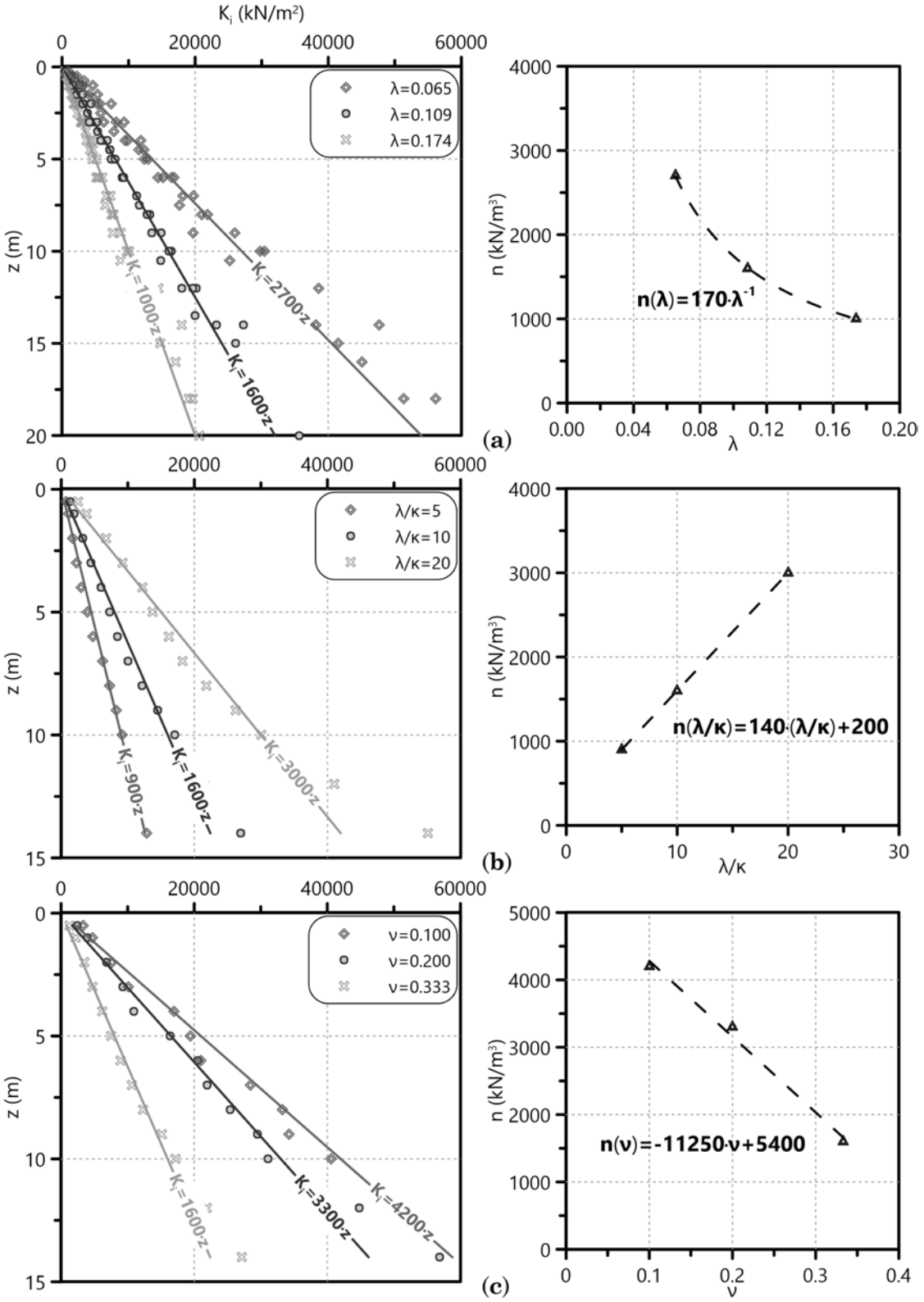

Figure 4.16: Determination of n-slope in the linear initial stiffness function $K_i(z) = n \cdot z$ of numerical p-y curves for NC clays. Effect of (a) NCL slope λ, (b) ratio λ/κ and (c) Poisson's ratio ν on n.

of n and its dependence from the aforementioned NC clay parameters respectively. The initial stiffness values depicted in Figure 4.16a (left) refer to FEA output from all the D under consideration, in order to verify once again the linear distribution of K_i with z and its independence from D (FEA output for NC clay with M=0.984, λ/κ=10 and ν=0.333 appear in this figure). For the effect of λ/κ on K_i, Figure 4.16b demonstrates results from FEA of a 1m-D laterally loaded pile in a NC clay with M=0.984, λ=0.109 and ν=0.333. For the corresponding influence of ν the K_i values of Figure 4.16c refer to the same pile and soil properties but with ν varying and λ/κ=10. As a result, the following equations represent the desired correlations of n with λ, λ/κ and ν:

$$n(\lambda) = 170 \cdot \lambda^{-1} \tag{4.2a}$$

$$n(\lambda/\kappa) = 140 \cdot (\lambda/\kappa) + 200 \tag{4.2b}$$

$$n(\nu) = 11250 \cdot \nu + 5400 \tag{4.2c}$$

Finally, Figure 4.17 depicts the ratio $n/\left[n(\lambda) \cdot n(\lambda/\kappa) \cdot n(\nu)\right]$ of the $K_i(z)$-slopes

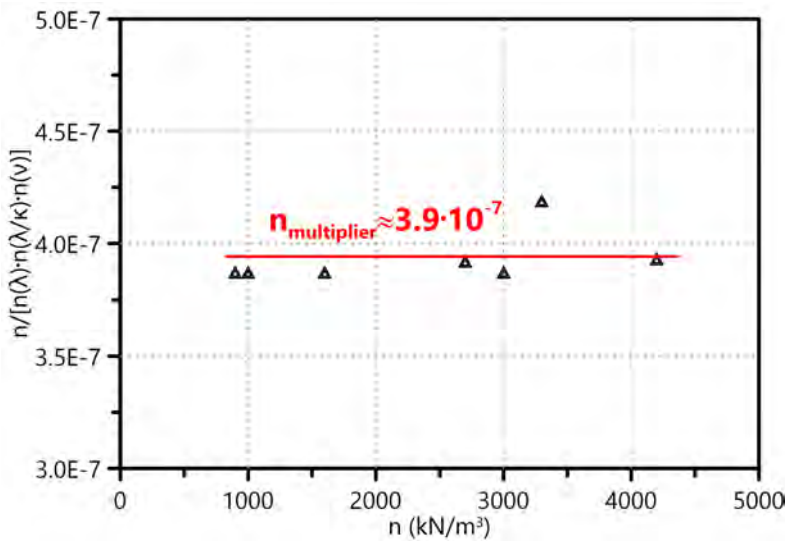

Figure 4.17: Determination of the n-slope multiplier for the grouping of the separate λ, λ/κ and ν effects on n and subsequently on K_i.

calculated from the aforementioned curve fitting process to the product of Equations 4.2 - for the corresponding λ, λ/κ and ν combinations - with the n estimations depicted in Figure 4.16. The average $n_{\text{multiplier}}$=$3.9 \cdot 10^{-7}$ multiplies the aforementioned product and the following equation of K_i occurs for the numerically developed NC

clay p-y curves.

$$K_{i,\mathrm{NC}}(z) = n \cdot z \quad (\mathrm{kN/m^2}) \tag{4.3a}$$

$$n = \left(71.6\,\frac{1}{\lambda} + 50.1\,\frac{1}{\kappa} - 149.2\,\frac{\nu}{\lambda} - 104.4\,\frac{\nu}{\kappa}\right) \quad (\mathrm{kN/m^3}) \tag{4.3b}$$

4.3.2 Ultimate lateral soil resistance p_u of p-y curves for NC clays

Apart from the determination of K_i, Equation 4.1 requires the estimation of p_u for the formulation of the p-y curve. The processing of the numerical p-y curves considers p_u as the p-value, the percentage difference of which from the following value is less or equal than 0.5% - practically negligible. The current numerical investigation normalizes the FEA derived p_u through the ultimate lateral soil resistance factor $N_p = p_u/(c_u\,D)$. Figures 4.7, 4.5, 4.10 and 4.11 imply the investigation of the effect M, λ, D and α may have on p_u respectively. Therefore, this paragraph presents the numerical N_p distribution with the non-dimensional depth z/D for various combinations of the aforementioned clay and pile parameters.

Initially, we examine the effect M and λ have on N_p for the rough pile-soil interface (α=1.0) and for all the pile diameters D of the FEA (Figure 4.18). More accurately, Figure 4.18a depicts the potential influence of M on N_p for various λ values, while Figure 4.18b demonstrates the opposite case. The specific investigation involves all the combinations of M and λ of Table 4.1 for D=1m. It also examines the corresponding favorable, intermediate and unfavorable NC clay properties for other pile diameters (D=0.5, 1.5 and 2.0m), i.e. M=0.772/λ=0.174, M=0.984/λ=0.109 and M=1.200/λ=0.065 respectively, in order to ascertain the D-effect on N_p. Figure 4.18a depicts that M affects more intensely the N_p factor - although only less than ±5% from a mean value along z/D-axis - in comparison with the corresponding effect of λ (Figure 4.18b) that seems rather insignificant. The specific observation is natural since M refers to the strength while λ to the stiffness of the NC clay. Nevertheless, the present elaboration concludes that neither M nor λ affect N_p crucially for NC clays. The effect of D is also not of concern, since the existing expression of N_p incorporates the specific influence satisfactorily.

Finally, the current paragraph investigates the effect of the adhesion factor α on N_p - actually the most significant one according to the literature (see Chapter 2). Figure 4.18 refers to FEA output of p_u for rough (α=1.0) pile-soil interaction - typical for soft clays. However, under certain circumstances this interface between the pile and the NC clay may correspond to lower adhesion values. Therefore,

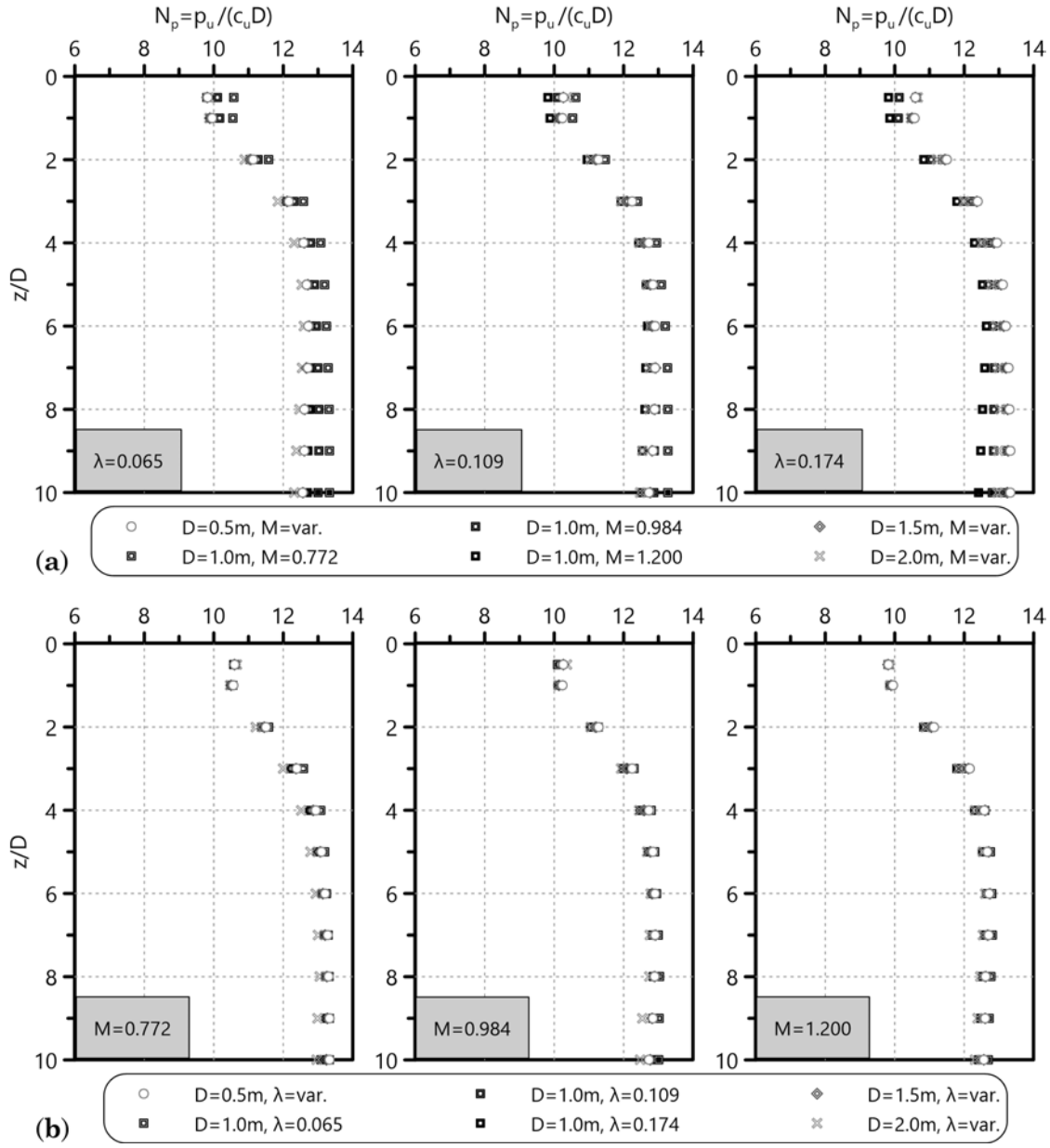

Figure 4.18: Distribution of the ultimate lateral soil resistance factor N_p with non-dimensional depth z/D derived from NC clay FEA. Effect of (a) CSL slope M and (b) NCL slope λ on N_p for various pile diameters D and rough pile-soil interface (α=1.0).

Figure 4.19 demonstrates the N_p distribution with z/D of all the NC clay FEA (see Table 4.1), distinguishing between α=1.0 and 0.3 cases. Since Figure 4.18 shows the insignificant effect of M, λ and D on N_p for α=1.0, the corresponding N_p distribution for α=0.3 in Figure 4.19 involves all the combinations of M and λ of Table 4.1 mainly for D=1m. For completeness purposes, the specific depiction, i.e for α=0.3, also includes the N_p calculations for piles with D=0.5, 1.5 and 2.0m from FEA with M=0.984/λ=0.109.

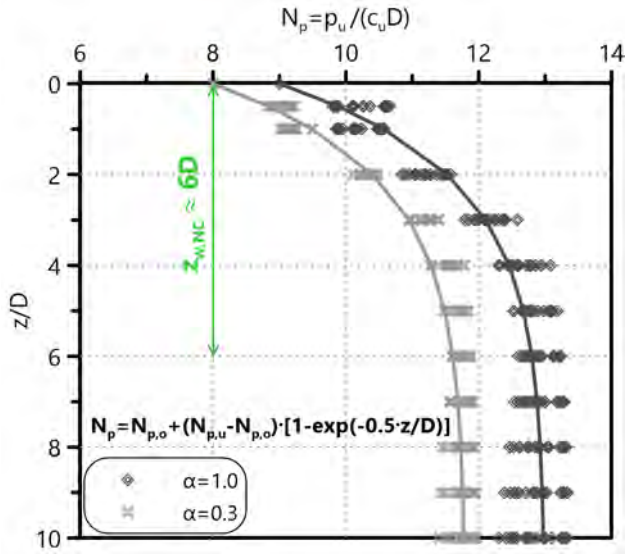

Figure 4.19: Effect of the adhesion factor α on the distribution of N_p with z/D from FEA of different pile diameters D in various NC clay simulations.

Consequently, the current numerical investigation proves that the adhesion factor α is the most significant parameter for the determination of p_u in p-y curves for NC clays. Figure 4.19 suggests a general exponential fit of N_p with z/D, where $N_{p,o}$ and $N_{p,u}$ the values of N_p at ground surface and below a certain depth respectively. As a matter of fact, this depth - where $N_p \approx N_{p,u}$ - agrees with the approximate transition depth from the wedge-type to the plane-strain failure mechanism $z_{w,\mathrm{NC}} \approx 6D$ for NC clays, according to Paragraph 4.2.3. Moreover, the investigation assigns $N_{p,o}$=8-9 and $N_{p,u}$=11.8-13.0 for α=0.3-1.0 respectively, assuming linear distribution of the aforementioned N_p values when in this range of adhesion factors. Thus, a set of equations occurs for the calculation of N_p:

$$N_p = \frac{p_u}{c_u \cdot D} = N_{p,o} + (N_{p,u} - N_{p,o}) \left(1 - \exp\left(-0.5\,\frac{z}{D}\right)\right) \tag{4.4a}$$

$$N_{p,o} = 7.57 + 1.43 \cdot \alpha \tag{4.4b}$$

$$N_{p,u} = 11.29 + 1.71 \cdot \alpha \tag{4.4c}$$

As a result, the current dissertation proposes the following expression for the N_p distribution with z/D for NC clays:

$$N_{p,\mathrm{NC}} = 7.57 + 1.43 \cdot \alpha + (3.72 + 0.28\alpha) \left(1 - \exp\left(-0.5\,\frac{z}{D}\right)\right) \tag{4.5}$$

4.3.3 Proposed monotonic p-y curves for NC clays

The current paragraph aims at summarizing the process for the formulation of the proposed monotonic NC clay p-y curves. The aforementioned numerical development of such p-y curves outlines the following steps:

1. First define the following NC clay and pile parameters: undrained shear strength distribution with depth c_u, NCL slope λ, NCL to swelling lines ratio λ/κ, Poisson's ratio ν, pile diameter D and pile-soil adhesion α.

2. Determine the initial stiffness K_i of the p-y curve at the desired depth z according to the equation:

$$K_i(z) = n \cdot z = \left(71.6\,\frac{1}{\lambda} + 50.1\,\frac{1}{\kappa} - 149.2\,\frac{\nu}{\lambda} - 104.4\,\frac{\nu}{\kappa}\right) \cdot z \quad (\mathrm{kN/m^2})$$

3. Calculate the ultimate lateral soil resistance p_u of the p-y curve at the specific depth through the equation:

$$p_u = N_p \cdot c_u \cdot D = \left[7.57 + 1.43 \cdot \alpha + (3.72 + 0.28\alpha)\left(1 - \exp\left(-0.5\,\frac{z}{D}\right)\right)\right] \cdot c_u \cdot D$$

   As Figure 4.8 indicates, the user of the proposed p-y curves for NC clays shall reduce the aforementioned p_u by 5% under the assumption of lower CSL line slope M in extension than in compression. Furthermore, another 5% reduction in p_u shall apply if the NC clay friction angle $\phi > 25°$ (equivalent to $M > 1$) according to Figure 4.18a, since some decrease occurs in N_p for such simulations - although not significant enough to incorporate the effect in the proposed N_p function (Equation 4.5).

4. Form the NC clay p-y curve using the proposed exponential relationship of the current chapter:

$$\frac{p}{p_u} = 1 - \exp\left(\frac{-K_i \cdot y}{p_u}\right)$$

Chapter 7 attempts to verify the numerically developed monotonic p-y curves for NC clays through the comparison of bending moment and horizontal displacement distributions along laterally loaded piles of specific large-scale or centrifuge experiments with the corresponding predictions of BNWF analyses incorporating the current proposals.

4.3.4 Comparison of proposed NC clay p-y curves with literature

The present paragraph compares the proposed NC clay p-y curves with corresponding literature methodologies (see Paragraph 2.9). The following comparison does not aim to criticise literature p-y curves for such soils but to indicate whether the proposals of the current dissertation are either conservative or radical compared to the existing ones. The comparison refers to a laterally loaded pile of D=1m, L=30m, α=1.0 in a NC clay with submerged unit weight γ=20kN/m^3, $c_u = 5 + 0.25 \cdot \sigma'_{vo}$ (kPa), λ=0.130 (C_c=0.30), λ/κ=10, ν=0.30 and water table at ground level. Figure 4.20 depicts that the proposed NC clay p-y curves deliver a p_u greater than all the literature methodologies, especially for shallow depths (p_u at least 20% higher than literature at z=2D). They also demonstrate K_i closer to the highest recommended values of literature.

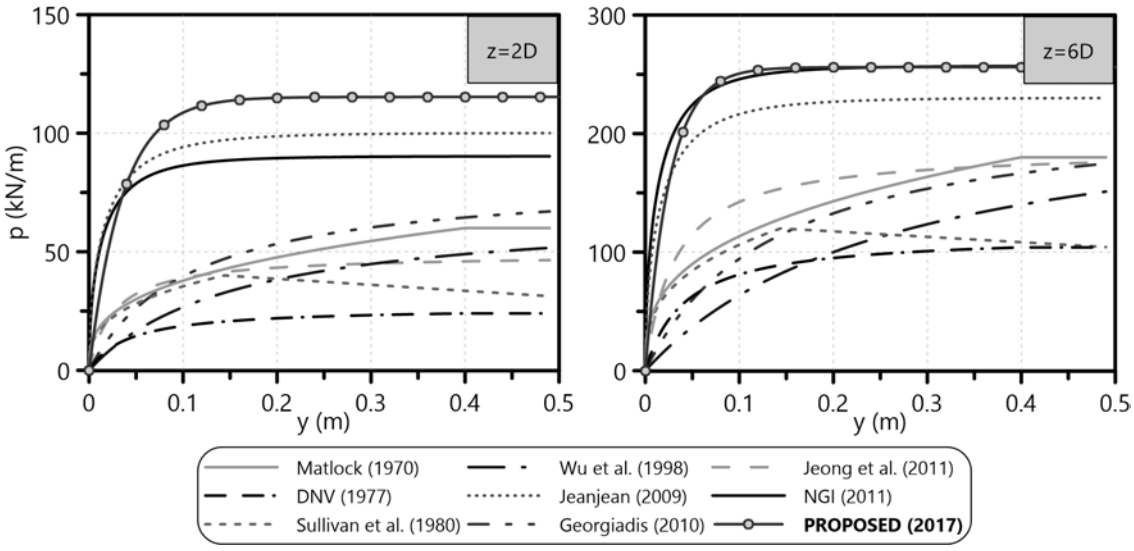

Figure 4.20: Comparison of the proposed monotonic p-y curves with corresponding literature methodologies for a pile of D=1m and α=1.0 in a fully saturated NC clay at shallow (z=2D) and greater depth (z=6D).

Another interesting comparison refers to the N_p and K_i distributions of the proposed p-y curves versus the corresponding literature values with the dimensionless depth z/D. Figure 4.21 confirms the aforementioned observations for the relatively high p_u and K_i of the proposed p-y methodology when compared with the literature recommendations. The latter seem to systematically underestimate the ultimate lateral soil resistance factor N_p for NC clays, potentially due to very low c_u values of such soils up to a certain depth of interest around 6-8D. However, it is always very important to carefully evaluate soil parameters at the construction site and

carry out large-scale load tests in order to choose the most appropriate p-y curve methodology for the final design of the laterally loaded piles.

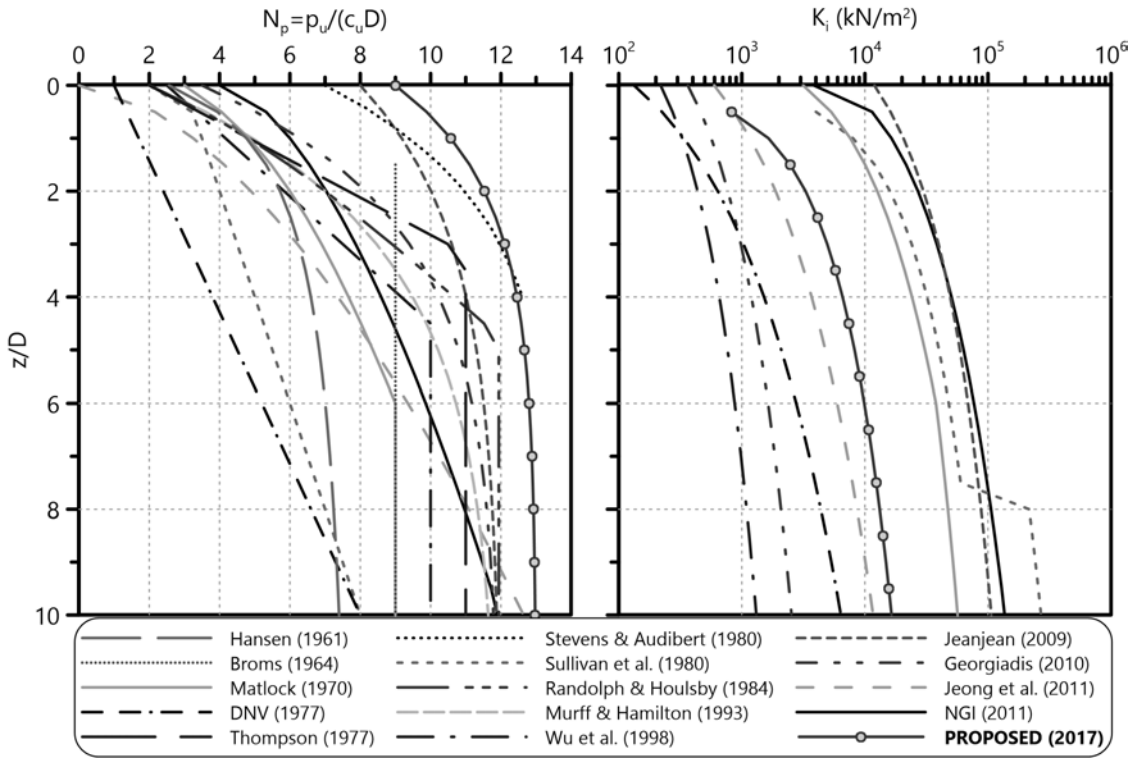

Figure 4.21: Comparison of the proposed N_p and K_i distributions with z/D versus corresponding literature methodologies for a pile of D=1m and α=1.0 in a fully saturated NC clay.

4.4 Concluding remarks on p-y curves for NC clays

Summarizing, the current chapter proposes an upgraded, exponential p-y curve relationship for soft, NC clayey soils under monotonic undrained loading conditions. The proposed curves correlate with certain compressibility parameters of the soil and interface properties of the pile-soil interaction. Especially for K_i, these correlations offer an alternative choice to the majority of the existing literature methods that assume an initial p-y stiffness mainly dependent from the characteristic axial strain ε_{50}. The utilized, effective stress, 3D FEM simulation captures successfully all the mechanisms mobilized during the external lateral loading of a long pile in such soils.

Chapter 4 concludes in the following points, referring to the proposed p-y curves for laterally loaded piles in soft, NC clayey soils (linearly increasing c_u with depth):

- The present dissertation proposes an exponential p-y form that fits the FEA derived curves in a manner more satisfactory than the renowned hyperbola relationship. Two parameters need to be defined for the exponential p-y curves applicable to NC clays: the initial p-y curve stiffness K_i and the ultimate lateral soil resistance factor N_p=$p_u/(c_u \cdot D)$.

- The FEA incorporate a significant range of soil (M, λ, λ/κ, ν) and pile (D, α) parameters for the numerical simulation of laterally loaded piles in NC clayey soils. An extensive parametric investigation reveals that the Critical State Line slope M - corresponding to $\phi = 20° - 30°$ - and the pile diameter D=0.5-2.0m do not affect the p-y curves derived from the FEA for undrained loading conditions. The rest of the parameters influence the p-y curves in a manner that is briefly explained in the following points.

- $K_{i,\mathrm{NC}}$ is a linear function of depth z with slope n and ground surface value 0, reflecting the corresponding distribution of the assumed undrained Young's modulus - also linear with depth - for the specific soil type. The initial p-y stiffness is actually a function of λ, λ/κ and ν (Equation 4.3): the slope λ of the virgin compression line rationally influences K_i since the curves refer to a NC clayey soil; the slope κ of the recompression line - incorporated in the ratio λ/κ - reflects the effect of the soil under unloading, which follows the deformation of the laterally loaded pile at the side opposite to the load direction; Poisson's ratio ν affects the initial stiffness of the soil and thus the corresponding p-y stiffness. K_i values of the proposed exponential p-y curves fall in the middle of the corresponding literature range for NC clays.

- $N_{p,\mathrm{NC}}$ is entirely a function of the pile-soil adhesion factor α (Equation 4.5). The FEA results confirm the existence of two soil failure mechanisms in front of the pile: a wedge failure extending from ground surface to a depth z=5-7D - highly dependent on α - and a plane-strain failure for greater depths. FEA generate N_p values that are consistently higher than the ones proposed in literature, both at ground level as well as at greater depth. N_p remains constant with the non-dimensional depth for $z/D > 6$, namely equal to the corresponding average depth of the NC clay wedge-type failure in front of the pile.

Chapter 5

Parametric investigation of monotonic p-y curves for OC clays

5.1 Introduction

The present chapter develops numerical p-y curves for monotonic laterally loaded piles in OC clay - almost constant c_u with depth - under undrained loading conditions, through effective stress coupled FEA. We investigate the effect of various soil and pile parameters on the two main parts of the p-y curves, namely the initial stiffness K_i and the ultimate lateral soil resistance p_u. The FEM code Simulia Abaqus 6.12 is utilized to simulate the problem, with the MCC constitutive law reproducing the OC clay behavior in the aforementioned parametric numerical investigation. However, since the MCC fails to reproduce strain-softening and small-strain stiffness characteristics of such soils, this study attempts to develop p-y curves by simulating OC clays through an MCC-type constitutive model that incorporates the aforementioned features (see Paragraph 3.2.2.2).

Consequently, the chapter delivers a hyperbolic form of p-y curves for OC clays, including certain strength, stiffness and geometry features of both the pile and the clay. The proposed p-y curve relationship for OC clays is compared with corresponding literature recommendations and its advantages and defects versus the latter are pointed out. Finally, the reader is referred to Chapter 7 for a validation of the proposed p-y curves with large-scale or centrifuge experimental results.

5.2 Parametric investigation of p-y curves for OC clays

In the current section we examine the parameters of the MCC constitutive law simulating the OC clay behavior (M, p_m, κ, etc.) as well as the features of the simulated laterally loaded pile (D, α, etc.). Furthermore, we investigate their effect on the numerically developed p-y curves, derived from the FEA. It is important to mention here that the specific parametric investigation takes place assuming constitutive behavior of the clay according to the MCC, i.e. no small-strain stiffness and structure degradation features. The following soil and pile parameters are of concern in this research attempt on p-y curves for OC clays:

- Average undrained shear strength $c_{u,avg}$ along a depth of $10D$ from the pile head
- Unloading-reloading lines slope κ
- The maximum coefficient of horizontal geostatic stress $K_{o,max}$
- Critical state line slope M
- Poisson's ratio ν
- Pile diameter D
- Pile-soil adhesion factor α
- Depth of differentiation for the OC clay failure mechanism z_w

Table 5.1 summarizes the range of the aforementioned parameters[1] - apart from z_w - examined in the current numerical investigation for the development of p-y curves in OC clays. Prior to carrying out FEA with all the potential parameter combinations depicted in Table 5.1, we initially consider their effect on the constitutive behavior of a single soil element at a representative depth (z=3D) in front of the laterally loaded pile, i.e. under compression. Thus, we determine the most influential of these OC clay parameters and we evaluate their effect on the derived p-y curves. Finally, the current chapter proposes an appropriate curve equation fitting the numerically developed p-y curves as well as specific N_p and K_i expressions for this p-y curve relationship, incorporating the parameters of the present numerical investigation. It is important to mention that NCL slope λ receives values between 0.065-0.174

[1] Appendix A contains the full extent of the parametric FEA carried out for OC clayey soils.

Table 5.1: OC clay properties of the FEA parametric investigation. The FEA involve piles of D=0.5, 1.0, 1.5 and 2.0m with pile-soil adhesion factor α=0.3, 1.0.

OC clay parameters				
$c_{u,\,avg}$[1] (kPa)	κ[2]	$K_{o,\,max}$[3]	M[4]	ν
50, 95, 190, 380	**0.0033, 0.0054, 0.0065, 0.0087, 0.0108, 0.0174**	1.5	1.2	0.100
190	0.0054	**0.7, 1.0**	1.2	0.100
190	0.0054	1.5	1.2	**0.200, 0.333**

[1] $c_{u,\,avg}$ values refer to the average undrained shear strength from ground level to a depth z=10D.
[2] κ values correspond to C_r=0.0075-0.04 ($\kappa = C_r/\ln 10$).
[3] $K_{o,\,max}$ is the maximum K_o assigned to shallow depths, where OCR is very high (see Equation 3.19).
[4] M=1.2 corresponds to ϕ=30° (Equation 3.3).

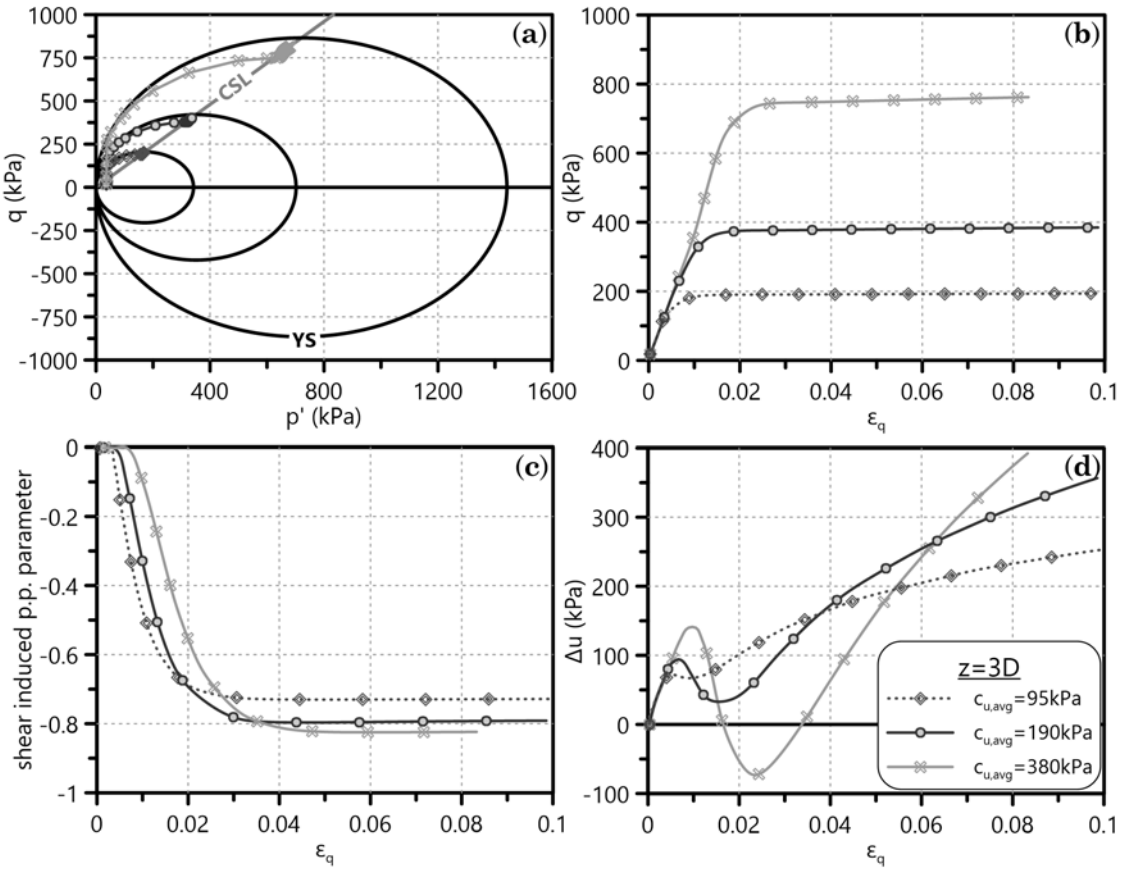

Figure 5.1: Effect of different $c_{u,\,avg}$ values (κ=0.0054, $K_{o,\,max}$=1.5, M=1.2, ν=0.1) on (a) stress paths, (b) deviatoric stress-strain curves, (c) volumetric-deviatoric strain curves and (d) excess pore water pressure development of a specific OC clay element under compression in front of the laterally loaded pile (z=3D).

- corresponding to C_c=0.15-0.40 - during the current numerical development of p-y curves for OC clays. Since the unloading-reloading lines slope κ dominates the compressibility of the heavily OC clays analyzed in the FEA of the present chapter, we assume λ/κ=10-20 in order to obtain a realistic undrained soil behavior on the $q-\varepsilon_q$ plane, i.e. peak strength (c_u=$q_{\max}/2$) at deviatoric strain ε_q=1-2% for the majority of the in situ stress states. According to Terzaghi et al. (1996), most values of the ratio C_c/C_r - thus λ/κ - are in the range of 5 to 50. Very high values of the ratio, even higher than 50, correspond to highly structured and bonded clay and silt deposits whereas low values refer to micaceous silts and fissured stiff clays and shales. Thus, the λ/κ ratios of the current numerical investigation are within the recommendations of the literature. In addition, λ only affects the equivalent c_u (see Equation 3.24), the average values of which along a pile length of $10D$ are parametrically investigated according to Table 5.1. Therefore, the current numerical investigation does not consider it necessary to examine the effect of λ on the derived p-y curves for OC clays.

5.2.1 OC clay parameters

The current paragraph describes the OC clay parameters examined in the current numerical simulation. The following parametric investigation indicates which OC clay properties it is necessary to take into account for the formulation of the corresponding numerical p-y curves. In consistence with the corresponding process followed for NC clay p-y curves (see Chapter 4) and prior to presenting an extensive investigation of the effect these properties ($c_{u,\,avg}$, κ, $K_{o,\,max}$, M, ν) have on the OC clay p-y curves, we demonstrate the following graphs at an average depth z=$3D$[1] (see Figure 3.34) of the FEA:

- stress paths $p-q$
- deviatoric stress-strain curves $q-\varepsilon_q$
- shear induced pore pressure parameter with the deviatoric strain $U_q-\varepsilon_q$[2]
- excess pore water pressure development with the deviatoric strain $\Delta u-\varepsilon_q$

All the aforementioned graphs represent the OC clay constitutive behavior of a laterally loaded pile with diameter D=1m and pile-soil adhesion factor α=0.3. Assuming such a low α - compared with the corresponding α=1.0 for NC clays - seems

[1] Assuming that the lateral loading of the pile affects the soil up to a depth $z \approx 6-8D$.

[2] The shear induced pore pressure parameter U_q stands for the percentage of the developed excess pore pressure Δu attributed to the shear stress. Assuming that $\Delta u = \Delta p + U_q \cdot \Delta q$ - where Δp=the difference in mean **total** stress - we calculate $U_q = -\Delta p^{'}/\Delta q$.

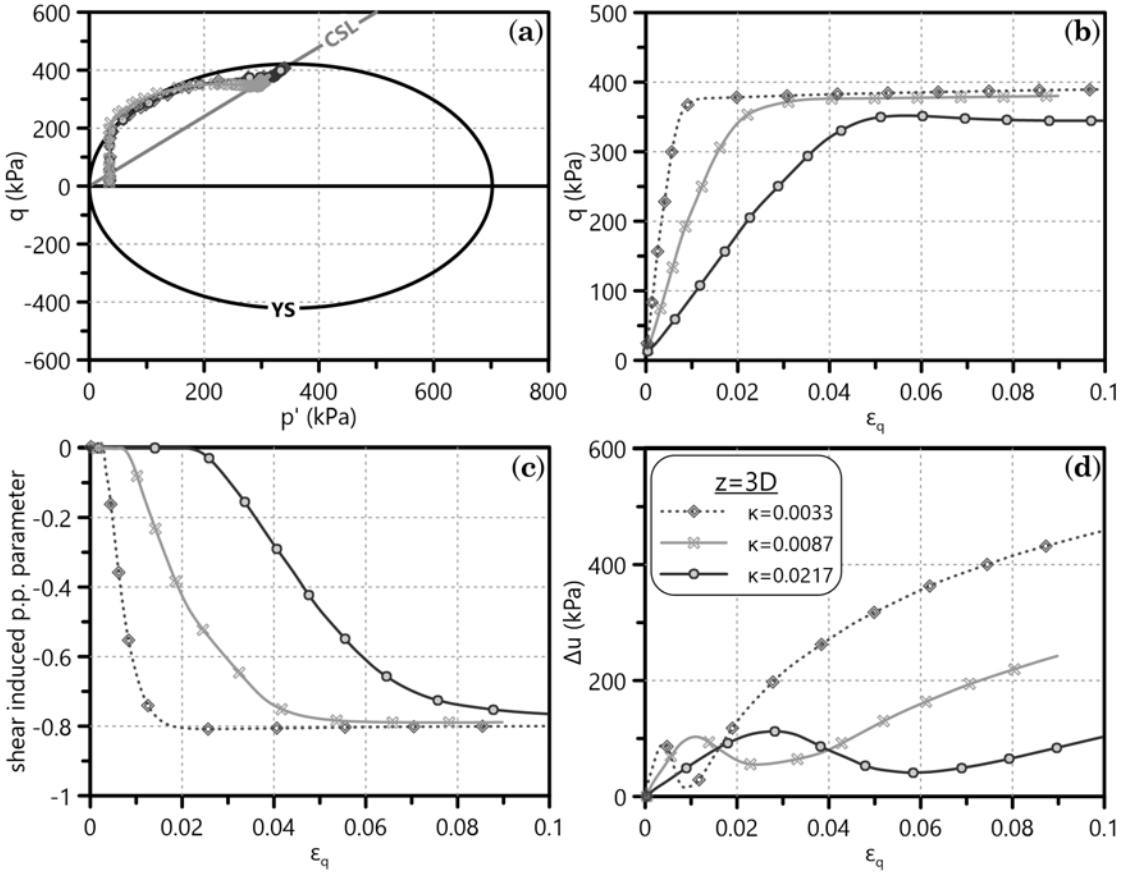

Figure 5.2: Effect of different unloading-reloading line slopes κ ($c_{u,\,avg}$=190kPa, $K_{o,\,max}$=1.5, M=1.2, ν=0.1) on (a) stress paths, (b) deviatoric stress-strain curves, (c) shear induced pore pressure parameter-deviatoric strain curves and (d) excess pore water pressure development of a specific OC clay element under compression in front of the laterally loaded pile (z=3D).

rational according to the trend the literature suggests for relatively high c_u values of OC clays (Figure 2.28), namely the general case of $c_{u,\,avg}$ >100kPa in the current dissertation. Paragraph 5.2.2 that follows examines the effect of pile characteristics on the numerical p-y curves for such clays. Figures 5.1, 5.2, 5.3, 5.4 and 5.5 depict the effect of $c_{u,\,avg}$, κ, $K_{o,\,max}$, M and ν respectively on the aforementioned graphs. Unloading-reloading lines slope κ clearly affects the initial slope of the $q-\varepsilon_q$, $U_q-\varepsilon_q$ and $\Delta u-\varepsilon_q$ curves thus playing the most crucial role on the stiffness of these graphs - supposedly on the stiffness of the corresponding p-y curves too. Poisson's ratio ν also affects the stiffness of the $q-\varepsilon_q$ and $\Delta u-\varepsilon_q$ curves, although not as intensely as κ. On the other hand, the average undrained shear strength $c_{u,\,avg}$ to a depth z=10D naturally influences the peak strength of the $q-\varepsilon_q$ curves since it corresponds to different yield surface sizes p_m. Finally, the effect of both the maximum coefficient of horizontal geostatic stress $K_{o,\,max}$ and the CSL slope M on the $q-\varepsilon_q$

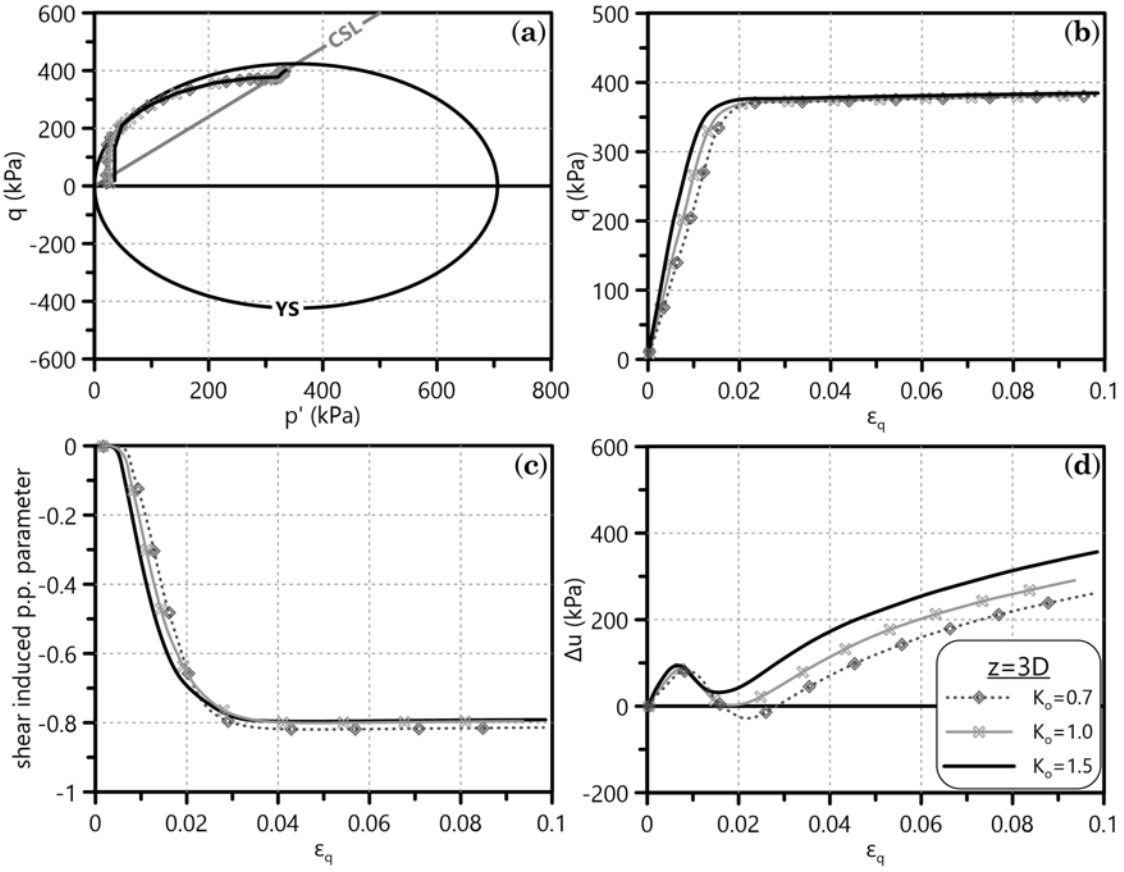

Figure 5.3: Effect of different maximum coefficients of horizontal geostatic stress $K_{o,max}$ ($c_{u,avg}$=190kPa, κ=0.0054, M=1.2, ν=0.1) on (a) stress paths, (b) deviatoric stress-strain curves, (c) shear induced pore pressure parameter-deviatoric strain curves and (d) excess pore water pressure development of a specific OC clay element under compression in front of the laterally loaded pile (z=3D).

plots is rather measurable. However, they seem to affect the $\Delta u - \varepsilon_q$ curves somehow and therefore the following investigation shall examine this effect, since the excess pore water pressure Δu affects the total lateral pressure p of the p-y curves under undrained loading.

The aforementioned OC clay simulation parameters demonstrate certain effect on the soil constitutive behavior. Thus, the following paragraphs present this effect on the numerically developed p-y curves parallel to $q - \varepsilon_q$ graphs for κ, ν and parallel to $\Delta u - \varepsilon_q$ graphs for $K_{o,max}$, M at depths z=2D, 4D, 6D and 8D.

5.2.1.1 Undrained shear strength (c_u)

The current paragraph attempts to explain the actual FEA simulation of an OC clay in terms of strength and how this simulation affects the derived p-y curves. At first, one has to understand the simulation process of such a clay as presented in

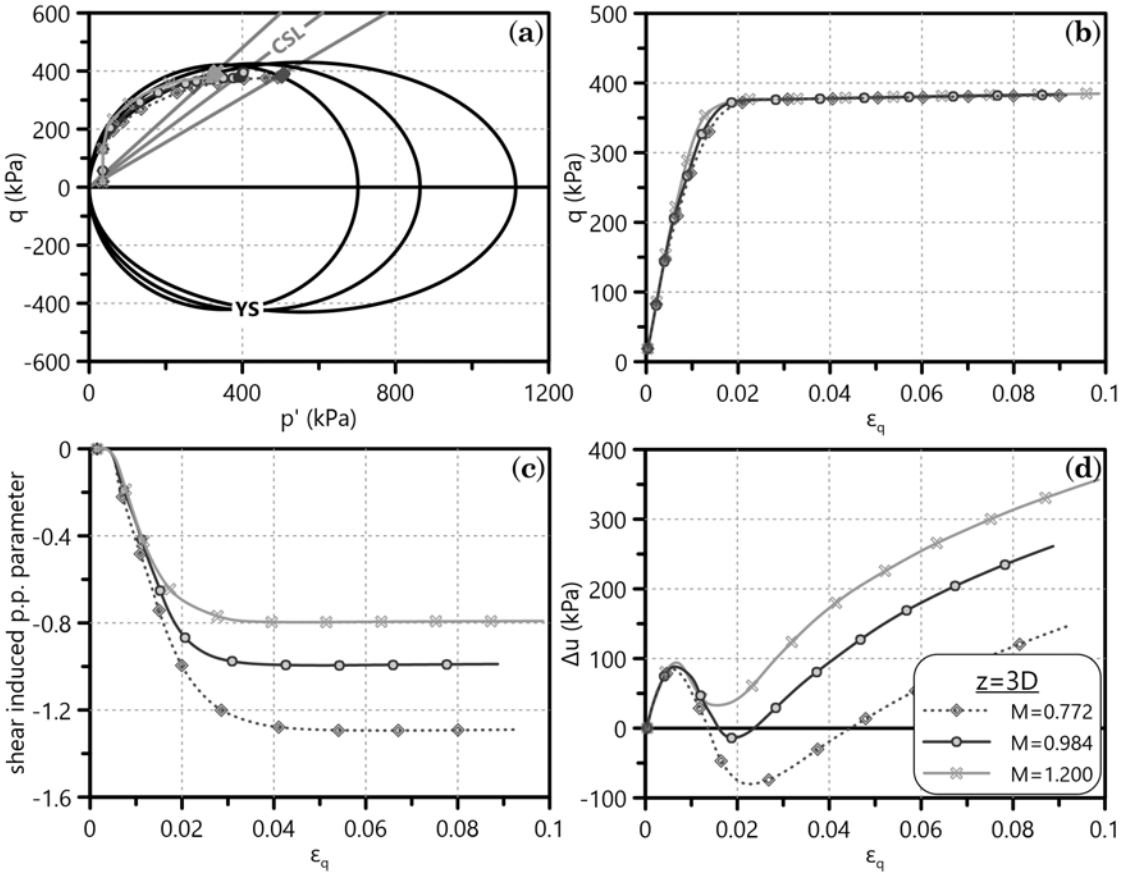

Figure 5.4: Effect of different CSL slopes M ($c_{u,\,avg}$=190kPa, κ=0.0054, $K_{o,\,max}$=1.5, ν=0.1) on (a) stress paths, (b) deviatoric stress-strain curves, (c) shear induced pore pressure parameter-deviatoric strain curves and (d) excess pore water pressure development of a specific OC clay element under compression in front of the laterally loaded pile (z=3D).

Paragraph 3.2.3.2. The geostatic stress field of the upper OC clay layer, namely up to z=10D that is crucial for a laterally loaded pile, refers to initial stress states inside the MCC yield locus and on an unloading-reloading line on the $p-q$ and $v-\ln p$ planes respectively (see Figure 3.14. Figure 5.6 demonstrates the four different c_u distributions simulated through the aforementioned process together with the corresponding $c_{u,\,avg}$ values examined in the current numerical investigation. Since c_u is the OC clay parameter representing the strength and affecting p_u, the FEA simulations for undrained lateral pile loading in such soils cover a wide range of this parameter - $c_{u,\,avg}$=50-380kPa according to Table 5.1.

Figure 5.7a confirms the assumption that $c_{u,\,avg}$ affects p_u of the derived p-y curves for certain realistic values of the rest OC clay parameters (κ=0.0054, $K_{o,\,max}$=1.5, M=1.2, ν=0.1) at the representative depth z=3D - D=1m, α=0.3. Furthermore Figure 5.7b validates the $c_{u,\,avg}$ values of the OC clays that the FEA of the current chapter simulate. It remains to ascertain if the difference in $c_{u,\,avg}$

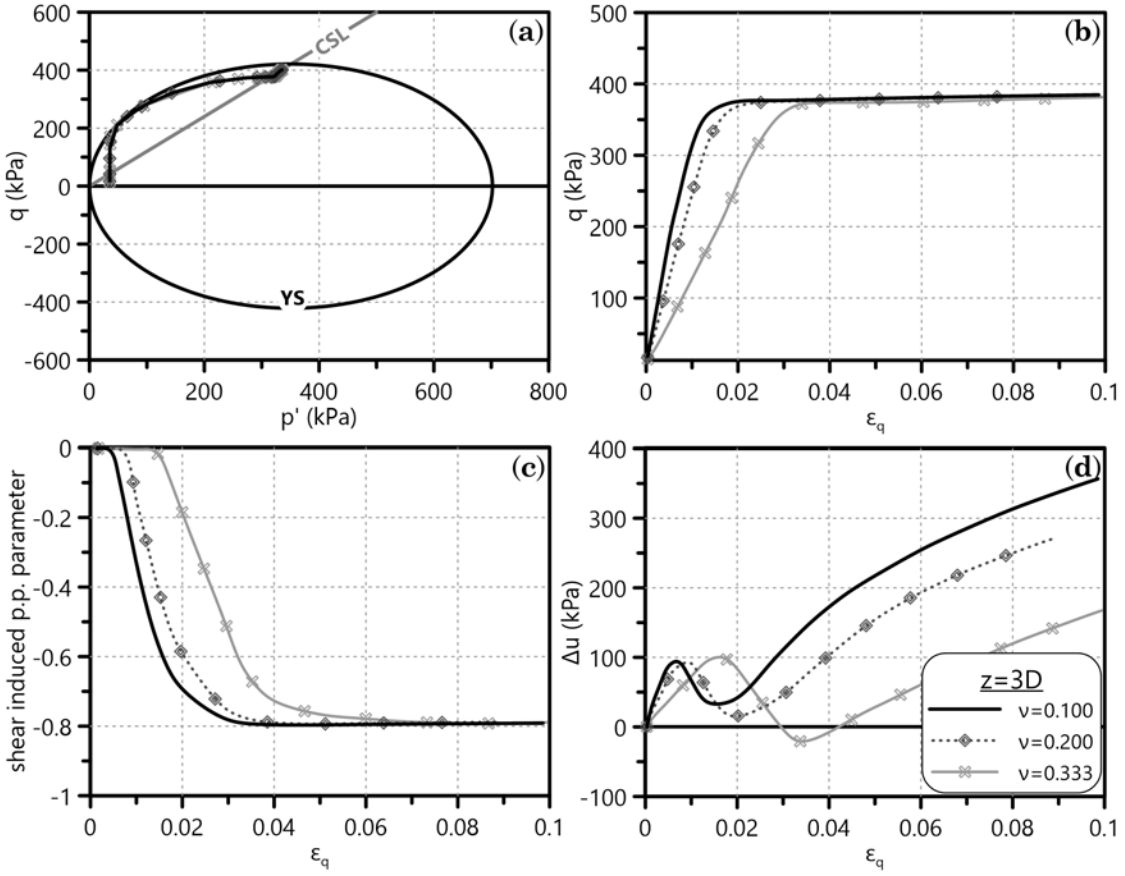

Figure 5.5: Effect of different Poisson's ratios ν ($c_{u,\,avg}$=190kPa, κ=0.0054, $K_{o,\,max}$=1.5, M=1.2) on (a) stress paths, (b) deviatoric stress-strain curves, (c) shear induced pore pressure parameter-deviatoric strain curves and (d) excess pore water pressure development of a specific OC clay element under compression in front of the laterally loaded pile (z=3D).

also affects N_p when it comes to the determination of the ultimate lateral OC clay resistance p_u.

5.2.1.2 Unloading-reloading lines slope (κ)

Paragraph 4.2.1.1 proved that the poroelasticity parameters λ and κ play a significant role in the stiffness of the NC clay and consequently in the estimation of K_i of the corresponding p-y curves. In accordance to that, the present paragraph examines the effect of κ on the p-y curves for OC clays. Figure 5.2 demonstrates how intensely κ affects both K_i and the initial stiffness of the $q-\varepsilon_q$ curves. Since the clays under concern are OC - some of them heavily OC in fact - alteration of λ does not influence the stiffness of the aforementioned curves, therefore we do not carry out a parametric investigation on it for such soils.

Figure 5.8 depicts the variation of p-y curves and the corresponding $q-\varepsilon_q$ plots at z=2, 4, 6 and 8D for a significant range of the unloading-reloading lines slope,

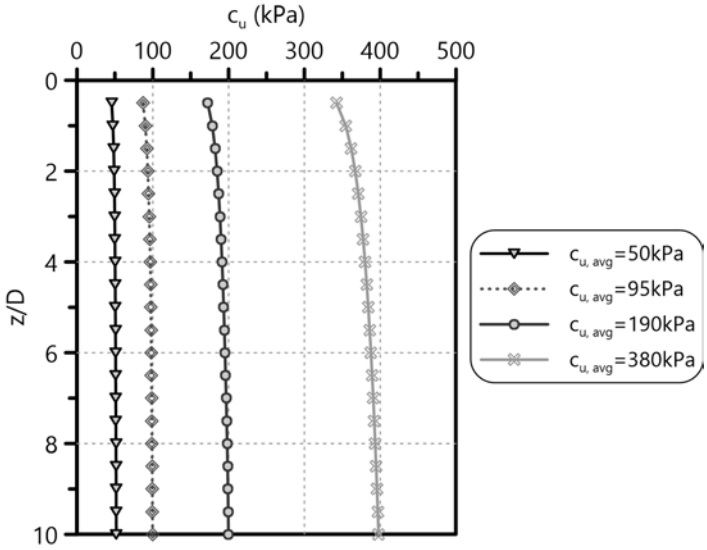

Figure 5.6: The parametric FEA for the numerical development of OC clay p-y curves examine four different values of $c_{u,\,avg}$=50, 95, 190 and 380kPa ($K_{o,\,max}$=1.5, M=1.2), considered from ground level to a depth z=10D.

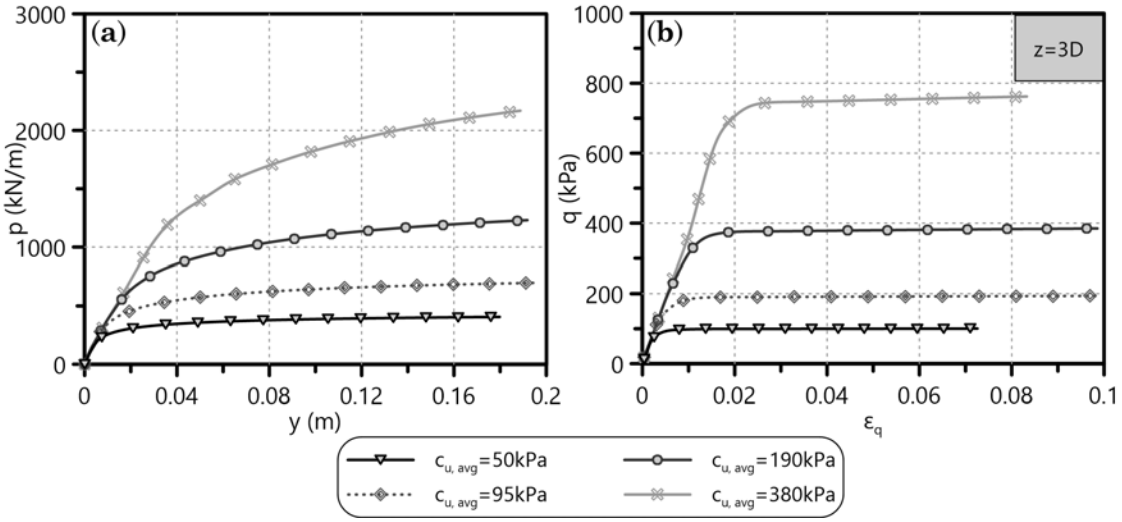

Figure 5.7: Effect of $c_{u,\,avg}$ on (a) the p-y curves and (b) the $q-\varepsilon_q$ curves at a representative OC clay depth z=3D, derived from FEA output.

namely κ=0.0033-0.0174 ($c_{u,\,avg}$=190kPa, $K_{o,\,max}$=1.5, M=1.2, ν=0.1). Despite the initial indications that κ just affects the stiffness (Figure 5.2) in terms of soil element behavior, Figure 5.8a shows a profound effect of this parameter on the ultimate strength too when referring to the system reaction, i.e. the p-y curves.

It is certain that the influence of κ on p_u is not attributed to differences in c_u. Figure 5.8b demonstrates negligible variation of $q_{\max}$=2c_u between the numerical simulations with different κ values at all the examined OC clay depths. Paragraph

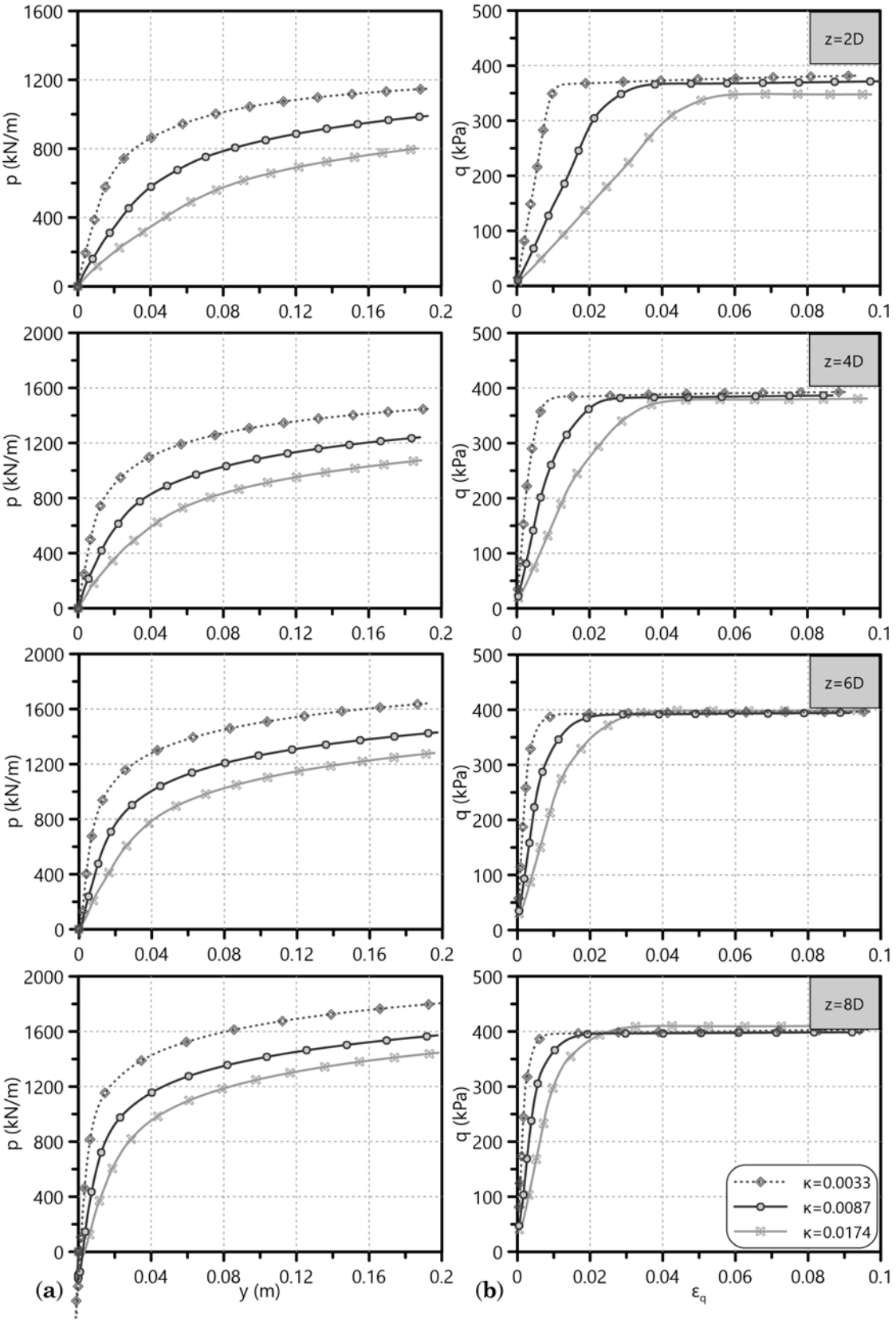

Figure 5.8: Effect of the unloading-reloading lines slope κ on (a) the p-y curves and (b) the $q - \varepsilon_q$ curves at different depths of OC clay, derived from FEA output.

5.4 handles quantitatively these effects by proposing a certain monotonic p-y curve equation for OC clays through the findings of this chapter.

5.2.1.3 Maximum coefficient of horizontal geostatic stress ($K_{o,\,max}$)

Another soil parameter of potential interest during the current numerical investigation is the maximum coefficient of horizontal geostatic stress $K_{o,\,max}$ assigned to the OC clay. The FEA of the present chapter simulate the OC clay geostatic stress field assuming a K_o according to the following equations (see Paragraph 3.2.3.2):

$$K_o = \begin{cases} K_{o,\,NC}, & \text{if } OCR = 1 \\ K_{o,\,OC} = K_{o,\,NC} \cdot \sqrt{OCR} \leq K_{o,\,max}, & \text{if } OCR > 1 \end{cases}$$

where $K_{o,\,NC}$=0.5 for NC clays. Since the OC clays under investigation are even very heavily overconsolidated, especially close to ground surface, the K_o values corresponding to high OCR are also high. It is reasonable to believe that such high values of K_o=2-5 for z <3m refer to actual horizontal stress coefficients of heavily OC clays at rest, although we cannot measure them in the laboratory due to potential deconfinement during sampling. However, we need to set a $K_{o,\,max}$ as a threshold value since the present dissertation aims at generating p-y curves through a certain parametric investigation. The current paragraph examines three different maximums of this kind, namely $K_{o,\,max}$=0.7, 1.0 and 1.5 ($c_{u,\,avg}$=190kPa, κ=0.0054, M=1.2, ν=0.1), applicable to the shallowest OC clay part. According to Figure 5.3, K_o seems to affect none of the depicted plots at the specific depth (z=3D) except for the $\Delta u - \varepsilon_q$ curve - and that only slightly.

As a consequence, we demonstrate the effect of $K_{o,\,max}$ on the numerical p-y curves and the corresponding $\Delta u - \varepsilon_q$ graphs in parallel at four different depths of the aforementioned OC clay, namely z=2, 4, 6 and 8D. Figure 5.9 points out the differences - although not striking ones - at all the examined depths for the aforementioned plots. Especially for the derived p-y curves, $K_{o,\,max}$ influences both K_i and p_u of the lateral OC clay response. Therefore, it is essential to identify exactly how the specific coefficient affects the p-y curves that the present chapter proposes for OC clays. Paragraph 5.4 proposes a certain p-y curve equation for OC clays and explains thoroughly the way that a specific mathematical formulation incorporates this effect on both parts of the curves (K_i and p_u).

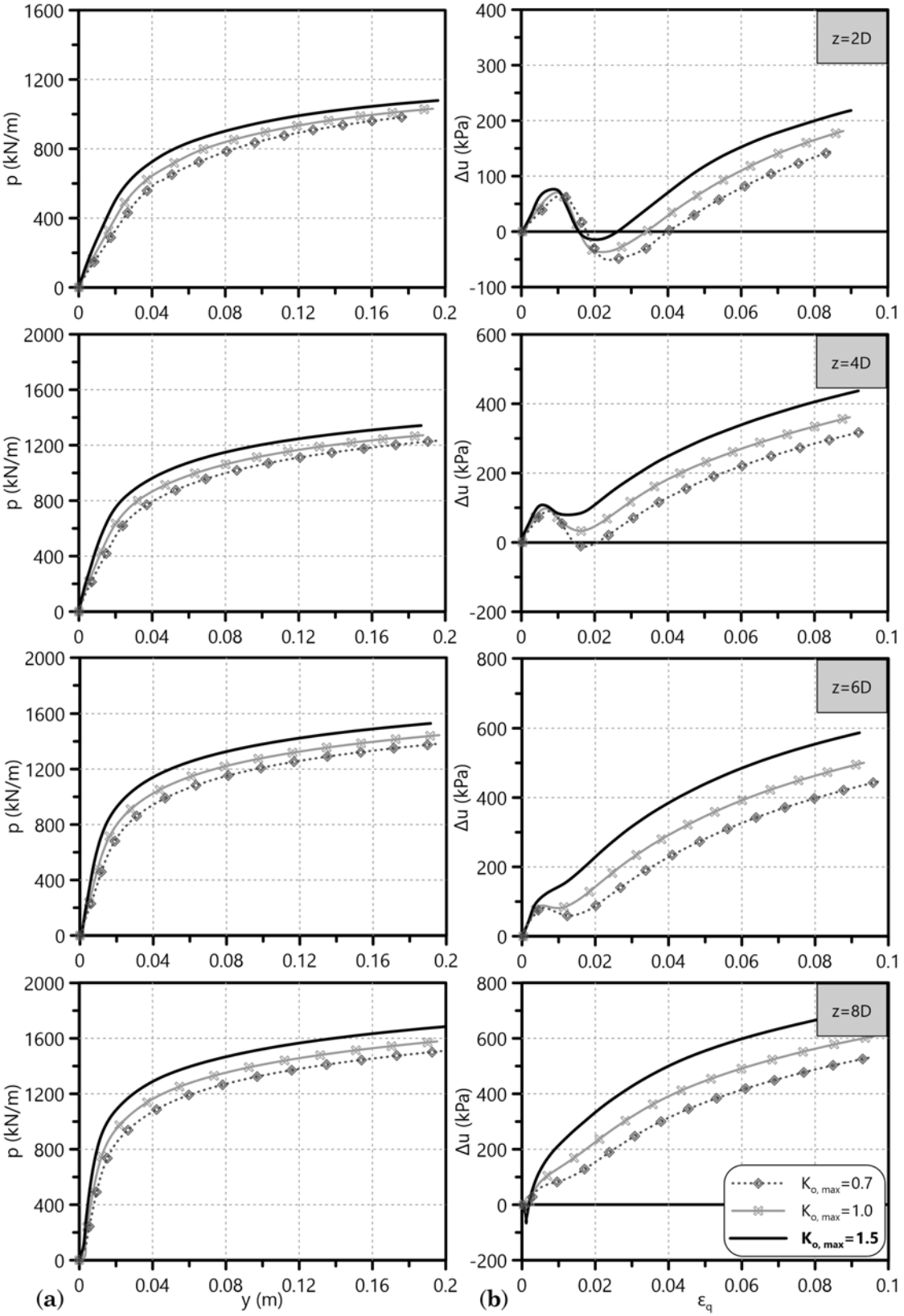

Figure 5.9: Effect of the maximum coefficient of horizontal geostatic stress $K_{o,max}$ on (a) the p-y curves and (b) the $\Delta u - \varepsilon_q$ curves at different depths of OC clay, derived from FEA output.

5.2.1.4 Critical state line slope (M)

As Figure 5.4 demonstrates, CSL slope M generally affects the OC clay excess pore water pressure development - $U_q - \varepsilon_q$ and $\Delta u - \varepsilon_q$ graphs. However, the stress-strain behavior of the soil element at the specific depth ($q - \varepsilon_q$) seems unaffected by the variation of M - corresponding to clay friction angles ϕ=20°, 25° and 30° (Equation 3.3). It remains to investigate whether this variation also influences the ultimate lateral soil resistance p_u of the numerical p-y curves. Figure 5.10 depicts in parallel the FEA derived p-y curves and soil $\Delta u - \varepsilon_q$ graphs at depths z=2, 4, 6 and 8D. The comparison unveils no effect of M differentiation on the numerical p-y curves for OC clays. This observation is reasonable since the equivalent $c_{u,\,avg}$ remains the same and equal to 190kPa (κ=0.0054, $K_{o,\,max}$=1.5, ν=0.1) for the three examined M values, despite the variation of p_m. Moreover, Paragraph 5.2.1.1 proved that $c_{u,\,avg}$ is the predominant OC clay parameter affecting p_u. As a result, the current numerical investigation does not consider M crucial for the development of OC clay p-y curves and therefore shall not include it in the corresponding proposed relationships - assuming that $c_{u,\,avg}$=190kPa is the mean and thus representative undrained strength examined in the FEA (see Table 5.1). From this point of the present chapter all the OC clay simulations involve M=1.2.

Another issue on the effect CSL slope M has on the p-y curves is its differentiation in compression (M_c) and extension (M_e) (see Equation 3.3). In order to investigate this effect, we carry out a FEA with M_e=0.8 · M_c ($c_{u,\,avg}$=190kPa, κ=0.0109, $K_{o,\,max}$=1.5, ν=0.1) and compare the derived p-y curves with the corresponding ones from the standard numerical simulation of the OC clays. Figure 5.11 observes infinitesimal difference on p_u of the numerical p-y curves between the two constitutive behaviors (M_e=M_c and 0.8 · M_c), namely less than 5% - with the ultimate lateral OC clay resistance measured at realistic lateral pile displacements ($y < 0.2D$). Consequently, this variation of M in compression and extension will no further employ the present investigation.

5.2.1.5 Poisson's ratio (ν)

The current paragraph exhibits the effect of Poisson's ratio ν on the FEA derived p-y curves for OC clays. This verification tests three values of Poisson's ratio, namely ν=0.10, 0.20 and 0.333 for an OC clay with $c_{u,\,avg}$=190kPa, κ=0.0054, $K_{o,\,max}$=1.5 and M=1.2, in terms of p-y and $q - \varepsilon_q$ curves - the latter for soil elements under compression in front of the pile (Figure 3.34). Although the lateral loading of the pile is undrained with $\varepsilon_{\text{vol}} \approx 0$ and thus $\nu_u \approx 0.5$ (see Paragraph 3.3.6), the actual ν of the soil controls its initial stiffness through the $2G/K$ ratio (Equation 3.9). Figure 5.12

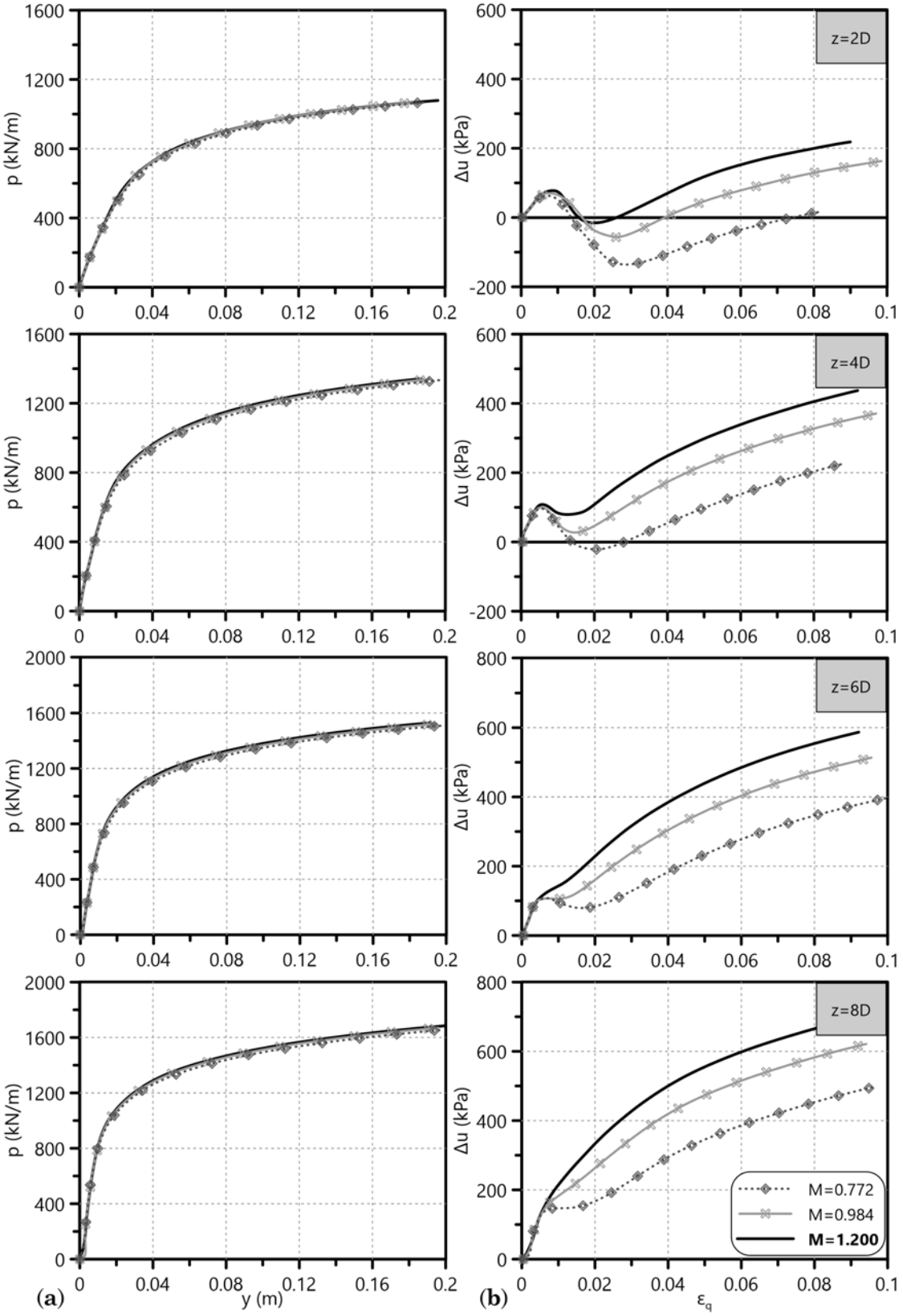

Figure 5.10: Effect of CSL slope M on (a) the p-y curves and (b) the $\Delta u - \varepsilon_q$ curves at different depths of OC clay, derived from FEA output.

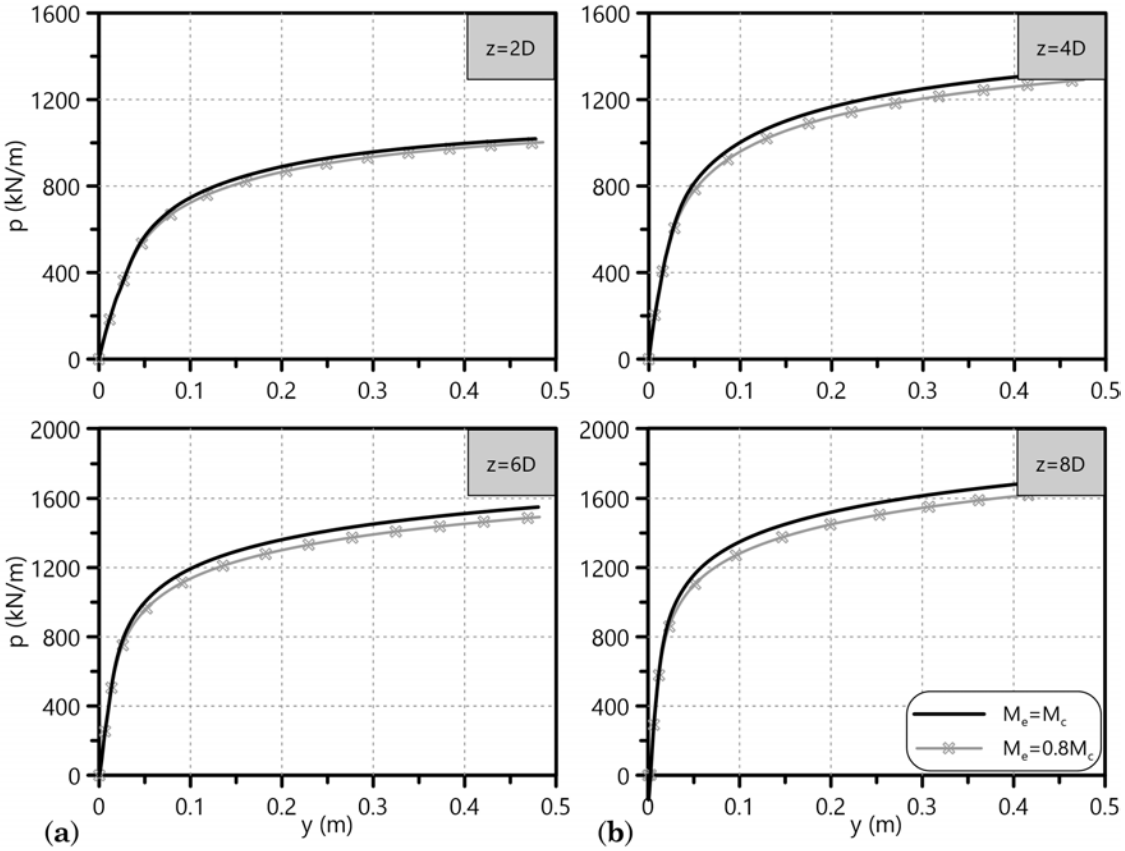

Figure 5.11: Effect of CSL slope M_e under extension on the numerical p-y curves for OC clays at various depths.

depicts the following correlation between the system and the soil element behavior: since ν has significant influence on the stress-strain curves of the soil (Figure 5.12b), it therefore clearly affects K_i of the numerical p-y curves derived from the FEA output (Figure 5.12a). Furthermore, it is obvious that the derived p-y curves refer to the total stress soil response on the laterally loaded pile. As long as the variation in ν also provokes different $\Delta u - \varepsilon_q$ curves for the OC clay (Figure 5.5d), the specific behavior adds to the the corresponding variation in K_i of the FEA derived p-y curves. Another observation regarding the effect of ν on the OC clay p-y curves involves the difference in p_u of the latter due to alteration of the first, especially for ν=0.333. However, values of ν=0.1-0.2 are more typical for OC clayey soils and for these values no significant p_u differentiation is observed. As a result, the derivation process of p-y curves for OC clays described in the following paragraphs does not investigate the effect of ν on the p_u for such curves.

Summarizing the findings of the aforementioned paragraph, the average undrained shear strength $c_{u,avg}$ along a depth of $10D$ from ground surface is the only OC clay parameter affecting just p_u of the derived p-y curves. On the contrary, the maximum

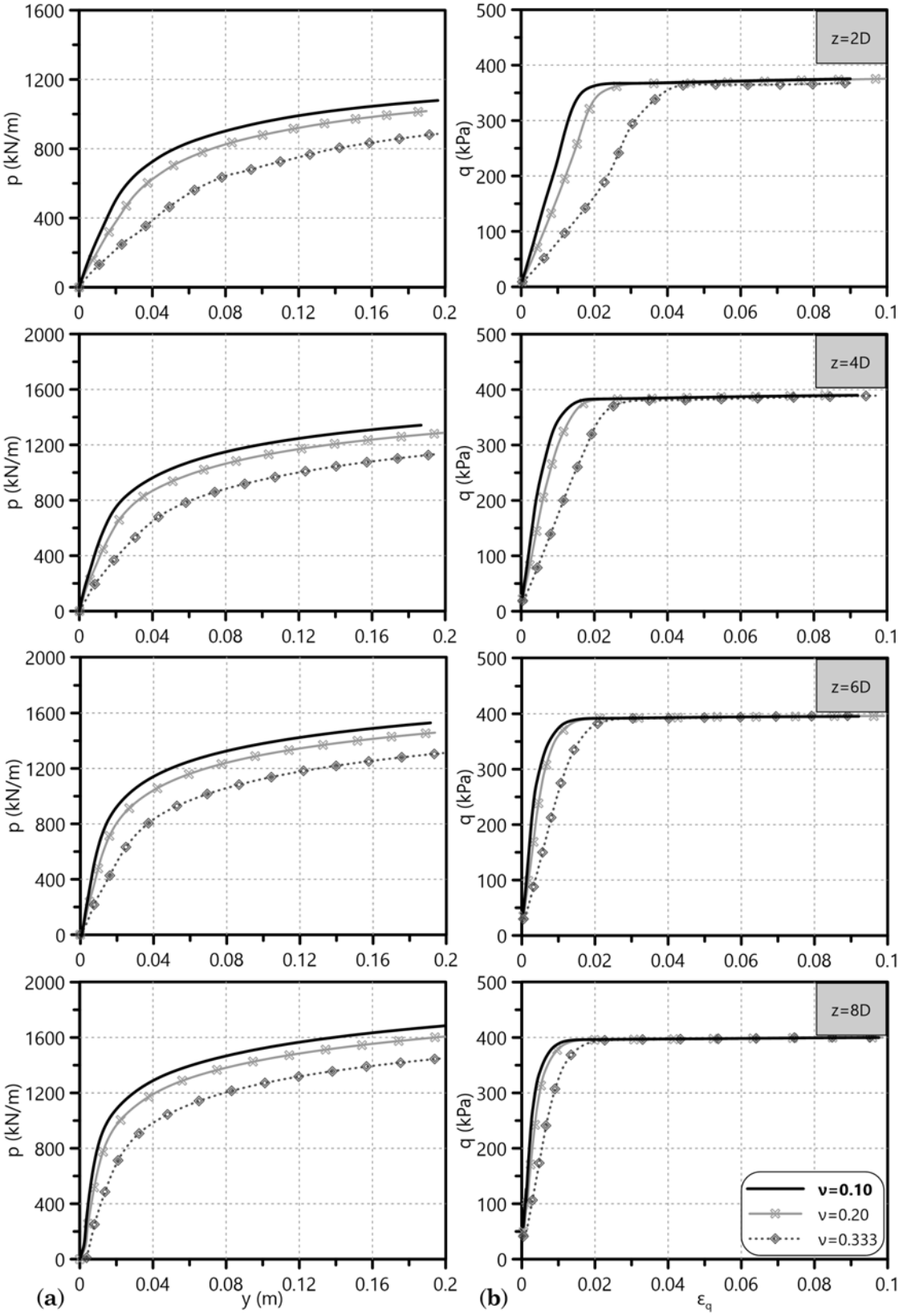

Figure 5.12: Effect of Poisson's ratio ν on (a) the p-y curves and (b) the $q - \varepsilon_q$ curves at different depths of OC clay, derived from FEA output.

coefficient of horizontal geostatic stress $K_{o,max}$, Poisson's ratio ν and the slope of the unloading-reloading lines κ demonstrate an effect on both K_i and p_u that becomes more profound and significant for the last two parameters. Finally, CSL slope M and its variation in extension show no effect on the numerical p-y curves, as long as $c_{u,avg}$ remains unchanged. The following paragraphs investigate the effect of certain pile characteristics, namely the diameter (D) and the pile-soil adhesion (α), on the derived OC clay p-y curves of the current FEA.

5.2.2 Pile parameters

The following paragraphs describe the laterally loaded pile parameters taken into account in the current numerical investigation. In more detail, they examine the effect the pile diameter D and the soil-pile adhesion factor α have on the derived p-y curves for OC clays.

5.2.2.1 Pile diameter (D)

As Paragraph 4.2.2.1 reminds, pile diameter D multiplies the actual lateral soil pressure thus delivering the renowned p of the p-y curves in kN/m. In order to evaluate the effect of D on the FEA derived p-y curves for OC clays the current paragraph demonstrates two different forms at two different depths (a shallow and a relatively deep one) of the same p-y curves: Figure 5.13a depicts the classic p-y form with p as a distributed load (kN/m) for four pile diameters D=0.5, 1.0, 1.5 and 2.0m at z=3 and 6m while Figure 5.13b demonstrates the same curves with p as pressure (kPa). It is evident that the differences we observe between the p-y curves of Figure 5.13a - in p_u as well as in K_i - seem to fade out in the corresponding expression of Figure 5.13b. However, the present chapter needs to examine further if D affects certain parameters of the mathematical form chosen to represent the numerical OC clay p-y curves of the current dissertation. Paragraph 5.4 follows a detailed procedure in order to incorporate the diameter effect - if there is any - together with the effects of other soil and pile parameters in the proposed p-y curves for OC clays.

5.2.2.2 Pile-soil adhesion factor (α)

The FEA of the current dissertation simulate the pile-soil adhesion as a function of the clay undrained shear strength c_u, since they investigate the undrained lateral pile response. Therefore, we have introduced the so-called adhesion factor α, controlling the shear strength on the pile-soil interface (see Paragraph 3.2.5). Figure 5.14 depicts

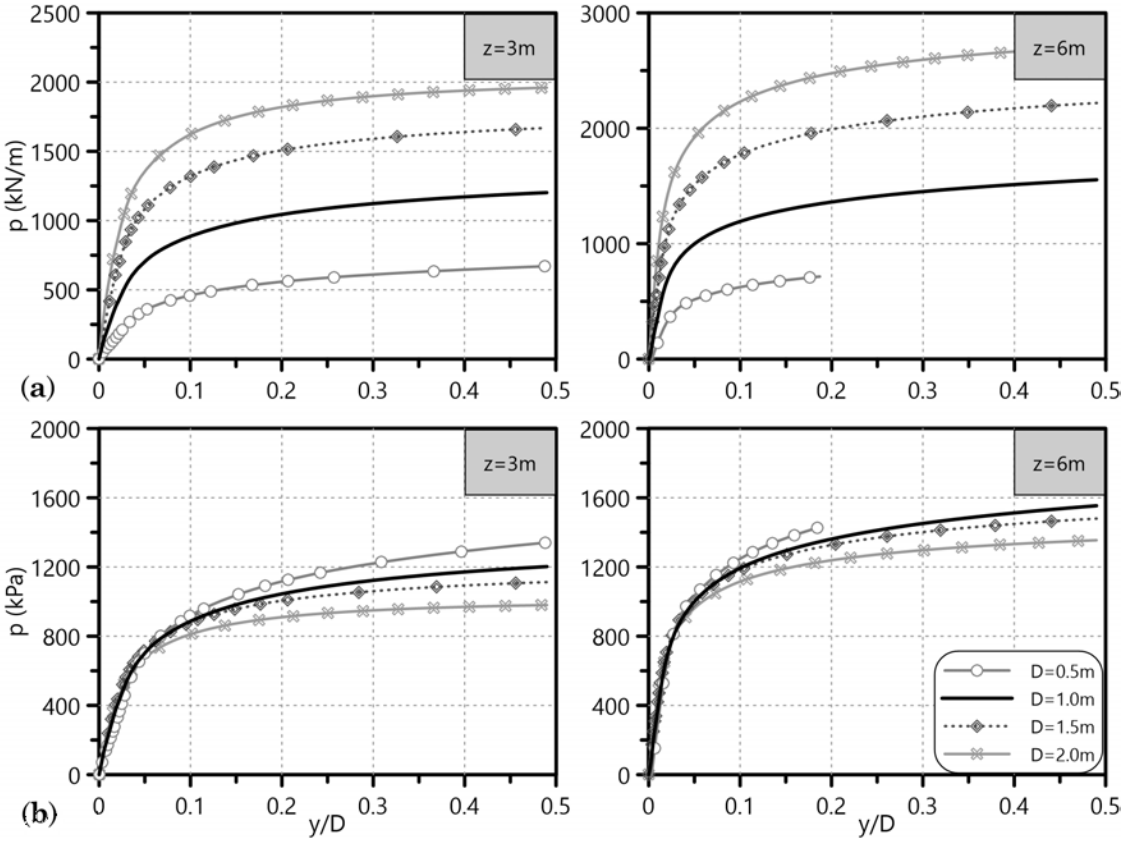

Figure 5.13: Effect of pile diameter D on the numerical p-y curves for OC clays at depth z=3 and 6m. Calculation of p as (a) distributed load (kN/m) - up - and (b) pressure (kPa) - down - along the laterally loaded pile.

the differences in p_u between the p-y curves of a smooth (α=0.3) and a rough (α=1.0) pile-soil interaction. The NC clay properties of the current investigation are the same with the ones used to examine the pile diameter effect on the corresponding p-y curves. Figure 5.14 shows that p_u of the rough pile-soil interface is almost 10% higher than that of the corresponding smooth interface (D=1m, $c_{u,avg}$=190kPa, κ=0.0109, $K_{o,max}$=1.5, ν=0.1).

O'Neill (2001) states that the estimation of α in clayey soils is quite uncertain for reasons associated with the characterization of shear strength profiles and the pile construction details. Therefore, the parametric investigation of the present chapter examines both smooth and rough pile-soil interactions for the numerical development of p-y curves in OC clays. Although the stiffer the clay, the closer α to value 0.3 (see Figure 2.28), the pile-soil interaction also concerns the pile surface and consequently Paragraph 5.4 proposes OC clay p-y curves for a range of adhesion factor α=0.3-1.0.

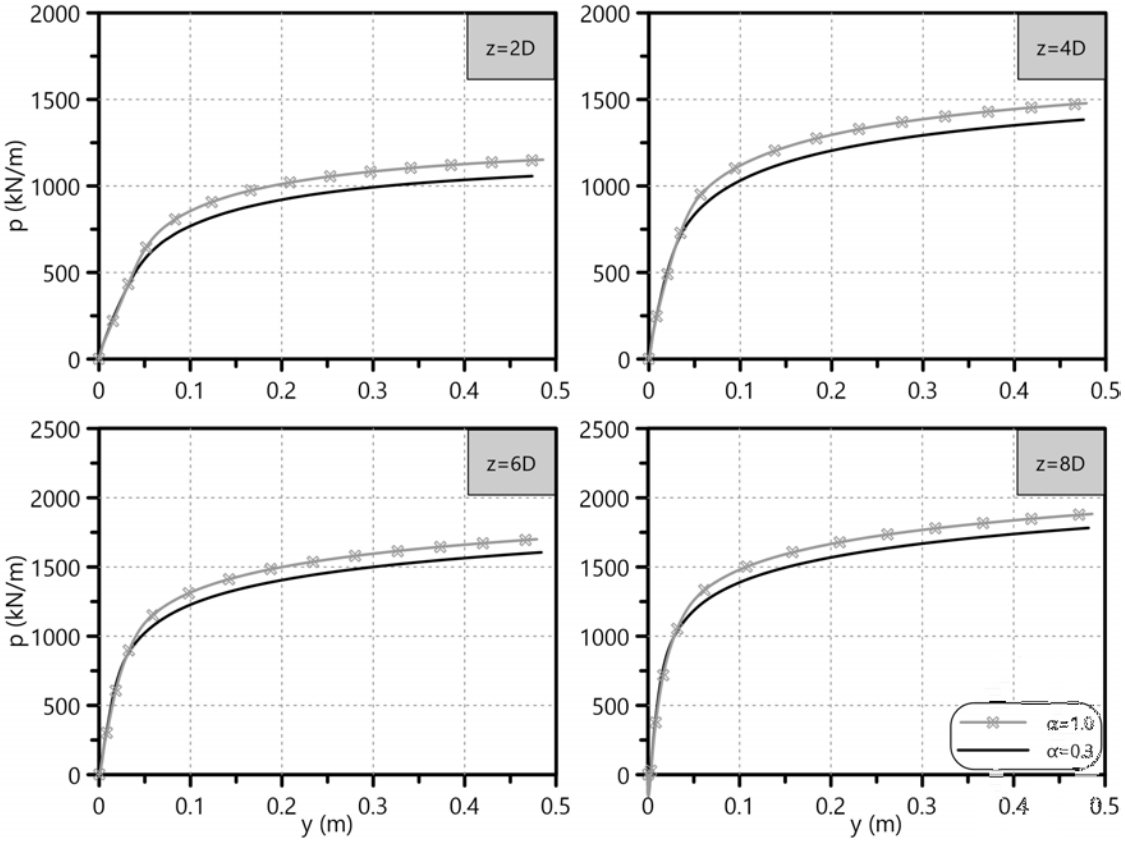

Figure 5.14: Effect of pile-soil adhesion factor α on the numerical p-y curves for OC clays at various depths.

5.2.3 OC clay failure mechanisms

The present paragraph distinguishes between two different failure mechanisms of the OC clay surrounding the laterally loaded pile, namely a shallow and a deep one. The shallow failure mechanism refers to a soil wedge in front of the pile that moves upwards when the clay reaches its ultimate lateral resistance. This failure type forms up to a certain depth, which the current investigation attempts to specify for various OC clay properties, pile diameters and pile-soil adhesion factors. For depths greater than the later the soil fails under plane-strain conditions. Figure 5.15 depicts the undeformed shape of the OC clay resultant displacements at a FEA loading frame with horizontal pile head deflection y_h equal to $50\%D$ - great enough to cause lateral OC clay failure up to a depth of $8D$. These displacements of the surrounding soil demonstrate two characteristic schemes:

- The distinction between a shallow wedge-type and a deep plane-strain failure mechanism in front of the pile. Figure 5.15 locates the transition from one failure type to the other at the depth where the vertical component u_z of the

resultant soil displacement fades out.

- The infinitesimal displacements of the OC clay at the back of the pile, obviously due to undrained shear strength adequate to allow for the vertical stability of that side during the pile-soil detachment (see Figure 3.16).

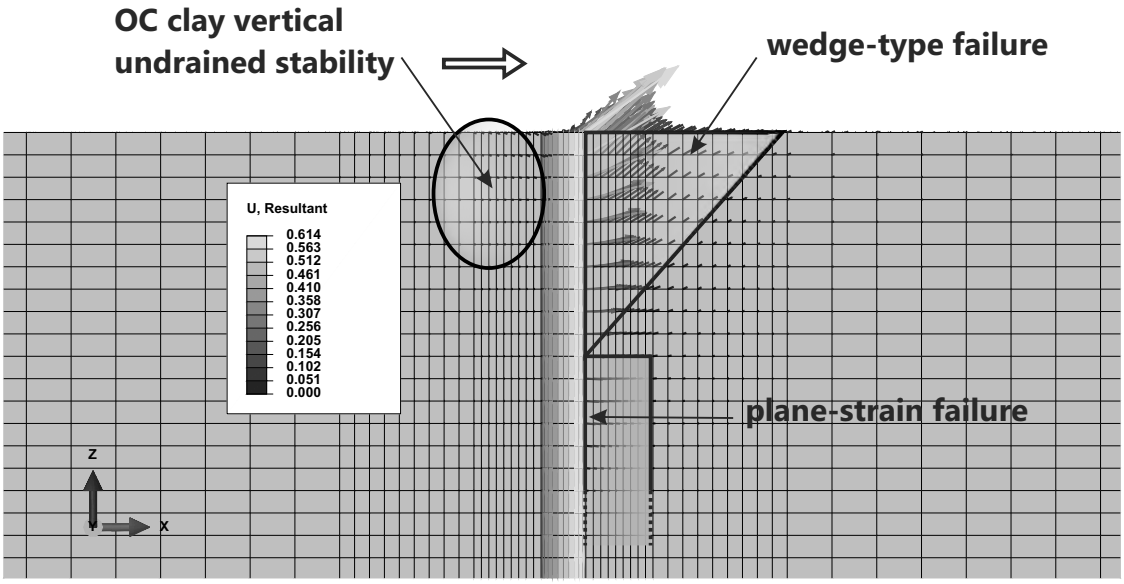

Figure 5.15: Undeformed shape of the OC clay resultant displacements at a FEA loading frame with horizontal pile head deflection y_h equal to 50%D (D=1m, α=0.3). Identification of two different failure mechanisms of the OC clay surrounding the laterally loaded pile.

For the determination of the aforementioned transition depth from the wedge-type to the plane-strain failure mechanism, we depict the the vertical OC clay displacement u_z normalized with the corresponding displacement of the ground surface $u_{z,\,top}$ - naturally assuming that the vertical deflection of the clay is maximum there - for FEA grid nodes in front of but not adjacent to the laterally loaded pile. These nodes represent all depths z of the same $x-y$ plan view point in the FEA. More accurately, Figure 5.16 plots the $u_z/u_{z,\,top}$ ratio of the soil nodes with the depth to pile diameter ratio z/D. The specific depiction refers to two different FEA loading frames with horizontal pile head deflection y_h=30%D and 50%D - significant in order to mobilize the ultimate lateral soil resistance p_u up to z=8D. We tested various potential $c_{u,\,avg}$, κ and α combinations ($K_{o,\,max}$=1.5, ν=0.1) of Table 5.1 for the OC clay. However, Figure 5.16 depicts FEA output of the 1m-diameter pile in OC clays with $c_{u,\,avg}$=95, 190, 380kPa and κ=0.0174, 0.0087, 0.0033 respectively for brevity. Furthermore, this graph also includes piles of D=0.5, 1.5 and 2.0m in a OC

clay with $c_{u,\,avg}$=190kPa and κ=0.0087. Thus, this investigation approximates the depth z_w of the failure wedge for both smooth and rough pile-soil interaction.

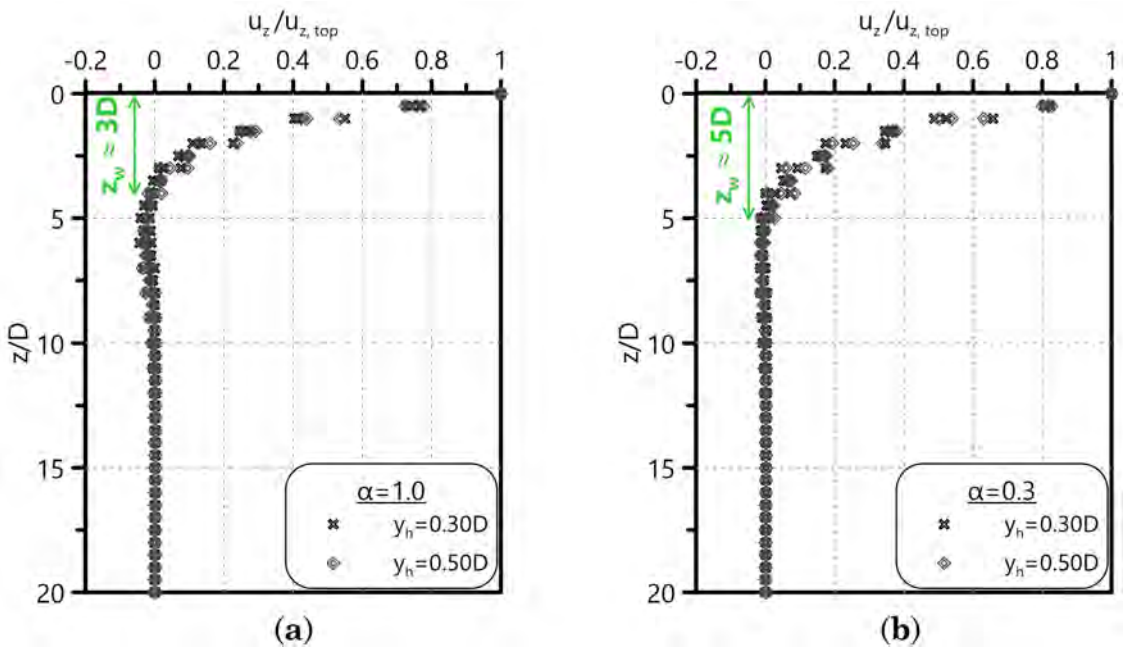

Figure 5.16: Normalized OC clay vertical displacement with the non-dimensional depth at two different FEA loading frames with horizontal pile head deflection y_h=30%D and 50%D. Parameters: $c_{u,\,avg}$=50-380kPa, κ=0.0033-0.0174, $K_{o,\,max}$=1.5, ν=0.1, D=0.5-2.0m. Estimation of the wedge-type failure depth (a) $z_w \approx 3D$ for rough (α=1.0) and (b) $z_w \approx 5D$ for smooth (α=0.3) pile-soil interaction.

The major observation of Figure 5.16 is that z_w differs between the smooth and the rough pile-soil interface simulation. More precisely, Figure 5.16a demonstrates minimization of $u_z/u_{z,\,top}$ at $z_w \approx 3D$ for the rough pile-soil interaction (α=1.0) while Figure 5.16b shows a $z_w \approx 5D$ for the corresponding smooth one (α=0.3). The specific behavior is natural - a simple analysis of the forces developing on the soil wedge clarifies that; the greater the friction between the pile and the clay, the shorter the wedge moving upwards during soil failure in front of the pile. A rough approximation of the transition depth from the wedge-type to the plane-strain failure mechanism indicates an average $z_{w,\,\mathrm{OC}} \approx 4D$ for OC clays according to the findings of the current numerical investigation, regardless of the soil-pile adhesion factor α.

5.3 Effect of small-strain stiffness and structure degradation on p-y curves for OC clays

Paragraph 3.2.2.2 thoroughly described the main principles and features of an advanced MCC-type constitutive law capable of controlling the small-strain stiffness (SSS) and the structure degradation (SD) of stiff, structured soils (Kalos, 2014). Since the current dissertation also deals with stiff, OC clays, the following paragraphs demonstrate a parametric investigation on these two features - SSS and SD - and how exactly they affect the corresponding numerically derived p-y curves. It is very important for the engineer to gain experience on the aforementioned effects through a realistic simulation of such soils and thus the specific evaluation aims towards that direction. The proposal of certain p-y curves for OC clays as an outcome of the present chapter shall incorporate the findings of this investigation. Characteristic frames of the FEA that depict the realistic simulation of the pile-soil interaction for OC clayey soils are included in Appendix C.

There are three main parameters that control the SSS and SD features of this MCC-type constitutive law:

- For the SSS, parameters ξ and λ^* correspond to the proportionality ratio of the PYE to the SSE and the interpolation rule between these two envelopes respectively.
- For the SD, ratio $B = p_m/p_m^*$ refers to the ratio of the SSE to the ISE size.

The investigation of the current section covers a wide range for these features, aiming to simulate both realistic and immoderate OC clay behavior. Thus, the dissertation ascertains which of these parameters significantly affect the corresponding OC clay p-y curves.

Prior to examining the effect of SSS and SD on the OC clay p-y curves, we verify that this advanced constitutive law is robust. For this purpose a decomposition of the specific law takes place. Since the advanced model actually works as an enhanced MCC constitutive law, the current verification must prove that it can successfully downgrade to the MCC framework through proper deactivation of its miscellaneous features.

The aforementioned verification involves a laterally loaded pile of D=1m and α=0.3 in an OC clay with $c_{u,avg}$=190kPa, κ=0.0065, $K_{o,max}$=1.5 and ν=0.1. In order to deactivate the SD characteristic, we assume B=1 that results in absolute coincidence of the ISE and the SSE. Thus, destructuring of the clay does not take place in the specific FEA. Furthermore, by choosing ξ=100% the PYE becomes

equal to the SSE≡ISE and thus no plastic strain accumulation occurs within the yield surface[1]. Figure 5.17 compares the results of the aforementioned FEA with the corresponding ones simulating the OC clay through the in-built MCC of Simulia Abaqus 6.12, both in terms of soil element and pile-soil system response at two different depths.

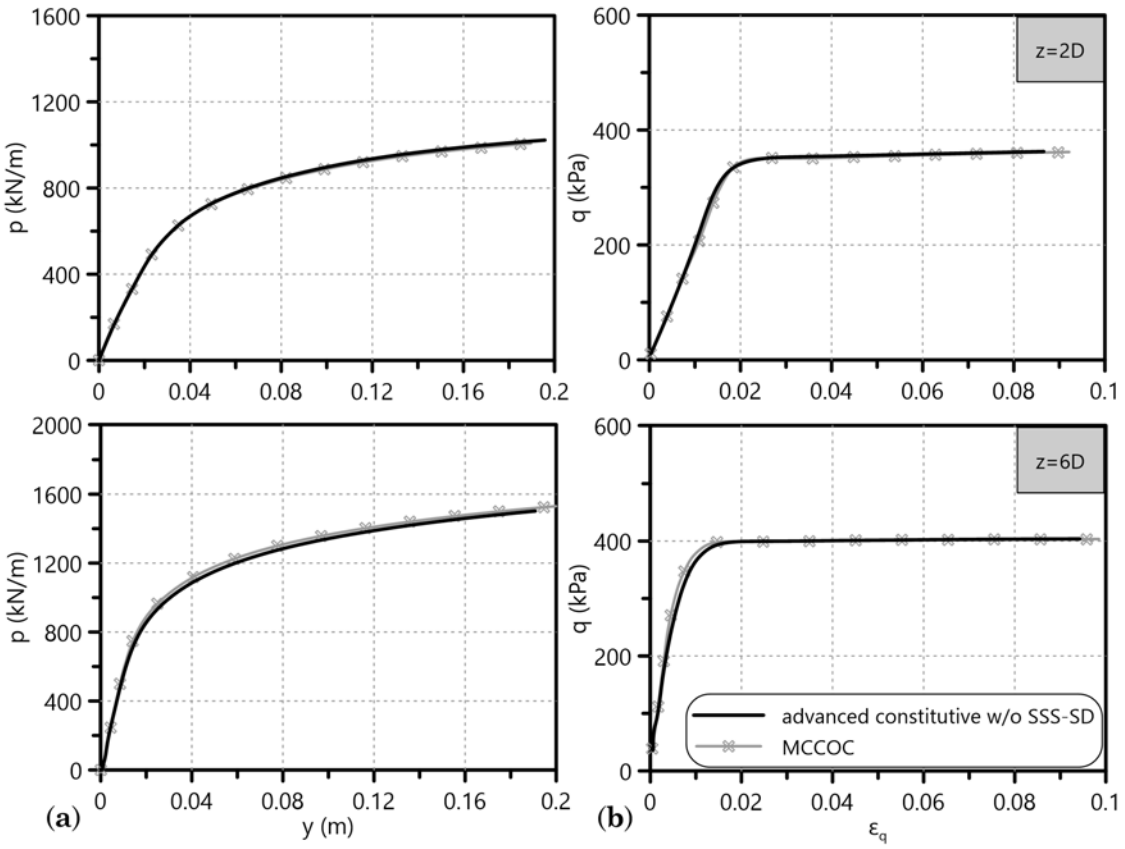

Figure 5.17: OC clay simulation through the MCC and the advanced constitutive law for structured soils downgraded to a MCC. Comparison of the FEA output in terms of (a) p-y curves and (b) $q - \varepsilon_q$ curves at depths z=2D, 6D.

The FEA results of the two OC clay simulations - through the MCC and the decomposed advanced MCC-type constitutive law for structured soils - coincide. This comparison confirms the robustness of the advanced constitutive law for OC clays from the scope of FEA p-y curves (Figure 5.17a) as well as in terms of soil behavior (Figure 5.17b). After the successful verification process of the utilized soil model the section carries on with the parametric investigation of the SSS and SD features.

[1]PYE coincides with SSE in this case and thus the interpolation rule between them does not affect the stress paths. Therefore, a value of λ^*=2 - within the proposed range - is assigned to the OC clay.

5.3.1 Effect of small-strain stiffness (SSS)

The current paragraph investigates the SSS effect on the OC clay constitutive behavior and consequently on the numerical p-y curves through three simple steps:

i Ascertain the effect of ξ (PYE to SSE size ratio) and λ^* (interpolation rule parameter between PYE and SSE) through numerical undrained triaxial tests on a specimen of structured OC clay (B=2) with OCR=3.

ii Determine the influence of the aforementioned parameters on the soil stress-strain curves as well as on the p-y curves through FEA of a laterally loaded pile in a structureless OC clay (B=1) from Table 5.1, assuming constant SSE≡ISE size with depth.

iii Examine how the SSS features affect the $q-\varepsilon_q$ and p-y curves of a structured OC clay (B=3) - within the range of Table 5.1 - through FEA and compare the findings with the remarks from the first process. Evaluate the SSS effect on the p-y curves quantitatively.

The initial purpose of examining the SSS effect on the soil behavior is achieved through numerical undrained triaxial tests (see Paragraph 3.2.2.3 and Figure 3.7 for details on the simulation). Step (i) of the parametric investigation deals with the actual influence that ξ and λ^* have on the stress paths and the stress-strain curves of the OC clay. More accurately, the process assumes a specimen of structured OC clay (B=2) with OCR=3 under vertical effective stress $\sigma_{vo}^{'}$ ≈20kPa (κ=0.0108, $K_{o,OC}$=0.866, M=1.2, ν=0.20) that is triaxially loaded up to relatively small total axial strain, namely ε_q <1%[1]. With axial strain increments of the order of 0.01% the specific numerical triaxial tests are capable of depicting variations of the small-strain stiffness for the soil. Although literature considers even strains of the order of 0.001-0.01% irreversible (Georgiannou, 1988; Jardine, 1995; Smith et al., 1992), such strains are not measurable in the FEA of the current dissertation. In addition, for the range of equivalent $c_{u,avg}$ under investigation by the present chapter (see Table 5.1) such strains definitely refer to the perfectly elastic response of the OC clay.

The triaxial tests of the current investigation step examine SSS parameters ξ and λ^* separately. Three different PYE to SSE ratios are under concern, namely ξ=0.1, 5 and 50% (λ^*=5). The greater the PYE the later the soil element starts accumulating plastic strains since its' initial state is located on the center of this envelope. The following equation accurately calculates the totally elastic deviatoric

[1]The investigation reminds that the axial strain during an undrained triaxial test is equal to the corresponding deviatoric strain of the specimen ($\varepsilon_a = \varepsilon_q$)

strain within the PYE under undrained triaxial loading conditions:

$$\varepsilon_{q,\,\mathrm{PYE}} = \frac{\sqrt{2/3}M \cdot \xi\, a_{\mathrm{SSE}}}{2G} \tag{5.1}$$

where a_{SSE}=$p_{m,/,\mathrm{SSE}}/2$ and G= the shear modulus of the soil. Values of ξ=0.1-5% are rational, while a proportionality ratio equal to 50% is rather exaggerated and aims at ascertaining the potential influence of the parameter on the constitutive behavior of the OC clay. Figure 5.18a demonstrates almost negligible effect of ξ both on the stress paths and the $q-\varepsilon_q$ curves of the soil element. Especially when referring to the SSS behavior - ε_q <0.2% - the size of PYE plays no role at all. Such an observation seems reasonable since ξ controls only the size of the PYE and therefore the initiation of plastic strain development, not the strain accumulation ratio. The latter is associated with the λ^* parameter. In more detail, λ^* controls how fast the PYE will touch the SSE; when it does so, the SSE and the ISE start moving towards each other and the destructuring process takes place. Three different interpolation rule parameters are examined, namely λ^*=0.1, 5 and 20 (ξ=5%). Figure 5.18b depicts the significance of λ^* in the SSS feature - influencing the small-strain behavior more intensely than ξ. The lower λ^* the slower the accumulation of plastic strains and the lower the peak strength reached at realistic ε_q. We also observe that a significant increase in λ^* - from 5 to 20 - reflects no actual effect on the SSS for ε_q <0.2%. Summarizing the findings of the numerical undrained triaxial tests for the SSS investigation, λ^* is profoundly the dominant SSS parameter and shall be examined further in the following steps - introducing the FEA of the laterally loaded pile. A value of ξ=5% is realistic and robust for the numerical simulation of the current problem.

It is clear that the three yield surfaces of the advanced constitutive law for structured soils are tightly related with one another, adding complexity to the interpretation of the OC clay stress-strain behavior. Therefore, the features of SSS and SD are disengaged from each other during the following parametric investigation of λ^*. Step (ii) examines the potential effect of the dominant SSS parameter, i.e. λ^*, on the OC clay p-y curves through FEA of the laterally loaded pile of D=1m. The numerical analyses simulate the SSS feature of the structureless OC clay ($c_{u,\,avg}$=190kPa, κ=0.0065, $K_{o,\,max}$=1.5, M=1.2, ν=0.1) - the SSE coincides with the ISE - with three different values of λ^*=0.1, 2 and 20 (ξ=5%). Figure 5.19 depicts (a) the behavior of the pile-soil system in terms of p-y curves and compares it with (b) the OC clay response at depth z=$2D$, $6D$ through the corresponding $q-\varepsilon_q$. The aforementioned graphs from the FEA utilizing the MCC for the OC

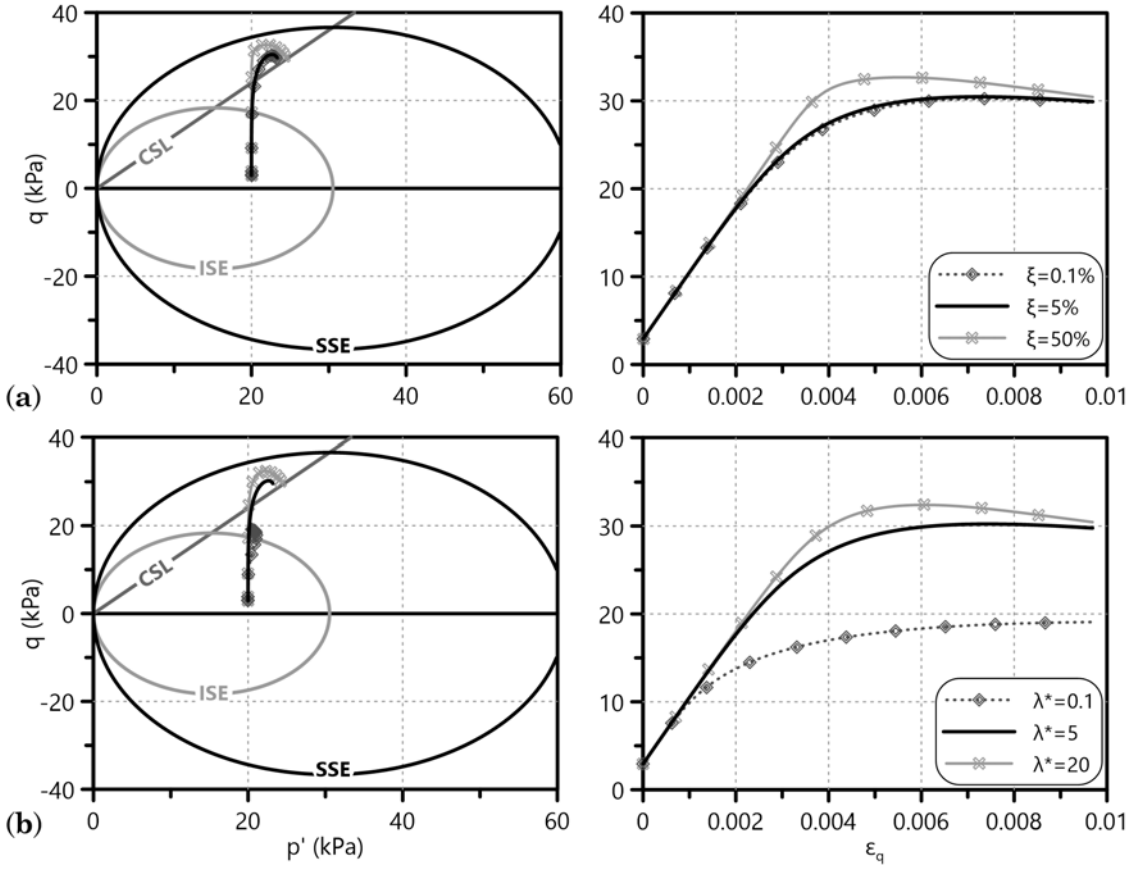

Figure 5.18: Parametric investigation of small-strain stiffness characteristics through numerical undrained triaxial tests on a structured OC clay specimen (OCR=3, σ'_{vo} ≈20kPa, κ=0.0108, $K_{o,OC}$=0.866, M=1.2, ν=0.20). Stress paths and deviatoric stress-strain curves for (a) various PYE to SSE proportionality ratios ξ (λ^*=5) and (b) various interpolation rule parameter values λ^* (ξ=5%) between the aforementioned envelopes.

clay simulation are also included in the previous figure for comparison purposes.

Starting from the OC clay constitutive behavior, Figure 5.19b demonstrates the already observed tendency of λ^* to smoothen the transition from the initial stiffness part to the failure stress plateau when receiving very low values - here 0.1. Although the ductile comportment for λ^*=0.1 is not typical of a stiff, OC clay, the specific depiction aims at presenting the SSS range that the sophisticated constitutive law can simulate. On the other hand, mid-range and high λ^* values exhibit no variation in $q-\varepsilon_q$ graphs compared to the corresponding behavior of the MCC soil simulation. It is very important to derive a realistic OC clay stress-strain behavior from the FEA, i.e. peak strength at ε_q <2%. Therefore, the FEA of the OC clay simulated with both SSS and SD features shall not utilize values of λ^* <2 according to the aforementioned plots.

Since λ^* controls the SSS behavior of the OC clay, one would expect significant

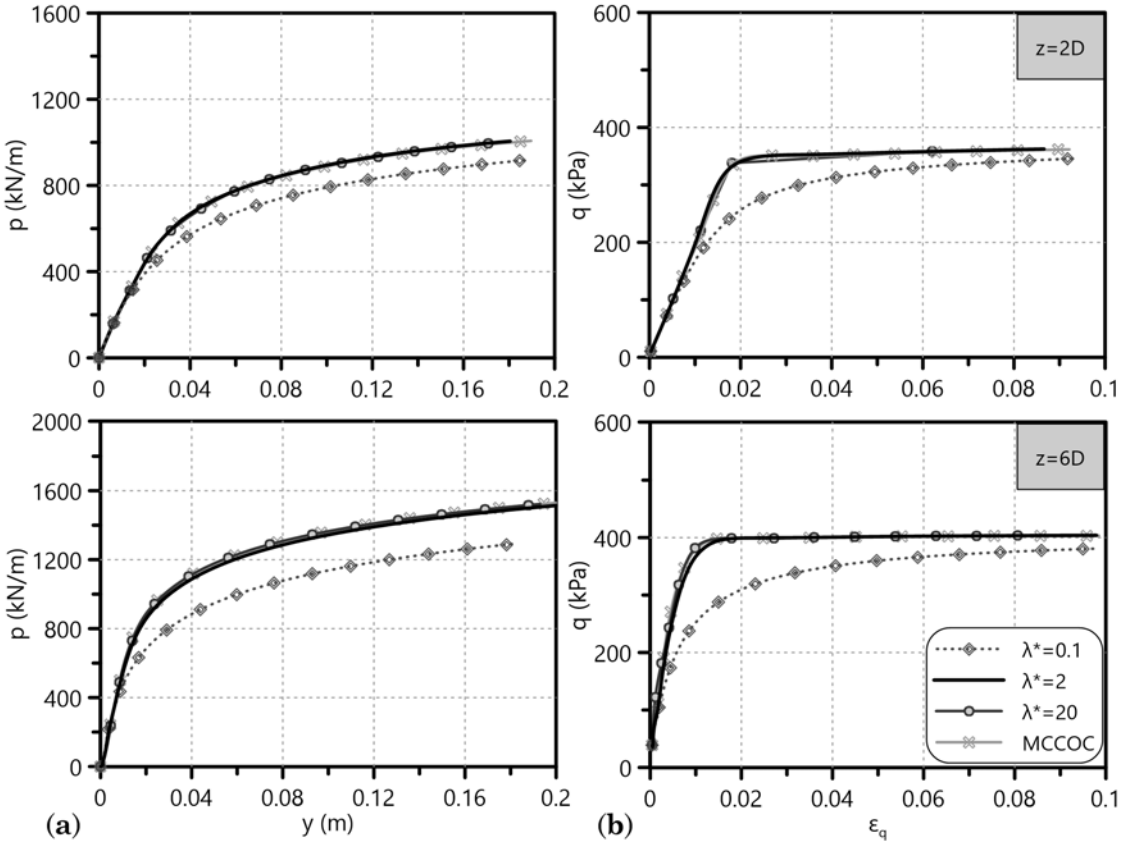

Figure 5.19: Effect of SSS parameter λ^* (ξ=5%) on (a) the p-y curves and (b) the $q-\varepsilon_q$ curves at two different depths of a structureless OC clay (B=1), derived from FEA output.

effect on K_i of the corresponding p-y curves at first thought. On the contrary, Figure 5.19a demonstrates an effect on the post-yield response of the p-y curves and thus on p_u for the lowest value of the parameter, i.e. λ^*=0.1. After considering the physical meaning of λ^*, the investigation comes up with the following explanation on this p-y curve effect: λ^* actually controls how much brittle or ductile the stress-strain behavior of the clay is. For a structureless OC clay simulation, where peak strength is independent from the SSE-ISE interaction since they coincide, the lower λ^* is the later the PYE reaches the SSE≡ISE and thus peak soil strength. As a consequence, the p-y curves corresponding to low λ^* values yield earlier than the others - at lower y - and thus demonstrate lower p_u at a specific lateral displacement assumed equal to y=20%D. The p-y curves of Figure 5.19a represent the pile-soil system behavior that transforms a low SSS (λ^*=0.1) in terms of soil stress-strain response into low p_u of the curves. However, such low λ^* values refer to the lower limit of the parameter range and therefore the current investigation will not deal further with its' influence on the ultimate lateral soil resistance of the p-y curves. It now remains to ascertain how λ^* affects the SSS in the complete advanced constitutive law, i.e. SSS and SD,

during the FEA of the laterally loaded pile in OC clay.

Step (iii) attempts to clarify the necessity - or not - of the SSS feature for the numerical development of OC clay p-y curves utilizing the sophisticated constitutive law (see Paragraph 3.2.2.2). FEA of the specific step involve the numerical simulation of a structured OC clay with SSE to ISE size ratio B=3 - corresponds to peak strength reduction around 50% - and the following strength and stiffness characteristics: $c_{u,\,avg}$=190kPa, κ=0.0054, $K_{o,\,max}$=1.5, M=1.2, ν=0.1. Values of λ^*=0.4, 2 and 20 alter the SSS of the OC clay in a sufficient range. Figure 5.20 depicts the derived numerical p-y curves together with the corresponding $q-\varepsilon_q$ curves at various soil depths, namely z=2, 4, 6 and 8D (D=1m). The aforementioned graphs from the FEA utilizing the MCC for the OC clay simulation are also included in this figure for comparison purposes.

Figure 5.20b locates the effect of λ^* on both the SSS and the peak strength of the clay. While the first is natural, the second is not that clear. Only if we consider the intense accumulation of plastic strains for low λ^* values does the lower peak strength in the $q-\varepsilon_q$ curves seem reasonable. The more the plastic strains at the same deviatoric stress level the longer the yield section of the clay and thus the smaller the size of the SSE when it starts destructuring towards the initial ISE[1]. Apart from this influence in the peak strength of the clay, the effect of λ^* on the SSS of the stress-strain behavior is rather insignificant. Figure 5.20a confirms that statement in terms of OC clay p-y curves; λ^* variation does not really affect the transition from the initial elastic part to the ultimate lateral soil resistance plateau of the numerical p-y curves. In addition, various λ^* values do not result in significant differentiation of p_u - among the results from the FEA of the structured soil - apart from the last depth examined (z=8D).

Summarizing the findings of the aforementioned parametric investigation on the SSS parameters (ξ, λ^*) of the sophisticated constitutive model to simulate stiff, structured, OC clays in the ongoing research, the following points are of concern:

- The size of the PYE is not important for the SSS since it controls the initiation and not the development rate of plastic strains. The latter is controlled by λ^* and results in significant variation of both the SSS and the peak strength of the OC clay, according to numerical undrained triaxial tests.

- The λ^* parameter affects the ultimate lateral soil resistance of the p-y curves according to FEA of the laterally loaded pile in a structureless (B=1) OC clay. However, λ^* values that led to this observation refer to non-realistic

[1]The shrinking of the SSE begins with the first deviatoric plastic strains that occur during the loading process.

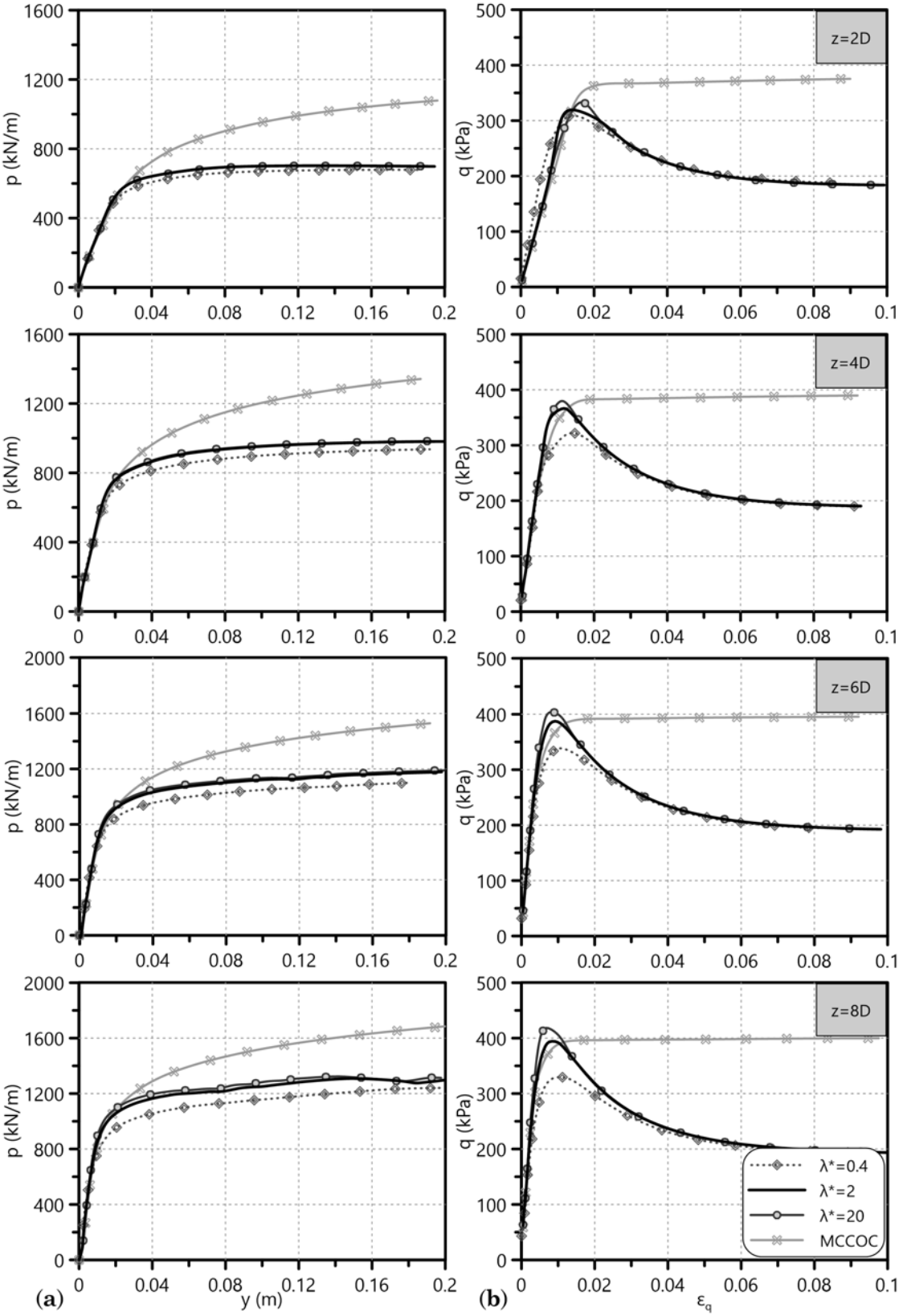

Figure 5.20: Effect of SSS parameter λ^* (ξ=5%) on (a) the p-y curves and (b) the $q-\varepsilon_q$ curves at various depths of a structured (B=3) OC clay ($c_{u,\,avg}$=190kPa, κ=0.0054, $K_{o,\,max}$=1.5, M=1.2, ν=0.1), derived from FEA output.

stress-strain curves of the soil - in terms of deviatoric strain, at which the clay reaches its' peak deviatoric stress. In general, the lower λ^* the more ductile the OC clay constitutive behavior.

- FEA of the laterally loaded pile in a structured, OC clay (B=3) demonstrate even less influence of λ^* in the numerical p-y curves - SSS and p_u. Consequently, as long as changes in the SSS of the soil do not affect the "yielding" part of the OC clay p-y curves significantly, the proposed p-y equations for such soils shall not include any parameters related to the SSS control.

According to these points, the pile-soil system response (p-y) overlies the constitutive behavior of the single soil element ($q-\varepsilon_q$) as far as small-strain stiffness is concerned. On the contrary, structure degradation seems very influential on p_u (Figure 5.20a) and thus the current dissertation shall investigate it further.

5.3.2 Effect of structure degradation (SD)

The following paragraphs attempt to clarify the effect of the potential OC clay structure degradation (SD) on the numerical p-y curves. Literature methodologies seem divided on whether the post-peak strength behavior of stiff clays, i.e. strength reduction of the soil, affects or not the corresponding p-y curves of the pile-soil system (see Figure 2.64). In more detail, Reese & Welch (1975), DNV (1977) and Sullivan et al. (1979) claim that p-y curves for stiff clays reflect the microscale post-peak strength reduction of the soil. The rest of the p-y methodologies applicable to stiff clays (Dunnavant & O'Neill, 1989; Georgiadis & Georgiadis, 2010; Jeong et al., 2011; Welch & Reese, 1972; Wu et al., 1998) propose p-y curves without any degradation of the p_u. Therefore, the current section investigates which approach is more realistic through FEA that utilize the aforementioned sophisticated constitutive law for the simulation of OC clays - incorporating the SD feature.

This advanced MCC-type constitutive model is capable of controlling the SD of the OC clay through the two following parameters:

- Parameter η that determines how steep or smooth the transition from the peak to the residual strength of the clay is - in terms of stress-strain behavior. The specific constitutive parameter relates itself to the accumulation of plastic strains, mainly deviatoric ones since the undrained loading of the soil leads to typically zero volumetric strain.

- Size ratio $B = p_m/p_m^*$ of the SSE to the ISE that controls the strength degradation percentage. B is not the actual residual-to-peak strength ratio itself

but different B values correspond to a variety of strength ratios, as the following paragraphs explain. For clarity's sake, the dissertation introduces the undrained shear strength degradation ratio RF, according to equation:

$$RF = \frac{q_{\text{residual}}/2}{q_{\text{peak}}/2} = \frac{c_{u,\,\text{res}}}{c_{u,\,\text{peak}}} \tag{5.2}$$

Since SSS does not affect significantly the derived p-y curves in the range of lateral displacements y that the current dissertation examines, the following parametric investigation on the SD feature assumes λ^*=2 and ξ=5%.

Initially, we perform numerical undrained triaxial tests on a structured OC clay specimen at vertical effective stress $\sigma_{vo}^{'}$ ≈50kPa ($c_{u,\,avg}$=190kPa, κ=0.0065, $K_{o,\,max}$=1.5, M=1.2, ν=0.1) in order to verify the effect of the aforementioned parameters on the constitutive behavior of the soil, i.e. stress paths and $q-\varepsilon_q$ curves. The specific stress field ($\sigma_{vo}^{'}$ ≈50kPa) corresponds to a depth z=5D for a pile diameter D=1m, thus representing the behavior trend of the loaded soil mass[1] in front of a laterally loaded pile. Figure 5.21 demonstrates how η and B affect the stress paths and deviatoric stress-strain curves of the OC clay specimen. The aforementioned graphs from the numerical tests utilizing the MCC for the OC clay simulation are also included in the previous figure for comparison purposes.

More accurately, Figure 5.21a displays the influence of various η values, namely 20, 50 and 150, on the strength degradation rate assuming a residual-to-peak strength ratio RF=0.5 (B=3). Higher η corresponds to more abrupt structure degradation and delivers peak strength at slightly lower axial strain, although practically insignificant. The stress paths initiate from the hypothetical K_o-line, follow the route of the PYE towards the diminishing SSE and turn towards the ISE on the CSL. It is important to observe how this characteristic hook form of the stress paths shrinks with increasing values of η. After the aforementioned parametric investigation we pick η=50 as the representative value controlling the transition from peak to residual strength for the OC clay simulation during the rest of the current chapter. Thus, the dissertation assumes that the simulated OC clay reaches its' residual undrained shear strength for axial (deviatoric) strain ε_q <10%, but also not much lower than that (see η=150). It is obvious that only experimental data from triaxial tests are capable of calibrating η successfully. However, the current dissertation focuses on the qualitative effect of the specific parameter on the stress-strain behavior - and through that on the derived p-y curves - and thus adopts this generally realistic

[1]The dissertation assumes a maximum depth of influence for the clay surrounding the laterally loaded pile equal to 10D.

strength degradation pattern for the OC clays of the following FEA.

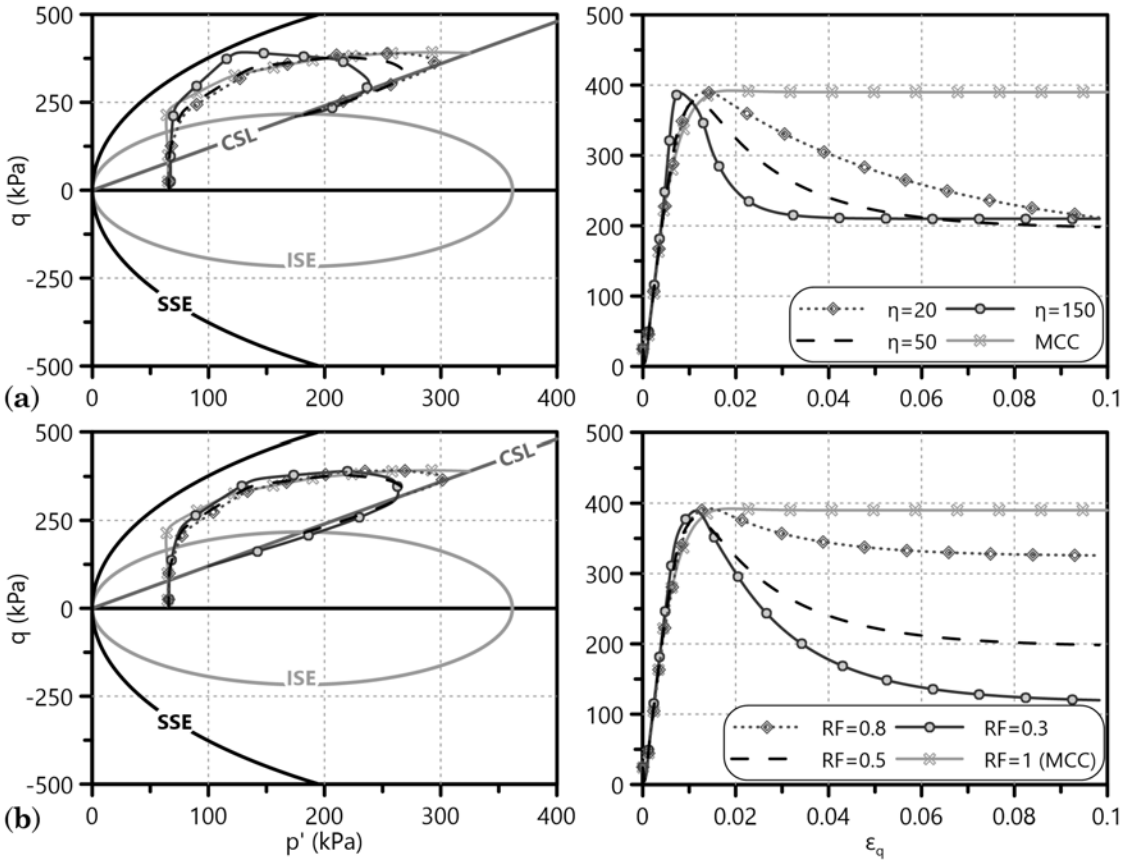

Figure 5.21: Parametric investigation of structure degradation characteristics through numerical undrained triaxial tests on a structured OC clay specimen (σ'_{vo} ≈50kPa, $c_{u,avg}$=190kPa, κ=0.0065, $K_{o,max}$=1.5, M=1.2, ν=0.1). Stress paths and deviatoric stress-strain curves for (a) various strength degradation rates controlled by η (B=3) and (b) various residual-to-peak strength ratios RF (η=50) - SSE and ISE of the latter refer to RF=0.5.

On the other hand, Figure 5.21b demonstrates the effect of B ratio on the behavior of the triaxially loaded OC clay specimen. The investigation examines three different values of B=1.5, 3 and 6 corresponding to RF=0.8, 0.5 and 0.3 respectively. The higher B the greater the undrained shear strength degradation of the clay. The general idea is to simulate three different destructuring patterns: a mild (RF=0.8), a moderate (RF=0.5) and an intense one (RF=0.3). Thus, the FEA of the laterally loaded pile to follow shall ascertain the quantitative effect of strength degradation on the derived p-y curves for the correspondingly simulated OC clays. Although there is no actual influence of B on the stress paths, its' effect on RF is profound - as expected.

The next step of the current parametric investigation on the SD feature refers to FEA of the laterally loaded pile in OC clays of various RF ratios. The FEA involve

a pile of D=1m and α=0.3 in an OC clay with the following strength and stiffness characteristics: $c_{u,\,avg}$=190kPa[1], κ=0.0054, $K_{o,\,max}$=1.5, M=1.2, ν=0.1. Figure 5.24 compares the derived p-y and $q-\varepsilon_q$ curves at depths z=2, 4, 6 and 8D for four different residual-to-peak undrained shear strength ratios RF=1.0, 0.8, 0.5 and 0.3, corresponding to of B=1 (the classic MCC), 1.5, 3 and 6 respectively. Similar graphs are derived from FEA output of the same pile on stiffer and softer OC clays, namely with $c_{u,\,avg}$=95 and 380kPa respectively, which the current parametric investigation does not include for brevity. Figure 5.22 confirms that for lateral pile displacement $y < 20\%D$ the OC clay in front of the pile has reached its' $c_{u,\,\mathrm{res}}$ both at z=2D and 6D (see Figure 3.34 for the exact soil element position on the plan view). It remains to ascertain how RF affects the numerical p-y curves. The derived p-y curves for the

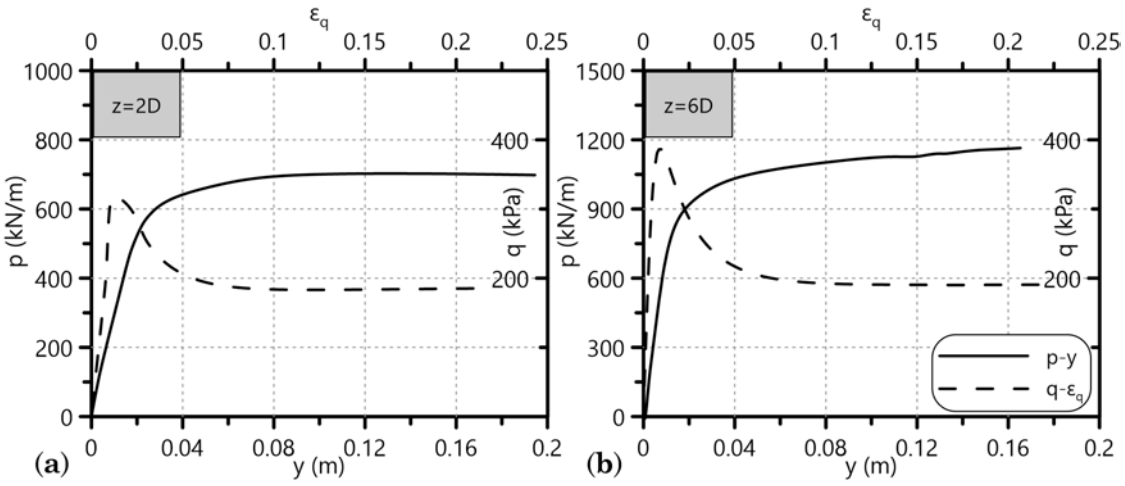

Figure 5.22: Parallel depiction of p-y and $q-\varepsilon_q$ curves for $y < 20\%D$ at (a) z=2D and (b) z=6D ($c_{u,\,avg}$=190kPa, κ=0.0054, $K_{o,\,max}$=1.5, M=1.2, ν=0.1), derived from FEA output.

OC clays with strength degradation naturally exhibit lower p_u than that of the MCC simulation. However, none of them reflects the strength degradation pattern of the corresponding $q-\varepsilon_q$ curves, except for the p-y curves of the intense RF=0.3 - and only slightly. Especially about RF=0.3 (B=6) one notices some smooth degradation of p_u on the numerical p-y curves of the order of magnitude around 10%. Such low p_u reduction for such intense - almost unrealistic - strength degradation of the OC clay supports the aforementioned observation concerning the effect of RF on the specific part of the p-y curves. This is a very important observation because it clarifies that the pile-soil response (p-y) dominates, causing the strength degradation pattern of the OC clay stress-strain behavior ($q-\varepsilon_q$) to fade out when projected to the system

[1]In the mid range of the OC clay strength values that the current chapter examines (see Table 5.1)

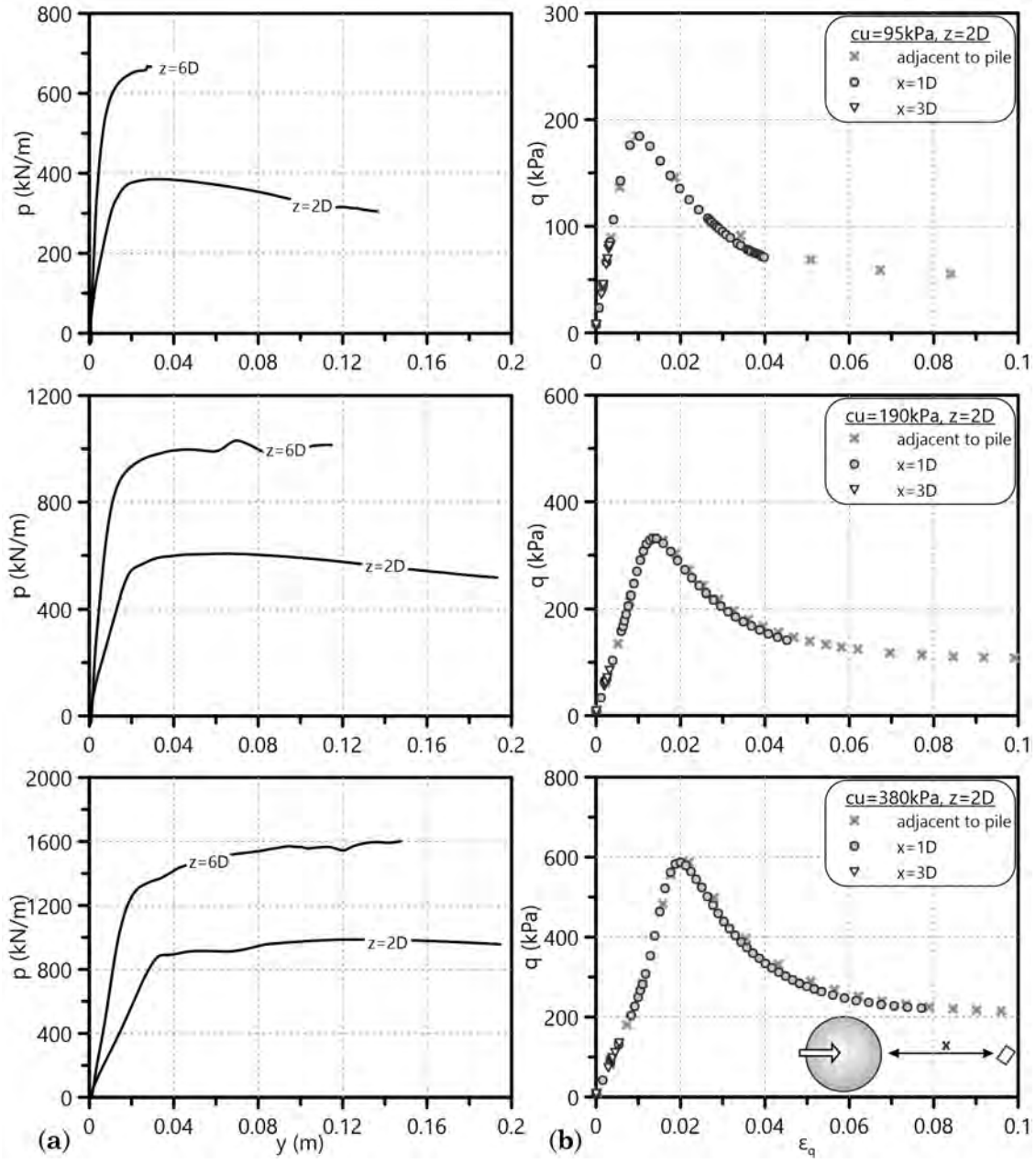

Figure 5.23: Parallel depiction of (a) p-y curves at z=2D, 6D and (b) $q - \varepsilon_q$ curves at z=2D at three different horizontal distances from the pile edge, namely x=0, 1 and 3D ($c_{u,\,avg}$=95, 190, 380kPa, RF=0.3, κ=0.0054, $K_{o,\,max}$=1.5, M=1.2, ν=0.1). All FEA output at the time frame when $y_{\mathrm{z=2D}} = 20\%D$.

behavior - according to the FEA output. As a matter of fact, only the soil elements at close proximity to the pile, i.e. up to $2D$ radial distance from the pile periphery, are loaded in such an intense manner to exhibit the strain softening behavior of Figure 5.24b. Figure 5.23a shows the derived p-y curves for three different OC clays with intense strength degradation (RF=0.3) at z=$2D$, $6D$, while Figure 5.23b confirms the aforementioned observation; soil elements at horizontal distance x=$3D$ do not even yield for pile head lateral displacement equal to 30%D. Thus, the current investigation concludes that the system behavior results in no actual degradation pattern of the OC clay p-y curves, just some p_u reduction depending on the RF level.

The following points summarize the observations of the aforementioned parametric investigation on the SD parameters (η, B) of the sophisticated constitutive model to simulate stiff, structured, OC clays:

- The constitutive law for the advanced simulation of structured OC clays offers the ability to control the strength degradation rate of the stress-strain curve, i.e. how steep or smooth the transition from peak to residual strength is. Parameter η of the model controls this transition. $q-\varepsilon_q$ curves from numerical undrained triaxial tests on an OC clay specimen under $\sigma_{vo}^{'}$ ≈50kPa for various η values lead to the following assumption: considering that the clay reaches its' residual strength $c_{u,\,\mathrm{res}}$ at an axial strain (deviatoric for undrained loading) ε_q <10%, η=50 delivers a quite realistic deviatoric stress-strain behavior and therefore the upcoming simulations for such soils will utilize the specific value. Future studies may calibrate η using experimental data from undrained triaxial tests on real OC clay specimens.

- The undrained shear strength degradation ratio $RF = c_{u,\,\mathrm{res}}/c_{u,\,\mathrm{peak}}$ is introduced and its effect on the numerical p-y curves is verified. The p-y curves derived from the FEA output depict that RF affects the p_u, i.e. lower RF (intense strength degradation) results in lower p_u compared to the corresponding ultimate lateral soil resistance of the MCC simulation - that delivers practically no strength degradation.

- Although OC clay stress-strain curves may exhibit very intense peak strength reduction (B=6), the corresponding numerical p-y curves tend to diminish such a pattern for the post-peak lateral response. Therefore, the current section concludes that for realistic lateral pile displacements, i.e. $y < 20\%D$, and physically rational RF no p_u reduction occurs in the proposed p-y curves for OC clays.

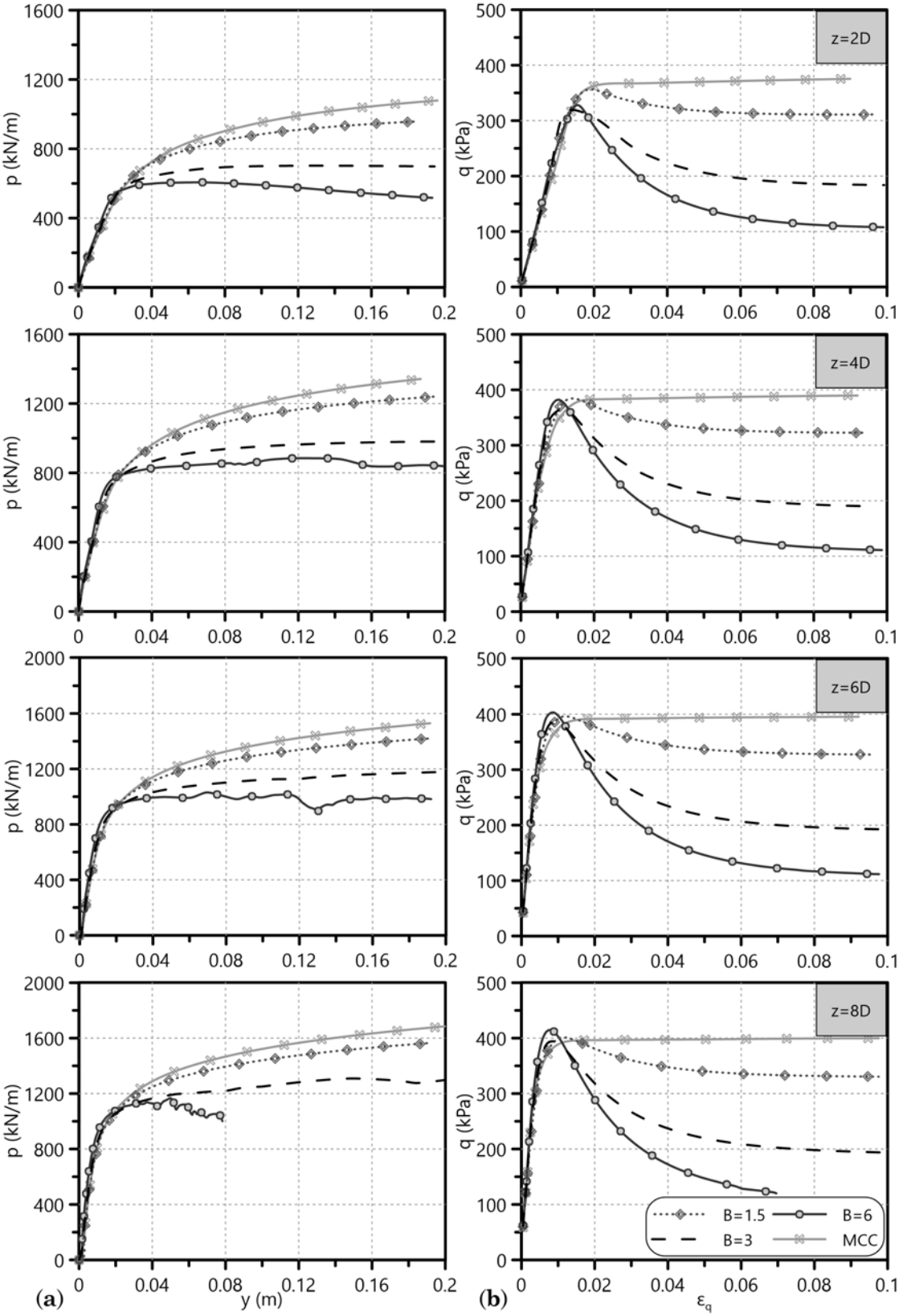

Figure 5.24: Effect of the SD parameter B (η=50) - representing the SSE to the ISE size ratio - on (a) the p-y curves and (b) the $q-\varepsilon_q$ curves at various depths of structured OC clays ($c_{u,\,avg}$=190kPa, κ=0.0054, $K_{o,\,max}$=1.5, M=1.2, ν=0.1), derived from FEA output.

As long as this section has ended up with certain remarks on the effect of the SSS and SD features on numerically derived OC clay p-y curves, the paragraphs to follow shall propose specific equations and processes for the accurate formulation of such curves.

Note: The aforementioned examination of the SSS and SD constitutive parameters requires a thorough calibration of the peak strength that the sophisticated law delivers - utilizing a certain combination of these parameters - with the corresponding OC clay strength simulated through the MCC. Such a calibration is quite complicated and demands the determination of the SSE and the ISE sizes through a trial-and-error procedure that exceeds the scientific boundaries of the present chapter. Therefore, Appendix B demonstrates the process followed in order to achieve this successful match of undrained peak strengths between the MCC simulation and that incorporating the advanced MCC-type constitutive law of Paragraph 3.2.2.2.

5.4 Monotonic p-y curves for OC clays

The current section presents the formulation procedure of p-y curves for OC clays, namely with almost constant undrained shear strength with depth, according to the corresponding numerical investigation of the dissertation. The renowned hyperbola Equation 5.3 (left) fits satisfactorily the numerical p-y curves for OC clays without strength degradation, i.e. FEA simulating the OC clay constitutive behavior through the MCC. In order to ascertain more accurately the initial stiffness K_i and the ultimate lateral soil resistance p_u of the numerical p-y curves we transform the hyperbola into a linear form (Equation 5.3). Figure 5.25 depicts this transformation and the corresponding calculations for K_i and p_u at two different depths (z=2D, 6D) of a stiff OC clay.

$$p = \frac{y}{\frac{1}{K_i} + \frac{y}{p_u}} \quad \Leftrightarrow \quad \frac{y}{p} = \frac{1}{K_i} + \frac{1}{p_u} \cdot y \tag{5.3}$$

Thus, this section gathers these two main p-y curve features (K_i, p_u) for the OC clays of the FEA (see Table 5.1 for the range of parameters) and relates them to certain soil and pile properties. This process also includes a parametric investigation on RF (Equation 5.2) and quantifies its' effect on the p-y form. Figure 5.26 demonstrates that the hardening p-y behavior of all the OC clays without strength degradation (RF=1) converts to a clear p_u plateau when taking the aforementioned

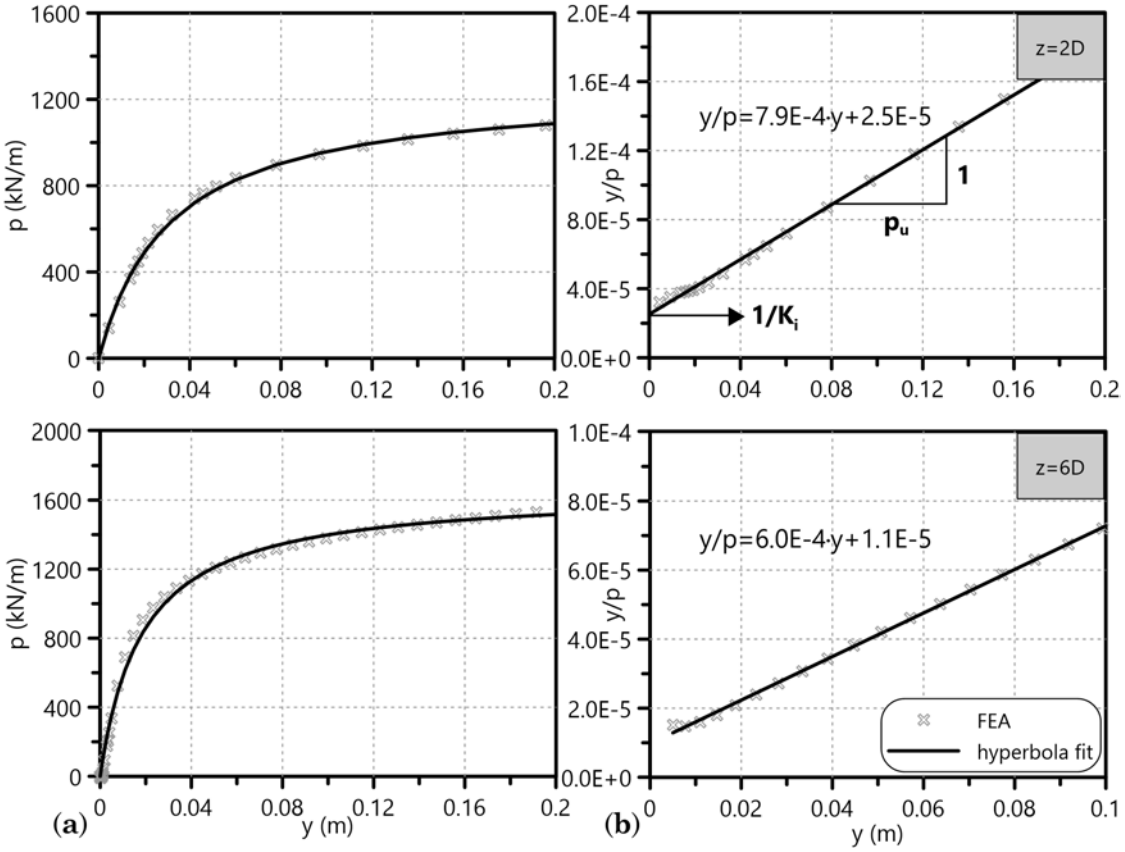

Figure 5.25: Hyperbola fit with FEA output in (a) the actual and (b) the linear form of the hyperbolic equation ($c_{u,\,avg}$=190kPa, κ=0.0054, $K_{o,\,max}$=1.5, M=1.2, ν=0.1).

feature into account ($RF < 1$). Therefore, the dissertation proposes the following exponential p-y form (applicable to NC clay p-y curves in Chapter 4) for stiff OC clays that exhibit strength softening during specimen testing:

$$\frac{p}{p_u} = 1 - \exp\left(\frac{-K_i \cdot y}{p_u}\right)$$

The following paragraphs introduce certain modifications of K_i and p_u to fit the FEA output of OC clays with $RF < 1$ through the exponential p-y form.

The section finishes with a step-by-step procedure for the formulation of OC clay p-y curves and a comparison of the FEA findings with the corresponding literature proposals.

5.4.1 Initial stiffness K_i of p-y curves for OC clays

This paragraph presents the FEA output processing in order to acquire K_i equations with certain OC clay stiffness parameters, i.e. unloading-reloading line slope κ and

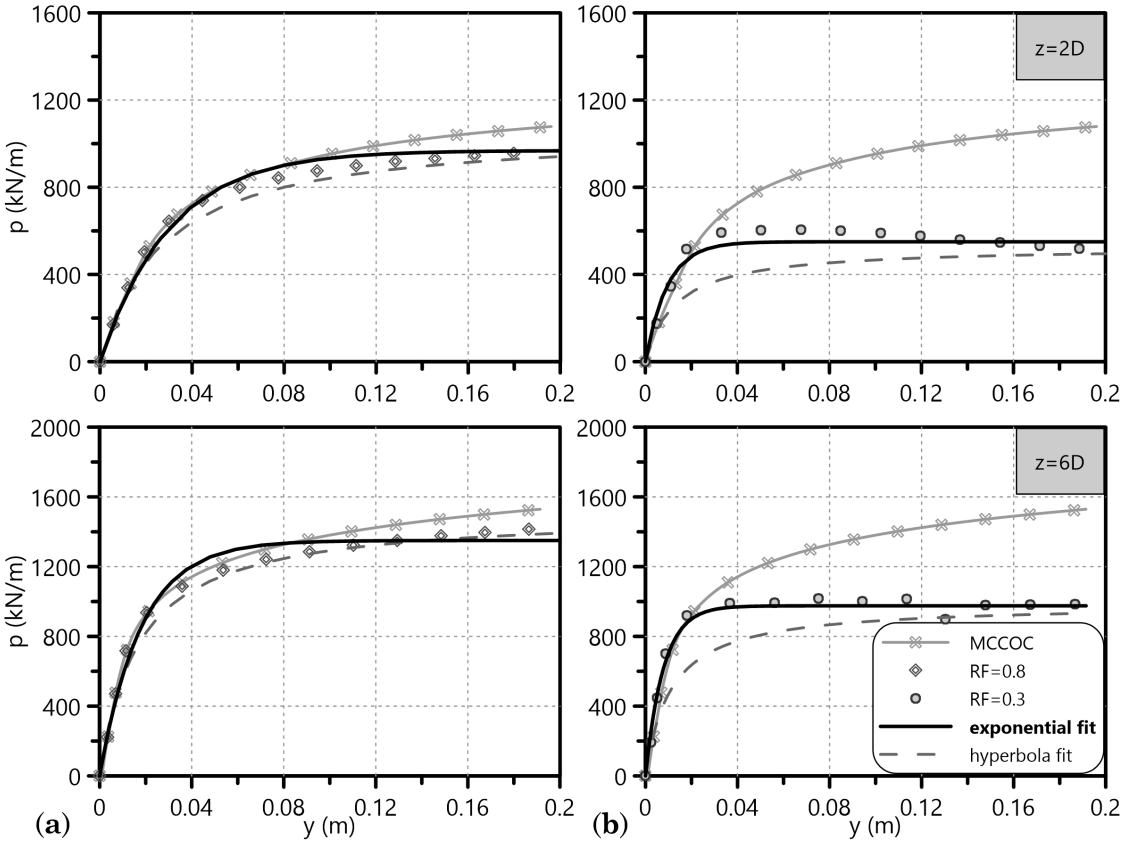

Figure 5.26: Better fitting capability of the exponential versus the hyperbolic form on the numerical p-y curves derived at z=2D and 6D for (a) RF=0.8 and (b) RF=0.3 ($c_{u,\,avg}$=190kPa, κ=0.0054, $K_{o,\,max}$=1.5, M=1.2, ν=0.1).

Poisson's ratio ν[1]. Compared to the corresponding formulations for NC clays, K_i follows a linear distribution with depth also for OC clays. However, while $K_i \approx 0$ at ground level for NC clays, it has an initial value $K_{i0} > 0$ for OC clays. Therefore, the thesis proposes the following equation:

$$K_i = n \cdot z + K_{i0} \tag{5.4}$$

As a result, the fitting process suggests specific correlations of n and K_{i0} with κ and ν. Figure 5.27a depicts the best fits of K_i with depth z for κ=0.0033, 0.0065 and 0.0174, constant ν=0.1, $c_{u,\,avg}$=50-380kPa and D=0.5-2.0m. In a similar manner - although for fewer FEA - Figure 5.27b correlates the parameters of Equation 5.4 with Poisson's ratio for ν=0.1, 0.2 and 0.333, constant κ=0.0054, $c_{u,\,avg}$=190kPa and D=1.0m. The procedure assumes that the adhesion factor does not affect K_i, thus the aforementioned fits refer to FEA of a smooth pile (α=0.3). All $K_i - z$

[1]Figures 5.8 and 5.12 imply that these two OC clay parameters significantly affect K_i.

distributions of Figure 5.27 correspond to $z \leq 10D$ since the lateral response of a flexible pile is of concern up to that maximum depth during design. The following equations represent the desired correlations of n and K_{i0} with κ and ν:

$$n(\kappa) = 270 \cdot \kappa^{-0.77} \tag{5.5a}$$

$$K_{i0}(\kappa) = 8.4 \cdot \kappa^{-1.3} \tag{5.5b}$$

$$n(\nu) = -30000 \cdot \nu + 17000 \tag{5.5c}$$

$$K_{i0}(\nu) = -66000 \cdot \nu + 24000 \tag{5.5d}$$

Finally, the parameters n and K_{i0} of the proposed Equation 5.4 for the initial stiffness of OC clay p-y curves receive the following form:

$$K_i = n \cdot z + K_{i0}$$

$$n = 270 \cdot \kappa^{-0.77} \cdot (-2.07 \cdot \nu + 1.17) \tag{5.6a}$$

$$K_{i0} = 8.4 \cdot \kappa^{-1.3} \cdot (-6.14 \cdot \nu + 2.23) \tag{5.6b}$$

Paragraph 5.4.3 examines whether strength degradation of stiff clays affects the K_i calculated during the aforementioned fitting process.

5.4.2 Ultimate lateral soil resistance p_u of p-y curves for OC clays

Since the shape of OC clay p-y curves represents a constantly hardening behavior - in contrast with p-y curves for NC clays that demonstrate a profound ultimate resistance plateau - the current investigation can only suggest a p_u at a specific y for such curves. The current dissertation aims to propose numerically developed p-y curves for realistic lateral pile displacements in terms of design. Thus, the following p_u calculations refer to $y \leq 0.2D$ at all the examined depths - a value that corresponds to failure even for the head of the laterally loaded pile.

The current numerical investigation normalizes the FEA derived p_u through the ultimate lateral soil resistance factor $N_p = p_u/(c_u\, D)$. Paragraphs 5.2.1 and 5.2.2 indicate significant effect of $c_{u,\,avg}$, κ, α and D on p_u (Figures 5.7, 5.8, 5.14 and 5.13 respectively). It remains to ascertain whether these parameters also affect the

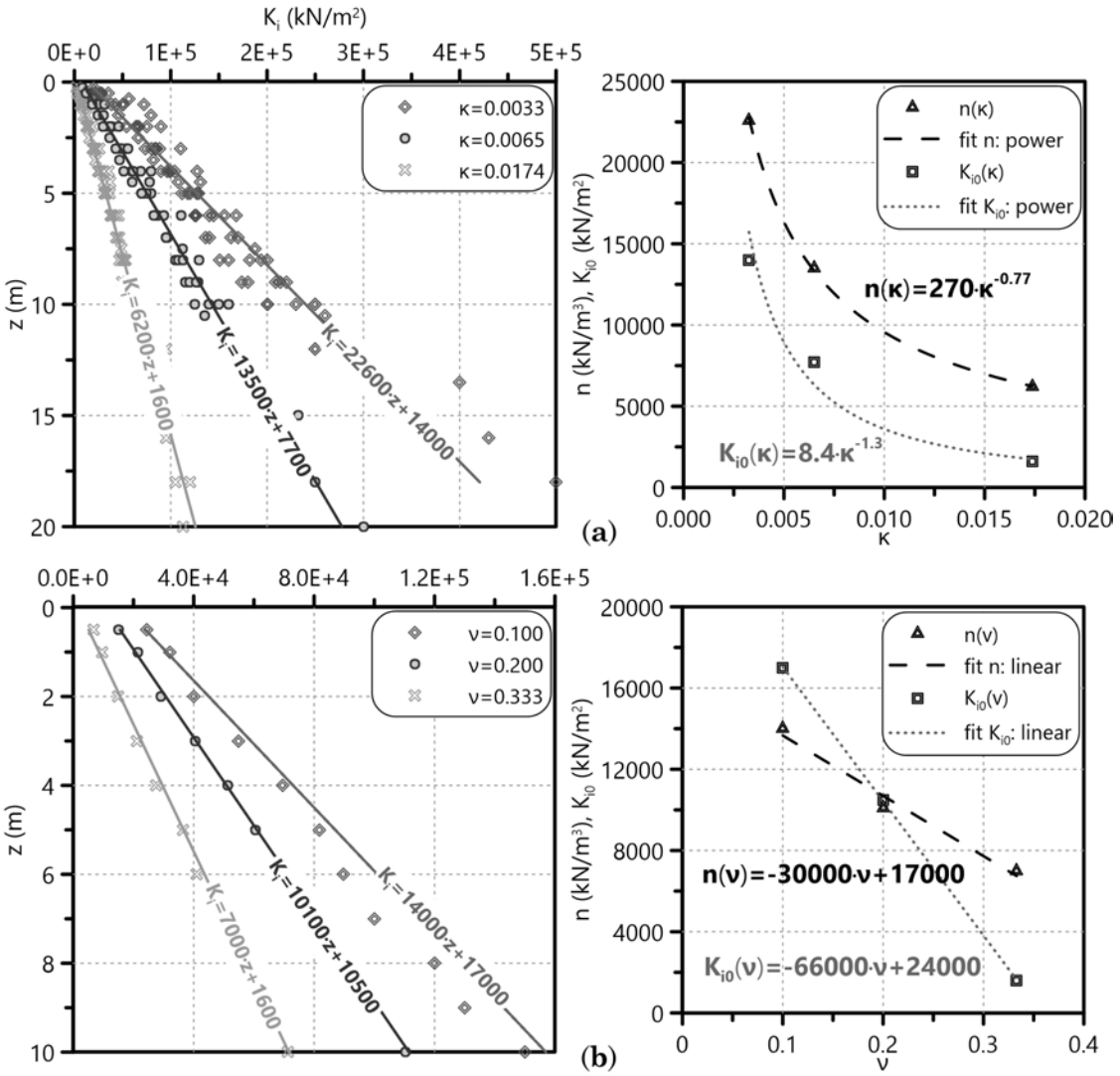

Figure 5.27: Determination of n-slope and ground level stiffness K_{i0} in the linear initial stiffness function $K_i(z) = n \cdot z + K_{i0}$ of numerical p-y curves for OC clays. Effect of (a) unloading-reloading lines slope κ and (b) Poisson's ratio ν on n and K_{i0}.

distribution of N_p with z/D. Figure 5.29 depicts these effects and implies that each of them has an important impact on N_p. The following curve fitting process aims at quantifying these effects, initially separately and finally combined into one relationship.

The following equation presents the general form of N_p with z/D for OC clays that fits best to the FEA output:

$$N_p = \frac{p_u}{c_u \cdot D} = N_{p,o} + (N_{p,u} - N_{p,o}) \left(1 - \exp\left(-0.333 \frac{z}{D}\right)\right) \tag{5.7}$$

where $N_{p,o}$ and $N_{p,u}$ are the values of N_p at ground surface and at a significantly great

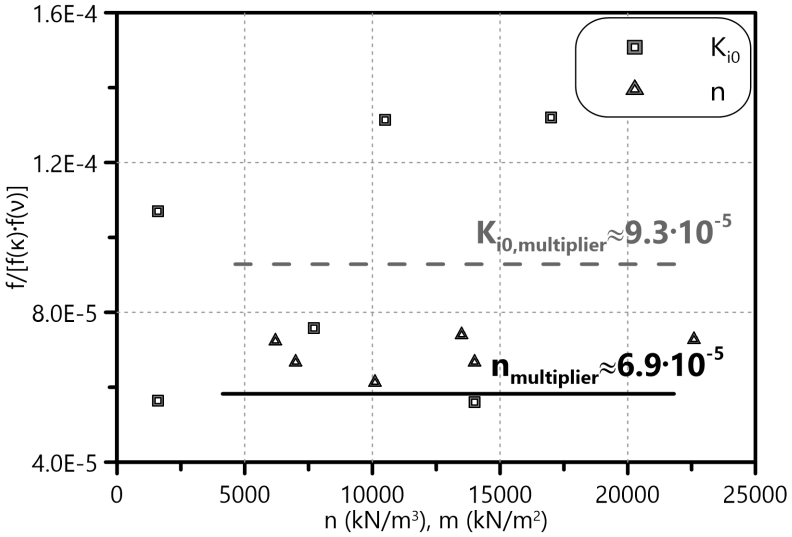

Figure 5.28: Determination of the n-slope and K_{i0} multipliers for the combination of the separate κ and ν effects on K_i.

depth ($z > 10D$) respectively. Figure 5.29 implies that $N_{p,o}$ is mainly influenced by $c_{u,\,avg}$ and α, while all the examined parameters of this figure seem to affect $N_{p,u}$. Processing of $N_{p,o}$ from all the OC clays under numerical investigation leads to the relationships of Figure 5.30 (Equation 5.8). Assuming $N_{p,o}$=4 and 5 for a smooth (α=0.3) and rough (α=1.0) pile-soil interaction respectively is a rather accurate simplification.

$$N_{p,o} = 0.6 \cdot \frac{c_{u,\,avg}}{p_a} + 0.9 \cdot \alpha + 2.5 \tag{5.8}$$

In a more complex manner, the curve fitting process attempts to quantify the effects of $c_{u,\,avg}$, κ, α and D on $N_{p,u}$. Since the combined influence of all these parameters obviously complicates the procedure, we decided to investigate them separately at the beginning. Finally, the process assumes that $N_{p,u}$ is the product of all the aforementioned isolated effects multiplied by a numeric factor. The following equation introduces this general idea:

$$N_{p,u} = X \cdot F_c \cdot F_\kappa \cdot F_D \tag{5.9}$$

where F_c, F_κ, F_D correspond to the isolated effects of $c_{u,\,avg}$, κ and D on $N_{p,u}$ respectively. X is the overall numeric factor to combine the aforementioned effects into one. The influence of α in $N_{p,u}$ is included in all the factors of Equation 5.9 as the curve fitting process demonstrates.

Figure 5.31 depicts the combined effect of $c_{u,\,avg}$ and κ on $N_{p,u}$. The diagrams

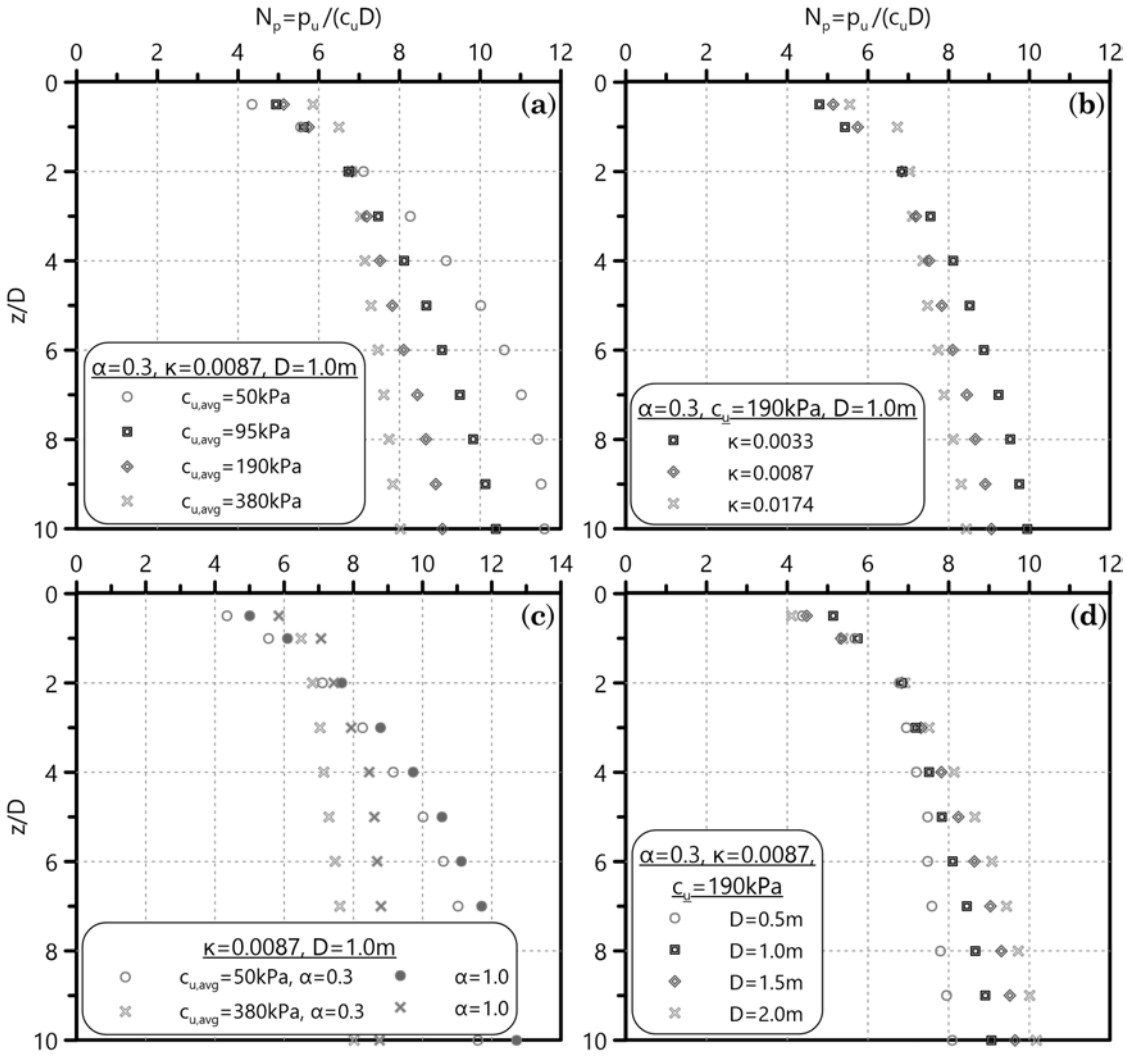

Figure 5.29: Distribution of the ultimate lateral soil resistance factor N_p with non-dimensional depth z/D derived from OC clay FEA. Effect of (a) average undrained shear strength $c_{u,\,avg}$ along a depth of $10D$ from the pile head, (b) unloading-reloading lines slope κ, (c) pile-soil adhesion α and (d) pile diameter D on N_p.

refer to all the values of $c_{u,\,avg}$ in Table 5.1 and include three κ values, namely 0.0033, 0.0087 and 0.0174, covering the whole range of the parametric investigation. The influence of α is examined separately for smooth and rough pile-soil interaction in Figures 5.31a and 5.31b respectively. The final verification of the $N_{p,u}$ expression showed that the effect of κ for smooth pile-soil interaction (α=0.3) fits best both the adhesion factors of the numerical investigation (Figure 5.32). It also revealed that the exponent -1/7 fits better the FEA output than the average of the exponents depicted in Figure 5.31, i.e. -1/6. The following equation reflects the aforementioned

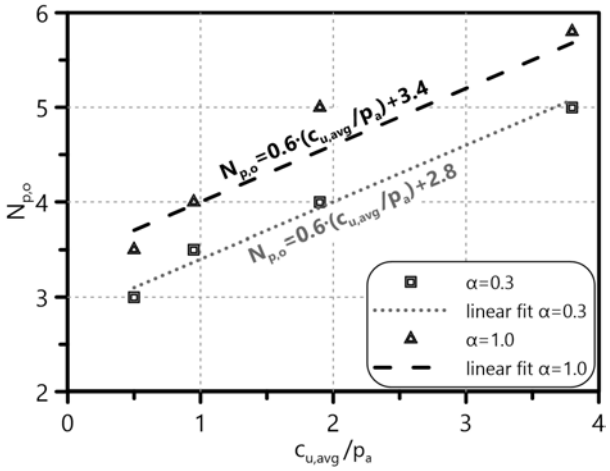

Figure 5.30: Relationship between $N_{p,o}$ (at ground surface) and parameters $c_{u,\,avg}/p_a$ (p_a=100kPa, the atmospheric pressure at sea level) and α from OC clay FEA output processing.

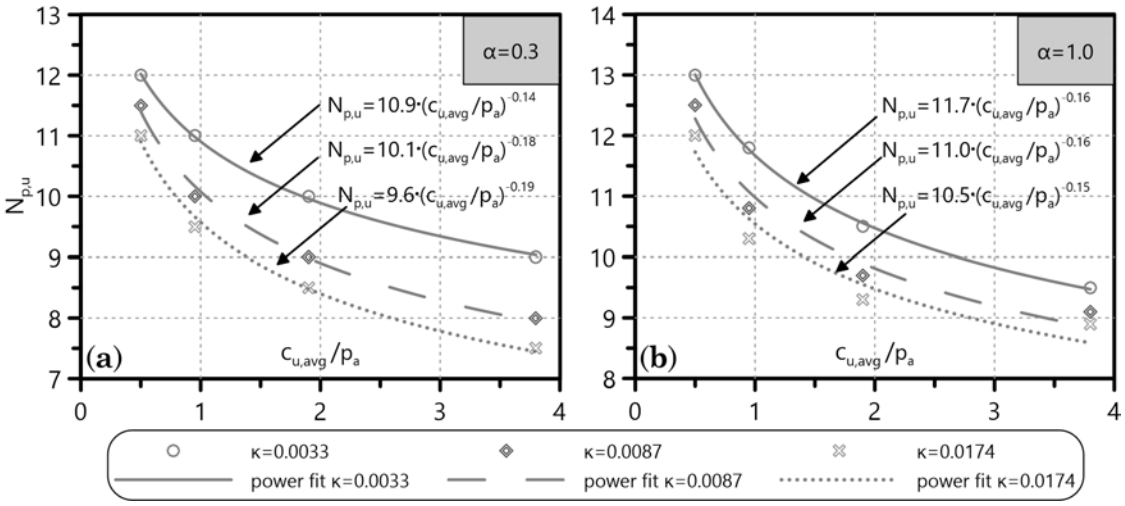

Figure 5.31: Combined relationship of $N_{p,u}$ (at $z > 10D$) with $c_{u,\,avg}/p_a$ (p_a=100kPa, the atmospheric pressure at sea level) and κ for (a) smooth (α=0.3) and (b) rough (α=1.0) pile-soil interaction, according to OC clay FEA output.

curve fitting procedure:

$$N_{p,u}(c_{u,\,avg},\,\kappa) = (-86 \cdot \kappa + 11) \cdot \left(\frac{c_{u,\,avg}}{p_a}\right)^{-\frac{1}{7}} \tag{5.10}$$

Figure 5.33 presents the diameter effect on $N_{p,u}$. More accurately, it depicts the linear function between the non-dimensional ratio D/D_1 (D_1=1m) and $N_{p,u}$ for pile diameters D=0.5, 1.0, 1.5 and 2.0m, for all the values of $c_{u,\,avg}$ simulated in the FEA and constant κ=0.0087 (mid-range value). The investigation actually concerns

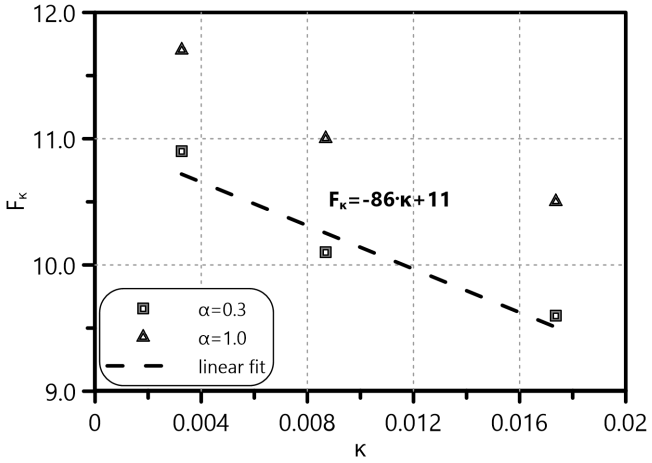

Figure 5.32: Determination of the effect κ has on $N_{p,u}$ for smooth (α=0.3) and rough (α=1.0) pile-soil interaction. Best-fit linear equation on the FEA output.

numerical results for α=0.3 and through a simple extrapolation one can predict the behavior for α=1.0. The following equation displays the implicit relationship between $N_{p,u}$ and the parameters D, $c_{u,\,avg}$ and α:

$$N_{p,u}(D,\, c_{u,\,avg},\, \alpha) = \left[7.9 + 0.9\alpha + \left(-0.5 \cdot \frac{c_{u,\,avg}}{p_a} + 2\right) \frac{D}{D_1}\right] \tag{5.11}$$

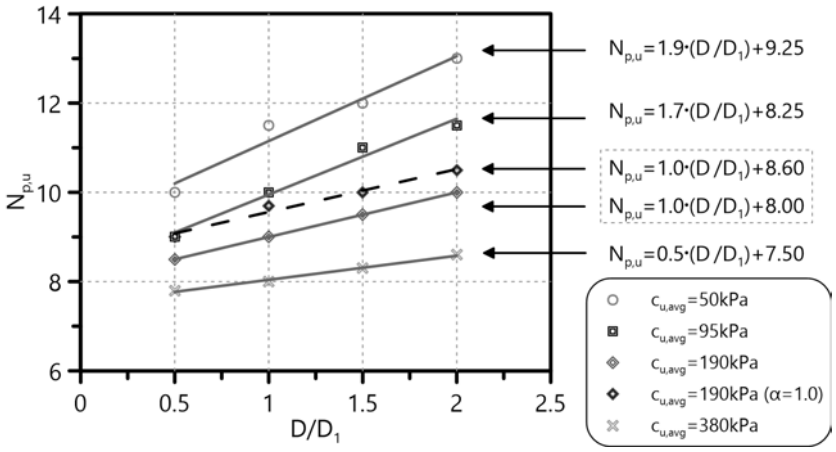

Figure 5.33: Linear relationship between $N_{p,u}$ and the non-dimensional diameter ratio D/D_1 for all $c_{u,\,avg}$ values of the FEA (κ=0.0087, α=0.3, 1.0).

Finally, we need to determine the multiplier X that combines Equations 5.10 and 5.11 into the general form of Equation 5.9. Figure 5.34 estimates the value of this numeric factor X=$N_{p,u\ \text{multiplier}} \approx 0.11$ in order to incorporate factors F_c, F_κ

and F_D (see Equation 5.9) into one mathematical expression. As a consequence, Equation 5.9 receives now the following form:

$$N_{p,u} = F_c \cdot F_\kappa \cdot F_D$$

$$F_c = \left(\frac{c_{u,\,avg}}{p_a} \right)^{-\frac{1}{7}} \tag{5.12a}$$

$$F_\kappa = -9.5 \cdot \kappa + 1.2 \tag{5.12b}$$

$$F_D = 7.9 + 0.9\alpha + \left(-0.5 \cdot \frac{c_{u,\,avg}}{p_a} + 2 \right) \frac{D}{D_1} \tag{5.12c}$$

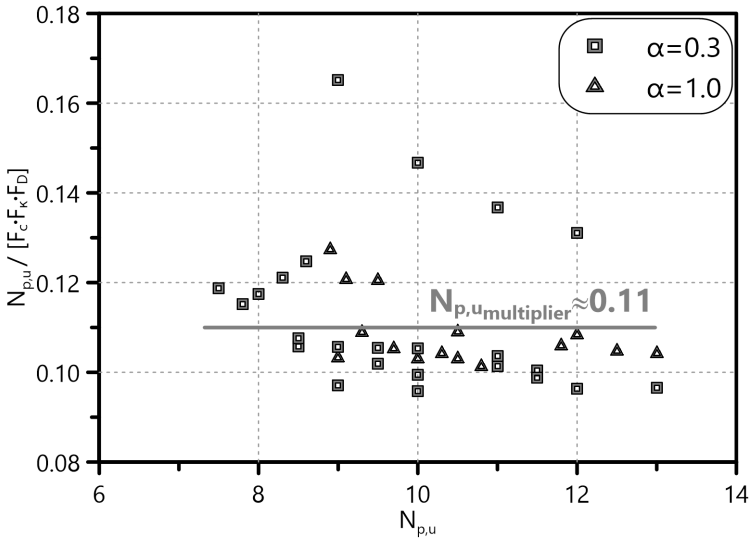

Figure 5.34: Determination of the multiplier for the combination of the separate $c_{u,\,avg}$, κ and D effects on $N_{p,u}$. The multiplier is applicable to both smooth (α=0.3) and rough (α=1.0) pile-soil interaction cases.

Figure 5.35 presents the capability of the proposed N_p function (Equations 5.7 to 5.12) to predict the N_p distribution with z/D of the OC clay FEA. Assuming a realistic error ±10% between the FEA output and the analytical prediction, the curve fitting process proves accurate regarding the whole range of OC clay and pile parameters in Table 5.1. Just the predictions for $c_{u,\,avg}$=380kPa seem a bit conservative, although only slightly.

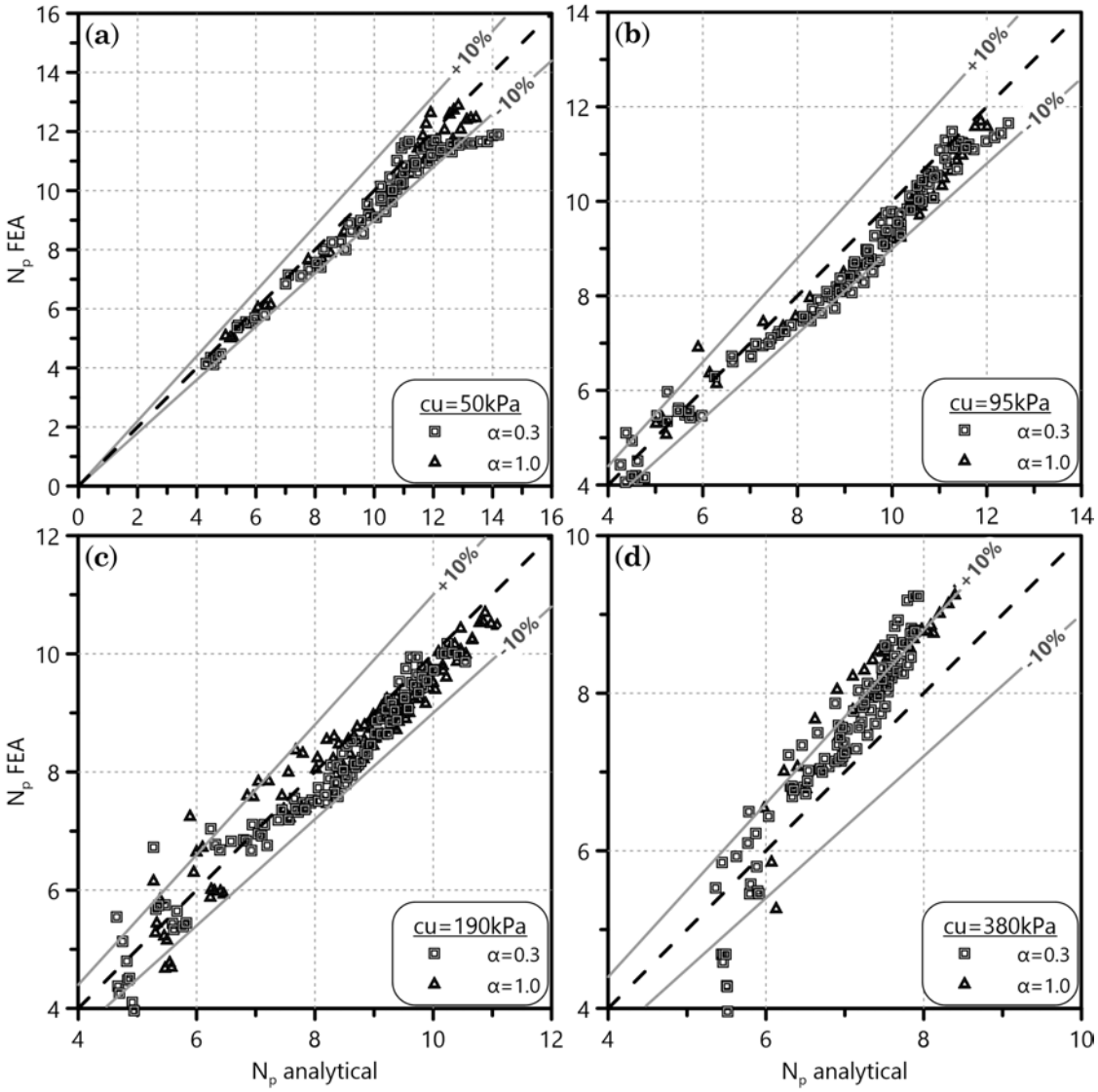

Figure 5.35: Comparison of the analytical prediction versus the FEA output regarding the ultimate lateral OC clay resistance factor N_p for (a) $c_{u,\,avg}$=50kPa, (b) $c_{u,\,avg}$=95kPa, (c) $c_{u,\,avg}$=190kPa and (d) $c_{u,\,avg}$=380kPa and varying values of parameters κ, α and D.

5.4.3 Effect of strength degradation on monotonic p-y curves for OC clays

The following paragraphs investigate the effect of OC clay strength degradation on K_i and p_u of the numerical p-y curves. Figure 5.26 proves that the exponential p-y equation fits better the corresponding FEA output for OC clays exhibiting strength degradation (SSS-SD) than the classic hyperbola form applicable to hardening soils (MCC). The FEA of the current investigation involve three different OC clays with $c_{u,\,avg}$=95, 190 and 380kPa, M=1.2, κ=0.0054, ν=0.1 and a pile of D=1m with smooth and rough pile-soil interaction (α=0.3, 1.0). The dissertation examines

three strength degradation ratios RF=0.8, 0.5 and 0.3 (Equation 5.2). Since the clay with $c_{u,\,avg}$=50kPa is actually medium - in the mid-range between soft and stiff clays - the investigation assumes that it exhibits no significant strength degradation and therefore excludes it from the following process.

It is rational to expect no significant effect of RF on K_i but for consistency reasons the current paragraph presents its distribution with z. Figure 5.36 depicts the K_i derived from the curve fitting process for the exponential p-y relationship (see Paragraph 4.3). The chart compares K_i values for all the examined $c_{u,\,avg}$ and RF combinations (α=0.3) with the case of no SD (RF=1.0) and the linear K_i-z distribution previously proposed for OC clays (Equations 5.4 and 5.6). It appears that the analytical expression for K_i is in agreement with the FEA output values of the specific parameter regardless of the RF.

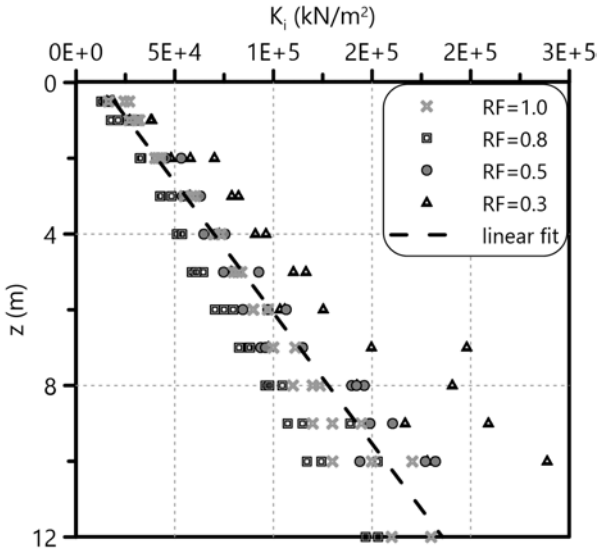

Figure 5.36: Comparison of $K_i - z$ distribution from FEA output using the exponential p-y relationship for various $c_{u,\,avg}$ and $RF < 1$ with the corresponding values for RF=1 and the proposed K_i linear equation for OC clays (Equations 5.4 and 5.6).

The section focuses now on quantifying the effect of RF on p_u, assuming that for $RF < 1$ the exponential p-y form fits the corresponding FEA output. Initially, we examine the influence of RF on N_p-z/D curves for all the $c_{u,\,avg}$ values under investigation. Figure 5.37 compares the N_p distribution of cases with $RF < 1$ (SSS-SD) to the ones with $RF = 1$ (MCC) for the OC clays. It is rather obvious that lower RF values, i.e. more intense strength degradation, yield lower N_p values at all depths. Thus, RF affects both $N_{p,o}$ and $N_{p,u}$ according to the relationships proposed in Figure 5.38 (Equations 5.13).

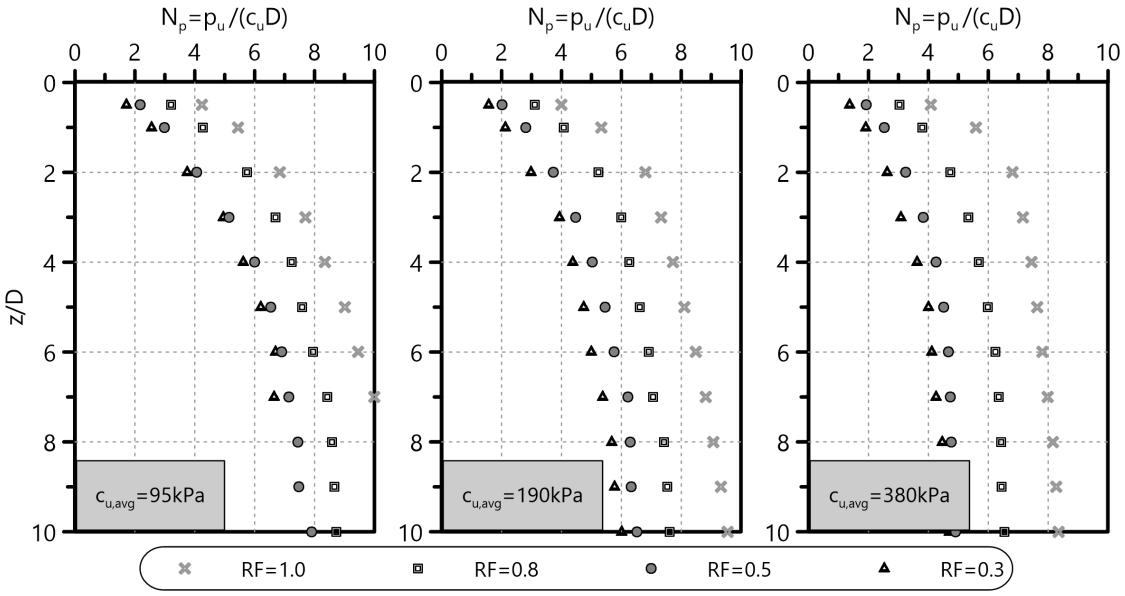

Figure 5.37: Effect of strength degradation ratio RF on N_p for OC clays with $c_{u,\,avg}$=95, 190 and 380kPa (M=1.2, κ=0.0054, ν=0.1, α=0.3, D=1m).

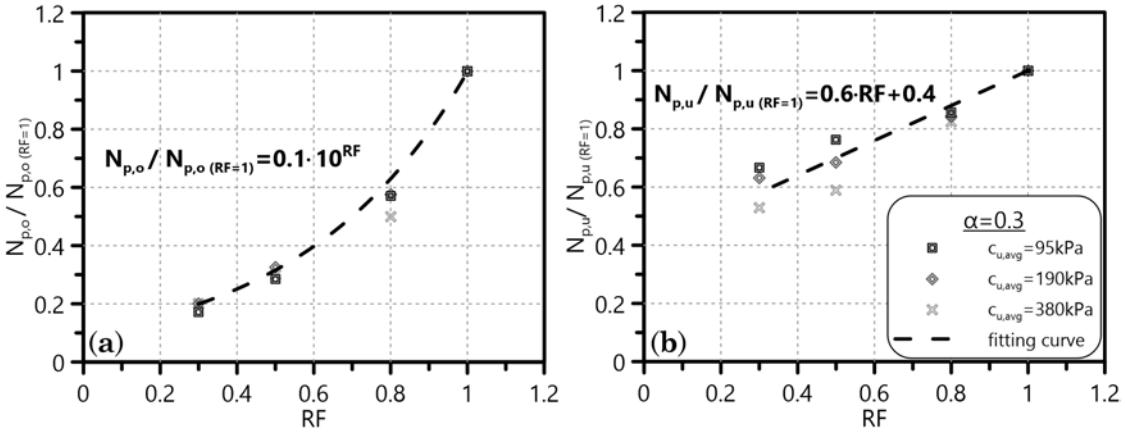

Figure 5.38: Ratios of $N_{p,o}$ and $N_{p,u}$ for $RF < 1$ to the corresponding values for RF=1 regarding all $c_{u,\,avg}$ values under investigation. Relationships of the ratios with RF.

$$\frac{N_{p,o}}{N_{p,o\ \mathrm{RF=1}}} = 0.1 \cdot 10^{RF} \tag{5.13a}$$

$$\frac{N_{p,u}}{N_{p,u\ \mathrm{RF=1}}} = 0.6 \cdot RF + 0.4 \tag{5.13b}$$

Figure 5.39 shows the high accuracy level of Equations 5.13 for smooth pile-soil interaction (α=0.3). The charts also include the cases with RF=1 in order to prove that the relationships fit successfully the FEA derived N_p for OC clays both with

and without strength degradation.

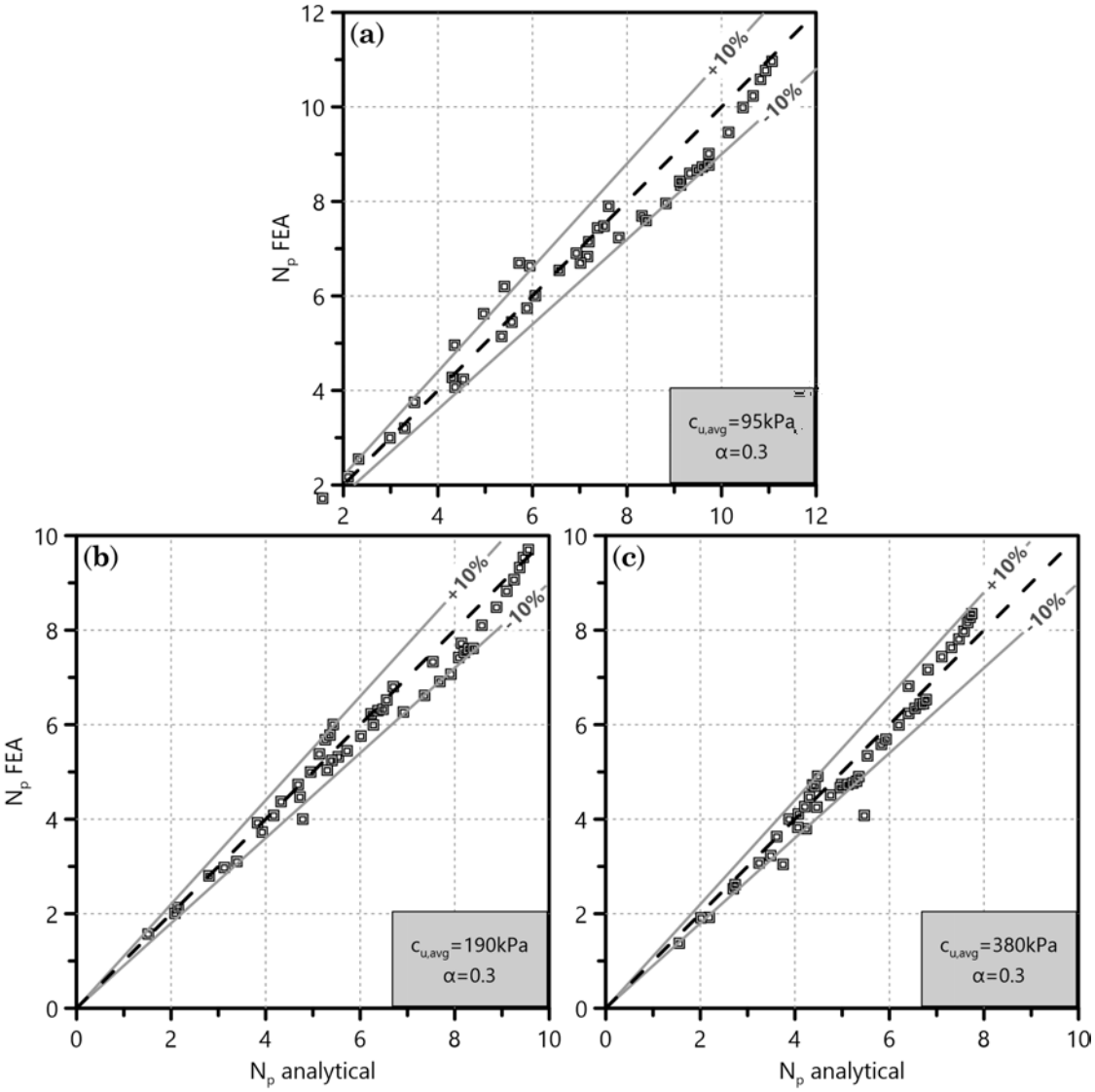

Figure 5.39: Comparison of the analytical prediction versus the FEA output regarding the ultimate lateral resistance factor N_p for OC clays with (a) $c_{u,\,avg}$=95kPa, (b) $c_{u,\,avg}$=190kPa and (c) $c_{u,\,avg}$=380kPa ($RF \leq 1$, α=0.3).

It remains to test whether the K_i-z function (Equations 5.4 and 5.6) together with the proposed reduction functions of $N_{p,o}$ and $N_{p,u}$ for $RF \leq 1$ (Equations 5.13) successfully fit the FEA derived p-y curves for the corresponding OC clays with rough pile-soil interaction (α=1.0). Figure 5.40 depicts the diminishing difference between the calculated p_u values for α=0.3 and 1.0 with decreasing RF. It shows the FEA p-y curves at z=2D, 6D for two OC clays at the limits of the numerical investigation, namely with $c_{u,\,avg}$=95, 380kPa and RF=0.3, 0.8. We observe that the more intense the strength degradation (RF=0.3) the smaller the p_u difference between

smooth and rough pile-soil interaction - a rather rational outcome considering that the behavior of the soil adjacent to the pile determines the interface deformation. As a consequence, one could just utilize $N_{p,o}$ and $N_{p,u}$ for α=0.3 (Equations 5.8 and 5.12) multiplied by the reduction factors of Equations 5.13 respectively in order to acquire the p_u values of the FEA derived p-y curves with α=1.0, but only for very intense strength degradation of the OC clay, i.e. $RF < 0.5$.

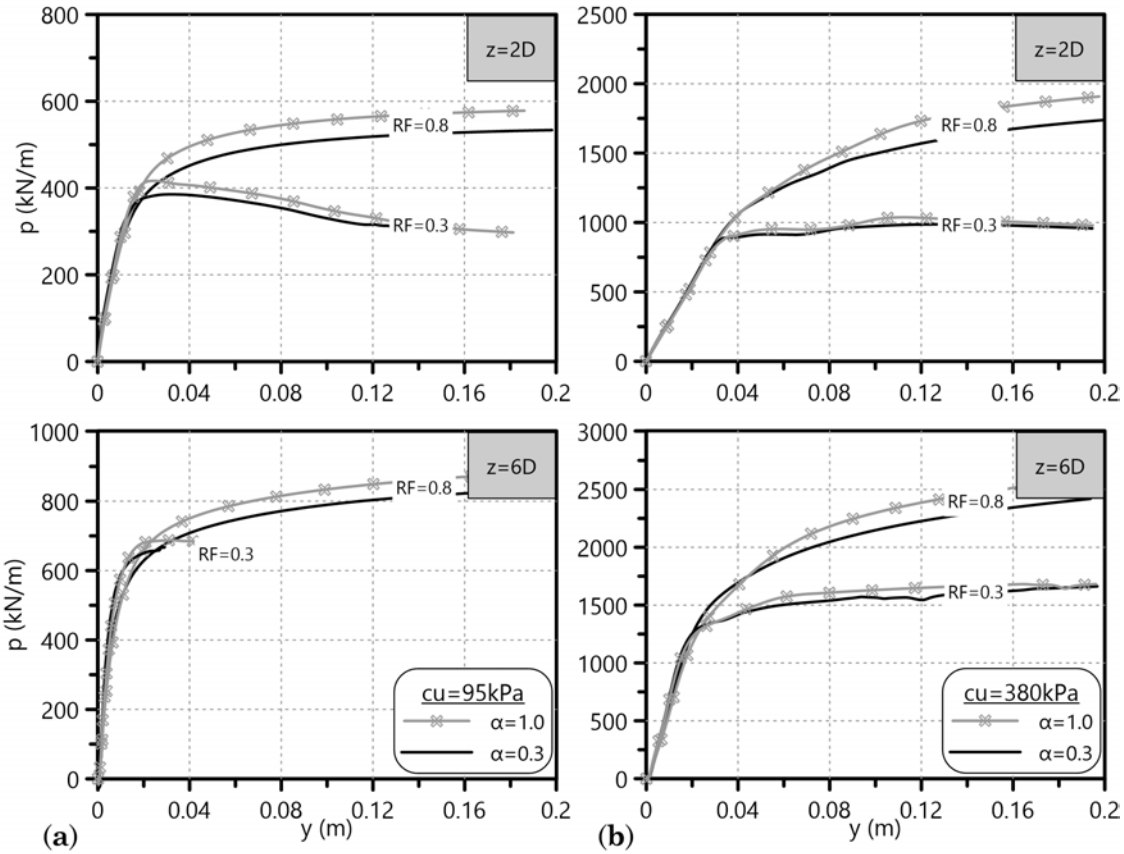

Figure 5.40: The more intense the strength degradation (RF=0.3) the smaller the p_u difference between smooth and rough pile-soil interaction. Observation from FEA p-y curves at depths z=2D, 6D for OC clays with (a) $c_{u,\,avg}$=95kPa and (b) $c_{u,\,avg}$=380kPa.

The reduction factors of Equations 5.13 are derived from FEA with α=0.3. It remains to ascertain if they also predict successfully the numerical p-y curves for rough pile-soil interaction. Figure 5.41 compares the rough pile p-y curves (α=1.0) from FEA output with the proposed exponential fit for all the OC clays under investigation in the current section ($c_{u,\,avg}$=95-380kPa, RF=0.3-0.8) at depths z=2D, 6D. The exponential p-y equation fits accurately the curves at shallow depths (z=2D) but exhibits some inconsistency deeper (z=6D), although just for low strength degradation (RF=0.8). Judging from Figures 5.39 and 5.41 the reduction factors of N_p for various RF values deliver exponential p-y curves that fit very well the ones

derived from FEA for both smooth and rough pile-soil interaction.

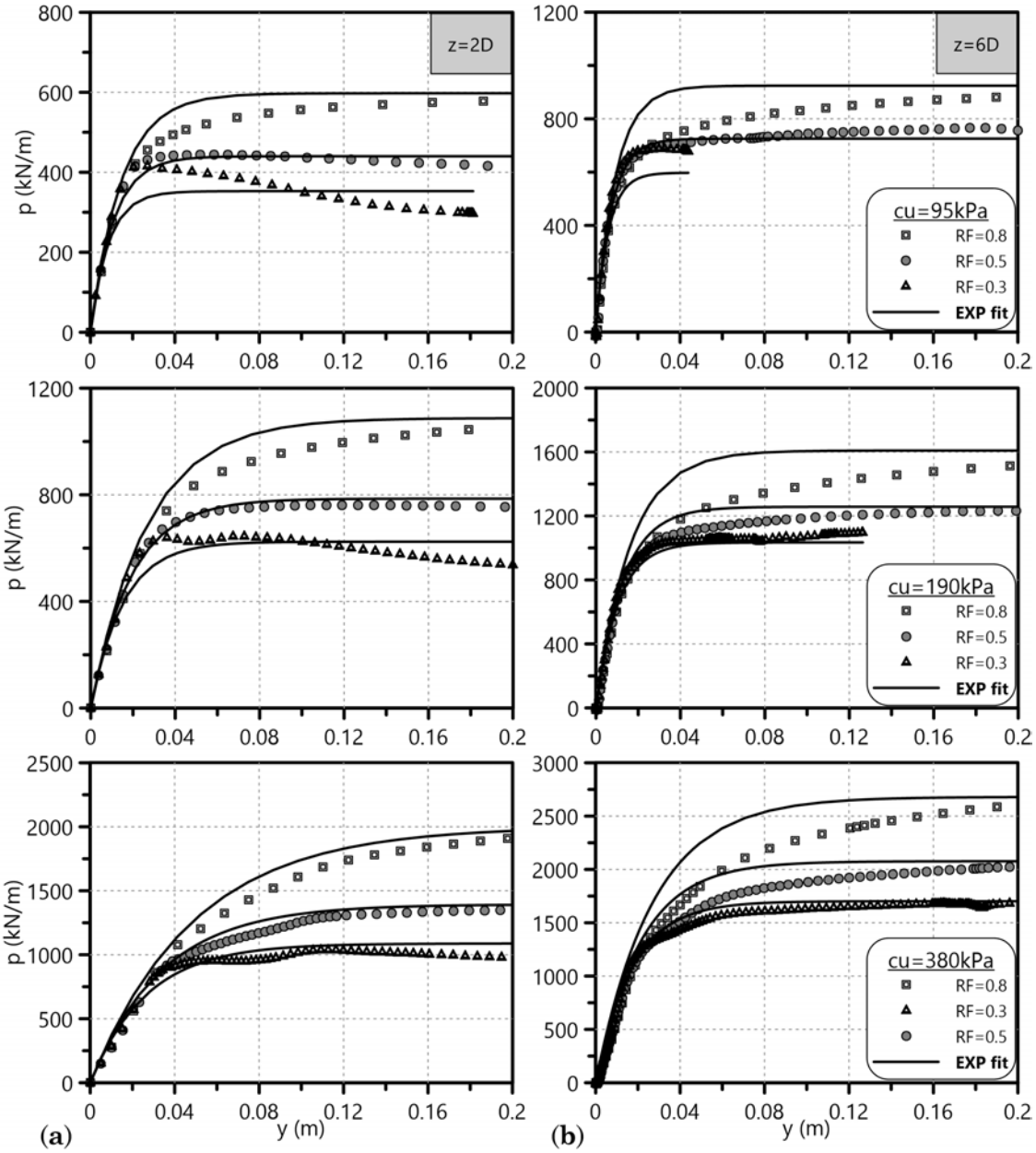

Figure 5.41: Comparison of rough pile p-y curves (α=1.0) from FEA output with the proposed exponential fit for OC clays with $c_{u,\,avg}$=95-380kPa and RF=0.3-0.8 at (a) z=2D and (b) z=6D utilizing the reduction factors of Equations 5.13 for N_p.

5.4.4 Proposed monotonic p-y curves for OC clays

The present paragraph aims at summarizing the process for the formulation of the proposed monotonic OC clay p-y curves. The aforementioned numerical development of such p-y curves outlines the following steps:

1. First define the following OC clay and pile parameters: average undrained shear strength $c_{u,\,avg}$ along a depth of $10D$ from the pile head, unloading-reloading lines slope κ, Poisson's ratio ν, pile diameter D and pile-soil adhesion factor α.

2. Determine the initial stiffness K_i of the p-y curve at the desired depth z according to the equation:

$$K_i = n \cdot z + K_{i0}$$

$$n = 270 \cdot \kappa^{-0.77} \cdot (-2.07 \cdot \nu + 1.17)$$

$$K_{i0} = 8.4 \cdot \kappa^{-1.3} \cdot (-6.14 \cdot \nu + 2.23)$$

3. Calculate the ultimate lateral soil resistance p_u of the p-y curve at the specific depth through the equations:

$$p_u = N_p \cdot c_u \cdot D = \left[N_{p,o} + (N_{p,u} - N_{p,o}) \left(1 - \exp\left(-0.333\,\frac{z}{D}\right)\right)\right] \cdot c_u \cdot D$$

$$N_{p,o} = \left(0.06 \cdot \frac{c_{u,\,avg}}{p_a} + 0.09 \cdot \alpha + 0.25\right) \cdot \left(10^{RF}\right)$$

$$N_{p,u} = (F_c \cdot F_\kappa \cdot F_D) \cdot (0.6 \cdot RF + 0.4)$$

$$F_c = \left(\frac{c_{u,\,avg}}{p_a}\right)^{-\frac{1}{7}}$$

$$F_\kappa = -9.5 \cdot \kappa + 1.2$$

$$F_D = 7.9 + 0.9\alpha + \left(-0.5 \cdot \frac{c_{u,\,avg}}{p_a} + 2\right) \frac{D}{D_1}$$

The procedure for the calculation of p_u outlines that the undrained shear strength c_u of the corresponding equation is the one at the desired depth of the p-y curve and might differ from $c_{u,\,avg}$ - average c_u from ground surface up to a depth

z=10D. Furthermore, the aforementioned expressions for $N_{p,o}$ and $N_{p,u}$ - ultimate lateral soil resistance factor at ground level and at $z > 10D$ respectively - include the OC clay strength reduction factor $RF = c_{u,\,\mathrm{res}}/c_{u,\,\mathrm{peak}}$. Thus, for clays that exhibit no strength degradation RF=1 while strain softening behavior corresponds to $RF < 1$.

4. Form the OC clay p-y curve according to the proposed distinction of the current chapter (regarding RF):

$$p = \frac{y}{\frac{1}{K_i} + \frac{y}{p_u}} \quad \text{for} \quad RF = 1$$

$$\frac{p}{p_u} = 1 - \exp\left(\frac{-K_i \cdot y}{p_u}\right) \quad \text{for} \quad RF < 1$$

Chapter 7 attempts to verify the numerically developed monotonic p-y curves for OC clays through the comparison of bending moment and horizontal displacement distributions along laterally loaded piles of specific large-scale or centrifuge experiments with the corresponding predictions of BNWF analyses incorporating the current proposals.

5.4.5 Comparison of proposed OC clay p-y curves with literature

The present paragraph compares the proposed OC clay p-y curves with corresponding literature methodologies (see Paragraph 2.9). The following comparison does not aim to criticise literature p-y curves for such soils but to indicate whether the proposals of the current dissertation are either conservative or radical compared to the existing ones. The comparison refers to a laterally loaded pile of D=1m, L=30m, α=1.0 in an OC clay with submerged unit weight γ=20kN/m^3, $c_{u,\,avg}$=c_u=100kPa, κ=0.0054 (C_r=0.0125), ν=0.10 and water table at ground level. Figure 5.42 depicts that the proposed OC clay p-y curves deliver a p_u almost similar to the highest one of the literature methodologies (Georgiadis & Georgiadis, 2010). They also demonstrate K_i closer to the highest recommended values of literature, although such a comparison is inconsistent since none of the existing methodologies correlates the initial stiffness of the p-y curves with poroelasticity parameter κ. The most crucial feature of the proposed p-y curves is that they neglect any potential strength degradation due to corresponding stiff OC clay behavior. The specific assumption

contrasts the literature p-y curves that suggest gradual p_u degradation, i.e. Reese et al. (1975), DNV (1977) and Sullivan et al. (1979).

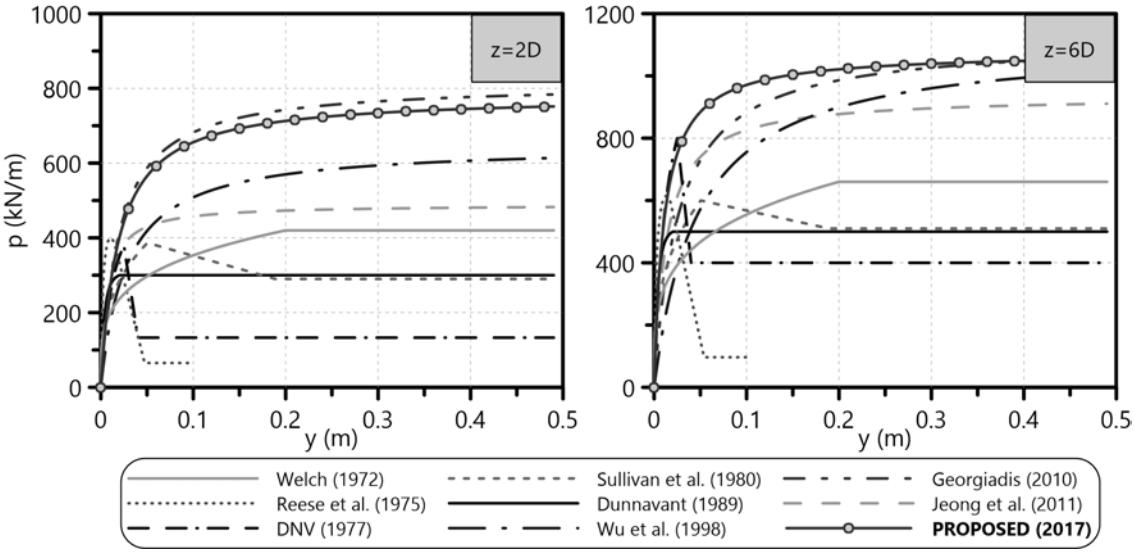

Figure 5.42: Comparison of the proposed monotonic p-y curves with corresponding literature methodologies for a pile of D=1m and α=1.0 in a fully saturated OC clay at shallow (z=2D) and greater depth (z=6D).

It is also interesting to compare the N_p and K_i distributions of the proposed p-y curves versus the corresponding literature values with the dimensionless depth z/D. Figure 5.43 confirms the aforementioned observations for the relatively high p_u and K_i of the proposed p-y methodology when compared with the literature recommendations. The ultimate lateral soil resistance factor N_p for OC clays according to the proposed methodology lies towards the peak values of the literature but not above them at all depths, a generally encouraging observation in terms of past design for laterally loaded piles.

5.5 Concluding remarks on p-y curves for OC clays

To sum up, the current chapter proposes an upgraded p-y curve relationship for medium-to-stiff, OC clayey soils under monotonic undrained loading conditions. The proposed curves correlate with a variety of soil, pile and pile-soil interface properties. Accordingly to the philosophy of the present thesis, these correlations offer an alternative choice to the majority of the existing literature methods. In addition, the aforementioned research elaborates on the effect that small-strain stiffness and strength degradation of the soil may have on the proposed p-y curves. The performed, effective stress, 3D FEA reproduce realistically the lateral response of a long

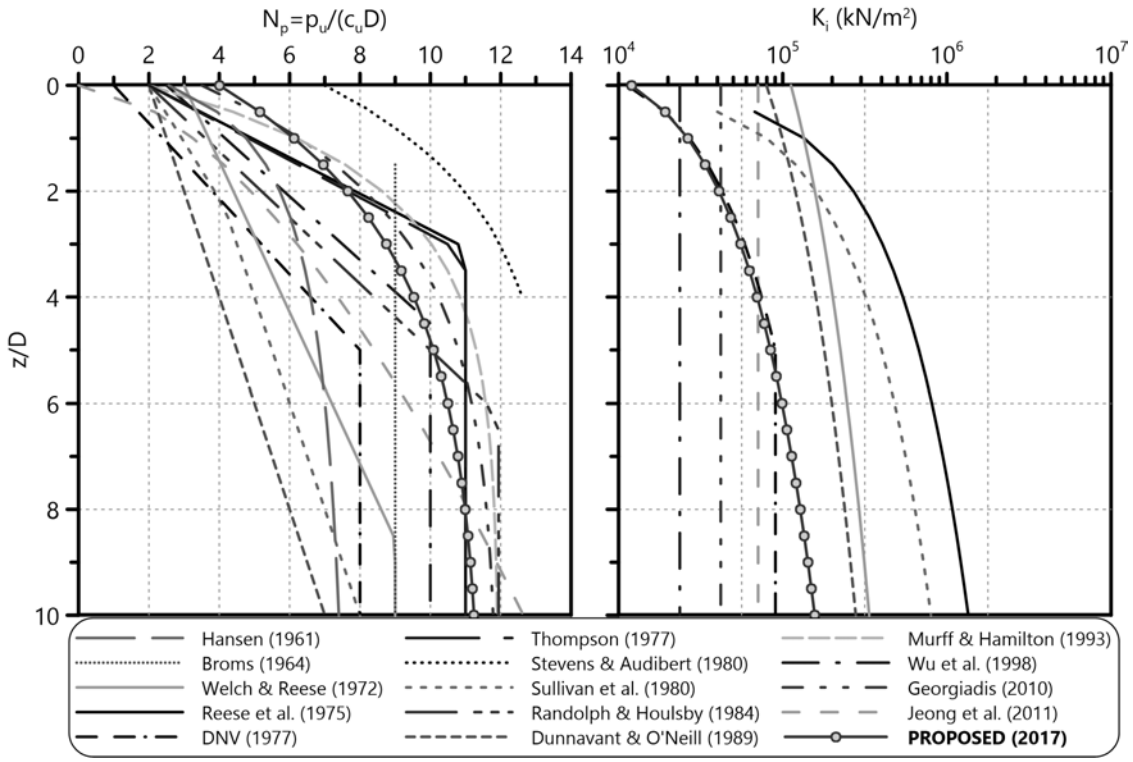

Figure 5.43: Comparison of the proposed N_p and K_i distributions with z/D versus corresponding literature methodologies for a pile of D=1m and α=1.0 in a fully saturated OC clay.

pile in such soils (soil failure, pile-soil detachment, excess pore pressure build-up, etc.).

Chapter 5 concludes in the following remarks referring to the proposed p-y curves for laterally loaded piles in OC clayey soils:

- The present dissertation proposes either the exponential or the hyperbolic p-y form for medium-to-stiff OC clays that do or do not exhibit strength degradation due to strain softening respectively, according to FEA results. Two parameters need to be defined for the p-y curves applicable to OC clayey soils: the initial p-y curve stiffness K_i and the ultimate lateral soil resistance factor N_p=$p_u/(c_u \cdot D)$.

- The FEA incorporate a significant range of soil ($c_{u,\,avg}$, M, κ, $K_{o,\,max}$, ν) and pile (D, α) parameters for the numerical simulation of laterally loaded piles in OC clays. A thorough parametric investigation reveals that the Critical State Line slope M - corresponding to $\phi = 20^\circ - 30^\circ$ - and the maximum coefficient of horizontal geostatic stress $K_{o,\,max}$=0.7-1.5 do not affect the p-y curves derived from the FEA for undrained loading conditions. The rest of

the parameters affect the p-y curves in a manner that is briefly explained in the following points.

- An advanced constitutive law is implemented in the FEA, allowing for the numerical simulation of small-strain stiffness (SSS) and structure degradation (SD) properties of the soil. Extensive parametric study on these two features shows that only SD plays significant role on p_u. The chapter correlates the decrease of p_u with $RF = c_{u,\,\mathrm{res}}/c_{u,\,\mathrm{peak}}$ of the stiff OC clays under investigation. This research claims that the numerically derived p-y curves do not reflect soil strength degradation, even of high intensity (e.g. RF=0.3). The specific observation is potentially attributed to the general pile-soil system behavior: only soil elements very close to the pile, i.e. distance less than $2D$ from pile periphery, exhibit post-peak behavior. As a consequence, the degradation of p_u from a peak to a residual value is considered negligible since it appears at very shallow depths ($z < 2D$) and only for very intense SD (RF=0.3).

- $K_{i,\mathrm{OC}}$ is a linear function of depth z with slope n and ground surface value $K_{i0} > 0$. Both parts are a function of κ and ν (Equation 5.6), reflecting the elasticity assumptions of the numerical simulation for such soils, i.e. pressure-dependent bulk modulus - and as a consequence Young's modulus. As a matter of fact, by assigning constant slope κ of the unloading-recompression line to the soil, the 3D FEA simulate a linearly increasing soil Young's modulus with depth. K_i values of the proposed p-y curves fall around the middle of the corresponding literature range for medium-to-stiff OC clays.

- $N_{p,\mathrm{OC}}$ is a composite function and depends on various soil and pile parameters - $c_{u,\,avg}$, κ, D, α and RF - (see Paragraph 5.4.4). Specific multipliers related to RF apply to the initial expression of N_p - for soils without strength degradation (RF=1) - when laboratory tests confirm strain-softening soil behavior ($RF <$ 1). FEA deliver N_p values close to the highest proposals of the literature.

Chapter 6

The effect of cyclic loading on p-y curves for clays

6.1 Introduction

The present chapter attempts to quantify the effect of cyclic loading on p-y curves for NC and OC clays. It examines how the repetitive lateral displacement or loading of the pile head affects the p-y curve stiffness and ultimate lateral soil resistance after a certain number of load cycles. Prior to simulating the actual problem we evaluate the capability of the utilized constitutive laws (see Paragraph 3.2.2) to capture cyclic soil behavior mechanisms. After drawing conclusions from the aforementioned process, the chapter moves on to the FEA of the cyclic (pseudostatic) laterally loaded pile. Finally, it presents the findings of this numerical investigation together with certain considerations on the realistic numerical simulation of the specific problem.

6.2 Nature of cyclic loading

The nature of cyclic lateral pile loading varies depending on the external cause and the number of load cycles. Cyclic lateral loading of piles generally occurs due to wave propagation and wind pressure (offshore structures). Storm events result in extensive wave and wind loading, last for some hundreds of cycles - or even thousands in extreme weather conditions - with almost constant intensity and are crucial for the design of offshore piled foundations.

The literature review of Chapter 2 describes p-y curve methodologies with specific guidelines for cyclic loading. Some of them assume degradation of both initial stiffness K_i and ultimate lateral soil resistance p_u due to cyclic loading - compared to static - (DNV, 1977; Reese et al., 1975) while others suggest that the specific load

type only reduces one of them, either K_i (Welch & Reese, 1972) or p_u (Dunnavant & O'Neill, 1989; Kim et al., 2016; Matlock, 1970; Sullivan et al., 1979). More specifically, Matlock (1970) proposes 28% reduction of the static p_u for cyclic p-y curves in soft clays[1]. In addition, the latter shows that p-y hysteresis loops in such soils stabilize after 10 load cycles according to laboratory model test (up to y_h=0.2D). Reese et al. (1975) and DNV (1977) distinguish between static and cyclic K_i and p_u for the corresponding p-y curves, while Welch & Reese (1972) correlates the cyclic y with the number of load cycles N for various p levels - thus affecting solely the cyclic K_i. Dunnavant & O'Neill (1989) claim that p_u of the cyclic p-y curves decreases for $y_h > 0.01D$, while they together with Kim et al. (2016) suggest correlations of the cyclic p_u with N.

Certain researchers propose exclusively cyclic p-y curves for clayey soils. Heidari et al. (2014) demonstrate a step-by-step procedure for the formulation of generalized cyclic p-y curves - applicable to both sands and clays - based on the implementation of a cyclic degradation model for the lateral soil reaction. Furthermore, Wang & Liu (2016) developed cyclic p-y curves for clays based on T-bar penetration test results, assuming that the cyclic response of the pile-soil system stabilizes after 10 load cycles. Research carried out by Janoyan et al. (2006), Stewart et al. (2007), Tuladhar et al. (2008), Chandrasekaran et al. (2010), Zhang et al. (2010), Memarpour et al. (2012) and Zhang & Ng (2016) regarding the cyclic lateral pile response in clays agrees on the following general observation: N=10-20 is a range of load cycles - of the same or almost the same amplitude - that allows for the cyclic response, i.e. hysteresis loops, to stabilize in terms of both pile and p-y behavior.

The current dissertation examines the effect of short-term cyclic loading (low number of cycles) on the lateral pile response, as well as on the post-cyclic p-y curves. FEA of the following numerical investigation simulate such loading in a pseudostatic manner through constant, two-way lateral displacement or concentrated load on the pile head for 20 cycles - significant enough to reflect any effect of cyclic loading on the derived p-y curves. Coupled FEA for monotonic lateral loading proved time-consuming even for computers with significant power - regarding the era of the thesis. Taking into account the demanding advanced clay constitutive laws, the specific number of cycles proves capable of providing us with some very interesting points.

[1] Sullivan et al. (1979) recommends the same modification

6.3 Cyclic undrained triaxial constitutive response

Prior to confronting the complex numerical problem of the cyclic laterally loaded pile in NC and OC clays, one shall examine whether the utilized constitutive laws (MCC and SSS-SD model respectively) can capture the cyclic soil response. Numerical undrained triaxial tests (see Paragraph 3.2.2.3) are carried out on specimens with NC and OC clay properties at depth z=3D (D=1m) - considering this depth representative of the soil behavior in front of the flexible laterally loaded pile. The properties of the NC and OC clay lay in the mid-range of the parametric investigation presented in Chapters 4 and 5 respectively:

- **NC clay:** M=0.984, λ=0.109, λ/κ=10, K_o=0.5, ν=0.333 (MCC, SSS)
- **OC clay ($RF = 1$):** M=1.2, $c_{u,\,avg}$=190kPa, κ=0.0054, $K_{o,\,max}$=1.5, ν=0.1 (MCC, SSS)
- **OC clay ($RF = 0.5$):** M=1.2, $c_{u,\,avg}$=190kPa, κ=0.0054, $K_{o,\,max}$=1.5, ν=0.1 (SSS-SD)

The following paragraph investigates the formulation of stress-strain loops and how excess pore pressure exhibits similar patterns during cyclic undrained triaxial loading. Furthermore, the accumulation of deviatoric plastic strain indicates how plasticity-based constitutive laws tend to respond during load cycles of the soil specimen. Since the intensity of the cyclic loading is always questionable during design, the numerical tests correspond to both small and significant imposed axial strains. In detail, 20 load-unload cycles of axial deformations $\varepsilon_{a,\,\mathrm{NC}}$=1%, 4% and $\varepsilon_{a,\,\mathrm{OC}}$=0.5%, 2% correspond to low and high intensity for the NC and the OC clay respectively. Figures 6.1, 6.2, 6.3 and 6.4 depict the undrained cyclic response of the clays under low and high axial strain in terms of the following curves:

(a) $p-q$: stress paths

(b) $\Delta u-\varepsilon_q$: excess pore pressure build-up with the deviatoric strain, i.e. axial strain for undrained conditions

(c) $S1-E1$: stress-strain curve in the generalized space, with $S1$=$(2\sigma_y-\sigma_x-\sigma_z)/\sqrt{6}$ and $E1$=$(2\varepsilon_y-\varepsilon_x-\varepsilon_z)/\sqrt{6}$ (the cyclic strain is applied along y-axis - see Figure 3.7)

(d) q–ε_{qp}: deviatoric stress-accumulated plastic deviatoric strain, with ε_{qp}=$\sum d\varepsilon_{qp}$

For comparison purposes, the aforementioned diagrams demonstrate the response of the soil simulated through both the MCC and the advanced SSS-SD constitutive

law. In more detail, clays without strain-softening - i.e. the NC clay and the OC with RF=1 - are simulated through the MCC and the small-strain stiffness feature of the advanced law (B=1). The complete SSS-SD model simulates only the stiff, OC clay with strength degradation.

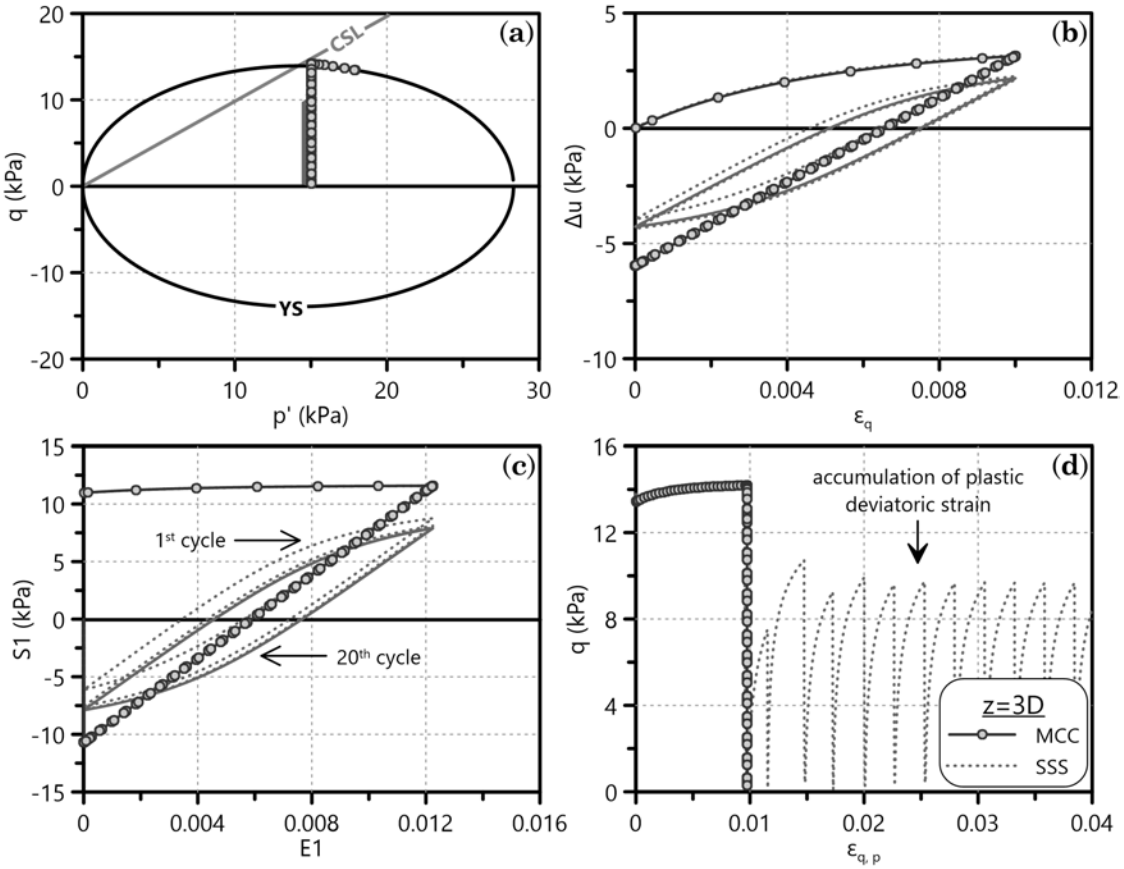

Figure 6.1: Effect of low intensity cyclic undrained triaxial loading (20 cycles, ε_a=1%) on (a) stress paths $p-q$, (b) excess pore pressure build-up $\Delta u-\varepsilon_q$, (c) stress-strain curve $S1-E1$ in the generalized space and (d) deviatoric stress-accumulated plastic deviatoric strain $q-\varepsilon_{qp}$ of a specific NC clay element under compression in front of the laterally loaded pile (z=3D).

For NC clays, either simulating them through MCC or the SSS feature of the SSS-SD constitutive model makes no actual difference in the cyclic soil response, apart from the formulation of hysteresis loops through the latter. The specific feature also allows for the accumulation of plastic strains (ε_{qp}) due to its limited yield surface (PYE - see Figure 3.6) that encloses the initial geostatic stress state - opposed to the MCC simulation that restricts the unloading-reloading of the soil element into the elastic domain of its yield surface YS (Figure 6.1a). The same observation applies to significant strains, where the NC clay strength is reached even from the first load cycle.

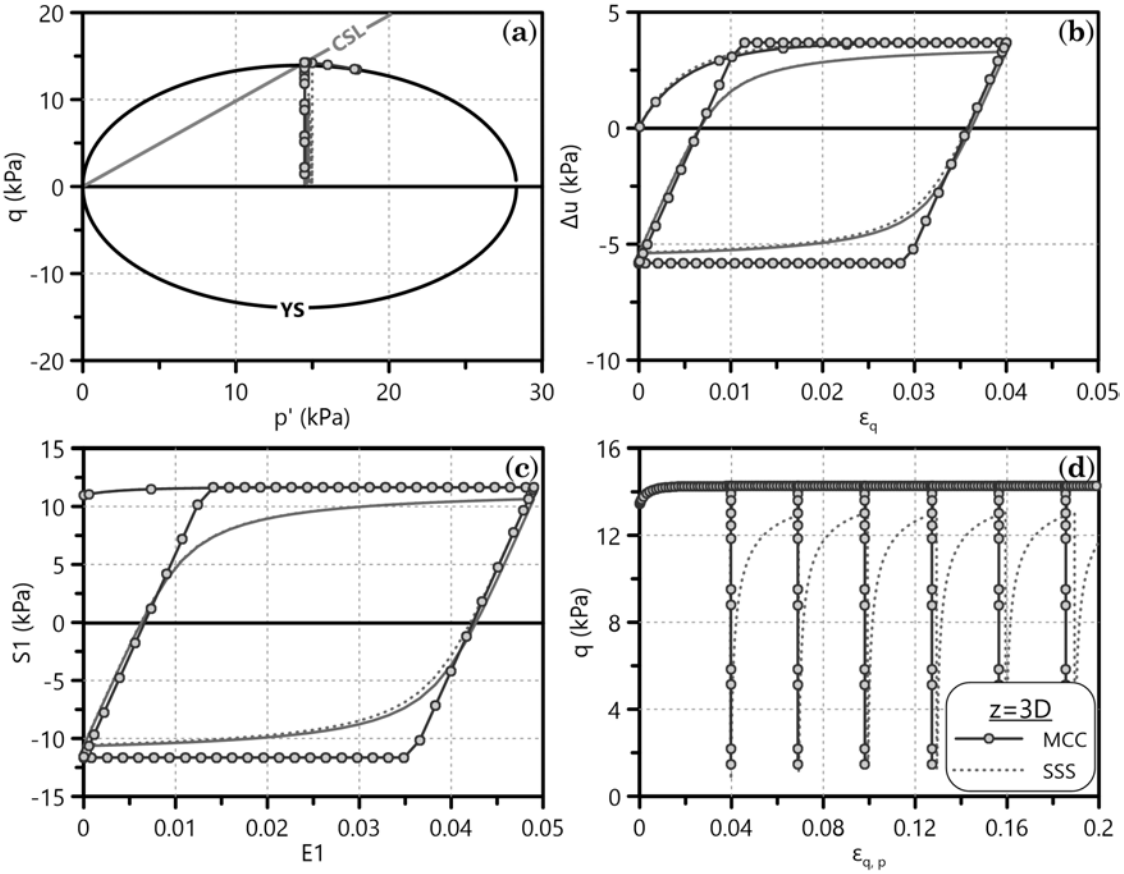

Figure 6.2: Effect of high intensity cyclic undrained triaxial loading (20 cycles, ε_a=4%) on (a) stress paths $p-q$, (b) excess pore pressure build-up $\Delta u-\varepsilon_q$, (c) stress-strain curve $S1-E1$ in the generalized space and (d) deviatoric stress-accumulated plastic deviatoric strain $q-\varepsilon_{qp}$ of a specific NC clay element under compression in front of the laterally loaded pile (z=3D).

On the other hand, OC clays seem to deliver a more realistic cyclic response when SSS-SD is utilized to simulate their constitutive behavior. Both in terms of $S1-E1$ and $q-\varepsilon_{qp}$ there are indications towards the aforementioned aspect. Especially for low strain intensity, the stress-strain loops stabilize at a rearranged stiffness lower than the initial. Moreover, the utilization of the SSS-SD law allows for structure degradation of the OC clay, namely a profound process during large strain cycles. Thus, the MCC and the SSS-SD will simulate NC and OC clay behaviors respectively in the cyclic loading FEA that follow.

6.4 Cyclic lateral pile head response

After validating the efficiency of the constitutive laws in capturing the undrained cyclic soil response, the numerical investigation moves on to the 3D simulation of

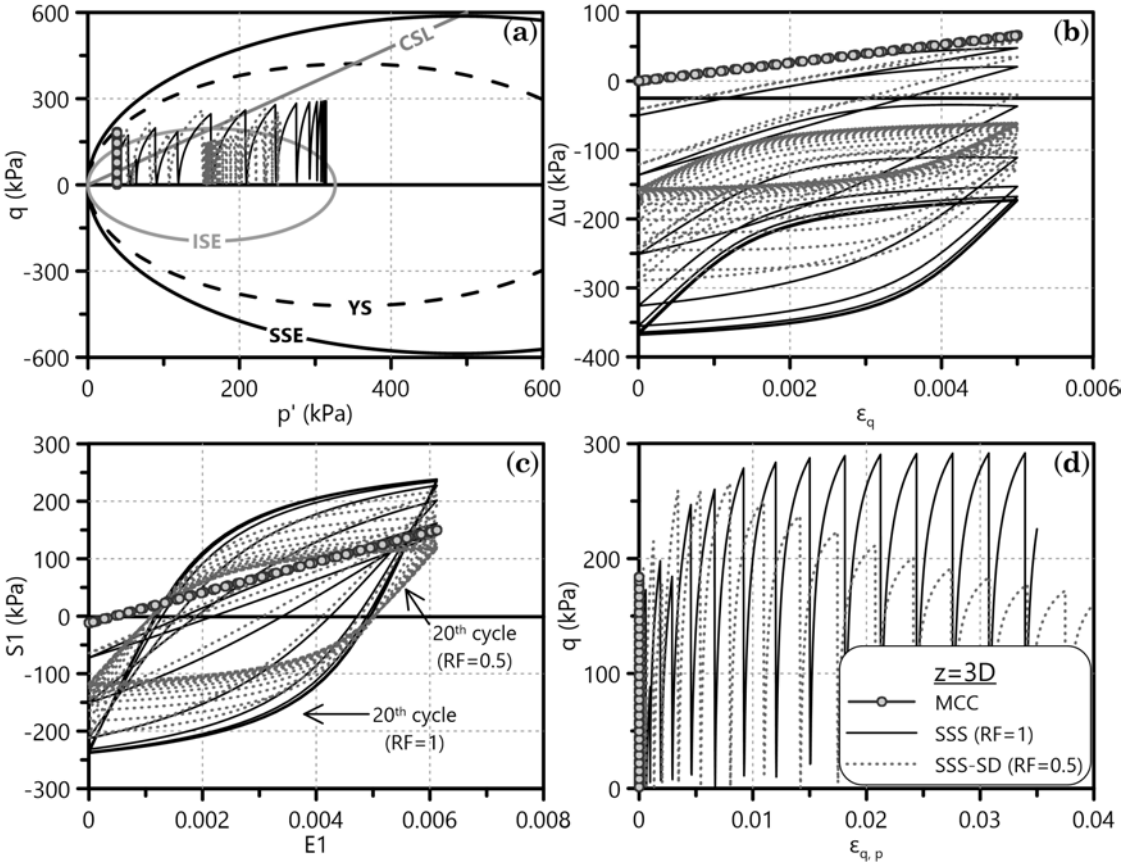

Figure 6.3: Effect of low intensity cyclic undrained triaxial loading (20 cycles, ε_a=0.5%) on (a) stress paths $p-q$, (b) excess pore pressure build-up $\Delta u-\varepsilon_q$, (c) stress-strain curve $S1-E1$ in the generalized space and (d) deviatoric stress-accumulated plastic deviatoric strain $q-\varepsilon_{qp}$ of a specific OC clay element under compression in front of the laterally loaded pile (z=3D).

the cyclic (pseudostatic) lateral loading of a 1m-diameter pile through FEA. The cyclic loading was initially simulated with horizontal displacement imposed on the pile head towards both directions of its initial state. However, the specific approach manipulates the equilibrium of the lateral pile response since the final position of the pile head is pre-defined. Therefore, the FEA impose a two-way, repetitive (for 20 load cycles), constant concentrated horizontal load H_c for a more realistic simulation of the problem. The magnitude of H_c per soil case is roughly equal to 1/3-1/2 of the ultimate lateral pile head load H_u during monotonic loading, i.e. H_c=600, 3000 and 2000kN for the NC, OC with RF=1 and OC with RF=0.5 clayey soils respectively.

Figure 6.5 compares the lateral monotonic and cyclic response of the pile head in terms of non-dimensional lateral displacement - shear force $y_h/D-H$ for the three clayey soils of the investigation. Simulating the NC clay with both constitutive laws (MCC, SSS) makes no actual difference on the specific diagram (Figure 6.5a),

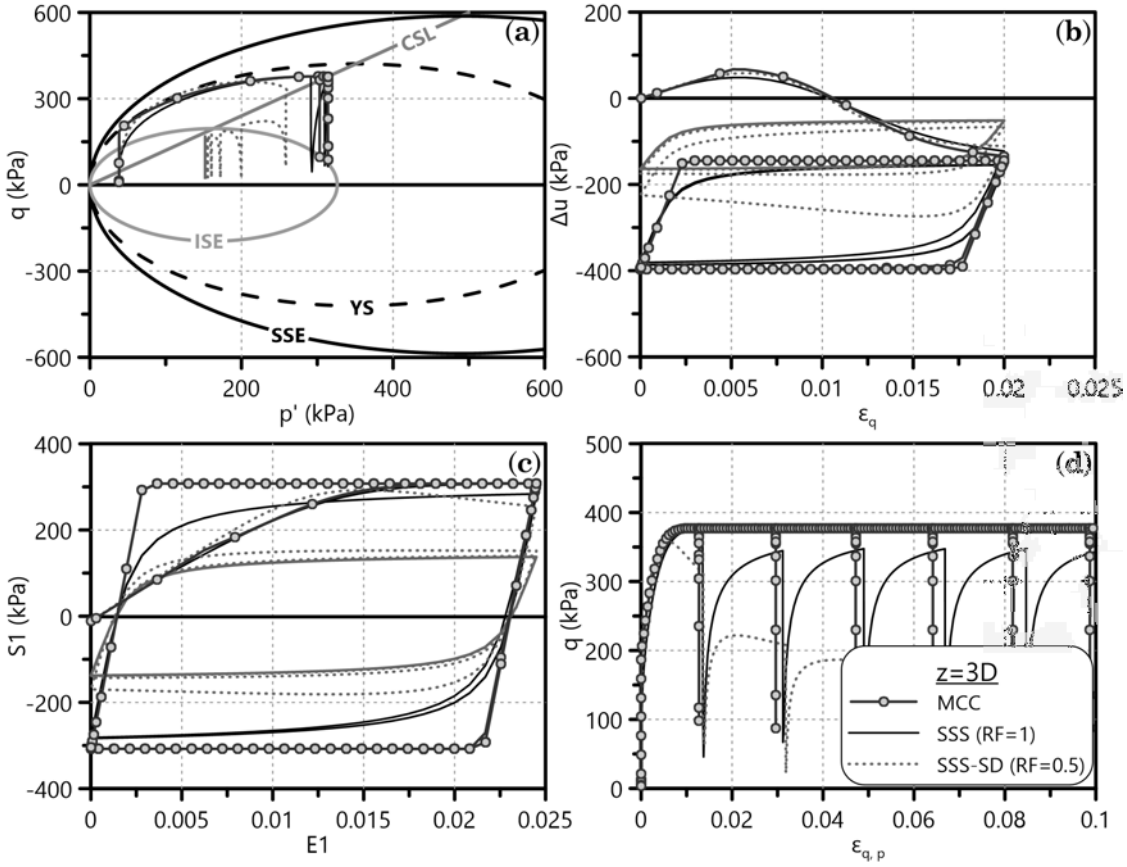

Figure 6.4: Effect of high intensity cyclic undrained triaxial loading (20 cycles, ε_a=2%) on (a) stress paths $p-q$, (b) excess pore pressure build-up $\Delta u-\varepsilon_q$, (c) stress-strain curve $S1-E1$ in the generalized space and (d) deviatoric stress-accumulated plastic deviatoric strain $q-\varepsilon_{qp}$ of a specific OC clay element under compression in front of the laterally loaded pile (z=3D).

despite the differences observed in terms of soil element response - potentially due to extensive soil deformation of the 3D FEA compared to the corresponding numerical triaxial tests. Furthermore, the cyclic loading does not seem to affect the post-cyclic H_u of all three soils.

The corresponding graphs of the stiff, OC clays (Figures 6.5b, c) depict clear indications of a stabilized pile-soil system response after a certain number of load cycles (the so-called plastic shakedown). In addition, we observe the reduced equivalent stiffness of the $y_h/D-H$ diagram if we take into account the interval of cyclic loading - definitely dependent on the number of the load cycles. Finally, the same diagram for the OC clay with strength degradation (RF=0.5) does not exhibit softening behavior, in contrast with the corresponding soil element stress-strain curves.

The aforementioned observations prove the capability of the 3D finite element model to simulate efficiently and realistically the pile response against external, lat-

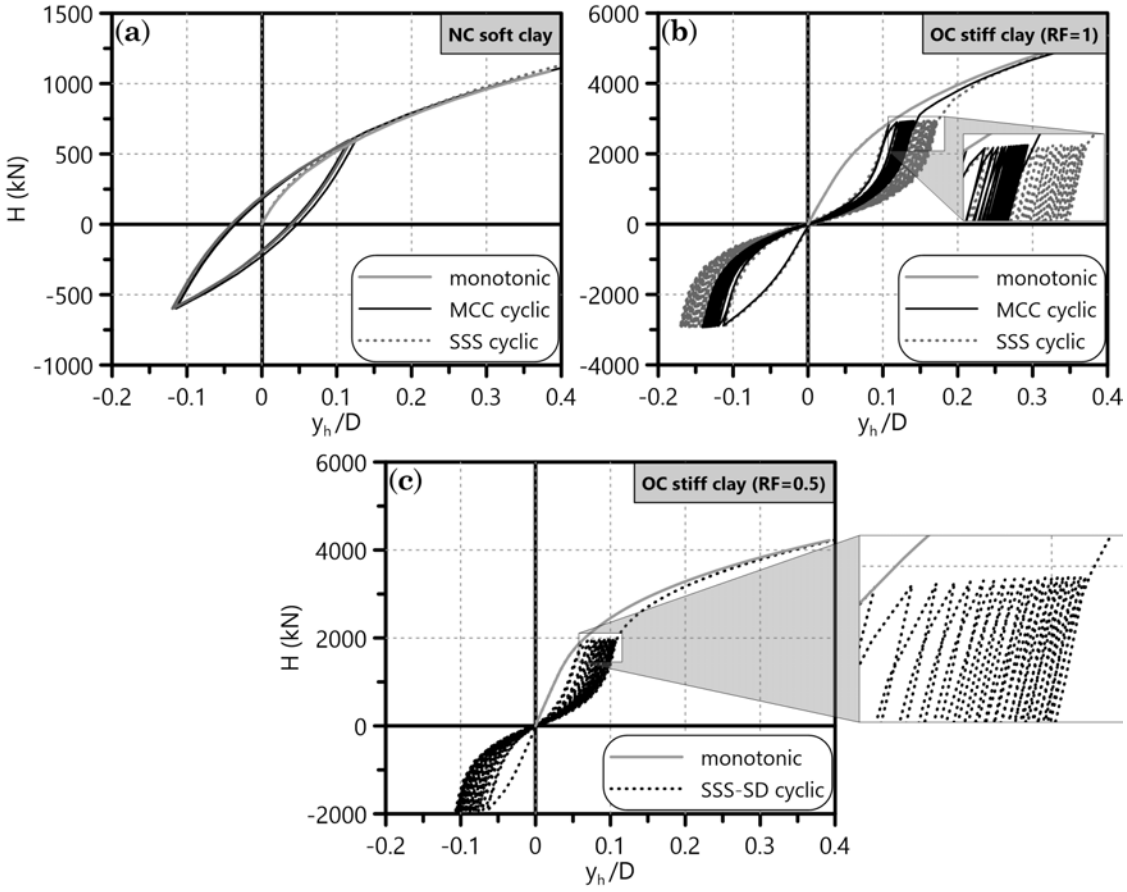

Figure 6.5: Diagrams of the non-dimensional lateral displacement - shear force of the pile head $y_h/D - H$ for monotonic and cyclic lateral loading in the following clayey soils: (a) soft, NC, (b) stiff, OC without strength degradation (RF=1) and (c) stiff, OC with strength degradation (RF=0.5).

eral, cyclic loads imposed on the pile head, regarding clayey soils under undrained loading conditions. Characteristic frames of the FEA that depict the realistic simulation of the cyclic pile-soil response are included in Appendix C.

6.5 Effect of cyclic loading on p-y curves for clays

The current paragraph deals with the effect of cyclic loading on the post-cyclic p-y curves, i.e. the curves derived from the final monotonic step of the aforementioned 3D FEA - after the imposed load cycles. More accurately, $H = H_u$ applies on the pile head - in accordance with the monotonic FEA (Chapters 4, 5) - after the 20 cycles of H_c, in order to observe potential differences of the post-cyclic p-y curves on this final step with corresponding monotonic ones. Before the examination of the numerical post-cyclic p-y curves, Figure 6.6 depicts the cyclic p-y curves (20 cycles)

at z=3D, derived from the FEA for the NC and the OC (RF=0.5) clayey soils. For comparative purposes, Figure 6.6a,b displays the cyclic p-y curves of the FEA with constant cyclic lateral pile head displacement y_h=0.2D while Figure 6.6c,d shows the corresponding curves for constant cyclic lateral load H_c.

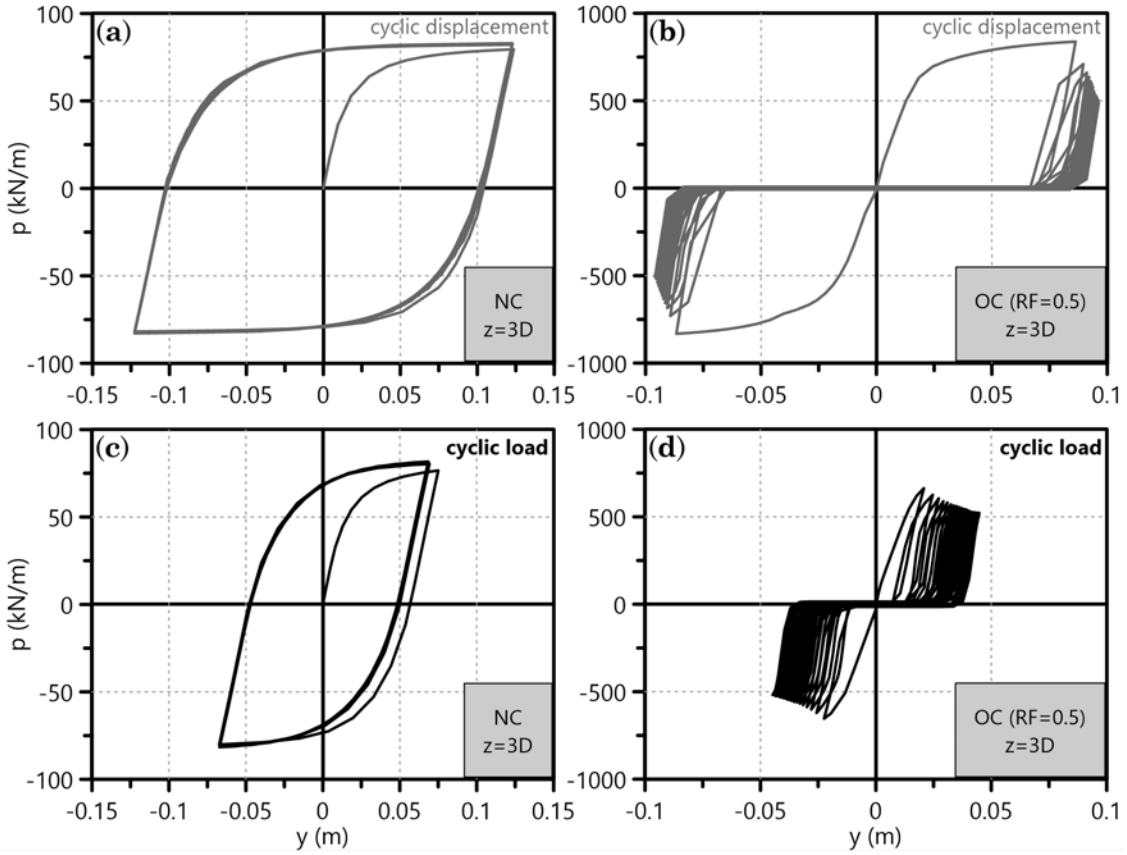

Figure 6.6: 20 load cycles of constant lateral pile head (a, b) displacement y_h=0.2D and (c, d) concentrated load H_c=0.3-0.5H_u in terms of p-y curves at z=3D for a NC (left) and an OC clay with RF=0.5 (right).

The aforementioned FEA examine the effect of twenty (20) displacement cycles - a rather small but indicative number - on both K_i and p_u of the post-cyclic p-y curves at various depths. The comparison applies between the pure monotonic p-y curves and the ones derived after the cyclic loading of the pile. Figure 6.6 justifies why the imposed cyclic load urges further investigation of the specific response, compared to the applied cyclic displacement - especially for OC clays. The following paragraphs present the effect of 20 load cycles on the post-cyclic p-y curves, together with certain reflections on the numerical simulation of the specific problem.

It is important to clarify that in the following investigation, the post-cyclic p-y curve is outlined by the final curve part, which indicates the transition of p from negative to positive values. Therefore, in order to compare the initial stiffness K_i

and the ultimate lateral soil resistance p_u between the monotonic and the post-cyclic p-y form, output processing needs to transpose the latter on the origin of the axes (see following paragraphs).

6.5.1 Cyclic numerical p-y curves for NC clays

The NC clay of the cyclic FEA has the following properties: M=0.984, λ=0.109, λ/κ=10, K_o=0.5, ν=0.333, namely the same ones tested under cyclic undrained triaxial loading in Paragraph 6.3. The soil surrounding the laterally loaded pile keeps falling in the gap that tends to form behind[1] the pile due to its very low strength.

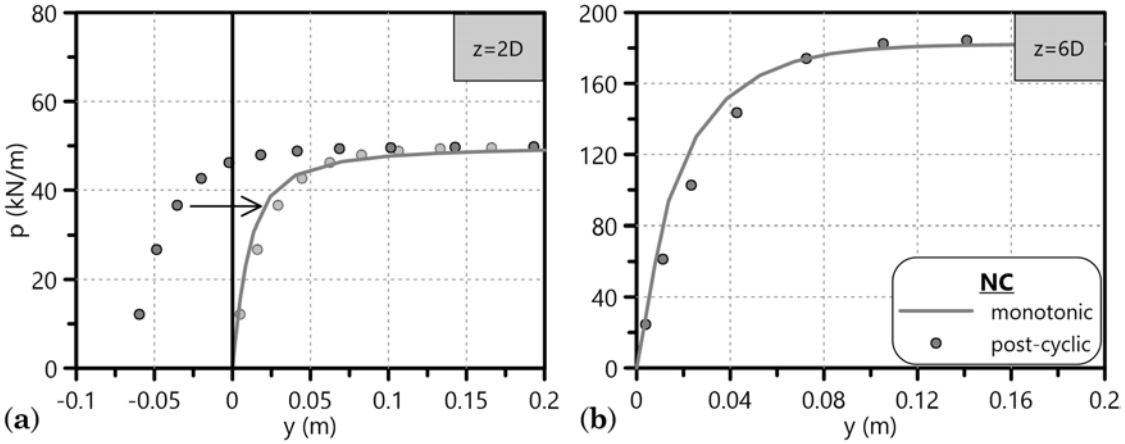

Figure 6.7: Comparison of monotonic p-y curves with the ones derived after 20 cycles of constant, lateral pile head concentrated load H_c=600kN for a NC clay at (a) z=2D and (b) z=6D.

Figure 6.7 depicts the comparison between monotonic and post-cyclic p-y curves at shallow (z=2D) and greater depth (z=6D). No significant difference is observed between the two p-y forms, even for the significant lateral displacement imposed to the pile head by the 20 cycles of H_c=600kN ($y_h \approx 0.1D$, Figure 6.5a). Cyclic loading with constant lateral pile head displacement (y_h=0.2-0.5D) led to the same observation - since the soil deformation mechanism of both simulations for such soft soils does not change.

6.5.2 Cyclic numerical p-y curves for OC clays

The OC clays of the cyclic FEA have the following properties: M=1.2, $c_{u,avg}$=190 kPa, RF=0.5-1, κ=0.0054, $K_{o,max}$=1.5, ν=0.1, namely the same ones tested under

[1] at the pile side opposite to the loading direction, since the pile deflects laterally back and forth during the load cycles

cyclic undrained triaxial loading in Paragraph 6.3. The soil surrounding the laterally loaded pile forms a "funnel" shape after stabilization of the cyclic pile-soil response.

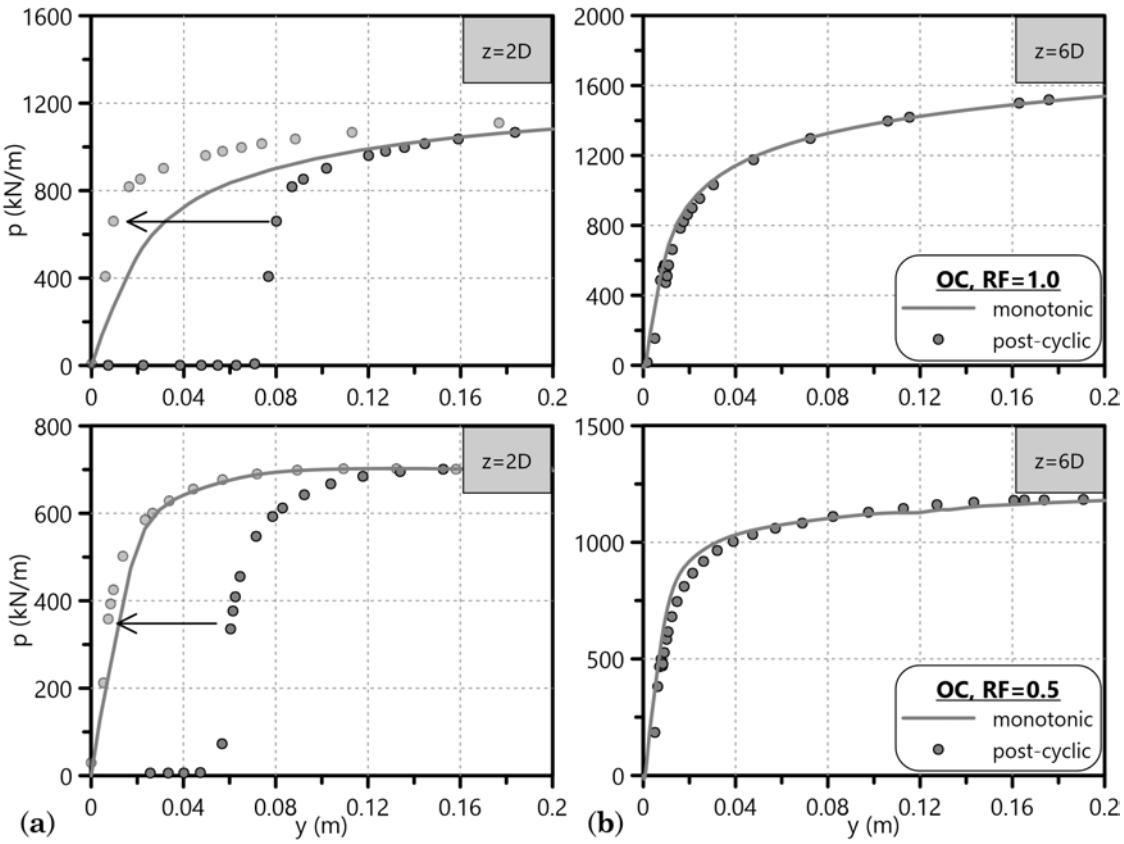

Figure 6.8: Comparison of monotonic p-y curves with the ones derived after 20 cycles of constant, lateral pile head concentrated load H_c for an OC clay without (up - RF=1, H_c=3000kN) and with strength degradation (down - RF=0.5, H_c=2000kN) at (a) z=2D and (b) z=6D.

Figure 6.8 depicts the comparison between monotonic and post-cyclic p-y curves at shallow (z=2D) and greater depth (z=6D). At the latter, the observation is the same with the corresponding p-y curves for the NC clay: no significant difference is observed between the two p-y forms. However, at z=2D the post-cyclic p-y curve exhibits higher K_i than the monotonic one - an effect that seems to fade with strength degradation (see RF=0.5 at the same depth). It is natural not to expect the same results from the FEA with cyclic constant lateral pile head displacement, since the imposed soil deformation mechanism allows for negligible alterations of the developed p from the stiff soil on the pile.

6.6 Concluding remarks on cyclic p-y curves for clays

FEA for cyclic (pseudostatic) lateral loading of a single 1m-diameter pile for twenty (20) load cycles - with constant concentrated horizontal force on the pile head - exhibit no significant differentiation of the post-cyclic against the monotonic numerical p-y curves for soft, NC clayey soils at all depths and for stiff, OC clayey soils at significant depth (z=6D). K_i of the post-cyclic p-y curves for stiff, OC clays without strength degradation is increased compared to the corresponding monotonic one at shallow depth (z=2D).

In more detail, Chapter 6 concludes in the following observations referring to numerically derived cyclic p-y curves for NC and OC clayey soils:

- Numerical undrained triaxial cyclic tests (strain-controlled) of both soil types are carried out in order to verify whether the utilized constitutive laws of the thesis - MCC and SSS-SD model by Kalos (2014) - capture successfully the corresponding behavior of the specimens. NC clay cyclic tests with both laws[1] exhibit no significant difference in terms of soil element cyclic response ($p-q$, $\Delta u-\varepsilon_q$, $S1-E1$) apart from the deviatoric plastic strain accumulation - MCC fails in this aspect. However, as long as the MCC reflects the general cyclic behavior of such soils it is utilized in the cyclic FEA of the laterally loaded pile. On the contrary, OC clays with strength degradation ($RF < 1$) exhibit significant differences compared to the corresponding MCC simulation. Features of non-linear elasticity (PYE) and strain-softening allow for the formulation of hysteresis loops during cyclic loading.

- Two different cyclic loading regimes apply on the pile head, namely a strain- and a stress-controlled. Regarding the first, two lateral deflections (y_h=0.2, 0.5D) are imposed on the pile towards both directions of its initial position. The conclusion is drawn that a constant cyclic pile head deflection may not trigger the mechanisms that alter the p-y curves after certain load cycles. Therefore, the chapter examines the effect of cyclic concentrated force for three soil types - one NC and two OC (with and without strength degradation), primarily on the lateral pile head response and secondarily on the post-cyclic p-y curves. The application of constant, two-way cyclic lateral force on the pile head delivers differentiated shallow post-cyclic p-y curves in terms of K_i for the OC clays, compared to the monotonic ones.

[1] the sophisticated constitutive law without strength degradation ($RF = 1$)

- The current numerical simulation is pseudostatic and does not account for time dependent phenomena. It only serves as an initial attempt to simulate undrained cyclic lateral loading of piles and examine potential effects on the derived post-cyclic p-y curves from a qualitative point of view. Further research is recommended on this topic, together with certain calibrations of the sophisticated constitutive law, especially regarding the rate dependency of the imposed cyclic loading. Finally, the absence of fatigue characteristics may be responsible for the behavior encountered in the aforementioned preliminary results.

Chapter 7

Experimental evaluation of the proposed p-y curves

7.1 General

The present chapter evaluates the efficiency of the proposed p-y curves for NC and OC clays through comparisons with centrifuge and large scale test results. These comparisons involve charts of the pile head lateral displacement vs. shear force ($y_h - H$) as well as the distribution of bending moment (M$-z$) and/or lateral displacement ($y - z$) along the laterally loaded pile. To do so, we apply the proposed p-y curves on a BNWF (Beam on Nonlinear Winkler Foundation) model taking into account all the soil and pile parameters described in the actual tests.

Part of this evaluation is also to verify whether the proposed p-y methodology is more effective than other literature methods (see Chapter 2) with reference to the aforementioned graphs. Since there is a wide variety of p-y methodologies applicable to both NC and OC clays, the current evaluation chooses to compare the p-y curves of this dissertation with corresponding curves from the upper and lower bound of the literature range. Thus, the following process also serves as guidelines for the design of laterally loaded piles in such clays.

7.2 Evaluation process

The laterally loaded pile is simulated as a BNWF on the $x-y$ plane[1] through Simulia Abaqus 6.12 in order to test the efficiency of the proposed p-y curves compared to other literature methodologies. The following paragraphs describe the numerical simulation and verify its accuracy in the calculation of shear forces, bending

[1] lateral load along x-axis, pile axis along y-axis

moments and lateral displacements along the pile.

7.2.1 The numerical BNWF simulation

The BNWF model is as simple as a single beam on non-linear springs, representing the pile and the lateral soil reaction respectively. Planar beam elements B21 simulate the pile and spring elements SPRING1 the horizontal soil response. Figure 7.1 displays the details of the numerical simulation regarding the p-y curves. Simulia Abaqus models the soil springs as force-displacement curves. However, p-y curves are usually expressed as distributed load-displacement curves in the literature (lateral soil pressure p multiplied by the pile width D). Therefore, the distributed lateral load p (kN/m) along the pile - depending on the depth of the p-y curve - is multiplied by the corresponding pile length of influence dz (m) in order to derive the required force-displacement SPRING1 curves.

Since the proposed monotonic p-y curves of the current dissertation involve compressibility parameters (λ, κ), Table 7.1 (Bowles, 1988) proposes certain correlations with natural soil characteristics such as Atterberg limits (PL, LL), water content w_N, specific gravity of soil grains G_s and initial void ratio e_o, in case the test reports lack information on the compressibility indexes. An average of these correlations provides us with a good estimate on the desired parameters and allows us to incorporate them in the proposed p-y curves. Poisson's ratio ν for all the clays of the experiments ranges between 0.10-0.30 if the test documentations do not suggest specific values for this parameter. The simulation of the pile takes into account the properties of the pile material, i.e. Young's modulus E_p, Poisson's ratio ν_p, yield strength f_y as well as moment-curvature graphs - if they are documented in the tests under investigation. Furthermore, the boundary conditions applied on the pile head and tip follow the observations of each experiment separately. Either free- or restrained-head conditions apply to the pile head. The pile tip rotates freely in the numerical simulation but if the test documentation states that the pile plugs then fixed conditions apply to its tip. Since all the test piles are not loaded vertically no boundary conditions apply to the pile tip in the vertical direction (y-axis). The aforementioned numerical simulation ensures that the BNWF model simulates the pile behavior as realistically as possible.

To gain confidence on the FEA output of this numerical simulation we cross-check the results of the BNWF model with the ones derived from the sophisticated 3D FEA of Chapters 4 and 5, regarding the distribution of shear forces, bending moments and lateral displacements along the pile in NC and OC clays.

Table 7.1: Correlation equations for soil compressibility

Compression index (C_c)	Comments	Source/Reference
$C_c = 0.009(LL - 10)^2$ ($\pm 30\%$ error)	Clays of moderate sensitivity	Terzaghi & Peck (1967)
$C_c = 0.37(e_o + 0.003LL + +0.0004w_N - 0.34)^3$	678 data points[5]	Azzouz et al. (1976)
$C_c = 0.141 G_s(\gamma_{\text{sat}}/\gamma_{\text{dry}})^{2.4}$	All clays	Rendon-Herrero (1983)
$C_c = 0.0093 w_N$	109 data points	Koppula (1981)
$C_c = -0.0997 + 0.009LL + 0.0014I_p + +0.0036w_N + 0.1165e_o + 0.0025C_p$[4]	109 data points[5]	Koppula (1981)
$C_c = 0.329[w_N G_s - 0.027PL + +0.0133I_p(1.192 + C_p/I_p)]^2$	All inorganic clays[5]	Carrier (1985)
$C_c = 0.046 + 0.0104I_p$	Best for $I_p < 50\%$	Nakase et al. (1988)
$C_c = 0.00234LL\,G_s$	All inorganic clays	Nagaraj & Srinivasa Murthy (1985, 1986)
$C_c = 1.15(e_o - 0.35)$	All clays	Nishida (1956)
$C_c = 0.009w_N + 0.005LL$	All clays	Koppula (1986)
$C_c = -0.156 + 0.411e_o + 0.00058LL$	72 data points	Al-Khafaji & Andersland (1992)
$C_c = (0.1849(G_s\,I_p)^{0.8021})\ln 10$	Intrinsic compressibility framework	Belokas & Kavvadas (2011)
Recompression index (C_r)		
$C_r = 0.000463LL\,G_s$		Nagaraj & Srinivasa Murthy (1985, 1986)
$C_r = 0.00194(I_p - 4.6) =$ $= 0.05$ to $0.1C_c$	Best for $I_p < 50\%$ In desperation	Nakase et al. (1988)

[1] All correlations by Bowles (1988) (Table 2-5), apart from Belokas & Kavvadas (2011).
[2] Use PL, LL, w_N, I_p as percent, not decimal.
[3] One may compute the in situ void ratio as $e_o = w_N\,G_s$ if $S_r \to 100\%$.
[4] C_p =percent clay (usually material finer than 0.002mm).
[5] Equations that use e_o, w_N and LL are for both normally and overconsolidated soils.

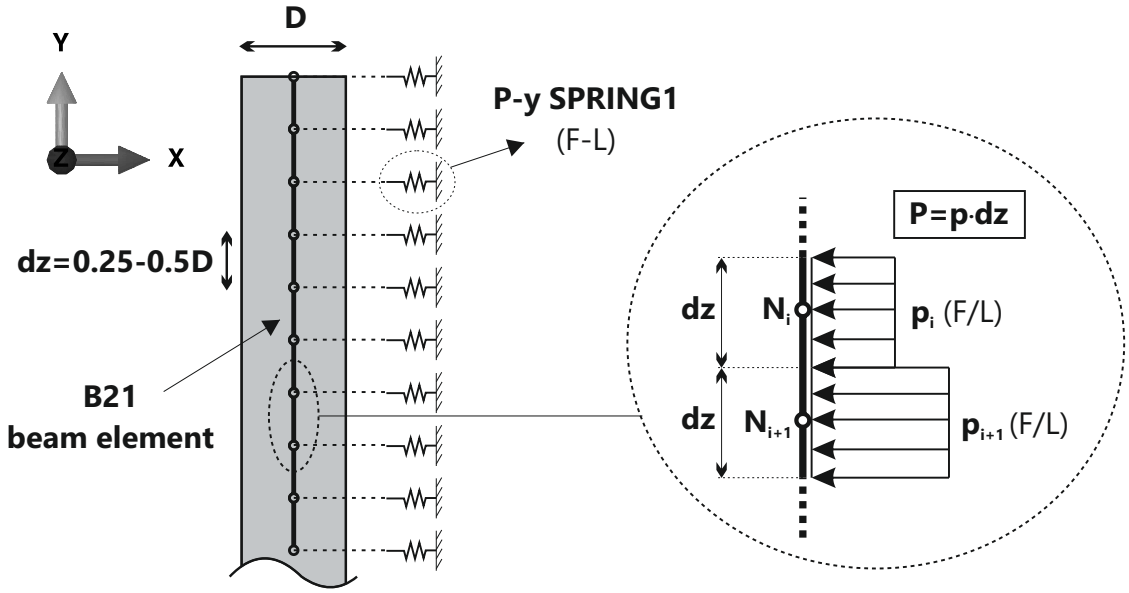

Figure 7.1: Numerical simulation of the laterally loaded pile as a BNWF (Beam on Nonlinear Winkler Foundation) and incorporation of the p-y curves in the FEA.

7.2.2 Verification of the BNWF model

The proposed p-y curves of this dissertation for NC and OC clays occurred from the numerical investigations described thoroughly in Chapters 4 and 5 respectively. The 3D FEA carried out to derive these curves serve here as a validation for the output of the simplistic BNWF simulation. The following paragraph compares the $y_h - H$, M$-z$ and $y - z$ graphs derived from the BNWF analyses with the corresponding diagrams of the 3D FEA for two different cases:

- a NC clay with M=0.984, λ=0.109 and pile-soil adhesion factor α=1.0,
- an OC clay with $c_{u,\,avg}$=190kPa, κ=0.065, ν=0.1 and pile-soil adhesion factor α=0.3.

The pile is considered elastic with reinforced concrete properties (E_p=30GPa, ν_p=0.2), its' head is free to rotate and a lateral displacement y_h=1D is applied on the pile head. Figure 7.2 compares the $y_h - H$ curves between the two simulations for both clays under consideration. Figures 7.3 and 7.4 compare the M$-z$ and $y - z$ distributions along the pile respectively between the BNWF and the 3D FE model for y_h=0.2D.

All the aforementioned comparisons demonstrate a very accurate numerical simulation of the actual 3D problem utilizing the 2D BNWF model together with the proposed p-y curves. Thus, the following paragraphs adopt this simulation in order to compare the experimental results of laterally loaded piles in soft NC and

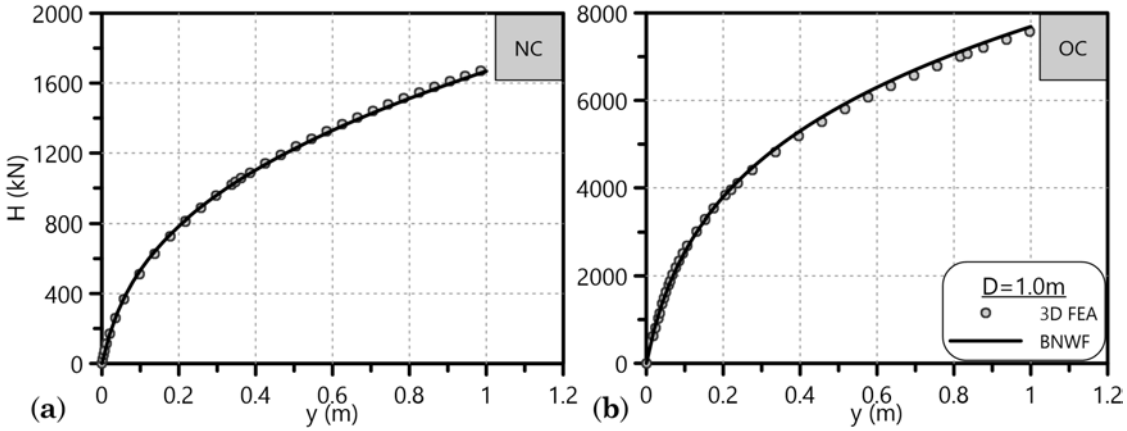

Figure 7.2: Comparison of pile head lateral load-displacement curves $y_h - H$ between the BNWF and the 3D FE simulations for (a) the NC and (b) the OC clay under consideration.

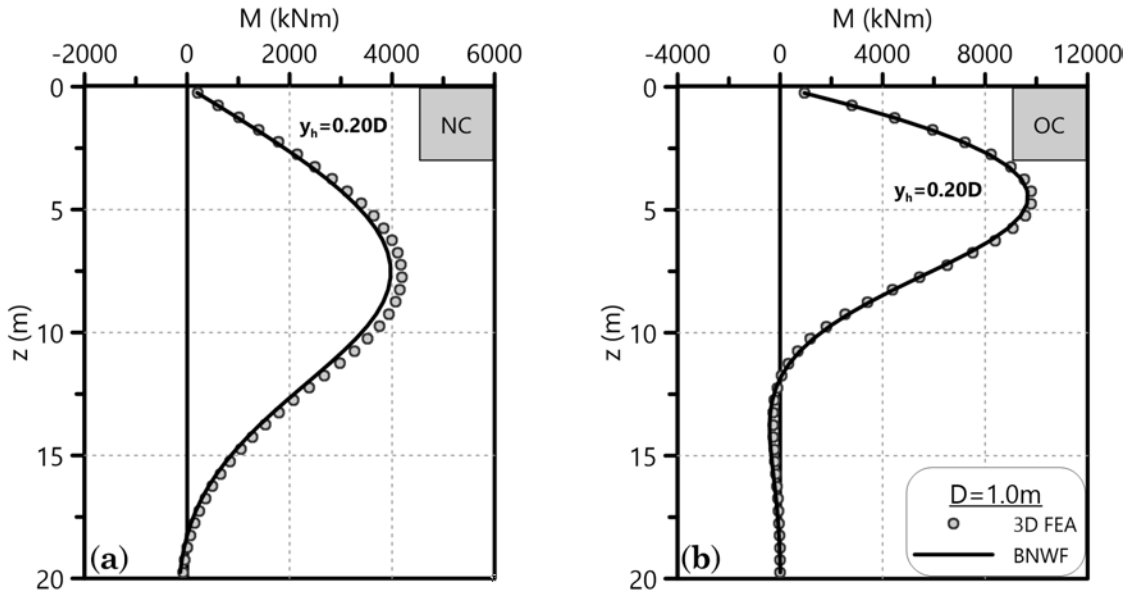

Figure 7.3: Comparison of bending moment distributions M$-z$ along the laterally loaded pile between the BNWF and the 3D FE simulations for (a) the NC and (b) the OC clay under consideration.

stiff OC clays with corresponding predictions using certain p-y curve methodologies (proposed here and from literature).

7.3 Evaluation of p-y curves for NC clays

Two different centrifuge tests by Ilyas et al. (2004) and Doyle et al. (2004) are chosen for the evaluation of the proposed p-y curves for soft NC clays. Both of them use kaolin slurry that consolidates under acceleration equal to that of the experiment.

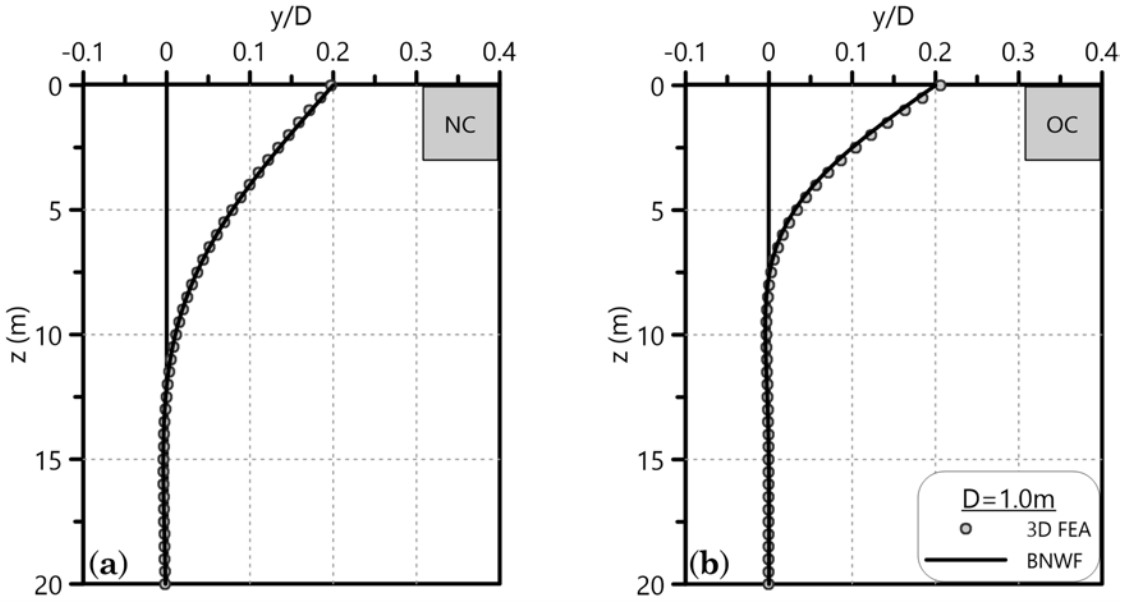

Figure 7.4: Comparison of lateral displacement distributions $y - z$ along the pile between the BNWF and the 3D FE simulations for (a) the NC and (b) the OC clay under consideration.

Thus, the consolidation process forms soft NC clay profiles with c_u that increases linearly with depth. Both experiment series attempt to clarify the effect of spacing on the lateral response of pile groups and compare it to the corresponding single pile behavior in such soils. The following evaluations utilize experimental results for the lateral response of the single pile and compare them with the BNWF predictions.

7.3.1 Centrifuge test by Ilyas et al. (2004)

Ilyas et al. (2004) carried out a series of centrifuge model tests in order to examine the behavior of laterally loaded pile groups in normally consolidated and overconsolidated kaolin clay. Apart from pile groups, lateral load tests were also conducted to single piles. Figure 7.5 depicts a schematic representation of the centrifuge test configuration. All the tests were conducted at 70g on the National University of Singapore (NUS) Geotechnical Centrifuge, which has a radius of 2 m and comprises a balanced arm with dual swing platforms.

The kaolin clay used to prepare the soft, NC clay profile in the test container had the following properties: average bulk unit weight $\gamma = 16kN/m^3$, average water content $w_N = 66\%$, plastic limit $PL = 35.1\%$, liquid limit $LL = 79.8\%$, virgin compression line slope $C_c = 0.55$, unloading-reloading line slope $C_r = 0.16$ and permeability $k = 2 \cdot 10^{-8} m/s$. The following stages were carried out for the preparation of the NC clay:

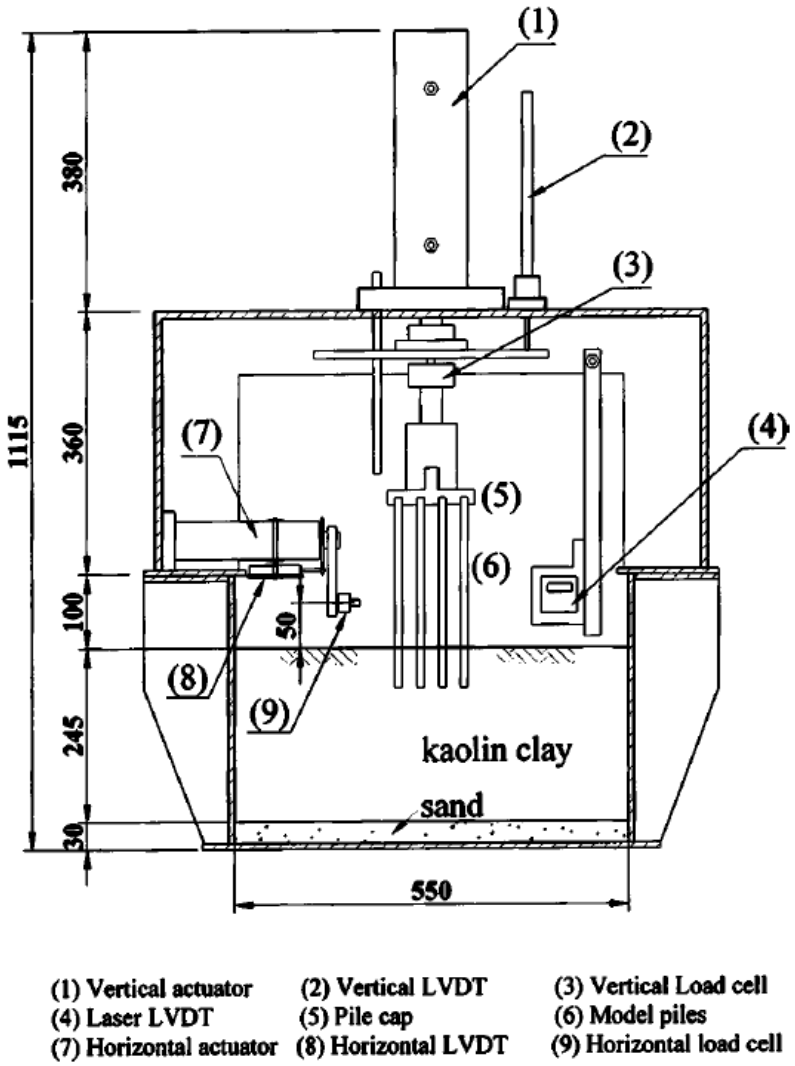

Figure 7.5: Centrifuge model setup of the laterally loaded pile tests carried out by Ilyas et al. (2004) (units in mm).

1. a 30-mm-thick sand layer (prototype 2.1m) was first placed at the bottom of the model container before placing the kaolin clay slurry.

2. the kaolin clay slurry was thoroughly mixed at 150% of its LL and deaired for 24h.

3. the slurry was then poured in the test container up to a thickness equal to 380mm and then consolidated under its self-weight in the centrifuge at 70g to allow the excess pore water pressure in the clay to dissipate through the clay surface and the openings located close to the bottom of the container via the bottom sand layer. After 6h of consolidation during flight and constant measurement of ground settlements and pore water pressures, the process reached

a degree of consolidation 95% resulting in a final clay thickness of about 245mm (prototype 17.15m).

4. T-bar penetrometer tests (Stewart & Randolph, 1991) that were conducted in-flight to determine the soil strength profile after consolidation, revealed that the c_u of the NC clay increased linearly with depth from 0 at ground surface to about 20kPa at prototype depth z=15m - thus the clay was considered soft.

Although the test reports do not mention any free water presence, it is possible that after completion of the consolidation progress some water content of the clay pores reached the ground surface. Thus, the following evaluation assumes that the centrifuge tests were carried out with free water above ground surface.

The model pile is a hollow aluminum square tube instrumented with ten levels of strain gauges to enable bending moment measurements along the pile shaft. At 70g, the simulated prototype pile has a width B=0.84m, embedded length L_b=14.7m in the clay, flexural rigidity $E_pI_p = 922MNm^2$[1] and the lateral load is applied on the pile head that lies 3.5m above ground surface - that results in a total pile length L=18.2m. All the test piles were jacked into the soil at 1g, assuming insignificant difference in pile capacity between 1g and 70g due to relatively small volume change of the clay - opposite to sand - during pile installation (Craig, 1985). The centrifuge was then spun up to 70g again for about 1h to enable the pore water pressure developed during pile installation to dissipate completely. A horizontal actuator (see Figure 7.5) pushes laterally the pile head until it reaches horizontal displacement y_h=1B.

Figure 7.6 depicts the p-y curves derived from all the methodologies applicable to soft, NC clays at two different depths, namely a shallow (z=2B) and a greater one (z=6B). The p-y curves proposed by Nichols et al. (2014) lie on the upper bound and close to the methodology of the current doctoral thesis ($\lambda = C_c/\ln 10 = 0.24$, $\lambda/\kappa = 3.9$, $\nu = 0.3$, $\alpha = 0.3$ for aluminium pile), while the p-y curves by Matlock (1970) (ε_{50} from Table 2.2) - also adopted by API (2007) - are located around the mid-range of the demonstrated plots. As long as the literature generally agrees that Matlock's p-y curves lead to a rather conservative design, we initially considered this methodology as the lower bound of the evaluation. The 2D simulations assume yield strength of the pile aluminium f_y=110MPa. By applying the three aforementioned p-y curve methods in the BNWF model, the following process compares their efficiency in predicting the lateral response of the single pile that was measured during the centrifuge test.

[1] assuming Young's modulus for the aluminium $E_{al} = E_p$=70GPa, the moment of inertia for the hollow square is I_p=0.0132m^4, resulting in prototype wall thickness t=0.0382m

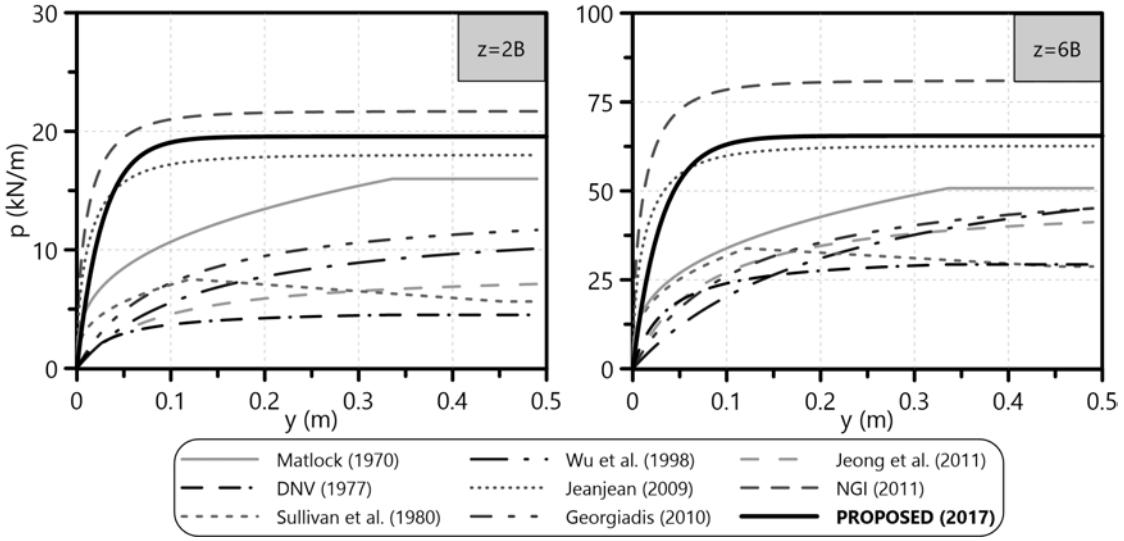

Figure 7.6: Comparison of the proposed monotonic p-y curves with corresponding literature methodologies for a square pile of B=0.84m and α=0.3 in the fully saturated soft NC clay described by Ilyas et al. (2004) at shallow (z=2B) and greater depth (z=6B).

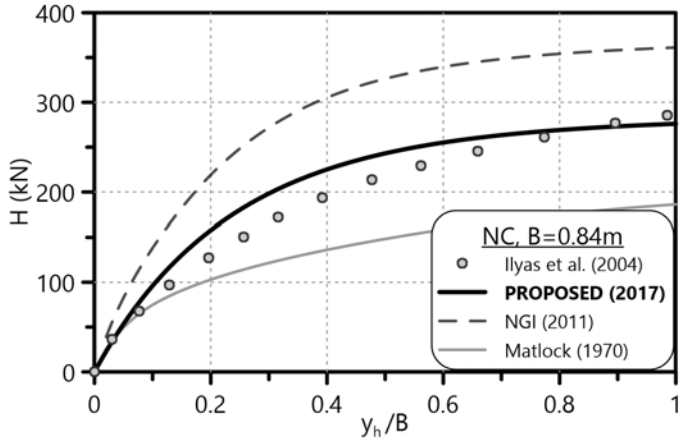

Figure 7.7: Comparison of dimensionless pile head lateral load-displacement curves $y_h/B-H$ between the centrifuge test measurements by Ilyas et al. (2004) and the BNWF simulations incorporating the p-y curves by Nichols et al. (2014), Matlock (1970) and the current dissertation.

Figures 7.7 and 7.8 demonstrate $y_h/B-H$ and M$-z$ curves of the experiment compared to the BNWF output from the simulation of the lateral NC clay response through the three aforementioned p-y curve methodologies. The p-y curves of the present dissertation deliver the closest plots to the experimental measurements. Moreover, they estimate very accurately both the ultimate pile head load and the maximum bending moment along the pile for two different lateral pile head displacements, namely y_h=0.1B and 0.5B. The BNWF analyses display that soil

failure dominates the lateral response of the pile-soil system, since no plastic hinge appears along the pile (pile deformation refers to short pile failure).

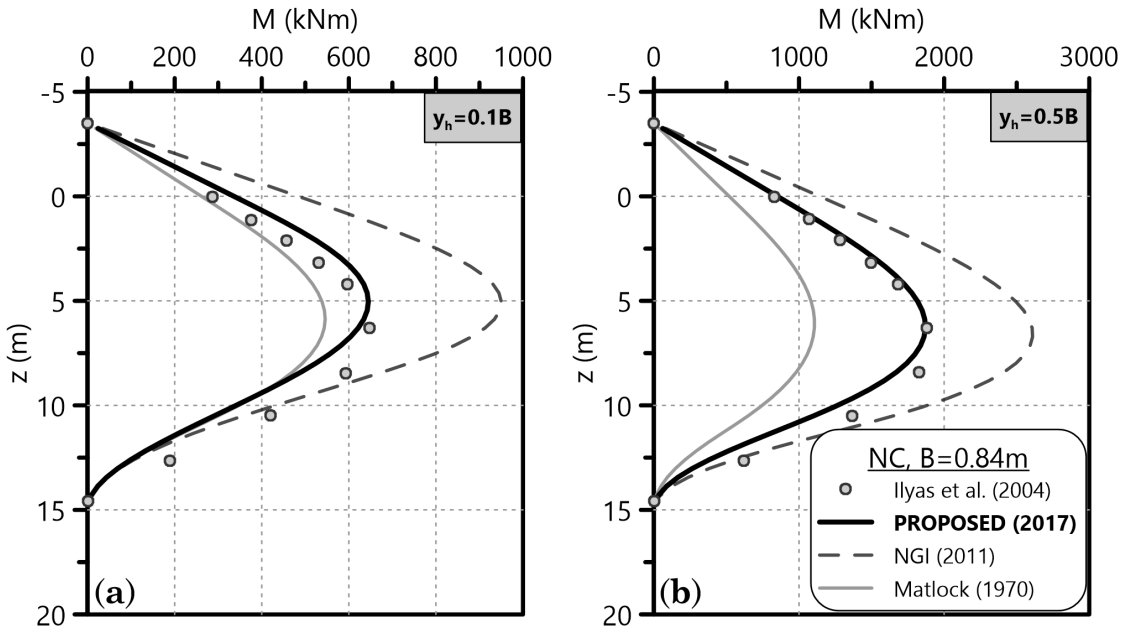

Figure 7.8: Comparison of bending moment distributions M$-z$ along the laterally loaded pile at (a) y_h=0.1B and (b) y_h=0.5B between the centrifuge test measurements by Ilyas et al. (2004) and the BNWF simulations incorporating the p-y curves by Nichols et al. (2014), Matlock (1970) and the current dissertation.

The aforementioned evaluation demonstrates how the proposed p-y curves for soft, NC clays successfully predict lateral pile head load-displacement curves and bending moment distribution along the pile for various load levels of the pile head. Furthermore, the significant divergence (around 50% from the experimental measurements) between the plots of Figures 7.7 and 7.8 outlines the need for more accurate p-y curves - take into account that only methods above the mid-range were chosen for the BNWF simulations.

7.3.2 Centrifuge test by Doyle et al. (2004)

Doyle et al. (2004) conducted four centrifuge model tests in order to examine the behavior of a single pile and a pair of piles under monotonic and cyclic lateral loading in normally consolidated kaolin clay. Figure 7.9 demonstrates the general configuration of the centrifuge tests together with a detail on the loading setup of the pile heads. All the tests were carried out at 100g in a 850mm diameter cylindrical tube at Cambridge University.

The speswhite kaolin clay used to prepare the soft, NC clay profile in the test tub

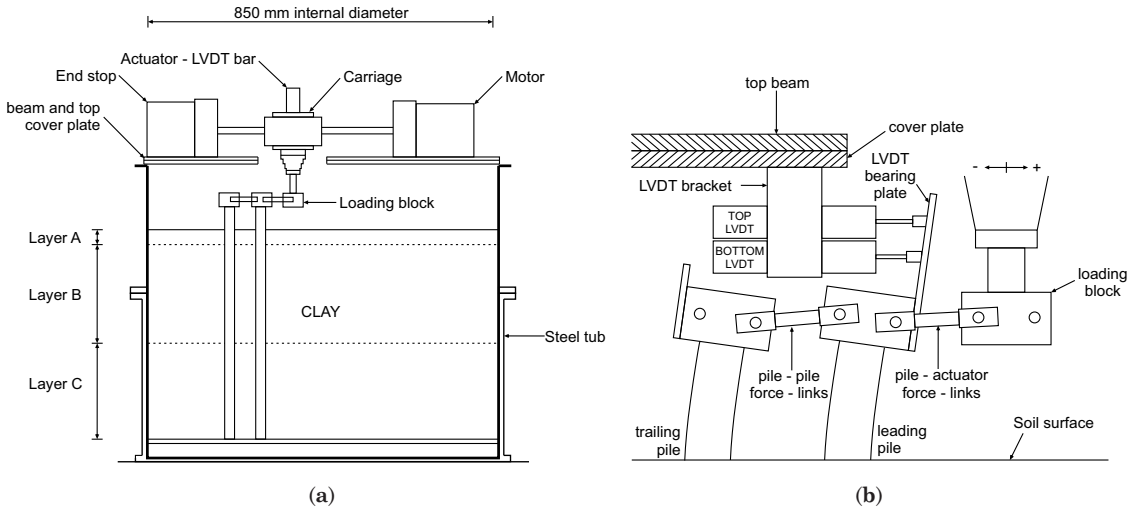

Figure 7.9: (a) Centrifuge model setup of the laterally loaded pile tests carried out by Doyle et al. (2004). (b) Detail of the link assembly between pile heads and the loading block.

was selected as being reasonably similar to "typical" Gulf of Mexico clays and has been used on previous model tests, see for example Murff & Hamilton (1993). The test report suggest the following properties for the clay: plastic limit $PL = 38\%$, liquid limit $LL = 69\%$ and specific gravity of the soil grains $G_s = 2.61-2.64\, Mg/m^3$. Figure 7.10b displays an average water content $w_N = 55\%$ and the present evaluation assumes initial void ratio $e_o{=}w_N \cdot G_s{=}0.55 \cdot 2.62{=}1.441$ (Bowles (1988), Table 2-5). Calculations according to Table 7.1 suggest average values of the compressibility indexes $C_c = 0.60$ and $C_r = 0.05$. The natural clay characteristics determine the average bulk unit weight of the clay through the following equation:

$$\gamma = G_s \frac{1+w_N}{1+e_o} g \quad \xrightarrow[e_o=w_N \cdot G_s]{w_N=55\%} \quad \gamma = 16.6 kN/m^3$$

The following stages were carried out for the preparation of the NC clay:

1. Mixing of kaolin powder with de-ionized water under partial vacuum produced a slurry at a moisture content of about twice the LL.

2. The kaolin slurry was poured and consolidated in the 850mm diameter steel tub at 1g in three layers (Figure 7.9). In more detail, layer C was consolidated to a uniform vertical effective stress of 350kPa. Layer B was poured onto the top of layer C and both layers were consolidated together by a downwards-hydraulic gradient method. Finally, just before Test 1 (single pile, static loading), layer A was poured as a slurry on top of layer B. The objective of the specific soil

profile formation was to create a layer with a shear strength varying linearly with depth, namely a NC clay.

3. At the beginning of each centrifuge test, the clay was allowed to re-consolidate at 100g for approximately 24h (around 27 years prototype time). Pore pressure transducers that were pre-installed in the clay during specimen preparation monitored the excess pore pressures. Despite the long consolidation time, the process did not achieve full dissipation of excess pore pressures.

4. In-flight vane tests measured the actual c_u profile of layer B, which had a linear distribution with depth c_u=$0.23\sigma'_{vo}$. Especially during Test 1, Layer B was under-consolidated according to vane measurements - they appear largely to the left of the aforementioned linear distribution assumed for c_u - potentially due to lack of total excess pore pressure dissipation (Figure 7.10a[1]). Layer C was supposed to have constant c_u=81kPa with depth based on consolidation.

Although the test reports do not mention any free water presence, it is possible that after completion of the consolidation progress some water content of the clay pores reached the ground surface. Thus, the following evaluation assumes that the centrifuge tests were carried out with free water above ground surface.

The model pile is a hollow duraluminium tube of prototype outer diameter D=2.54m consisting of two parts - upper and lower - with different internal diameters and finalized with a solid plug at its tip. The pile is instrumented with fifteen levels of strain gauges (see Figure 7.10c) to enable bending moment measurements along the pile shaft. At 100g, the prototype length and stiffness of the three aforementioned parts are the following:

- upper part of embedded length $L_{1,b}$=30.0m, length extruding from ground surface 7.5m (point of lateral load application), flexural rigidity $E_pI_{p,1} = 60263MNm^2$ and equivalent wall thickness[2] t_1=0.04953m.

- lower part of embedded length $L_{2,b}$=17.5m, flexural rigidity $E_pI_{p,2} = 46776MNm^2$ and equivalent wall thickness[2] t_2=0.0381m.

- solid plug with length L_{plug}=4.0m, diameter decreasing from D=2.54m to D=2.39m with depth and flexural rigidity $E_pI_{p,\text{plug}} > 86090MNm^2$.

[1]Vane test measurements refer to both small and large strain, delivering peak and residual c_u of the NC clay respectively. The BNWF simulation fits only peak strength values, since the proposed methodology takes these into account.

[2]equivalent wall thickness calculated on the basis of matching the prototype E_pI_p to a steel pile (E_p=200GPa).

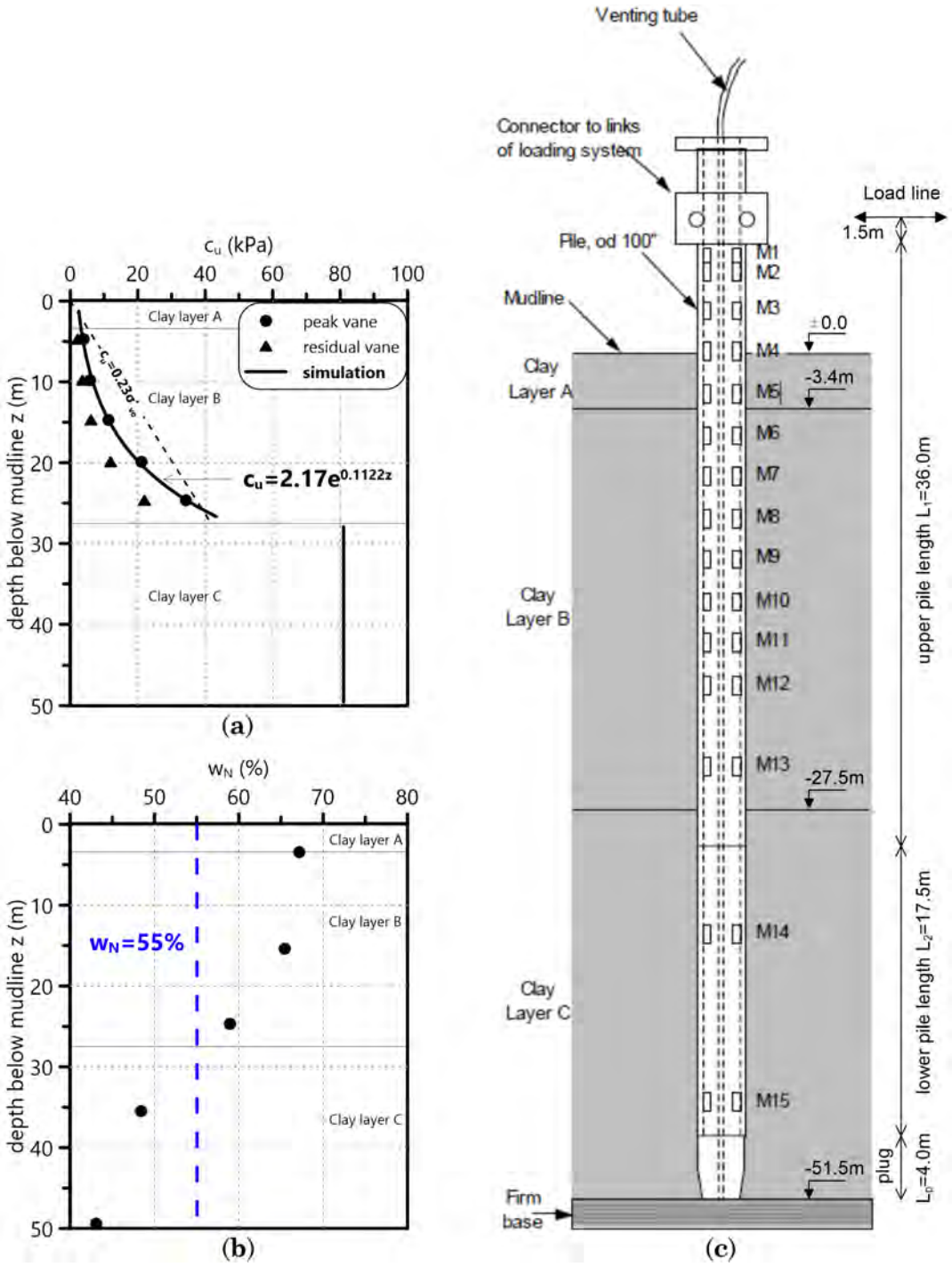

Figure 7.10: Details on centrifuge Test 1 by Doyle et al. (2004): (a) distribution of undrained shear strength c_u and (b) natural water content w_N measurements with prototype depth, together with simulation values. (c) Model pile instrumentation and prototype lengths of separate parts.

The aforementioned pile parts result in a total pile length L=59m. The model piles were driven in pre-augered holes in the clay. Clay samples extracted from the holes were tested in order to determine the moisture content of the soil. An electric motor applied lateral displacements to a carriage, which imposed the lateral load to the piles through a loading block properly linked to their heads (Figure 7.9b).

The first static test loaded the single pile to failure, since the bending moment distribution along the pile calculated from the readings of the strain gages under elastic conditions became inaccurate for $H > 95\%H_u$ - H_u=the ultimate pile head lateral load. After the specific loading point, yield moments appeared between z=23-30m below mudline. The test reports duraluminium stress at the elastic limit equal to 235MPa and ultimate stress 430MPa. The corresponding yield (M_y) and ultimate (M_u) bending moments[1] of the pile parts are calculated: (a) for the upper part $M_{y,1} = 156MNm$, $M_{u,1} = 395MNm$ and (a) for the lower part $M_{y,2} = 121MNm$, $M_{u,2} = 303MNm$. Inspection after Test 1 indicated that after lateral pile head deflection $y_h = 3.66m \approx 1.5D$ the pile had developed a plastic hinge at $z = 30m \approx 12D$ below ground surface with total hinge rotation of 1.9^o. Comments on this test suggest the usage of M_y values together with the corresponding yield curvature for the most accurate back-calculation of the measured M and y distributions.

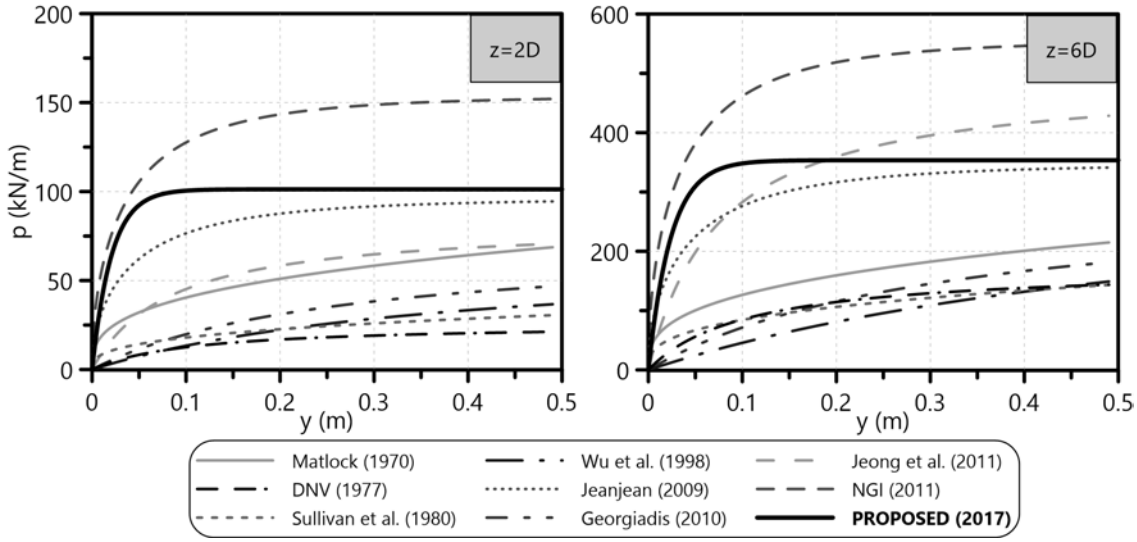

Figure 7.11: Comparison of the proposed monotonic p-y curves with corresponding literature methodologies for a circular pile of D=2.54m and α=0.3 in the fully saturated soft NC clay described by Doyle et al. (2004) at shallow (z=2D) and greater depth (z=6D).

Figure 7.11 depicts the p-y curves derived from all the methodologies applicable to soft, NC clays at two different depths, namely a shallow (z=2B) and a greater one

[1] M_y with duraluminium stress at the elastic limit and M_u with its ultimate stress.

(z=6B). The p-y curves proposed by Nichols et al. (2014) lie on the upper bound and close to the methodology of the current doctoral thesis ($\lambda = C_c/\ln 10 = 0.26$, $\lambda/\kappa = 12$, $\nu = 0.3$, $\alpha = 0.3$ for duraluminium pile), while the p-y curves by Matlock (1970) (ε_{50} from Table 2.2) - also adopted by API (2007) - are located towards the lower bound of the demonstrated plots. By applying the three aforementioned p-y curve methods in the BNWF model, the following process compares their efficiency in predicting the lateral response of the single pile that was measured during centrifuge Test 1.

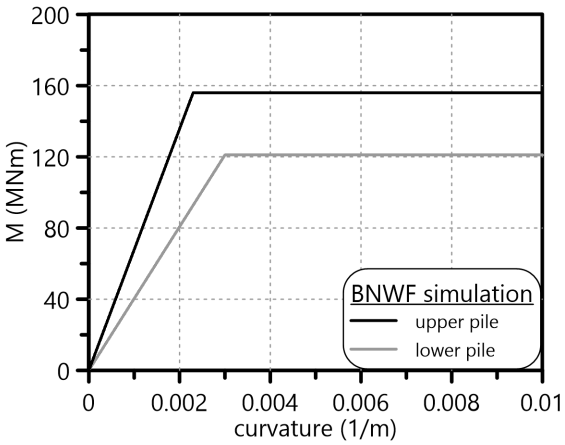

Figure 7.12: Bending moment-curvature behavior assumed in the BNWF simulations for the upper and the lower pile part, according to centrifuge test measurements and observations by Doyle et al. (2004).

The 2D simulations assume two different behaviors for the pile material: i) totally elastic behavior with the equivalent steel properties described for the model pile and ii) elastic-perfectly plastic behavior controlled by the bending moment-curvature diagrams of Figure 7.12. The peak bending moment values of these elastoplastic relationships are the yield moments $M_{y,1}$ and $M_{y,2}$ of the upper and the lower pile part respectively. The curvature values 0.0023 and 0.003 (1/m) corresponding to these moments occurred after double differentiation of the $y - z$ distribution with z (at z=22.0 and 30.5m), delivered by the test report at $H = 95\%H_u$ (assumed lateral pile head load at first pile yield). However, since the $y - z$ curves of the report were calculated through double integration of the bending moment profile - derived from the strain gages measurements, considerable uncertainties accompany the specific graphs. Thus, a primary evaluation of the proposed methodology takes place assuming elastic pile response and further observations follow incorporating the pile material non-linearity.

Figure 7.13 depicts $y_h/D - H$ curves of the static centrifuge Test 1 compared to the BNWF output from the simulation of the lateral NC clay response through

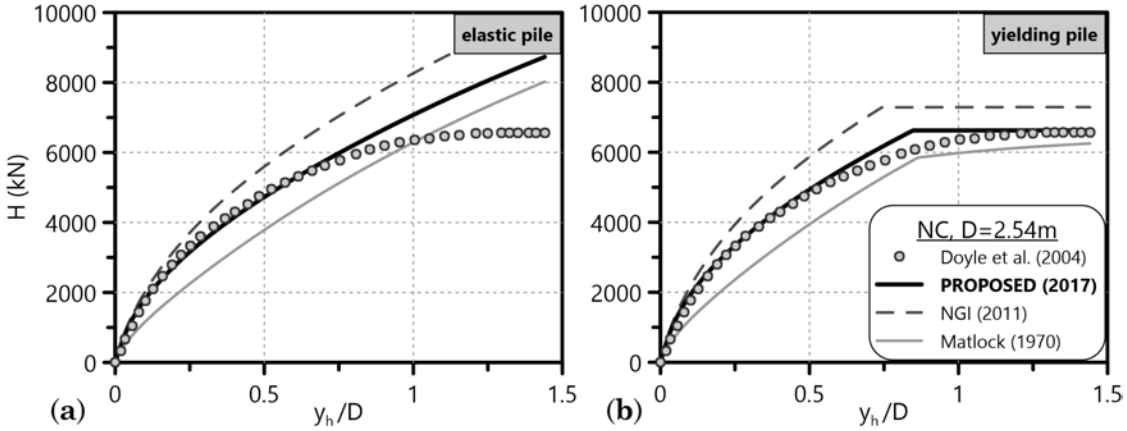

Figure 7.13: Comparison of dimensionless pile head lateral load-displacement curves $y_h/D-H$ between the centrifuge test measurements by Doyle et al. (2004) and the BNWF simulations incorporating the p-y curves by Nichols et al. (2014), Matlock (1970) and the current dissertation, assuming (a) elastic pile and (b) yielding pile in the 2D analyses.

the three aforementioned p-y curve methodologies, for both elastic and yielding pile behavior. The p-y curves of the current dissertation match the experimental measurements more accurately than the other two literature methodologies up to $y_h \approx 0.8D$ of the elastic steel pile. For greater y_h all methods overestimate H_u since they do not take pile yield into account. Assuming moment-curvature behavior of Figure 7.12 for the pile of the simulations, the proposed p-y curves of the thesis for soft NC clays deliver again the closest pile head lateral load-displacement response to the experiment. The p-y curves by Matlock (1970) match almost accurately the experimental H_u but predict a ductile pile head lateral response at lower H levels compared to the test. The methodology by Nichols et al. (2014) overestimates H_u but only by 10%. Indicatively, at y_h=0.2-0.5D Figure 7.13b shows deviations $\pm 15-25\%$ of the $y_h/D-H$ predictions by the two aforementioned literature p-y curve methodologies.

For the BNWF simulations that take into account the elastoplastic pile material behavior, Figures 7.14 and 7.15 compare the M$-z$ and $y/D-z$ distributions along the pile respectively at $H=40$, 80%H_u - H_u=6565kN (the ultimate pile head lateral load measured in the centrifuge test). The corresponding results through utilization of the proposed p-y curves again match successfully the experimental measurements. The other two methodologies also predict M_{max} close to the test, especially for $H=80\%H_u$. Finally, the p-y curves of the dissertation lead to more accurate lateral displacement distributions, although the accuracy of the experimental y profiles is questionable even by the test report.

To conclude, the p-y curves proposed by the current dissertation for soft, NC

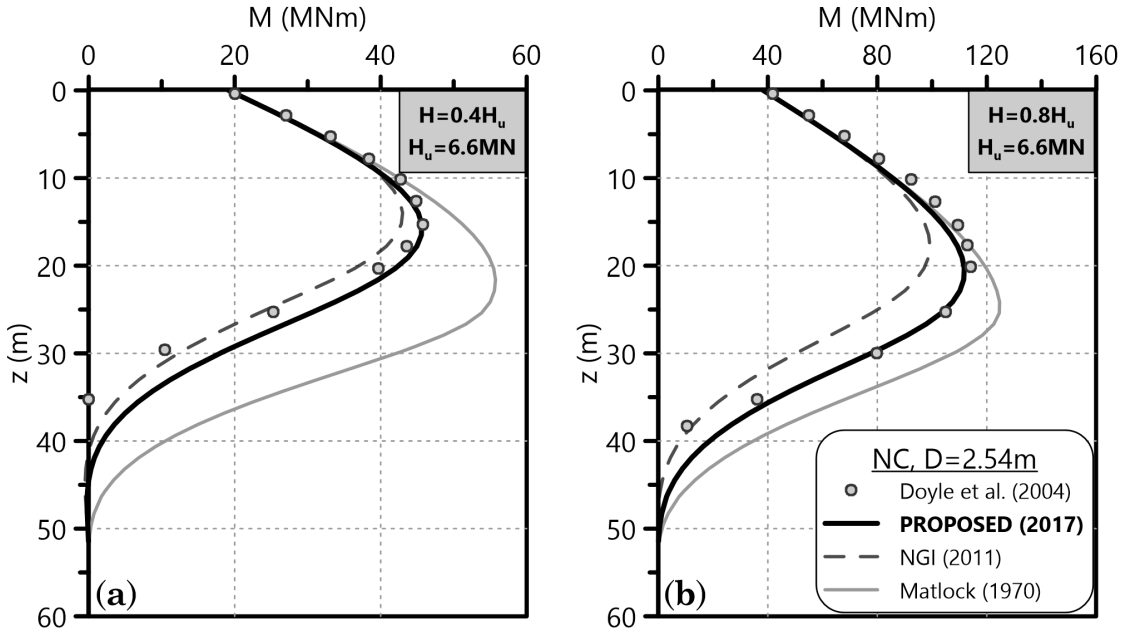

Figure 7.14: Comparison of bending moment distributions M$-z$ along the laterally loaded pile at (a) $H = 40\%H_u$ and (b) $H = 80\%H_u$ (H_u=6565kN from centrifuge test) between the centrifuge test measurements by Doyle et al. (2004) and the BNWF simulations incorporating the p-y curves by Nichols et al. (2014), Matlock (1970) and the current dissertation, assuming elastoplastic pile behavior.

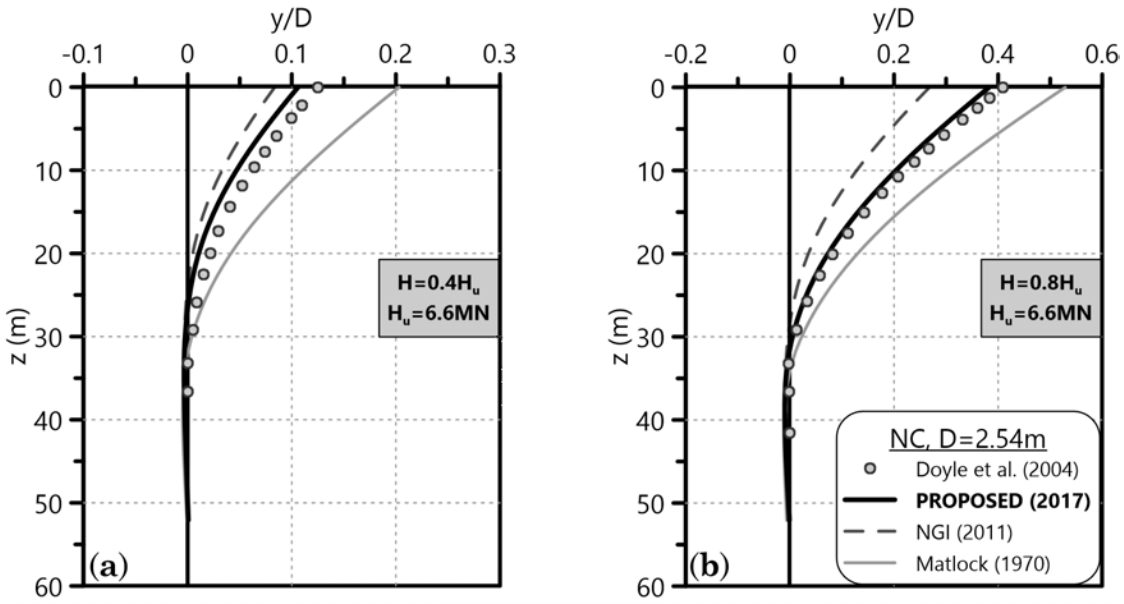

Figure 7.15: Comparison of non-dimensional lateral displacement distributions $y/D - z$ along the laterally loaded pile at (a) $H = 40\%H_u$ and (b) $H = 80\%H_u$ (H_u=6565kN from centrifuge test) between the centrifuge test measurements by Doyle et al. (2004) and the BNWF simulations incorporating the p-y curves by Nichols et al. (2014), Matlock (1970) and the current dissertation, assuming elastoplastic pile behavior.

clays deliver reliable predictions of the lateral pile response in terms of $y_h - H$, M$-z$ and $y - z$ diagrams. The results of the BNWF simulation utilizing these curves match successfully the experimental measurements of the centrifuge tests by Ilyas et al. (2004) and Doyle et al. (2004). Despite yielding of the pile tested in the second case, the proposed p-y curves simulate accurately the pile behavior under intense static lateral loading. The p-y curves by Matlock (1970) - adopted by API (2011) - seem conservative once more, while the stiffest curves by Nichols et al. (2014) usually overestimate H_u and thus underestimate the maximum M and y along the pile.

7.4 Evaluation of p-y curves for OC clays

Two field test series of laterally loaded piles in stiff clayey soils by Rollins et al. (1998) and a research group in the University of California, Los Angeles (UCLA) (Janoyan et al., 2006; Lemnitzer et al., 2010; Stewart et al., 2007) are chosen for the evaluation of the proposed p-y curves for stiff OC clays. The soil profiles of the test sites mainly involve stiff clayey soils of almost constant c_u with depth. The experiment series by Rollins et al. (1998) attempted to clarify the effect of spacing on the lateral response of pile groups and compare it to the corresponding single pile behavior in such soils. The UCLA tests were carried out on reinforced concrete (RC) piles until structural failure, i.e. extensive lateral loading. The following evaluations utilize experimental results for the lateral response of the single pile and compare them with the BNWF predictions.

7.4.1 Full-scale tests by Rollins et al. (1998)

Rollins et al. (1998) carried out a static lateral load test on a full-scale pile group and on a single pile, aiming to compare the lateral responses of the two. The tests were conducted on mixed steel-concrete piles, driven in a thoroughly documented medium to stiff OC clay under undrained conditions. This evaluation compares the results of certain BNWF simulations of the single pile load test with the corresponding experimental measurements. Figure 7.16 depicts the composite soil profile of the tests based on the results of all the field and laboratory investigations. Prior to pile driving, the surficial gravel fill (up to z=1.6m) was excavated, with the excavation pit extending significantly from the test site. The natural ground below the aforementioned gravel layer consisted mainly of silty clay underlain by a sand layer. Atterberg limits and natural water content of the clayey soil resulted in the following average values: $PL = 18\%$, $LL = 37\%$ and $w_N = 30\%$. Assuming $G_s = 2.7\,Mg/m^3$ and $e_o = w_N\,G_s = 0.81$ (for the fully saturated soil), Table 7.1 suggests C_r=0.018-0.046.

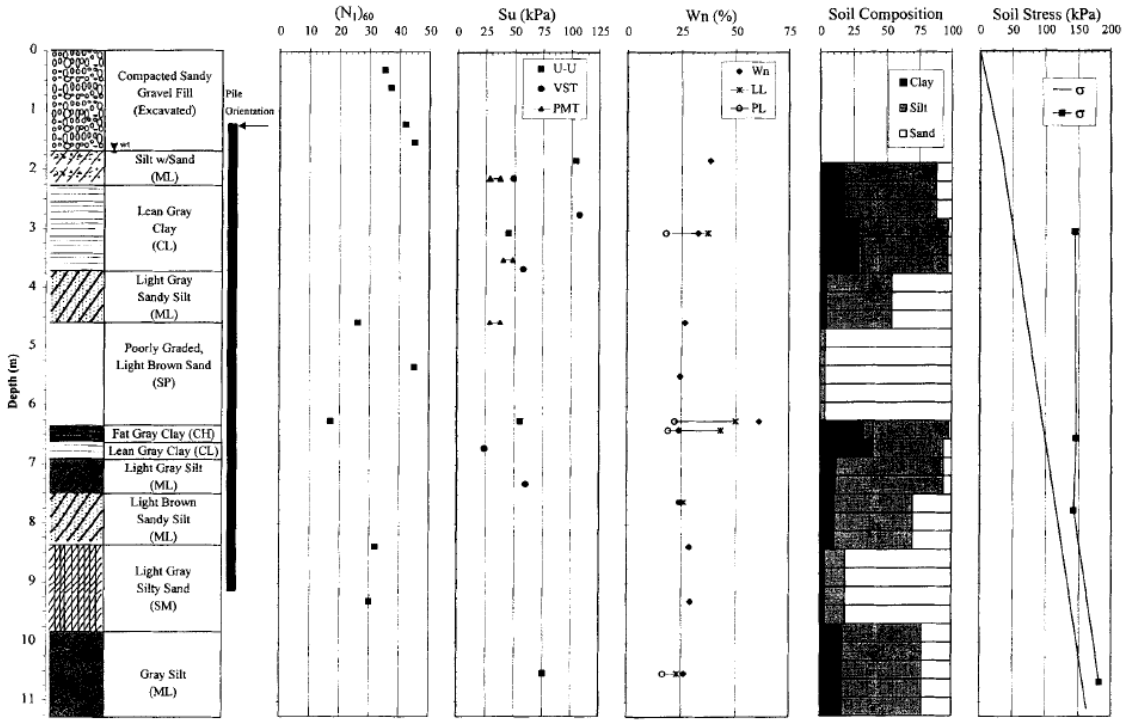

Figure 7.16: Geotechnical site characterization by Rollins et al. (1998). From left to right: Soil profile, SPT measurements $(N_1)_{60}$, c_u estimates (S_u), Atterberg limits and natural wet content (W_n), soil composition and effective soil stress distribution with pre-consolidation pressure measurements $(\sigma^{'} - \sigma)$.

According to $\sigma^{'}_{vo} - z$ from Figure 7.16, average bulk unit weight is $\gamma = 15kN/m^3$ below (wet) and $\gamma_d = 14kN/m^3$ above the water table (dry). The soil was overconsolidated (OC) down to z=10m, with c_u measurements ranging between 25-100kPa - derived from laboratory (UU), vane shear (VST) and pressuremeter (PMT) testing. The first sand layer (z=4.6-6.4m)[1] has a friction angle $\phi_1 = 38^o$ and the second one (z=8.3-9.7m) $\phi_2 = 36^o$, both with relative density $D_r = 65 - 80\%$ according to the geotechnical site report of the tests. Correlations of $(N_1)_{60}$=20-40 with ϕ, D_r by Meyerhof (1956) generally agree with the aforementioned sand properties. The ground water table was met at z=1.6m, right on top of the first clayey layer (Figure 7.16).

The piles were closed-end steel pipes of inner diameter d=0.305m and thickness t=9.5mm, thus resulting in actual D=0.324m. Prior to instrumentation and load testing, the pipes were filled with concrete. The separate materials of the mixed steel-concrete pile cross-section had the following properties:

- Steel: elastic modulus $E_{p,s}$=200GPa and minimum yield stress $f_{y,s}$=331MPa

[1] depth z counts from gravel fill surface, prior to its excavation

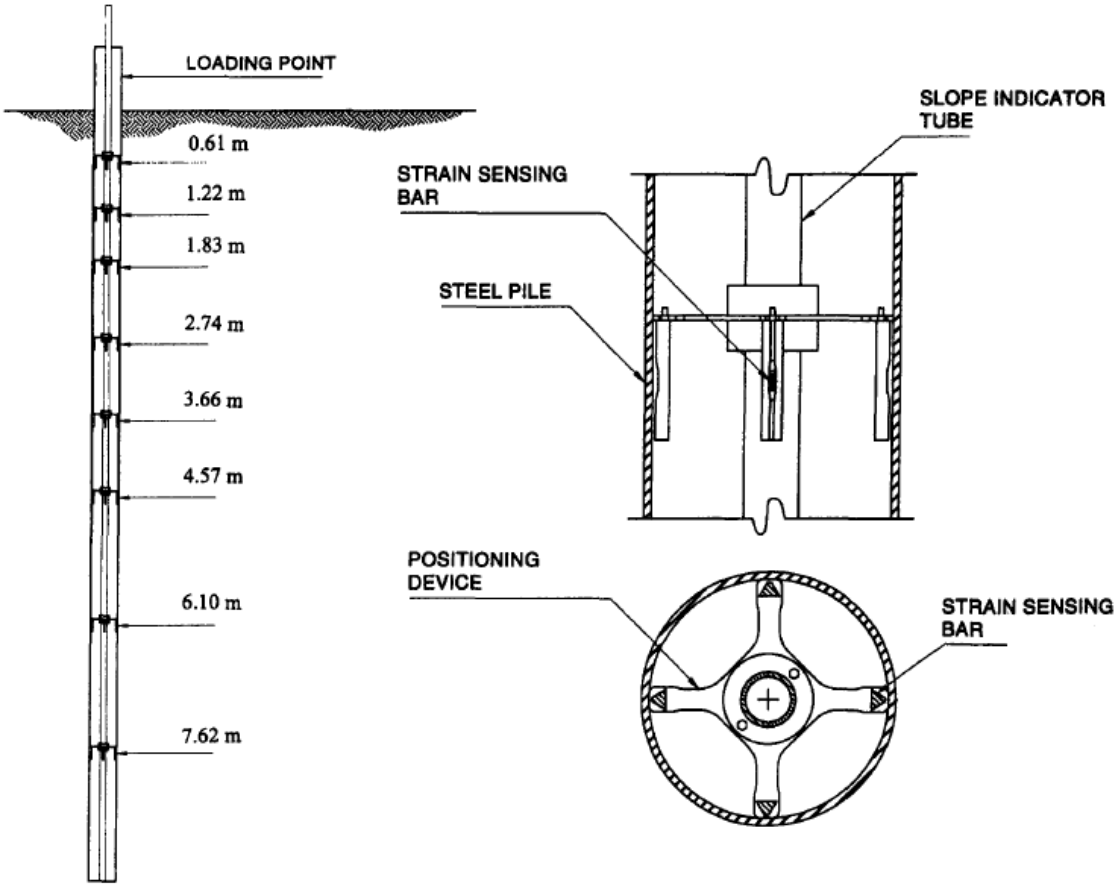

Figure 7.17: Test pile instrumentation with details by Rollins et al. (1998).

- Concrete: elastic modulus $E_{p,c}$=17.5GPa and compressive strength $f_{y,p}$=20.7MPa

Total length of the test piles was L=7.9m - they were driven down to almost half the thickness of the second sand layer - with the point of lateral load application at 0.4m above the surface of the first natural soil layer (after gravel fill excavation). Figure 7.17 depicts the pile instrumentation consisting of: strain gages cast in sensing bars[1], a slope indicator tube (inclinometer) and mounting brackets ensuring the pre-defined positioning of the two aforementioned instruments. Free-head loading conditions applied on the pile heads and the lateral load was imposed through a 1.34MN capacity hydraulic jack. The total applied load was measured through a load cell placed immediately behind the jack, while displacements measurements were documented through a certain LVDT configuration.

In order to incorporate the aforementioned complex soil profile and pile cross-section into the BNWF simulation, certain simplifications needed to take place.

[1]The strain sensing bars were manufactured from fiberglass/vinylester composite materials, designed with an elastic modulus approximately equal to the corresponding anticipated concrete modulus in order to avoid local reinforcing of the latter.

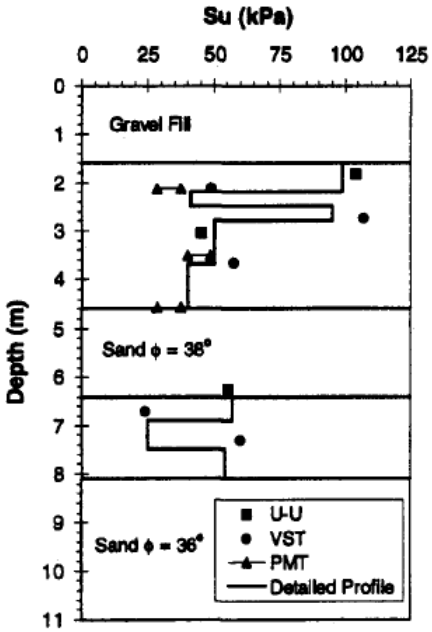

Figure 7.18: Distribution of c_u with depth for the BNWF simulations, corresponding to a detailed soil profile by Rollins et al. (1998).

Regarding the soil profile, Figure 7.18 displays the assumed c_u distribution with depth - corresponding to a detailed soil profile. The BNWF models simulate only the steel part of the pile, assuming that the concrete - with properties of one order of magnitude lower than the ones of the steel - does not influence significantly the total stiffness of the mixed cross-section.

Figure 7.19 depicts the p-y curves derived from all the methodologies applicable to stiff, OC clays at two different depths, namely a shallow (z=2D) and a greater one (z=6D). The p-y curves proposed by the current dissertation ($\kappa = C_r/\ln 10 = 0.008 - 0.02$, $\nu = 0.10$, $\alpha = 0.3$ for steel pile) lie on the upper bound and close to the methodology by Georgiadis & Georgiadis (2010), while the p-y curves by Reese et al. (1975) (ε_{50} from Table 2.4) are located at the lower boundary of the demonstrated plots regarding the residual p. Despite the presence of Welch's p-y curves close to the upper bound of the range, the specific methodology (Welch & Reese, 1972) refers to stiff clays with no free water. Since ground water table of the test site was documented almost on ground surface, Welch's p-y curves were judged inapplicable to the BNWF simulation of this experiment. The sand layers were initially represented from p-y curves by API (2011). However, the BNWF output did not alter either using the API p-y curves for sand or assuming OC clay of c_u=50kPa - a rather conservative assumption according to Rollins et al. (1998) - at the specific layers. By applying the three aforementioned p-y curve methods in

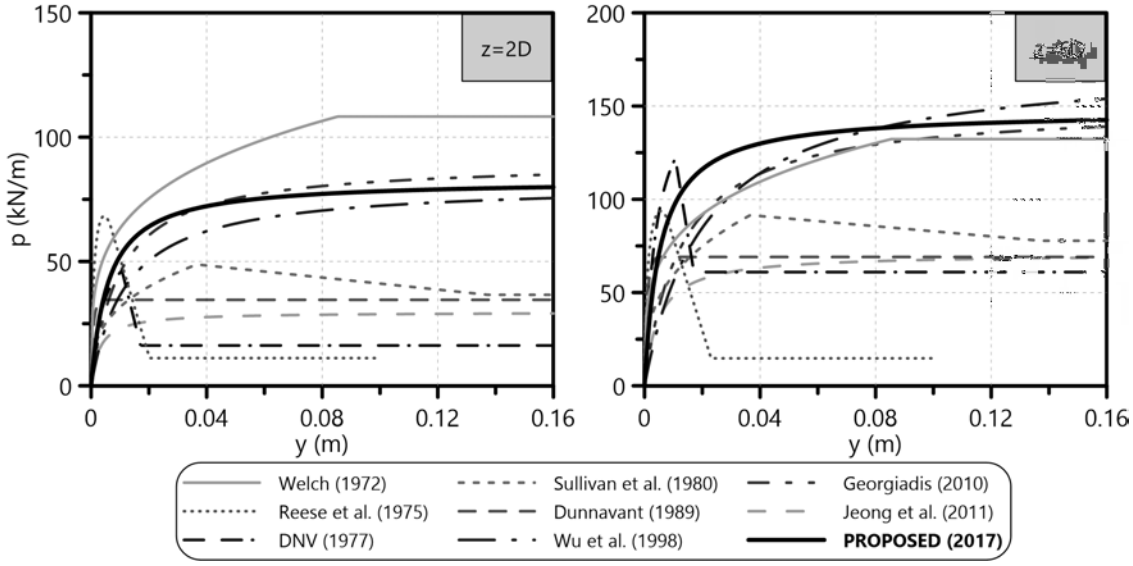

Figure 7.19: Comparison of the proposed monotonic p-y curves with corresponding literature methodologies for a circular pile of D=0.324m and α=0.3 in the fully saturated medium-stiff OC clay described by Rollins et al. (1998) at shallow (z=2D) and greater depth (z=6D).

the BNWF model, the following process compares their efficiency in predicting the lateral response of the single pile that was measured during the full-scale test.

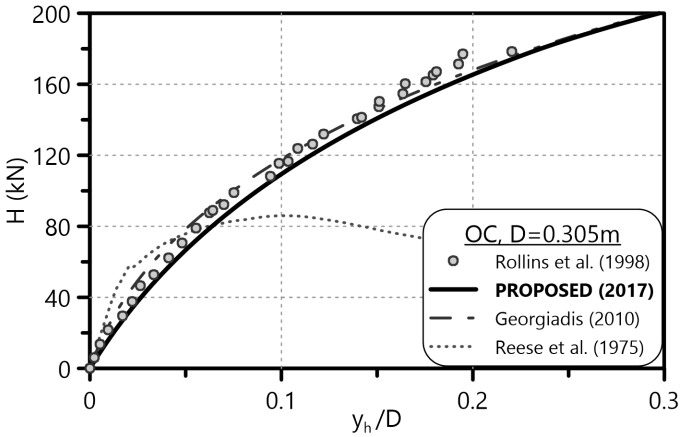

Figure 7.20: Comparison of dimensionless pile head lateral load-displacement curves $y_h/D - H$ between the field test measurements by Rollins et al. (1998) and the BNWF simulations incorporating the p-y curves by Georgiadis & Georgiadis (2010), Reese et al. (1975) and the current dissertation.

Figures 7.20 and 7.21 demonstrate $y_h/D - H$ and M$-z$ curves of the experiment compared to the BNWF output from the simulation of the lateral OC clay response through the three aforementioned p-y curve methodologies. The p-y curves of the present dissertation deliver diagrams that are very close to the experimental mea-

surements. Moreover, they estimate very accurately the maximum bending moment along the pile, particularly for H=53.4kN. At the specific pile head load (Figure 7.20a) the two literature methodologies predict M_{max} values that deviate from the test results by 20-40%. Lateral pile head displacement (y_h) does not exceed $0.2D$ and thus no yield of the pile material occurs.

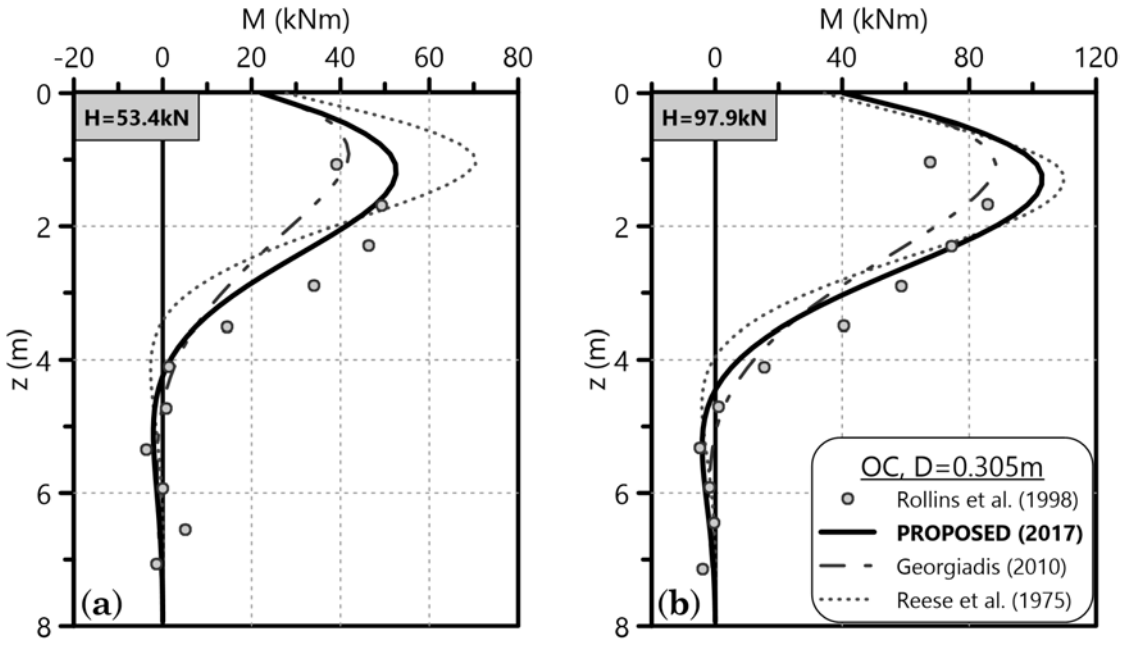

Figure 7.21: Comparison of bending moment distributions M$-z$ along the laterally loaded pile at (a) H=53.4kN and (b) H=97.9kN between the field test measurements by Rollins et al. (1998) and the BNWF simulations incorporating the p-y curves by Georgiadis & Georgiadis (2010), Reese et al. (1975) and the current dissertation.

The aforementioned evaluation demonstrates how the proposed p-y curves for medium-stiff, OC clays successfully predict lateral pile head load-displacement curves and bending moment distribution along the pile for various load levels of the pile head. Furthermore, it addresses the issue of p-y curve forms (e.g. Reese et al., 1975) that fail to reproduce the $y_h/D - H$ measured during the experiment - potentially due to the assumption of post-peak strength degradation.

7.4.2 Full-scale tests by UCLA (1998-2006)

A research group of the civil engineering faculty in the University of California, Los Angeles (UCLA) (Janoyan et al., 2006; Lemnitzer et al., 2010; Stewart et al., 2007) carried out a series of four (4) full-scale cyclic lateral load tests on bridge foundation components (a pile group and three single piles) in order to examine their lateral response in stiff, overconsolidated clayey soils. All tests were conducted

at a Caltrans-owned test site in Hawthorne, California. The following evaluation focuses on the single piles, namely two 0.61m-diameter piles - a free-head (flagpole) and a fixed-head - and one free-head 2.0m-diameter pile, that are addressed as three separate cross-checks. Figure 7.22 depicts a schematic representation of the field tests configuration. All test specimens were standard concrete bored piles and no groundwater or soil caving was encountered over their depth, during their construction.

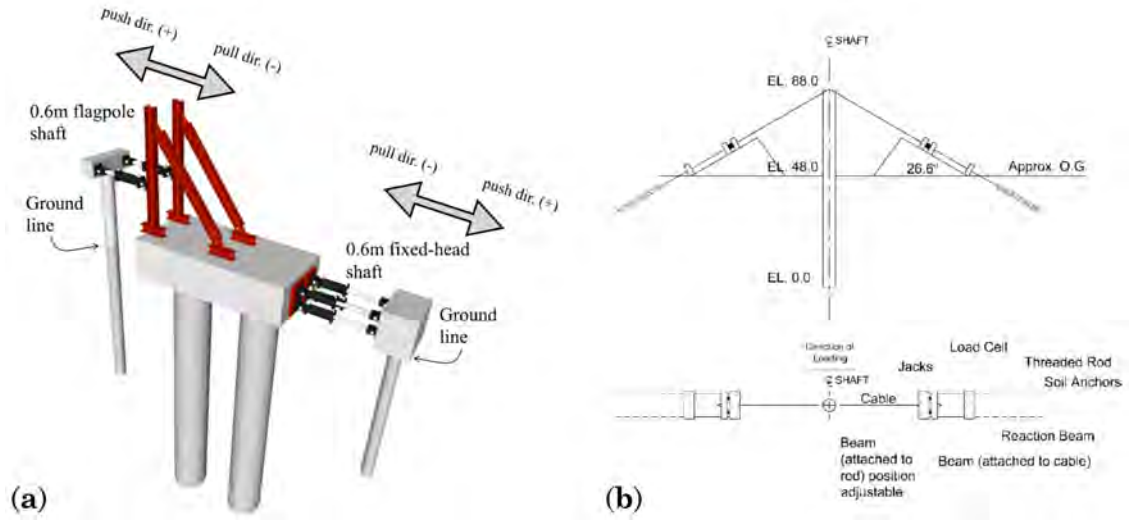

Figure 7.22: Setup of the full-scale singe laterally loaded pile tests carried out by the UCLA research group (1998-2006). (a) 0.61m-diameter piles and (b) 2.0m-diameter pile.

Prior to the evaluation of the proposed p-y curves with the three single pile tests, the current paragraph describes briefly the geotechnical conditions of the site. The test site was near the Los Angeles International Airport and consists of quaternary alluvial soils that extend to great depth. As depicted in Figure 7.23, the geotechnical investigation revealed a soil profile consisting of a surficial layer of uncontrolled fill with asphalt and concrete debris (generally 1.2m thick) underlain by partially saturated and overconsolidated silty and sandy clay that extends to a depth of 7.3m, with occasional thin sand seems. The ground water table was met at z=14.6m from the fill surface according to Stewart et al. (2007) - below all pile tips. The GIR involves the results of CPTs, PMTs, consolidation and triaxial testing of specimens from the clay layer. Relatively high degree of saturation ($S_r = 86-100\%$), low hydraulic conductivity and sufficiently fast rate of loading imply undrained conditions of the clay. Generally conservative assumptions lead to $c_u \approx 200$kPa - constant with depth - and $OCR \approx 2-6$, indicating that the clayey soils at the site are OC within the depth range of interest. Laboratory UU triaxial testing of clay specimens indicated failure strains $\varepsilon_q = 0.6-1\%$. Atterberg limits and

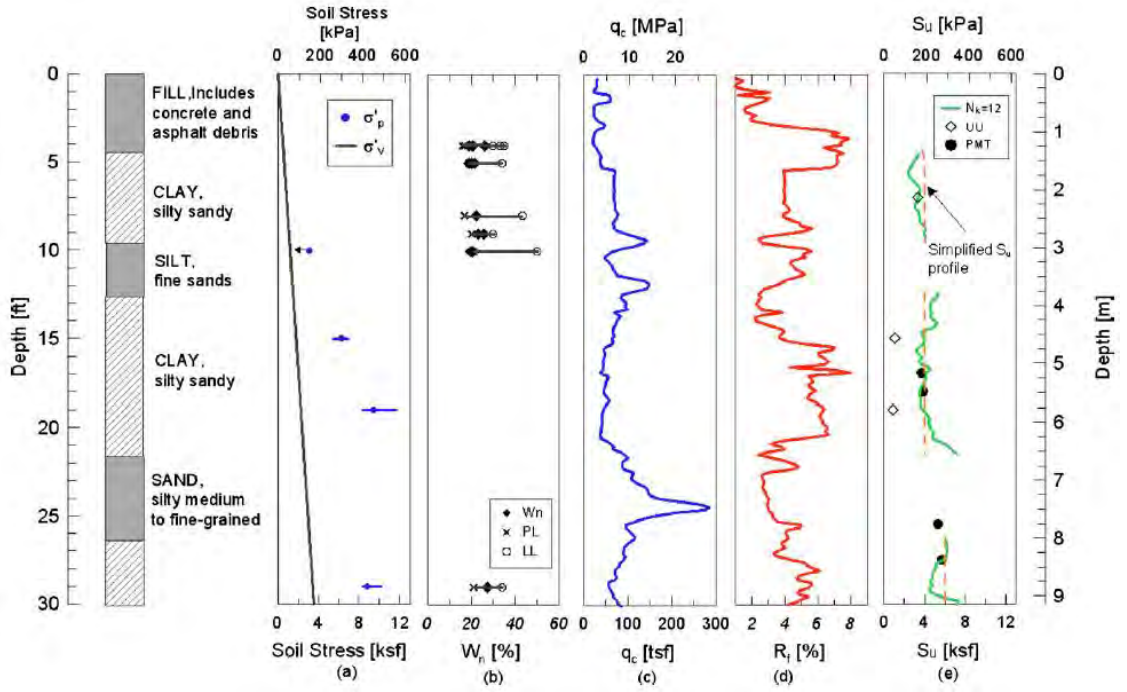

Figure 7.23: Geotechnical site conditions of the UCLA tests by Lemnitzer et al. (2010). From left to right: Soil profile, (a) effective soil stress distribution with preconsolidation pressure measurements ($\sigma_v^{'} - \sigma_p^{'}$), (b) Atterberg limits and natural wet content (W_n), (c) CPT measurements (q_c), (d) friction ratio from CPT soundings (R_f) and (e) c_u estimates together with a corresponding simplified profile (S_u).

natural water content of the clayey soil resulted in the following average values: $PL = 20\%$, $LL = 35\%$ and $w_N = 25\%$. Assuming $G_s = 2.7\,Mg/m^3$, Table 7.1 suggests C_r=0.015-0.044. However, back analyses of numerical undrained triaxial tests on the specific clay at various depths resulted in ε_q much higher than the ones observed in the laboratory. Therefore, the recompression slope is corrected in order to deliver peak strength at average failure strain 0.8% and thus the following evaluation assumes C_r=0.004 for the clayey soils of the specific site.

RC piles of D=0.61m

These full-scale tests involve two 0.61m-diameter, bored piles of the same embedded length L_b=7.62m. The specific length counted from the top of the first natural soil, i.e. silty sandy clay, since the surficial fill layer was excavated during this series of load tests. The toes of both piles were in the last silty sand layer of Figure 7.23. The actual differences between these piles were the height of the heads above ground surface and the rotational constraints of the latter. The so-called flagpole pile was free-head with length extruding from ground surface 4.06m (point of lateral load application), thus resulting in total pile length $L_{\text{free-head}}$=11.68m. The other pile

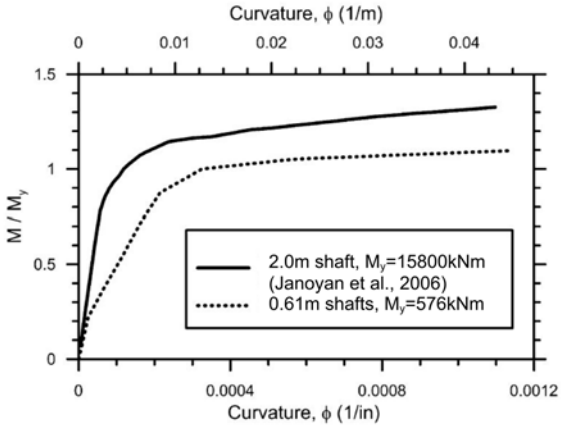

Figure 7.24: Normalized bending moment-curvature behavior assumed in the BNWF simulations for the 0.61m- and the 2.0m-diameter concrete piles, according to test measurements and observations by Janoyan et al. (2006) and Stewart et al. (2007).

was fixed-head and its top was constrained against rotation exactly on ground surface. The BNWF simulations assume yielding behavior for the reinforced concrete of the piles, controlled by the normalized bending moment-curvature diagram of Figure 7.24 (D=0.61m). Cyclic loading of the aforementioned piles was carried out in a quasi-static manner, under displacement control through a properly configured reaction system (see Figure 7.22a). Only 3 lateral load cycles took place and the loading/unloading-displacement curves of Figure 7.25 were derived from pile head measurements. The marked backbone curves are defined as the average of the applied load at the peak displacement for the first half-cycle in each loading direction (the difference in peak load due to cyclic loading was typically small).

Figure 7.26 depicts the p-y curves derived from all the methodologies applicable to stiff, OC clays at two different depths, namely a shallow (z=2D) and a greater one (z=6D). The p-y curves proposed by the current dissertation ($\kappa = C_r/\ln 10 = 0.0017$[1], $\nu = 0.15$, $\alpha = 1.0$ for bored pile) lie on the upper bound and close to the methodology by Georgiadis & Georgiadis (2010), while the p-y curves by Dunnavant & O'Neill (1989) are located at the lower boundary of the demonstrated plots ($E_{50} = c_u/\varepsilon_{50}$ with ε_{50} from Table 2.4). Despite the presence of Reese's p-y curves close to the lower bound of the range (regarding the residual p), the specific methodology (Reese et al., 1975) refers to stiff clays with presence of free water. Since ground water table of the test site was documented way below the tips of the specific piles, Reese's p-y curves were judged inapplicable to the BNWF simulation of this experiment. The sand layers were initially represented from p-y curves by

[1] C_r=0.004 is the corrected value in order to reach peak strength at $\varepsilon_q = 0.8\%$.

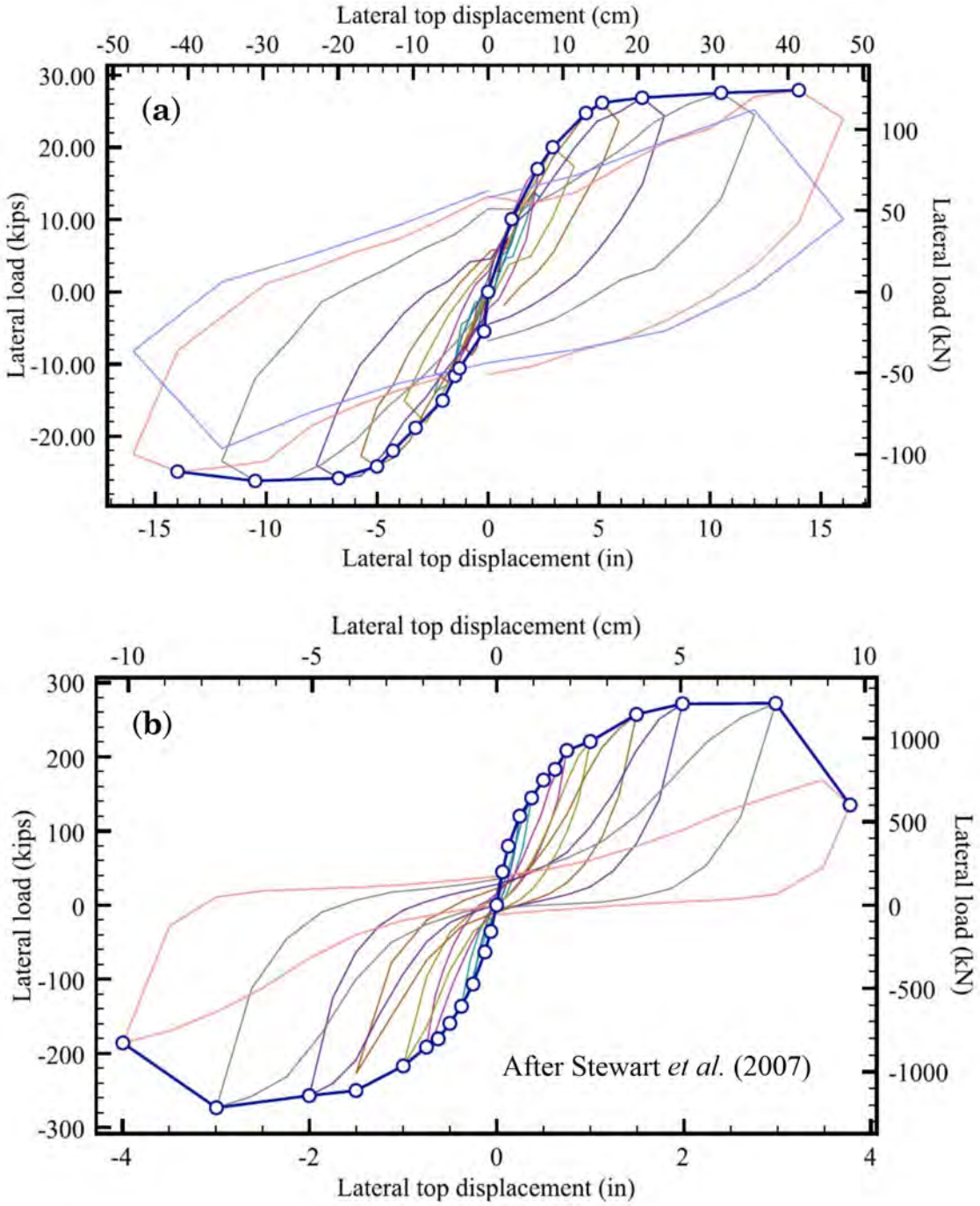

Figure 7.25: Measured load-displacement curves at selected cycles and backbone curves for test piles of D=0.61m: (a) free- and (b) fixed-head (Stewart et al., 2007).

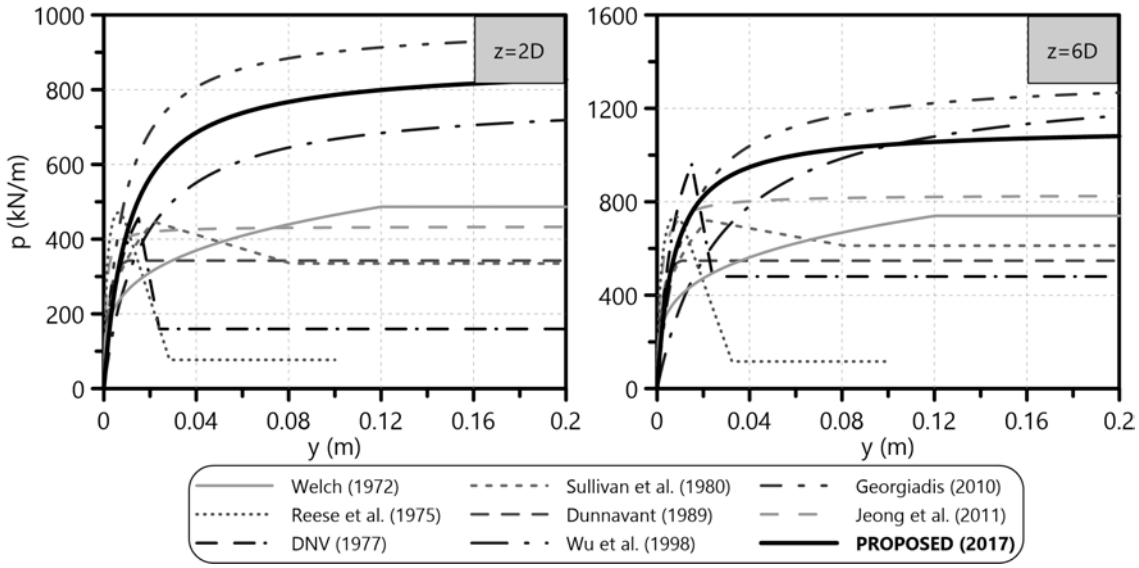

Figure 7.26: Comparison of the proposed monotonic p-y curves with corresponding literature methodologies for a circular pile of D=0.61m and α=1.0 in the stiff OC clay described by Stewart et al. (2007) at shallow (z=2D) and greater depth (z=6D).

API (2011). However, the BNWF output did not alter either using the API p-y curves for sand or assuming OC clay of c_u=200kPa - a rather conservative assumption according to Lemnitzer et al. (2010) - at the specific layers. By applying the three aforementioned p-y curve methods in the BNWF model, the following process compares their efficiency in predicting the lateral response of the single piles (free- and fixed-head) that was measured during the full-scale tests.

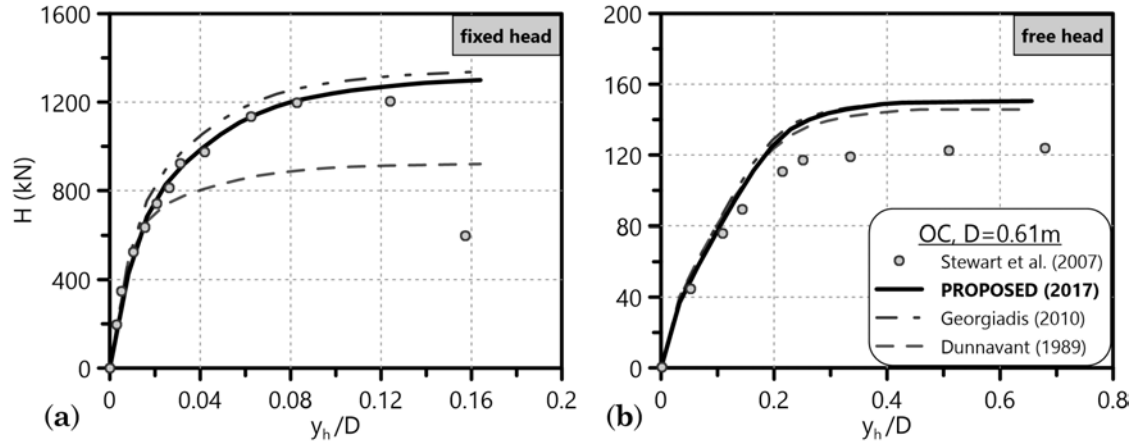

Figure 7.27: Comparison of dimensionless pile head lateral load-displacement curves $y_h/D-H$ for the 0.61m-diameter piles, between the full-scale test measurements by Stewart et al. (2007) and the BNWF simulations incorporating the p-y curves by Georgiadis & Georgiadis (2010), Dunnavant & O'Neill (1989) and the current dissertation. (a) fixed- and (b) free-head pile.

Figure 7.27 compares the $y_h/D - H$ backbone curves of the cyclic load tests - for the piles with D=0.61m - to the BNWF output from the simulation of the lateral OC clay response through the three aforementioned p-y curve methodologies, for both fixed- and free-head conditions. The 2D analyses simulate the reinforced concrete cross-section of the piles according to the moment-curvature behavior depicted in Figure 7.24. Furthermore, the loading of the pile heads is monotonic during the simulations, since the low number of load cycles in the full-scale tests did not affect the ultimate lateral load H_u. The p-y curves of the current dissertation together with the ones by Georgiadis & Georgiadis (2010) match the experimental measurements for the fixed-head pile very accurately. On the contrary, the methodology by Dunnavant & O'Neill (1989) underestimates H_u by 25% for the same pile. For the free-head pile, all the utilized p-y curves predict an ultimate lateral load almost 30% higher than the measured H_u of the actual test. The specific deviation is potentially attributed to a corresponding overestimation of c_u at the depth range of interest, since the results of the GIR refer to overburden conditions prior to the excavation of the surficial fill layer.

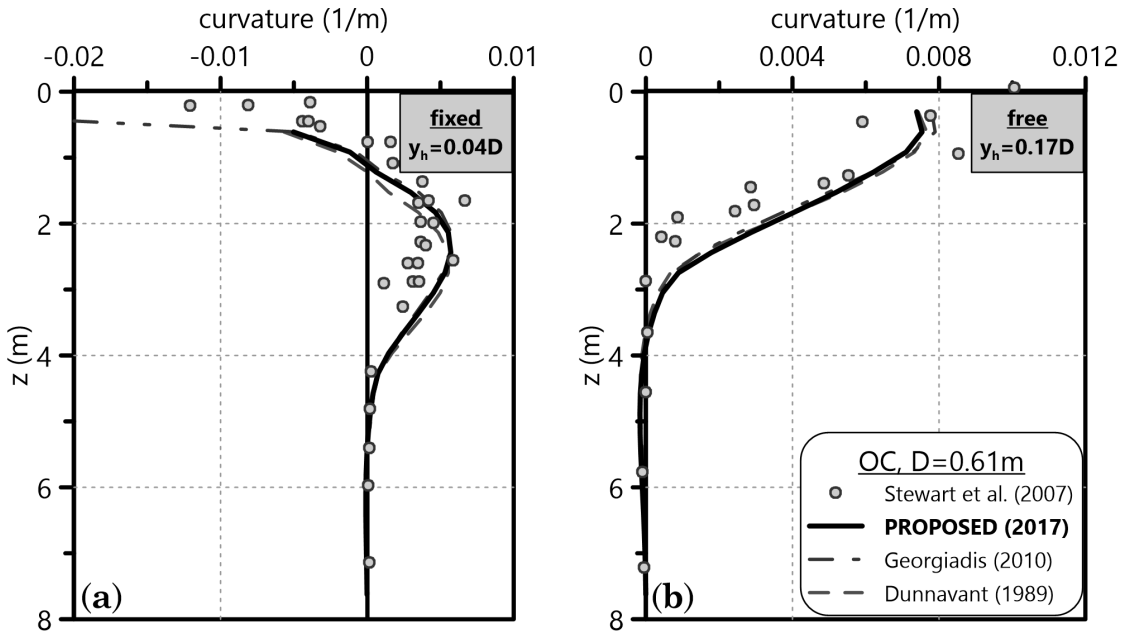

Figure 7.28: Comparison of curvature distributions along the laterally loaded piles of D=0.61m, between the full-scale test measurements by Stewart et al. (2007) and the BNWF simulations incorporating the p-y curves by Georgiadis & Georgiadis (2010), Dunnavant & O'Neill (1989) and the current dissertation. (a) fixed-head pile at y_h=0.04D and (b) free-head pile at y_h=0.17D.

Figure 7.28 depicts curvature distributions of the experiment along the 0.61m-diameter piles compared to the BNWF output from the simulation of the lateral OC

clay response through the three aforementioned p-y curve methodologies. All the p-y curves deliver curvature patterns with depth that are very close to the experimental measurements. Moreover, they estimate very accurately the maximum curvature along the pile, especially for the fixed-head specimen. However, this uniformity in curvature despite the striking differences between the p-y curves - particularly between Dunnavant & O'Neill (1989) and the other two - might occur due to yield of the pile material ($y_h > y_{h,\,\text{yield}}$).

RC pile of D=2.0m

A full-scale cyclic lateral load test was conducted on a cast-in-drilled-hole 1.8m-diameter pier-column that continued below ground surface to a shaft of slightly greater diameter, namely D=2.0m. The embedded length of the shaft (D=2.0m) was L_b=14.62m while the pier-column (D=1.8m) extruded 12.2m above ground surface - the surficial fill was not excavated during this test - thus resulting in a total length L=26.82m of the specimen. The BNWF simulations assume yielding behavior for the reinforced concrete of the monolithic pier-column, controlled by the normalized bending moment-curvature diagram of Figure 7.24 (D=2.0m). Cyclic loading of the pier-shaft system was carried out quasi-statically, using anchored cables that imposed lateral displacement on top of the column (see Figure 7.22b). The geometry of this loading system (inclined tension cables) imposed axial forces simultaneously with the horizontal ones on the test pile. However, the axial loads on the pile were not significant relatively to its axial capacity. Only 2 lateral load cycles were performed at most displacement levels (0.05-2.75m), apart from y_h=0.152 and 0.457m that were imposed for 12 cycles each. Thus, the loading/unloading-displacement curves of Figure 7.29 were derived from pier head measurements together with the corresponding marked backbone curve[1]. Janoyan et al. (2006) states that potential impact of vertical ground motions on the lateral pile response was not addressed with the specific test setup and loading protocol.

Figure 7.30 depicts the p-y curves derived from all the methodologies applicable to stiff, OC clays at two different depths, namely a shallow (z=2D) and a greater one (z=6D). The p-y curves proposed by the current dissertation ($\kappa = C_r/\ln 10 = 0.0017$[2], $\nu = 0.15$, $\alpha = 1.0$ for bored pile) lie on the upper bound and close to the methodology by Jeong et al. (2011) (K_c=800 for average OCR=4 and PI=15), while the p-y curves by DNV (1977) are located at the lower bound of the range regarding the residual p (ε_{50} from Table 2.4). The p-y curves by Reese et al. (1975) were judged inapplicable to the BNWF simulation of this experiment for the same

[1] see explanation of backbone curve for the piles of D=0.61m

[2] C_r=0.004 is the corrected value in order to reach peak strength at $\varepsilon_q = 0.8\%$.

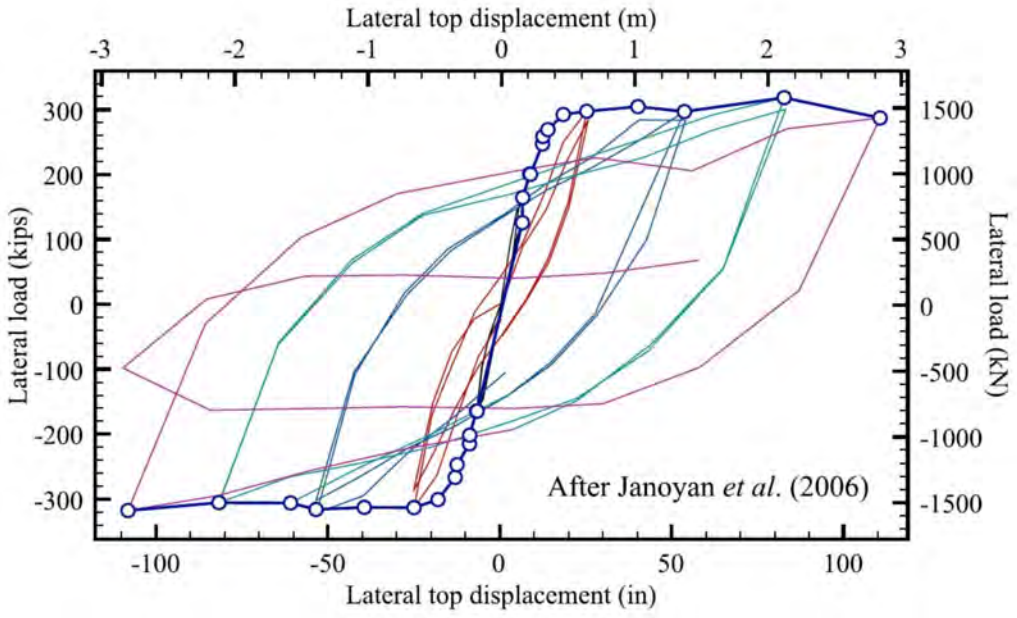

Figure 7.29: Measured load-displacement curves at selected cycles and backbone curve for test pile of D=2.0m (Janoyan et al., 2006).

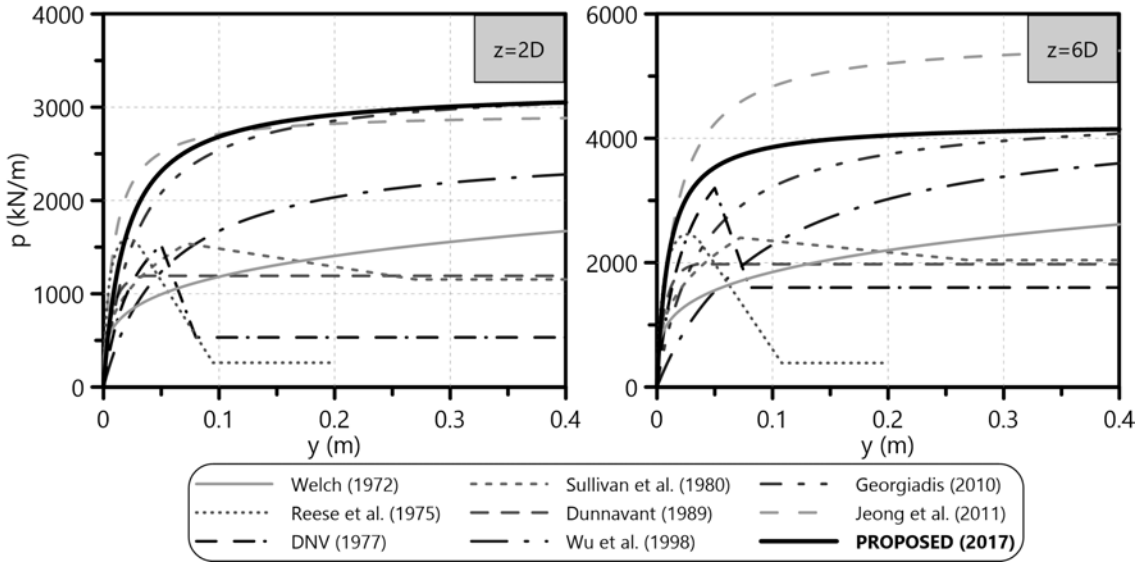

Figure 7.30: Comparison of the proposed monotonic p-y curves with corresponding literature methodologies for a circular pile of D=2.0m and α=1.0 in the stiff OC clay described by Janoyan et al. (2006) at shallow (z=2D) and greater depth (z=6D).

reason they were not used for the 0.61m-diameter piles (water table below pile tips). The sand layers were initially represented from p-y curves by API (2011). However, the BNWF output did not alter either using the API p-y curves for sand or conservatively assuming OC clay of c_u=200kPa at the specific layers. By applying the three aforementioned p-y curve methods in the BNWF model, the following process compares their efficiency in predicting the lateral response of the single pile that was measured during the full-scale tests.

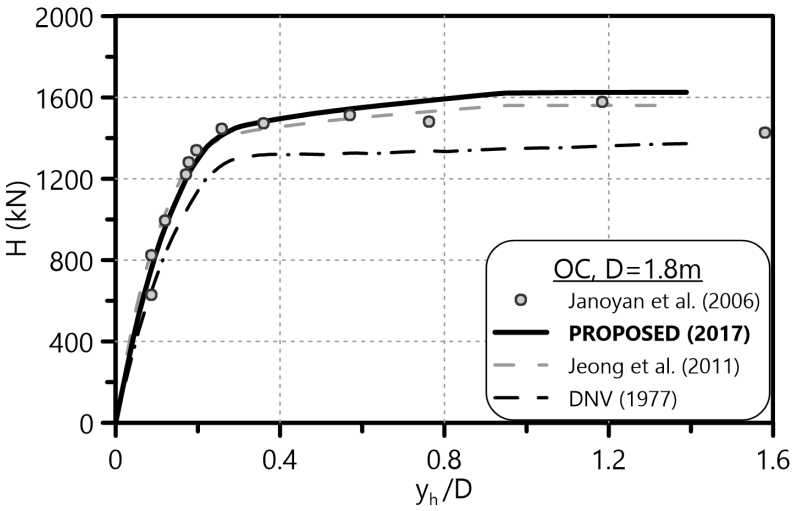

Figure 7.31: Comparison of dimensionless pile head lateral load-displacement curves $y_h/D - H$ for the 1.8m-diameter pier head, between the full-scale test measurements by Janoyan et al. (2006) and the BNWF simulations incorporating the p-y curves by Jeong et al. (2011), DNV (1977) and the current dissertation.

Figure 7.31 compares the $y_h/D - H$ backbone curve of the cyclic load test on the pier-column head (D=1.8m) to the BNWF output from the simulation of the lateral OC clay response through the three aforementioned p-y curve methodologies. The 2D analyses simulate the reinforced concrete cross-section of the piles according to the moment-curvature behavior depicted in Figure 7.24. Furthermore, the loading of the pile heads is monotonic during the simulations, since the low number of load cycles in the full-scale test did not affect the ultimate lateral load H_u. The p-y curves of the current dissertation together with the ones by Jeong et al. (2011) match accurately the experimental measurements. On the other side, the guidelines by DNV (1977) underestimate H_u by almost 20% for the same pile. The specific deviation potentially derives from the assumption made by DNV (1977) that peak strength degrades after a certain value of y for OC clays.

Figure 7.32 depicts curvature distributions of the experiment along the 2.0m-diameter piles compared to the BNWF output from the simulation of the lateral

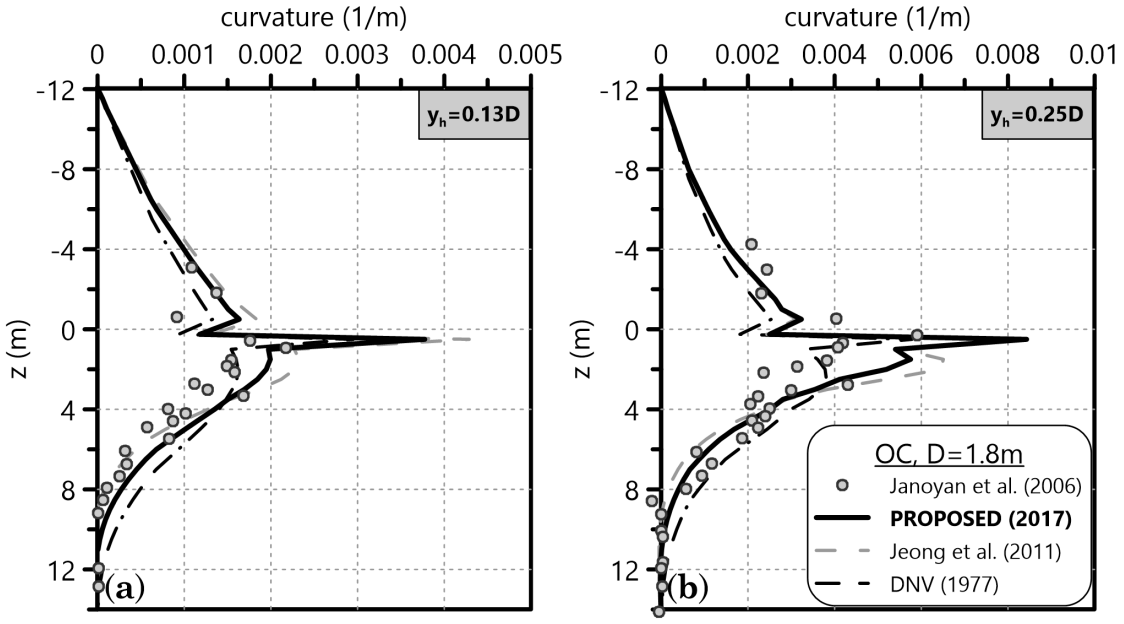

Figure 7.32: Comparison of curvature distributions along the laterally loaded pile of D=2.0m, between the full-scale test measurements by Janoyan et al. (2006) and the BNWF simulations incorporating the p-y curves by Jeong et al. (2011), DNV (1977) and the current dissertation. Pier-column head lateral displacement (a) y_h=0.13D and (b) y_h=0.25D ($D = D_{\text{upper}} = 1.8m$).

OC clay response through the three aforementioned p-y curve methodologies. The utilized p-y curves predict curvature patterns with depth that are very close to the experimental measurements. Excessive curvature at ground level (z=0) probably occurs due to underestimation of p-y stiffness at the specific depth range by all the methods used in the evaluation. However, we observe a constant trend of the p-y curves by DNV (1977) to deliver generally higher curvature along the embedded pile. Jeong et al. (2011) estimates pile curvature accurately for $z > 4m = 2D$, while the p-y curves proposed by the current dissertation seem to predict a curvature distribution that is generally in the closest agreement with the test results along the whole embedded pile length.

The evaluation of the proposed p-y curves for stiff, OC clays through the UCLA experimental results proved successful. In addition, it provided us with useful conclusions regarding the efficiency of other p-y curve methodologies in the specific tests. Apart from the small diameter free-head pile (D=0.61m), $y_h/D - H$ and curvature distributions were reproduced satisfactorily by the BNWF simulation utilizing p-y curves around the upper bound of the corresponding range. The methodology of the current dissertation performed very well in the BNWF simulations of piles with a wide range of diameters D=0.61-2.0m that were loaded to failure.

7.5 Concluding remarks on the evaluation of the proposed p-y curves for clays

Chapter 7 concludes in the following remarks regarding the evaluation of the proposed p-y curves of the present thesis and their comparison with corresponding literature methodologies:

- The validation of the BNWF simulation, i.e. a laterally loaded pile simulated as a beam on a non-linear Winkler soil (p-y curves), with 3D FEA results of Chapters 4 and 5 is successful. The p-y curves of the current dissertation for NC and OC clays, when utilized in the BNWF simulations, reproduce exactly the lateral response of the elastic piles analyzed in the aforementioned chapters for both soil types.

- Two experiments of laterally loaded piles per clay category (soft, NC and stiff, OC) are simulated through the BNWF model that uses certain p-y curve methodologies to reproduce the lateral soil response. Apart from the proposed methodology, which generally lies close to the upper bound, we choose two more p-y curve methods at the boundaries - upper and lower - of the range for comparative purposes. The experiments involve piles of various diameters (D=0.305-2.54m), materials (concrete/ steel) and flexural behavior (elastic/ yielding).

- The proposed p-y curves reproduce quite accurately the lateral pile response of all four load tests, in terms of lateral load-displacement graphs and bending moment/ lateral displacement/ curvature distribution along the pile. It is important to mention here that the proposed methodology seems independent from pile yielding, flexural rigidity and pile head fixity conditions. Furthermore, it predicts a lateral response of the pile very close to the experimental measurements, regardless of the groundwater table depth. Finally, it also captures maximum bending moments of the test piles - the most significant magnitude of long piles design under such loading conditions - with significant accuracy compared to the majority of the existing p-y curves. Thus, it offers a trustworthy alternative in the BNWF simulation of laterally loaded piles in NC and OC clayey soils, utilizing common compressibility (C_c, C_r, ν) and strength parameters (c_u).

- In general, p-y curves with K_i and p_u among the upper bound of the corresponding range (Georgiadis & Georgiadis, 2010; Jeong et al., 2011; Nichols

et al., 2014) prove capable of reproducing accurately the experimental lateral pile response of the aforementioned tests, although with some minor deviations from the measurements. On the contrary, p-y methodologies below the average of the range underestimate by 25-40% design magnitudes of interest (H_u, M_{max}). As a result, the proposed p-y curves of the current dissertation support the following idea: designing laterally loaded piles in clayey soils with p-y curves that adopt p_u close to the upper bound of the range is highly recommended under the condition that a thorough groung investigation has preceded.

Chapter 8

Conclusions

8.1 Summary of main points

As stated in the introduction, the current dissertation attempts to provide the engineer with clear guidelines for the design of laterally loaded piles in clayey soils through numerically derived (3D FEA) p-y curves. Two (2) main objectives were pursued towards this direction. The first was to develop a sophisticated and reliable three-dimensional finite element model in the commercial code Simulia Abaqus 6.12 for the realistic simulation of a single, laterally loaded pile in clayey soils. The second was to propose a new set of upgraded p-y curves through the results of "numerical experiments", using the undrained shear strength distribution of the clayey soil as criterion (NC and OC soils). Thus, the proposed p-y curves of the present thesis correlated the lateral response of the soil-pile system with widely used strength and compressibility parameters for clayey soils.

The current dissertation achieved both the aforementioned objectives according to the following points. Initially, the main characteristics of the proposed monotonic p-y curves for clayey soils are summarized:

1. The proposed p-y curves follow the notations of renowned corresponding international literature methodologies, regarding the initial stiffness K_i and the ultimate lateral soil resistance p_u. The parameters of the problem affecting these two main features are described in the next points.

2. The methodology distinguishes between soft, normally consolidated (NC) and stiff, overconsolidated (OC) clayey soils. The criterion of this categorization is the distribution of the undrained shear strength c_u with depth, i.e. linearly increasing for NC and constant for OC soils. It is noted here that we may come across stiff NC as well as soft OC clays in nature. However, the thesis adopted

the practical consideration that most NC clayey soils are soft while OC ones are stiff. The proposed p-y curves for NC soils are an exponential function of K_i and p_u, which exhibits clear plateau for extensive lateral displacement y - typical characteristic of soft soils. On the other side, the p-y curves proposed for OC soils follow the renowned hyperbola - used by many other literature methods - between y, K_i and p_u, which is quite representative of soils with hardening comportment.

3. The initial stiffness K_i is affected by the compressibility parameters of the soil (C_c, C_r) for both clay types. Furthermore, it increases linearly with depth correspondingly to the Young's modulus of the soil that also follows the same pattern according to the utilized poroelasticity framework (the Modified Cam-Clay (Roscoe & Burland, 1968) constitutive law - MCC - simulates the fully saturated clay behavior in the 3D FEA).

4. The dimensionless coefficient of ultimate lateral soil resistance $N_p = p_u/(c_u \cdot D)$ - non-dimensional p_u form - correlates with various parameters of the problem for the two clayey soil types under investigation (soft NC, stiff OC):

   i. for soft NC clayey soils the numerical analyses concluded that N_p depends entirely from the adhesion factor α between the pile and the surrounding soil.

   ii. for stiff OC clayey soils the parameters that influence N_p are the following (in order from the most to the less significant one): the average undrained shear strength $c_{u,\,avg}$ from ground surface to a depth z=10D, the pile diameter D, the adhesion factor α of the pile-soil interaction and the slope κ=C_r / ln 10 of the recompression line from the oedometer test curve $v - \ln p'$ - $v = 1 + e$ the specific volume, e the void ratio and p' the mean effective stress of the soil.

5. Particular attention was given to the effect of small-strain stiffness (relatively small strains, $\varepsilon < 0.1\%$) and strength degradation - after a certain level of deformation (strain softening) - on the numerical p-y curves for stiff, OC clays. The following findings occurred from this thorough investigation:

   i. intense changes in soil stiffness at relatively small strains (small-strain stiffness) do not affect respectively equally the K_i of the p-y curves.

   ii. undrained shear strength degradation greater than 20% (with reference to peak strength) transforms the form of the p-y curve from hyperbolic to exponential. The corresponding reduced value of p_u correlates exclusively with the strength reduction factor $RF = c_{u,\,\mathrm{res}}/c_{u,\,\mathrm{peak}}$. It is obvious that for

the cases of stiff OC clays without any strain softening one shall consider RF=1.

For the validation and evaluation of the proposed p-y curves the dissertation carried out the following works:

1. A 2D simulation of the pile-soil system as a Beam on Non-linear Winkler Foundation (BNWF) - beam on p-y curves - was designed in the finite element code Simulia Abaqus 6.12, aiming to predict the lateral pile response (pile head lateral load-displacement curve, bending moment, horizontal displacement and/or curvature distribution along the pile) of physical lateral load tests in clayey soils under undrained conditions. For the initial verification of the simulation, we compare the pile response of the 2D BNWF model incorporating the proposed p-y curves with the corresponding 3D FEA that produced these curves. These comparisons displayed that the BNWF simulation is reliable and can predict successfully the lateral response of the pile. As a result, it is capable of simulating with accuracy the real experiments.

2. Through the aforementioned BNWF technique, four (4) lateral pile load tests are simulated. The experiments involve piles of various materials and dimensions installed in clayey soils with a wide range of strength and compressibility parameters. More accurately:

    i. for the evaluation of the proposed p-y curves for soft NC clayey soils two centrifuge tests are modelled (Doyle et al., 2004; Ilyas et al., 2004), involving metallic laterally loaded piles of physical diameters D=0.8, 2.5m. The soil profile of the NC materials was represented by kaolin slurry layering in the model container of the centrifuge tests.

    ii. for the assessment of the proposed p-y curves for stiff OC clayey soils two full-scale tests are simulated (Rollins et al., 1998; Stewart et al., 2007), involving steel and reinforced concrete piles, of diameters D=0.3, 2.0m in real soil profiles with undrained shear strength range c_u=40-200kPa.

3. Apart from the validation of the proposed p-y curves, the thesis attempts to evaluate their predictions of the lateral pile response in comparison with corresponding predictions that utilize typical p-y methods of the international literature. For this particular purpose, we chose literature p-y curves around the upper and the lower bound of the total range and applied these curves on the aforementioned BNWF model. Thus, comparisons of the lateral pile response occurred (bend-

ing moments, lateral forces, horizontal displacements and curvature) between the predictions of the proposed and the literature p-y curves.

The aforementioned validation process of the proposed p-y curves proved the developed numerical tools trustworthy and in accordance with the exhibited experimental behaviour of centrifuge and full-scale lateral pile load tests in clayey soils. Consequently, the main points of the current thesis are summarized in the following:

1. Comparative assessment of the literature methodologies up to depth z=10D reveals significant divergence of the existing p-y curves for clayey soils. Indicatively, the comparison demonstrates differences up to two orders of magnitude for the initial stiffness K_i and up to 150% for the ultimate lateral soil resistance p_u. The aforementioned deviations refer to z=3D (the lateral soil response is more critical close the ground surface).

2. The proposed p-y curves for soft, NC clayey soils correlate with: slopes λ and κ of the virgin compression and the unloading-recompression lines respectively, Poisson's ratio ν and the pile-soil adhesion factor α ($\tau_{u,\,\text{interface}} = \alpha \cdot c_u$). The slope of the critical state line (CSL) M and the pile diameter D do not affect essentially these p-y curves.

3. The proposed p-y curves for stiff, OC clayey soils correlate with: the slope κ of the unloading-recompression line, Poisson's ratio ν, the pile-soil adhesion factor α, the pile diameter D and the average undrained shear strength $c_{u,\,avg}$ from ground surface to a depth z=10D. Strength degradation of the OC soil due to strain softening is not reflected on the corresponding p-y curves (residual strength down to 30% of peak strength.

4. Fixity conditions of the pile head (fixed, free) and geometrical non-linearities of the problem (large strain analysis) do not influence the numerical development of p-y curves for clayey soils under undrained loading.

5. Pseudostatic cyclic lateral displacement of the pile head $y_h = 5 - 50\%D$ does not affect significantly the numerical p-y curves, as they were derived from 3D FEA that simulate the clayey soils of the current dissertation through the MCC and the sophisticated model by Kalos 2014 (with small-strain stiffness and structure degradation features). However, the application of constant, two-way cyclic lateral force on the pile head delivers differentiated shallow post-cyclic p-y curves in terms of K_i for the OC clays, compared to the monotonic ones.

6. The proposed p-y curves simulate very accurately the lateral pile response (horizontal displacement, bending moment, curvature) in soft NC and stiff OC clayey

soils through the simplistic 2D BNWF model, as it occurred from comparisons with real experimental data. Despite the fact that the 3D FEA of the present thesis assume a fully elastic pile behavior, the numerically developed p-y curves predict successfully deformations and bending moments along the piles of the physical load tests that carry on even after failure of the pile material (plastic hinge).

7. The current thesis supports the modern aspect that the design of piles under lateral loading is over-conservative. Thus, it encourages the use of p_u around the upper bound of the literature methodologies for a safe, accurate and cost-effective design, as long as a thorough geotechnical investigation has taken place before.

8. The existing p-y curve methods overlook the effect of certain soil parameters (C_c, C_r, ν), leading to conservative design solutions. On the contrary, the proposed p-y curves of the current thesis incorporate the aforementioned effects, thus improving the cost and the reliability of the design.

8.2 Recommendations for future research

Future research can focus on two different axes, namely: a) improving the numerical tools utilized for the development of the p-y curves (finite element types, soil/ pile constitutive laws) and b) broaden the field of application regarding the proposed p-y curves (ground conditions/ geometry, loading type). The following shortcomings of the present thesis form the corresponding needs for further research:

1. The use of higher order finite elements (quadratic C3D20P) is required for a more detailed numerical simulation of the problem under investigation. The numerical analyses of the current dissertation utilize linear, three-dimensional finite elements with pore-pressure calculation (C3D8P) because the use of quadratic elements demands higher computational cost and usually causes numerical instabilities of the code under the regime of extensive deformation and material failure - for the estimation of p_u in the p-y curves.

2. Certain features of the poroelasticity theory and the MCC constitutive law imposed the assumption of specific distributions on some soil parameters that are investigated:

    i. assuming constant slope κ of the unloading-recompression line, the 3D FEA simulate a linearly increasing soil Young's modulus with depth. Increasing κ with depth is required for the simulation of constant modulus of elasticity.

ii. constant yield surface magnitude is utilized to simulate almost constant c_u of OC clayey soils with depth. This assumption sometimes leads to excessive (non-realistic) overconsolidation ratios (OCR) close to ground surface, especially during the simulated cases of hard clayey formations ($c_u > 200$kPa).

3. The constitutive laws of the 3D FEA in the current thesis (simplified but classic Modified Cam-Clay law and an advanced model recently proposed by Kalos 2014) are based on Critical State Soil Mechanics and do not incorporate fatigue features, required to simulate potential hysteresis loops of the soil-structure interaction curves during cyclic loading of many cycles. In addition, the developed numerical simulation is pseudostatic and does not account for time dependent phenomena. Therefore, the conclusions for the influence of cyclic loading (with few cycles) on the numerical p-y curves are more or less qualitative and reflect the limitations of the utilized constitutive laws regarding this type of loads. The guidelines by Andersen (2015) hold as a potential reference in an attempt to quantify the effect of cyclic loads on the corresponding numerically developed p-y curves.

4. Further investigation of the effect of the partially saturated surficial soil zone on the proposed p-y curves is highly recommended. The present thesis examines fully saturated clayey soils ($S_r = 100\%$) and thus probably neglects potential strength increase of the soil close to ground surface due to partial saturation - an area that is crucial for the lateral response of the pile-soil system. Research carried out by Georgiadis et al. (2003), Jostad et al. (2015), Bardanis (2016) and Sitarenios (2016) could offer significant aid towards the specific direction.

5. The proposed p-y curves of the thesis assume horizontal ground surface. However, it is possible to construct piles in sloping ground and certain modifications shall apply on the p-y curves in that case (see Georgiadis & Georgiadis, 2010; Matlock & Reese, 1960). Therefore, improvement of the numerically developed p-y curves of the dissertation is required towards this direction.

6. The dissertation overlooks potential alterations of the soil stress field due to the pile installation. As a result, the proposed p-y curves mainly refer to bored piles. However, the proposed p-y curves also performed satisfactorily in physical lateral load tests of driven piles by predicting their lateral response quite accurately. The specific performance is probably attributed to the extended soil area that reacts to the lateral loading of the pile. The pile installation process affects only the vicinity of the pile and thus its effects are localized at the closely surrounding clayey soil. Nevertheless, further investigation of the specific pile-soil interaction and its influence on numerically developed p-y curves for such soils is required

and research conducted by Chaloulos et al. (2013) on sandy soils could prove very useful referring to this goal.

Appendix A

List of parametric FEA

A.1 Description

The present appendix presents the tables of FEA carried out within the parametric investigation, which Chapters 4 and 5 describe thoroughly for soft, NC and medium-to-stiff, OC clayey soils respectively. The wide range of soil and pile parameters covered in these parametric FEA allows for the detailed definition of the corresponding numerical p-y curves.

A.2 List of FEA for soft, NC clays

The parametric investigation of soft, NC clays involves the following soil and pile parameters:

- Critical state line (CSL) slope M
- Normal compression line (NCL) slope λ
- NCL to unloading-reloading line slope ratio λ/κ
- Poisson's ratio ν
- Pile diameter D
- Pile-soil adhesion factor α

The actual range of the aforementioned parameters is indicated through coloured cells in the following table.

No.	NC clay parameters				Pile parameters	
	M	λ	λ/κ	ν	D (m)	α
1	0.772	0.065	10	0.333	1.0	0.3
2	1.2	0.065	10	0.333	1.0	0.3
3	0.984	0.065	10	0.333	1.0	0.3
4	0.772	0.174	10	0.333	1.0	0.3
5	0.772	0.109	10	0.333	1.0	0.3
6	0.984	0.109	10	0.333	1.0	0.3
7	0.984	0.174	10	0.333	1.0	0.3
8	1.2	0.109	10	0.333	1.0	0.3
9	1.2	0.174	10	0.333	1.0	0.3
10	0.772	0.065	10	0.333	1.0	1.0
11	0.772	0.109	10	0.333	1.0	1.0
12	0.772	0.174	10	0.333	1.0	1.0
13	0.984	0.065	10	0.333	1.0	1.0
14	0.984	0.109	10	0.333	1.0	1.0
15	0.984	0.174	10	0.333	1.0	1.0
16	1.2	0.065	10	0.333	1.0	1.0
17	1.2	0.109	10	0.333	1.0	1.0
18	1.2	0.174	10	0.333	1.0	1.0
19	0.772	0.174	10	0.333	0.5	1.0
20	0.772	0.174	10	0.333	2.0	1.0
21	0.772	0.174	10	0.333	1.5	1.0
22	1.2	0.065	10	0.333	0.5	1.0
23	1.2	0.065	10	0.333	1.5	1.0

No.	NC clay parameters				Pile parameters	
	M	λ	λ/κ	ν	D (m)	α
24	1.2	0.065	10	0.333	2.0	1.0
25	0.984	0.109	10	0.333	0.5	0.3
26	0.984	0.109	10	0.333	1.5	0.3
27	0.984	0.109	10	0.333	2.0	0.3
28	0.984	0.109	5	0.333	1.0	1.0
29	0.984	0.109	20	0.333	1.0	1.0
30	0.984	0.109	10	0.1	1.0	1.0
31	0.984	0.109	10	0.2	1.0	1.0

A.3 List of FEA for medium-to-stiff, OC clays

The parametric investigation of medium-to-stiff, OC clays involves the following soil and pile parameters:

- Average undrained shear strength $c_{u,\,avg}$ along a depth of $10D$ from the pile head
- Unloading-reloading lines slope κ
- The maximum coefficient of horizontal geostatic stress $K_{o,\,max}$
- Critical state line (CSL) slope M
- Poisson's ratio ν
- Reduction factor of the peak undrained shear strength $RF = c_{u,\,\mathrm{res}}/c_{u,\,\mathrm{peak}}$
- Pile diameter D
- Pile-soil adhesion factor α

The actual range of the aforementioned parameters is indicated through coloured cells in the following table.

No.	OC clay parameters						Pile parameters	
	$c_{u,\,avg}$ (kPa)	κ	$K_{o,\,max}$	M	ν	RF	D (m)	α
1	50	0.0033	1.5	1.2	0.1	1.0	1.0	0.3
2	380	0.0033	1.5	1.2	0.1	1.0	1.0	0.3
3	95	0.0033	1.5	1.2	0.1	1.0	1.0	0.3
4	190	0.0033	1.5	1.2	0.1	1.0	1.0	0.3
5	50	0.0174	1.5	1.2	0.1	1.0	1.0	0.3
6	50	0.0054	1.5	1.2	0.1	1.0	1.0	0.3
7	50	0.0087	1.5	1.2	0.1	1.0	1.0	0.3
8	95	0.0054	1.5	1.2	0.1	1.0	1.0	0.3
9	95	0.0065	1.5	1.2	0.1	1.0	1.0	0.3
10	95	0.0087	1.5	1.2	0.1	1.0	1.0	0.3
11	95	0.0108	1.5	1.2	0.1	1.0	1.0	0.3
12	95	0.0174	1.5	1.2	0.1	1.0	1.0	0.3
13	190	0.0054	1.5	1.2	0.1	1.0	1.0	0.3
14	190	0.0065	1.5	1.2	0.1	1.0	1.0	0.3
15	190	0.0087	1.5	1.2	0.1	1.0	1.0	0.3
16	190	0.0108	1.5	1.2	0.1	1.0	1.0	0.3
17	190	0.0174	1.5	1.2	0.1	1.0	1.0	0.3
18	380	0.0054	1.5	1.2	0.1	1.0	1.0	0.3
19	380	0.0065	1.5	1.2	0.1	1.0	1.0	0.3
20	380	0.0087	1.5	1.2	0.1	1.0	1.0	0.3
21	380	0.0108	1.5	1.2	0.1	1.0	1.0	0.3
22	380	0.0174	1.5	1.2	0.1	1.0	1.0	0.3
23	50	0.0033	1.5	1.2	0.1	1.0	1.0	1.0

No.	OC clay parameters						Pile parameters	
	$c_{u,\,avg}$ (kPa)	κ	$K_{o,\,max}$	M	ν	RF	D (m)	α
24	380	0.0033	1.5	1.2	0.1	1.0	1.0	1.0
25	95	0.0033	1.5	1.2	0.1	1.0	1.0	1.0
26	190	0.0033	1.5	1.2	0.1	1.0	1.0	1.0
27	50	0.0174	1.5	1.2	0.1	1.0	1.0	1.0
28	50	0.0054	1.5	1.2	0.1	1.0	1.0	1.0
29	50	0.0087	1.5	1.2	0.1	1.0	1.0	1.0
30	95	0.0054	1.5	1.2	0.1	1.0	1.0	1.0
31	95	0.0065	1.5	1.2	0.1	1.0	1.0	1.0
32	95	0.0087	1.5	1.2	0.1	1.0	1.0	1.0
33	95	0.0108	1.5	1.2	0.1	1.0	1.0	1.0
34	95	0.0174	1.5	1.2	0.1	1.0	1.0	1.0
35	190	0.0054	1.5	1.2	0.1	1.0	1.0	1.0
36	190	0.0065	1.5	1.2	0.1	1.0	1.0	1.0
37	190	0.0087	1.5	1.2	0.1	1.0	1.0	1.0
38	190	0.0108	1.5	1.2	0.1	1.0	1.0	1.0
39	190	0.0174	1.5	1.2	0.1	1.0	1.0	1.0
40	380	0.0054	1.5	1.2	0.1	1.0	1.0	1.0
41	380	0.0065	1.5	1.2	0.1	1.0	1.0	1.0
42	380	0.0087	1.5	1.2	0.1	1.0	1.0	1.0
43	380	0.0108	1.5	1.2	0.1	1.0	1.0	1.0
44	380	0.0174	1.5	1.2	0.1	1.0	1.0	1.0
45	190	0.0054	0.7	1.2	0.1	1.0	1.0	0.3
46	190	0.0054	1.0	1.2	0.1	1.0	1.0	0.3

No.	OC clay parameters						Pile parameters	
	$c_{u,avg}$ (kPa)	κ	$K_{o,max}$	M	ν	RF	D (m)	α
47	190	0.0054	1.5	0.772	0.1	1.0	1.0	0.3
48	190	0.0054	1.5	0.984	0.1	1.0	1.0	0.3
49	190	0.0054	1.5	1.2	0.333	1.0	1.0	0.3
50	190	0.0054	1.5	1.2	0.2	1.0	1.0	0.3
51	95	0.0054	1.5	1.2	0.1	0.3	1.0	0.3
52	95	0.0054	1.5	1.2	0.1	0.5	1.0	0.3
53	95	0.0054	1.5	1.2	0.1	0.8	1.0	0.3
54	190	0.0054	1.5	1.2	0.1	0.3	1.0	0.3
55	190	0.0054	1.5	1.2	0.1	0.5	1.0	0.3
56	190	0.0054	1.5	1.2	0.1	0.8	1.0	0.3
57	380	0.0054	1.5	1.2	0.1	0.3	1.0	0.3
58	380	0.0054	1.5	1.2	0.1	0.5	1.0	0.3
59	380	0.0054	1.5	1.2	0.1	0.8	1.0	0.3
60	95	0.0054	1.5	1.2	0.1	0.3	1.0	1.0
61	95	0.0054	1.5	1.2	0.1	0.5	1.0	1.0
62	95	0.0054	1.5	1.2	0.1	0.8	1.0	1.0
63	190	0.0054	1.5	1.2	0.1	0.3	1.0	1.0
64	190	0.0054	1.5	1.2	0.1	0.5	1.0	1.0
65	190	0.0054	1.5	1.2	0.1	0.8	1.0	1.0
66	380	0.0054	1.5	1.2	0.1	0.3	1.0	1.0
67	380	0.0054	1.5	1.2	0.1	0.5	1.0	1.0
68	380	0.0054	1.5	1.2	0.1	0.8	1.0	1.0
69	50	0.0087	1.5	1.2	0.1	1.0	0.5	0.3

No.	OC clay parameters						Pile parameters	
	$c_{u,\,avg}$ (kPa)	κ	$K_{o,\,max}$	M	ν	RF	D (m)	α
70	50	0.0087	1.5	1.2	0.1	1.0	2.0	0.3
71	50	0.0087	1.5	1.2	0.1	1.0	1.5	0.3
72	95	0.0087	1.5	1.2	0.1	1.0	0.5	0.3
73	95	0.0174	1.5	1.2	0.1	1.0	0.5	0.3
74	95	0.0087	1.5	1.2	0.1	1.0	1.5	0.3
75	95	0.0174	1.5	1.2	0.1	1.0	1.5	0.3
76	95	0.0087	1.5	1.2	0.1	1.0	2.0	0.3
77	95	0.0174	1.5	1.2	0.1	1.0	2.0	0.3
78	190	0.0065	1.5	1.2	0.1	1.0	0.5	0.3
79	190	0.0065	1.5	1.2	0.1	1.0	0.5	1.0
80	190	0.0087	1.5	1.2	0.1	1.0	0.5	0.3
81	190	0.0087	1.5	1.2	0.1	1.0	0.5	1.0
82	190	0.0065	1.5	1.2	0.1	1.0	1.5	0.3
83	190	0.0065	1.5	1.2	0.1	1.0	1.5	1.0
84	190	0.0087	1.5	1.2	0.1	1.0	1.5	0.3
85	190	0.0087	1.5	1.2	0.1	1.0	1.5	1.0
86	190	0.0065	1.5	1.2	0.1	1.0	2.0	0.3
87	190	0.0065	1.5	1.2	0.1	1.0	2.0	1.0
88	190	0.0087	1.5	1.2	0.1	1.0	2.0	0.3
89	190	0.0087	1.5	1.2	0.1	1.0	2.0	1.0
90	380	0.0033	1.5	1.2	0.1	1.0	0.5	0.3
91	380	0.0087	1.5	1.2	0.1	1.0	0.5	0.3
92	380	0.0033	1.5	1.2	0.1	1.0	1.5	0.3

No.	OC clay parameters						Pile parameters	
	$c_{u,\,avg}$ (kPa)	κ	$K_{o,\,max}$	M	ν	RF	D (m)	α
93	380	0.0087	1.5	1.2	0.1	1.0	1.5	0.3
94	380	0.0033	1.5	1.2	0.1	1.0	2.0	0.3
95	380	0.0087	1.5	1.2	0.1	1.0	2.0	0.3

Appendix B

Equivalency between the MCC and the SSS-SD constitutive laws

B.1 Description

The current appendix aims at presenting the process that the dissertation followed for the determination of a size ratio A between the Structure Strength Envelope (SSE) and the yield locus of the MCC simulating OC clays. Since the MCC cannot reproduce significant strain-softening, the thesis utilizes a sophisticated constitutive law for the simulation of stiff, structured clays - see Paragraph 3.2.2.2 - that incorporates small-strain stiffness (SSS) and structure degradation (SD) features. The main assumption is that both the MCC and the advanced constitutive model deliver the same peak undrained shear strength for the OC clay, with the latter capable of simulating also various levels of strength degradation. Therefore, the necessity occurred for the correlation of certain yield surface sizes between the two constitutive laws.

B.2 Theoretical approach of A

Figure B.1 explains schematically the meaning of ratio A. It is nothing more than the ratio of the initial SSE size to the size of the MCC yield locus simulating a certain $c_{u,\,avg}$ and is represented by the following equation:

$$A = \frac{p_{m,\,\mathrm{SSE}}}{p_{m,\,\mathrm{MCC}}} \tag{B.1}$$

The general idea lying behind this equation is that the SSE begins to shrink with the accumulation of plastic strains, i.e. the stress path reaches the bounding surface of

the PYE. While the stress path carries the PYE onto the SSE, the size of the latter becomes significantly smaller than its' initial. At the point of "return" towards the ISE[1], that is exactly when the destructuring process begins, the SSE must have the same - or almost the same - size with the corresponding MCC yield surface in order to achieve similar $c_{u,\,\mathrm{peak}}$ between the two simulations. As a consequence, the present appendix attempts to specify the correlation of A with various parameters of the problem, such as depth z, average undrained shear strength $c_{u,\,avg}$ and of course the size ratio $B = p_m/p_m^*$ of the SSE to the ISE.

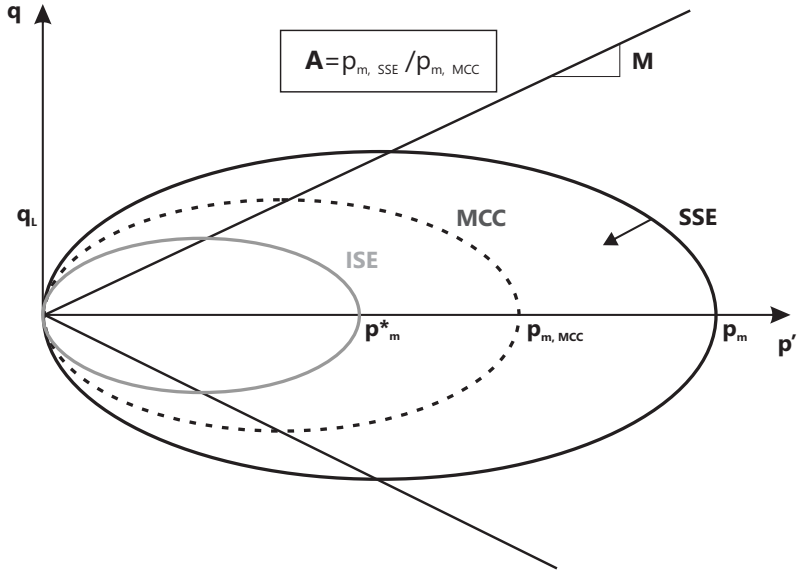

Figure B.1: Schematic representation of the general idea behind A ratio. The concept for the equivalency in peak undrained shear strength between the MCC and the SSS-SD constitutive law for OC clays.

B.3 Trial-and-error process for the determination of A

The appendix carries out a set of numerical undrained triaxial tests (see Paragraph 3.2.2.3 for details) in the FEM code Simulia Abaqus 6.12 at two different depths z of the three average undrained shear strengths $c_{u,\,avg}$ examined in Chapter 5. More accurately, the investigation involves undrained triaxial tests of "specimens" at z=1, 4m, with $c_{u,\,avg}$=95, 190 and 380kPa (κ=0.0054, $K_{o,\,max}$=1.5, M=1.2, ν=0.1). The FEA simulate the OC clay through both the MCC and the advanced constitutive

[1]The ISE hardens only narrowly due to lack of volumetric strains under undrained loading conditions - similar to the slight hardening of the MCC in the same case.

model (SSS-SD). The OC clay simulation through the sophisticated SSS-SD constitutive law involves three different B ratios, namely 2, 5 and 10 in order to cover all potential intensities of structure degradation, that is mild, moderate and intense. A is not a ratio that one can calculate directly since it refers to peak strength, i.e. at failure. Therefore, we assume three values of the ratio, A=1.5, 2.0, 2.5, and compare the two constitutive simulations (MCC and SSS-SD) in terms of stress paths and $q - \varepsilon_q$ curves. It is important to clarify that during the specific trial-and-error process certain parameters of the sophisticated model are assumed constant: ξ=0.05, λ^*=2 and η=50. According to Paragraph 5.3, the aforementioned parameters reproduce a physical constitutive behavior of the simulated OC clays. However, in case of variation - especially for λ^* and η - one needs to repeat the procedure. Thus, the developed process serves as a guideline and not as a quantitative proposal.

B.3.1 A for average undrained shear strength 95kPa

Figures B.2, B.3 and B.4 depict the comparison of (a) effective stress paths and (b) $q - \varepsilon_q$ curves for $c_{u,\,avg}$=95kPa and B=2, 5 and 10 respectively.

B.3.2 A for average undrained shear strength 190kPa

Figures B.5, B.6 and B.7 depict the comparison of (a) effective stress paths and (b) $q - \varepsilon_q$ curves for $c_{u,\,avg}$=190kPa and B=2, 5 and 10 respectively.

B.3.3 A for average undrained shear strength 380kPa

Figures B.8, B.9 and B.10 depict the comparison of (a) effective stress paths and (b) $q - \varepsilon_q$ curves for $c_{u,\,avg}$=380kPa and B=2, 5 and 10 respectively.

B.4 Determination of A

The findings of the aforementioned trial-and-error process demonstrate a correlation of A with B and z. As expected, the tested values of A did not deliver stress paths and peak deviatoric strength that matched exactly with the corresponding MCC simulation. As a result, the specific study compiled the following table to summarize the correlations that occured with these parameters. It seems that depth z plays some role in the determination of A, which is a natural effect since z is indicative of the in situ stress field. However, the most profound correlation of A is that with the destructuring ratio B. Figure B.11 presents A as a function of B, either taking into account its' variation with z (Figure B.11a) or not (Figure B.11b). The

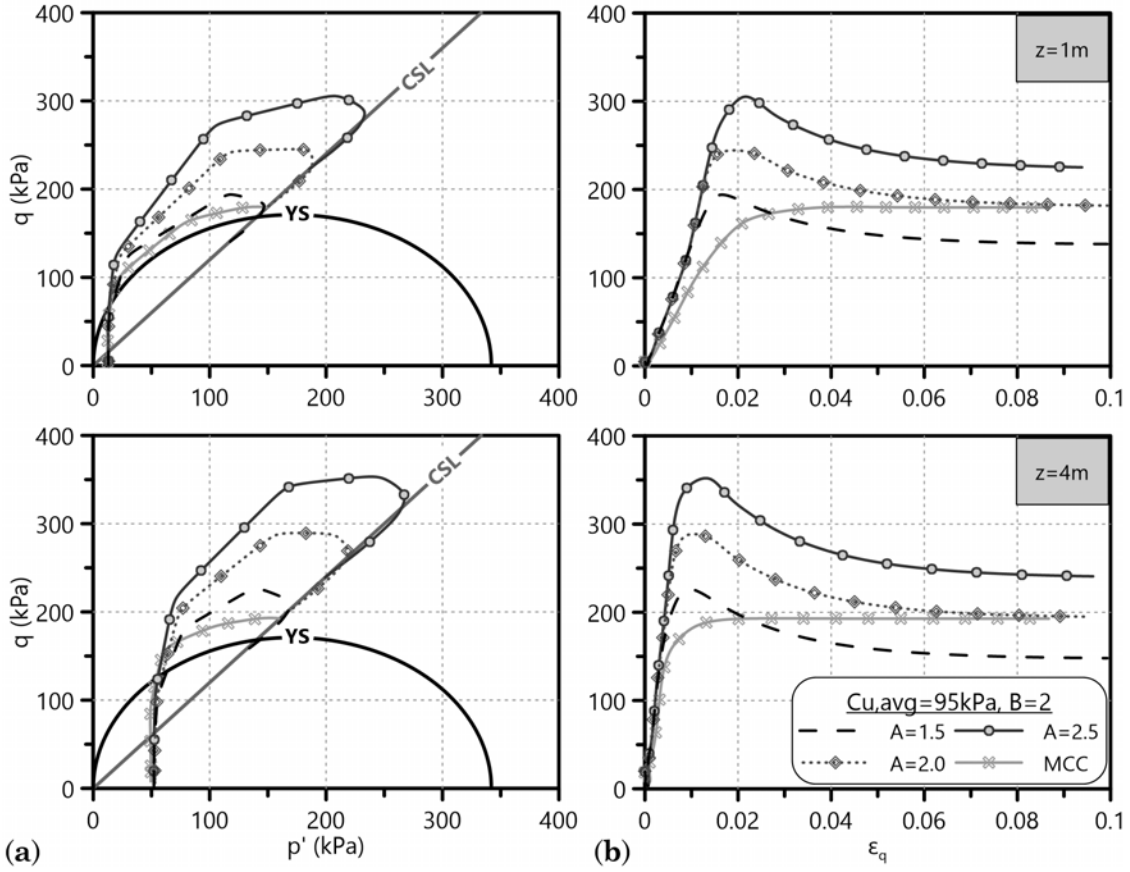

Figure B.2: Trial-and-error determination of A ratio through numerical undrained triaxial tests on OC clay specimens ($c_{u,\,avg}$=95kPa, κ=0.0054, $K_{o,\,max}$=1.5, M=1.2, ν=0.1) simulated by the MCC and the sophisticated SSS-SD constitutive law (B=2). (a) Stress paths and (b) deviatoric stress-strain curves for various ratios A at depths z=1 and 4m.

Table B.1: Determination of A ratio according to the trial-and-error results of the numerical undrained triaxial tests.

$c_{u,\,avg}$ (kPa)	B	A (z=1m)	A (z=4m)
95	2	1.3	1.2
	5	1.7	1.4
	10	1.8	1.5
190	2	1.5	1.3
	5	1.8	1.5
	10	1.9	1.6
380	2	1.5	1.4
	5	1.8	1.7
	10	2.0	1.8

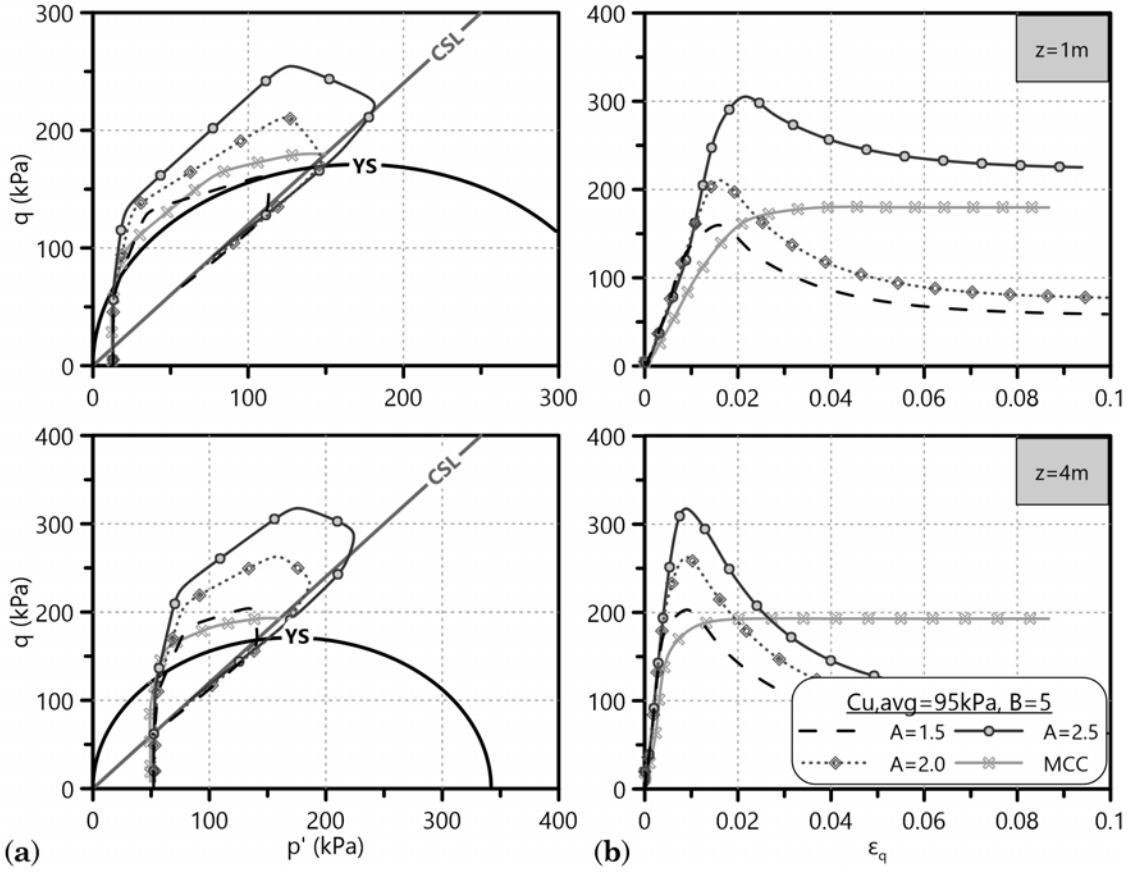

Figure B.3: Trial-and-error determination of A ratio through numerical undrained triaxial tests on OC clay specimens ($c_{u,\,avg}$=95kPa, κ=0.0054, $K_{o,\,max}$=1.5, M=1.2, ν=0.1) simulated by the MCC and the sophisticated SSS-SD constitutive law (B=5). (a) Stress paths and (b) deviatoric stress-strain curves for various ratios A at depths z=1 and 4m.

specific study assumes that this differentiation is not significant enough to produce a complex equation for A, reminding the reader that it is a conventional and not a constitutive parameter after all. Thus, the current appendix proposes the following equation correlating ratio A with B, applicable for the $c_{u,\,avg}$ range (95-380kPa) that the present dissertation utilizes to simulate OC clays.

$$A = 0.25\ln(B) + 1.22 \tag{B.2}$$

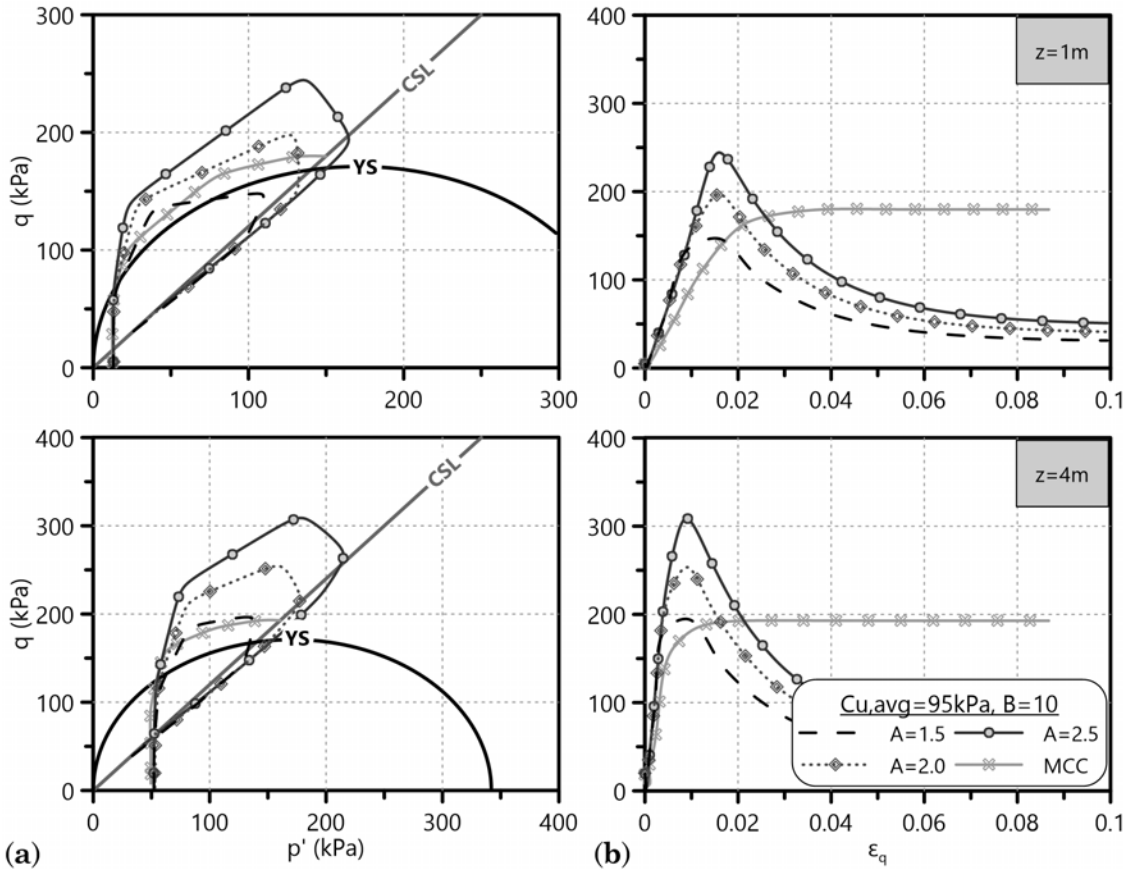

Figure B.4: Trial-and-error determination of A ratio through numerical undrained triaxial tests on OC clay specimens ($c_{u,\,avg}$=95kPa, κ=0.0054, $K_{o,\,max}$=1.5, M=1.2, ν=0.1) simulated by the MCC and the sophisticated SSS-SD constitutive law (B=10). (a) Stress paths and (b) deviatoric stress-strain curves for various ratios A at depths z=1 and 4m.

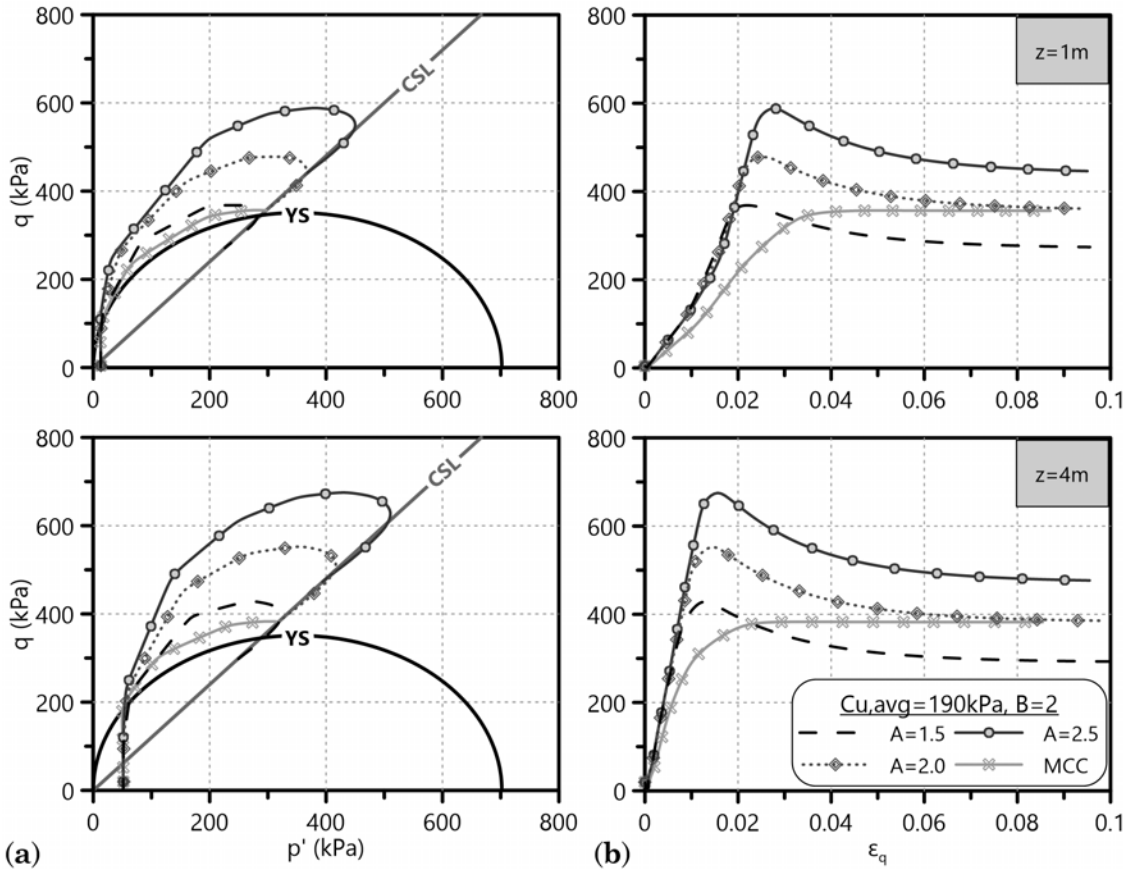

Figure B.5: Trial-and-error determination of A ratio through numerical undrained triaxial tests on OC clay specimens ($c_{u,\,avg}$=190kPa, κ=0.0054, $K_{o,\,max}$=1.5, M=1.2, ν=0.1) simulated by the MCC and the sophisticated SSS-SD constitutive law (B=2). (a) Stress paths and (b) deviatoric stress-strain curves for various ratios A at depths z=1 and 4m.

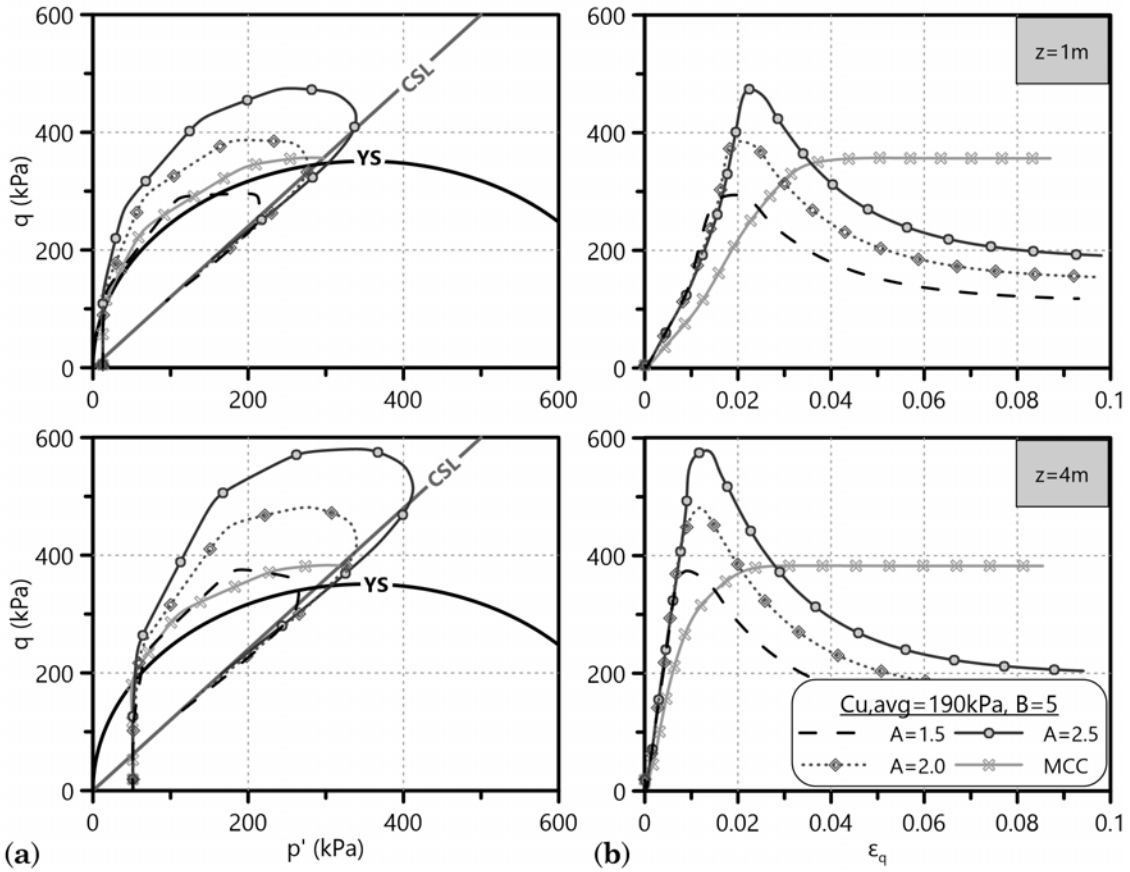

Figure B.6: Trial-and-error determination of A ratio through numerical undrained triaxial tests on OC clay specimens ($c_{u,\,avg}$=190kPa, κ=0.0054, $K_{o,\,max}$=1.5, M=1.2, ν=0.1) simulated by the MCC and the sophisticated SSS-SD constitutive law (B=5). (a) Stress paths and (b) deviatoric stress-strain curves for various ratios A at depths z=1 and 4m.

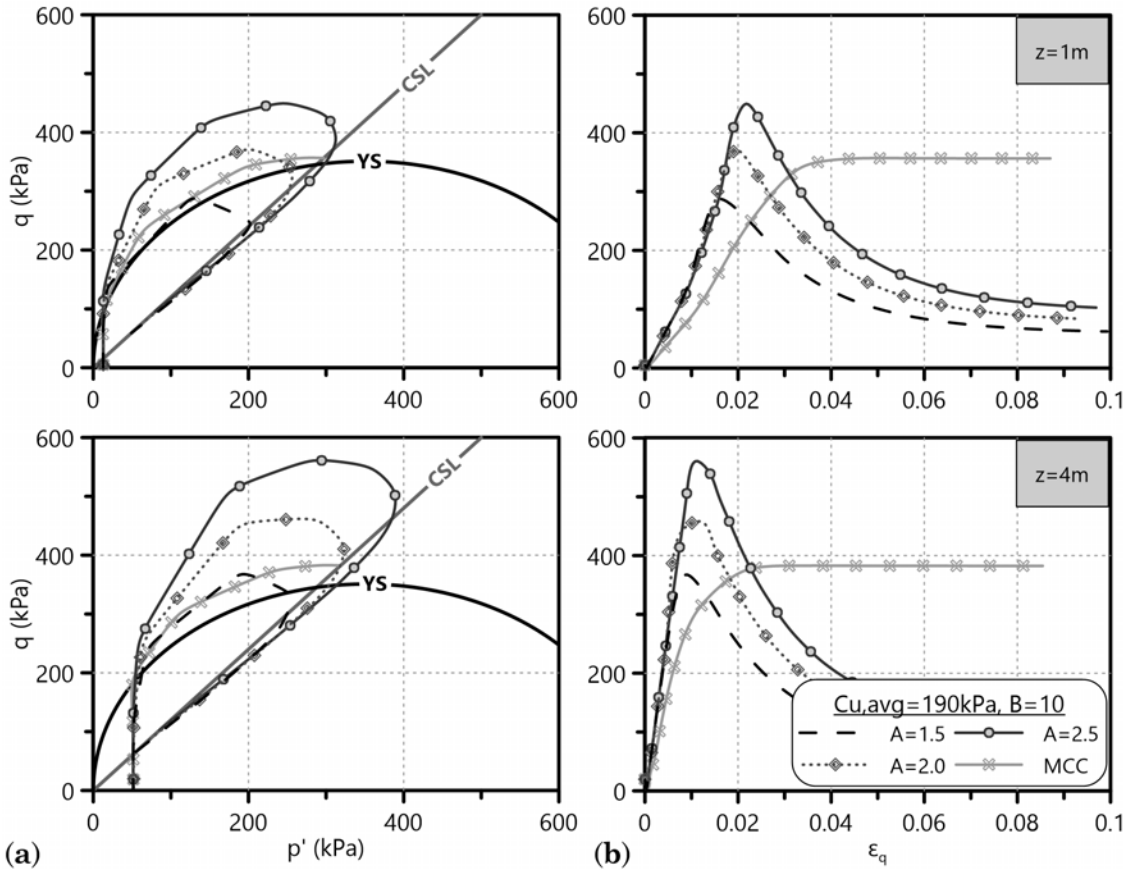

Figure B.7: Trial-and-error determination of A ratio through numerical undrained triaxial tests on OC clay specimens ($c_{u,\,avg}$=190kPa, κ=0.0054, $K_{o,\,max}$=1.5, M=1.2, ν=0.1) simulated by the MCC and the sophisticated SSS-SD constitutive law (B=10). (a) Stress paths and (b) deviatoric stress-strain curves for various ratios A at depths z=1 and 4m.

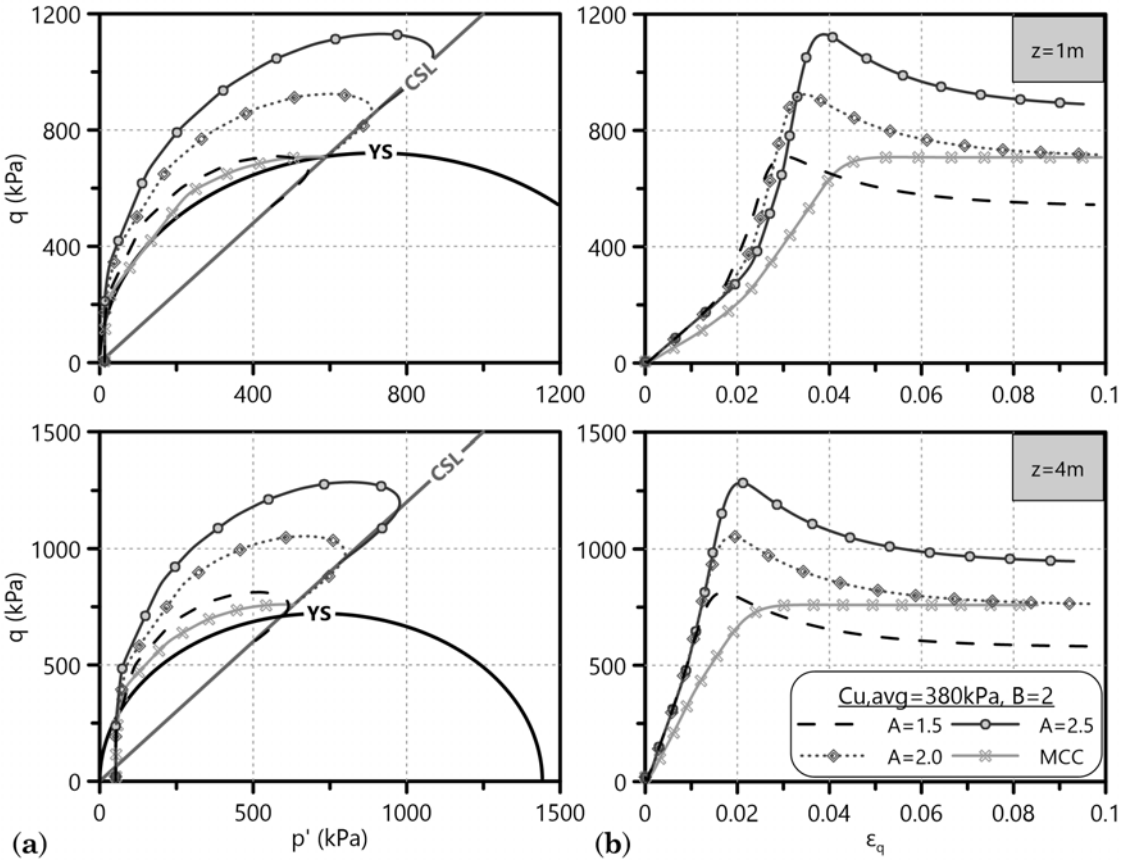

Figure B.8: Trial-and-error determination of A ratio through numerical undrained triaxial tests on OC clay specimens ($c_{u,\,avg}$=380kPa, κ=0.0054, $K_{o,\,max}$=1.5, M=1.2, ν=0.1) simulated by the MCC and the sophisticated SSS-SD constitutive law (B=2). (a) Stress paths and (b) deviatoric stress-strain curves for various ratios A at depths z=1 and 4m.

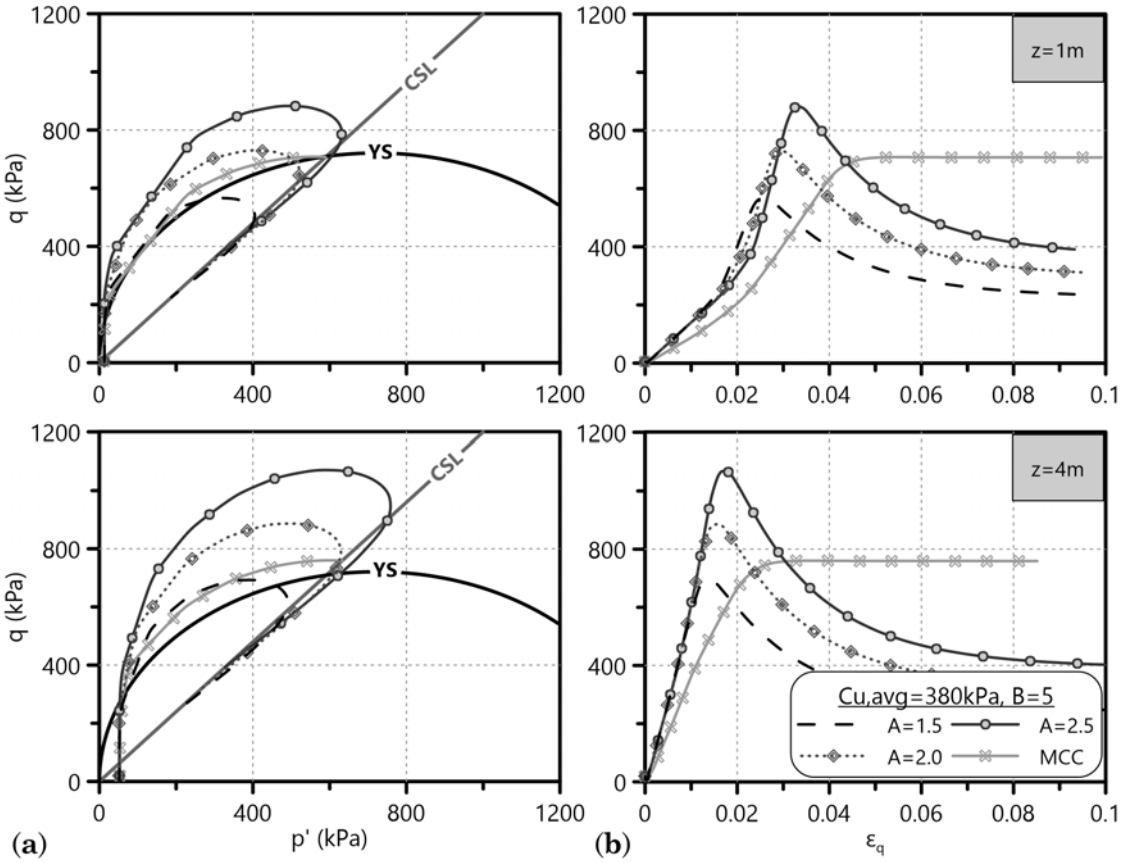

Figure B.9: Trial-and-error determination of A ratio through numerical undrained triaxial tests on OC clay specimens ($c_{u,\,avg}$=380kPa, κ=0.0054, $K_{o,\,max}$=1.5, M=1.2, ν=0.1) simulated by the MCC and the sophisticated SSS-SD constitutive law (B=5). (a) Stress paths and (b) deviatoric stress-strain curves for various ratios A at depths z=1 and 4m.

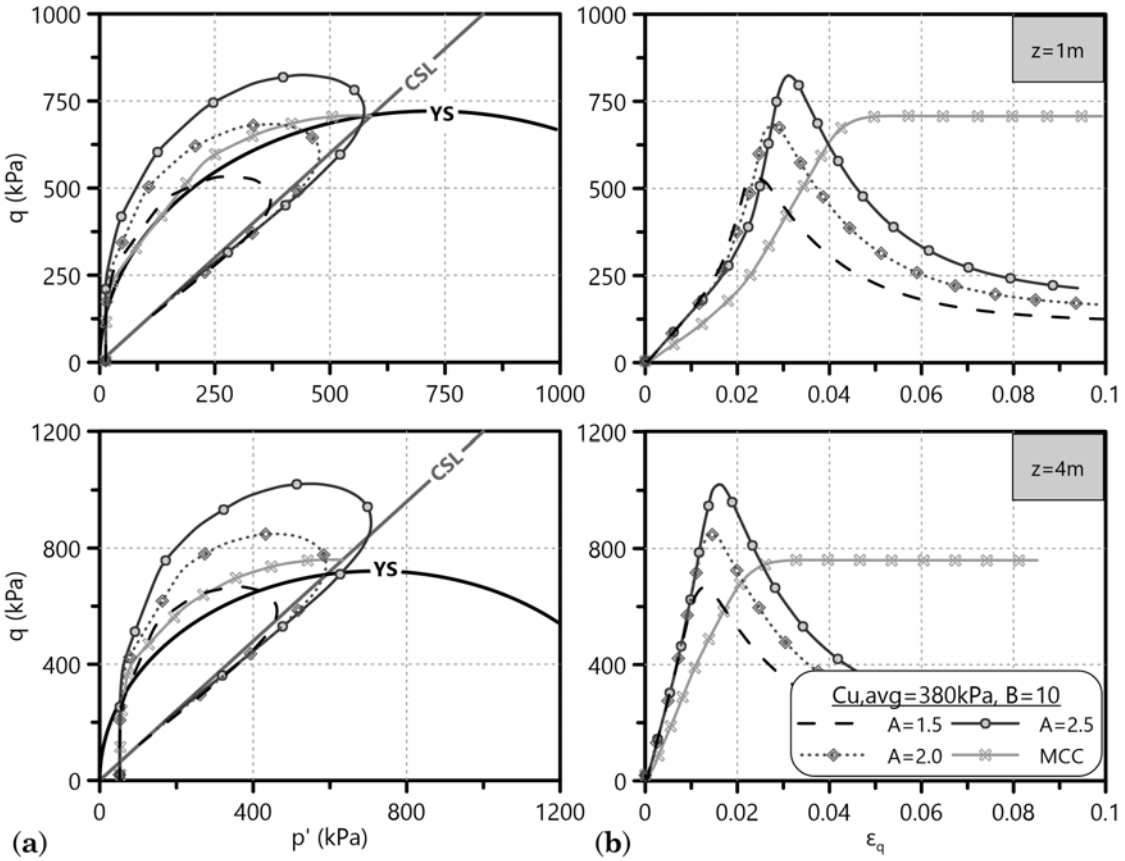

Figure B.10: Trial-and-error determination of A ratio through numerical undrained triaxial tests on OC clay specimens ($c_{u,\,avg}$=380kPa, κ=0.0054, $K_{o,\,max}$=1.5, M=1.2, ν=0.1) simulated by the MCC and the sophisticated SSS-SD constitutive law (B=10). (a) Stress paths and (b) deviatoric stress-strain curves for various ratios A at depths z=1 and 4m.

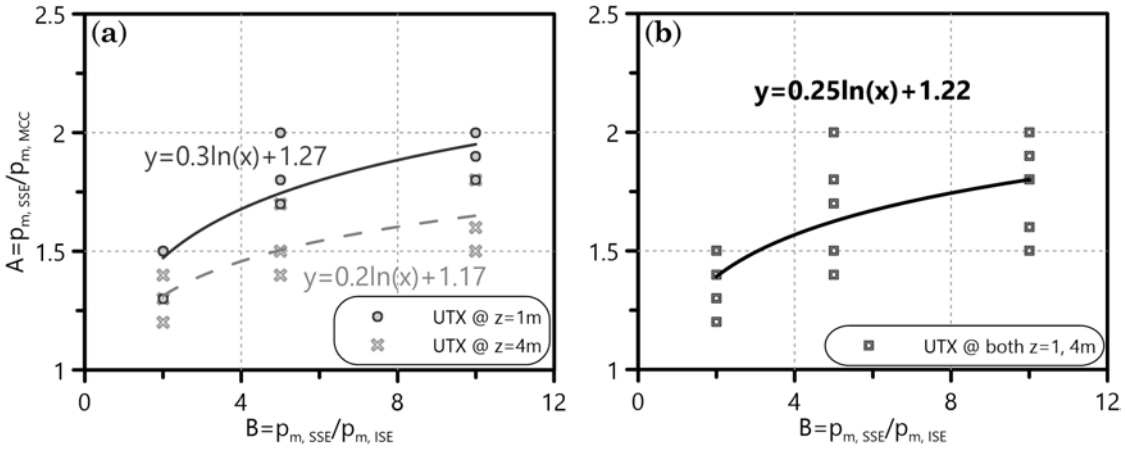

Figure B.11: Correlation of A ratio with the destructuring ratio $B = p_m/p_m^*$ (a) varying with depth z and (b) unique for all depths, according to the finally assumed values from Table B.1.

Appendix C

Characteristic frames of the FEA

C.1 Description

The current appendix presents indicative contours from characteristic frames of the FEA carried out within the parametric investigation that is thoroughly described by Chapters 3 to 6. Although the following figures do not cover the parametric numerical investigation in full extent, they depict certain output variables representative of the lateral pile and soil response. The FEA frames demonstrate contours of the resultant displacement (U, Magnitude), the plastic strain magnitude (PEMAG) and the developed soil pore pressure (POR) on the deformed shape of the mesh. A 1m-diameter pile together with the following two (2) soils are included in the present appendix, with parameters in the mid-range of the extensive parametric study:

- **soft, NC clay:** M=0.984, λ=0.109, λ/κ=10, K_o=0.5, ν=0.333
- **stiff, OC clay:** M=1.2, $c_{u,\,avg}$=190kPa, κ=0.0054, $K_{o,\,max}$=1.5, ν=0.1, RF=1

C.2 Characteristic FEA frames

The FEA frames refer to the following three (3) simulations, both for soft NC and stiff OC clayey soils:

- external monotonic lateral loading of a free-head flexible pile
- external monotonic lateral loading of a fixed-head flexible pile
- external cyclic lateral loading of a free-head flexible pile

Figures of the aforementioned simulations are depicted separately in the paragraphs ahead. In order to avoid the depiction of excessive mesh deformation, load frames

of pile head displacements y_h=0.5D and y_h=2.0D are presented with scale factors 2 and 0.5 respectively.

C.2.1 Monotonic lateral loading of a free-head pile in soft NC clay

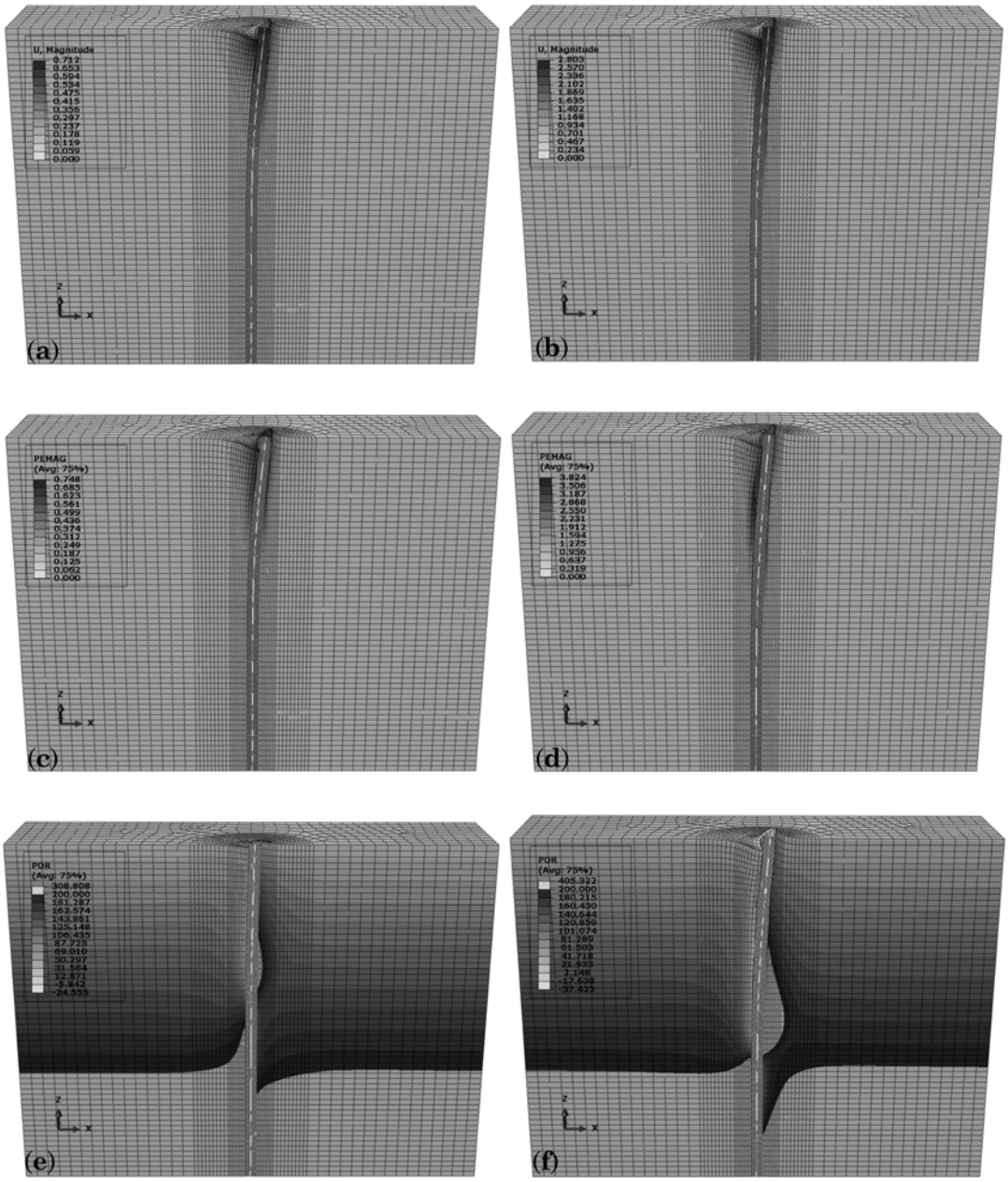

Figure C.1: Deformed mesh contours of (a,b) the resultant displacement (U, Magnitude), (c,d) the plastic strain magnitude (PEMAG) and (e,f) the developed soil pore pressure (POR) of two different load frames: monotonic horizontal pile head displacement y_h=0.5D (left) and y_h=2.0D (right) of a free-head flexible pile in a soft, NC clay.

C.2.2 Monotonic lateral loading of a free-head pile in stiff OC clay

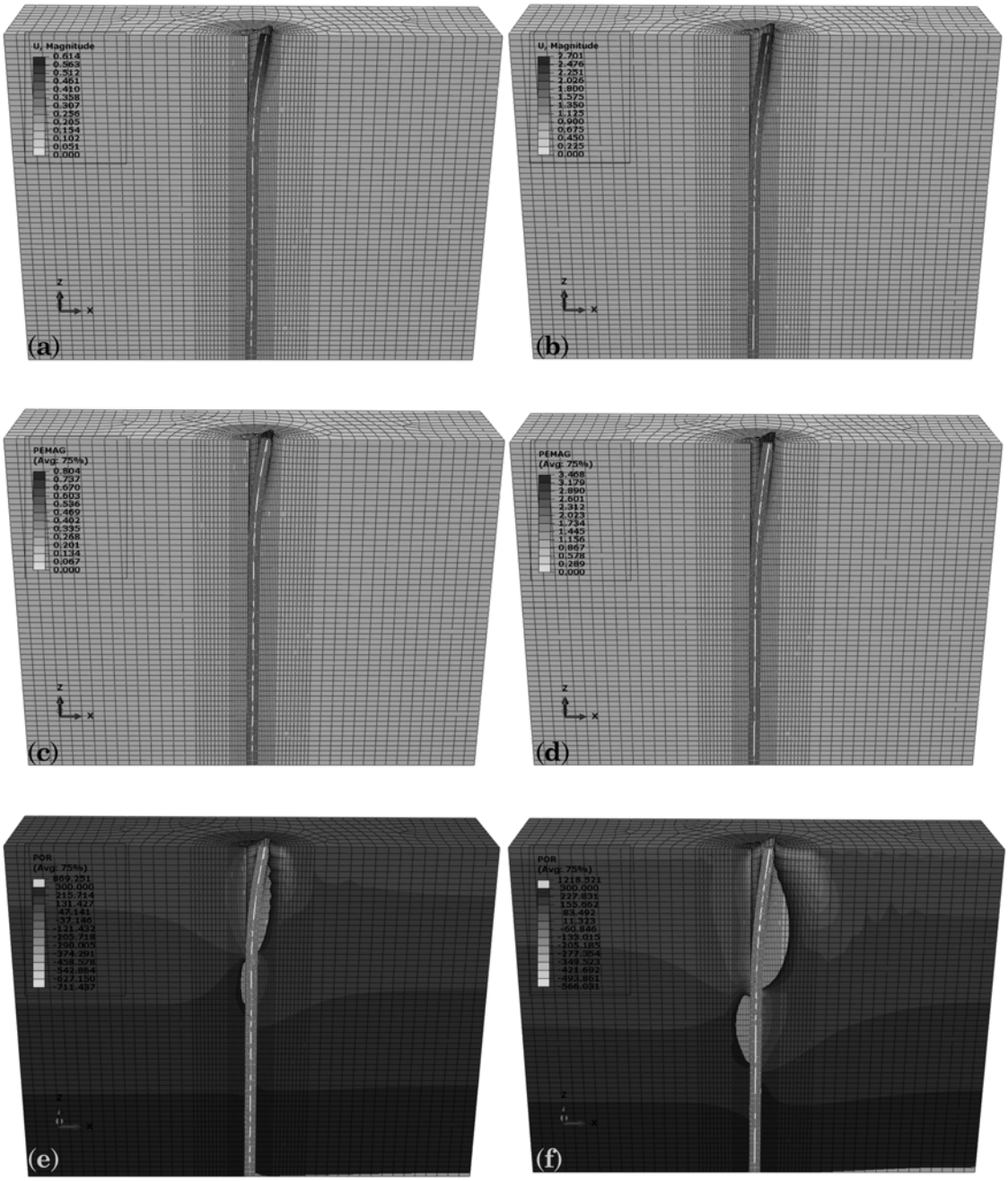

Figure C.2: Deformed mesh contours of (a,b) the resultant displacement (U, Magnitude), (c,d) the plastic strain magnitude (PEMAG) and (e,f) the developed soil pore pressure (POR) of two different load frames: monotonic horizontal pile head displacement y_h=0.5D (left) and y_h=2.0D (right) of a free-head flexible pile in a stiff, OC clay.

C.2.3 Monotonic lateral loading of a fixed-head pile

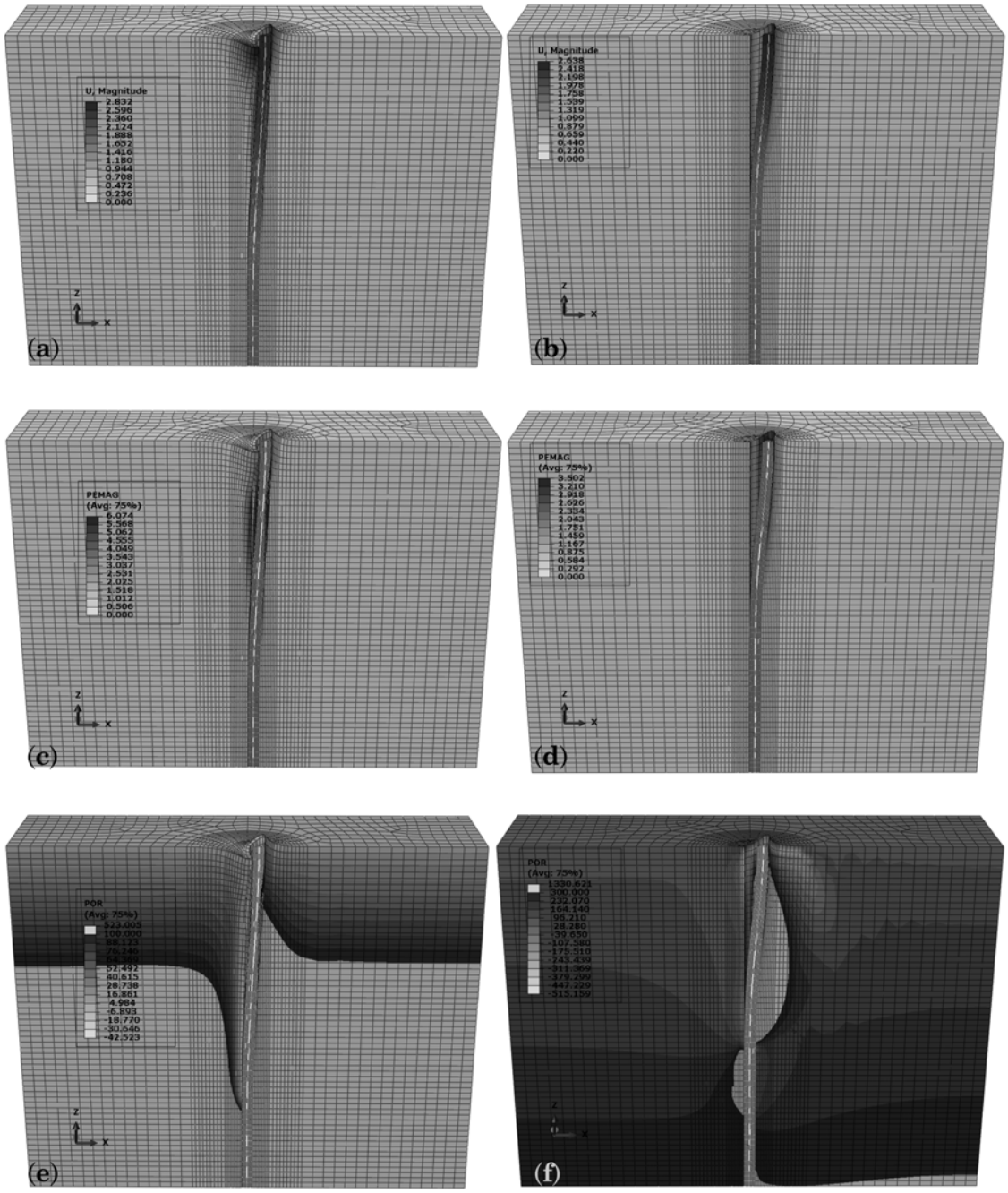

Figure C.3: Deformed mesh contours of (a,b) the resultant displacement (U, Magnitude), (c,d) the plastic strain magnitude (PEMAG) and (e,f) the developed soil pore pressure (POR) for the soft, NC (left) and the stiff, OC clay (right) - monotonic horizontal pile head displacement y_h=2.0D.

C.2.4 Cyclic lateral loading of a free-head pile

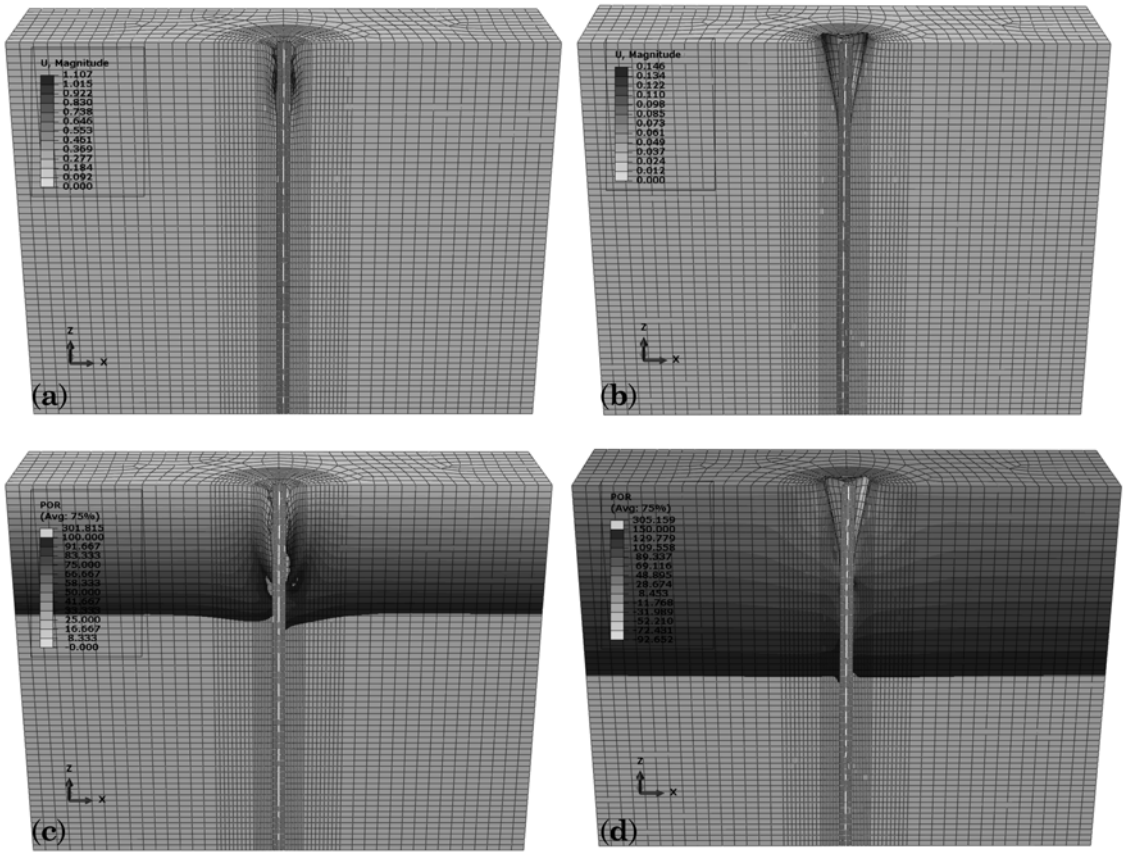

Figure C.4: Deformed mesh contours of (a,b) the resultant displacement (U, Magnitude) and (c,d) the developed soil pore pressure (POR) for the soft, NC (left) and the stiff, OC clay (right), representing the state after 20 cycles of two-way pile head lateral loading.

References

Ahmadi, M. & Ahmari, S. (2009). Finite-element modelling of laterally loaded piles in clay. *Proceedings of the Institution of Civil Engineers-Geotechnical Engineering 162*(3), 151–163.

Amerasinghe, S. (1973). *The stress-strain behaviour of clay at low stress levels and high overconsolidation ratio*. Ph. D. thesis, Cambridge University.

Andersen, K. (2015). Cyclic soil parameters for offshore foundation design. *Frontiers in Offshore Geotechnics III 5*.

API (2007). American petroleum institute recommended practice for planning, designing and constructing fixed offshore platforms—working stress design. *RP2A-WSD*.

API (2011). Geotechnical and foundation design considerations. *2GEO-2011*.

Ashour, M. & Norris, G. (2000). Modeling lateral soil-pile response based on soil-pile interaction. *Journal of Geotechnical and Geoenvironmental Engineering 126*(5), 420–428.

Ashour, M., Norris, G., & Pilling, P. (1998). Lateral loading of a pile in layered soil using the strain wedge model. *Journal of Geotechnical and Geoenvironmental Engineering 124*(4), 303–315.

Atkinson, J. & Bransby, P. (1977). The mechanics of soils, an introduction to critical state soil mechanics. Technical report.

Baguelin, F., Frank, R., & Said, Y. (1977). Theoretical study of lateral reaction mechanism of piles. *Géotechnique 27*(3), 405–434.

Belokas, G. (2008). *Simulating the Mechanical Behaviour of Structured and Anisotropic Soils*. Ph. D. thesis, School of Civil Engineering, National Technical University of Athens (NTUA).

Belokas, G. & Kavvadas, M. (2011). An intrinsic compressibility framework for clayey soils. *Geotechnical and Geological Engineering 29*(5), 855–871.

Bouafia, A. (2013). PY curves from the prebored pressuremeter test for laterally loaded single piles. *Proceedings of the 18th International Conference on Soil Mechanics and Geotechnical Engineering*, Number 1714.

Bowles, J. E. (1988). *Foundation analysis and design*.

Briaud, J. L., Smith, T., Meyer, B., et al. (1983). Using the pressuremeter curve to design laterally loaded piles. *Proceedings of the 15th Offshore Technology Conference*. OTC.

Broms, B. B. (1964). Lateral resistance of piles in cohesive soils. *Journal of the Soil Mechanics and Foundations Division 90*(2), 27–64.

Brown, D. A. & Shie, C.-F. (1990). Three dimensional finite element model of laterally loaded piles. *Computers and Geotechnics 10*(1), 59–79.

Burland, J. (1990). On the compressibility and shear strength of natural clays. *Géotechnique 40*(3), 329–378.

Chaloulos, Y. K., Bouckovalas, G. D., & Karamitros, D. K. (2013). Analysis of liquefaction effects on ultimate pile reaction to lateral spreading. *Journal of Geotechnical and Geoenvironmental Engineering 140*(3), 04013035.

Chandrasekaran, S., Boominathan, A., & Dodagoudar, G. (2010). Experimental investigations on the behaviour of pile groups in clay under lateral cyclic loading. *Geotechnical and Geological Engineering 28*(5), 603–617.

Chen, L. & Poulos, H. (1993). Analysis of pile-soil interaction under lateral loading using infinite and finite elements. *Computers and Geotechnics 15*(4), 189–220.

Comodromos, E. M., Papadopoulou, M. C., & Rentzeperis, I. K. (2009). Pile foundation analysis and design using experimental data and 3-D numerical analysis. *Computers and Geotechnics 36*(5), 819–836.

Craig, W. (1985). Modeling pile installation in centrifuge experiments. *Proceedings of the 11th International Conference on Soil Mechanics and Foundation Engineering*, pp. 1101–1104.

Dafalias, Y. & Popov, E. (1975). A model of nonlinearly hardening materials for complex loading. *Acta Mechanica 21*(3), 173–192.

Davies, M. P. (1987). *Predicting axially and laterally loaded pile behaviour using in-situ testing methods*. Ph. D. thesis, University of British Columbia.

Dewaikar, D., Salimath, R., & Sawant, V. (2009). A modified py curve for the analysis of a laterally loaded pile in stiff clay. *Australian Geomechanics 44*(3), 91.

DNV (1977). *Rules for the Design, Construction and Inspection of Offshore Structures*. Det Norske Veritas.

DNV (2010). *Design of Offshore Wind Turbine Structures*. Det Norske Veritas.

Doyle, E., Dean, E., Sharma, J., Bolton, M., Valsangkar, A., Newlin, J., et al. (2004). Centrifuge model tests on anchor piles for tension leg platforms. *Proceedings of the Offshore Technology Conference 2004*. OTC.

Dunnavant, T. W. & O'Neill, M. W. (1989). Experimental p-y model for submerged, stiff clay. *Journal of Geotechnical Engineering 115*(1), 95–114.

Frank, R. (2009). Design of foundations in france with the use of menard pressuremeter tests (MPM). *Soil Mechanics and Foundation Engineering 46*(6), 219–231.

Gabr, M., Lunne, T., & Powell, J. (1994). P-y analysis of laterally loaded piles in clay using dmt. *Journal of Geotechnical Engineering 120*(5), 816–837.

Gazetas, G. (1991). Foundation vibrations. *Foundation Engineering Handbook*, pp. 553–593. Springer.

Gazetas, G. & Dobry, R. (1984). Horizontal response of piles in layered soils. *Journal of Geotechnical Engineering 110*(1), 20–40.

Gazioglu, S. M. & O'Neill, M. W. (1984). Evaluation of py relationships in cohesive soils. *Analysis and Design of Pile Foundations:*, pp. 192–213. ASCE.

Georgiadis, K. & Georgiadis, M. (2010). Undrained lateral pile response in sloping ground. *Journal of Geotechnical and Geoenvironmental Engineering 136*(11), 1489–1500.

Georgiadis, K., Potts, D., & Zdravkovic, L. (2003). The influence of partial soil saturation on pile behaviour. *Géotechnique 53*(1), 11–25.

Georgiannou, V. N. (1988). *The behaviour of clayey sands under monotonic and cyclic loading*. Ph. D. thesis, Imperial College London (University of London).

Gerolymos, N. & Gazetas, G. (2006). Development of Winkler model for static and dynamic response of caisson foundations with soil and interface nonlinearities. *Soil Dynamics and Earthquake Engineering 26*(5), 363–376.

Guo, F., Lehane, B., & Ju, J. (2014). Experimentally derived CPT-based p-y curves for soft clay. *The 3rd International Symposium on Cone Penetration Testing. Las Vegas:[sn]*, pp. 1021–1028.

Hansen, J. (1961a). A general formula for bearing capacity. *Danish Geotechnical Institute Bulletin* (11).

Heidari, M., El Naggar, H., Jahanandish, M., & Ghahramani, A. (2014). Generalized cyclic p–y curve modeling for analysis of laterally loaded piles. *Soil Dynamics and Earthquake Engineering 63*, 138–149.

Hetényi, M. (1971). *Beams on elastic foundation: theory with applications in the fields of civil and mechanical engineering*. University of Michigan.

Ilyas, T., Leung, C., Chow, Y., & Budi, S. (2004). Centrifuge model study of laterally loaded pile groups in clay. *Journal of Geotechnical and Geoenvironmental Engineering 130*(3), 274–283.

Janoyan, K. D., Wallace, J. W., & Stewart, J. P. (2006). Full-scale cyclic lateral load test of reinforced concrete pier-column. *ACI structural journal 103*(2), 178.

Jardine, R. (1995). One perspective of the pre-failure deformation characteristics of some geomaterials. *Pre-Failure Deformation of Geomaterials. Proceedings of the International Symposium, 12-14 September 1994, Sapporo, Japan. 2 Vols*.

Jeanjean, P. et al. (2009). Re-assessment of py curves for soft clays from centrifuge testing and finite element modeling. *Proceedings of the Offshore Technology Conference 2009*. OTC.

Jeong, S., Kim, Y., & Kim, J. (2011). Influence on lateral rigidity of offshore piles using proposed p–y curves. *Ocean Engineering 38*(2–3), 397 – 408.

Jostad, H., Grimstad, G., Andersen, K., & Sivasithamparam, N. (2015). A FE procedure for calculation of cyclic behaviour of offshore foundations under partly drained conditions. *Frontiers in Offshore Geotechnics III*, 153–172.

Kalos, A. (2014). *Investigation of the nonlinear time-dependent soil behavior*. Ph. D. thesis, School of Civil Engineering, National Technical University of Athens (NTUA).

Kavvadas, M. & Amorosi, A. (2000). A constitutive model for structured soils. *Géotechnique 50*(3), 263–273.

Kavvadas, M. & Gazetas, G. (1993). Kinematic seismic response and bending of free-head piles in layered soil. *Géotechnique 43*(2), 207–222.

Kim, G., Kyung, D., Park, D., Kim, I., & Lee, J. (2016). CPT-based py analysis for piles embedded in clays under cyclic loading conditions. *KSCE Journal of Civil Engineering 20*(5), 1759–1768.

Kim, Y. & Jeong, S. (2010). Analysis of soil resistance on laterally loaded piles considering soil continuity. *Journal of Korean Society of Civil Engineers (KSCE) 26*(12), 31–40.

Kitazume, M. (1994). Lateral resistance of long pile in soft clay. *Proceedings of the International Conference Centrifuge 94*, pp. 485–490.

Kourkoulis, R., Gelagoti, F., Anastasopoulos, I., & Gazetas, G. (2010). Slope stabilizing piles and pile-groups: parametric study and design insights. *Journal of Geotechnical and Geoenvironmental Engineering 137*(7), 663–677.

Lee, J., Seo, K., Kang, B., Cho, S., & Kim, C. (2010). Application of effective cone factor for strength characterization of saturated clays. *GeoFlorida 2010: Advances in Analysis, Modeling & Design*, pp. 1029–1036. ASCE.

Lee, P. Y. & Gilbert, L. W. (1979). Behavior of laterally loaded pile in very soft clay. *Proceedings of the 11th Offshore Technology Conference*. OTC.

Lemnitzer, A., Khalili-Tehrani, P., Ahlberg, E. R., Rha, C., Taciroglu, E., Wallace, J. W., & Stewart, J. P. (2010). Nonlinear efficiency of bored pile group under lateral loading. *Journal of Geotechnical and Geoenvironmental Engineering 136*(12), 1673–1685.

Liang, R., Shatnawi, E. S., & Nusairat, J. (2007). Hyperbolic p-y criterion for cohesive soils. *Jordan Journal of Civil Engineering 1*(1), 38–58.

Malandraki, V. & Toll, D. (1994). Yielding of a weakly bonded artificial soil. *Proceedings of the International Symposium on Pre-Failure Deformation Characteristics of Geomaterials, Hokkaido, Japan*, Volume 1, pp. 315–20. Balkema, Rotterdam.

Marchetti, S. (1980). In situ tests by flat dilatometer. *Journal of the Geotechnical Engineering Division 106*(3), 299–321.

Matlock, H. (1970). Correlations for design of laterally loaded piles in soft clay. *Offshore Technology in Civil Engineering's Hall of Fame Papers from the Early Years*, 77–94.

Matlock, H. & Reese, L. C. (1960). Generalized solutions for laterally loaded piles. *Journal of the Soil Mechanics and Foundations Division 86*(5), 63–94.

McClelland, B. & Focht, J. A. (1958). Soil modulus for laterally loaded piles. *Transactions of the American Society of Civil Engineers 123*(1), 1049–1063.

Memarpour, M. M., Kimiaei, M., Shayanfar, M., & Khanzadi, M. (2012). Cyclic lateral response of pile foundations in offshore platforms. *Computers and Geotechnics 42*, 180–192.

Meyerhof, G. (1956). Penetration tests and bearing capacity of cohesionless soils. *Journal of the Soil Mechanics and Foundations Division 82*(1), 1–19.

Murff, J. D. & Hamilton, J. M. (1993). P-ultimate for undrained analysis of laterally loaded piles. *Journal of Geotechnical Engineering 119*(1), 91–107.

Mylonakis, G., Nikolaou, A., & Gazetas, G. (1997). Soil-pile-bridge seismic interaction: kinematic and inertial effects. Part I: soft soil. *Earthquake Engineering & Structural Dynamics 26*(3), 337–359.

Nichols, N. W., MJ, R., Mukherjee, K., Ayob, B., Sapihie, M., Clausen, C. J., Lunne, T., et al. (2014). Effect of lateral soil strength and stiffness on jacket foundation integrity and design for south china sea sites. *Proceedings of the Offshore Technology Conference-Asia 2014*. OTC.

O'Neill, M. W. (2001). Side resistance in piles and drilled shafts. *Journal of Geotechnical and Geoenvironmental Engineering 127*(1), 3–16.

Peck, R. B., Hanson, W. E., & Thornburn, T. H. (1974). *Foundation Engineering*, Volume 10. Wiley New York.

Poulos, H. G. (1971). Behavior of laterally loaded piles I. Single piles. *Journal of Soil Mechanics and Foundations Division*.

Randolph, M. F. & Houlsby, G. (1984). The limiting pressure on a circular pile loaded laterally in cohesive soil. *Géotechnique 34*(4), 613–623.

Reese, L. C., Cox, W. R., Koop, F. D., et al. (1975). Field testing and analysis of laterally loaded piles om stiff clay. *Proceedings of the 7th Offshore Technology Conference*. OTC.

Reese, L. C. & Van Impe, W. F. (2010). *Single piles and pile groups under lateral loading*. CRC Press.

Reese, L. C. & Welch, R. C. (1975). Lateral loading of deep foundations in stiff clay. *Journal of the Geotechnical engineering division 101*(7), 633–649.

Robertson, P. K., Davies, M. P., & Campanella, R. G. (1989). Design of laterally loaded driven piles using the flat dilatometer. *Geotechnical Testing Journal 12*(1), 30–38.

Rollins, K. M., Olsen, R. J., Egbert, J. J., Jensen, D. H., Olsen, K. G., & Garrett, B. H. (2006). Pile spacing effects on lateral pile group behavior: load tests. *Journal of Geotechnical and Geoenvironmental Engineering 132*(10), 1262–1271.

Rollins, K. M., Peterson, K. T., & Weaver, T. J. (1998). Lateral load behavior of full-scale pile group in clay. *Journal of Geotechnical and Geoenvironmental Engineering 124*(6), 468–478.

Roscoe, K. & Burland, J. (1968). On the generalized stress-strain behaviour of wet clay.

Roscoe, K. H., Schofield, A., & Wroth, C. (1958). On the yielding of soils. *Géotechnique 8*(1), 22–53.

Schofield, A. & Wroth, P. (1968). Critical State Soil Mechanics.

Scott, R. F. (1980). Analysis of centrifuge pile tests; simulation of pile-driving.

Scott, R. F. (1981). *Foundation Analysis*. Prentice-Hall London.

Simulia, D. S. (2012). Abaqus 6.12 documentation. *Providence, Rhode Island, US*.

Skempton, A. (1951). The bearing capacity of clays.

Smith, P., Jardine, R., & Hight, D. (1992). The yielding of bothkennar clay. *Géotechnique 42*(2), 257–274.

Stevens, J. & Audibert, J. (1979). Re-examination of py curve formulations. *Proceedings of the 11th Offshore Technology Conference*. OTC.

Stewart, D. & Randolph, M. (1991). A new site investigation tool for the centrifuge. *Proceedings of the International Conference Centrifuge 91*, pp. 531–538.

Stewart, J. P., Taciroglu, E., Wallace, J. W., Ahlberg, E. R., Lemnitzer, A., Rha, C., Tehrani, P., Keowen, S., Nigbor, R. L., & Salamanca, A. (2007). Full scale cyclic large deflection testing of foundation support systems for highway bridges. Part I: Drilled shaft foundations. *Structural and Geotechnical Engineering Laboratory, University of California, Los Angeles.* (Report No. UCLA-SGEL 2007/01,).

Sullivan, W. R., Reese, L. C., & Fenske, C. W. (1979). Unified method for analysis of laterally loaded piles in clay. *Numerical Methods in Offshore Piling, London 22*(23).

Templeton, J. S. et al. (2009). Finite element analysis of conductor/seafloor interaction. *Proceedings of the Offshore Technology Conference 2009*. OTC.

Terzaghi, K. (1943). *Theoretical soil mechanics*. Wiley.

Terzaghi, K. (1955). Evalution of coefficients of subgrade reaction. *Géotechnique 5*(4), 297–326.

Terzaghi, K., Peck, R. B., & Mesri, G. (1996). *Soil mechanics in engineering practice*. John Wiley & Sons.

Thompson, G. R. (1977). *Application of the Finite Element Method to the Development of py curves for Saturated Clays*. Ph. D. thesis, University of Texas at Austin.

Timoshenko, S. (1934). *Theory of Elasticity*. Engineering societies monographs. McGraw-Hill.

Tuladhar, R., Maki, T., & Mutsuyoshi, H. (2008). Cyclic behavior of laterally loaded concrete piles embedded into cohesive soil. *Earthquake Engineering & Structural Dynamics 37*(1), 43–59.

Vaughan, P., Maccarini, M., & Mokhtar, S. (1988). Indexing the engineering properties of residual soil. *Quarterly Journal of Engineering Geology and Hydrogeology 21*(1), 69–84.

Wang, T. & Liu, W. (2016). Development of cyclic p–y curves for laterally loaded pile based on T-bar penetration tests in clay. *Canadian Geotechnical Journal 53*(10), 1731–1741.

Welch, R. C. & Reese, L. C. (1972). Lateral load behavior of drilled shafts. Technical report, University of Texas at Austin.

Wood, D. M. (1990). *Soil behaviour and critical state soil mechanics*. Cambridge University Press.

Wu, D., Broms, B. B., & Choa, V. (1998). Design of laterally loaded piles in cohesive soils using py curves. *Soils and Foundations 38*(2), 17–26.

Yang, Z. & Jeremić, B. (2002). Numerical analysis of pile behaviour under lateral loads in layered elastic–plastic soils. *International Journal for Numerical and Analytical Methods in Geomechanics 26*(14), 1385–1406.

Yegian, M. & Wright, S. G. (1973). Lateral soil resistance displacement relationships for pile fundation in soft clays. *Proceedings of the 5th Offshore Technology Conference*. OTC.

Zhang, C., White, D., & Randolph, M. (2010). Centrifuge modeling of the cyclic lateral response of a rigid pile in soft clay. *Journal of Geotechnical and Geoenvironmental Engineering 137*(7), 717–729.

Zhang, Y. & Ng, C. W. (2016). Centrifuge modeling of single pile response due to lateral cyclic loading in kaolin clay. *Marine Georesources & Geotechnology* (just-accepted).